

**Design and synthesis of
multifunctional ligands to study and
prevent aggregation processes in
Amyotrophic Lateral Sclerosis
proteins**

Dissertation

for the award of the degree

“Doctor rerum naturalium”

of the Georg-August-Universität Göttingen

within the doctoral program Chemistry

of the Georg-August University School of Science (GAUSS)

submitted by

Viktorija Mrđen Debono

from Siverić, Croatia

Göttingen, 2020

Thesis Committee

Prof. Dr. Ulf Diederichsen

Institute of Organic and Biomolecular Chemistry, University of Göttingen

Jun.-Prof. Dr. Franziska Thomas

Organisch-Chemisches Institut, Ruprecht-Karls-Universität Heidelberg

Members of the Examination Board

Referee:

Prof. Dr. Ulf Diederichsen

Institute of Organic and Biomolecular Chemistry, University of Göttingen

Referee:

Jun.-Prof. Dr. Franziska Thomas

Organisch-Chemisches Institut, Ruprecht-Karls-Universität Heidelberg

Further members of the Examination Board

Prof. Dr. Kai Tittmann

Department of Molecular Enzymology, University of Göttingen

Prof. Dr. Lutz Ackermann

Institute of Organic and Biomolecular Chemistry, University of Göttingen

Dr. Felipe Opazo

Center for Biostructural Imaging of Neurodegeneration (BIN), University Medical Center Göttingen

Dr. Holm Frauendorf

Institute of Organic and Biomolecular Chemistry, University of Göttingen

Date of oral examination: 11.12.2020

The work described in this thesis was carried out under the supervision of Prof. Dr. Ulf Diederichsen and Prof. Dr. Franziska Thomas at the Center for Biostructural Imaging of Neurodegeneration of University Medical Center Göttingen, and at the Institute of Organic and Biomolecular Chemistry of the Georg-August University of Göttingen. It was done in collaboration with Lisa-Marie Funk and Prof. Dr. Kai Tittmann at the Department of Molecular Enzymology of the University of Göttingen between May 2016 and October 2020.

Declaration of Authorship

Hereby, I declare that I prepared the doctoral thesis entitled “Design and Synthesis of multifunctional ligands to study and prevent aggregation processes in Amyotrophic Lateral Sclerosis proteins” on my own, and with no other sources and aids than quoted.

This dissertation is the result of my own work and includes nothing, which is the outcome of work done in collaboration except where specifically indicated in the text. It has not been previously submitted, in part or whole, to any university or institution for any degree, diploma, or other qualification.

Göttingen, November 4, 2020

Signed:

Viktoria Mrđen Debono

To my parents

ABSTRACT

Amyotrophic lateral sclerosis (ALS) is an incurable lethal disease that affects motor neurons and its heterogeneity is reflected in various mutations among the sporadic ALS (sALS) and familial ALS (fALS) disease types. Superoxide dismutase-1 (SOD1), as a cell guardian, is an essential protein needed for the antioxidative cellular homeostasis but is many times a silent traitor in both types of ALS. The exact mechanisms by which SOD1 mutations contribute to ALS are still not fully understood, but structural investigations have interestingly revealed that the protein is a homodimer. It is suggested that the most severe mutations disrupt the dimer interface, causing dissociation, misfolding, and protein aggregation, which are the main sources of toxicity. Additionally, the aggregation processes trigger many other mechanisms, and correlation between the mutants' structural damage and aggregation pathways remains a puzzle.

In this thesis, *in silico* docking studies are done to design multifunctional ligands, whose biphenyl core structures mitigate the aggregation of a severe dimer interface mutant. A modular synthetic approach is developed, and different ligands are synthesized to anchor the protein dimer while preventing protein dissociation. Protein-ligand interactions, affinity, and their behaviour are then investigated via microscale thermophoresis, isothermal calorimetry, and aggregation assays. It is shown that synthesized ligands with aromatic substituents have a higher binding affinity toward the protein, and that they could reduce the aggregation of the SOD1 mutant. Additionally, the principle that the ligands can mediate a transfer of a fluorescent dye onto a target amino acid shows their multifunctionality. The design of affinity-based fluorogenic probes is envisaged as an extended approach and should assist to understand the mechanisms leading to SOD1-related ALS.

ACKNOWLEDGEMENTS

This journey toward the doctorate would not have been possible without the support of various people, that I would like to thank.

Firstly, I would like to thank my supervisors Prof. Dr. Ulf Diederichsen and Prof. Dr. Franziska Thomas. I thank Prof. Dr. Ulf Diederichsen for giving me the opportunity to work on this thesis for the last years, his valuable and realistic input in this project, and his confidence by allowing me a lot of freedom in my research. Particularly, I would like to thank Prof. Dr. Franziska Thomas for the interesting interdisciplinary project. Without her guidance, support, inspiring discussions, and fruitful input until the end, this thesis would have been impossible.

Furthermore, I would like to thank Prof. Dr. Kai Tittmann for being part of the examination board, for the nice collaboration on this project, his experience and knowledge in the enzymology part, and always welcoming atmosphere in his labs. His knowledgeable experience and contribution to the enzymology part are highly appreciated.

I would like to thank Dr. Felipe Opazo for being a member of the examination board, and for the ability to use devices of his department, and his readiness to share the knowledge and assist in fluorescence microscopy. I also thank Prof. Dr. Lutz Ackermann, and Dr. Holm Frauendorf for their acceptance to be the members of the examination board. I also thank Prof. Dr. Claudia Höbartner for being a third supervisor in the initial phase of this project, before leaving the University of Göttingen.

I would like to thank the whole Diederichsen and Thomas group for the really nice time, their acceptance, welcoming atmosphere, and willingness to speak English whenever was needed. Here, I would like to especially thank the “BIN” team: Robert Schirmacher, Dr. Selda Glowacki, and Vanessa Reusche, your commitment and willingness to always come to an agreement made it possible to work and establish a nice working environment in the new BIN labs. Robert, thank you for being a great colleague in this ALS project, your support and help since the early phases. It was fun to share the lab with you, and the synthesis discussions we had, and your ideas were always helpful. Furthermore, thank you for proofreading parts of this thesis. Selda, thank you for sharing your knowledge and experience, your high safety standards in the BIN labs made it possible to work in

clean, safe and tidy labs. And, thank you for always being there for me, whenever needed, whichever topic occurred I always could count on your support, also thank you for proofreading this thesis, your valuable comments are highly appreciated. Vanessa, it was fun sharing the labs and office with you, I am grateful for your understanding and enthusiasm to discuss all my assay troubles at any time.

I would like to thank all members of Prof. Tittmann group, for the nice and always welcoming atmosphere. Here, I am honestly grateful to Lisa-Marie Funk, for close collaboration, her expertise and great support in all protein-related questions. Thank you for your great commitment and patience with my ligands and the ITC experiments, also for familiarizing me with the protein crystallization it would be impossible to overcome the problems with our tricky SOD and get “my” first protein crystals without your support.

I would like to thank all lab rotation students and my Bachelor students Vanessa Theuer, Robert Keller and Franziska Otto. I hope you enjoyed your time and could learn a thing or two, I thank you for your high commitment and support in certain experiments and studies.

I would also like to acknowledge all my former and present colleagues in the IOBC lab, Dr. Barbara Hübrich, Dr. Jan-Dirk Wehland, Dr. Dina Zanbot, Brigitte Worbs and Mike Groth for a great atmosphere and tidy lab, and always keeping a place for me whenever BIN labs were out of order. Here I would also like to thank Mathis Rink, thank you for making me feel part of the Thomas group and for all discussion and interesting papers, and always welcome atmosphere in the “Mathis lab”. I also thank Benedikt Kugler for proofreading part of this thesis.

I would also like to acknowledge Aoife Neville and Angela Heinemann for their great organisational support and eagerness to always find a solution. My acknowledgements extend to analytics facilities, NMR service, Dr. Michael John and his team for all measured NMR spectra, and Mass department service run by Dr. Holm Frauendorf for all the mass spectra as well as for our test with protein measurements.

Furthermore, thank all my family and friends for their support even on a distance, throughout these years. Aoife Neville, Anastasiya and Robert Schirmacher thank you for all late food deliveries and chocolates for keeping me fit.

Especially, I would like to thank my parents for always supporting me and giving me freedom in all my decisions, even thousands of kilometres apart they are always with me.

Last but not least, I would like to thank my husband, Michael, for proofreading this thesis, his help with formatting and putting finishing touches onto it. Thank you for always believing in me, your sincere faith encouraged me in the most critical moments. Thank you for your support and staying always by my side.

CONTENTS

1 INTRODUCTION	1
2 STATE OF THE ART	3
2.1 Amyotrophic Lateral Sclerosis.....	3
2.1.1 Disease patterns and epidemiology	3
2.1.2 Pathophysiology and neuro mechanisms	5
2.1.3 Therapeutic approaches and ALS treatments	6
2.2 Superoxide Dismutase-1 (SOD1).....	8
2.2.1 Structure and function.....	8
2.2.2 SOD1 in familial ALS.....	11
2.2.3 ALS and SOD1 aggregation.....	13
2.2.4 Insight into current SOD1 therapeutic approaches.....	15
3 AIM OF THE WORK	21
4 BIOPHYSICAL AND COMPUTATIONAL METHODS	23
4.1 In silico design	23
4.2 Molecular docking	24
4.2.1 AutoDock Vina	25
4.3 Microscale Thermophoresis	26
4.4 Isothermal Calorimetry	28
5 RESULTS AND DISCUSSION	29
5.1 Ligands design and molecular docking.....	29
5.1.1 Analysis of the hSOD1 protein cavity and ligands design.....	29
5.1.2 Molecular docking to the hSOD1 protein.....	33
5.2 Synthesis	52
5.2.1 Modular synthesis approach.....	52
5.2.2 Retrosynthetic approach of lead structure A	53
5.2.2.1 Synthesis development toward the ligands A	54
5.2.3 Retrosynthesis and synthesis of lead structure B.....	60
5.2.4 Retrosynthesis and synthesis of lead structure C.....	63
5.2.5 Improved synthesis strategy A for a library enlargement.....	66
5.2.6 Proof of concept - NBD transfer reaction.....	72
5.3 Biophysical and Protein studies	74
5.3.1 Expression and purification of the hSOD1 proteins	74
5.3.2 Activity analysis of hSOD1wt and A4V proteins.....	76

5.4 Binding affinity assays and aggregation studies	82
5.4.1 <i>Microscale Thermophoresis (MST)</i>	82
5.4.2 <i>Isothermal Titration Calorimetry (ITC)</i>	96
5.4.4 <i>Ligands influence on the SOD1 aggregation</i>	100
5.5 X-ray crystallographic studies of hSOD1wt and ligands.....	105
6 SUMMARY AND OUTLOOK	107
7 EXPERIMENTAL SECTION	113
7.1 Materials.....	113
7.1.1 <i>Utilized Primers</i>	118
7.1.2 <i>Devices</i>	119
7.2 Methods.....	121
7.2.1 <i>Molecular Biology</i>	121
7.2.1.1 Plasmid Transformation	121
7.2.1.2 Isolation of Plasmid DNA	122
7.2.1.3 Determination of DNA Concentration.....	122
7.2.1.4 DNA Sequencing.....	122
7.2.1.5 Polymerase Chain Reaction.....	123
7.2.1.6 Horizontal Agarose Gel Electrophoresis	123
7.2.2 <i>Protein preparation</i>	123
7.2.2.1 Expression of hSOD1 and variants.....	123
7.2.2.2 Purification of the hSOD1 proteins.....	124
7.2.2.3 SDS-Polyacrylamide Gel Electrophoresis (SDS-PAGE)	125
7.2.2.4 Protein concentration determination.....	125
7.2.2.5 Reconstitution of hSOD1 with Cofactors	125
7.2.2.6 Activity assay of the SOD1 proteins	126
7.2.2.7 Size exclusion chromatography (SEC).....	126
7.2.3 <i>X-Ray Crystallography</i>	127
7.2.3.1 Crystallization conditions for hSOD1 proteins.....	127
7.2.3.2 X-ray Data Collection and Refinement	127
7.2.4 <i>Biophysical studies</i>	128
7.2.4.1 Thermal shift assay.....	128
7.2.4.2 Microscale Thermophoresis	128
7.2.4.3 Isothermal titration calorimetry (ITC)	130
7.2.4.4 Aggregation assay	130
7.3 <i>In silico</i> design and molecular docking.....	131
7.3.1 <i>Preparation of protein and ligands structure for docking</i>	131
7.3.2 <i>Docking procedure with AutoDock Vina</i>	132
7.4 Synthesis of ligand molecules.....	132

7.4.1	<i>Analytics</i>	132
7.4.2	<i>Synthetic procedures</i>	134
7.4.2.1	3-Iodo-4-nitrophenol (1)	134
7.4.2.2	<i>Tert</i> -butyl(3-iodo-4-nitrophenoxy)diphenylsilane (2).....	135
7.4.2.3	1-Bromo-4-(<i>tert</i> -butoxy) benzene (4)	136
7.4.2.4	4-(<i>Tert</i> -butoxy)phenyl)boronic acid (5).....	136
7.4.2.5	((4'-(<i>Tert</i> -butoxy)-6-nitro-[1,1'-biphenyl]-3-yl)oxy)(<i>tert</i> -butyl)diphenylsilane (13)	137
7.4.2.6	4'-(Benzyloxy)-6-nitro-[1,1'-biphenyl]-3-ol (18)	138
7.4.2.7	6-Nitro-4'-(trifluoromethyl)-[1,1'-biphenyl]-3-ol (19)	139
7.4.2.8	6-Nitro-[1,1'-biphenyl]-3-ol (21)	140
7.4.2.9	6-Nitro-[1,1'-biphenyl]-3-yl propionate (22).....	141
7.4.2.10	6-Amino-[1,1'-biphenyl]-3-yl propionate (23).....	142
7.4.2.11	2-(4-(Benzyloxy)phenyl)acetic acid (26).....	143
7.4.2.12	2-(4-((Tetrahydro-2H-pyran-2-yl)oxy)phenyl)acetic acid (27).....	144
7.4.2.13	6-(2-(4-(Benzyloxy)phenyl)acetamido)-[1,1'-biphenyl]-3-yl propionate (28)	145
7.4.2.14	4'-(Benzyloxy)-6-nitro-[1,1'-biphenyl]-3-yl propionate (29)	146
7.4.2.15	6-Amino-4'-(benzyloxy)-[1,1'-biphenyl]-3-yl propionate (30)	147
7.4.2.16	4'-(Benzyloxy)-6-(2-(4-(benzyloxy)phenyl)acetamido)-[1,1'-biphenyl]-3-yl propionate (31).....	148
7.4.2.17	6-Amino-4'-(trifluoromethyl)-[1,1'-biphenyl]-3-yl propionate (32).....	149
7.4.2.18	6-(2-(4-((Tetrahydro-2H-pyran-2-yl)oxy)phenyl)acetamido)-4'-(trifluoromethyl)-[1,1'-biphenyl]-3-yl propionate (33).....	151
7.4.2.19	2-(4-(Benzyloxy)phenyl)- <i>N</i> -(5-hydroxy-[1,1'-biphenyl]-2-yl)acetamide (34).....	152
7.4.2.20	<i>N</i> -(5-Hydroxy-4'-(trifluoromethyl)-[1,1'-biphenyl]-2-yl)-2-(4-((tetrahydro-2H-pyran-2-yl)oxy)phenyl)acetamide (35).....	153
7.4.2.21	2-(4-(Benzyloxy)phenyl)- <i>N</i> -(5-((7-nitrobenzo[<i>c</i>][1,2,5]oxadiazol-4-yl)oxy)-[1,1'-biphenyl]-2-yl)acetamide (36)	155
7.4.2.22	<i>N</i> -(5-((7-Nitrobenzo[<i>c</i>][1,2,5]oxadiazol-4-yl)oxy)-4'-(trifluoromethyl)-[1,1'-biphenyl]-2-yl)-2-(4-((tetrahydro-2H-pyran-2-yl)oxy)phenyl)acetamide (37).....	156
7.4.2.23	2-(4-Hydroxyphenyl)- <i>N</i> -(5-((7-nitrobenzo[<i>c</i>][1,2,5]oxadiazol-4-yl)oxy)-4'-(trifluoromethyl)-[1,1'-biphenyl]-2-yl)acetamide (38).....	158
7.4.2.24	<i>N</i> -(5-Hydroxy-4'-(trifluoromethyl)-[1,1'-biphenyl]-2-yl)-2-(4-hydroxyphenyl)acetamide (L9)	159
7.4.2.25	<i>N</i> -(4',5-Dihydroxy-[1,1'-biphenyl]-2-yl)-2-(4-hydroxyphenyl)acetamide (L1)	160
7.4.2.26	<i>N</i> -(5-Hydroxy-[1,1'-biphenyl]-2-yl)-2-(4-hydroxyphenyl)acetamide (L10)	162
7.4.2.27	2-Bromo-1-(4-(<i>tert</i> -butoxy)phenyl)ethan-1-one (40).....	163
7.4.2.28	2-Bromo-1-(4-((tetrahydro-2H-pyran-2-yl)oxy)phenyl)ethan-1-one (43)	163
7.4.2.29	6-((2-Oxo-2-phenylethyl)amino)-[1,1'-biphenyl]-3-yl propionate (44)	164
7.4.2.30	6-((4-Nitro- <i>N</i> -(2-oxo-2-(4-((tetrahydro-2H-pyran-2-yl)oxy)phenyl)ethyl)phenyl)sulfonamido)-[1,1'-biphenyl]-3-yl propionate(47).....	165
7.4.2.31	4-Aminophenyl benzoate (56).....	166

7.4.2.32 4-Amino-3-bromophenyl benzoate (57)	167
7.4.2.33 4-(((Benzyloxy)carbonyl)amino)-3-bromophenyl benzoate (58)	168
7.4.2.34 Benzyl (2-bromo-4-hydroxyphenyl) carbamate (59).....	169
7.4.2.35 Benzyl (5-hydroxy-4'-((tetrahydro-2H-pyran-2-yl)oxy)-[1,1'-biphenyl]-2-yl)carbamate (60)	170
7.4.2.36 6-(((Benzyloxy)carbonyl)amino)-4'-((tetrahydro-2H-pyran-2-yl)oxy)-[1,1'-biphenyl]-3-yl benzoate (61).....	171
7.4.2.37 6-Amino-4'-((tetrahydro-2H-pyran-2-yl)oxy)-[1,1'-biphenyl]-3-yl benzoate (62)	172
7.4.2.38 6-(2-(3,5-Dimethoxyphenyl)acetamido)-4'-((tetrahydro-2H-pyran-2-yl)oxy)-[1,1'-biphenyl]-3-yl benzoate (63)	174
7.4.2.39 6-(2-(2,5-Dimethoxyphenyl)acetamido)-4'-((tetrahydro-2H-pyran-2-yl)oxy)- [1,1'-biphenyl]-3-yl benzoate (64)	175
7.4.2.40 4'-((Tetrahydro-2H-pyran-2-yl)oxy)-6-(2-(o-tolyloxy)acetamido)-[1,1'-biphenyl]- 3-yl benzoate (65).....	176
7.4.2.41 <i>N</i> -(4',5-Dihydroxy-[1,1'-biphenyl]-2-yl)-2-(5-methyl-2,4-dioxo-3,4-dihydropyrimidin-1(2H)-yl)acetamide (67).....	178
7.4.2.42 6-(3-Methylbutanamido)-4'-((tetrahydro-2H-pyran-2-yl)oxy)-[1,1'-biphenyl]-3-yl benzoate (68)	179
7.4.2.43 6-Isobutyramido-4'-((tetrahydro-2H-pyran-2-yl)oxy)-[1,1'-biphenyl]-3-yl benzoate (69)	180
7.4.2.44 <i>N</i> -(4',5-Dihydroxy-[1,1'-biphenyl]-2-yl)-2-methoxyacetamide (70)	181
7.4.2.45 3-Bromo-4-(2-(2,5-dimethoxyphenyl)acetamido)phenyl benzoate (71)	182
7.4.2.46 2-(2,5-Dimethoxyphenyl)- <i>N</i> -(5-hydroxy-4'-(trifluoromethyl)-[1,1'-biphenyl]-2-yl)acetamide (72).....	184
7.4.2.47 2-(2,5-Dimethoxyphenyl)- <i>N</i> -(5-hydroxy-4'-nitro-[1,1'-biphenyl]-2-yl)acetamide (73).....	185
7.4.2.48 <i>N</i> -(4',5-Dihydroxy-[1,1'-biphenyl]-2-yl)-2-(3,5-dimethoxyphenyl)acetamide (74)	186
7.4.2.49 <i>N</i> -(4',5-Dihydroxy-[1,1'-biphenyl]-2-yl)-2-(o-tolyloxy)acetamide (75)	188
7.4.2.50 <i>N</i> -(4',5-Dihydroxy-[1,1'-biphenyl]-2-yl)-2-(2,5-dimethoxyphenyl)acetamide (76)	189
7.4.2.51 <i>N</i> -(4',5-Dihydroxy-[1,1'-biphenyl]-2-yl)-3-methylbutanamide (77).....	190
7.4.2.52 <i>N</i> -(4',5-Dihydroxy-[1,1'-biphenyl]-2-yl)isobutyramide (78)	192
7.4.2.53 4'-((Tetrahydro-2H-pyran-2-yl)oxy)-6-(2-(4-((tetrahydro-2H-pyran-2-yl)oxy)phenyl)acetamido)-[1,1'-biphenyl]-3-yl benzoate (81)	193
7.4.2.54 <i>N</i> -(5-((7-Nitrobenzo[c][1,2,5]oxadiazol-4-yl)oxy)-4'-((tetrahydro-2H-pyran-2-yl)oxy)-[1,1'-biphenyl]-2-yl)-2-(4-((tetrahydro-2H-pyran-2-yl)oxy)phenyl)acetamide (82)	195
7.4.2.55 <i>N</i> -(4'-Hydroxy-5-((7-nitrobenzo[c][1,2,5]oxadiazol-4-yl)oxy)-[1,1'-biphenyl]-2-yl)-2-(4-hydroxyphenyl)acetamide (83) LS A1.....	196

8 BIBLIOGRAPHY 199

9 APPENDICES 213

9.1 Expression and purification data of hSOD1 214

9.2 Free binding energies of the lead structures..... 216

9.3 Biophysical and protein studies 218

9.4 Binding affinity assay development.....	219
9.5 Aggregation assay data	224
9.6 Analytics	225

LIST OF ABBREVIATIONS AND ACRONYMS

ALS	Amyotrophic Lateral Sclerosis
AU	absorption unit
calc.	calculated
δ	chemical shift (NMR)
DCM	dichloromethane
DIPEA	<i>N, N'</i> -diisopropylethylamine
DMF	dimethylformamide
DMSO	dimethyl sulfoxide
ε	extinction coefficient
EDTA	ethylenediaminetetraacetic acid
eq	equivalents
ESI-MS	electrospray ionisation mass spectrometry
fALS	familial ALS
FTIR	Fourier-transform infrared spectroscopy
HEPES	4-(2-hydroxyethyl)-1-piperazineethanesulfonic acid
HIC	hydrophobic interaction chromatography
HOBt	hydroxybenzotriazole
HPLC	high performance liquid chromatography
HR-MS	high resolution mass spectrometry
HTS	high throughput screening
ITC	Isothermal Titration Calorimetry
IPTG	Isopropyl β -D-1-thiogalactopyranoside
MeCN	acetonitrile
MeOH	methanol

MND	motor neuron disease
MST	Microscale Thermophoresis
MTBE	methyl- <i>tert</i> -butylether
<i>m/z</i>	mass-to-charge ratio
NBD	7-nitro-2-1,3-benzoxadiazole
NMR	nuclear magnetic resonance
PG	protection group
PEG	polyethylene glycol
PPTS	pyridinium <i>p</i> -toluenesulfonate
QSAR	quantitative structure-activity relationship
R_f	retention factor
RMSD	root-mean-square deviation
ROS	reactive oxygen species
rt	room temperature
sALS	sporadic ALS
SDS	sodium dodecyl sulfate
SEC	size exclusion chromatography
SOD	superoxide dismutase
tBu	<i>tert</i> -butyl protection group
THF	tetrahydrofuran
TLC	thin layer chromatography
t_R	retention time
<i>v/v</i>	volume/volume ratio
<i>w/v</i>	weight/volume ratio
wt	wild type
Z (CBz)	carboxybenzyl protection group

1 INTRODUCTION

Communication between nerve cells in the human brain and muscle nerves is a crucial step needed for voluntary muscle movements. Despite the high number of neurons and their continuous impressive performance and signalling in the brain, damage of motor neurons can be fatal very quickly. These fatalities are seen in many neurodegenerative diseases, and among them, the deterioration and loss of upper and lower motor neurons is still the main characteristic of Amyotrophic lateral sclerosis (ALS).^[1,2] When the motor neurons stop sending a signal, the muscles are weakened, which leads to paralysis. And, when the skeletal muscles of the diaphragm are affected, the outcome becomes mortal very fast. Now, there are only two approved drugs for the treatment of ALS, and while the cause remains unknown, there is no cure for this disease. It was initially thought that ALS is an only sporadic disease (sALS), however, it is shown that some people inherited the disease from their parents, also known as familial ALS (fALS).^[3] The research identified different processes in the neurons by studying the modified genes from those patients, that might cause the disease. It is not clear which processes are the result of the disease and which could be causing it. Also, different epidemiology and heterogeneity involved do not go hand in hand with fast revelation in curing the diseases.^[4] However, since that time, many breakthroughs in different areas of science have also contributed to the knowledge of the ALS disease.

The most impact on ALS development was the discovery of the first gene *sod1*, related to this pathogenic disease. Since then, more than 50 years ago, different genes were discovered.^[5] However, research has shown that SOD1 is still the second most present protein involved in many processes related to the ALS as well as other neurodegenerative

diseases. Moreover, up until now, there are no treatments for SOD1-ALS related disease. With the resolution of the crystal structure of the SOD1 protein, research has focused on the structural investigation of the protein and its mutations that occur in fALS and sALS patients. Multiple mechanisms were indicated into the toxicity of the SOD1, and as a protein involved in antioxidative regulation, initially, it was assumed that the main problem is a functional loss of the protein. However, now it is generally accepted that the main pathogenicity of the SOD1-mutant proteins is rather causing toxic gain of function, either in single or dependent processes, maturation, misfolding, stability and aggregation.^[6] Lack of stability has been discussed as a reason for SOD1 malfunction, and so far, groups proposed that it is possible to stabilize the protein itself. Our approach toward potential therapeutically interesting targets is presented in the following chapters, firstly, through an *in silico* design approach to structurally understand the SOD1 protein and to identify potential sites for protein stabilization by small-molecule binding, secondly, through a synthesis of potential lead structures and lead structure libraries, and thirdly through testing of synthesized ligands for their affinity to the protein and their ability to stabilize the protein structure and slow down ALS relevant toxic protein aggregation.

2 STATE OF THE ART

2.1 Amyotrophic Lateral Sclerosis

2.1.1 Disease patterns and epidemiology

In the early 19th century neurologist Jean-Martin Charcot reported to his medical colleagues, after reassuring his patient of recovery, “...we can and must speak amongst ourselves in total frankness. The prognosis is deplorable; alas, he is a lost soul...”^[7] This followed from their earlier studies, in which life of other ALS patients from first indications until the end was not more than three years. Furthermore, they found that lesions in different parts of the spinal cord, lateral and frontal horn, have distinct manifestation, chronic progressive paralysis, muscle contractures and spasticity without atrophy, whereas in the latter one paralysis with muscle atrophy.^[7] Until today, fundamental description in the clinical picture of the amyotrophic lateral sclerosis (ALS), also known as Charcot, Lou Gehrig’s or motor neuron disease (MND) did not change much.^{[7][8][9]} However, crucial patterns and characteristics evolved throughout the years, like weakness, muscle wasting, fasciculations, weakness in anti-gravity muscle or spasticity, which could be attributed to the upper motor neurons.^[1] Even though that only approximately 27-28% of disease onsets show bulbar symptoms, which combine difficulty of speaking and swallowing (dysarthria and dysphagia), while 58-80% is usually manifested in the limb-onset, and the remaining 8-23% is a combined onset, the effect on bulbar functions usually have more detrimental consequences.^[2,7,9,10] Additionally, patients with bulbar onset are usually diagnosed earlier than the others. However, because of nonspecific early symptoms, delay in ALS diagnosis still ranges

from 9 to 24 months.^[10] Usual disease onset is between 51 and 66 years, and only 10% of diagnosed patients live 10 years or longer, while the majority has only 24 - 50 months to live after diagnosis.^[10] A yearly incidence of 0.6 to 3.8 per 100 000 individuals worldwide is reported; however only in Europe, the initial range rate is two times higher. Even though the incidence and prevalence numbers vary significantly between the continents and countries, mostly because there are not enough real population studies outside of Europe, the number of diagnosed patients is increasing, and risks emerge also from different environmental factors that are still poorly understood.^[1,10,11] ALS disease is divided into two major groups, sporadic ALS (sALS) that covers 90% of all the cases, and familial ALS (fALS) with 10% of all cases. While sALS occurs with no familial history, in fALS at least one additional family member has inherited disease either in an autosomal dominant or recessive manner.^{[3,12][13]} So far, clinically it is not possible to distinguish between these two types; however, advanced research in molecular genetics, ensures a better understanding of familial ALS, which on its own provides also a little more insight into cases with sALS.^[14] Today, with more than 50 genes classified as potentially causative, 40-55% of all fALS cases are attributed to four genes and their pathogen variants *sod1*, *c9orf72*, *fus* and *tardbp*.^[4,12,14] Additionally, as shown in Figure 2.1, meta-analysis among diverse studies shows that in European population almost 34% of fALS cases are linked to *c9orf72* gene, 3-4% to *fus* and *tardbp*, respectively, and 15% to *sod1*, while the rest is still unknown. However, the numbers for the two most represented genes linked to fALS are quite different for the Asian population, 30% are attributed to the *sod1* gene, and only 2.3% to the *c9orf72* gene.^[4] The anatomy of sALS remains unknown, as only 11% can be attributed to the most common genes classified in fALS. Therefore the difference across populations is negligible.^[4,12]

Up to date research was conducted toward understanding and correlation of genetic risks for sALS, yet a huge part remains undiscovered, beside complexity of the disease itself, lack in more advanced technologies and some environmental factors also play a role that is not easily correlated.^[12,15]

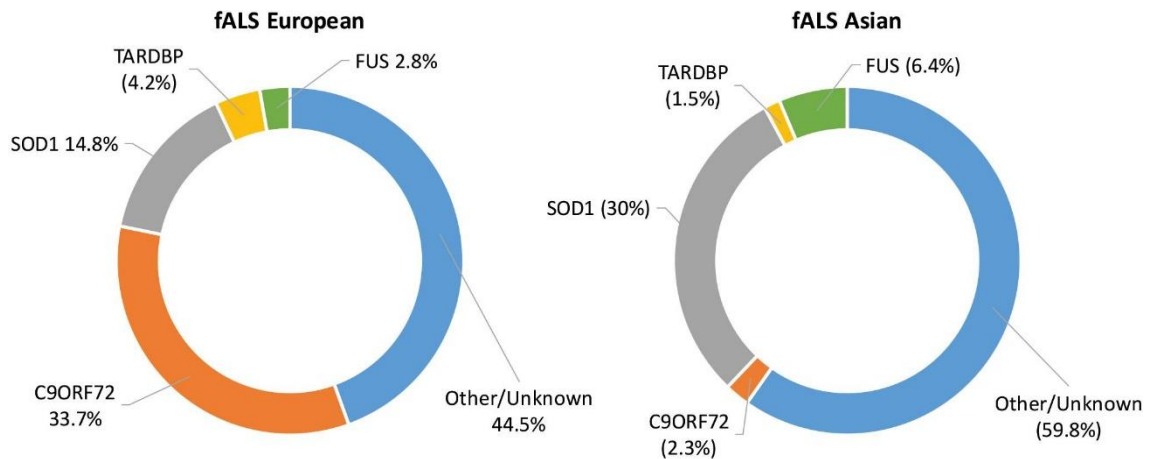


Figure 2.1 Distribution of fALS with most common genetic variation in European (*left*) and Asian (*right*) population. Adapted from ^[12], Copyright © 2019 with permission from Mezzini, Flynn, Pitout, Fletcher, Wilton and Akkari.

2.1.2 Pathophysiology and neuro mechanisms

The complexity of all pathophysiological mechanisms, genetic findings and symptoms related to the ALS disease is vast, even so, that is preferably named, neurodegenerative syndrome, rather than disease.^[16] Generally, genetic mutations are associated into mostly three pathophysiological processes: disturbance in RNA mechanisms, protein degradation pathways and impaired axonal function and transport.^[12,17] Yet, these are just part of the mechanisms proposed to influence ALS. How exactly they are correlated, and what is more causative, remains an unsolved puzzle. Here, some mechanisms are described, and shown in Figure 2.2.^[18] A gain of toxic RNA species, intracellular aggregates and nuclear transport defect is usually caused by mutations and depletions of *c9orf72*, *tardbp* and *fus* genes, which alter transcription and translation processes.^[12,13,16] Williamson and Cleveland^[19] showed axonal impaired function of SOD1 mutants, early, before the onset of symptoms. Now it is known that accumulation of neurofilaments, as well as loss or gain of function in glial cells, disrupt cytoskeletal architecture and impair axonal function.^[12,17] Mutations in SOD1 and other genes have interference with protein degradation pathways, and destruction of proteostasis, mostly due to aggregate accumulation and disruption of the protein clearance mechanisms.^[11,12,18] The processes related to SOD1 will be discussed further in Section 2.2. Glutamate excitotoxicity is a pathological response onto the impaired function of EEAT2 receptor and reduced clearance of glutamate from the synaptic cleft, which leads to an increased damage of AMPA and NMDA glutamate receptors and induces neurodegeneration through an increased flow of Ca^{2+} .^[12,18] This process triggers mitochondrial dysfunction and

oxidative stress, by the accumulation of Ca^{2+} in mitochondria, which results in generating neuronal toxic hydroxyl and free radicals, yet the effects of SOD1 mutants on mitochondrial dysfunction seem to result from misfolded proteins rather than impaired enzymatic activity.^[18,20] Other mechanisms such as oligodendrocyte dysfunction and neuroinflammation have also been implicated in ALS pathophysiology, contributing axonal impairment, and neuronal loss by microglia and astrocytes inflammatory response.^[12,17,18,21]

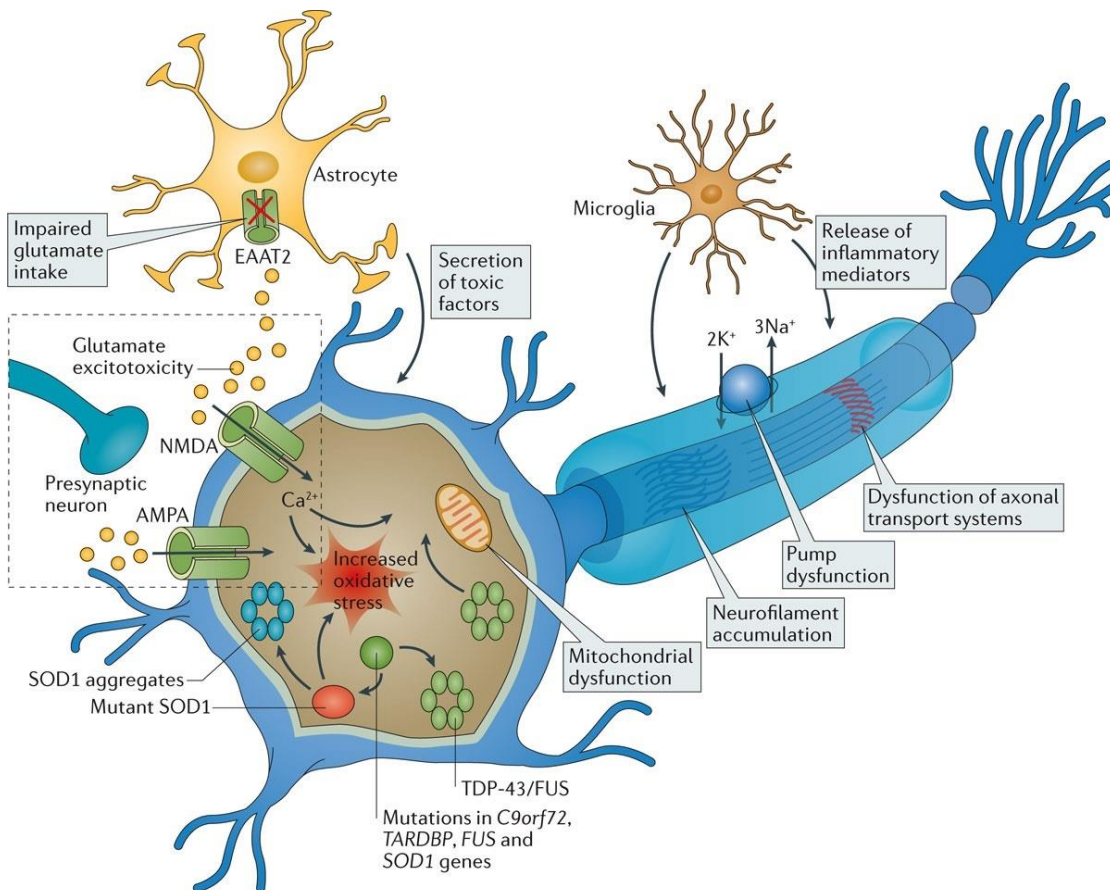
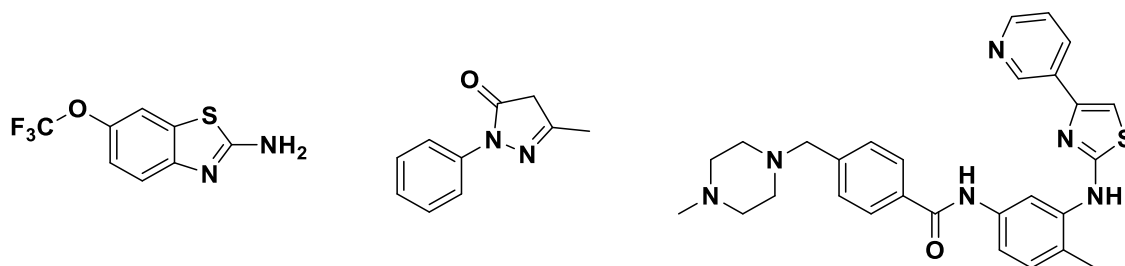


Figure 2.2 Some pathophysiological mechanisms involved in Amyotrophic Lateral Sclerosis neurodegeneration. Adapted from^[18], Copyright © 2016, Springer Nature

2.1.3 Therapeutic approaches and ALS treatments

Currently, there are only two drugs, which are approved as a treatment for ALS, and only Riluzole^[22] reached the market worldwide (see Scheme 2.1). It was approved in 1995 as a first drug for ALS, and, in the first trial, showed improvement of limb function in comparison with the placebo group; however, it only prolongs patients survival about three months.^[12,22,23] Riluzole influences glutamate excitotoxicity pathways. Nowadays, the theory of blocking mechanisms on the glutamate receptors^[24] is not accepted anymore,

yet it is proposed that the effect is mostly obtained by stimulating glutamate uptake from the synapse.^[25,26] Edaravone^[27], is a drug, which has been approved as a free radical scavenger and antioxidative agent in 2017 for the US and Japan market.^[12,28] One of the reasons, why the drug still did not reach EU market is due to the failure in a first clinical phase 3 trial. Two additional trials showed impact in treated patients compared to the placebo control. However, the trials were completed only on Japanese population, which, epidemiologically, differs from European countries.^[26] In the 25 years from first drug approval more than sixty compounds have been researched, and mostly tested for anti-inflammatory, anti-oxidative or neuroprotective treatment, however, the most common failure of efficiency was in human clinical trials, which is another indication for the complexity of the disease and its heterogeneity.^[26] Masitinib is potentially next in line to be approved as a drug for ALS treatment. It is known as a selective tyrosine kinase inhibitor, and, in preclinical studies showed an impact on neuroinflammation mechanisms, as well as prolonged survival in mutated sod1 mice, even if delivered after the disease onset.^[26] The second larger phase 3 clinical trial for Masitinib was approved and started this year (2020) with an estimated duration of two years.^[29]



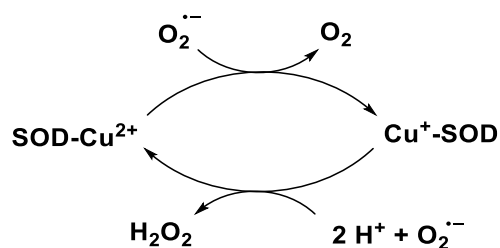
Scheme 2.1 Drugs approved for treatment in ALS, Riluzole (*left*), Edaravone (*centre*) and drug in phase 3 of clinical trials Masitinib (*right*).

New approaches for ALS treatment evolved particularly in RNA therapeutics, with antisense oligonucleotide drugs, in which the first drug for the treatment of ALS is already in clinical trials with estimated primary results in summer 2021.^[12,30] So far, there are still many pathophysiological mechanisms unexplored in terms of treatments of ALS, and because of the heterogeneity and complexity involved, it might be required to act simultaneously on different mechanisms and pathways to achieve notable results.

2.2 Superoxide Dismutase-1 (SOD1)

2.2.1 Structure and function

In the late 1960s McCord and Fridovich discovered the enzyme, superoxide dismutase. The main breakthrough was the attribution of the function to the ubiquitous blue-green copper protein (erythrocyuprein), which, until that time, was assumed to be only a copper storage without any enzymatic function.^[31,32] By studying the reduction of cytochrome c with the enzyme xanthine oxidase (XO), they confirmed that inhibition of the reaction is not occurring *via* the binding site of XO as originally thought, rather a superoxide radical is the product of the xanthine oxidase and inhibition occurs in a competing reaction between the SOD enzyme and cytochrome c.^[31,33] They concluded that the enzyme SOD catalyses the dismutation of superoxide to hydrogen peroxide and oxygen.^[31] Furthermore, the catalytic cycle, in which SOD catalyses the disproportionation of two superoxide molecules, was later called “ping-pong mechanism”, Scheme 2.2.^[34,35]

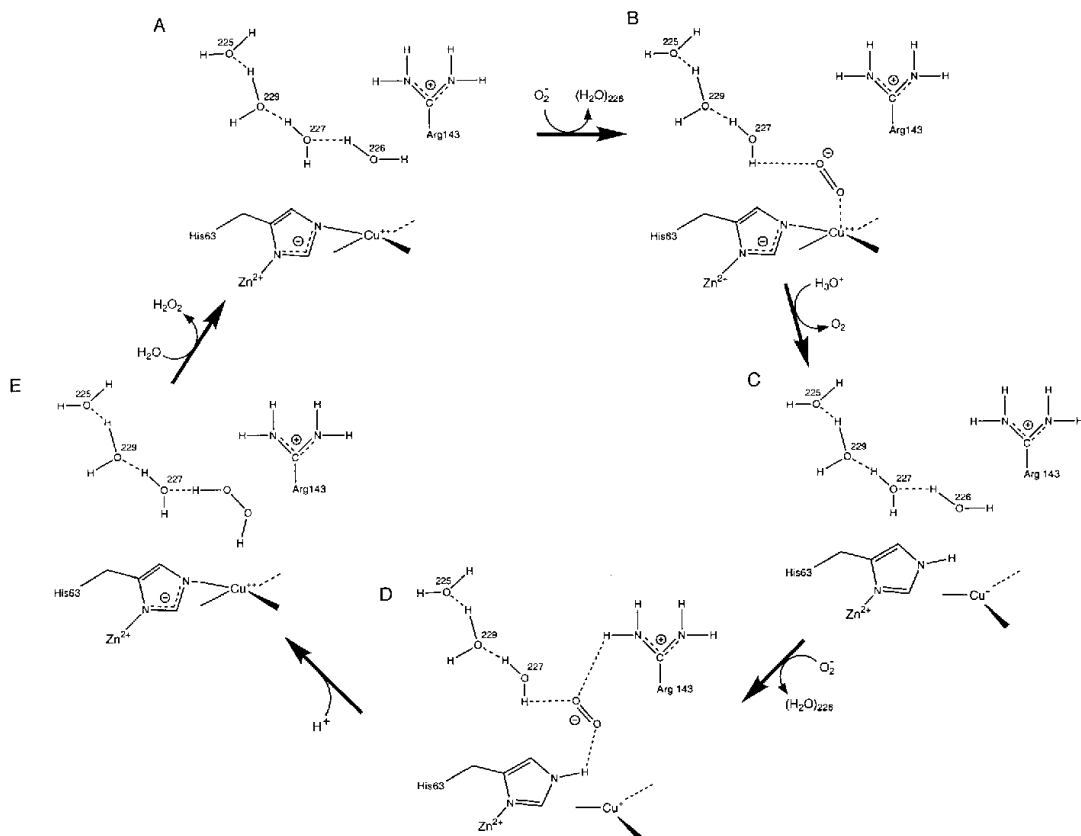


Scheme 2.2 Disproportionation of superoxide anion in SOD1 catalysed mechanism

The importance of the SOD enzyme was recognised very quickly as it could not be found in anaerobic organisms, yet in almost all biological aerobic organisms, to serve as a bodyguard from reactive oxygen species (ROS) of the oxygen metabolism.^[35–37,37] With a 10^4 higher rate than spontaneous dismutation, the SOD1 catalysed reaction is also regarded as diffusion-controlled ($2 \times 10^9 \text{ M}^{-1}\text{s}^{-1}$).^[38] SOD enzymes are divided in different families according to their metals in the active sites. In humans, there are three different forms of SOD: SOD2 (Mn-SOD) is localised in the mitochondria and contains Mn as a cofactor in the active site. The Cu and Zn family is subdivided in two forms: EC-SOD is found in the extracellular space, and the Cu,Zn-SOD1 protein is located intracellular e.g. the cytoplasm and nucleus.^[39,40,40] Today, SOD1 is known as a 32 kDa homodimeric protein, which consists of 153 amino acids per monomer. From the early crystallographic structures of the bovine, later human SOD1 it was found that each monomer unit contains an eight-stranded anti-parallel β -barrel forming the hydrophobic core.^[34,41] (see Figure

2.3) In the active centre of each monomer, copper and zinc coordinating sites are linked by His63 in the oxidized Cu(II) state, Figure 2.3 (bottom). They are balanced among two loops, which are both contributing to the active site, the electrostatic loop VII (amino acids 122-143) shown in orange-red and the zinc loop IV (amino acids 49-84) in blue. Furthermore, the zinc-loop has also a structural role by which the β -barrel sheet is stabilized *via* a (Cys57-Cys146) disulphide bond, shown in yellow, Figure 2.3 (top). In the catalytic process, both loops are involved by forming the active site and enhancing the interaction with a substrate *via* electrostatic forces.

The mechanism of the reaction starts by water displacement at copper (II) when the superoxide enters the cavity, and binds to a copper, stabilized by Arg143. Copper (II) is then reduced to copper (I), and oxygen is released simultaneously. Consequently, His63 is protonated and binds the second superoxide which also forms hydrogen bonds to Arg143, due to bond rearrangements and a proton transfer from the water in the active site, copper (I) is oxidised and hydrogen peroxide is released, Scheme 2.3.^[42,43,43]



Scheme 2.3 SOD1 mechanism cycle in the active site, taken from.^[43]

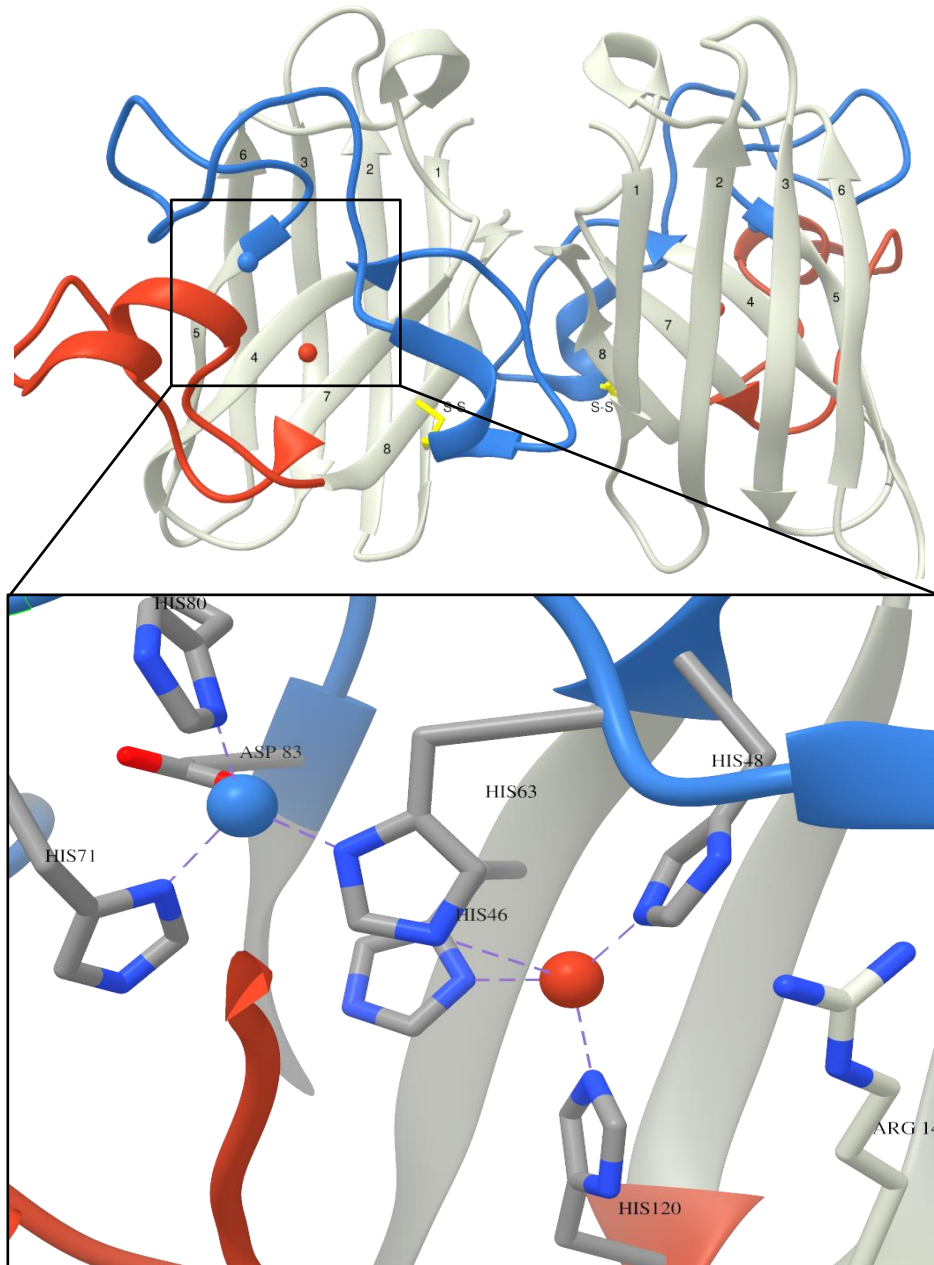


Figure 2.3 Human SOD1 homodimer and its active site, top and bottom. Zinc and loop IV (blue), Cu and electrostatic loop VII (orange), disulphide bridge between strand 8 of the β -barrel and loop IV (yellow). PDB code 2V0A, model visualized *via* UCSF Chimera^[44].

The fully metallated SOD1 protein with an intact intra-molecular disulphide bond is a very stable homodimer with a melting temperature ranging from 77 °C up to 100 °C, which is also likely to be buffer influenced.^[34,45,46]

2.2.2 SOD1 in familial ALS

A new era in ALS disease research began almost 30 years ago with the discovery of the 21q22.1 chromosomal locus of the *sod1* gene. 11 mutations in the primary *sod1* sequence were associated with familial ALS.^[5] Now 187 mutations in *sod1* are known to be linked to ALS disease, as last accessed from the ALSod database (October 2020).^[47] However, it is not confirmed if all of them are also pathogenic. Many groups showed that the mutations influence structural integrity of the β -barrel, the dimer interface and the loops leading to an overall destabilization of the protein structure, later known as “*framework destabilization*”.^{[48][49]}

Uniform arguments were observed throughout the years from many experiments that mutations indeed influence the unfolding properties, causing dimer destabilisation, and the formation of soluble and insoluble oligomers. Aggregation was also correlated to the lack of the intramolecular disulphide bridge and/or cofactors in the active site.^[49,50,51–53,53] Interestingly, the most common mutations Ala4Val (A4V) and Ile113Thr (I113T) are located at the dimer interface. The survival of patients with A4V or I113T SOD1 mutations is very short with 1.2 to 4.3 years after onset. Other mutations such as H46R go along with a survival rate of 17.6 years in average.^[54] Furthermore, I113T can also appear as sporadic phenotype and can have a different onset and variability, where more than 90% people that carry the mutation, will have developed the disease after the age of seventy. Characteristics among the mutations throughout the protein are different even among those in the same region. On the other hand, similarities are shown among the mutations at particular sites such as the dimer interface, the metal region, the β -barrel and the loops. They all interfere with the structural integrity, and the protein is not possible to mature into the wild-type structure. Although, many destabilisation processes are involved in structural perturbation, including removal of hydrogen bonding, salt bridges or disturbance of hydrophobic interactions, repulsive steric clashes induced by mutations are shown among all of them, and it result in varying but relatively short survival times, as shown in Figure 2.4.^[55]

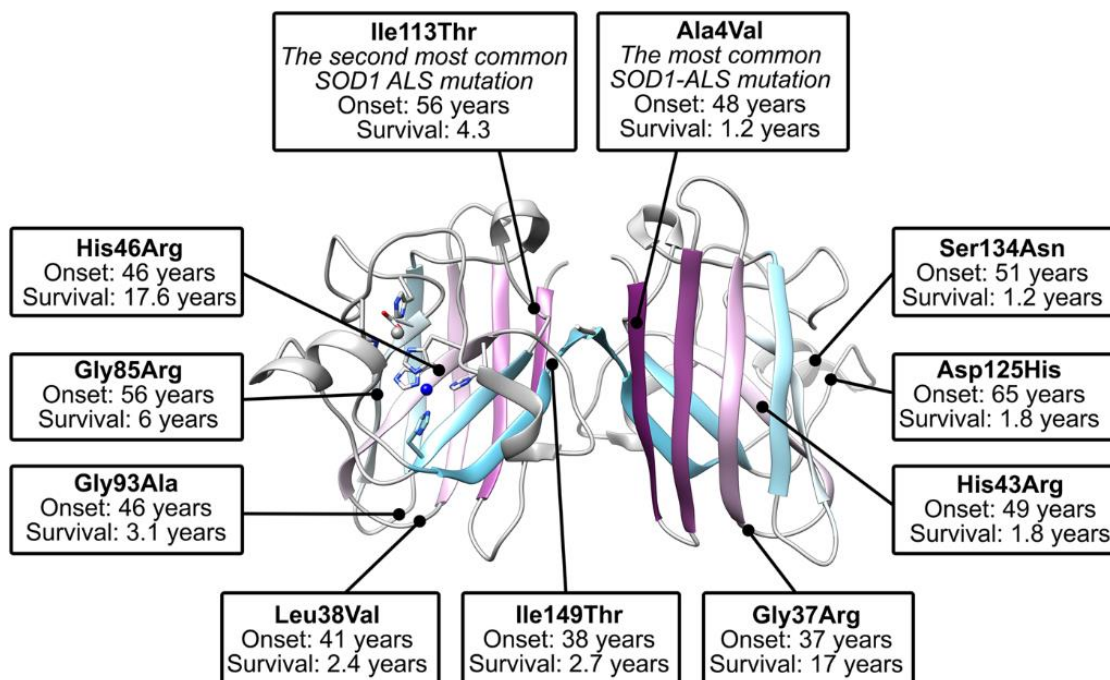


Figure 2.4 ALS mutants at different SOD1 dimer sites. Taken from^[55] Copyright © The Author(s) 2019

Hough *et al.* showed differences in the conformation between wildtype and A4V and I113T, respectively, where the opening of the dimer interface is observed for both mutants and even more pronounced in the latter one, where the observed conformation of the dimer is elongated. Their conformation difference dictates the orientation of the monomers.^[51] Both mutations have an influence on the hydrogen bond between Ile151-Gly114; however, variation in hydrogen-bond distance is more observed in the A4V mutation. Another important effect of I113T was that the influence on the nearby residues was minimal, yet the major perturbation was observed due to the loss of hydrophobic contact at dimer interface between the carbon atoms of Ile113 and Ala4.^[51] Different findings and crystal structures of the mutants of the zinc-loop dimer interface can have significant impact on the destabilization of the dimer and the β -barrel structure, thus trigger aggregation processes. A similarity to dimer interface mutants and the importance of preserving hydrophobic interactions can be observed in Leu38Val mutation, in which the side chain is usually inserted into the hydrophobic core and has a stabilising van-der-Waals interaction with Val114 and nearby residues at the β -turn. However, those interactions are disrupted in the mutated protein.^[56] Cardoso *et al.* observed the same effect with the A4V mutation, which resulted in a movement of the subunits, thus, caused structural opening on the other side of the β -barrel at Leu106. Depending on the mutation, interactions will be reduced or clashes and repulsion inside the β -barrel will interfere with the structural integrity and initiate aggregation.^[57] Generally, findings indicate that ALS-

correlated mutations are more likely to occur in the functional parts, such as the interface, the metal binding, the β -barrel root and the disulphide region as part of the zinc loop, while more solvent-exposed and not protected regions are less likely to be mutated.^[55] This indicated that SOD1 involvement in ALS is not only through reduced activity and loss of function but rather to many correlated processes that could have a gain of toxic function. This all correlates well to the earlier findings from the complete knock-out of SOD1 in mice that did not show any symptoms of ALS.^[58,59] Moreover, it was already shown by Bruijin *et al.* that formation of aggregates in G85R mice increases the progress of the disease.^[59] All this led to the conclusion that SOD1 toxicity probably results from gain of function resulting in misfolded, oligomerised and aggregated species of SOD1.

Therefore, SOD1 related ALS correlates with aggregation as a hallmark of many neurodegenerative diseases.

2.2.3 ALS and SOD1 aggregation

To expand and understand the underlying mechanisms of the aggregation observed and implicated in SOD1-related disease, many cells and *in vitro* models were developed. Rakhit *et al.* reported pronounced aggregation of the zinc-deficient wildtype as a consequence of oxidation, while in the other mutants the effect was much less pronounced. Light scattering of the metal deficient wild-type at 350 nm showed the formation of big aggregates, even with the copper present in the active site.^[60] Furthermore, the lack of oxidants still showed a small amount of aggregation in the zinc-depleted control, indicating the importance of metal in the aggregation process. Many aggregates confirmed in correlation with SOD1-ALS resembled an amyloid fibril structure as known from other neurodegenerative diseases.^[49,51,61] Interestingly, rather amorphous than amyloid-like aggregates have been observed in the spinal cord, resembling unfolded and monomeric structures of SOD1.^[62] This is also an indication that formation of aggregates of SOD1 not necessarily has to be typically fibrillar, as it is mostly observed for α -synuclein or other aggregation prone proteins. The structures might highly differ depending on the mutations and processes by which they occur. It was shown that mutations within different protein sites have generally different influence on the overall structure.^[63] Additionally, the lack of metals affects aggregation of the SOD1 and the formation of soluble oligomers. The protein structure of the apo form is perturbed and much more flexible, with the buried Cys6 and Cys111 more likely to be exposed and

oxidized to form soluble oligomers, either by disulphide bonds or noncovalent interactions between the β -sheets.^[64,65,65] Furthermore, similarities between aggregates observed *in vitro* versus *in vivo* were confirmed in which they share similar fibrillar features.^[66] Yet, the aggregates, heterogeneity and initiation of fibril formation were also shown in self-assembling peptides particularly the segments of the β -strand 8 (147-153), and the loop VI (101-107), in which the hydrophobic side chains induced a zippering effect.^[67] This also suggests that the solvent exposure of the dimer interface can have a significant effect on the aggregation of the SOD1 protein. Even more, if the internal disulphide bond is broken, flexibility is induced in the loop, and the dimer contacts are loosened, which can easily trigger aggregation, as shown for the peptide segments.

Unfolded monomeric SOD1 was also shown to influence the aggregation gained by either oxidative response or dimer dissociation, by which cellular toxicity due to formation of soluble low molecular aggregates was confirmed.^[46,51,52,68] Monomer formation can result in monomer association with a dimeric non-disulphide bonded SOD1 to first form trimers, and later higher toxic oligomeric species.^[69,70]

Different mechanisms and pathways, by which the mature proteins aggregate have been described, which occur either dependent or independent of each other. As shown in Figure 2.5 those aggregation processes can be roughly divided into three pathways. Demetallation and reduction of the internal disulphide bond effect the stability of the protein by leading to solvent exposure of all cysteine residues, and, hence, to oligomer assembly. Additionally, the induced structural perturbation aligns β -barrel sheets in an ideal position for fibrillation and aggregation. Furthermore, they all affect the dimer interface, which leads to destabilization of the intact dimer: reduced disulphide bonds induce flexibility into the zinc subloop at the dimer interface causing clashes, while demetallation initiates barrel perturbation, and, hence, dissociation into monomers. Dissociation of the folded wild-type, on the other hand, is very unlikely on its own, as the binding dissociation constant is very low in a range of 10^{-8} to 10^{-10} M.^[71,72] However, mutations on the dimer interface influence dissociation and destabilization of the dimer, subsequently causing aggregation.^[72,73] Furthermore, demetallated wildtype and mutant SOD1 protein have an even higher propensity to dissociate.^[74]

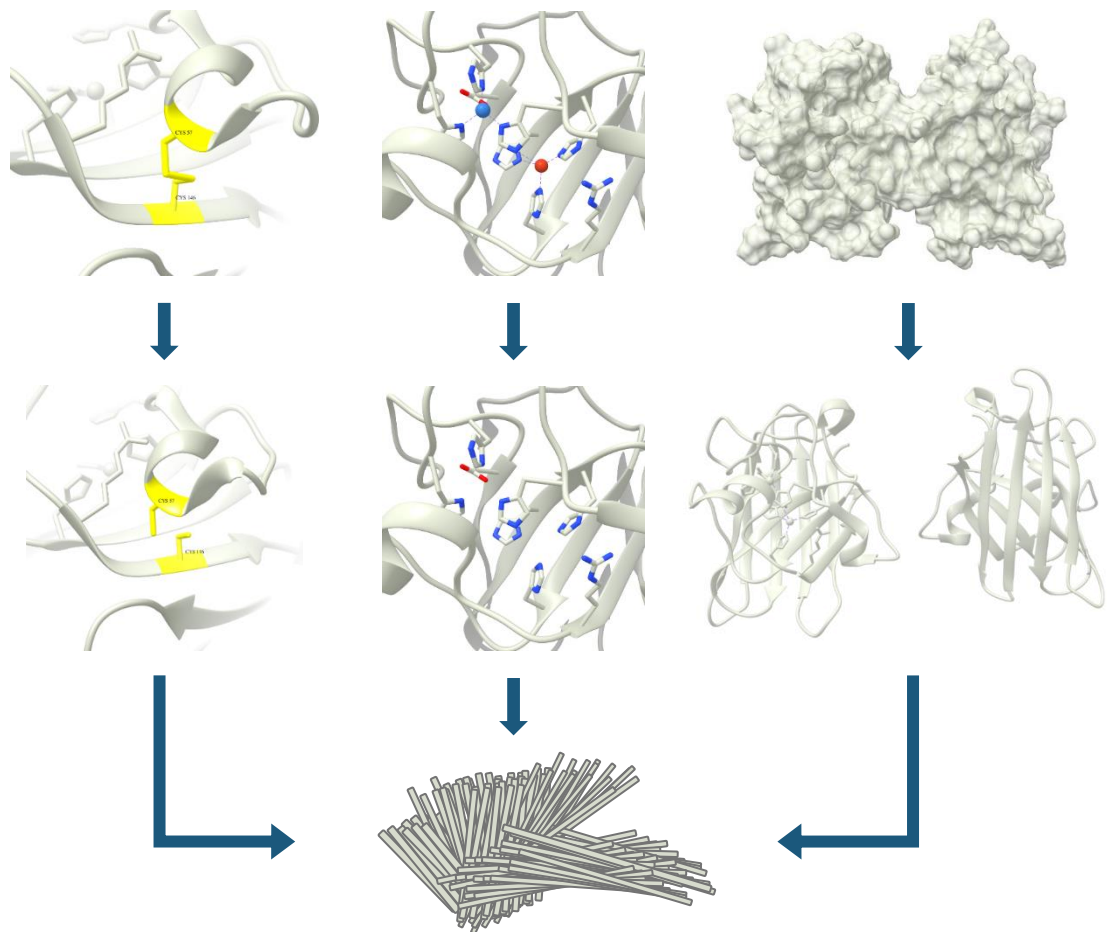


Figure 2.5 Discussed aggregation pathways of SOD1 protein (from left to right: disulphide (Cys57-Cys146) bond reduction, demetallation and destabilization of the dimer).

2.2.4 Insight into current SOD1 therapeutic approaches

In the last fifty years of SOD1-ALS related research, many structural and functional properties have been revealed and knowledge was gained. With the first approved drug for the treatment of ALS, therapeutic approaches and investigations on SOD1 were also directed toward that area, considering all structural and functional properties as well as the ubiquity of the protein in many ALS-related mechanisms. Yet, until now there is no drug or therapeutic approved in correlation with the SOD1 protein. On the other hand, several approaches have been developed to address critical structural and functional properties implicated in ALS.

Regulation of copper and zinc levels in the metal active site is important for the functional protein, yet the mutants usually reveal impaired ability to correctly metalate in the folding process. Researchers showed that zinc dose dependency in transgenic G93A mice has to be carefully balanced to have a beneficial effect on deficiency, and survival rate, but it

should not exceed more than 11 mg per day.^[75] Others showed that promoting copper increase might have more influence, especially when taken into account the reduced ability of mutants to interact with a copper chaperon for SOD1 protein (CCS). Studies indicate a scavenging capability of CuATSM (diacetylbis(N(4)-methylthiosemicarbazonato) copper(II) toward peroxyxynitrite, a product of the reaction of superoxide and nitric acid, that damages cells in the process of protein nitration.^{[76][77]} Furthermore, mutated G93A, G37R and G93A mice co-expressing human CCS showed an increase in survival upon controlled treatment with CuATSM, which resulted in higher copper levels and activity in the majority of mutants.^{[78][79]} In cellular experiments, CuATSM resulted in increased cell survival and lower aggregation levels, however, it was only specific for mutants with wildtype similarities and not for metal-binding region mutants.^[80] The mechanisms involved are still not clear and are currently investigated, yet treatments with CuATSM are already in phase I and II of clinical trials in Australia.^[80]

Ray *et al.* showed that instability and dissociation of the A4V mutant SOD1 protein could be minimized by harnessing the amino acids at the dimer interface by a disulphide bond.^[52] While engineering a V148C substitution they were able to retain a dimeric structure comparable to the wildtype protein. In the low concentration range the A4V mutant was confirmed to be monomeric and in an amyloid pore-like aggregated species. Similarly, Auclair *et al.* showed covalent bridging of monomers by maleimide functional groups. They used a small-molecule approach to cross-link two exposed cysteine residues (Cys111) and stabilize G93A and G85R mutants by approximately 20 and 45 °C, respectively.^[81] Additional approaches were shown to target solvent-exposed and oxidation-susceptible Cys111 site. In 2012 Banci *et al.* confirmed the influence of cisplatin, a known therapeutic in cancer treatments, has a positive effect on apo SOD1 proteins. Even though crystallographic data revealed steric clashes at the dimer interface and a distortion of the structure between the Cys111 residues, protein thermal stability was improved by 8 °C with a binding affinity of approximately 37 µM. Besides dimer stabilization and aggregation inhibition, already formed SOD1 aggregates were dissolved.^[82]

Two years ago, Capper *et al.* showed antioxidative ebselen and ebsulphur to act as a chaperone in SOD1 folding, by increasing the dimer affinity. The effect of increased dimer affinity was most pronounced for the A4V SOD1 variant with an almost 60-fold increase in association strength in the presence of ebselen. A slight increase in the association strength of the dimer, 1 to 3 fold depending on the compound, was also shown

with the zinc-metallated wild-type.^[73] Beside balancing dimer stability to suppress dissociation and unfolding processes that lead to aggregation, an experiment in living human cells indicated intramolecular disulphide bond formation of reduced zinc metallated SOD1 mutants when treated with ebselen. This enabled proper folding of immature monomers, which were impaired, if the amount of copper chaperone in the cytosol was inadequate.^[73] So far, all tested small molecules which lead to an increase in stability or promote folding and reduce aggregation, are not specific enough and could bind to other proteins or are unstable in cellular environment.

In 2005 Ray and Lansbury, after their earlier disulphide bridging in V148C substitution, performed *in silico* studies and screened a library of 1.5 million small molecules.^[83] They addressed the cavity of the SOD1 protein at the dimer interface opposite to the earlier described cysteine 111 proximity site. From the top 100 hits of the initial library screen, they narrowed it down to 15 molecules which appeared adequate in stabilizing and lowering aggregation of the A4V dimer under induced unfolding conditions. They confirmed the importance of the Val148 site for the binding affinity of the tested molecules by mutating Val7 and Val148 residues with Phe, in which aggregation inhibition was not observed. From the structural similarity of the tested compounds, an aromatic moiety was shown to be important for the binding to the hydrophobic core between the valine residues and the stability of the protein.^[83] Five years later they presented improved molecules with binding specificity toward SOD1 mutants, while enlarging the *in silico* screen of a commercially available database of 2.2 million compounds.

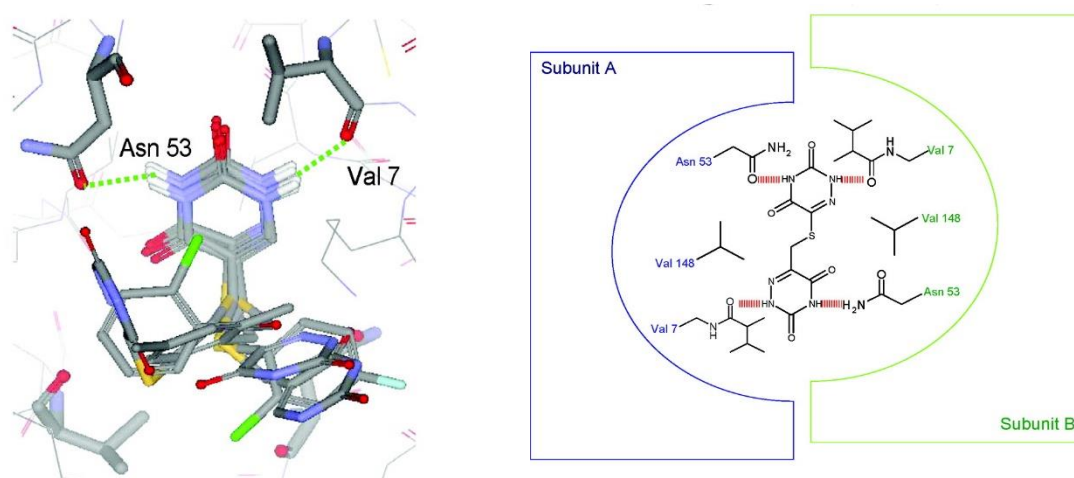


Figure 2.6 Binding site Val148 and compounds with aza-uracil like moieties, adapted from.^[84]

Docking was performed iteratively with the flexible target and also with hydrogen bond constraint parameters on Val7 and Asn53 residues in the cavity. Fourteen obtained compounds showed an increased binding affinity for the A4V and a high efficiency to block aggregation. Six of them showed high specificity toward the SOD1 in comparison to the blood plasma. Structurally, the compounds were similar to previously reported compounds with aromatic moieties, but contained uracil or aza-uracil like moieties that could be involved hydrogen bonding with Asn53 and Val7 of the opposing monomer units.^[84] (Figure 2.6) They also indicated that *in silico* design could be a potent tool for new drug design. However, compared to the previously described cysteine site studies, the binding behaviour of the compounds was not structurally confirmed.

Consequently, these findings were challenged by Antonyuk *et al.* when they attempted to structurally inspect these ligands *via* cocrystallization experiments with the mutants. They obtained 1.7 Å resolution crystal structures of the SOD1 L38V mutant with uridine 5'-monophosphate (UMP) chosen to compare the similarity of uracil-like structures, proposed earlier in ligand screening.^[56] The UMP binding site was located farther from the dimer interface between the electrostatic and zinc-binding loops. During structural investigation, they discovered a “druggable” site in proximity of the Trp32 residue from crystal structures of G93A and L38V with 1.55 Å to 1.65 Å resolutions, respectively. They were able to provide structural information of binding with SOD1 mutants.^[56] Later, they showed that isoproterenol and 5-fluorouridine do not have a tremendous effect on the guanidine induced unfolding of A4V and I113T SOD1 mutants. Furthermore, the crystal structure revealed a binding site in between the β -strands 2, 3 and 6 close to Trp32.^[69] These compounds were shown to have a high ability to block the aggregation of A4V SOD1 and were specific for SOD1 in blood plasma.^[84] These experiments clearly show the importance of crystal structures for drug design and the need for relevant methods to test the binding affinity of small molecules for SOD1. Afterwards, Manjula *et al.* reported different compounds to bind to Trp32 in the low micromolar range and inhibit oxidation.^[85,86] Pokrishevsky *et al.* also showed the importance of that site, they confirmed that a Trp32Ser mutation diminishes SOD1 aggregation, induced by Trp32 self-seeded aggregation, despite the generally reduced stability of the mutants and wildtype proteins. Additionally, they tested 5-fluorouracil and 5-fluorouridine onto Trp32 aggregation and confirmed high potency of those chemotherapeutics to reduce aggregation in SOD1, and up to now, they seem to be the most prominent candidates for SOD1-ALS treatment.^[87]

As described above, many approaches were developed for the treatment of SOD1 related ALS over the years. In Figure 2.7 all cavities and sites reported are visualized that could be potential therapeutic targets in SOD1. The metal site is shown in red, the dimer interface with two possible cavities, Cys111 (yellow) at the top of the protein, and Val148 (blue) at the core between two monomers, and the Trp32 site shown in green.

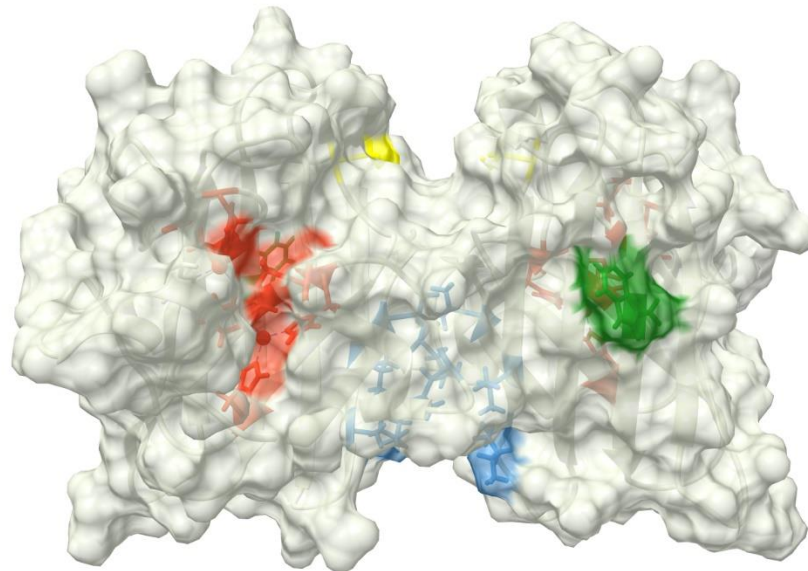


Figure 2.7 Potential therapeutic sites in SOD1 protein: metal (red), Cys111 (yellow), Trp32 (green), Val148 (blue). PDB code 2V0A, visualization by UCSF Chimera.^[44]

The understanding of SOD1 functional and structural properties has improved extensively since its gene discovery. It is now known that the metal-binding site, the dimer interface and β -barrel structure influence the SOD1-related ALS disease. Furthermore, CuATSM, ebselen and 5-fluorouracil were shown to be potent small molecules in intervening aggregation. Although these important findings are milestones in the therapeutic development of SOD1, the question of delivery, specificity and affinity to SOD1 is yet to be answered in order to develop sensible therapeutic strategies. The revelation of SOD1 aggregation on ALS might be the main breakthrough. Mutations were found across the whole protein, yet not all of them are propagating aggregation. Those at the critical sites of the protein are promoting dissociation, unfolding and prevention of folding into stable dimers, which will lead to inclusions, as well as fibrillar and amorphous aggregates. The actual structure-toxicity relation is still a puzzle and might differ because of different initiation points and propagation mechanisms. Additionally, differences in sALS and fALS epidemiology of SOD1 are huge, and many mechanisms of aggregate formation are still unknown, contradictory and cannot always be correlated. Hence, it can be

2 State of the art

concluded that there is still much more that we do not yet know, and basic research in different areas is important to answer further questions and help to deliver proper therapeutic approaches.

3 AIM OF THE WORK

Superoxide dismutase-1 (SOD1) is a well-known protein that is involved in fatal ALS disease. However, throughout the years of structural and functional discoveries, there are still unanswered questions of its pathogenicity in ALS as well as other neurodegenerative diseases.

Early structural investigations of SOD1 proteins indicated the importance of the dimer interface between the two monomer units.^[88] Initial studies of interfacial SOD1 mutants, such as A4V revealed a destabilization and possible dissociation into monomers that could propagate the aggregation.^[51] Various strategies have been proposed in order to prevent undesired dissociation in SOD1 mutants. For instance, the introduction of an artificial disulphide-bridge was found to stabilize the A4V mutant (see Section 2.2.4). Furthermore, small molecules, which bind to the interfacial cavities showed structure stabilizing effects. However, the V148 cavity was not yet successfully addressed by small molecules.

The aim of this work is the development of an affinity-based stabilization as a labelling approach for SOD1 A4V. To achieve this, we intended to design multifunctional ligands with an affinity for the cavity of interest that could influence protein aggregation. Furthermore, the ligands are planned to be tagged with a fluorogenic dye and, thus, be transformed into an affinity-based probe (see Figure 3.1).

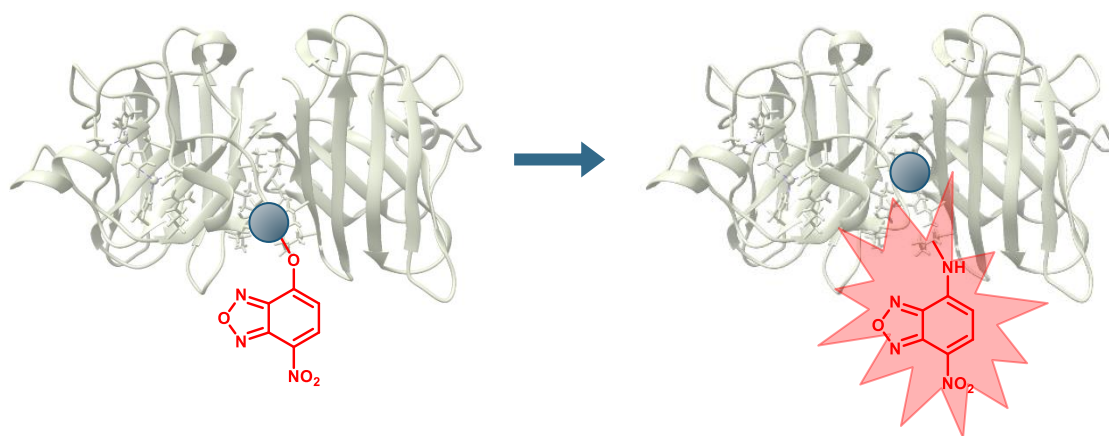


Figure 3.1 Schematic overview of the aim of this work. A small ligand molecule with an affinity for the cavity of interest precludes the fluorescence on the lysine residue.

To achieve this goal, several tasks have to be addressed: 1) structural analysis of the protein cavity Val148; 2) *in silico* design of the ligands; 3) ligand synthesis; and 4) assessment of binding properties and aggregation studies.

Structural analysis of the protein cavity is important as there are no crystal structures of small molecules reported to bind to the cavity. Therefore, different protein crystal structures are planned to be analysed prior to molecular docking. For *in silico* design studies, molecular docking of AutoDock Vina is used for prediction of ligand binding followed by analysis of their bound conformations in the protein cavity. Ligand synthesis is planned to be performed in a modular approach so that the ligand library can easily be enlarged. Lastly, the obtained ligands are assessed for their binding properties in microscale thermophoresis, isothermal calorimetry and thermal shift assays. Aggregation studies are then performed to assess their influence on protein aggregation.

4 BIOPHYSICAL AND COMPUTATIONAL METHODS

4.1 In silico design

In the present work, *in silico* design also known as computer-aided drug design ^[89] was used for the rational design of small molecules. The capacity of the method has been shown in a broad area of drug research and medicinal chemistry. Essentially, the efficacy of *in silico* design is to shorten the time needed for the identification of lead structures by using computational tools if compared to the traditional laboratory experiments and high-throughput screening (HTS).^[90] Through *virtual screening*, an important technique of *in silico* drug design, methodical docking of a broad range of the drug candidates is performed for the identification of potential ligands. ^[89,90]

There are mainly two categorizations of virtual screening methods: ligand-based and structure-based methods, also known as molecular docking. In the case of ligand-based methods, information of the target, usually, a macromolecule or protein is very limited, therefore pharmacophore modelling and quantitative structure-activity relationship (QSAR) methods are used.^[91] Molecular docking can be chosen for different but complementary approaches. When the structure of the target is known, large libraries of the compounds are evaluated against the target. Therefore, hit molecules can be obtained in a relatively short time. Furthermore, molecular docking is valuable for the binding mode analysis of the small molecules to a specific target site, as well as the study of the binding interactions to predict and model characteristics of the drug lead structures i.e.,

absorption, distribution, metabolism, elimination and toxicity (ADMET).^[92] One interesting concept of *in silico* design used in the field of drug design development is called *inverse* virtual screening. It can be part of both previously mentioned categories, besides the concept where one ligand is evaluated versus many targets to identify its presumed nonspecific targets, as well as identify possible specific targets, multiple libraries of ligands are tested against many targets to determine specific pharmacological activity.^{[93][94]}

4.2 Molecular docking

Throughout the years docking theories were evolving, from “*lock-key*” mechanisms^[95] according to which ligand and target should be rigid in docking simulations, followed by the “*induced-fit*” theory^[96], in which it is proposed that the active site is changing upon ligand binding. In agreement with that, either, ligand and target or only ligand should be considered as flexible in docking calculations.^[91] The “*Conformational selection*” model combines pre-equilibrated structures and the random fluctuation of target and ligands.^{[97][98]} To obtain the best characterisation of the interaction between ligand and target, a combination of the induced fit and conformational selection model was proposed.^[99]

To predict ligand conformation in the docking, and to evaluate its binding affinity to a target protein, the docking software gives outputs according to the combination of the docking theories, and balances between accurate simulations and required computing time. Therefore, the perspective of molecular docking theory can be explained with the complementary methods: the sampling method, and the scoring function method.^[91,100]

The sampling method is inspecting conformations of the ligand in the active site using different algorithms, which are mainly varying in how they map the ligand into an active site; i.e., matching algorithm (MA) is using the molecular shape map of a ligand as pharmacophore where the distance between a ligand and a protein is calculated. Incremental construction (IC) does fragmentation of the ligand and then incremental addition of the other functional groups in different orientations, in which they fit to the binding site. Multiple Copy Simultaneous Search (MCSS) performs multiple copies and randomization of the functional groups. Consequently, new binding sites and ligand conformations are calculated from the favourable interaction energies of the multiple placed functional groups.^[91]

Scoring functions have a judge role, in which it is crucial to define the correct poses, as well as to eliminate non-binders from the poses obtained and rank the predicted ligand poses. This process is important for reliable molecular docking evaluation. So far, there are three main categories (force-field based scoring function, empirical, and knowledge-based function), which are being constantly developed to improve their efficiency.^{[91][100,101]}

4.2.1 AutoDock Vina

In this work, molecular docking was used to predict the binding of the ligands to the hSOD1 target protein and analyse their bound conformations. For the docking, different software (SwissDock^[102], Mcule^[103], AutoDock Vina^[104]) was evaluated. There are several differences; however, one main difference was that SwissDock and Mcule are web-based docking servers, whereas AutoDock Vina is an offline docking software. From the web-based docking servers, SwissDock has user-friendly interface and suppresses information on how the system is designed. Furthermore, the computational setup was at disposal.^[105] Therefore it was used as a confirmation of the molecular docking with the AutoDock Vina.

The stochastic methods that are used in AutoDock are Monte Carlo (MC) and Genetic algorithms (GA). These methods perform searches of the space by randomization of the ligand conformation. Conformations in MC are generated *via* bond rotation and rigid-body translation or rotation. A further selection of the conformations is based on the energy barriers principle. In GA new conformations are represented when a change in the structure occurs due to some mutation or depletion. If that new structure passes the energy threshold it will be used for further sampling.^[91]

AutoDock Vina implements simple scoring functions for the estimation of the protein-ligand affinity, and the search is based on the stochastic MC and GA methods. Vina uses a combination of knowledge-based and empirically weighted scoring functions; that includes hydrophobic interactions (van-der-Waals), hydrogen bonding, torsion degree and repulsion.^[106,107] High impact and improvements in speed and precision over the previous version (AD4) were achieved with a local search algorithm; where the conformations are calculated by the iterative local gradient-based search.^[107] Conformation pose with the highest binding affinity, also the most negative affinity, is

ranked as the top pose. The poses are approved or rejected if the next iteration has a lower free energy than the previous iteration.^[106]

4.3 Microscale Thermophoresis

Microscale thermophoresis (MST) has lately been developed as a very powerful method for determining binding dissociation constants at different interactions, i.e. protein-protein, DNA-protein, and protein-small molecules.^[108,109] It is also used as a high-throughput screening method, along with other biophysical methods to compare and confirm promising binding hits.^[110]

The concept is based on the different movement of the molecules through a temperature gradient induced by an IR-laser, in which the rate of motion is different between a single molecule and complex.^[111] The effect of thermophoresis, also known as Soret effect is dependent on a change in size, charge, solvation entropy of the molecules, and it is detectable in constant buffer conditions.^[112] The advantage of the experimental setup is that the change of the thermophoretic effect is monitored by fluorescence inside a glass capillary, through an objective coupled onto a dichroic mirror when the heat effect is induced by an IR-laser.^[113] As shown in Figure 4.1, the IR-laser is applied onto all capillaries with serial dilution, and, simultaneously, molecular movements are detected by fluorescence detection. A microscopic view of the molecular interactions through different stages is shown. In the initial state, also known as F_{cold} , the IR laser is off and fluorescence distribution is homogeneously detected inside the capillary and there is no directed movement of the molecules at the sample. By inducing a temperature gradient with the IR-laser, fluorescence distribution F_{hot} is obtained from two effects. Drop-in dye fluorescence depending on its intrinsic temperature dependence is induced by thermal relaxation time, which is usually very fast, and in the diffusion effect, in which the labelled sample moves out (positive thermophoresis) or toward (negative thermophoresis) the heated region until a steady-state is reached. Back diffusion occurs in the last stage when fluorescence jumps back to a homogenous distribution, due to IR-laser being deactivated.^[111,113,114]

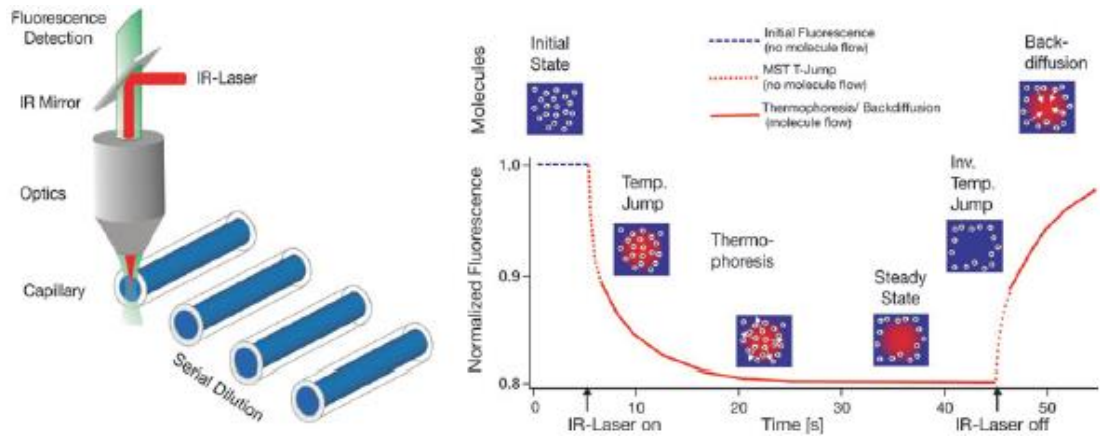


Figure 4.1 MST assay setup. *Left:* Macroscopic view of the experimental setup; *Right:* Microscopic view of the molecular interactions in the MST assay shown through different stages. Adapted from.^[114]

For binding affinity analysis, ligand-dependent changes in the MST trace at each capillary is shown as normalized fluorescence (ΔF_{norm}) in which is calculated by dividing F_{hot} by F_{cold} whereas F_{hot} and F_{cold} values correlate to the average fluorescence between the hot and cold areas marked as red and blue cursors, respectively. Furthermore, the concentration of the titrated non-labelled ligand is plotted against the normalized fluorescence to determine a binding constant from a binding curve, as shown in Figure 4.2.^[108]

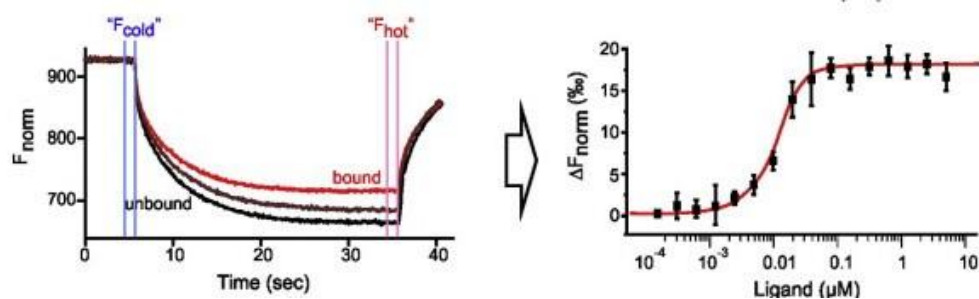


Figure 4.2 MST binding experiment and analysis. *Left:* Thermophoretic movement of a fluorescent molecule within MST-on time of 20 s, in which the IR-laser is on. *Right:* Binding curve derived from normalized fluorescence and concentration of the titrated ligand. Adapted by permission from CC BY licence; The Authors. Published by Elsevier B.V. (2014).^[108]

MST-on time can be used for two different time points in MST measurements, first, it defines a period, where the IR-laser is on, which is described as the measured time, and second, it defines the analysed MST-on time. In Figure 4.2 MST-on times are the same, indicated by the red F_{hot} cursor. To minimize a possible structural destabilization of the molecules by applied temperature from IR laser intensity, a shorter MST-on time should be used.^[113,115] From the difference between unbound and bound values, a response amplitude is obtained. In combination with a signal to noise ratio (S/N) which is

calculated by dividing the response amplitude by noise (standard deviation of the fit residuals), those parameters are used to estimate the validity of the assay. For a consistent analysis of all assays, analysed MST-on time was used at 1.5 s as described in Section 7.2.4.2.

4.4 Isothermal Calorimetry

Isothermal Calorimetry (ITC) is a method which is used to determine how tightly a ligand is bound to i.e. a protein measuring the heat that is released or consumed upon the binding process.^[116] The heat change is monitored and maintained to zero temperature difference between the reference and sample cell. The sample cell contains one of the analytes of the binding reactions, and a syringe which contains a solution of the ligand is attached to it. The reference cell usually contains water. In Figure 4.3, the basic setup of the calorimeter is shown, as well as typical raw data obtained after ligand injection into the sample cell as heat pulses. The heat pulse is integrated over time and normalized to a concentration where the resulting isotherm is obtained, and fitted to determine the binding affinity, as well as stoichiometry and enthalpy of the reaction.^[117]

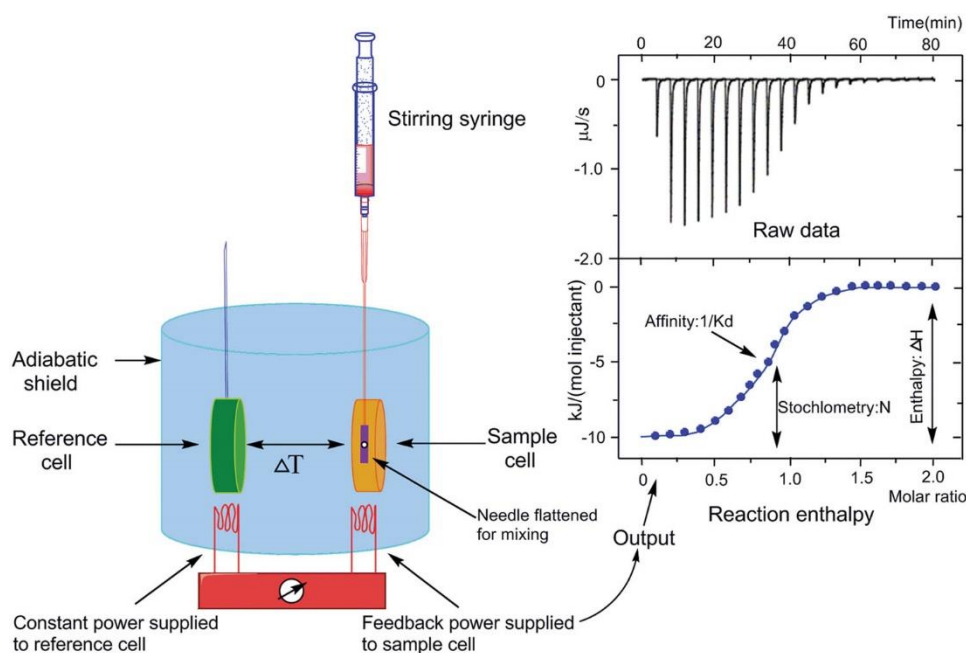


Figure 4.3 Basic ITC experiment setup, adapted from^[118] Copyright © 2015 Song, Zhang and Huang, licence CCBY

5 RESULTS AND DISCUSSION

This chapter is divided into three main sections. Firstly, the ligands' design through analysis of the hSOD1 protein cavity and evaluation of molecular docking simulation studies are described (Section 5.1). Secondly, retrosynthetic approaches and synthesis strategies towards a ligand library are proposed (Section 5.2). Thirdly, biophysical studies of the ligands and the proteins are reported with a focus on protein studies (Section 5.3), binding affinity and aggregation (Section 5.4), and structural investigation as well as structural analysis and X-ray crystallization (Section 5.5).

5.1 Ligands design and molecular docking

5.1.1 Analysis of the hSOD1 protein cavity and ligands design

Our first molecular docking approach was not a blind docking^[93,105], as the cavity of interest has already been known, but there were no crystal structures of small molecules reported to bind to the cavity. The Lansbury group^[83,84,119] reported binding of small molecules at the dimer interface in the cavity of Val148, this was later challenged by the reports on the Trp32 residue.^[69] These findings caught our attention mainly for two reasons: 1) an investigation of the controversial cavity, and 2) the presence of a lysine residue that can be targeted for NBD fluorescent labelling. The fluorogenic properties of the NBD dye, as a “*turn-ON*” fluorescence concept was reported earlier to be successful in a biotin-avidin complex, as well as selective labelling of mitochondria in living cells.^[120] The X-ray structure of the hSOD1 protein and an enlarged bottom-up view of the cavity are depicted in Figure 5.1.

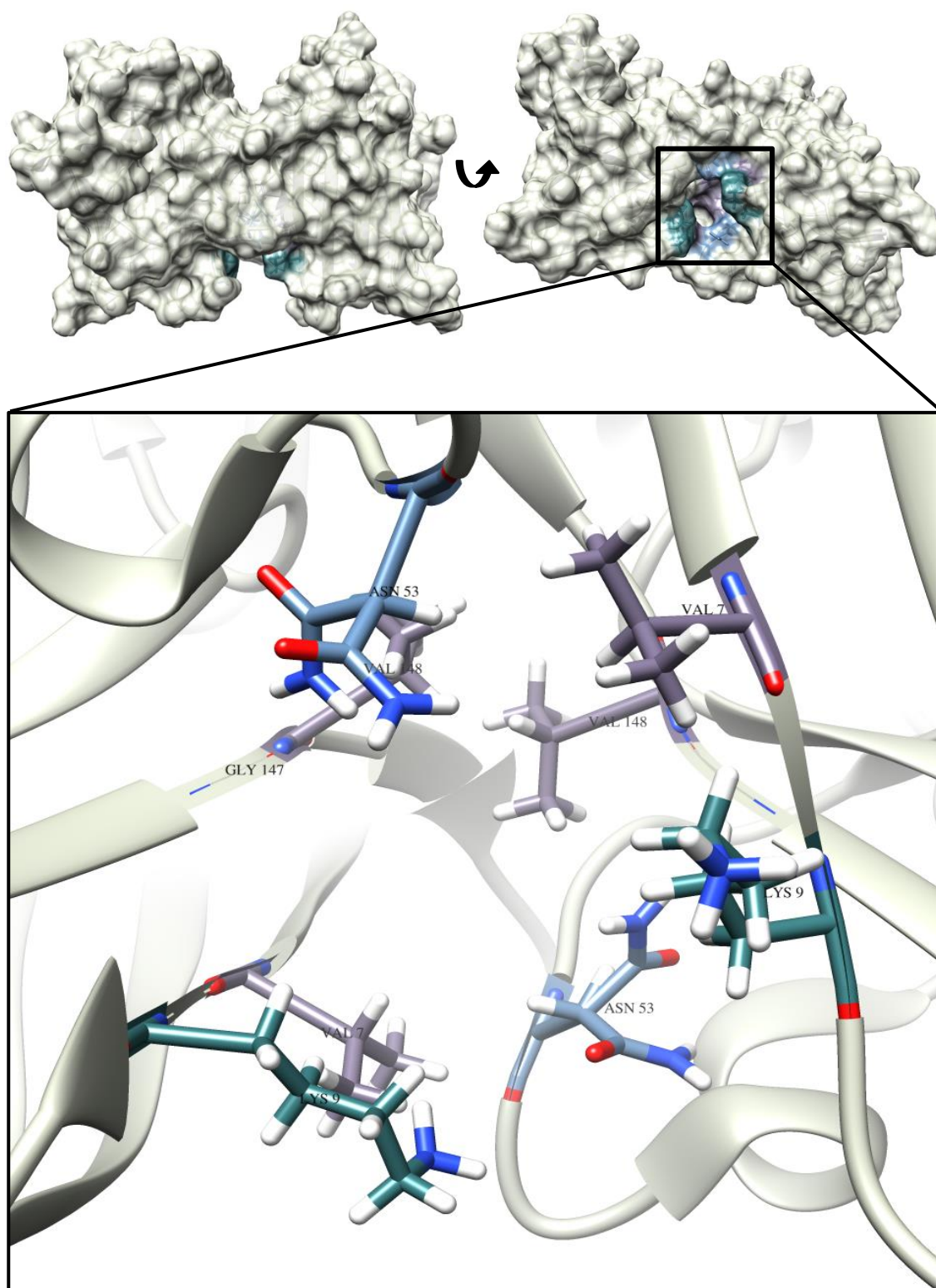


Figure 5.1 hSOD1 protein dimer centred at Val148, and enlarged bottom view into the cavity. Valine residues are depicted in purple, asparagine in blue and lysine residues in green. PDB code 2V0A, visualization by UCSF Chimera.^[44]

In the enlarged representation, the residues pointing into the cavity are depicted at the dimer interface, with Val148, Val7 (purple) and Gly147 (light grey) forming the hydrophobic cavity. The entrance to the cavity is comprised of polar amino acids with

Lys9 shown in green on the left (monomer strand A) and right side (monomer strand F) and Asn53 in blue at the top (monomer strand A) and bottom (monomer strand F) of the cavity. The approximate distance between Val7 and Val148 of the same monomer is $\sim 8\text{\AA}$, while the distance of Val148 of each monomer is $\sim 3.8\text{\AA}$. This can be seen as the top of a funnel-like cavity at the dimer interface, where hydrophobic interactions of the ligands would be necessary to ensure binding. At the periphery of the cavity, the distance between the lysine residues is approximately $\sim 11.3\text{\AA}$, similar to the distance between the polar asparagine residues ($\sim 11.7\text{\AA}$). This cavity with the hydrophobic core and the respective peripheral amino acids was used in our docking studies, and, hence, for the ligands design.

Rules for designing ligands, which bind to the cavity of interest Cav(V148) are as follows:

- 1) hydrophobicity to ensure binding to the inner core of the cavity;
- 2) the possibility to form hydrogen bonds with the backbone of the residues;
- 3) the possibility of transfer of a fluorophore attached to the ligand to Lys9 to achieve labelling of the protein; and
- 4) design of a ligand core structure that can easily be modified taking into account conformational favourable interaction of the functional groups and the possibility of library enlargement.

Figure 5.2 (top) shows two 3D models of the lead structures, coloured according to the elements: oxygen in red, nitrogen in blue, carbon in grey, and hydrogen in white. If both molecules are centred on the respective molecule origin, the differences can be observed. For instance, the amide bond in molecule A is on the y- axis and the methylene group is arranged in x- direction. In lead structure B, the methylene group between the amine and the carbonyl group is more flexible and in a different torsion angle, and the aromatic ring in y-direction is in an orientation that enables π - π stacking. Both structures are designed to bind to Cav(V148). It would be interesting to see how the flexibility of the molecules affect their dockings. In Figure 5.2 (bottom), lead structure C is positioned similarly to the two previous structures through the 0° plane. Here, the difference is in the position of the amide bond next to the aromatic ring, which is now in the direction of the y-axes, and also represents, an ideal geometry to point into Cav(V148).

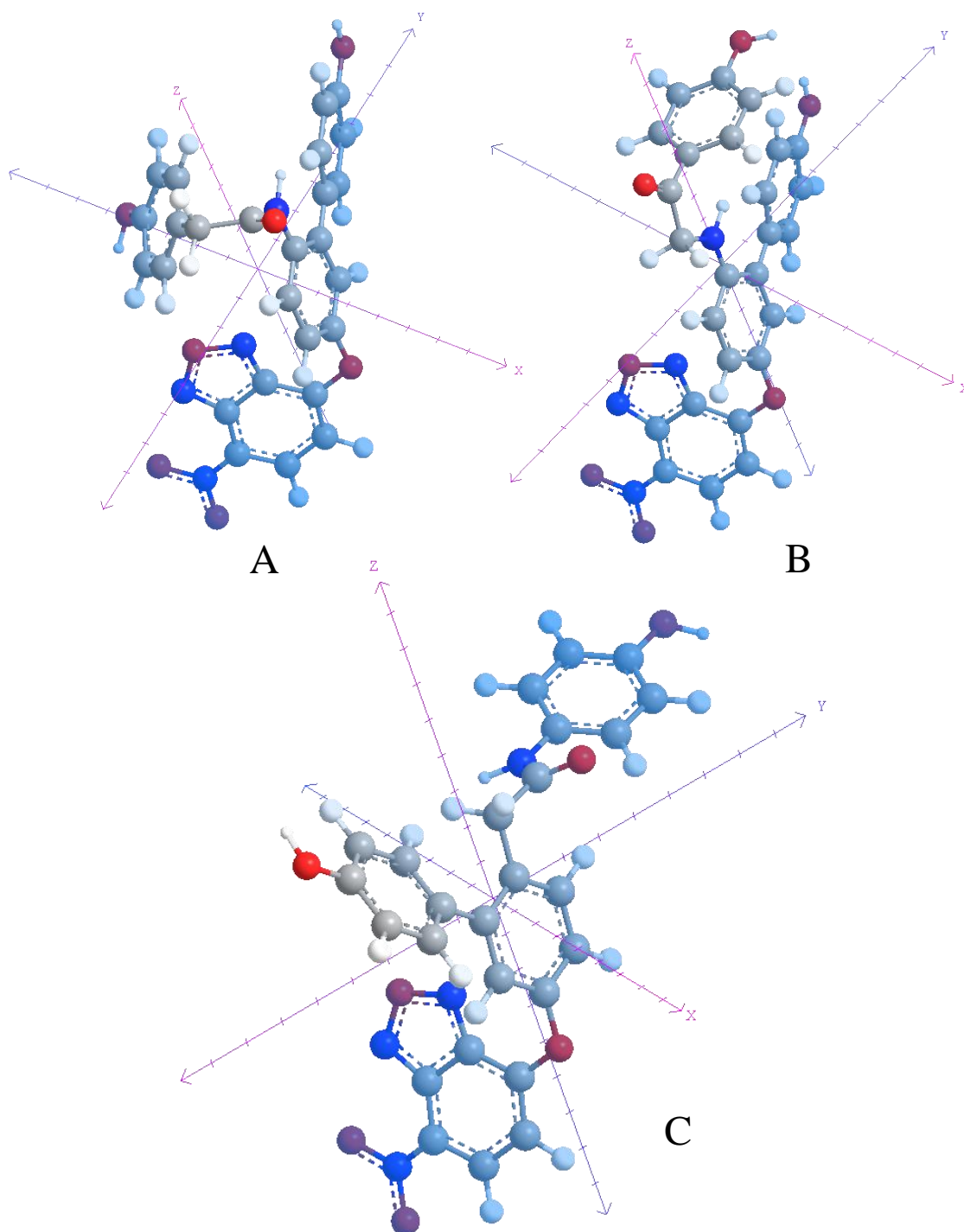


Figure 5.2 Designed lead structures centred on the respective structures at 0° in x-, y- and z-axes. *Top:* Lead structure A (left) and B (right). *Bottom:* Lead structure C.

The described ligands were designed in such a way that the core structure including the biphenyl rings and the third aromatic ring, which are connected *via* an amide or an amine bond, are inside the cavity and the fluorophore (*O-NBD*) is outside the cavity, close to Lys9 for fluorescent labelling.

5.1.2 Molecular docking to the hSOD1 protein

Molecular docking simulations of the structures of interest were performed with AutoDock Vina as explained in Section 7.3 and were comparable to the results from the SwissDock web-based server.

Molecular docking included a simulation search with the lead ligand structures and ligand scaffold structures, without a fluorophore attached, and were divided into several stages. It was reported that the selection of a bigger grid-box^[90] includes more *off-target* binding search and shows more clearly the true ligand-favoured site.^[121] The molecular docking, in simulation with a big grid resulted in 25-50% off-target binding, for all ligands when the exhaustiveness, the computational power to search the space, was small. However, the initial poses were in Cav(V148). With an increase of exhaustiveness, the results were more consistent and *off-target* binding was reduced to 10%. Again, the first two to three binding poses were in the cavity of interest. For a deeper docking analysis of the lead structures, the search space was minimized and centred according to the amino acids in the Cav(V148), Val148, Gly147, Asn53, Lys9 and Val7 from both monomers as described in the experimental section. A difference within the docked lead structures was observed in their first poses; however, the variation of the negative Gibbs energy was in a maximum range of ± 1 kcal/mol. Analyses of the lead structures in the cavity revealed that structures A and B are properly aligned in the cavity. (Figure 5.3 and Figure 5.4)

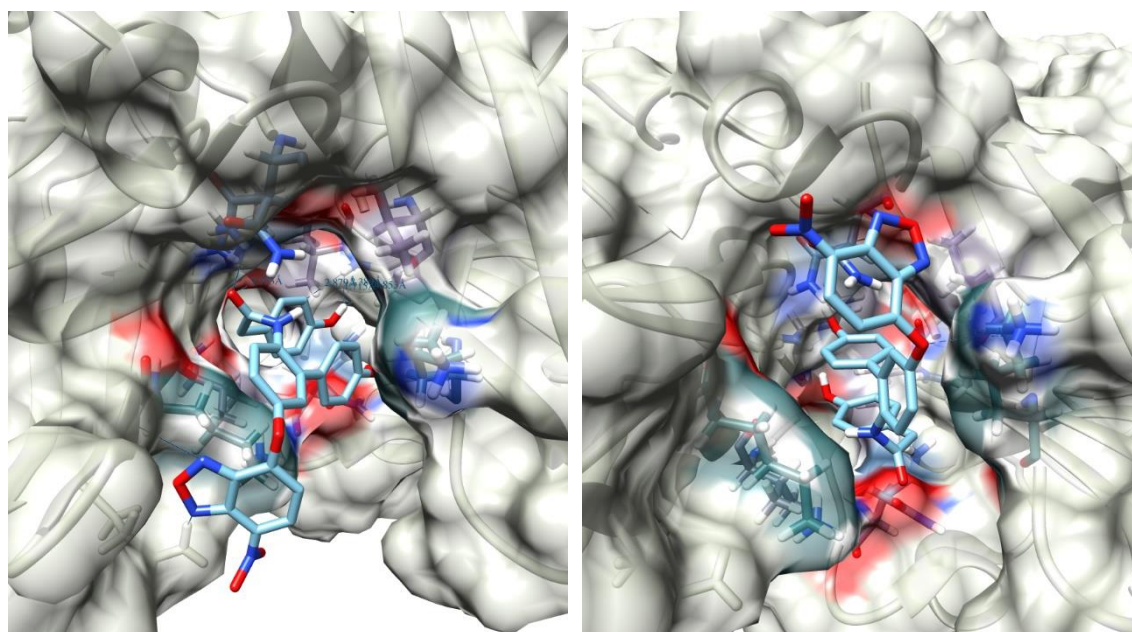


Figure 5.3 Lead structures A in the cavity of interest. *Left:* 1st docking pose with free binding energy of - 9.0 kcal/mol. *Right:* 2nd docking pose with free binding energy of -8.6 kcal/mol.

In Figure 5.3, lead structure A (LS A) is shown in the first (left) and the second (right) docking pose, which revealed the smallest distance to the Lys9. The NBD fluorophore's oxygen atom of the ligand is in approximate distance of 3.5 Å. While the ligand scaffold, which is designed for the hydrophobic interaction with the amino acids of Cav(V148), is positioned in such a way, that the mentioned π - π stacking of the molecule is observed. Furthermore, ~85 polar and non-polar interactions within the protein Cav(V148) are formed with distances of 2.0 - 4.0 Å. The hydrogen bonds to the backbone of the protein are mostly affirmed with Val148 and Val7 residues and the -OH groups of the aromatic rings along with the amide bond of the ligand and Asn53 of the respective protein chain and depend on the obtained binding affinity pose. Moderate and weak non-covalent interactions result from the hydrophobic effect of the ligand and the respective amino acids in the protein cavity.

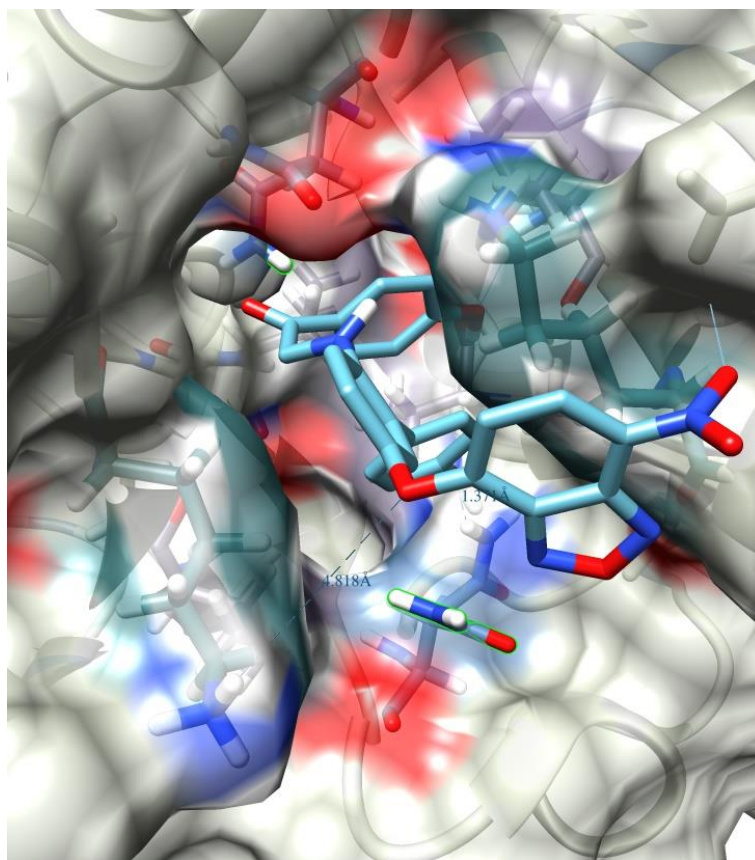


Figure 5.4 Lead structure B in the cavity of interest Cav(V148) with a free binding energy of -9.1 kcal/mol.

The docking studies with LS B (Figure 5.4), also revealed an affinity to the Cav(V148). Interestingly, all poses of the docking showed the fluorophore part of the molecule to point out of the cavity toward the lysine residues. This is in contrast to structure A where 30% were inside the cavity. However, the RMSD values of these poses in structure A

differed by 8.0 Å from the most energetically favoured pose of 0 Å RMSD. Our accepted limit for upper and lower bound of the pose studied was set to a maximum of 4.0 Å. The binding affinity of the lead structures was not significantly different in the poses within the evaluated limits. It ranged from 0.1 kcal/mol up to 0.4 kcal/mol in the last pose (Appendix 9.2). The difference in conformational orientation between the lead structures A and B can be observed in the binding affinity poses, particularly, with respect to the amide and amine bond of the structures. This results in similar poses, which are classified differently depending on the highest affinity and favourable position with regard to the binding energy between the two structures. However, lead structure B has similar interactions with the protein, except that they are observed in different ranking poses in comparison to the lead structure A. Examination of lead structure C revealed an affinity of the fluorophore unit of the structure for the cavity of interest, while the proposed affinity scaffold of the molecule was pointing out indicating that it was not in the ideal position for fluorescent labelling on any of the lysine residues. Additionally, the energy of binding was significantly lower than for the other two lead structures, and within a range of -8.5 kcal/mol to -7.9 kcal/mol.

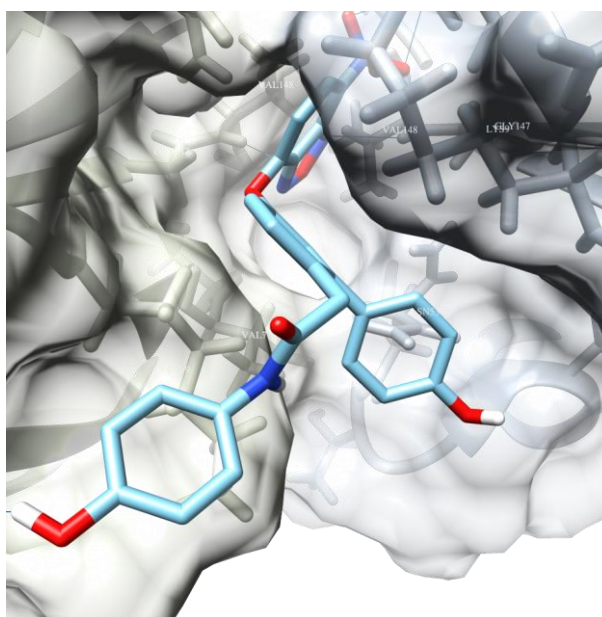


Figure 5.5 Lead structure C in the cavity of interest, Cav(V148) with a free binding energy of -8.5 kcal/mol.

The evaluation of the molecular docking of the designed lead structures confirms the affinity to the cavity of interest, and in case of structures A and B, desired multifunctionality of the ligands, to direct the fluorophore to Lys9 while stabilizing protein dimer in Cav(V148). Further developments with *in silico* design and molecular docking were mainly based on the scaffolds of lead structures A and B as an affinity site

without a fluorophore attached. It is important to test the ligand scaffolds in the cavity alone to ensure a good binding affinity, thus enhancing the possibility to stabilize the protein and slow down the protein aggregation.

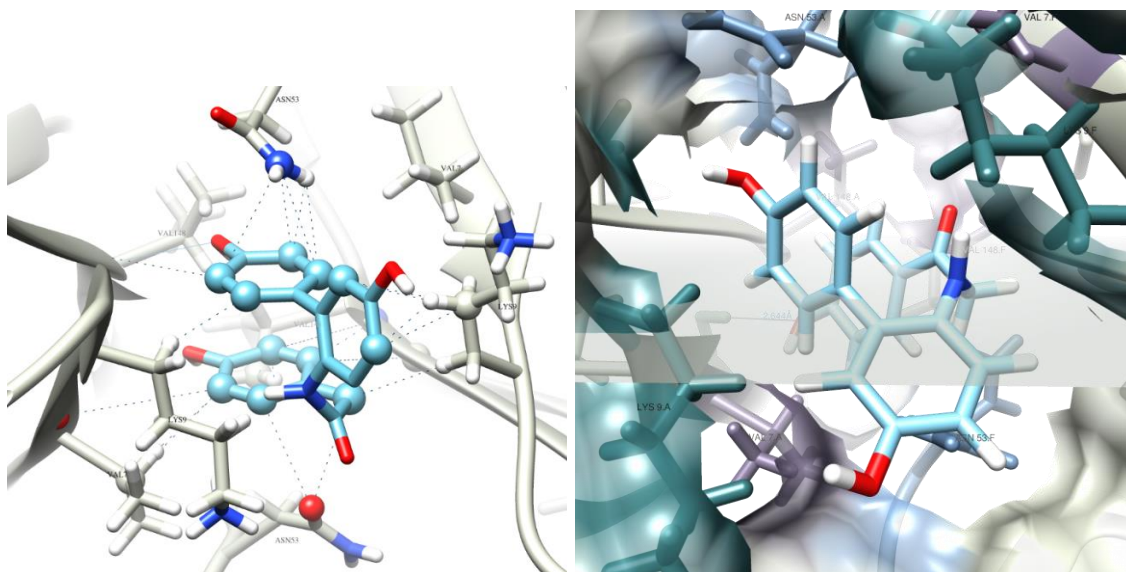
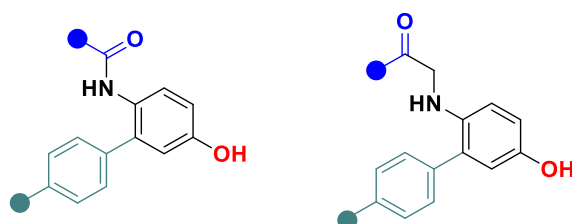


Figure 5.6 Ligand scaffolds in the cavity of interest, Cav(V148). *Left*: Lead structure A with free binding energy of -8.0 kcal/mol; *Right*: Lead structure B with free binding energy of -8.6 kcal/mol.

Figure 5.6 shows the first binding pose of lead structures A and B and the atoms involved in polar and non-polar contacts to the amino acids in the protein cavity. The docking of the lead structures A and B shown in Figure 5.6 results in calculated free binding energies in all poses for both ligands in the range from -8.6 to -6.9 kcal/mol. The first poses with the lowest free binding energy were visualized. Furthermore, other poses with an RMSD difference up to max 4.0 Å for each upper and lower bound were checked and their position in the cavity was taken into consideration. The analysis revealed that the benzyl ring attached to the amide or amine bond, which seem to be involved in π - π stacking in both ligands as shown in Figure 5.6, would be suitable for modification to enable an enhancement of hydrophobic interactions to Val148 of the protein monomers and to increase the overall affinity for the cavity.



Scheme 5.1 Schematic view of the scaffold structures A (left) and B (right).

Molecular docking was performed with both, the basic scaffolds of LS A and LS B as shown in Scheme 5.1. Variation of the functional groups was performed on the benzyl ring connected to an amide and amine bond, here depicted in blue, and the biphenyl rings, depicted in green. In Table 5.1, the diversification of the functional groups on LS A and LS B structures is summarized with the respective free binding energies of the ligand-protein complex being in their most stable conformation and highest binding affinity according to AutoDock Vina predictions.

The ΔG -values of the reported functional groups indicate an increased affinity to Cav(V148), with blue being aromatic-aliphatic functional groups fall in the lower range of -7.3 kcal/mol. In the complex of ligand L1A and hSOD1 a free binding energy of -8.0 kcal/mol is obtained. The ligand forms hydrogen bonds to the Val148 main chain peptide bond (-OH---N-Val148, 2.0 Å) of strand A, and to the asparagine side chain amide group (-CO---H-Asn53, 2.8 Å) of strand F. Asparagine amide group (-OH---H-Asn53, 3.2 Å) of strand A is not considered a true hydrogen bond, because the angle is not optimal. The bonding to the asparagine residues on both strands has to be considered carefully, as it is not clear, how they are conformed for all the PDB structures tested (Section 7.3.1).

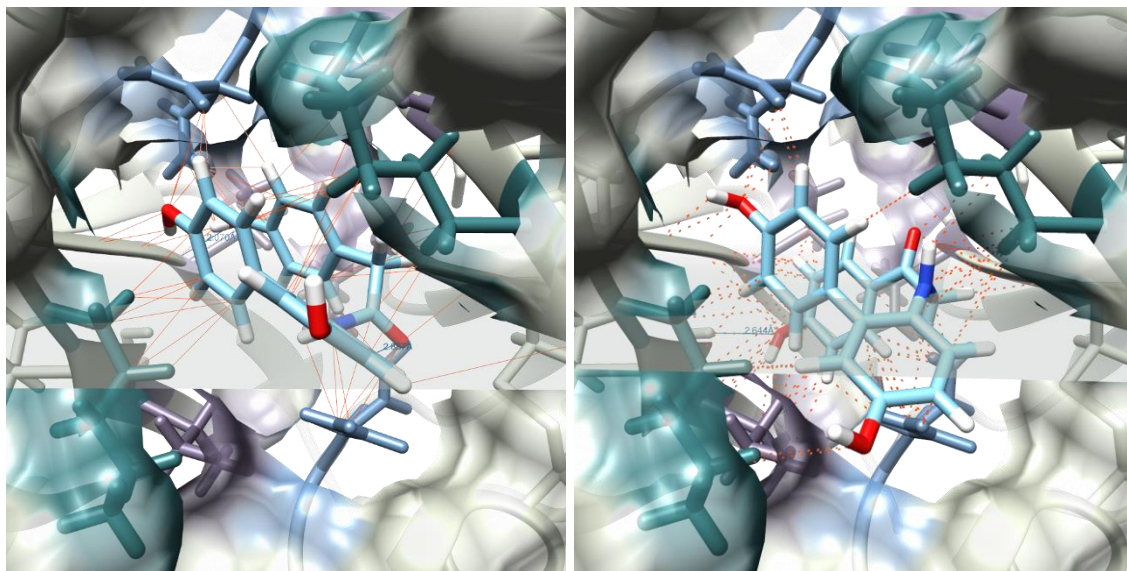
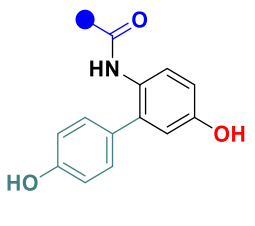
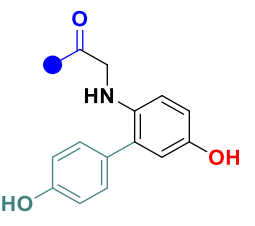
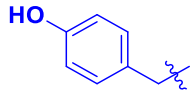
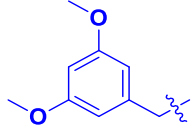
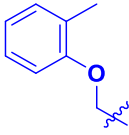
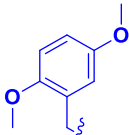
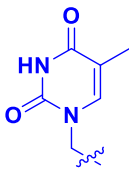
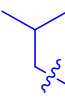
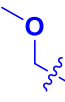


Figure 5.7 Docking of ligands L1 in the cavity of interest, Cav(V148) with their polar and non-polar interactions. *Left*: L1A with free binding energy of -8.0 kcal/mol; *Right*: L1B with free binding energy of -8.6 kcal/mol.

Table 5.1 Comparison of ligands estimated free binding energies for lead structures A and B.

		-ΔG (kcal/mol)	
			
		A	B
L1		8.0	8.6
L2		8.4	8.5
L3		8.6	8.4
L4		8.3	8.5
L5		8.6	8.6
L6		7.3	7.5
L7		7.5	7.2
L8		7.5	7.3

The ligand L1B shows a free binding energy, which is increased by 0.6 kcal/mol compared to L1A. From the position in the cavity we can observe a difference in amide vs amine bond flexibility. The active torsion of L1B brings the amine above the plane, and more flexibility on the aromatic ring inside as shown in Figure 5.7 (right). This could be one of the main reasons for such a difference in binding among the ligands as well as more total interactions with Cav(V148). From the position of L1A in the cavity, it can be seen how the hydrophobic part of the ligand is oriented toward the inner cavity, where non-polar contacts with the amino acids are attained. Polar contacts with the more hydrophilic part of the cavity (mostly lysine and asparagine) are also formed. Contacts are shown as orange-red dotted line. The difference between ligands L1A and L1B could be designated to a higher hydrophobic interaction that contributes to the entropic binding and free energy calculation. When the free energy (-8.4 kcal/mol) of L2A is compared to the L1A, an increase in binding affinity to the cavity is confirmed. The additional hydrogen bond with the asparagine amide side chain (-OMe---H-Asn53, 2.3 Å) of strand A together with the amide on the asparagine on strand F (-CO---H-Asn53, 2.6 Å) contribute to a higher affinity to the cavity. However, what seems to result in a higher affinity is the binding of the hydrophobic methyl groups to the inner cavity.

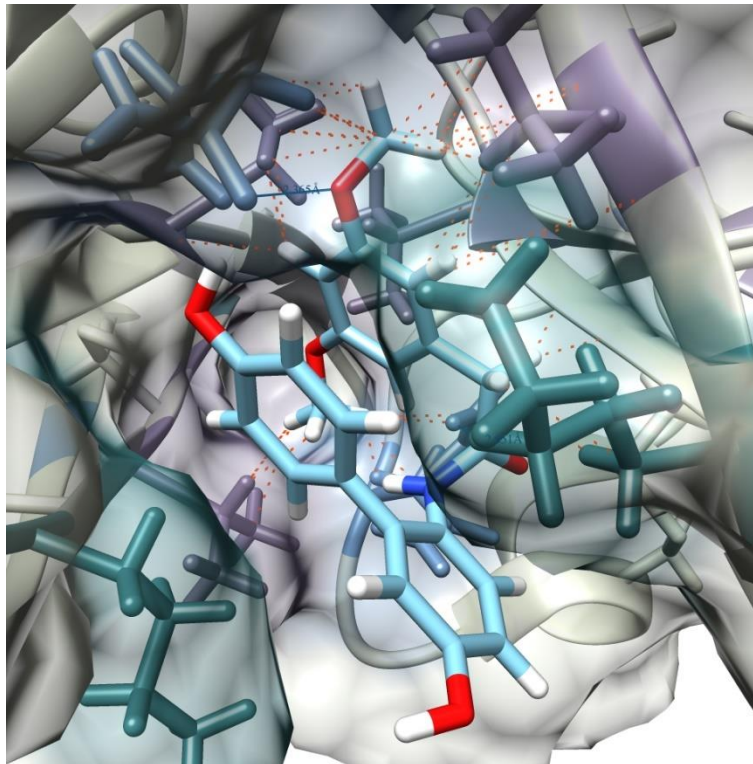


Figure 5.8 Ligand L2A in the cavity of interest with free binding energy of -8.4 kcal/mol, polar and non-polar contacts are shown with orange-red dotted lines.

As shown in Figure 5.8, non-polar contacts are contributing to the interaction with the valine residues (purple) of both protein strands. For all docking poses, π - π stacking of the aromatic rings within the ligand is observed, except in the pose with the lowest affinity, when the RMSD value exceeds the set limit, at which the ligand stretches vertically along the cavity, while forming four hydrogen bonds with both monomers of the protein. No additional interactions were identified for L1B, and the position within the cavity was practically the same. This could also indicate that the position of the methylene group does not have a tremendous impact on the binding itself rather on the flexibility of the ligand. Docking of ligand L4A (Figure 5.9), in which hydrogen bonding from dimethoxy groups to the protein strands is omitted, gave a binding free energy difference of - 0.1 kcal/mol compared to ligand L2A, and a lower estimated affinity of L4A. However, a higher affinity of L4A (-8.4 kcal/mol), compared to L1A (- 8.0 kcal/mol) is likely due to the hydrophobic interactions with the amino acids in the protein's inner cavity, because the total number of hydrogen bonds is the same.

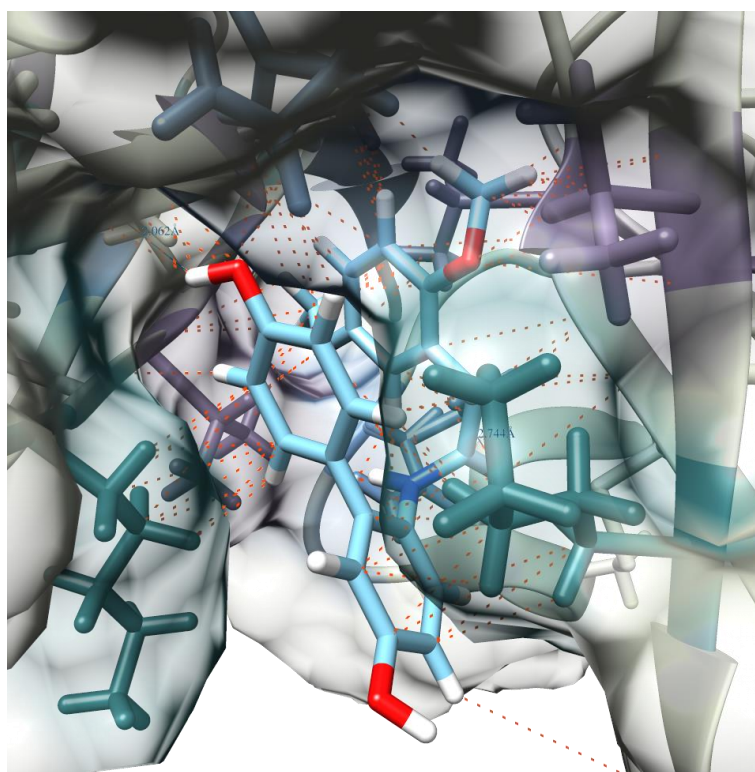


Figure 5.9 Ligand L4A in the cavity of interest, Cav(V148) with -8.3 kcal/mol free binding energy; red-orange dotted lines indicate contacts within the cavity.

Furthermore, the conformation of ligand L3A complements earlier conclusions. A free binding energy of -8.6 kcal/mol is obtained in the most stable pose scored that showed no hydrogen bonding with any of the abovementioned amino acids in the cavity. However, the distances of the polar and non-polar contacts of the Cav(V148) amino acids are in the range of 1.3 - 4.0 Å and the total number of interactions is high compared to the ligands previously described. The interactions are shown in Figure 5.10. It can be seen that the benzyl ring directly connected to the amide bond points in other directions and that π - π stacking interaction between the biphenyl rings is configured parallel-displaced.

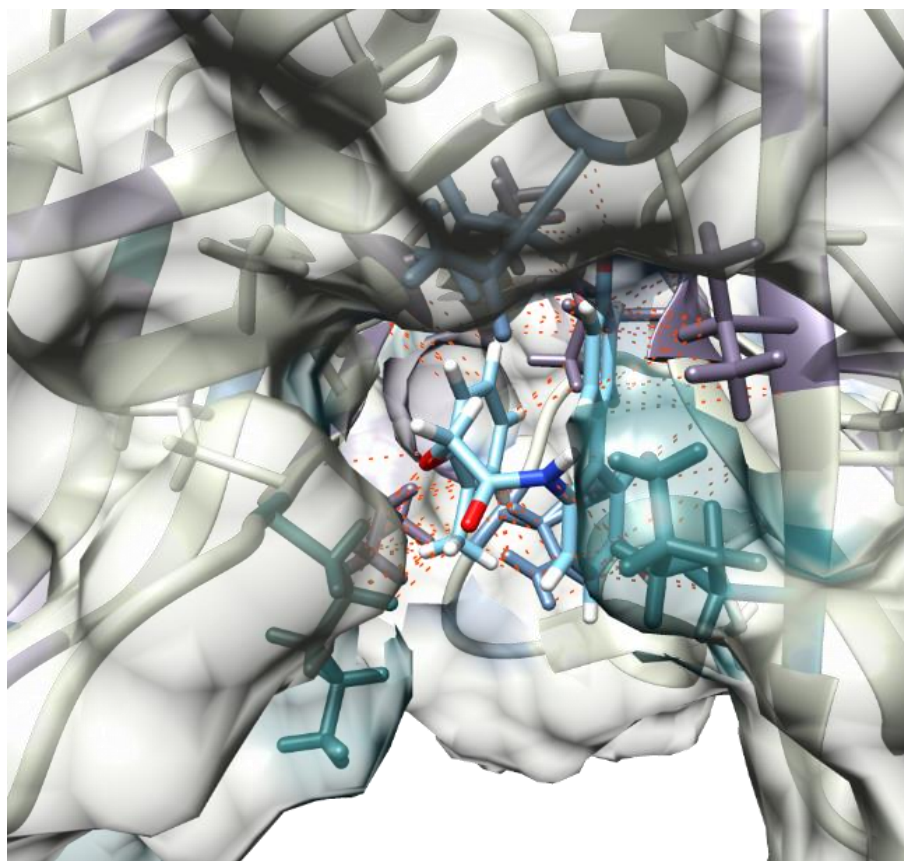


Figure 5.10 Ligand L3A in the cavity of interest, Cav(V148), with -8.6 kcal/mol free binding energy.

The binding affinity of the ligand L5A has the same score as L3A, but the obtained binding energy results from hydrogen bonds and from hydrophobic interactions. In the pose with the most stable conformation Figure 5.11 the ligand forms hydrogen bonds to the amide bond of the asparagine (-CO---H-Asn53, 3.0 Å) of strand F. Furthermore, two hydrogen bonds are formed between the carbonyl group of the thymine-based structure and with the asparagine amide side chain and the main chain of the valine residue on strand A (-CO---H-Asn53, 2.1Å, -CO---H-Val148, 2.2 Å).

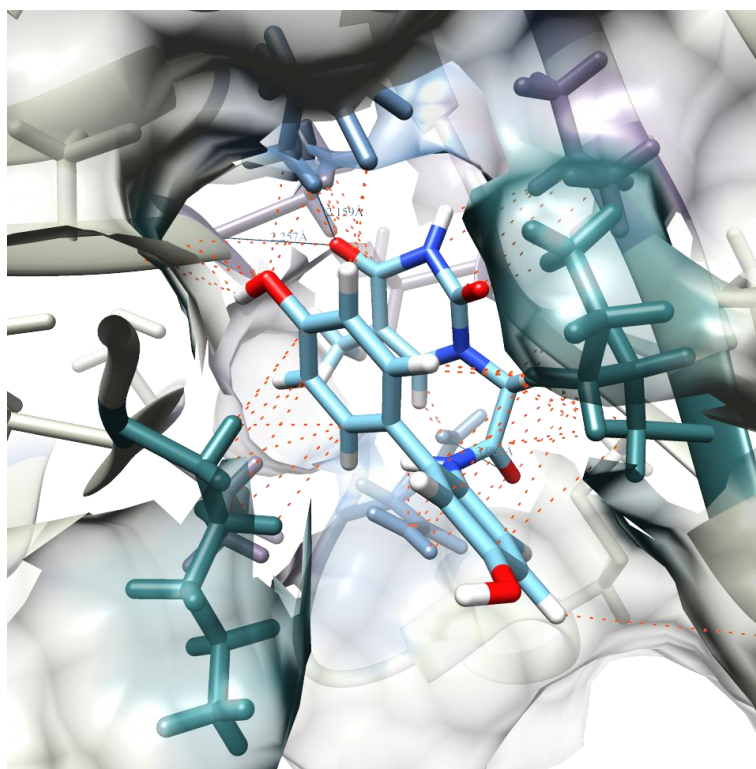


Figure 5.11 Ligand L5A in the cavity of interest, Cav(V148) with a free binding energy of - 8.6 kcal/mol. Hydrogen bonds are depicted with a straight lines (blue), other interactions are depicted with orange-red dotted lines.

It is interesting to compare the binding affinity between the ligands with the same highest-ranking score; in one, the binding seems to be completely obtained through largely hydrophobic interaction, while the other binding is occurring mostly from hydrogen bonds. To achieve higher affinity, both, enthalpy and entropy, have to be favoured in the binding. The conformation of the ligands with the aliphatic chains (L6, L7, L8) in Table 5.1 showed a lower binding affinity for both lead structures with a higher free binding energy in the range of -7.5 kcal/mol to -7.3 kcal/mol. Ligand L8A has a lower binding energy of -7.5 kcal/mol contributed from one hydrogen bond to the asparagine amide side chain of strand F (-CO---H-Asn53.F, 2.1 Å) and 79 polar and non-polar contacts to the other amino acids in the cavity, (Figure 5.12, left).

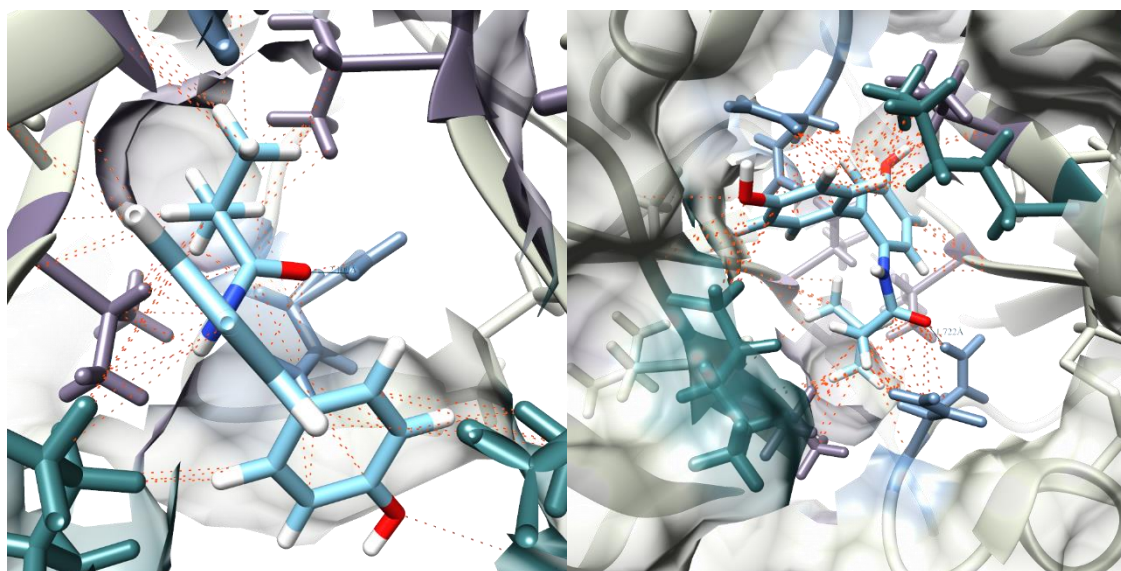


Figure 5.12 Ligands of lead structure A in the cavity of interest, Cav(V148) with their free binding energies. *Left: L8A (- 7.5 kcal/mol), Right: L6A (- 7.3 kcal/mol).*

In the binding conformation of L7 (Figure 5.13), hydrogen bonding from the oxygen of the carbonyl group as well as the ether group are directed to differently positioned amide side chains of the same asparagine on strand F. Therefore, it could be assumed that only one of these hydrogen bonds can possibly be formed. The angle of 3° and the length difference of 0.2 \AA , respectively, are relatively small just to eliminate one of them. However, it can be concluded that the position of the ligand in the cavity is in proximity to the Asn53 with the possibility to form hydrogen bonds. Although, the number of hydrogen bonds in L7A is the same and additional 26 polar and non-polar contacts are observed compared to the L8A, there is no difference in the calculated binding energies of both ligands.

The binding affinity of ligand L6A to the protein was estimated to have the highest free binding energy according to the AutoDock Vina. From the interaction with the amino acids in the cavity, ligand L7A has the most non-polar and most polar contacts compared to the other two ligands with the aliphatic functional groups. If we add the hydrogen bond to the amide side chain of the asparagine of strand F ($-\text{CO}---\text{H-Asn53}$, 1.7 \AA) it is difficult to conclude on the better binding affinity among them. However, it can be observed that the space in the cavity is not completely occupied by any of the ligands with aliphatic groups (Figure 5.12 and Figure 5.13), and the enthalpic contributions to the binding can be improved.

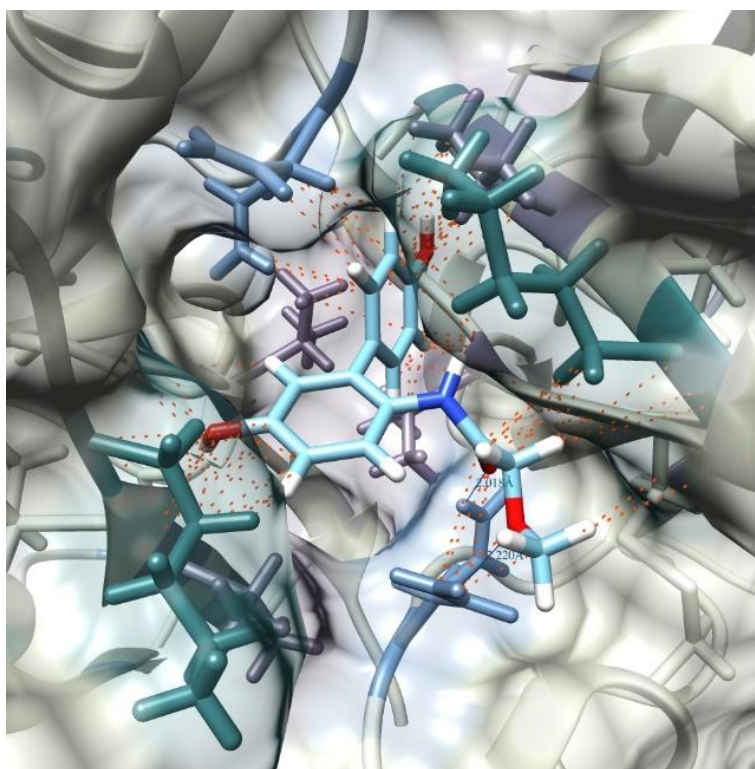
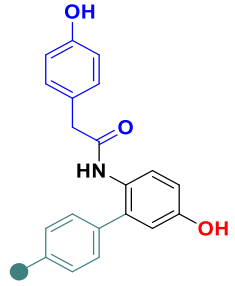
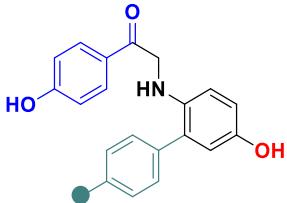


Figure 5.13 Ligand L7A in the cavity of interest, Cav(V148) with a free binding energy of - 7.5 kcal/mol.

From the analysis of the ligands shown in Table 5.1, it can be concluded that the aromatic functional groups are necessary for a high binding affinity to Cav(V148). Furthermore, the ranking among the best ligands with the lowest free binding energies can be based not only on enthalpic interactions, which mostly take hydrogen bonding into account, but also on entropic binding, as seen in the case of L5 and L3. Especially as Cav(V148) is hydrophobic at the inner core and more hydrophilic at the periphery. The flexibility of the ligands has to be considered carefully, especially if the space is not fully occupied, which could lead to greater discrepancies among the scored poses, and the accuracy of the docking is more likely to be compromised. Additionally, the positioning of the functional groups that influence the affinity by entropic and enthalpic binding is important, as can be seen from the docking of ligands L2 and L4. Moreover, ligand L1 is shown to be a good starting point for ligand optimization, considering that the *in silico* design is half the reality, in which a lot of important aspects are simplified that contribute to the real binding.

The previous paragraphs were focused on variation of the blue structural moiety (Scheme 5.1). Additionally, molecular docking was also performed with functional group diversification on the biphenyl ring marked in green (Table 5.2) to be able to compare the influence of functional groups on the binding to Cav(V148). In the analysis of the ligand L10A (Figure 5.14), a certain contribution to the free binding energy (-8.4 kcal/mol) is obtained from hydrogen bonding of the hydroxyl group to the Val7 main chain (-OH---H-Val7, 1.8Å) and another 120 interactions were identified within the cavity. L10A also shows a π - π stacking, but the black benzyl ring points inside the cavity, which results in a hydrogen bond to Val7. From the docking obtained for L10 it can be seen that the impact of the functional group on the binding to Cav(V148) is rather small, as it points outside the cavity in both lead structures.

Table 5.2 Comparison of the ligands estimated free binding energies for lead structures A and B with diversification on biphenyl ring (green).

ID	●	- Δ G (kcal/mol)	
			
		A	B
L1	HO	8.0	8.6
L9	F ₃ C	8.3	8.8
L10	H	8.4	8.4
L11	H ₃ C	8.9	8.4
L12	O ₂ N	8.8	8.6

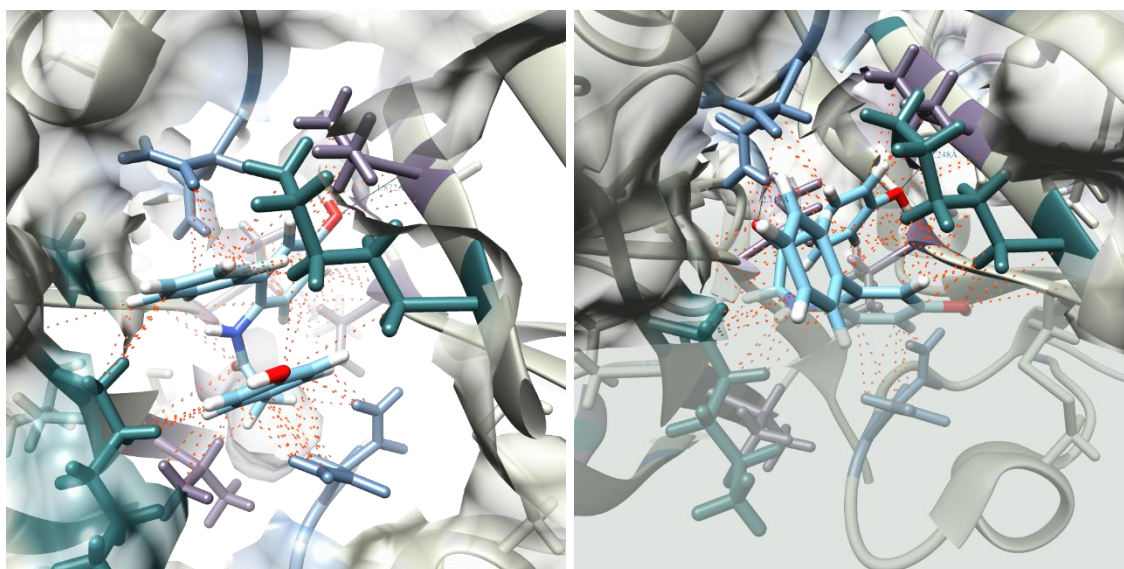


Figure 5.14 Ligands L10 in the cavity of interest, Cav(V148) with their free binding energies of - 8.4 kcal/mol. *Left:* lead structure A; *Right:* lead structure B.

If a CF₃ group is placed in the *para*- position, as seen in L9, the free binding energy difference to L10 is still low, while it is more significant compared to L1. The interaction of the CF₃ group in L9A is to the valine and asparagine residues of only one monomer of the protein. Moreover, the position of the core benzyl ring is pointed inside Cav(V148) and it is involved in π - π stacking with the aromatic ring with the CF₃ group in *para*-position, which is positioned above the plane (Figure 5.15, left). In contrast, ligand L9B gives a lower free binding energy in molecular docking, and a better positioning of the ligand inside Cav(V148) with interactions to Val148 of both monomers of the protein and to Val7 and Asn53 on one monomer, with distances ranging from 2.3 Å to 3.5 Å. The difference is also visible in the arrangement of the core aromatic ring, which is now positioned toward the periphery of the cavity, (Figure 5.15, right). However, hydrophobicity of the CF₃ results in burial into the hydrophobic interior, which leads to a decrease in binding energy.

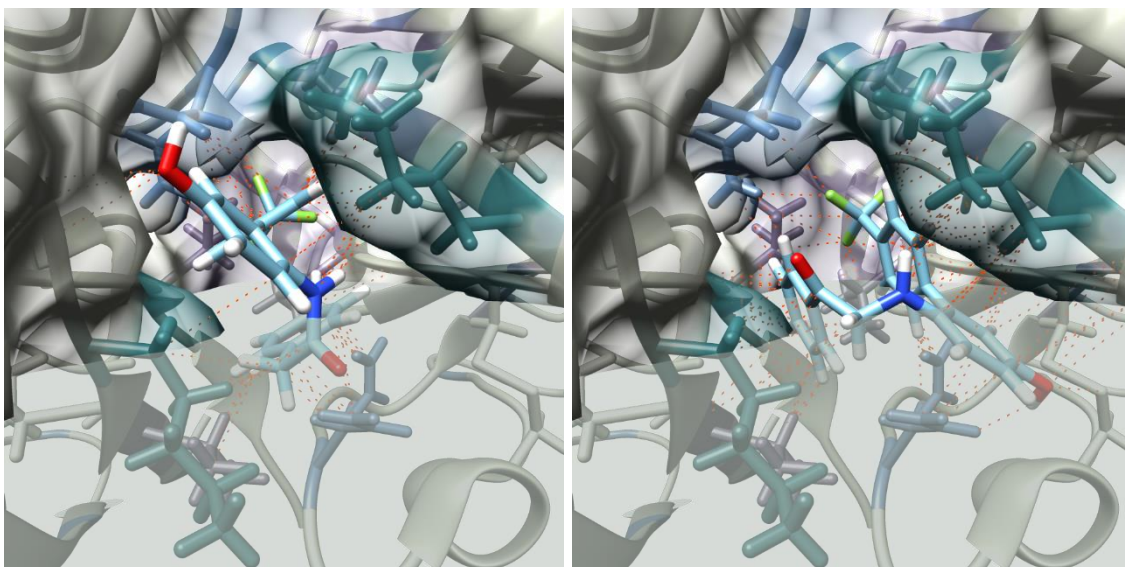


Figure 5.15 Ligands L9 in the cavity of interest, Cav(V148). *Left:* L9A with free binding energy of - 8.3 kcal/mol; *Right:* L9B with free binding energy of - 8.8 kcal/mol.

If a methyl group is placed in *para*- position of the aromatic ring, the ligand L11A in the most stable scoring pose has a free binding energy of -8.9 kcal/mol, potentially results from two additional hydrogen bonds to strand F of the protein, including the amide side chain of the asparagine and the carbonyl in the lysine main chain; (-CO---H-Asn53, 2.2 Å), (-OH---O-Lys9, 2.2 Å). On the other hand, ligand L11B has a higher free binding energy, which could be explained by the lack of hydrogen bonding and other weak interactions with the cavity. However, the methyl group is still buried inside the cavity and forms interactions with non-polar amino acids, Figure 5.16.

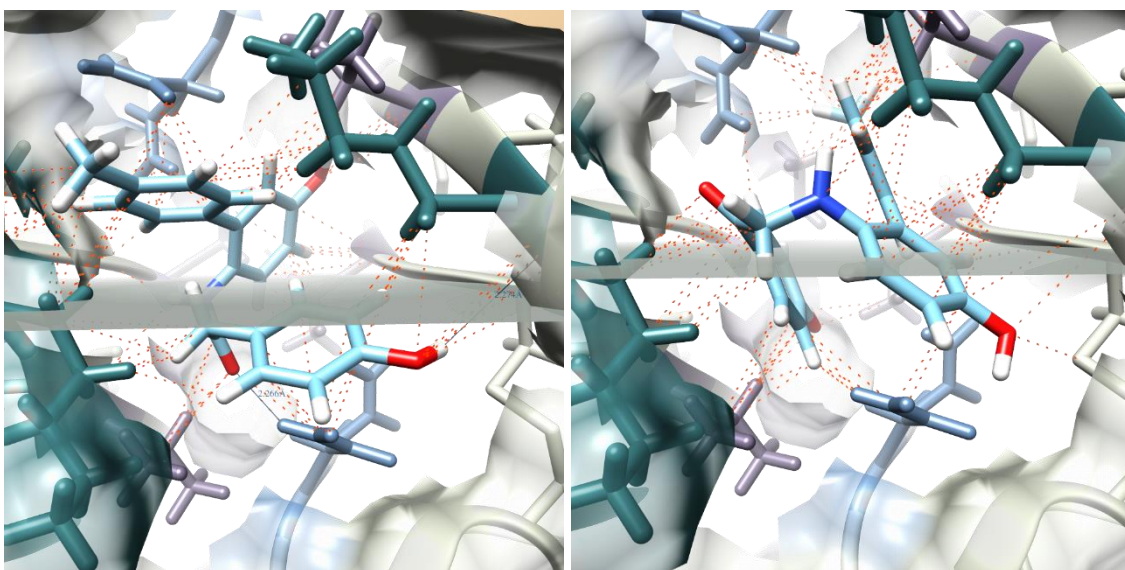


Figure 5.16 Ligands L11 in the cavity of interest, Cav(V148). *Left:* L11A with free binding energy of - 8.9 kcal/mol; *Right:* L11B with free binding energy of - 8.4 kcal/mol.

The free binding energy of L12A with a nitro group in *para*- position is similar to L12B with a difference of 0.2 kcal/mol. Additionally, both ligands form two hydrogen bonds with the protein, but L12B has fourteen additional interactions. However, if we compare their conformation in the cavity (Figure 5.17), it is clear that L12B (right) may occupy a more favourable position with the nitro group being buried in the cavity and forming hydrogen bonds to two strands of the protein: (-NO---H-Val7, 2.1 Å), (-NO---H-Asn53, 2.4 Å). In contrast, the nitro group of L12A (left) is directed out of the cavity and reveals interactions with the Lys9 and Gly10 with an approximate distance in the range of 2.5 Å to 3.8 Å.

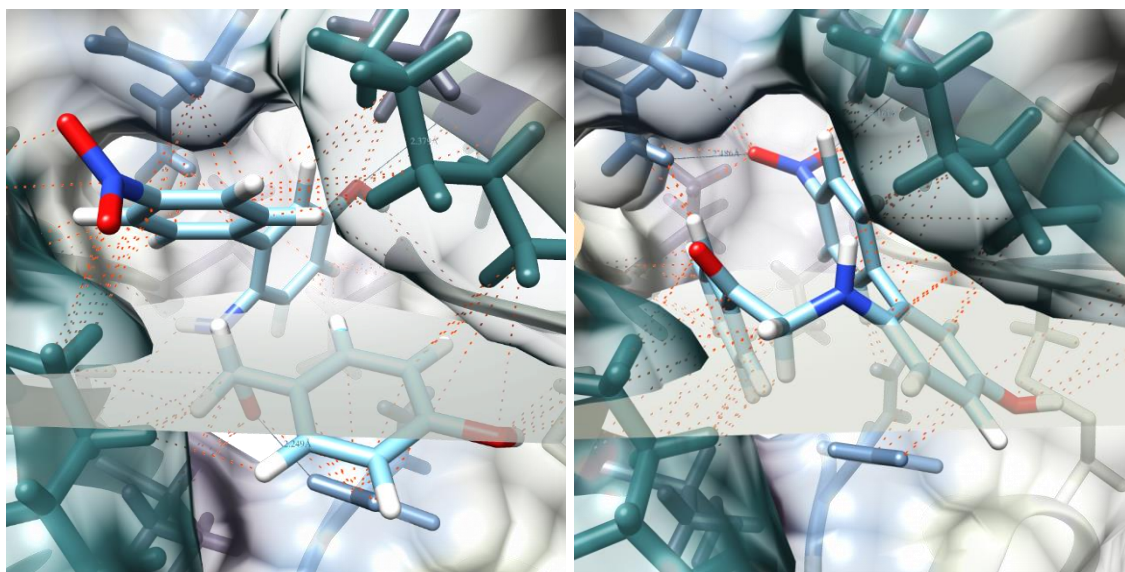
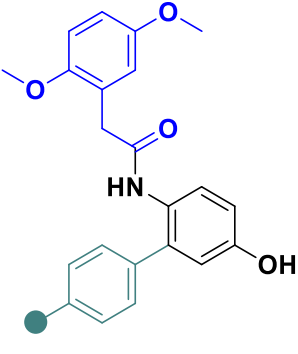


Figure 5.17 Ligands L12 in Cav(V148) with polar and non-polar contacts < 3.8 Å (orange-red dotted lines), and hydrogen bonding < 2.4Å (blue straight lines). *Left*: L12A with free binding energy of - 8.8 kcal/mol; *Right*: L12B with free binding energy of - 8.6 kcal/mol.

If we compare ligand L12A, Figure 5.17 (left) and L9A Figure 5.15 (left), it can be observed how the polar nitro- group is positioned at the periphery and the binding energy is 0.5 kcal/mol lower than the one of L9A.

Some *in silico* studies were conducted upon indication of better binders after *in vitro* binding experiments, see Section 5.4. Improved binding affinity was confirmed for ligand L4A. Therefore, the blue building block was introduced first, and diversification with a nitro or a CF₃ group was performed at the green building block especially due to their different position in molecular docking. (Table 5.3)

Table 5.3 Estimated free binding energies for putative ligands of lead structure A

	●		
			
ID	L4	L13	L14
-ΔG (kcal/mol)	8.3	8.3	8.7

The interaction of the methoxy groups of L14A is visible in Figure 5.18. The interaction with valine residues of both protein strands, and the nitro group in *para*- position results in hydrogen bonding to the amide side chain of Asn53. Interestingly, L13 positioned opposite with the CF₃-group being buried inside the Cav(V148).

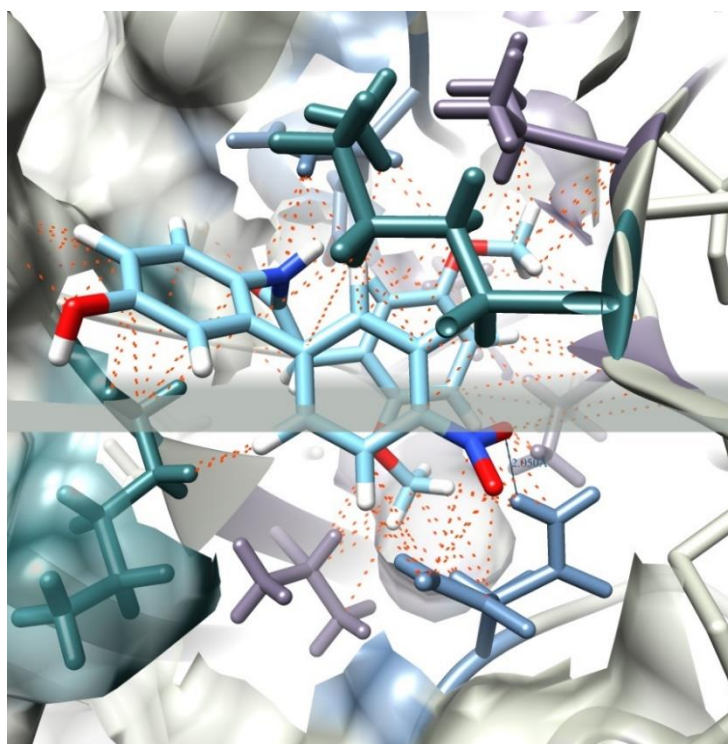


Figure 5.18 Ligand L14A in Cav(V148) with the free binding energy of - 8.7 kcal/mol; orange-red dotted lines represent the interaction within the cavity, and hydrogen bonding between the nitro- group and Asp53.F is shown with blue straight line.

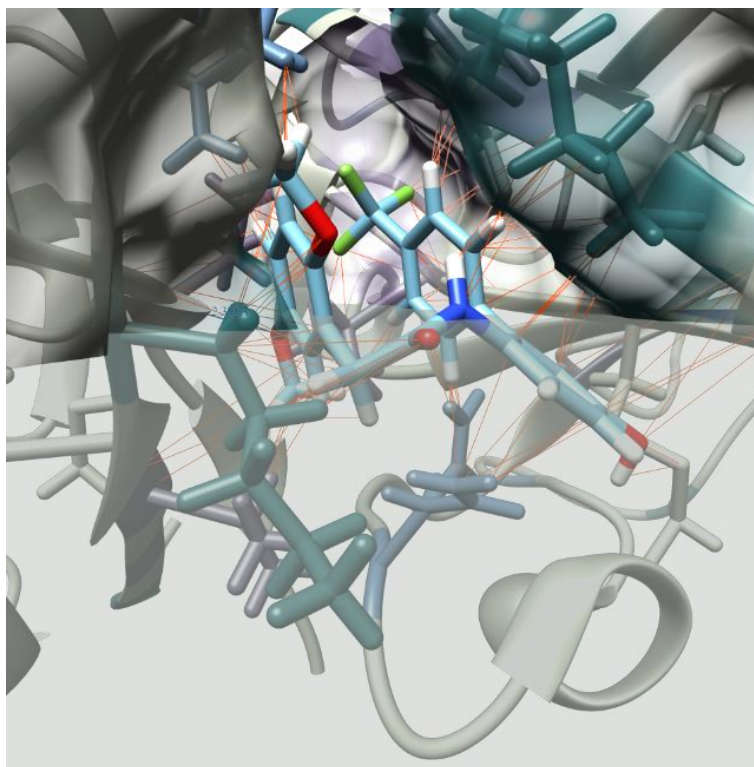


Figure 5.19 Ligand L13 in Cav(V148) with free binding energy of -8.3 kcal/mol.

Furthermore, both ligands, L13 and L14, and their conformation in the cavity could be influenced by the restricted position and the interaction of the methoxy functional groups on the blue aromatic ring. This could also be compared with L9A (Figure 5.15) and L12A (Figure 5.17), which lack these substituents.

From the *in silico* design and the molecular docking of different ligands we were able to confirm putative interactions within the cavity of interest. Also, different functional groups have impact on the binding, as seen in the comparison of aliphatic and aromatic moieties. This is consistent for both lead structures. The cavity of interest is hydrophobic and peripheral area hydrophilic. Due to the interactions with the presented ligands, the hydrophobic/hydrophilic interactions were matching the protein cavity. Furthermore, analysis of binding energies is not definite and does not have complete tolerance for each individual interaction. In reality, additional attractive and repulsive interactions between protein and ligands could easily be misinterpreted, if not all conformational changes are considered. To improve the affinity of the ligands for the hydrophobic cavity of our protein of interest, it would be strategically ideal to first prove the interaction and then design the functional group. We have observed much conformational flexibility during the scored poses with AutoDock Vina; however, it can be difficult to take the boundaries for flexibility into consideration. We have seen from already approved drugs, that it is necessary to lock them in the active conformation in order to enhance the interaction. One

example is diclofenac, which inhibits the enzyme cyclooxygenase more efficiently compared to ketoprofen because it is in a more preferred conformation.^[122] From an example of other inhibitors by Llorens *et.al.* it can be seen, how the omitted halogens in the aromatic fenoprofen allow more flexibility and free rotation of an ether bond between two rings. Diclofenac restricts the flexibility with two chlorine atoms in *ortho*- positions on the aromatic ring.^[123] Both inhibitors interact with the enzyme, but the fenoprofen affinity is lower, because more energy is required to reach the optimal conformation for the interaction. In our docking studies, most attention was given to the first scored poses, but also to the other poses with the lowest RMSD difference compared to the first zero value. However, restricting flexibility without any confirmation of the real binding would be immature, as the other enthalpy-entropy compensation cannot be fully encountered in the simulation, and we would need biophysical studies to examine possible interactions in the cavity, and ideally a structural validation.

The major limitations in computational docking are correlated with molecular conformation sampling and scoring functions, especially, because the flexibility of the target is mostly excluded, which can cause inaccurate pose prediction. Additionally, the solvent might be of great importance for ligand binding. It could serve as a chaperone to allow hydrogen bonding between ligands and target or simply add an entropic effect in the binding site. Crystal structures can also have a big impact on the reliability of the modelled binding if differences in crystal packing are not considered properly.^{[124][89]}

Altogether, it is crucial to keep the drawbacks in mind that molecular docking is bearing, to overcome the obstacles and have reliable studies. Finally, a combination of different biophysical and structural studies should be obtained and verified to confirm the reliabilities of the docking studies.

5.2 Synthesis

In order to validate the *in silico* analysis and library design, ligands had to be synthesized. Therefore, a synthesis approach was proposed, and revised along the way. This section describes the retrosynthetic approach and the synthesis design of the lead structures (LS) as well as their synthesis and library development. From the schematic view of the lead structures (Figure 5.20) it is possible to subdivide them into a basic structural unit, which consists of a biphenyl unit shown in black and green, which carries either a secondary amine (structure B) or an amide (structure A) in *ortho*- position of the core phenyl ring. In lead structure C (LS C), a methylene group is bound in *ortho*- position to the core phenyl ring, while the amide bond originates from the third aromatic ring shown in blue. The final lead structures (LS) are connected to the fluorophore *O*-nitrobenzoxadiazole. The advantage of the presented structures is the possibility of a modular synthesis approach, which facilitates the variation of functional groups and library enlargement.

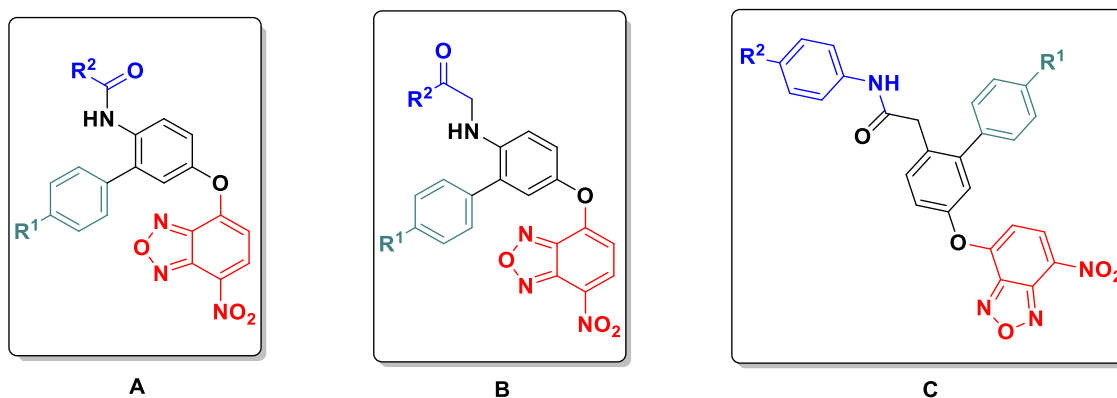
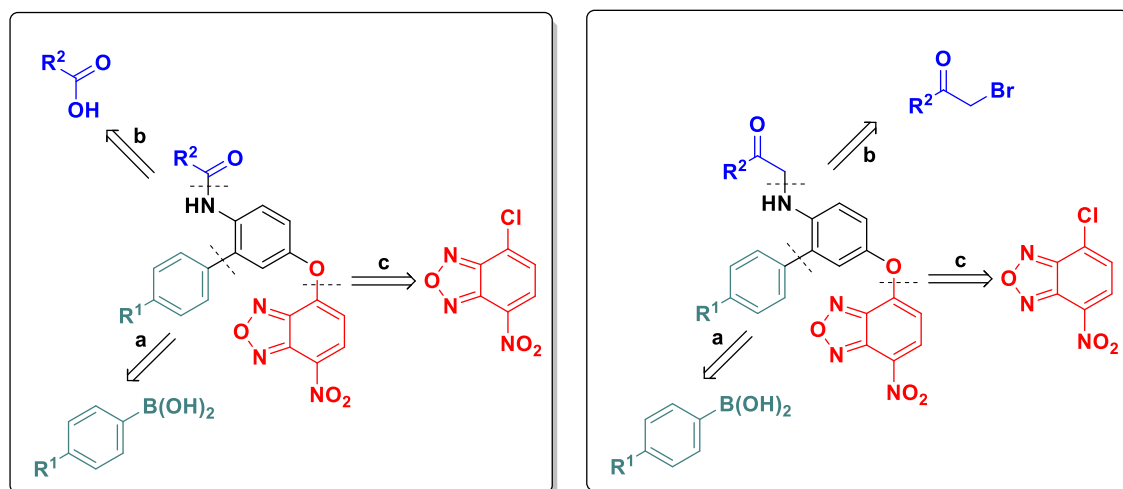


Figure 5.20 Lead structures A, B and C. The four basic structural units are shown in green, black, blue and red colour.

5.2.1 Modular synthesis approach

Predicting and planning synthetic pathways is a key step for a synthetic chemist, yet in medicinal chemistry and drug development, the task could be even more challenging. To optimize a non-binding ligand to a drug, sometimes only one functional group needs to be varied. Therefore, a modular approach should be considered and implemented in the early stages of synthesis planning. A possible modular synthesis of lead structures A (LS A) and (LS B) is shown in Scheme 5.2. The building block *O*-nitrobenzoxadiazole shown in red represents the previously mentioned fluorogenic dye for the labelling of lysine residues, and will be attached in a last synthesis step by C-O bond formation *c*. Furthermore, the ligand scaffold branches into three main building blocks as described

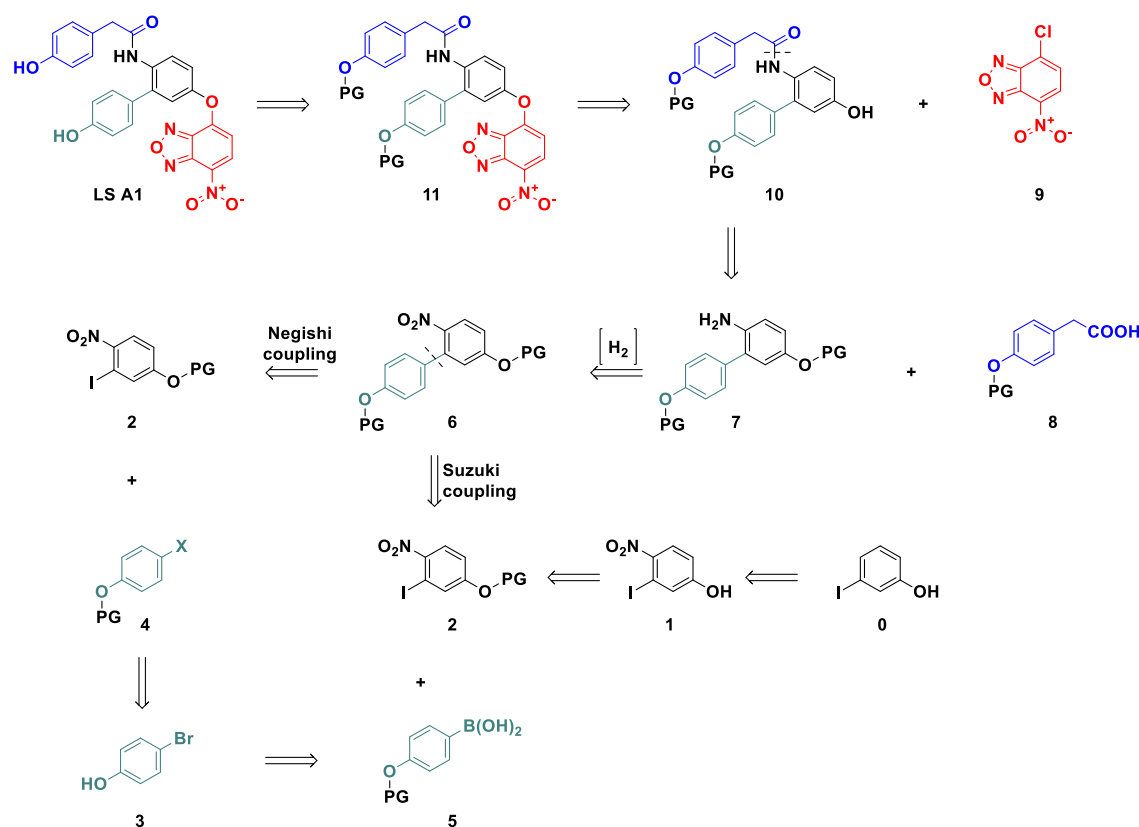
earlier and could be synthesized by amide bond formation or a nucleophilic substitution reaction marked in **b**, and the biphenyl ring can be obtained in a C-C coupling reaction **a**.



Scheme 5.2 Modular synthesis strategy of the lead structures. *Left: LS A; Right: LS B.*

5.2.2 Retrosynthetic approach of lead structure A

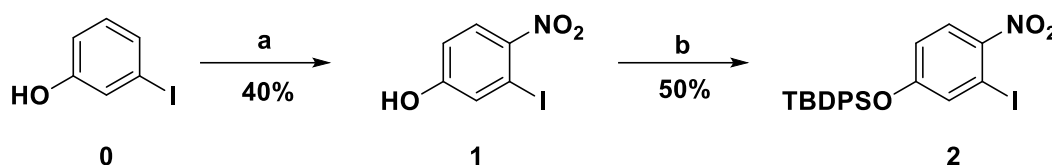
The retrosynthesis of lead structure **A** focuses on the synthesis of ligand structure **10** (Scheme 5.3), which will be tested as potential ligand for hSOD1. Later, the ligand structure **10** could be combined with the NBD fluorophore in a nucleophilic substitution reaction^[125], followed by the deprotection of the protecting groups (PG) of structure **11** in the final step. Tetrahydropyran ether as PG group can be easily removed under mildly acidic conditions.^[126] It is important to choose appropriate PGs, as this could be a critical reaction step. Ideally, the removal of the PGs should be performed in one step. For the synthesis of ligand **10**, an amide bond formation on structure **7** with a protected synthesized or a commercially available acid **8** and a further deprotection step will be employed. Aniline **7** can be obtained by reducing a nitro group in *ortho*- position on the biphenyl system **6**, which can be obtained by Negishi or Suzuki coupling.^[127] This leaves us with three structures that are either commercially available, as in 3-iodo-4-nitrophenol (**1**), 4-bromophenol (**3**), and boronic acids (**5**), or could be functionalized and synthesized from aryl halides.

Scheme 5.3 Retrosynthetic route of lead structure **A**.

5.2.2.1 Synthesis development toward the ligands **A**

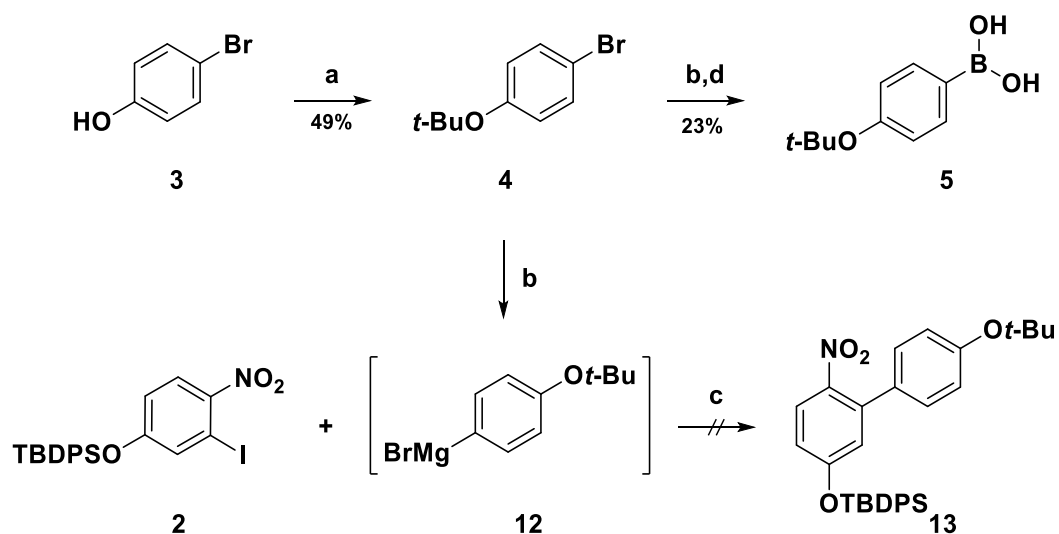
From the retrosynthetic analysis of lead structure **A**, the synthesis was divided into three building blocks (**2**, **7** and **8**), which will be combined to the final structure. The core building block 3-iodo-4-nitrophenol (**1**) was initially obtained by electrophilic aromatic substitution from 3-iodo phenol (**0**) with nitric acid as a nitro source in acetic acid, as well as by reaction of **0** with sodium nitrite and sulfuric acid.^{[128][129]} The product **1** was obtained in 37-40% yield under both reaction conditions. The moderate yield is the result of the unspecific nitration of 3-iodophenol in *o*-, and *p*- positions, as well as the difficulties of separating the *ortho*- product from the other substituted compounds. However, the product could be obtained, and further protecting groups were deployed. It is important to notice that the PG on structure **2** had to be orthogonal to the other PGs of the building blocks, to allow selective deprotection prior to the nucleophilic substitution with the NBD fluorophore. Furthermore, it should be stable to the basic conditions that were required in the next synthesis steps. As shown in Scheme 5.4, the *tert*-butyldisopropylsilyloxy group was used to protect **1**, as a relatively stable and robust protecting group toward acidic and basic conditions.^[130] Although the yield of 93% was obtained after purification by column chromatography, NMR analysis confirmed only

~50% of product **2**, that was purified portionwise by HPLC. The protection with TBDPS was not always straightforward, and the yield of the pure substance was only ~50%, which was due to the electron poor character of **1**.



Scheme 5.4 Reaction scheme of compound **2**. a) HNO_3 , HOAc , rt; b) NEt_3 , TPDPSCl , CH_2Cl_2 .

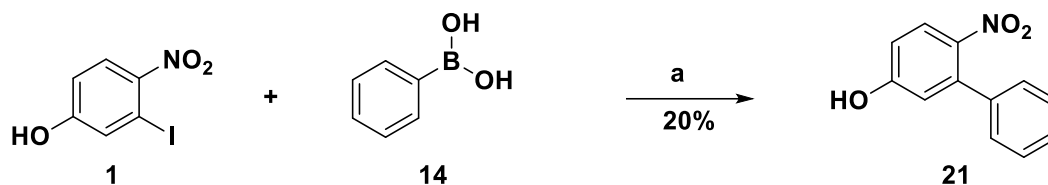
For the synthesis of the biphenyl structure in compound **6**, it was necessary to first synthesize the aryl halide, which could be further converted into the *tert*-butyl Grignard for a Negishi cross coupling or into a boronic acid for a Suzuki coupling.^{[131][132]} Scheme 5.5 shows the protection reaction **a** of 4-bromophenol (**3**) with *tert*-butyl bromide in pyridine to obtain compound **4**, which was further used in reactions **b** and **d** to obtain the reactant **5** for the Suzuki coupling, and **b** for Negishi.



Scheme 5.5 Protection of aryl halides as a precursor in Negishi and Suzuki coupling a) *t*-BuBr, pyridine; b) Mg, LiCl, THF; d) triethylborate, HCl.

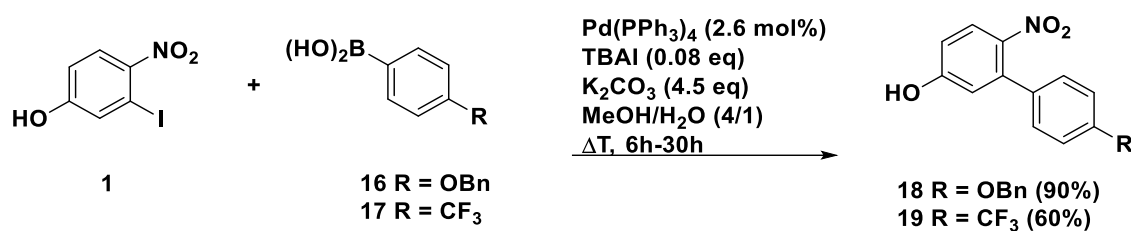
Tert-butyl bromide in pyridine was used in the reaction **a** to obtain **4** in 49% yield. The unreacted 4-bromophenol was recovered by distillation. The intermediate compound **12** was prepared by a Grignard reaction in **b** with LiCl and Mg in anhydrous THF, which was further used with triethyl borate and hydrochloric acid to convert it into the boronic acid **5**. However, only a low yield of 23% was obtained. The Negishi coupling **c** was tried with ZnCl_2 , $\text{Pd}(\text{dba})_2$ as an air stable Pd complex and Grignard intermediate **12**, yet the reaction was not successful. There could be several reasons involved, the bulky protecting

group TBDPS or the nitro group as a very deactivating and *m*-directing substituent, as well as the effect of nitro group to form an indole in a Bartoli reaction.^[133] The Suzuki coupling of compounds **5** and **2** with *tetrakis*(triphenylphosphine) palladium as a catalyst, and barium hydroxide in aqueous dioxane gave coupling products without *tert*-butyl and TBDPS groups as well as *tert*-butyl diphenyl silanol as detected by mass spectrometry. However, the main product was not observed, and no further purification of the resulting mixture was continued. Therefore, a step backwards was taken and a Suzuki coupling without protecting groups on any of the reactants was performed, as shown in Scheme 5.6. Here, the commercially available reactants 3-iodo-4-nitrophenol and phenylboronic acid were used applying the same reaction conditions as previously tested. The product was isolated successfully but with a low yield of only 20%.



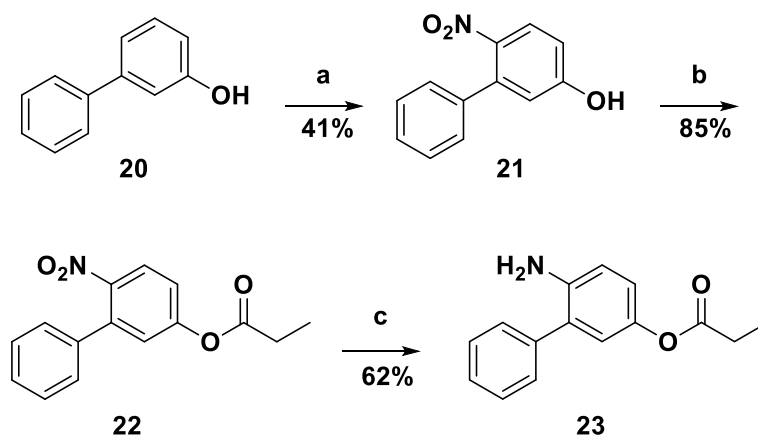
Scheme 5.6 Suzuki coupling of compound 21. a) Ba(OH)₂ (2.8 eq), Pd(PPh₃)₄, dioxane/H₂O.

In this exploration phase of the coupling reaction and the formation of C-C bonds, we decided to optimize the Suzuki reaction. Some advantages include a high functional group tolerance, nontoxic conditions, and commercial reactant availability, among others.^[132] *Schmidt* and *Riemer* investigated different phenols and phenol boronic acids for coupling with Pd/C in water.^[134] They also showed potassium carbonate to be a very good base for the coupling with varying equivalents of the reactants under different conditions. The conditions from different approaches were adapted to our system.^{[135][136]} We introduced potassium carbonate as a base with *tetrakis*(triphenylphosphine) palladium as a catalyst in a methanol/water mixture and added tetrabutylammonium iodide as an additive. It has been reported that the reaction of aryl bromide is facilitated, while the reaction with aryl iodides has no positive effect on the completion of the reaction with palladium acetate as a catalyst.^[135] In the planned coupling reaction shown in Scheme 5.7 the biphenyl structures **18** and **19** were obtained in 60-90% yield with different functional groups in *para*-position. The coupling with aryl iodide and aryl boronic acid bearing an electron-withdrawing group led to a moderate yield of 60% and required prolonged reaction time, while with a moderate electron-donating group on the aryl boronic acid gave a yield of 90% and the reaction was completed after six hours at reflux.



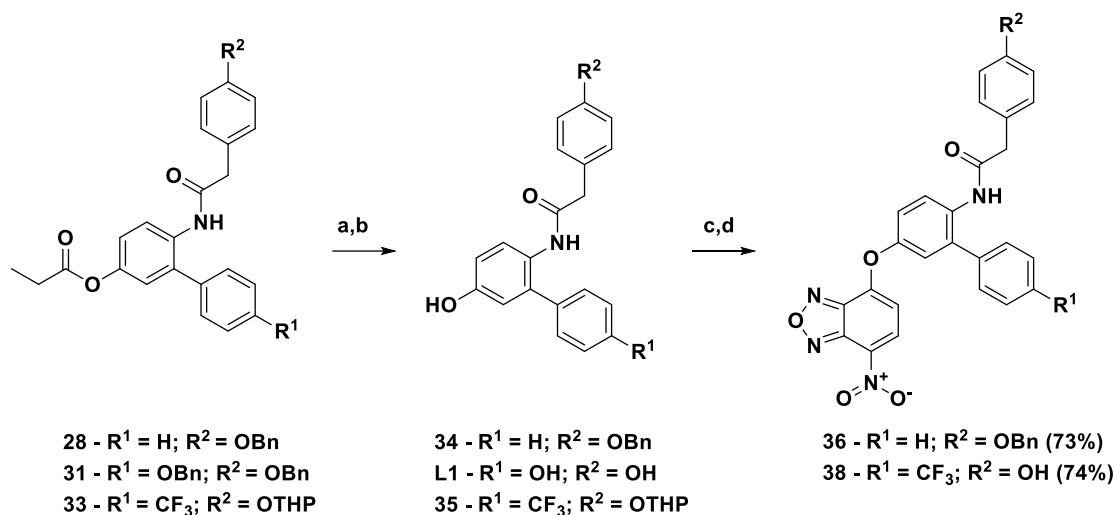
Scheme 5.7 Suzuki coupling of 3-iodo-4-nitrophenol and aryl boronic acids to corresponding biphenyls **18** and **19**.

On the retrosynthetic route of the lead structure **A**, the biphenyl amine structure **7** was required for an amide bond formation reaction and the synthesis of ligand **10**. As the amine functionality was planned to be obtained from the reduction of the nitro group, an initial test reaction was performed to optimize this step. Therefore, 3-phenylphenol was converted into **21**. The reaction proceeded in acetic acid with an overall yield of 81%, with the compound of interest **21** being obtained in 41% while *o*- and *p*- positions were substituted in 14% and 26%.^[137] Furthermore, the protection of the hydroxyl group was carried out prior to the reduction of the nitro group, since this could easily be deprotonated. Subsequent esterification with propionic acid^[138] was obtained without difficulty in 85% yield, followed by the reduction in 62% yield using Pd/C and H₂ (Scheme 5.8).



Scheme 5.8 Synthesis toward the biphenyl amine **23**: a) HNO₃, HOAc, 0°C → rt.; b) C₃H₆O₂, EDC-HCl, DMAP; c) Pd/C, H₂.

For the amide coupling with the amine biphenyl derivatives **4**, acids were synthesized that had benzyl or tetrahydropyran ether as protection groups in *p*- position. Initially, a benzyl protection was applied because of the benzyl protected hydroxyl group on the aryl boronic acid to ensure simultaneous deprotection in the last step after the ether synthesis. However, this was not compatible with the reduction of the nitro group. Therefore, the tetrahydropyran group was used for hydroxyl protection, with the advantage of an easy

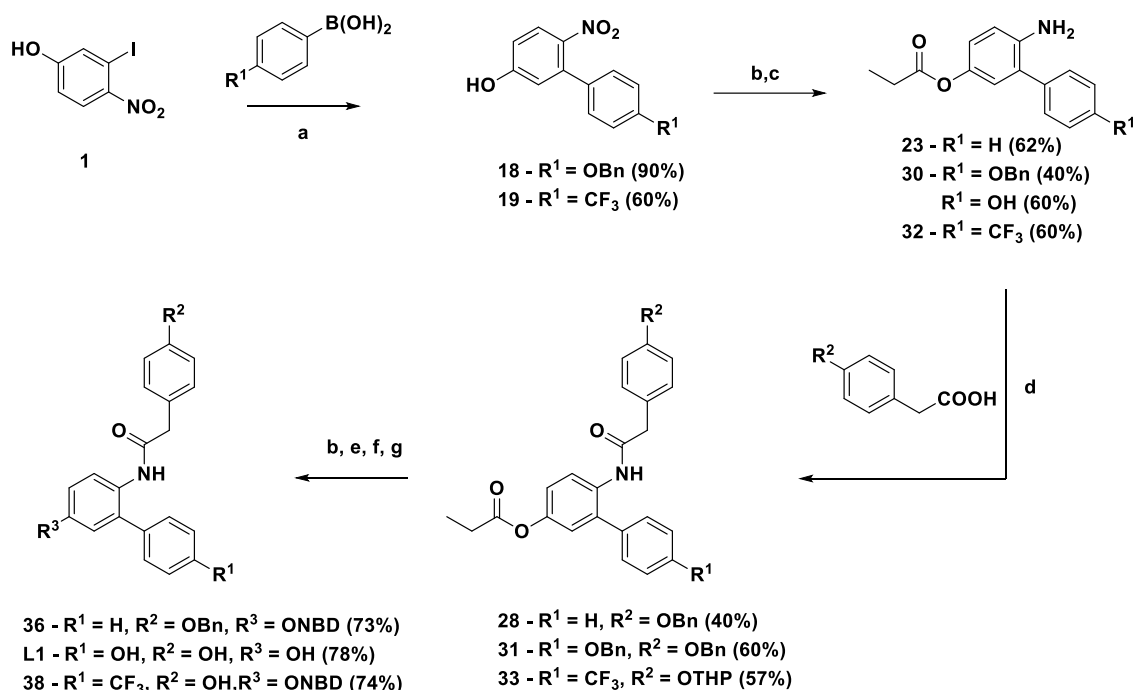


Scheme 5.11 Synthesis toward the compounds **34**, **L1**, **35** and lead structures **36**, **38**. a) KOH, MeOH; b) Pd/C, H₂; c) NBD-Cl, Et₃N, MeCN d) PPTS, MeOH.

The hydrolysis **a** proceeded smoothly in methanol and potassium hydroxide as a base in 99% yield. In the hydrogenation **b**, the benzyl groups were removed with palladium on charcoal and hydrogen under atmospheric pressure to obtain **L1** in quantitative yields. Ligand **34** with a benzyl group underwent further reaction with NBD-Cl to form lead structure **A** in 73% yield while maintaining the benzyl protection. Here, our attempt to remove the protecting group by hydrogenation was successful, but it also resulted in reduction of the nitro group in NBD. It was therefore necessary to rethink the protecting group strategy. The attachment of the NBD on the ligand bearing a CF₃ group and the further removal of the THP in the last step went well with 62% overall yield of the lead structure **38**.

The following Scheme 5.12 shows the complete synthesis of lead structure **A** with diversification of the functional groups in *para*- position of the biphenyl ring. In reaction **a**, Suzuki cross coupling was performed, and the product was obtained in 60-90% yield, depending on the functional group on the aryl boronic acid. Furthermore, the esterification of the phenol **b** proceeded smoothly in 92-95% yield, for both, the electron-withdrawing group, CF₃ and the electron-donating group benzylether. In the hydrogenation **c**, the reduction of the nitro group went well, but difficulties were encountered with the benzyl deprotection which reduced the yield to 40%. The amide bond formation **d** with different protected hydroxyl group was successful, but only in moderate yields of 55-60% and relatively long reaction times of up to two days. The hydrolysis reaction **e** with potassium hydroxide as a base, and the removal of the protection group under acidic conditions **g** were quantitative for all ligands. The ether

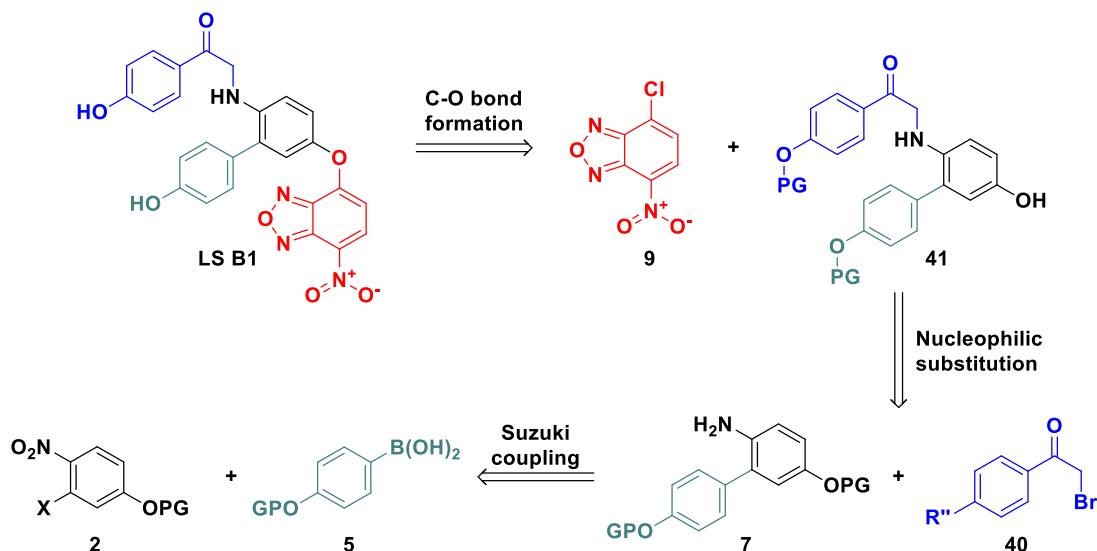
synthesis in reaction *f* on the aromatic phenol was successful and gave moderate yields (50-75%).



Scheme 5.12 Synthesis toward the lead structures **A**: a) Pd(PPh₃)₄, TBAI, K₂CO₃, MeOH/H₂O; b) EDC-HCl, DMAP, CH₂Cl₂ c) Pd/C, H₂, EtOH/EtOAc; d) EDC-HCl, HOBT, CH₂Cl₂; e) KOH, MeOH; f) NBD-Cl, Et₃N, MeCN; g) PPTS, MeOH.

5.2.3 Retrosynthesis and synthesis of lead structure **B**

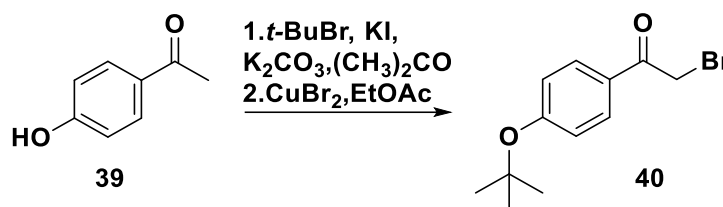
As already shown in Figure 5.20, a major difference between lead structures **A** and **B** is the methylene bridge, which for lead structure **B** is between the secondary amine and a carbonyl group, and, hence, requires a different retrosynthetic approach (Scheme 5.13).



Scheme 5.13 Retrosynthesis approach of the lead structure **B**.

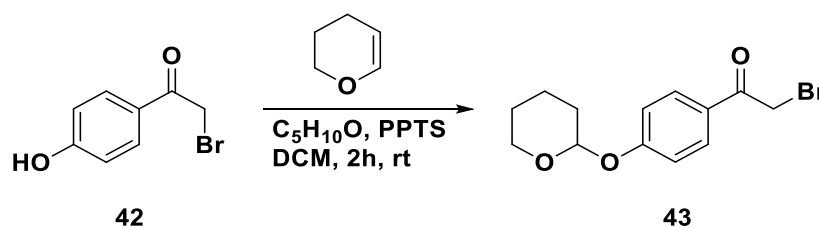
The key step in the synthesis of lead structure **B** (**LS B1**) is the nucleophilic substitution of the aniline **7** and the haloalkane **40** after the Suzuki coupling. The rest of the synthesis is similar to **LS A**. Therefore, the nucleophilic substitution toward the secondary amine **41** is discussed only.

The first approach toward **40** was the α -bromination of 4-hydroxy acetophenone with pyridinium tribromide as the bromine source in acetic acid; however, only a dibrominated product was obtained. Following different attempts with copper (II) bromide and previously *tert*-butyl protected 4-hydroxyacetophenone, mono- and dibrominated products in 79% yield were obtained, but the isolation was not straightforward, as the purification via flash column chromatography was not possible, and isolation by HPLC was not an efficient option, too.



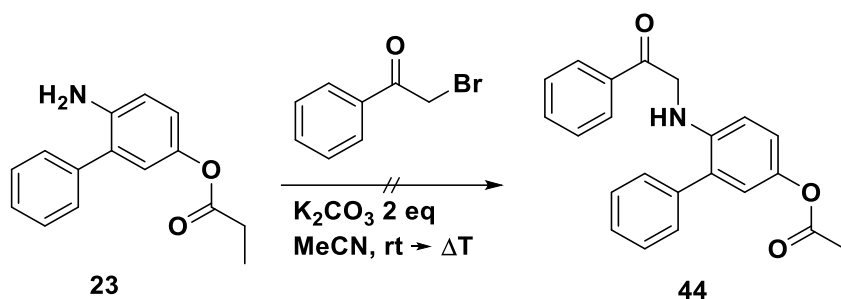
Scheme 5.14 Synthesis of compound **40** for the nucleophilic substitution reaction.

To avoid costly purification procedures between mono- and dibrominated products, commercially available 2-bromo-4-hydroxy acetophenone was protected as tetrahydropyranyl ether group in 60% yield,^[143] (Scheme 5.15).



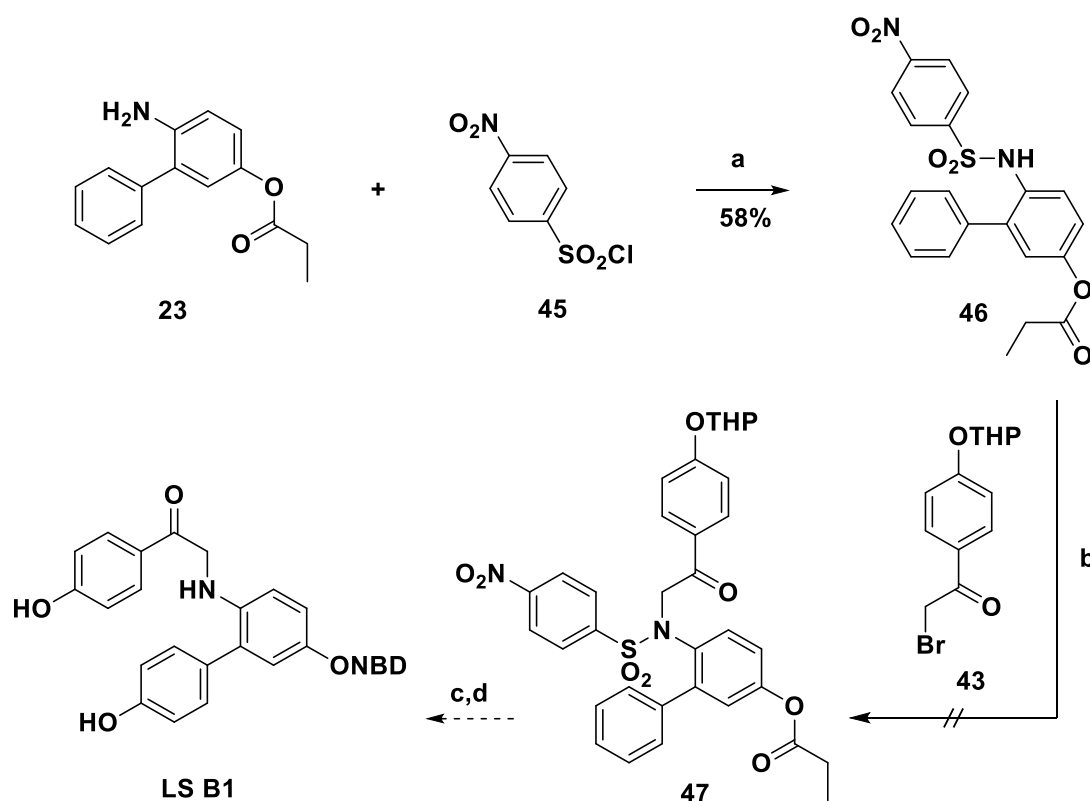
Scheme 5.15 Synthesis of compound **43**.

The key reaction of this synthesis strategy toward lead structure **B** is nucleophilic substitution to obtain the lead structure for further testing. Some initial tests were performed evaluating nucleophilic substitution conditions, in which potassium carbonate and triethyl amine were used as a base in various solvents and varying temperatures. However, no conversion was observed.



Scheme 5.16 Attempted nucleophilic substitution reaction toward compound **44**.

Another approach to the secondary amine was applied through 4-nitrobenzenesulfonyl chloride, which was reacted with a primary amine in pyridine as basic solvent. The mono-substituted sulfonamide **46** was obtained in 58% yield. The secondary amine was planned to be obtained from alkylation of the sulfonamide **46** and subsequent cleavage of *p*-nitro phenylsulfonic acid in **47** via Meisenheimer complex.^[144] However, the alkylation step **b** was not successful. (Scheme 5.17).



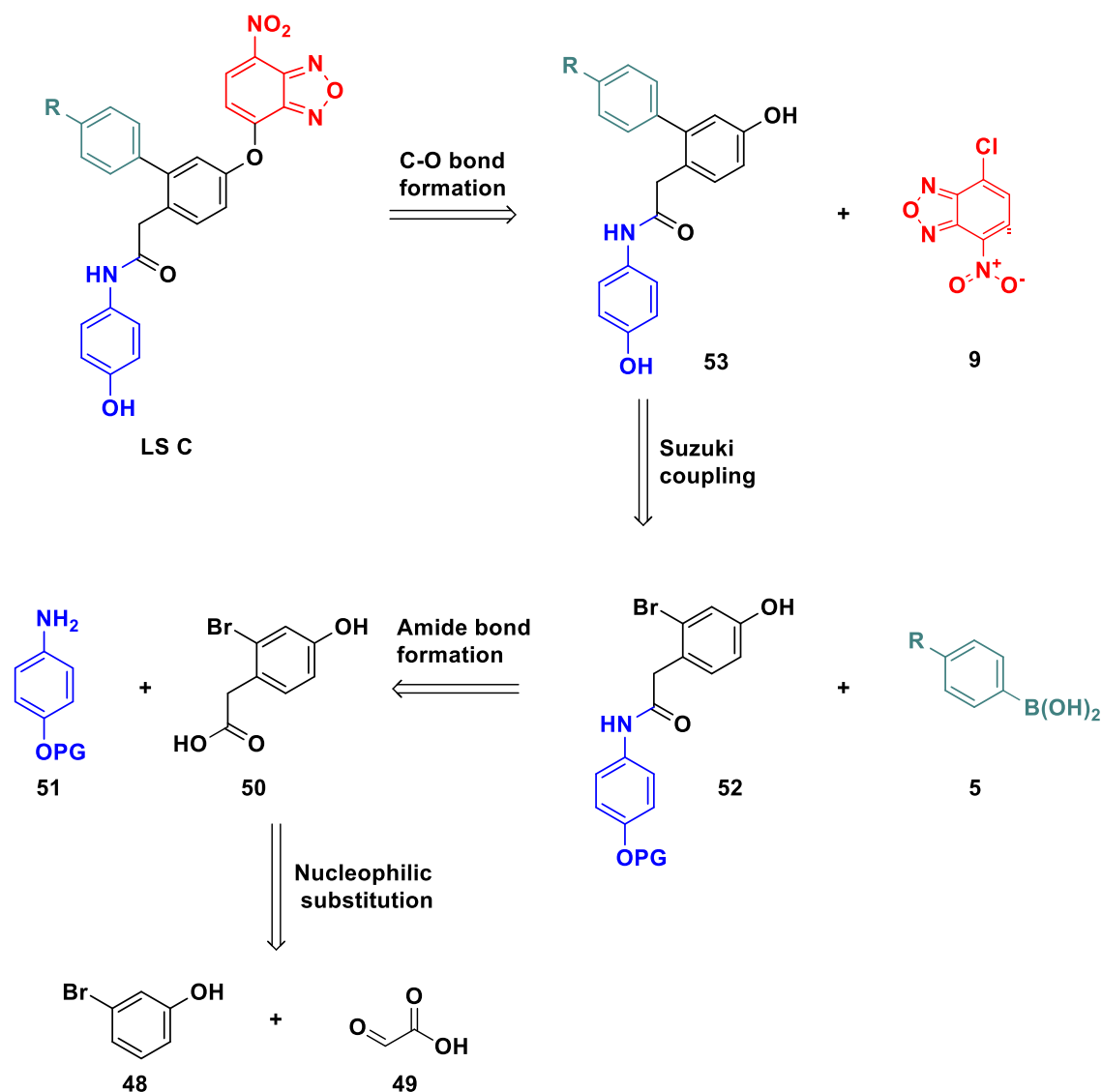
Scheme 5.17 Attempt toward secondary amine synthesis: a) pyridine, DCM ΔT ; b) K_2CO_3 , MeCN.

Further synthesis approaches were not tested because the idea was to compare the best ligands from proposed, designed and modelled ligands. The aim of this work was not only to synthesise the ligands, but to test their function and to establish a binding affinity assay.

Therefore, at this point, the focus was laid on the further development of the lead structure **A**.

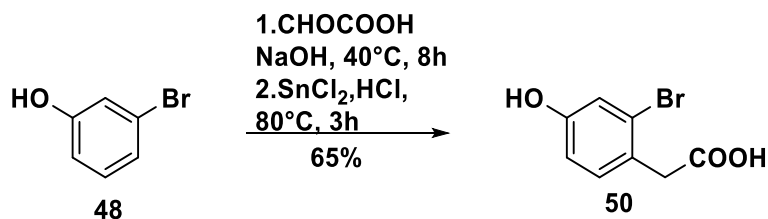
5.2.4 Retrosynthesis and synthesis of lead structure C

The difference of this lead structure compared to the two previously described structures is the position of the amide bond in the molecule. As it can be seen in the Scheme 5.18, an amide bond is formed from a primary amine attached to the aromatic building block **51** in blue and the acid on the 3-bromophenol as the core building block **50** shown in black. The flexibility of the molecule is slightly changed, because the biphenyl has no restraint from the amide bond and can rotate freely on the C-C bond of the methylene group and the carbonyl carbon. Therefore, to obtain the structure **52** an amide bond formation was envisaged on compound **51** with a previously synthesized or commercially obtained building block **50**. In the following step, the lead structure was planned to be synthesized by a Suzuki coupling with the commercially obtained or modified boronic acid **5**. The lead structure was further optimized for a coupling to fluorophore **9** to obtain the final structure for fluorescent dye transfer, as well as for the binding affinity tests, for which the protecting groups on the molecule had to be removed. This synthetic strategy was pursued by V. Theuer during her bachelor thesis.^[145]



Scheme 5.18 Retrosynthesis of the lead structure C.

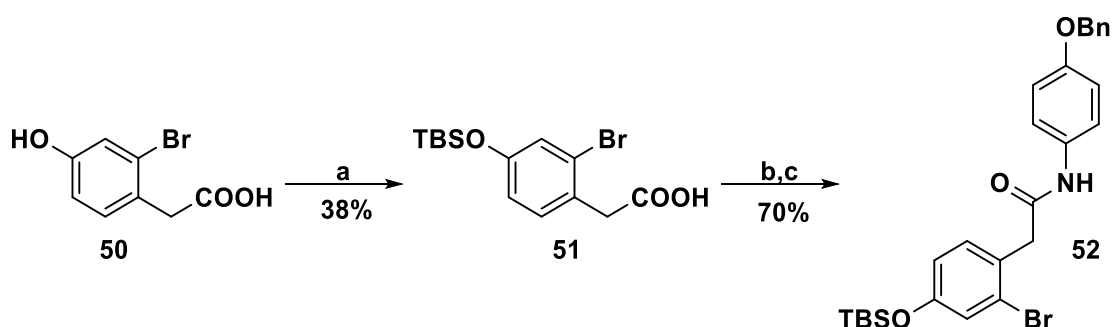
The acid of the core building block was obtained in two steps according to a literature-known procedure.^[146] In the nucleophilic reaction step with sodium hydroxide and glyoxylic acid, the product was isolated in 63% yield. Furthermore, the acid **50** was obtained upon reduction with tin chloride and gave a yield of 67%, (Scheme 5.19).



Scheme 5.19 Synthesis of compound 50.^[146]

Prior to the formation of the amide bond with commercially available benzyloxy aniline, protection of the phenolic OH-group with *tert*-butyldimethylsilyl chloride was necessary

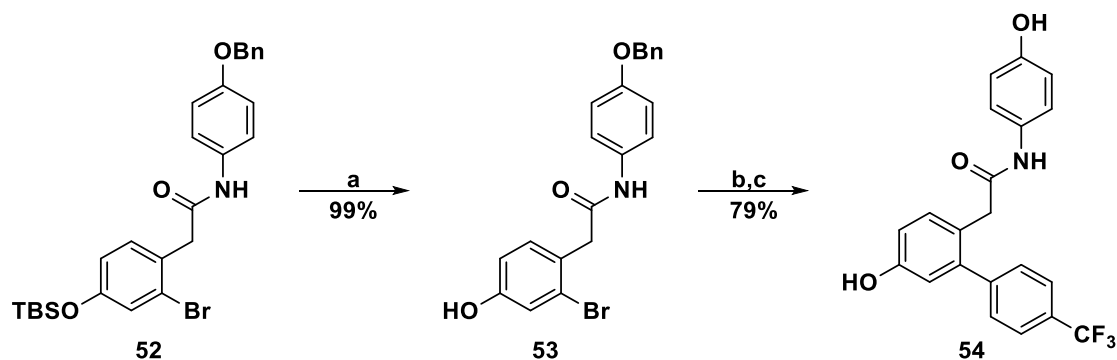
in order to avoid side reactions in the following step. In the first step of the amide bond synthesis, oxalyl chloride was used to prepare the corresponding acyl chloride, which was then reacted further with 4-benzyloxylaniline to obtain the product **52** in 70% yield.



Scheme 5.20 Synthesis of compound **52**: a) TBSCl (1.5 eq), Et₃N (2.0 eq), THF; b) C₂Cl₂O₂ (1.5 eq), DMF cat., dioxane; c) 4(benzyloxy)anilin (1.2 eq), K₂CO₃ (4 eq), dioxane.^[145]

Prior to the next critical step, the Suzuki coupling, the TBS protecting group was removed, the Suzuki product **54** was obtained in a 79% yield as shown in the Scheme 5.21.

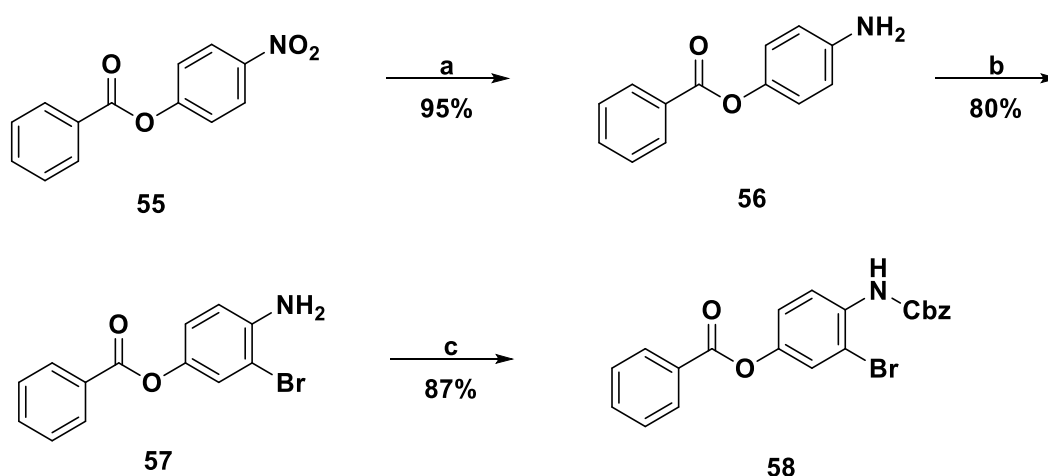
In the next step, compound **53** was reduced with palladium on charcoal and lead structure **C** was obtained in 98%. The introduction of the fluorophore in **54** was not performed, as the ligand was first submitted to binding affinity tests.



Scheme 5.21 Synthesis of compound **54**: a) TBAF(3.0 eq), THF, rt;b) Pd(PPh₃)₄ (10 mol%), K₂CO₃ (4.5 eq), (4-(trifluoromethyl)phenyl)boronic acid (1.5 eq), 24h, MeOH/H₂O; c) Pd/C, H₂.^[145]

5.2.5 Improved synthesis strategy A for a library enlargement

In the previously established synthesis, some problems and disadvantages were encountered from the protecting group strategy, purification steps and expensive starting material. It was also observed that one way around the steric hindrance of the PG in the amide bond formation could be to change the reaction sequence to perform the Suzuki coupling reaction after the amide bond formation. Furthermore, this strategy made it possible to introduce various functional groups and building blocks on the core aromatic ring and, hence, simplified a library enlargement. In addition, we were able to start from inexpensive compounds. The following synthesis route shows, how we can reach the main starting point in just 2 to 3 synthesis steps and, from there, decide, which building block we want to vary. This gives us more options for a faster library synthesis.

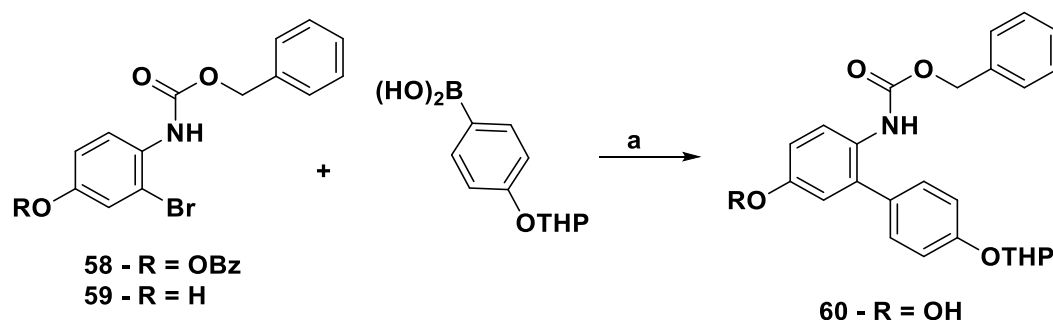


Scheme 5.22 Synthesis toward core scaffold for improving synthesis strategy: a) Pd/C, H₂, (2.5 bar), EtOH/EtOAc, 3.5h; b) NBS, DCM, rt; c) CBzCl, pyridine, EtOAc, rt.

The first hydrogenation step from commercially available **55** to 4-aminophenyl benzoate went smoothly in 95% yield. The reduction was also carried out with tin (II) chloride, but the basic work up led to the cleavage of the benzoate, and to a moderate yield of only 50% compared to the reaction with palladium on charcoal and hydrogen. In the next step, bromination with *N*-bromosuccinimide (NBS) was performed, which resulted in 80% yield. Since double bromination was confirmed by mass spectrometry, this could be avoided by adding the NBS in portions, in order to give a better yield. From this compound it was possible to proceed with the amide bond formation or with the Suzuki coupling. Before Suzuki coupling, an amine protecting group had to be introduced to restrain its basic and nucleophilic properties, as initial Suzuki trials with unprotected amine showed no product formation.

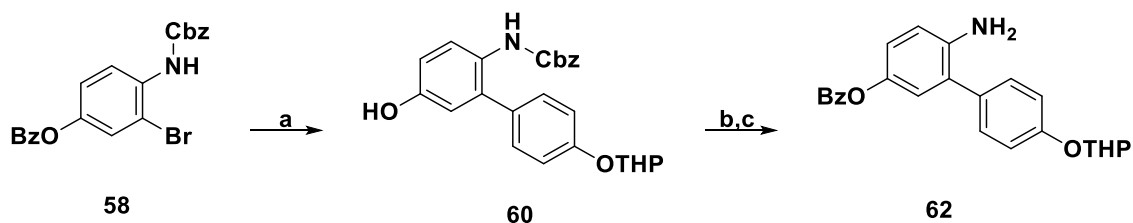
It was assumed that the reactivity of bromine is reduced compared to iodine for the Suzuki coupling. However, this could have resulted in prolonged reaction times, but less likely in no product formation after days of reaction monitoring. The reaction with benzyl chloroformate in pyridine **c** was obtained in 87% yield.

Blaise et al. ^[147] reported the successful regioselective Suzuki coupling on very electrophilic chloropyridazines with different solvents under microwave irradiation. Furthermore, other research groups reported that dimethoxyethane had a reductive effect on palladium.^{[148][149]} In view of this, the Suzuki coupling was tested under slightly different conditions under microwave irradiation and we were able to obtain our biaryl products in yields of 70 - 90 % with reaction times of 10 min. Furthermore, the reactions were also successful under reflux, by increasing the reaction times to eight hours. (Scheme 5.23).



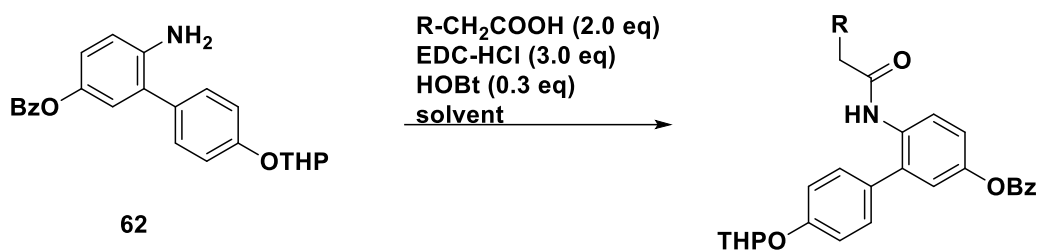
Scheme 5.23 Synthesis of biaryl structure **60** in Suzuki coupling. a) Pd(PPh₃)₄ (5 mol%), Na₂CO₃ (2.0 eq), DME/H₂O, 110 °C, 10 min, $\mu\text{w}/\Delta\text{T}$, 8h.

Due to the basic conditions of the Suzuki coupling the benzoate group was partially saponicated. Therefore, reprotection was required. In summary, the biphenyl core can be synthesized in three steps of which two are PG insertion and removal. In the first step **a** conversion with tetrahydropyran aryl boronic acid *via* Suzuki coupling to the biphenyl products was performed in a total yield of 90 %. In the second step **b**, the obtained hydrolysed biphenyl products were reacted with 2-fold excess of benzoic acid in a Steglich esterification. EDC·HCl was used because of its water soluble by-products in the workup process.^[150] The benzyl alcohol protected ester was obtained in 83% yield. In the final step **c**, the carbamate protecting group was removed in a hydrogenation reaction in 94% yield. Overall, a total yield of 82% was obtained in the synthesis of biphenyl **62** (Scheme 5.24).



Scheme 5.24 Synthesis toward biphenyl amine a) R-B(OH)_2 , $\text{Pd(PPh}_3)_4$, (5 mol%), Na_2CO_3 , $\text{DME/H}_2\text{O}$; b) $\text{EDC}\cdot\text{HCl}$ (1.1 eq), DMAP (0.1 eq), DCM ; c) Pd/C , H_2 , EtOH/EtOAc .

The ligands previously described in terms of *in silico* studies were synthesized via amide coupling. In the general Scheme 5.25, derivatisation of the ligands with different commercially available acids was obtained with some slight variations on the solvent system and the equivalents of the activation agents. The acid derivatisation is shown in Table 5.4.



Scheme 5.25 Synthesis by amide bond formation; entry 1-7, Table 5.4.

In entry 1, biphenyl amine **62** and 3,5-dimethoxyphenylacetic acid were reacted in toluene as a solvent with a higher boiling point than dichloromethane to shorten the reaction time compared to dichloromethane and chloroform. Here, the reaction was refluxed for 6 h and stirred at room temperature for an additional 12 h and the product **63** was obtained in 85% yield. The reaction with 2,5-dimethoxyphenylacetic acid in entry 2 was performed under reflux for a total of 24 h and the product **64** was obtained in 76% yield. In entry 3, reaction with 2-methylphenoxy acetic acid in chloroform the product was obtained after 22 h in 80% yield. The same reaction in DMF led to the deprotection of the THP protected phenol. With 1-thymine acetic acid, entry 4, reaction gave no conversion after two days under reflux in toluene. In another attempt with DMF, the reaction was performed at 160 °C for 6 h until no more starting material was observed. Mass analysis confirmed the reactants and the products in which the protecting groups were completely or partially cleaved. The reason could be the excess of acid and high temperature, which is beneficial for tetrahydropyran removal, however, the benzoate group is usually removed under basic conditions, but under high temperature and low pH it could be more labile. Therefore, the yield of final ligand **67** was only 30% after column chromatography followed by HPLC, but it was sufficient for subsequent biophysical studies. Further synthesis with nucleic-

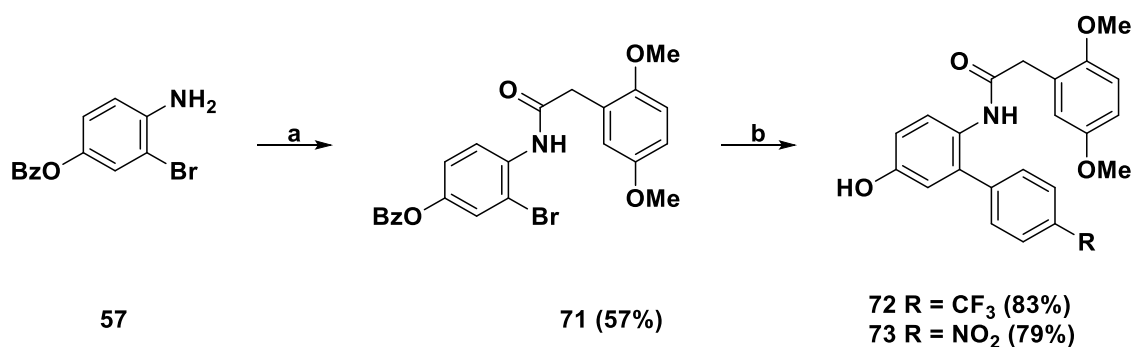
acid-like structures should be done under less acidic conditions, more monitoring and temperature-controlled conditions. In reaction with aliphatic acids, entry 5, 6 and 7, reactions were performed in chloroform and resulted in high yields for isobutyric acid, entry 6, and isovaleric acid 5; however, with much longer reaction times compared to the aromatic acids. Reaction with methoxyacetic acid (entry 7) in DMF resulted in complete cleavage of the protecting groups, and compound **70** was obtained in 50% yield, while partial cleaving of benzoate group was obtained in 30% yield.

Table 5.4 Acid derivatisation via amide bond formation. (Entries 2, 3, 5, and 6 were made by R. Keller during his bachelor thesis).^[151]

Entry	1	2	3	4	5	6	7
Acid (R)							
Solvent system	toluene	toluene	CHCl ₃	DMF	CHCl ₃	CHCl ₃	DMF
Time	18 h	27h	12h	72h	36h	40h	12h
Yield	85%	76%	80%	30%	93%	83%	50%
Product	63	64	65	67	68	69	70

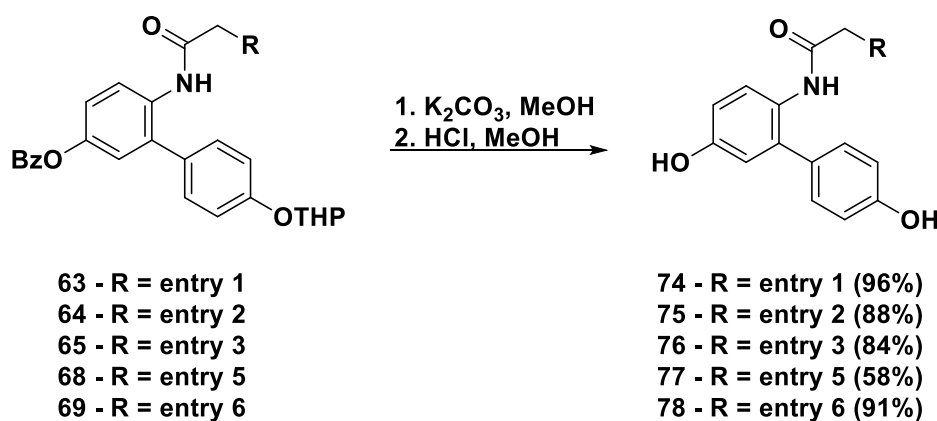
In the synthesis of lead structures with variation on the biphenyl unit, amide bond reaction was performed prior to Suzuki coupling (Scheme 5.26).

Starting from ligand **57** the amide bond reaction succeeded under conditions similar to those discussed above. A slightly reduced yield of 57% was observed with 2,5-dimethoxyphenylacetic acid, as can be seen from Scheme 5.26. Here, the order of reactions has been changed, and in *o*- position we have weakly deactivating bromine, which might reduce the reactivity of **57**. In the second step **b**, Suzuki coupling was performed under the conditions described above. Here, the amount of acid was reduced to 1.1 eq in order to reduce unreacted boronic acid and to ease the workup process.



Scheme 5.26 Synthesis of **72** and **73**: a) 2,5-dimethoxyphenyl acetic acid (2.0 eq), EDC-HCl (3.0 eq), HOBT (0.3 eq), CHCl₃; b) R-B(OH)₂ (1.1 eq), Pd(PPh₃)₄ (5 mol%), Na₂CO₃ (2.0 eq), DME/H₂O.

The final steps of the ligand synthesis required removal of protected groups. As shown in the following scheme in the first step, the benzoate group was removed under basic conditions using potassium carbonate in methanol and the reactions were terminated after 3 h at room temperature. In case of insoluble reactants, it was heated to 60 °C.



Scheme 5.27 Final synthesis steps toward the ligands.

In the next step, the acidic removal of the tetrahydropyran ether under acidic conditions with 1 mM aq. hydrochloric acid was also straight forward and the reactions were quantitative. The reaction order was switched for the ligands **77** and **75**, however the reason for the lower yield might be use of too high concentrated hydrochloric acid (6 M) which resulted in 20% of hydrolysed amide. The Figure 5.21 shows the synthesized library of ligands from lead structure A.

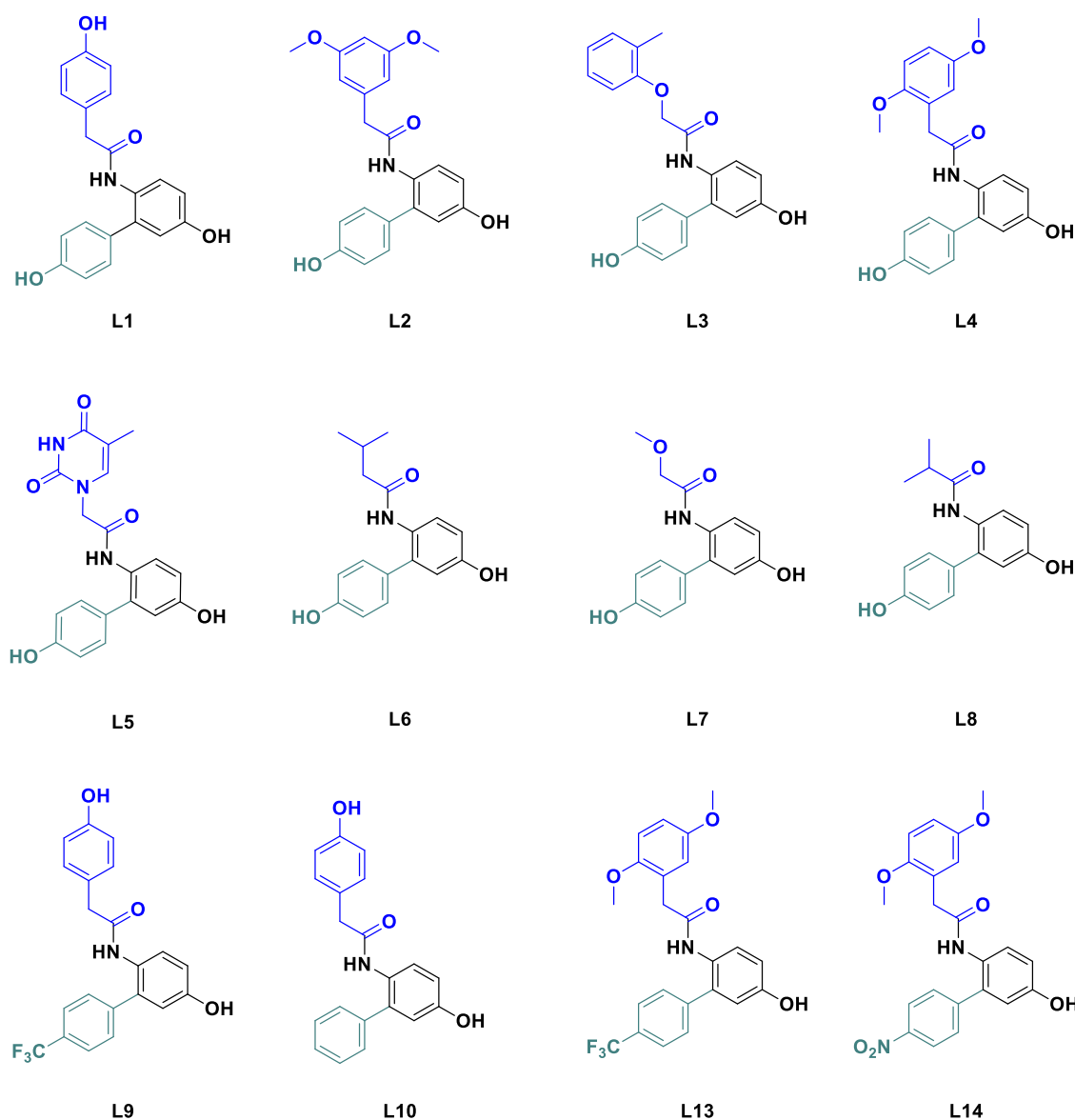


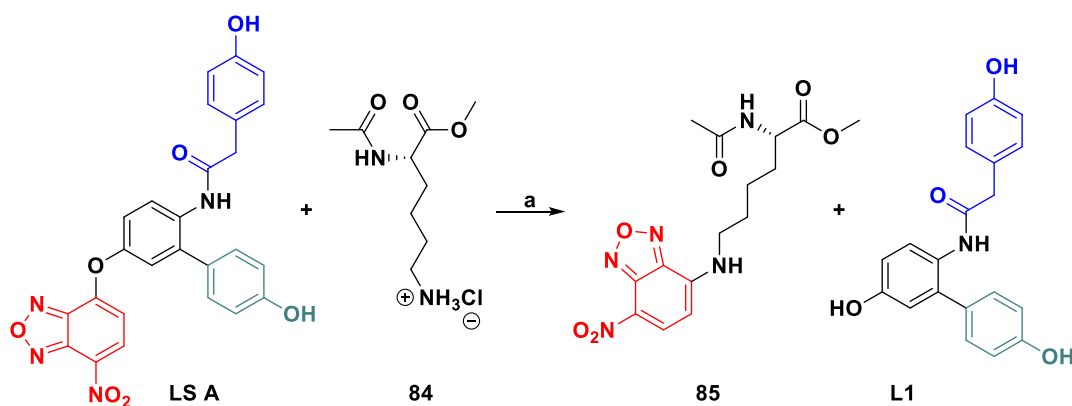
Figure 5.21 Ligands library of the lead structure A.

Different approaches toward the lead structures using a modular synthesis strategy were shown in the previous sections. In the early stages of the synthetic approach to lead structure A, problems with the formation of the C-C bond arose. The attempts by Negishi and Suzuki coupling reactions did not result in the desired biphenyl structure. One of the problems was the reproducibility of the Grignard formation. Furthermore, the bulky silyl protecting groups hindered the reaction. We changed the strategy to protect functional groups using the benzyl protecting group, yet it was not the ideal group due to the further reduction reactions. To overcome that problem the benzoate and tetrahydropyranyl ether protecting groups were used for hydroxyl protection.

The early synthesis towards lead structure B was hampered by unsuccessful formation of the secondary amine positioned *ortho* to sp²-sp² carbon bond of the biaryl. With an improved synthetic approach towards lead structure A more modularity was introduced, which paved the way for an easier library synthesis and enlargement. The synthesized ligands have diverse functional groups with electron donating and withdrawing character, which influenced the synthesis of the ligand and is differently reflected the synthesis reaction time and the overall yield. Furthermore, fine-tuning and synthesis optimization was not the only goal of this thesis, and as the synthesis was revised along the way, more attention could be paid to its improvement in the later stage upon confirmation of the protein-ligand interactions.

5.2.6 Proof of concept - NBD transfer reaction

As mentioned earlier, the goal of the fluorophore moiety was to label the protein on the lysine residue in the proximity of the cavity of interest. With the improved synthesis A ligand **LS A** was obtained and tested in a model system shown in Scheme 5.28.



Scheme 5.28 Proof of concept reaction, mediating fluorescence on the lysine residue in a model system; a) DIPEA (5.0 eq), DMSO, 25 °C, 2h.

The main advantage of this process is that the *O*-NBD moiety does not exhibit fluorescence but upon binding to the lysine residue fluorescence emission is observed, as described earlier in Section 5.1.

In the model system, reaction of the nucleophilic lysine with the *O*-NBD moiety gives compound **85** after 2 h reaction time at 25 °C while **L1** is simultaneously released. This reaction was monitored by HPLC, Figure 5.22. Compound **85**, at 450 nm, is observed with a retention time (t_R) of 18.5 min, while **L1** was confirmed at 14.5 min and 280 nm. **LS A** has (t_R) of 24.5 min, and it is visible that there is no absorbance at 450 nm.

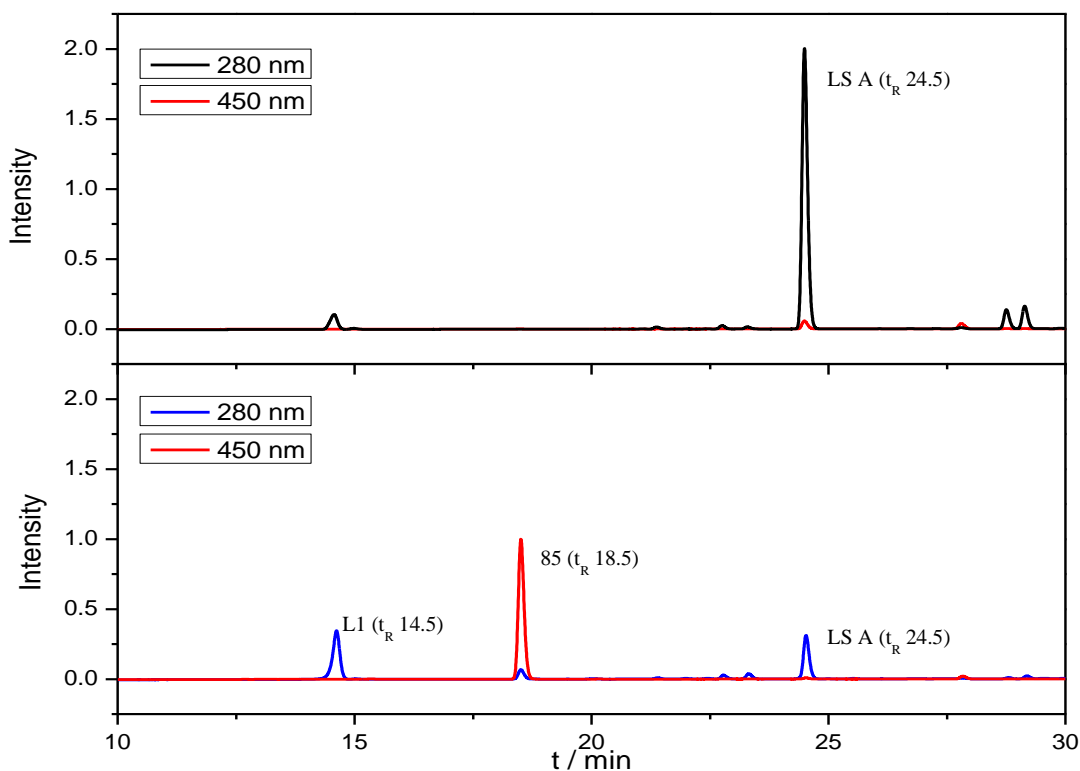


Figure 5.22 HPLC chromatograms of LS A (100 μM) with 85 (100 μM) in DMSO, as a proof of concept reaction after 2h incubation at 25 $^{\circ}\text{C}$, (analytical C-18; 20 \rightarrow 100% MeCN in 35 min); full chromatogram (see Figure 9.15).

The general proof of concept was successful. The reaction monitoring showed product formation after 2 h at 25 $^{\circ}\text{C}$, for which, analytical C-18 column with a gradient of 20% to 100% MeCN in 35 min was used. With the model system, we confirmed that the basic principle of fluorogenic labelling should work, and further fluorescence studies on SOD1 proteins should be conducted. However, it would be beneficial first to confirm the affinity of the ligand to the cavity of interest.

5.3 Biophysical and Protein studies

Protein studies and biophysical investigation were performed in close collaboration with Lisa-Marie Funk in the group of Prof. Dr. Kai Tittmann.

5.3.1 Expression and purification of the hSOD1 proteins

In the present work, the expression and purification protocol from the group of Prof. Hasnain were optimized to obtain a respectable amount of the active protein, hSOD1 wt and the A4V variant. The pET303C-hSOD1wt plasmid was expressed in *E. coli* BL21 Star™ (DE3) controlled by IPTG induced T7 expression. For the analysis of the expression, samples were taken hourly, and cell growth was followed by optical density at wavelength of 600 nm, (Figure 9.1). The cells were harvested after 20 h of incubation, see Figure 5.23 and yielded in ~32 g cells from 6 L culture, which is 5.28 g/L.

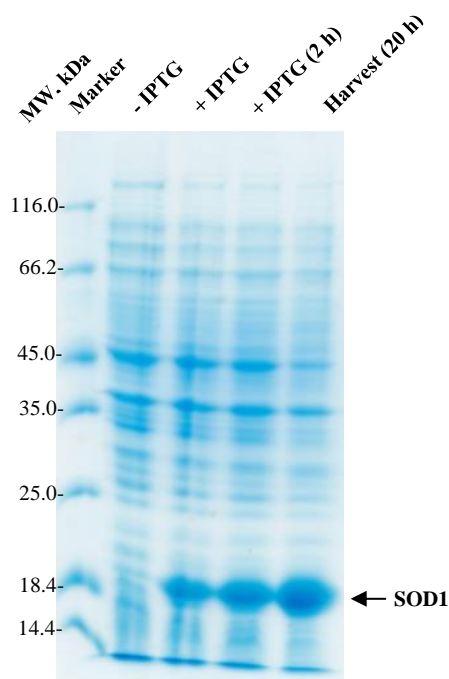


Figure 5.23 Expression of the hSOD1wt protein from the pET303C-hSOD1wt plasmid (SDS-PAGE, 15%). -/+ IPTG: before and after induction with 0.4 mM IPTG, respectively.

Subsequently, the cell pellets were disrupted and purified as described in Section 7.2.2.2. For purification fractions samples were taken and analysed on a 15% SDS-gel (Figure 5.24). It can be seen that a considerable amount of the hSOD1 protein is in the

supernatant, whereas the loss of the insoluble protein in the pellet is very small. Furthermore, it can be observed that the largest amount of the purified protein is obtained in the elution step with a high purity.

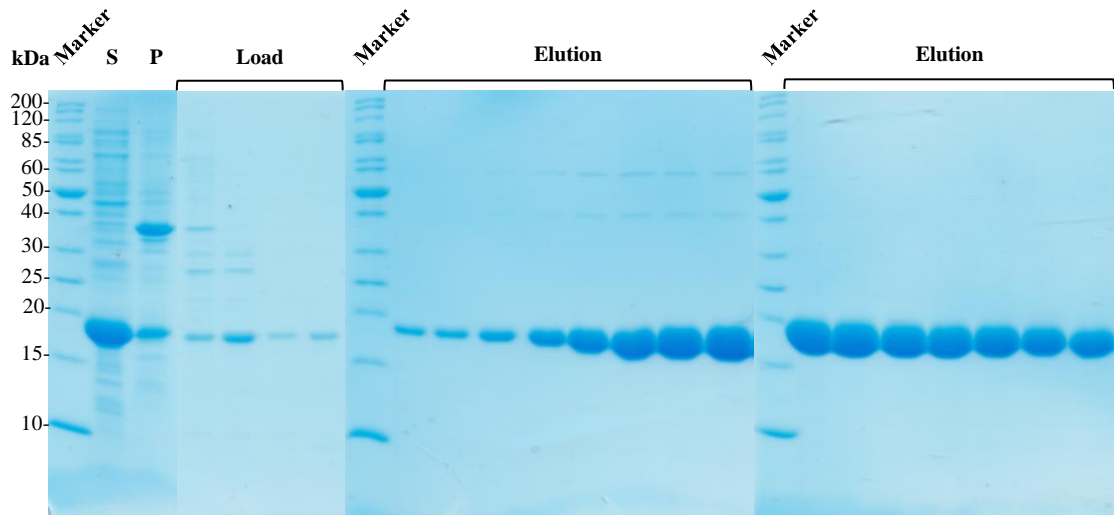


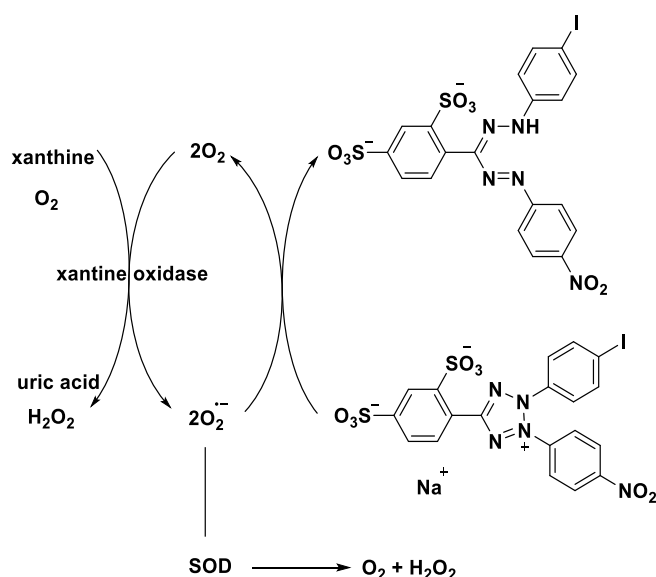
Figure 5.24 Purification of the hSOD1wt (SDS-PAGE 15%). S and P: supernatant and pellet fractions after cell disruption. Load, Elution: fractions of the TMAE chromatography.

From gel electrophoresis, it can be observed that the amount of protein in the loading step is considerably small. In the early elution steps, slight impurities with a molecular weight of 40 and 60 kDa can be observed; however, at this point such impurities were negligible, especially, as most of the protein eluted in the later steps was pure. The protein was purified yielding ~60 mg protein per 1 g cell pellet. Following reconstitution of the cofactors (Cu and Zn), as explained in Section 7.2.2.5, fully reconstituted protein was obtained with a homogeneity yielding 17-20 mg hSOD1 wt protein per 1 g cells.

The expression and purification of the hSOD1A4V variant was performed similar to the wildtype protein. We confirmed the instability of the variant before the cofactor exchange, which led to a higher aggregation and, additionally, to a 15% lower yield of the purified variant in comparison to the hSOD1 wt. One of the reasons might be a reduced affinity for Zn, which is shown in A4V to be almost 30-fold decreased compared to the wt protein.^[152] Compared to previous research throughout the years, the expression of the protein in different systems and the purification protocol have changed and were required to be adapted, but the expression and purification yield of the SOD1 proteins is still comparable.^{[153][154]} Recently, the group showed periplasmic expression of SOD1 proteins and purification with HIC which resulted also in 16 - 23 mg/L culture.^[155]

5.3.2 Activity analysis of hSOD1wt and A4V proteins

The activity analysis of the purified proteins was carried out according to Section 7.2.2.6, in which the activity of the protein was determined by inhibition of the reduction reaction, which was measured spectrophotometrically by absorbance depletion of the WST-1 dye.^[156] The principle of the assay is based on an indirect measurement of the SOD1 activity. As shown in Scheme 5.29, xanthine and xanthine oxidase generate superoxide radicals, which are oxidized upon reaction with 2-(4-iodophenyl)-3-(4-nitrophenyl)-5-(2,4-disulfophenyl)-2H-tetrazolium monosodium salt, also known as water soluble tetrazolium salt (WST-1), producing WST-1 formazan as yellow dye. The SOD1 activity is measured by the inhibition of the reduction reaction, where absorbance depletion of the WST-1 formazan dye is determined spectrophotometrically at 440 nm.^[157]



Scheme 5.29 Schematic view of the activity assay

We confirmed the activity of the fully reconstituted protein, as well as the reduced activity of the protein with only zinc as a cofactor, which was comparable to the control of bovine SOD1, Figure 5.25. Although impaired activity of hSOD1 in zinc deficient cells was observed by 50%, it was confirmed that only a 10-fold higher zinc concentration compared to the copper concentration is required to achieve a specific activity.^[158] Yet, it was shown much earlier with the bovine SOD1 that stoichiometric zinc increases the possibility of folding and has an effect on the structure, while copper is essential for the activity of the protein.^{[45][159]}

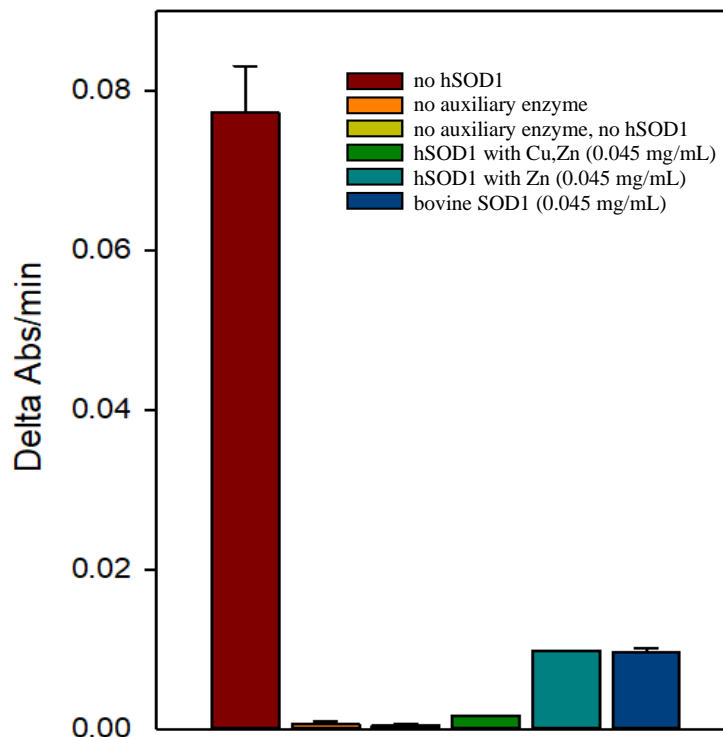


Figure 5.25 Activity assay of hSOD1 wt protein with both cofactors (Cu, Zn), and Zn only.

We have also investigated the influence of DMSO on the activity of the hSOD1 proteins as one of the important co-solvents used to increase the solubility of small molecules and drugs for hydrophobic macromolecules.

From the results obtained and shown in Figure 5.26 a reduced reaction inhibition was confirmed, which indicates a lower activity for both, apo and holo wt proteins with 20% DMSO in 50 mM sodium phosphate (SP) buffer. The reaction inhibition was reduced by almost 50% as compared to the activity obtained without co-solvent, which is shown in blue on the left. The decrease in the activity of the apo proteins compared to the holo under the same conditions was less than 10%. The activity of the A4V apo and holo protein was similar in buffer and with 20% DMSO. However, the lower activity of the A4V apo variant compared to the holo is more pronounced; approximately 40% of the activity was lost under the same conditions (shown in red on the right side of Figure 5.26). When comparing the A4V variant and the wt protein in buffer, the activity of the holo and apo variants is 30 to 40% less than for the wt proteins, respectively. However, this effect is different in DMSO; the activity of holo A4V is approximately 18% less compared to holo wt, while the apo A4V variant kept its activity decrease compared to the wt holo protein of around 40%. Furthermore, it must be stated that the concentration of the variants is 10-fold higher, as indicated in the diagram, however this was necessary,

because the activity of the A4V variant at a concentration of 0.02 $\mu\text{g/mL}$ was so low that the standard error deviation was higher than the signal (data not shown).

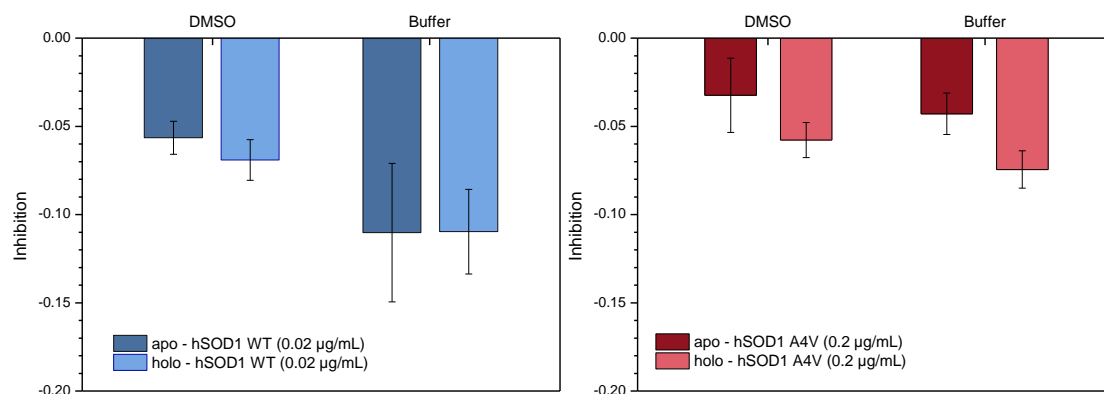


Figure 5.26 Activity of the hSOD1 proteins shown as reaction inhibition in 50 mM sodium phosphate buffer, pH 7.4 with 20% DMSO, and buffer with 0% DMSO. Left: hSOD1 wt holo and apo proteins with 0.02 $\mu\text{g/mL}$ concentration; Right: hSOD1 A4V holo and apo proteins at a concentration of 0.2 $\mu\text{g/mL}$ (experiments performed with *F. Otto*)

The data confirmed a higher DMSO influence on the activity of the wt protein, yet this effect was less pronounced in the mutant. Moreover, it was still acceptable to use DMSO for the ligand solubility, since the wt activity, with its higher 10-fold concentration, was only impaired to a range of the mutant's normal activity. Furthermore, we have confirmed the influence of DMSO on the protein stability in different buffers. In experiments with proteins in 100 mM hepes buffer, 150 mM NaCl, pH 7.4 as well as with aforementioned 50 mM sodium phosphate buffer without DMSO, there was no significant difference (data not shown), whereas for the wt and A4V proteins with DMSO, impairment observed in sodium phosphate (SP) buffer was approximately only 5 to 10%, respectively (Figure 5.27).

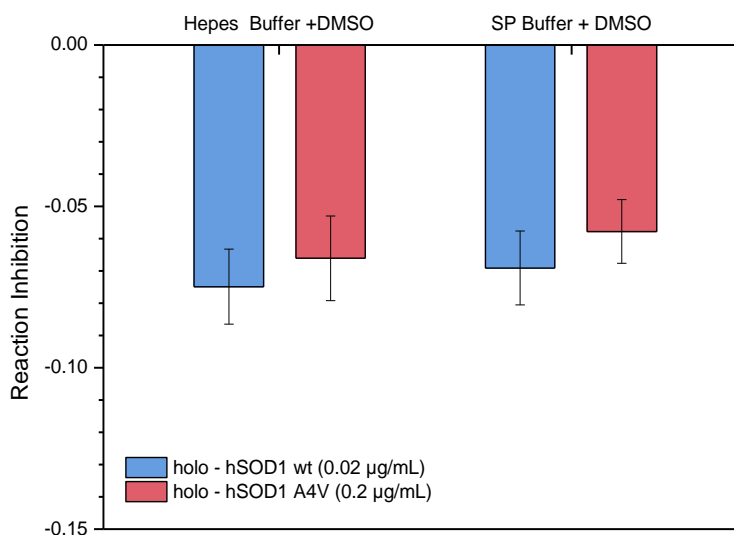


Figure 5.27 Activity of the hSOD1 proteins shown as reaction inhibition with 20% DMSO in 100 mM hepes buffer, 150 mM NaCl, pH 7.4 and 50 mM sodium phosphate (SP) buffer, pH 7.4

The influence of DMSO on the enzymatic activity of the hSOD1 proteins was rather negligible when the concentration was taken into account. Besides, it is known that decreased enzymatic activity of the SOD1 proteins is not a direct cause for ALS but can alter the disease.^[6] Moreover it is also reported that the influence of DMSO on enzymatic activity does not always correlate with the binding affinity and protein misfolding. Even amounts less than 5% lead to a change in the stability and unfolding in bacterial NAD⁺ synthetase.^[160] There is not much literature reported on the influence of DMSO on SOD1 proteins, which is usually used as a co-solvent in various *in vitro* experiments. However, the efficiency of polyphenol, resveratrol, dissolved in 25% DMSO was tested onto mutated mice intraperitoneal, to see the effect on motor neuron loss, and no negative effect on DMSO concentration was reported.^[161] However, in the native-MS experiment, it was shown that a low percentage of 0 to 1% DMSO can stabilize the SOD1 apo proteins, while with higher concentration the effect is destructive.^[162] Overall, the effect of DMSO on the SOD1 proteins should be considered individually according to the experiments conducted.

Initially, multiangle light scattering (MALS) experiment was performed for hSOD1 protein size confirmation, and a tight dimer (~28 kDa) was confirmed, Figure 5.28.

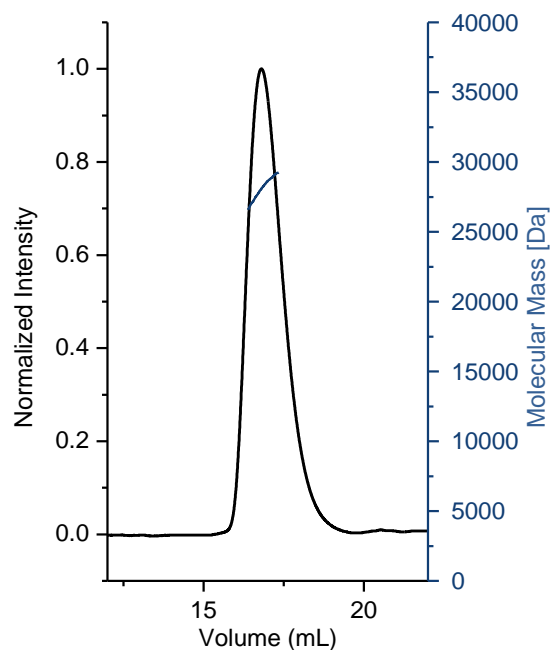


Figure 5.28 Confirmation of hSOD1wt protein by MALS experiment

Afterwards, prior to binding studies, proteins were also analysed by size exclusion chromatography (SEC), as explained in Section 7.2.2.7. It was also in agreement with initial MALS data, as shown in Figure 5.29.

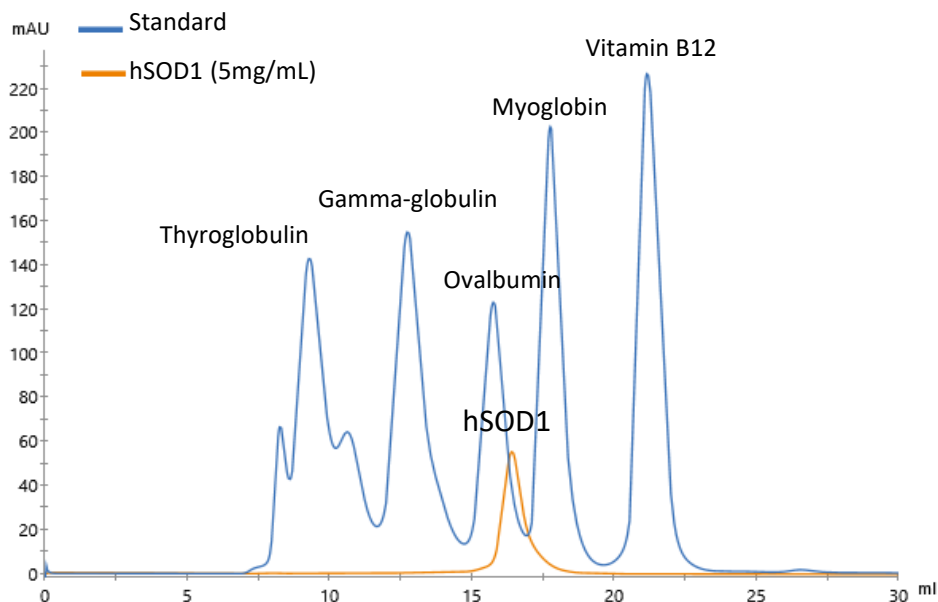


Figure 5.29 Size exclusion chromatography: hSOD1 wt 5 mg/mL (orange), Biorad-Standard (blue)

We confirmed an impaired stability of the A4V variant and its high propensity for aggregation compared to the wt protein. We could also observe a higher instability of the

A4V apo protein at lower concentrations and after 48 h incubation at 37 °C. Furthermore, the A4V apo monomer-dimer equilibrium was not distinguishable as the protein aggregated towards a 100 kDa species Figure 5.30 (bottom). This was consistent with literature data on the A4V aggregation potential and the wt stability.^[52,69]

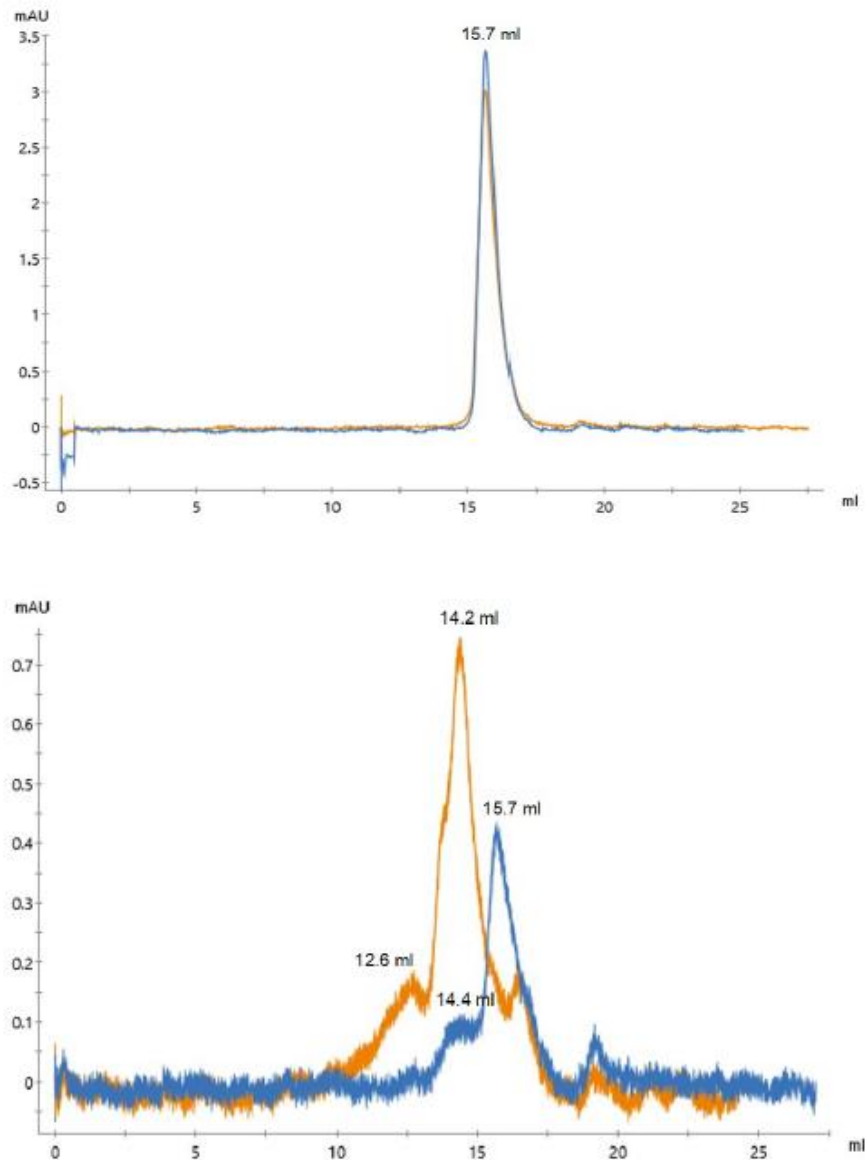


Figure 5.30 SEC studies after 48 h incubation at 37 °C. *Top:* hSOD1 wt; *Bottom:* hSOD1 A4V; holo and apo proteins showed in blue and orange, respectively. (Experiments performed with F. Otto during her bachelor thesis)

5.4 Binding affinity assays and aggregation studies

Determination of the binding affinity is a very important approach in drug design and development. It indicates an interaction between the identified hit molecules and the protein. To ensure a better understanding of the ligand-protein interaction and its characteristics, and to confirm whether there are any interactions at all, the binding affinity of ligands was measured. Therefore, different approaches were examined and developed to answer questions about the ligand affinity and the aggregation processes with hSOD1 proteins.

5.4.1 Microscale Thermophoresis (MST)

As described in Section 4.3, an MST assay was used to confirm the interaction of synthesized ligands with the hSOD1 protein. In various publications, binding studies of the reported compounds with hSOD1 proteins were omitted, whereas they obtained crystal structures with the compounds.^{[56][69]} Recently, Manjula and Sruthi showed ligand interactions with the hSOD1 Trp32 site using MST.^[86] In our approach, we wanted to confirm the interactions of the ligands we have designed with the hSOD1 protein, and continue with structural investigations. Initial experiments involved labelling of the protein with different fluorophores that are suitable for the channel set-up of the instrument. The early tests were performed on a label-free instrument, in which fluorescence was detected intrinsically from the tryptophan amino acids of hSOD1. This approach was dismissed, because of the interfering autofluorescence of the ligands. For the measurements on the instrument with pico-red channel, Atto647N dye was initially tried due to the strong absorption, the high fluorescence efficiency and the photostability.^[163] The protein was preferably labelled on a lysine residue via an NHS ester instead of a cysteine residue via maleimide. The latter is not an option because the available cysteine residues (Cys111) are at the dimer interface and the dye attachment could also induce protein misfolding, and aggregation, which was also confirmed in our MST experiment (Figure 9.8). Furthermore, it was not applicable in a parallel project in the group that is focused on Cav(C111). Ultimately, labelling the lysine residues was a lower risk, as hSOD1 has in total twenty-two lysine residues, eleven per monomer, and the possibility to attach the dye on both lysine residues in our cavity of interest was only ~10%.

Experiments with Atto647 cysteine labelled hSOD1 showed strong aggregation of the target, as expected, even in the absence of the ligands. In this case, an MST optimized buffer was used (50 mM Tris-HCl pH 7.4, 150 mM NaCl, 10 mM MgCl₂, 0.05% Tween-20). Additional optimization by adjusting the buffer conditions and the detergent concentrations did not help with the aggregation problems. Ligands were tested in the same setup to determine the influence and behaviour with the protein. However, aggregates were detected in most of the capillaries (Figure 9.8). Labelling with Atto647N *via* an NHS ester on a lysine residue prevented immediate aggregation of the target protein, which confirmed the hypothesis with the cysteine residues. However, some difficulties were still obtained, such as the low fluorescence intensity of the target, and reduced but still significant aggregation. Furthermore, ligands showed autofluorescence. Attempting to make use of the ligand autofluorescence and titrate the protein instead of the ligand was not an option, as the fluorescence intensity of the ligands was too low for a valid assay.

An increase in the concentration of one of the fluorescent targets was limited by the low solubility of the ligands in aqueous buffer. In the case of an increase in the target protein concentration, it was required to enhance the ligand concentration as well, since otherwise, the binding curve would not reach saturation. Even with the highest possible concentration of DMSO that the protein could tolerate (25%), ligand concentration was not sufficient to achieve high fluorescence intensity. Therefore, the labelling strategy was changed and a labelling kit with a red NHS ester dye was used by applying a slightly modified protocol as described in Section 7.2.4.2. Then the influence of the dye on the misfolding and aggregation of the labelled protein by separating the monomer and dimer using size exclusion chromatography was excluded (Section 7.2.2.7). In addition, we confirmed that the enzymatic activity was not reduced, (Figure 9.6). The next steps in assay development included validation of the labelled protein, its adequate fluorescence, stability, and buffer optimization. In Figure 5.31, a difference in fluorescence intensity can be observed for each individual labelled protein batch at the same or different concentrations. Batch 3, with a concentration of 5 nM was comparable to batch 2 with the same MST power. Here, the fluorescence was consistent, except the largest discrepancy for batch 1, as shown in green. To avoid such effects, a minimum of three independent measurements was conducted for each binding experiment.

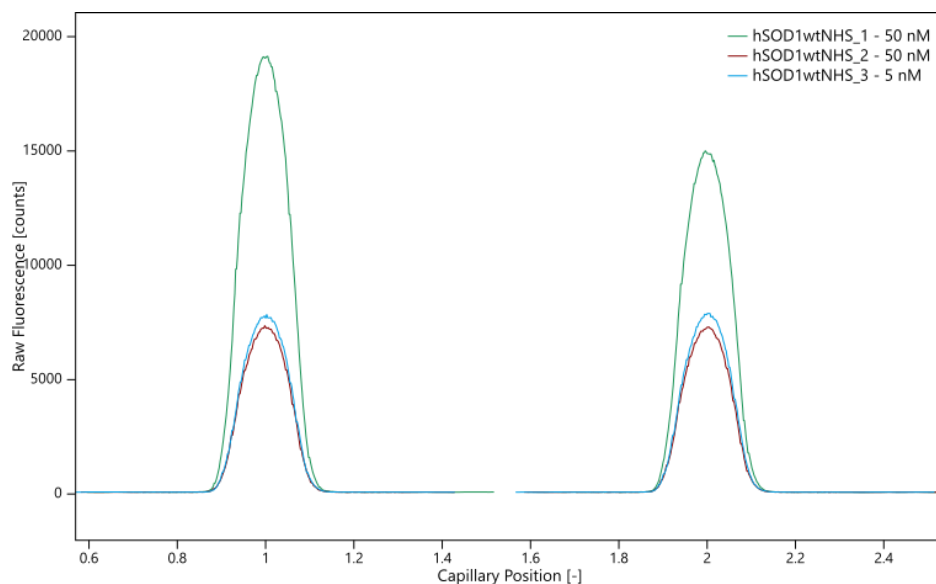


Figure 5.31 Raw fluorescence signal from different batches of hSOD1wt protein labelled with red NHS ester labelling kit.

Another point in assay development was to confirm and exclude protein aggregation. As can be seen from the thermophoretic trace of the labelled protein, no aggregation was observed (Figure 5.32).

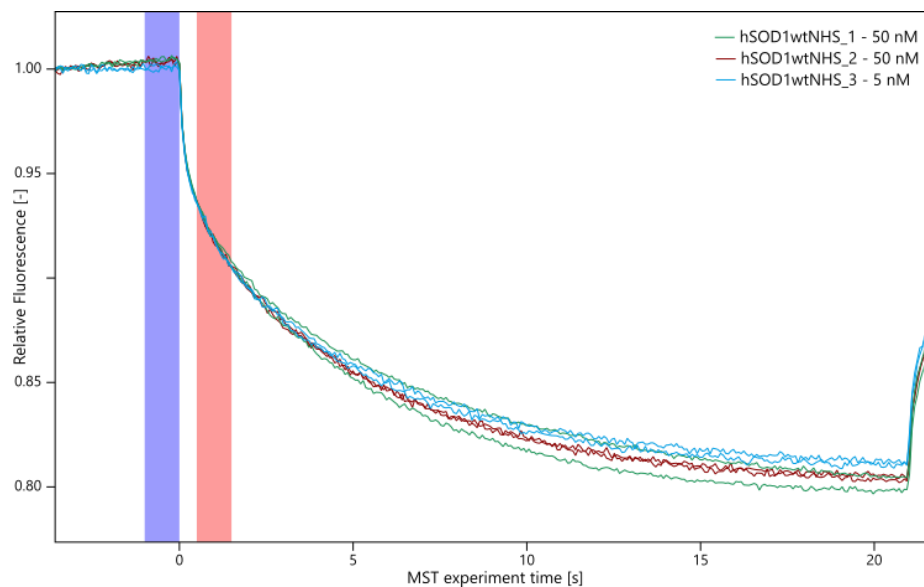


Figure 5.32 Thermophoretic traces of NHS ester labelled hSODwt protein batches.

Buffers also play a crucial role in biophysical studies^{[164][165]}, and can influence the stability and assay performance. In view of the stability of the hSOD1 protein in the cellular and cytosolic environment, different buffers were tested for *in vitro* assays and some of them were excluded. As previously shown, SOD1 proteins were active in both, the HEPES and sodium phosphate buffers, the latter one being used for the MST binding assays, as it performed well in the initial screening phase with the ligand.

The initial testing of the assay was approached with a single test screening in which only the highest concentration of ligands was titrated with a labelled protein, incubated for 15 to 30 min, and measured. However, this method was not reliable as many possible ligands were omitted, mostly because their highest concentration was not sufficient to reach saturation. When full titration experiments were carried out, usually sixteen concentrations were measured. Best to our knowledge, a validation of the assay with a reference standard was not possible because not many binding assay studies were performed with hSOD1 proteins. Lately, some groups have reported that small molecules affect the oxidative effects on the SOD1 proteins^{[166][86]}, but there was no accessible standard available for testing.

Our MST binding studies were largely established with ligand L1. At the beginning, we tested different incubation times, to confirm the optimal equilibrium time, shown in Figure 5.33. Here, the L1 with 10% DMSO in concentration ranged from 6.69 mM to 0.204 μ M while the concentration of the labelled protein target was kept constant at 5 nM.

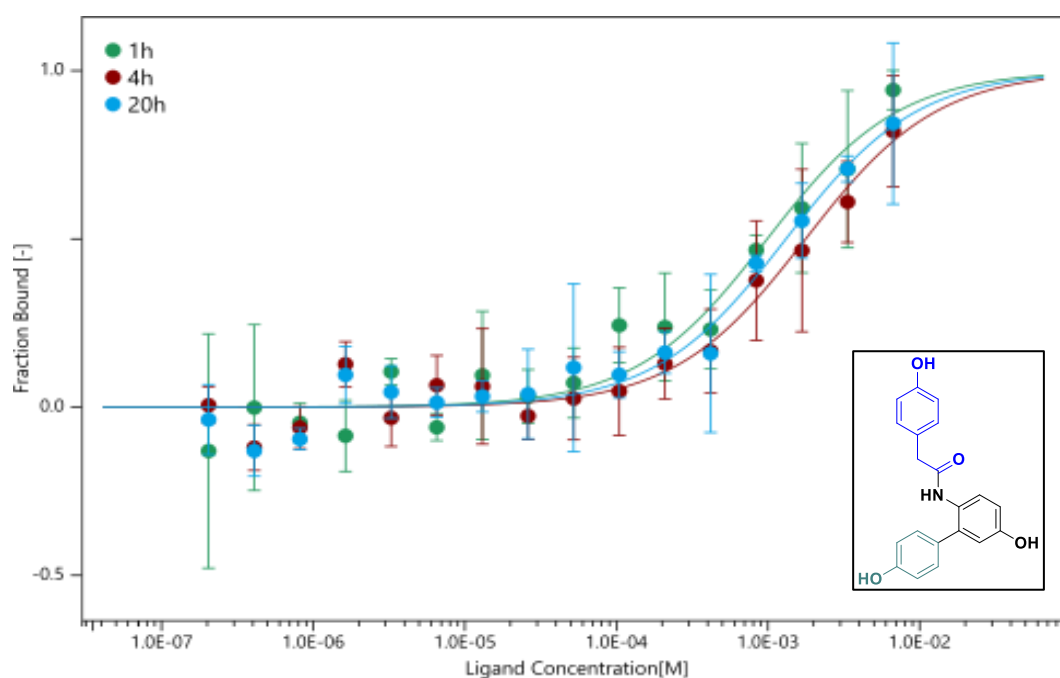


Figure 5.33 MST binding affinity data of ligand L1. Development of the assay through incubation time screening with the ligand and the protein.

The difference in the obtained K_d values was mostly in the range of the error, 0.988 mM \pm 0.349 mM for 1 h incubation time (green), 1.77 mM \pm 0.589 mM for 4 h (red) and 1.31 mM \pm 0.400 mM for 20 h incubation time (blue). However, the best K_d value with an incubation time of 1 h had the lowest signal-to-noise (S/N) ratio of 12.93 compared to 17.08 and 16.51 for the incubation at 4 h and 20 h, respectively. Moreover, a similar range of S/N ratio was observed in the analysis with different MST-on time (up to 5 s). In our

analyses the MST-on time was kept at 1.5s to minimize the effect of a possible structural destabilization on the K_d values, (Figure 9.9). Therefore, it was concluded that the incubation time can range from 1h and 4h, and, in itself, is likely not to be a crucial parameter for the ligand binding affinity in the concentration range used. The error discrepancy between the individual replicates was still high, with the high DMSO concentration and the low ligand concentration being the most likely reasons. Unfortunately, the requirement of DMSO was the main issue in the assay due to the low solubility of the ligands without DMSO. A DMSO tolerance test was performed with the hSOD1 proteins and we observed a slightly impaired protein activity as shown earlier in Section 5.3.2. Even with DMSO, the hSOD1 wt was even more active compared to the variant. Quality tests and the influence of DMSO against the labelled protein target were done to exclude negative effects, i.e. fluorescence, adsorption, aggregation and photobleaching. The thermophoretic effect was observed in the titration experiment with 0% to 20% DMSO, where we were able to confirm the importance of a constant concentration across the capillaries during the binding affinity measurements. When the concentration in our binding assay was kept constant, there was no DMSO influence on the binding affinity in comparison to the negative control measurements of DMSO and protein. (Figure 5.34).

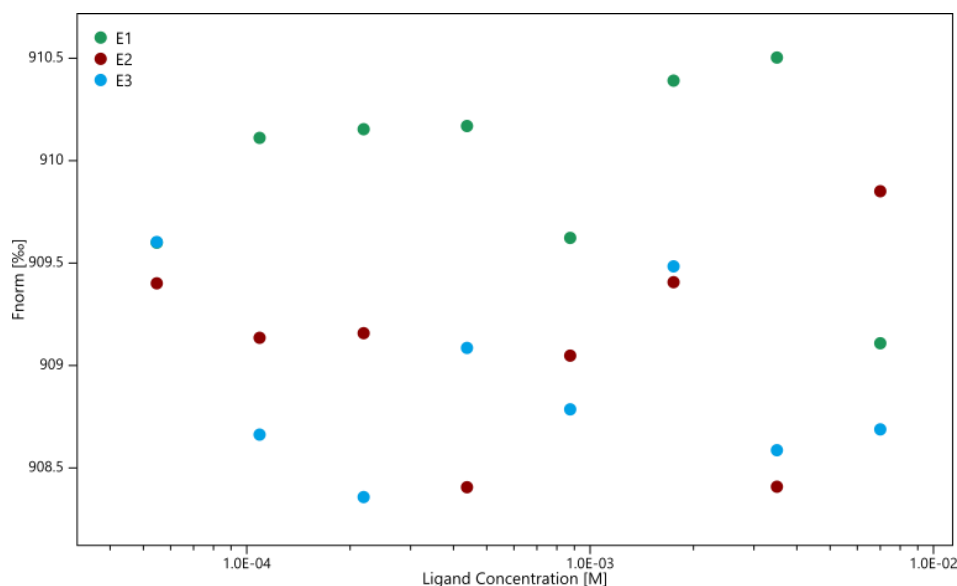


Figure 5.34 MST experiment without a ligand as a control measurement. Experiments performed in triplicates (E1-E3), titrated as 1:1 serial dilution with constant DMSO concentration (20%) in 50 mM sodium phosphate buffer and labelled hSOD1wt protein.

On the one hand, DMSO did not have a detrimental effect on protein functionality and stability, and it was acceptable to use it for the benefit of the ligand solubility in the MST

assay. However, an influence on the fluorescence was observed, thus affecting the data quality, the discrepancy between individual replicates, which led to a high error and a large range of K_d confidence.

In the literature, the influence of DMSO on a non-covalent protein ligand complex was reported, pointing to an increase of the K_d value of about an order of magnitude, which masked the real binding affinity of the complex.^[167] Other studies suggested the effect of DMSO on the stability of the protein and apparent binding, yet with a contrasting effect upon concentration adjustment.^{[168][169][170]} Recently, Zhao *et al.* showed the effect of aprotic solvents on the hSOD1 apo protein by native electrospray ionization–ion mobility–mass spectrometry (ESI-IM-MS). There, the influence of DMSO and DMF on the stabilization, unfolding and dissociation of apo SOD1 depends strongly on the percentage concentration of the added solvents. Up to 1% of the results indicate an increase in the apo SOD1 stability, while from 1 - 20% the effect is opposite.^[162] This effect of DMSO was not confirmed in our MST assay, as the labelled protein was holo, which is structurally already more stable than apo protein.

Furthermore, the binding affinity analysis of the synthesized ligands was assessed with the MST. However, to overcome the solubility problem, the DMSO percentage concentration had to be increased. As already discussed, it did not have a big impact on the protein stability, but rather on the data quality. For consistent analysis and comparison of the ligands, the reference ligand L1 was tested with 20% DMSO concentration. From the binding affinity curves of the ligand L1 with 10 and 20% DMSO shown in Figure 5.35, we were not able to see any significant difference in the binding affinity. The ligand concentration for the dilution series of L1 with 20% DMSO ranged from 7.00 mM to 0.214 μ M, while the concentration of the target protein was kept constant at 25 nM, after an incubation time of 2h, measurements were performed using 10% excitation power and medium MST power (40%), shown in green. The MST-on time was 1.5s and the obtained K_d was 0.634 mM \pm 0.235 mM, which is in the same range as previously described. A slight difference between the different percentage concentration of DMSO is observed in a lower S/N ratio (10.89) for ligand L1 with 20% DMSO (green). However, this had no influence on further analysis, as we could not confirm any drastic impact of DMSO on the binding affinity of the reference ligand and on the protein stability. Therefore, the ligand L1 was used as a reference for further binding affinity studies with the other ligands, after which we ranked the ligands with the best to worst binding affinity to the protein and their respective K_d values.

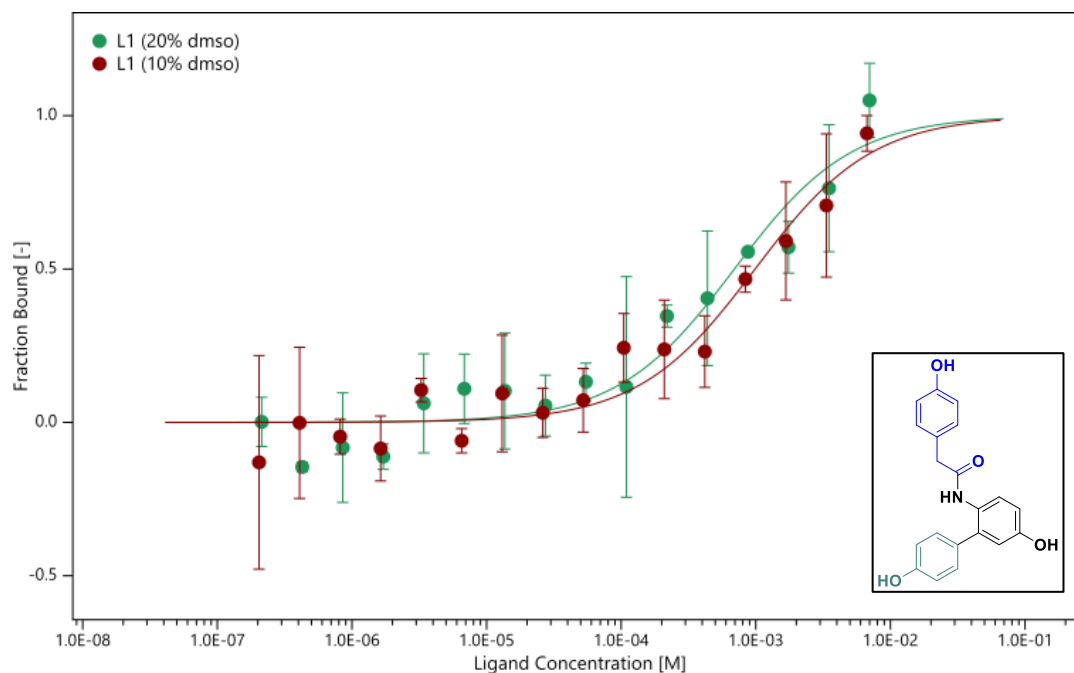


Figure 5.35 MST binding experiments of L1 to hSOD1wt labelled protein. Comparison of L1 with different DMSO concentration 20% (green) and 10% (red); error bars represented as the standard deviation of three individual replicates in each experiment.

The MST assay was performed with ligands L9 and L10, in which the difference in their structure compared to L1 was in the functional groups in *p*- position of the biphenyl ring structures (Figure 5.21). For the ligand L9 with trifluoromethyl group, the measurement was not possible under the established conditions, because the solubility of the molecule was very poor, and when the concentration of DMSO was higher than 20%, the protein started to aggregate, and the concentration was low. Solubility of ligand L10 was obtained with 20% DMSO in 50 mM sodium phosphate buffer, pH 7.4, and the maximal ligand concentration obtained was in the range from 5.27 mM to 0.161 μ M. Compared to L1, L10 had a higher S/N ratio (15.32) and an almost two times higher response amplitude, which resulted in better fitting of the binding affinity curve ($K_d = 1.73 \text{ mM} \pm 0.71 \text{ mM}$), Figure 5.36. This indicated that L10 (red) has a weaker binding affinity than L1 (green) for hSOD1, yet is still in a very narrow range when the standard deviation of three individual replicates (represented in error bars) is taken into account.

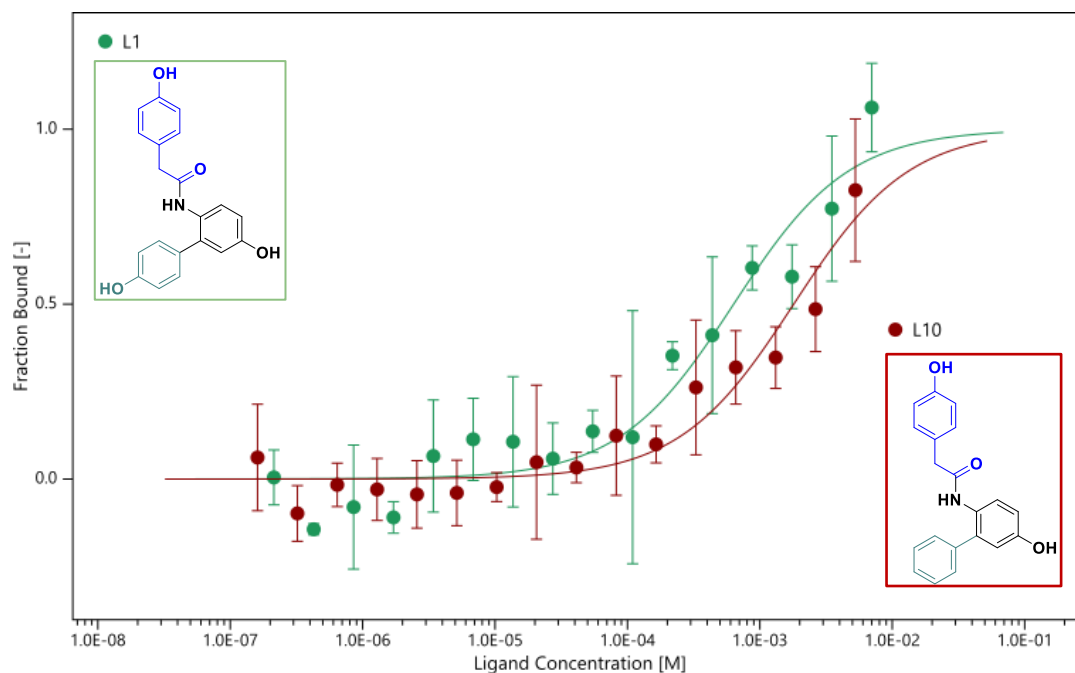


Figure 5.36 MST binding experiment of ligand L10 (red) and comparison with the reference ligand L1 (green); K_d (L10) = $1.7 \text{ mM} \pm 0.7 \text{ mM}$; S/N 15.32; response amplitude: 6.24.

Ligands previously elaborated with the aromatic moiety showed better predicted binding affinities by *in silico* simulations; this trend was also observed in the MST assays. Ligand L4 (Figure 5.37) shows a binding affinity with a dissociation constant of $K_d = 315 \text{ } \mu\text{M} \pm 115 \text{ } \mu\text{M}$, and with a slightly lower S/N ratio of 10.76 compared to L1. However, this S/N ratio is still higher than the validity limitation of the quality of the data. The K_d fit was not affected, whereas for ligand L2, the S/N ratio was just above the limit, and the fitted data obtained were very noisy. The standard deviation from triplicates was in the same range as the fitted K_d value ($168 \text{ } \mu\text{M} \pm 146 \text{ } \mu\text{M}$). The most likely reason for this difference between the two ligands (L4 and L2) lies in a lower concentration of L2 in the binding experiment ($1.0 \text{ mM} - 0.032 \text{ } \mu\text{M}$), which is actually four times lower than for ligand L4, and saturation could not be reached. No aggregation was observed from the MST traces and the raw data, meaning there was not an influence on the affinity (Figure 9.10).

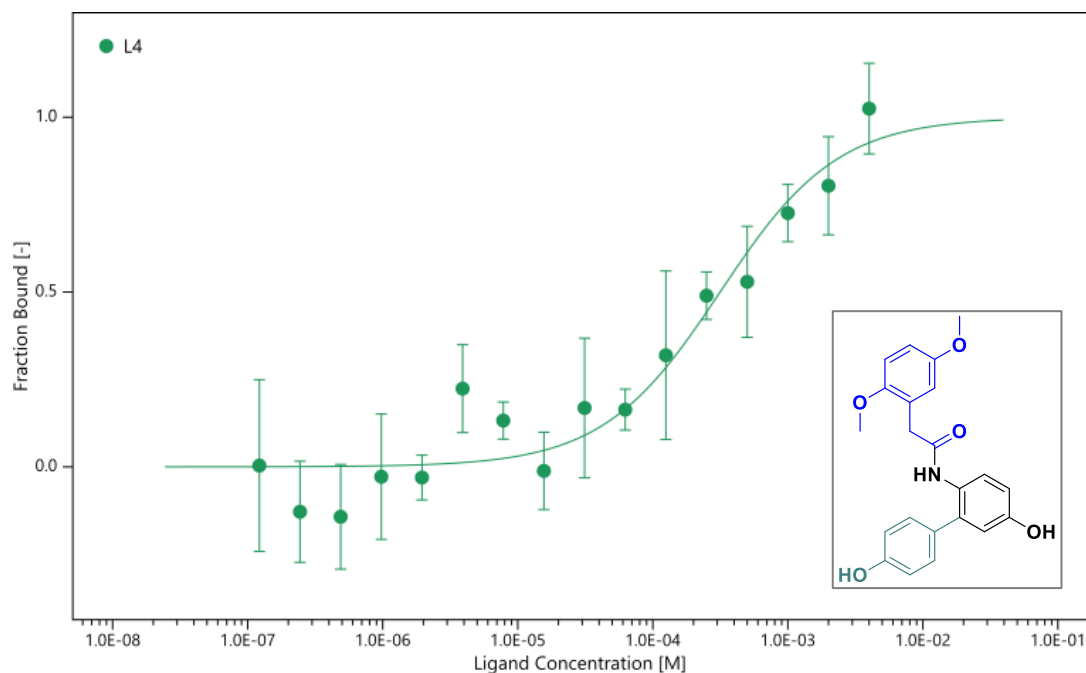


Figure 5.37 MST binding experiment of ligand L4. Binding curve obtained from three independent measurements; error bars calculated as their standard deviation; Compared to L1 ligand, K_d value of L4 is lower ($315 \mu\text{M} \pm 115 \mu\text{M}$; $S/N = 10.76$).

Ligands L13 and L14 are structurally very similar to L4, with the exception of the functional group in *p*- position of the biphenyl ring. Ligand L13 with a trifluoromethyl group in this position had a lower binding affinity according to the *in silico* data and a low solubility, as already confirmed with L9. Therefore, we continued the assay with L14 and the nitro group in *p*- position. Figure 5.38 shows three independent binding affinity assays of L14 and labelled target protein. In all MST experiments, the concentration of the labelled protein was kept constant (5 nM or 25 nM), while the concentration of the ligand L14 was in the range from 0.50 mM to 15.3 nM. This ligand indicated an increased binding affinity toward hSOD1 compared to the other ligands with a binding constant of $21.0 \mu\text{M} \pm 7.4 \mu\text{M}$, shown with the green curve, S/N ratio was 10.15 and response amplitude 3.66 which was still in the range of our reference ligand L1. (Error bars are represented as standard deviation from three independent measurements). The entire assay was repeated with different batches to confirm reproducibility. The concentration of the ligand could not be increased, due to its low solubility, nor high errors could be eliminated between individual measurements. The MST assay with L14 shown in brown had a worse S/N ratio than previously discussed, only 6.47, and a response amplitude of 2.74, which explains the binding constant, where the confidence was half its value ($K_d = 14 \mu\text{M} \pm 7 \mu\text{M}$). In the binding affinity assay with the curve shown in blue, the binding constant for the ligand L14 was the highest ($K_d = 108 \mu\text{M} \pm 32 \mu\text{M}$). However, in this assay we have obtained the best S/N ratio of 17.53 with a response amplitude of 3.85.

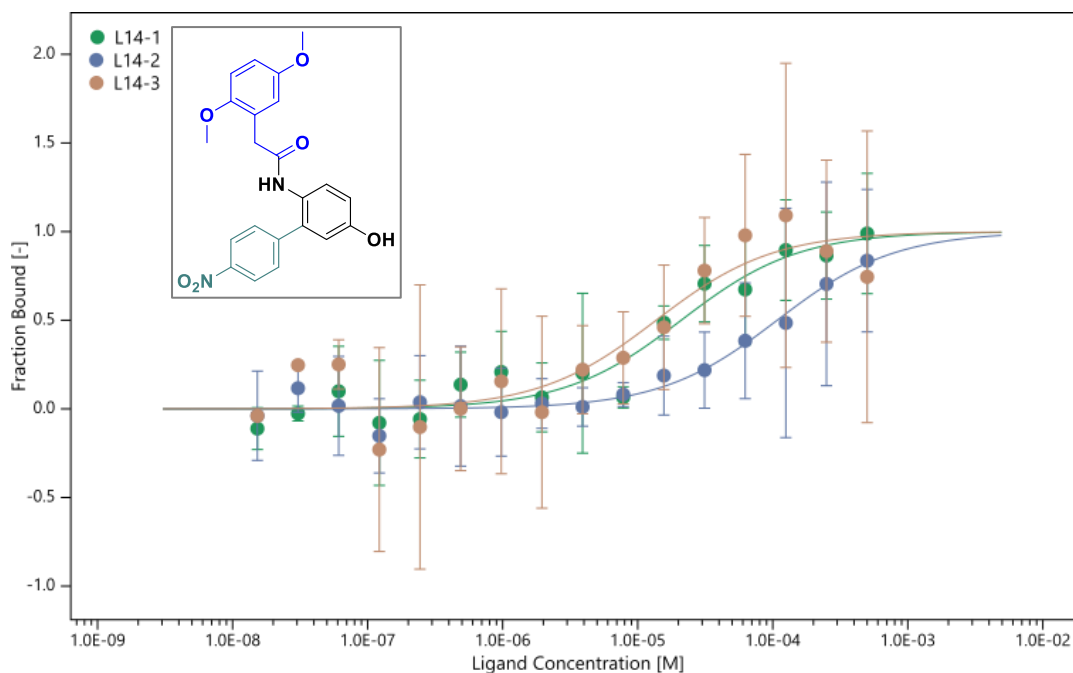


Figure 5.38 MST binding experiments of ligand L14 to different batches of the labelled hSOD1wt protein. Binding curves obtained from three independent measurements; error bars calculated as their standard deviation; obtained dissociation constants: $K_d = 14 \mu\text{M} \pm 7 \mu\text{M}$ (green, batch-1), $K_d = 108 \mu\text{M} \pm 32 \mu\text{M}$ (blue, batch-2), $K_d = 60.28 \mu\text{M} \pm 36.51 \mu\text{M}$ (light brown, batch-3).

From the MST assay with ligand L14 we could confirm a better binding than with reference ligand L1, which is also consistent with the theoretical *in silico* predictions. However, we cannot establish a definite binding constant among those obtained for ligand L14. It can only be concluded that the range lies between 20 and 100 μM , and further experiments and methods would be required to confirm whether this ligand really has such affinity toward the protein. In the experiment with ligand L3 with a concentration range of 1.00 mM – 30.50 nM a similar effect was observed. The difference in the binding constants obtained from different experiments varied between three to six times. For ligand L3 we also observed the influence of the incubation time, in which, after 24h incubation, with the same sample S/N ratio increased from 6.17 to 10.81, compared to 2h, respectively increasing the K_d value to $108.69 \mu\text{M} \pm 42.24 \mu\text{M}$ from previously obtained $60.28 \mu\text{M} \pm 36.51 \mu\text{M}$ for a shorter incubation time. In another experiment from a different batch, the binding constant was in a higher range with a K_d of $380.89 \mu\text{M} \pm 206.29 \mu\text{M}$, and S/N ratio of 12.65. (Figure 5.39) A comparison with the reference L1 showed that the ligand L3 has a higher affinity for the hSOD1wt protein, and it is most likely in the range of the ligands L4 and L14.

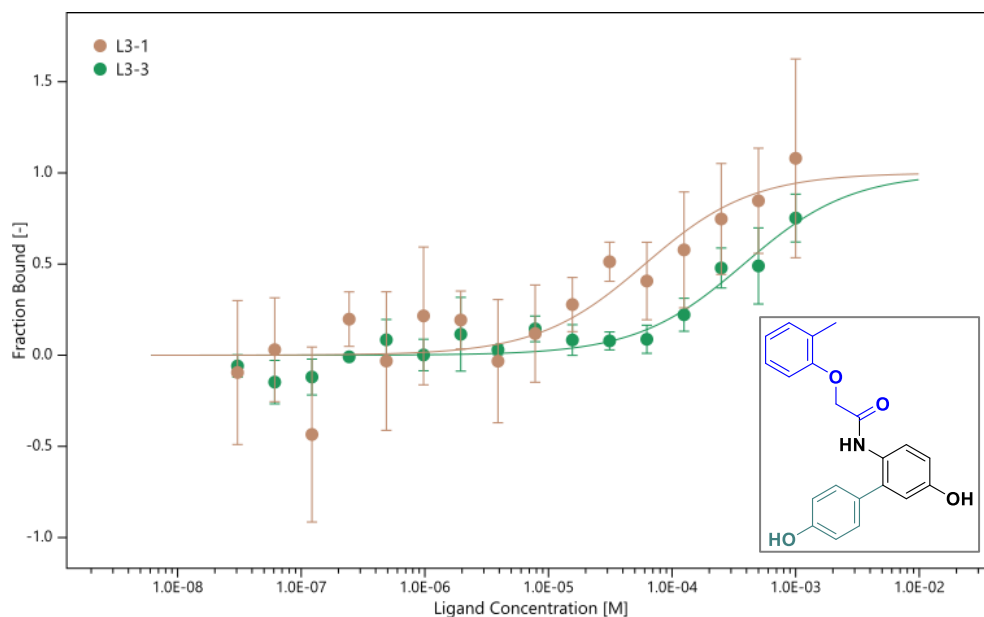


Figure 5.39 Binding affinity curves of ligand L3 in MST experiments with different batches of the labelled protein; obtained dissociation constants: $K_d = 60.28 \mu\text{M} \pm 36.51 \mu\text{M}$ (light brown, batch-1), $K_d = 380.89 \mu\text{M} \pm 206.29 \mu\text{M}$ (green, batch-3).

For ligand L5, which was also ranked the same as L3 from the predicted *in silico* studies, the binding constant was also in a similar range compared to the other ligands with the aromatic moiety. The concentration of ligand L5 was higher (10.00 mM – 0.305 μM) due to the better solubility under the assay conditions, but the error among individual experiment was still high as can be seen in Figure 5.40. The obtained dissociation constant ($K_d = 555.56 \mu\text{M} \pm 181.11 \mu\text{M}$), was lower compared to the reference ligand L1, but the binding affinity was not significantly improved, yet we obtained the result that indicates the binding affinity of the ligand with a thymine-like moiety to the protein.

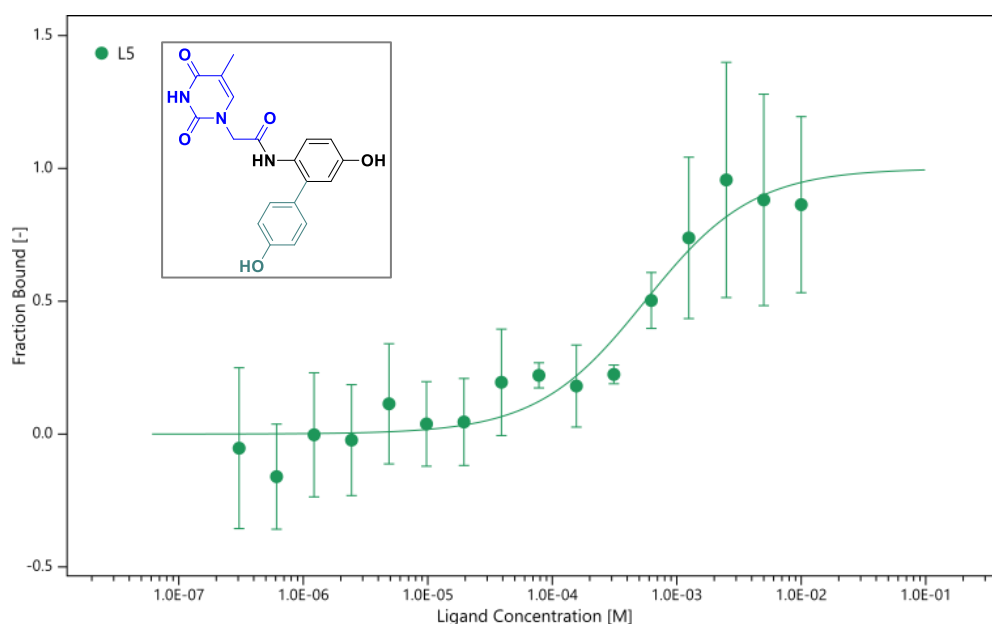


Figure 5.40 Ligand L5 in the MST experiment with labelled hSDO1wt protein.

Ligands with aliphatic moieties, L6, L7 and L8 (Figure 5.21), generally showed lower binding affinities. By comparing L6 and L8, the latter indicated an almost three times lower binding constant in the assay with 10% DMSO. However, the S/N ratio was also lower. Taking that into account, the K_d obtained for the ligand L6 was more a representation of the true value. Furthermore, in the MST experiment with ligand L6 in 20% DMSO, the concentration was increased to a range from 10 mM to 0.305 μ M, which result in an better S/N ratio (31.99) and a more reliable dissociation constant, $K_d = 2.7 \text{ mM} \pm 0.5 \text{ mM}$; Figure 5.41.

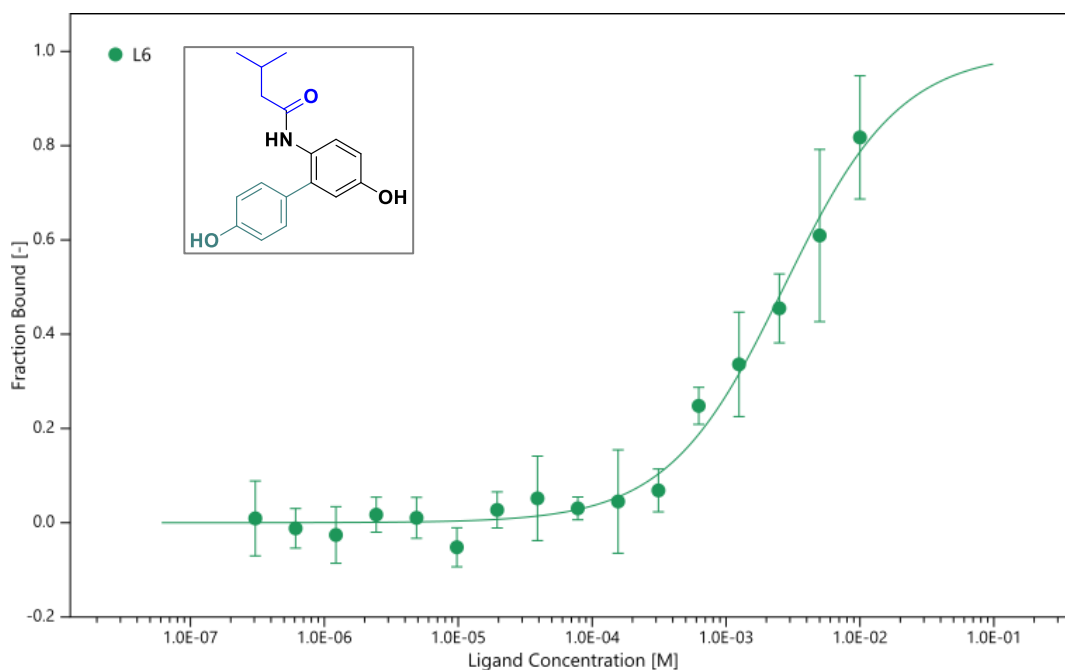


Figure 5.41 MST binding experiment of L6 to hSOD1wt protein and obtained binding constant ($K_d = 2.70 \text{ mM} \pm 0.484 \text{ mM}$).

In the experiment with ligand L7, the initial fluorescence signal was not constant, indicating a concentration dependent change, as shown in Figure 5.42. After performing the SD-test, a specificity test, in which it is confirmed if the ligand induced fluorescence change is an artefact and the assay needs to be optimized or whether the increase was part of the binding affinity^[171], it was confirmed that the ligand induces fluorescence upon binding (see Figure 9.12). Hence, the initial fluorescence was used to derive the binding constant. The initial fluorescence and binding affinity curve of ligand L7 are shown in Figure 5.42, with a fitted K_d of 4.7 mM, whereas the confidence of the fit was not applicable. The concentration of the ligand was in a range of 9.30 mM to 0.284 μ M. This result supports and opens up additional questions regarding the labelled protein site, which may indicate a different location of L7 than *in silico* predictions.

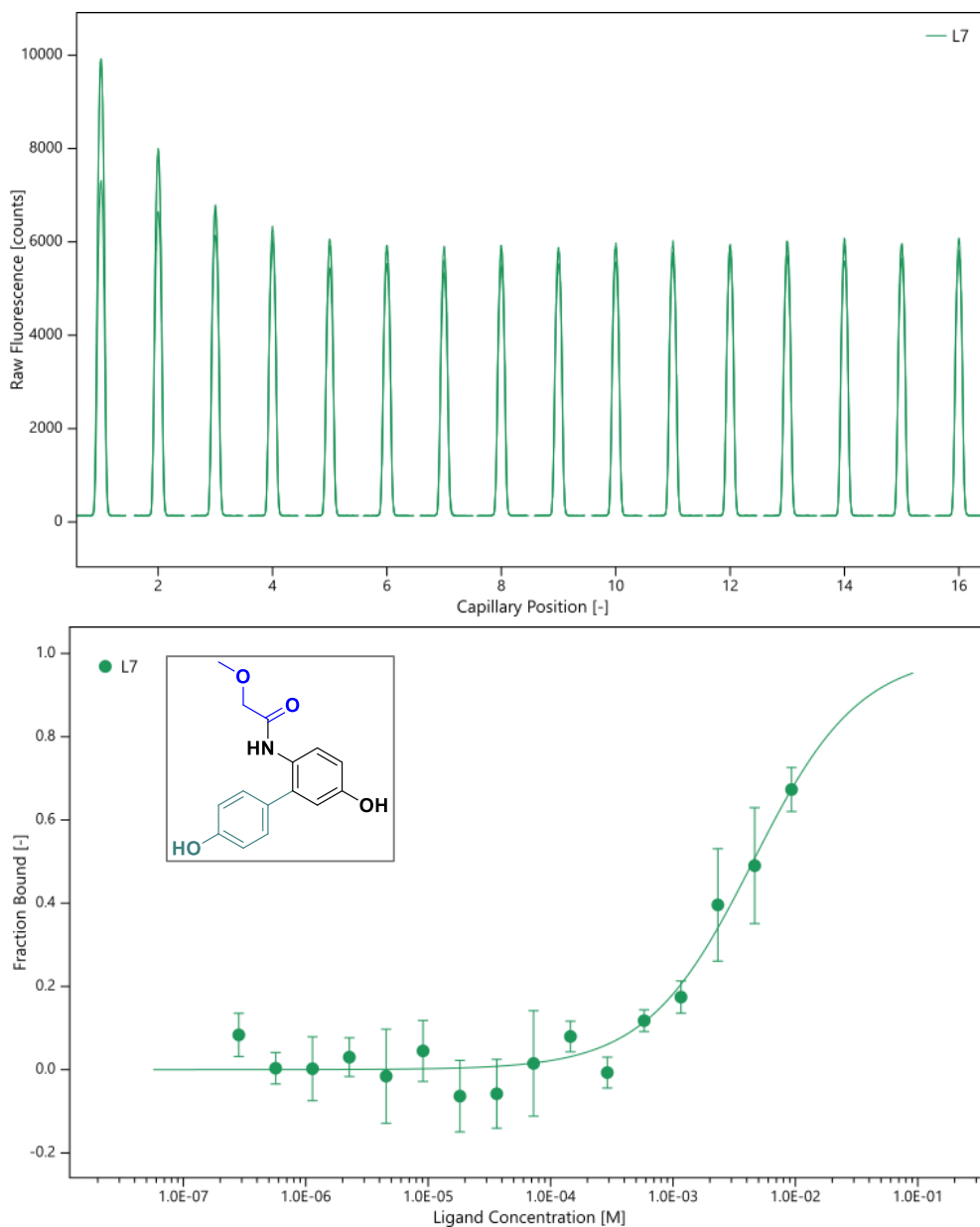


Figure 5.42 MST experiment with ligand L7. *Top*: The initial raw fluorescence obtained as an concentration increase. *Bottom*: Binding affinity curve with dissociation constant ($K_d = 4.7$ mM) derived from values of the initial fluorescence.

The binding curves of the most promising ligands are plotted with the reference ligand L1, (Figure 5.43). The concentration range varies due to the different ligand solubilities. However, the increase in the binding affinity for the proposed ligands can also be seen even with the errors of the experiment. This indicates that the initial *in silico* results were valid, and that our design approach was set in the right direction. We have confirmed that solubility of the ligands is very important, as a good ligand solubility eases the binding assay. In Table 5.5 the most promising ligands are ranked according to their averaged K_d values from the MST assay.

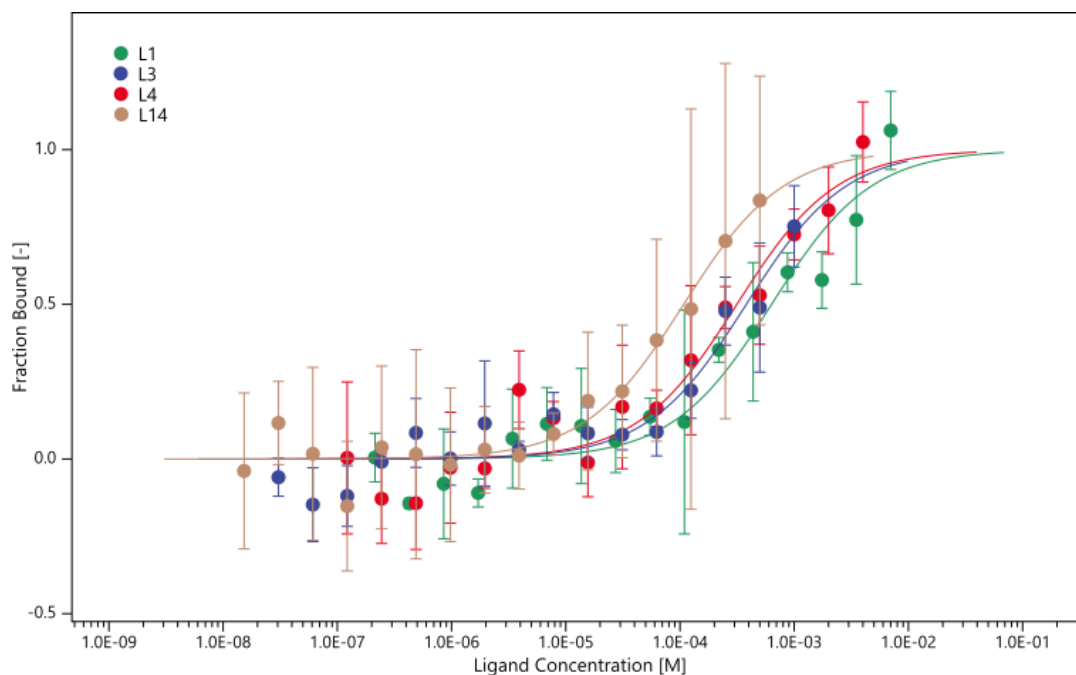
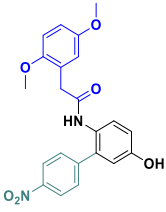
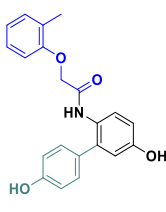
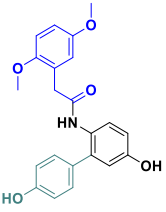
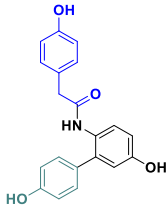


Figure 5.43 MST experiment, ligands with the best binding affinity toward the hSOD1wt protein.

Table 5.5 The most promising ligands and the averaged binding constants

Ligands				
	L14	L3	L4	L1
conc. [mM]	0.50 - 1.53e-05	1.00 - 3.05e-05	4.00 - 1.22e-04	7.00 - 2.14e-04
K_a value	48 μM ± 15 μM	182 μM ± 95 μM	315 μM ± 115 μM	634 μM ± 235 μM
S/N	11.38	9.07	10.71	10.89
Response amplitude	3.42	3.78	4.05	3.67

As previously shown, one of the main problems in microscale thermophoresis is the large difference in the results consistency. During the measurements, individual repeats, obtained the same day and treated similarly showed different thermophoretic response. This was also confirmed for measurements repeated with different batches. On the one

hand, we might conclude that some ligands may need to be treated differently and optimizing the buffer system may not work for all ligands in the library. On the other hand, this poses a problem of comparability among them, and the ranking system according to their affinity for the protein cannot be established. Similar problems with data reproducibility and inconsistencies with aggregation prone proteins, were already reported in the literature, when small molecule interaction on α -synuclein protein was studied.^[172] Moreover, we have also confirmed the influence of DMSO on the data quality. Removing this effect from the measurements could be beneficial for further investigation of binding affinities and reproducibility. Like any other biophysical method, MST has its advantages and disadvantages. With very small amounts required, it is an attractive method, for initial screening and development. With this method, we could confirm the binding of the designed ligands. However, in order to obtain more precise binding affinities and a better understanding of the investigated system, a combination with other methods is required to reach a final conclusion.

5.4.2 Isothermal Titration Calorimetry (ITC)

As described in Section 4.4, ITC is a well-established method for analysing binding affinities. Another incentive beside confirmation of the MST studies was to obtain thermodynamic information of the binding affinity of the ligands and the SOD1 proteins, and possibly to be able to evaluate the contribution of different functional groups. In addition, the correlation with the *in silico* design could open up the possibility of improving their affinity prior to structural studies.

Early experimental investigation with reference ligand L1 indicated a binding to hSOD1wt, and the fitted binding constant was in the higher micromolar range ($104 \mu\text{M} \pm 38.5 \mu\text{M}$), as shown in Figure 5.44. At that point we have already observed problems of a high DMSO concentration in the control experiment during the titration of the ligand into the buffer, yet the effect was not that high, so it was possible to subtract it from the protein data, (Figure 9.7).

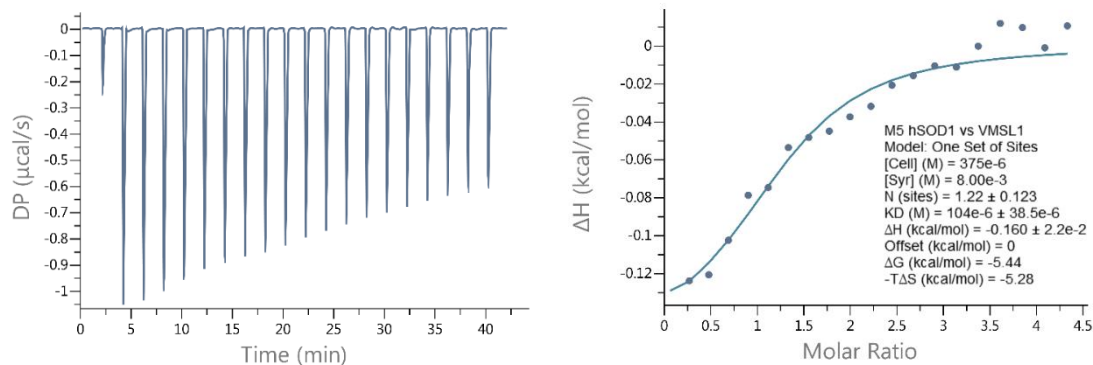


Figure 5.44 Binding affinity in 100 mM hepes buffer, 150 mM NaCl, pH 7.4 including 20% DMSO with L1 (8 mM) in syringe and hSOD1 wt (375 μ M) concentration in cell (ITC experiments performed and evaluated by Lisa-Marie Funk)

The following attempts to reproduce the data were not successful, as the effect of DMSO resulted in a higher signal in the control measurements. Further, experimental investigations to find suitable solvents with acceptable ligand solubility for the ITC assay confirmed that glycerol (GOL) was a good match. Figure 5.45 shows the high signal in the experiment with DMSO and the better baseline obtained with glycerol.

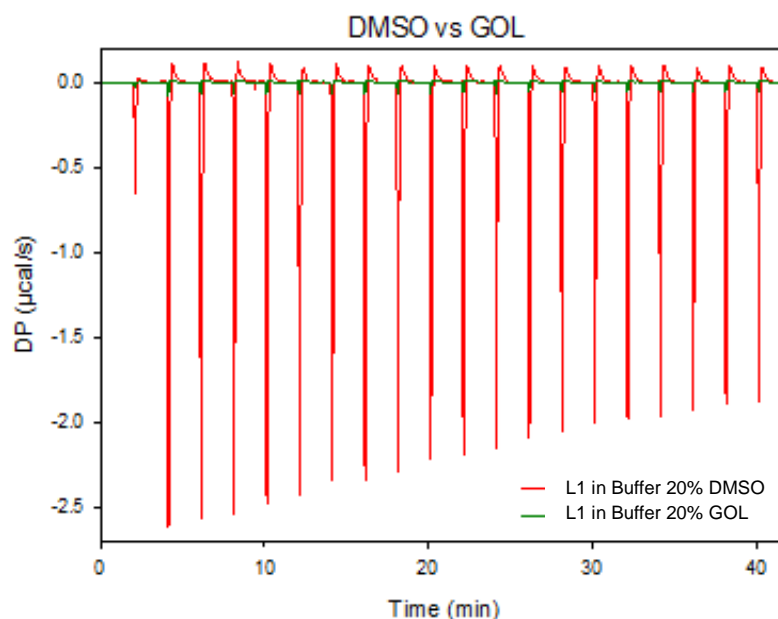


Figure 5.45 Comparison of heat signal produced by titrating ligand L1 into buffer (100 mM hepes buffer, 150 mM NaCl, pH 7.4) with 20% DMSO (red) or glycerol (green)

Furthermore, binding experiments with ligand L1 and glycerol as a co-solvent showed no binding. Rather, we have confirmed the importance of cell flushing before loading to avoid mismatch and reduce the background noise (data not shown). From the data shown in Figure 5.46, a higher endothermic signal is observed for the ligand in buffer (shown in red). One possibility why the binding with the ITC is undetectable could be the

unfavourable desolvation upon binding to the cavity. This effect was confirmed in other studies on trypsin and resulted in complete loss of the binding affinity with benzamidine derivative.^[173] Moreover, the challenge of the ITC binding assay with the SOD1 protein has already been recognized, even for soluble ligands that have been structurally confirmed to be bound to the Trp32 binding site it was not successful.^[69] Recently, a group reported the binding affinity of quercitrin to A4V protein with a binding constant of $\sim 34 \mu\text{M}$, which was obtained from ITC assay measurement. However, prior to the assay, the concentration of the DMSO used for the solubility of the ligand was unclear.^[166]

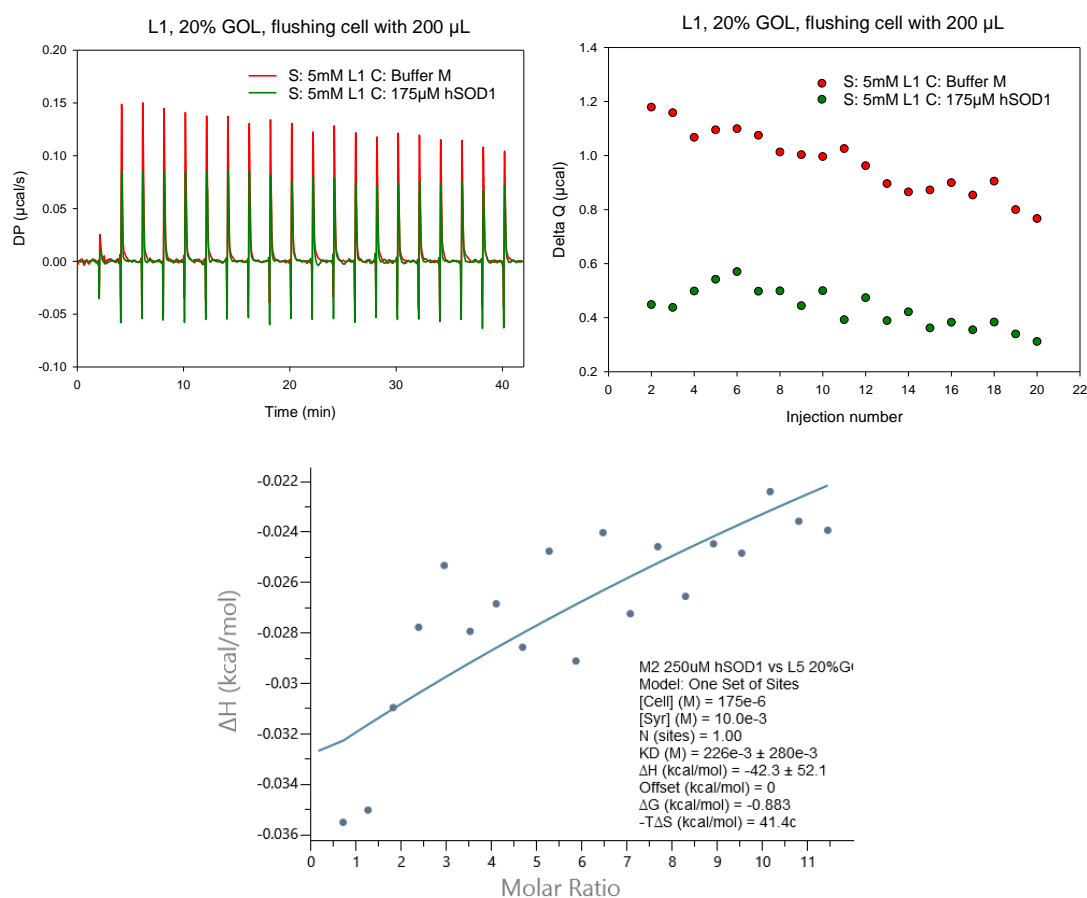


Figure 5.46 ITC binding affinity assay; ligand L1 (5 mM) and hSOD1 wt (175 μM) with 20% glycerol as a co-solvent in buffer M (100 mM hepes buffer, 150 mM NaCl, pH 7.4).

At this point, further ligand tests in the ITC assay were stopped, mainly because of their low solubility even in glycerol, in which the highest concentration was still not sufficient to observe weak interactions.

5.4.3 Thermal shift assay

The principle of this method is to determine protein stability by measuring the melting temperature of the protein upon thermal denaturation. It is based on the fluorescence signal of the SYPRO Orange stain, which is observed upon dye interaction with the hydrophobic regions of unfolded protein. To answer the question of ligand influence on the hSOD1 protein stability the following assay was conducted as described in Section 7.2.4.1.

Initial screening concentration range tests were performed on the hSOD1 holo enzymes. Enzymes were tested in the respective concentration range with and without addition of DMSO to obtain the protein concentration. The assay with ligands was performed with the A4V apo protein; however, high ligand interference with a dye hampered the real output, as can be seen from the fluorescence signal (Figure 5.47) even when the respective ligand controls were subtracted. Followed by calculation of the 1st and 2nd derivative melting temperatures of ligands were obtained in the temperature range of 31- 35°C.

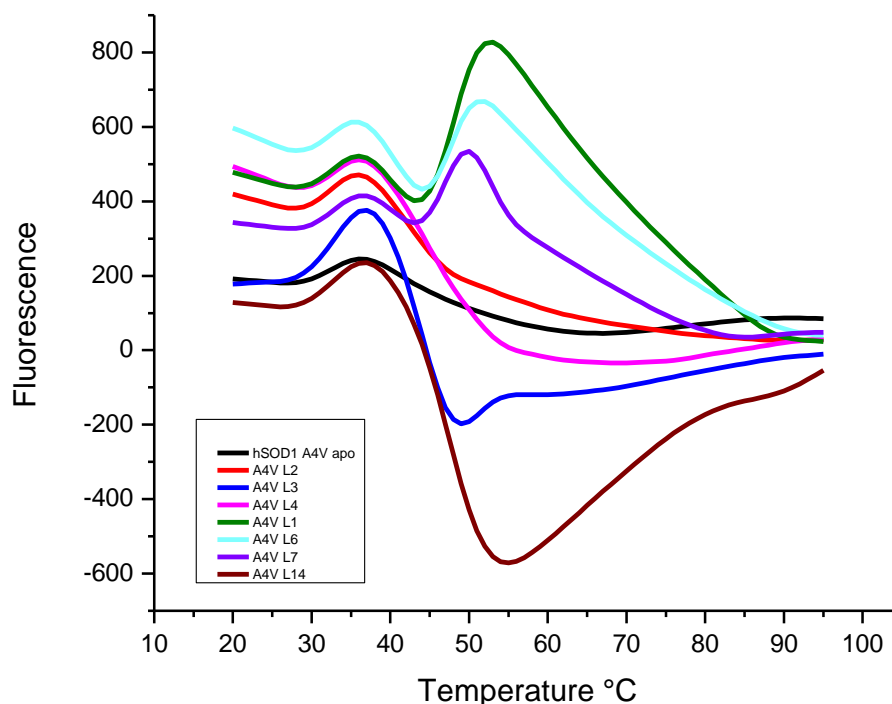


Figure 5.47 Fluorescence intensities in thermal shift assay with ligands (1 mM) and hSOD1 A4V apo protein (1 μ M) with 20% DMSO in 50mM sodium phosphate buffer, pH 7.4.

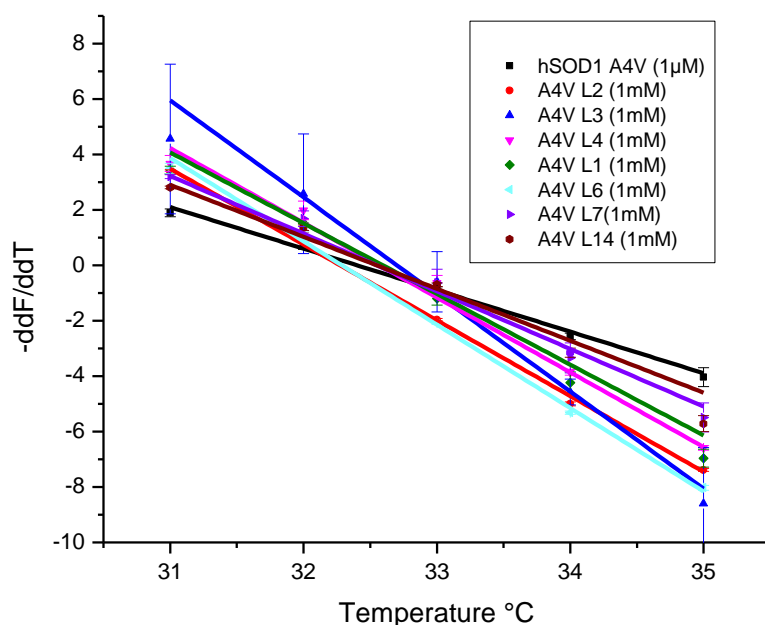
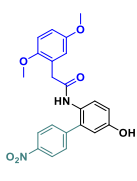
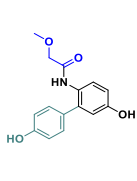
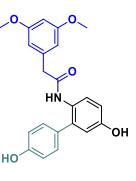
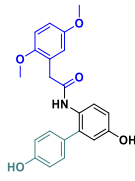
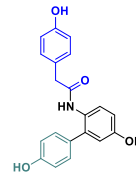
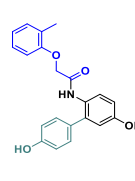


Figure 5.48 Linear fit of the thermal shift data as 2nd derivative.

Table 5.6 Melting temperature obtained from thermal shift assay. Ligand influence on the hSOD1A4V apo stability. (A4V apo; $T_m = 32.40 \pm 0.07$ °C)

						
	L14	L7	L2	L4	L1	L3
T_m (°C)	32.55±0.12	32.55±0.12	32.55±0.06	32.56±0.10	32.60±0.23	32.70±0.24

From the obtained results it can only be concluded that there might be slight tendency for ligand L3, as the difference of 0.03°C between A4V apo protein is the highest. However, this would not be enough to stabilize the protein, and more tests should be performed.

5.4.4 Ligands influence on the SOD1 aggregation

In order to confirm the influences of the ligands on aggregation processes, aggregation assays were conducted as described in Section 7.2.4.4. As already reported in the literature, mutations have strong influence on the protein aggregation.^{[51][61]} We have confirmed earlier that the apo variant A4V is more unstable and easily prone to aggregation. Therefore, the influence of ligands on the apo A4V variant was tested. In the

aggregation assay, the A4V apo variant was tested with two different detection reagents, the ThT dye and commercially available PROTEOSTAT reagent dye in order to detect aggregated protein as amyloid fibrils. In this assay, dyes show an increase in fluorescence when bound to the aggregated fibrillar proteins. This structure has been reported as a cross- β spine quaternary structure.^[174]

Münch and Bertolotti previously showed the influence of low pH and high temperature on the aggregation of the A4V protein.^[175] Here, the aggregation of the A4V apo protein incubated at different temperatures and times was also confirmed. The amount of aggregates was calculated from the aggregated reference IgG standard. Aggregation of the A4V protein was confirmed after 48h incubation at 0 °C in both assays, while the sensitivity of the PROTEOSTAT dye is approximately two times higher than that of the ThT dye at all incubation times. Interestingly, in the aggregation assay with the ThT dye less aggregates were detected after 48h incubation at 50 °C than after 24h, a possible reason is that the amount of fibrillar aggregates was reduced and not detected due to the lower sensitivity of the ThT dye. However, the purpose of the chosen assay setup was to confirm the aggregation of the A4V protein and capability of the ThT dye to detect aggregates already after 24h incubation at 50 °C, Figure 5.49.

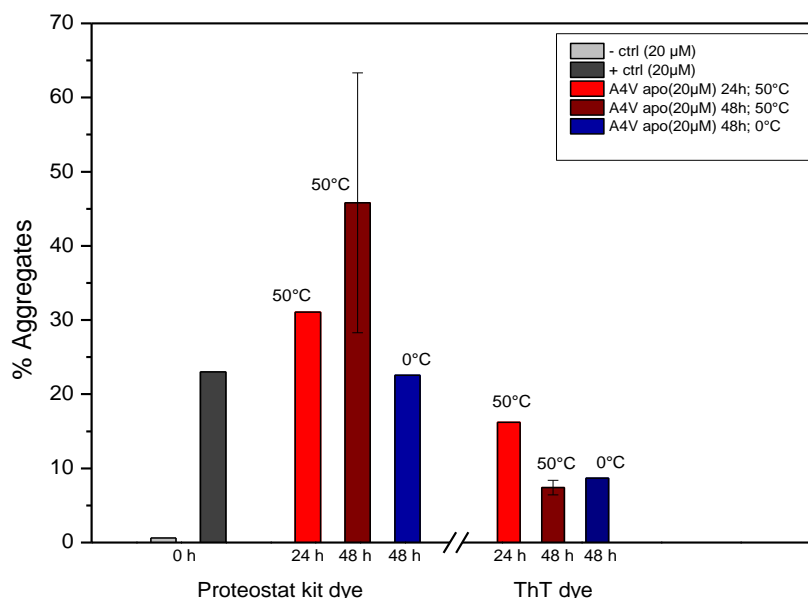


Figure 5.49 Aggregation assays with PROTESOTAT and ThT dye conducted in 50 mM sodium phosphate buffer, pH 7.4 with incubation times 24 to 48 h, at 0 °C and 50 °C, with 20 μ M final concentration of A4V apo protein.

The aggregation assay with the ThT dye was used to determine the aggregation of the A4V variant in the presence of the ligands with the best binding affinities (Figure 5.43). In the assay, apo A4V protein (20 μ M), ligands (1 mM) and the respective controls were

incubated in 50 mM sodium phosphate including 20% DMSO for 24h at 50 °C. As it was confirmed to be enough time to detect the aggregates. From the results obtained, a strong influence of DMSO on the aggregation of the A4V apo variant was observed, as shown in Figure 5.50. The amount of A4V aggregated with the addition of DMSO is approximately 5% less than hSOD1wt holo protein, which was used as a negative control. These results were also confirmed in the assay with the PROTEOSTAT dye, in which the amount of aggregates in the presence of DMSO was approximately 25% less than in the assay with buffer only, (Figure 9.13). However, it was important to establish the assay and obtain the same effect for both tested dyes, because it did not depend on the commercially available PROTEOSTAT dye.

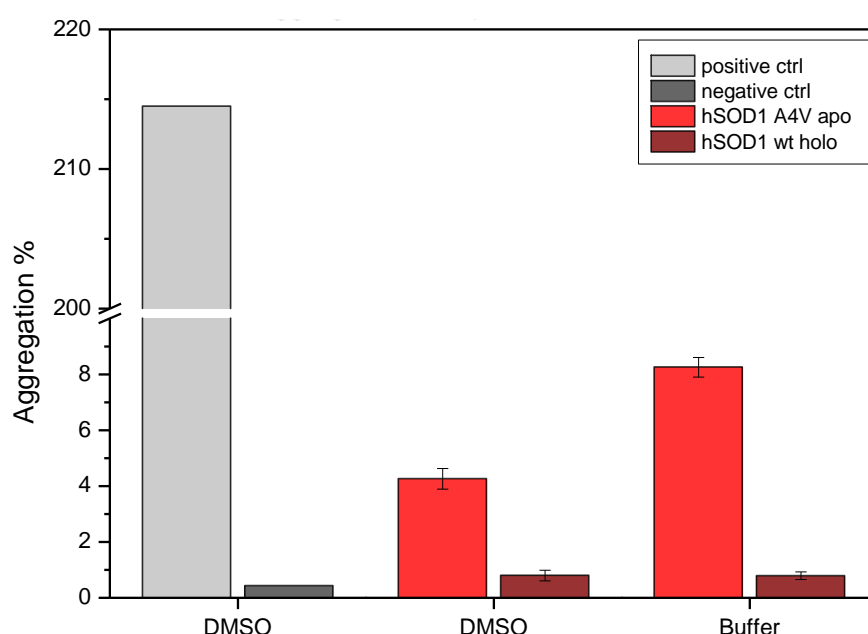


Figure 5.50 Aggregation assay of hSOD1 proteins with ThT dye; conducted in Buffer (50 mM sodium phosphate buffer, pH 7.4) and in DMSO (Buffer + 20% DMSO) at 50 °C for 24 h, with a final protein concentration (20 μM). Aggregated and monomeric lysozyme was used as a positive and negative control, respectively.

Additionally, from the data recorded for A4V incubated with the ligands in DMSO, the same amount of aggregates was detected with or without ligands (L4, L1 and L14). Yet, in the presence of ligand L3, effect on aggregation was different. We observed no difference to the A4V variant in buffer, (Figure 9.14). How does DMSO effect the aggregation and what really happens with the ligand L3, where this effect is completely diminished? It is known that DMSO can have different effects on proteins and can stabilize the enzymes by increasing their preferential hydration. Moreover, with thermal denaturation, it is unfavourable since more free energy is required for unfolding in a system with DMSO as co-solvent.^{[176][177]} Besides, it has been reported that a decrease in

protein charge induced by a low concentration of DMSO has a stabilizing effect on protein unfolding for lysozyme and myoglobin.^[169] This effect was indicated for apo SOD1 proteins, but the others showed that an increased concentration of DMSO promotes destabilization for the apo SOD1 dimer.^[162]

Different additives were tested in order to obtain a solvent that does not have an effect on the aggregation and in which the solubility of the ligands was no longer impaired. Figure 5.51 shows the data for the aggregation of the apo A4V variant with different additives (20%). Again, a lower aggregation with DMSO was confirmed. Importantly we could observe that PEG additives did not have an effect on the aggregation as there was no significant difference compared with the A4V apo protein in buffer control.

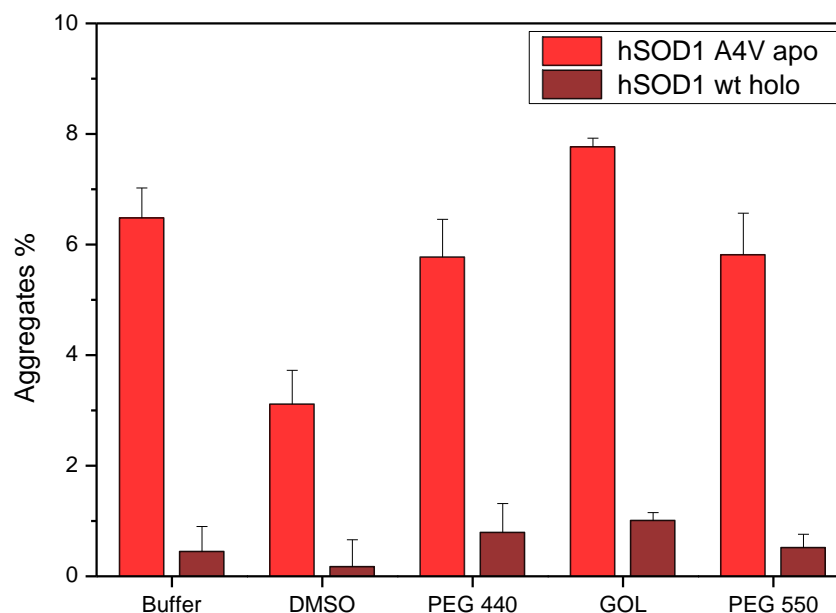


Figure 5.51 Aggregation assay screen of hSOD1 proteins with various additives (20%) and their influence as co-solvents on aggregation. Samples with a final protein concentration 20 μ M were incubated for 24 h at 50°C in 50 mM sodium phosphate buffer pH 7.4, including 20% of respective additive.

In the following, the most promising ligands were tested according to their binding affinity, with 20% PEG550. From the data obtained and shown in Figure 5.52, it can be seen that the effect of the reference ligand on the aggregation is rather low. Statistically, there was no significant difference observed for the ligands L4, L1 and L14, whereas the effect on aggregation was confirmed for the ligand L3. If we correlate these results with the binding affinity data, we cannot observe an exact similar pattern. L3 had a binding constant in the lower μ M range compared to the other ligands, L14 had by far the best binding constant \sim 50 μ M but it also had the highest error so that the K_d varied from 20-

100 μM . Moreover, L4 ($\sim 315 \mu\text{M}$) also showed better binding than L1 ($\sim 640 \mu\text{M}$), the tendency is visible here, but there is no significant difference to the control sample.

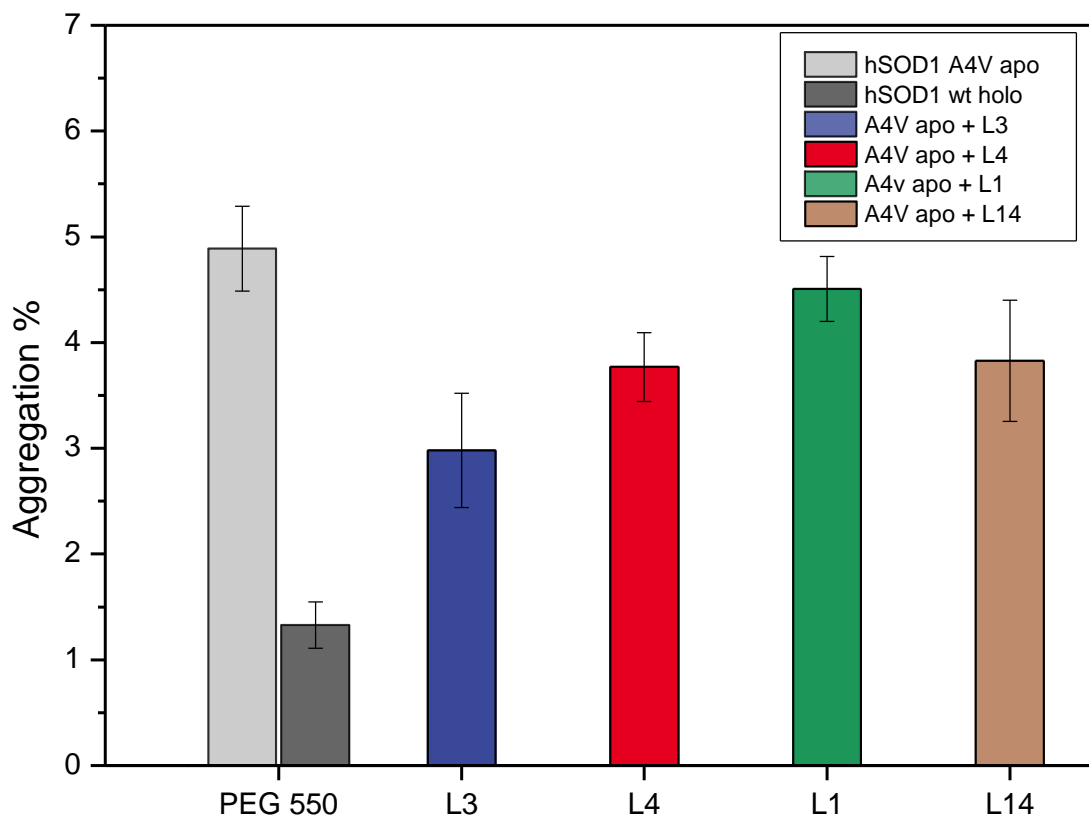


Figure 5.52 Ligands influence on the aggregation of the hSOD1 A4V apo protein. Assay conducted at 50 °C for 24 h with a final protein (20 μM) and ligands (1 mM) concentration in 50 mM sodium phosphate buffer, pH 7.4 and 20% PEG550.

However, we could confirm an effect of the ligands on the aggregation of the A4V apo protein. Moreover, the binding affinity does not necessarily need to correlate with the aggregation studies, if ligands slow down aggregation by association with undetectable aggregates and prolonging time to form insoluble aggregates. Earlier it was shown that the aggregation morphology of apo SOD1 protein is kinetically dependent ^[178], which also means that the amount of fibrillar or amorphous aggregates is dependent on the first initiated pathway. Additional studies of the most promising ligands with the fluorophore attached could provide a clear picture on the aggregation phase and association with the ligands.

5.5 X-ray crystallographic studies of hSOD1wt and ligands

For a deeper understanding and confirmation of the real ligand binding site, various literature reported conditions were tested for X-ray crystallization; however, these could not be reproduced. [69,85]

In order to find the crystallization conditions for hSOD1 proteins different approaches were applied, i.e., (manual screen, additive screen, and automated crystallization screen). The manual and additive screens did not give satisfying results; therefore, an automated screen was performed. The screen was carried out by Elham Paknia in the group of Prof. Holger Stark (*Structural Dynamics*) at Max Planck Institute for Biophysical Chemistry (MPI). For the automated screen, 1 μ L of the hSOD1wt protein (10 mg/mL) in 20 mM Tris buffer pH 8.0 was mixed with 1 μ L of the kits reservoir solutions on the 96-well plate (Intelli - Art Robbins Instruments LLC, Sunnyvale, CA, USA) using crystallization robot Crystal Gryphon LCP (Art Robbins Instruments LLC, Sunnyvale, CA, USA). Sitting-drop diffusion method was used, and the crystallization screen was performed at 20 °C. Following, positive screen conditions which revealed bigger crystals, crystal were reproduced manually using the sitting and hanging drop vapour diffusion approach. In Figure 5.53 first crystals are shown in 0.2 M ammonium sulfate, 0.1 M MES buffer, pH 6.5, 20% PEG 8000 as one of the conditions obtained by the hanging-drop method, observed after three and ten days incubation time in a well with a precipitant solution of 0.2 M ammonium sulfate, 0.1 M MES buffer, pH 6.5, 20% PEG 8000 and a final hSOD1 concentration of 0.04 mg/mL.

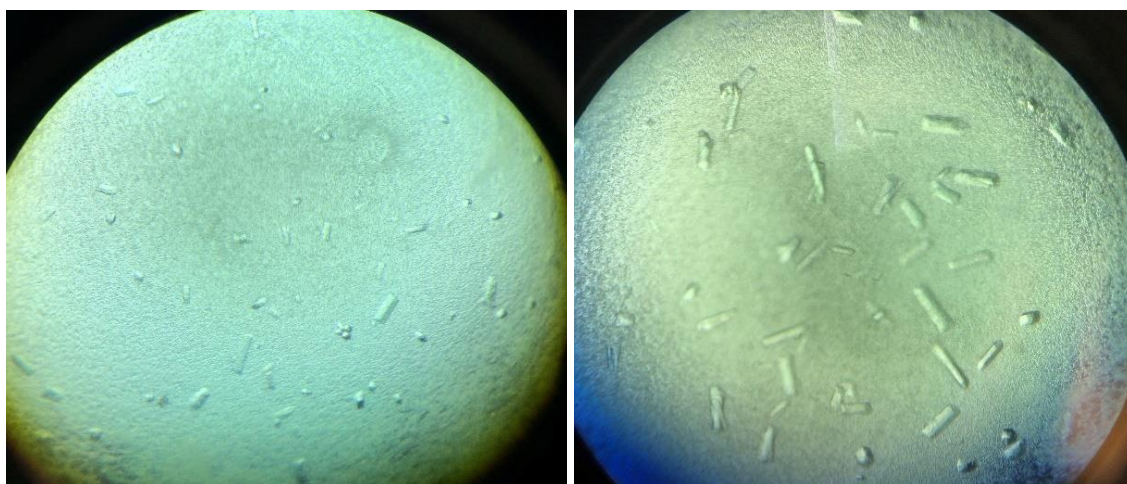


Figure 5.53 hSOD1 wt crystals obtained in 0.2 M ammonium sulfate, 0.1 M MES buffer, pH 6.5, 20% PEG 8000, after three (left) and ten (right) days.

Acquiring crystals itself is a challenging process as even a small change in pH, protein concentration, precipitant concentration, or temperature can shift the equilibrium, which is not ideal for supersaturation.^[179] Furthermore, crystals must be stable and resistant to the solvents used in soaking experiments. Here we have also encountered problems with DMSO when looking for a good cryoprotectant solution that would not have to affect the impact on diffraction. Initially, the crystals burst and broke apart in less than 5s, yet after more optimized soaking conditions, we were able to increase the time to 4 min. Unfortunately, until now we have not yet been able to structurally confirm any ligands bound to the protein sites. One of the reasons could be a short soaking time, Manjula *et al.* reported much longer ligand soaking time ranging from 3h to 20h.^[85] Also, to be able to obtain structural information, a higher resolution would be ideal, as our crystals have so far been diffracted from 2.3 – 3.2 Å. The entire X-ray data processing, reduction, refinement evaluation and building of the hSOD1 model (Figure 5.54) was done by Lisa-Marie Funk.

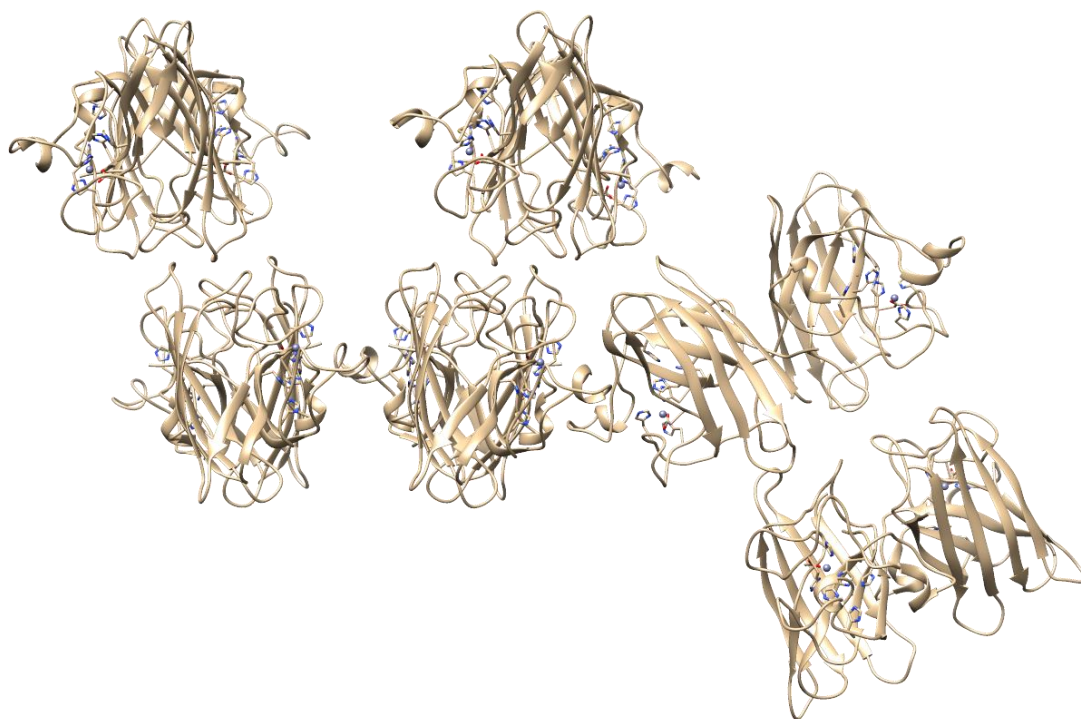


Figure 5.54 Refined structure of the obtained crystal structure of hSOD1wt (*Evaluation was done by Lisa-Marie Funk*).

6 SUMMARY AND OUTLOOK

In this work, ligands with a binding affinity to hSOD1 and the potential to inhibit the aggregation of hSOD1 mutants in amyotrophic lateral sclerosis (ALS) were designed and synthesized. The lead ligands were designed after a computational structural investigation of the hSOD1 protein cavity Cav(V148) using molecular docking with AutoDock Vina. They exhibit two key units, the ligand scaffold unit, through which the stability of the protein and the affinity for the cavity was intended to be achieved, and the fluorophore unit, which would give a turn-on fluorescence response upon binding to the protein

The development of the lead ligands required confirmation of the affinity of the ligand scaffold to the protein before the fluorophore unit was attached. Putative ligand binders were obtained by iterative *in silico* docking simulation studies. Ligand scaffolds were then ranked according to the highest score of the predicted binding energies and interactions within the cavity. Ligand L14 with the lowest binding energy is shown in Figure 6.1.

Different synthesis strategies toward the three lead structures A, B and C were performed. While the synthesis was successful for two of them, further studies were pursued on the variation of lead structure A, which could then be studied in terms of their binding properties to hSOD1 and their potential to reduce hSOD1 aggregation. An improved modular synthesis strategy granted easier library enlargement. As shown in overall Scheme 6.1, it is possible to achieve the main amine compound in two steps, and further proceed with a Suzuki coupling or the amide bond reaction formation. The variation of the aromatic and aliphatic functional groups on the ligand scaffold enabled a higher binding affinity to the protein. A total of 13 ligands bearing H-bond donors and acceptors

were synthesized, keeping in mind the overall hydrophobicity required for the cavity, and the Lipinski rule^[180] of tolerance, (Figure 5.21).

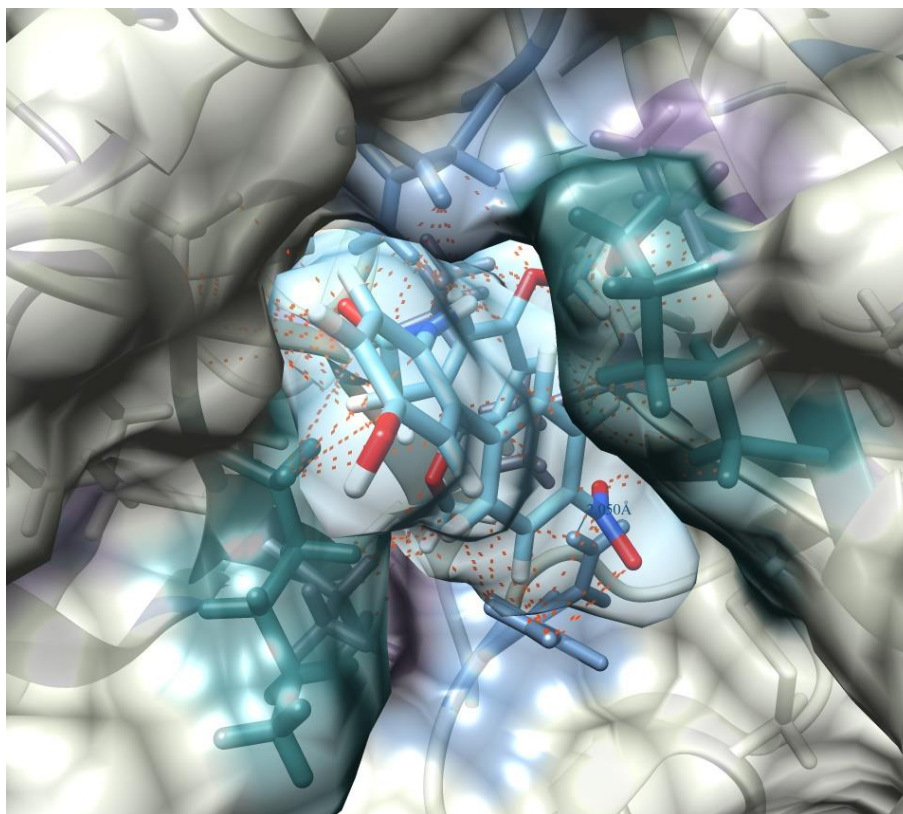
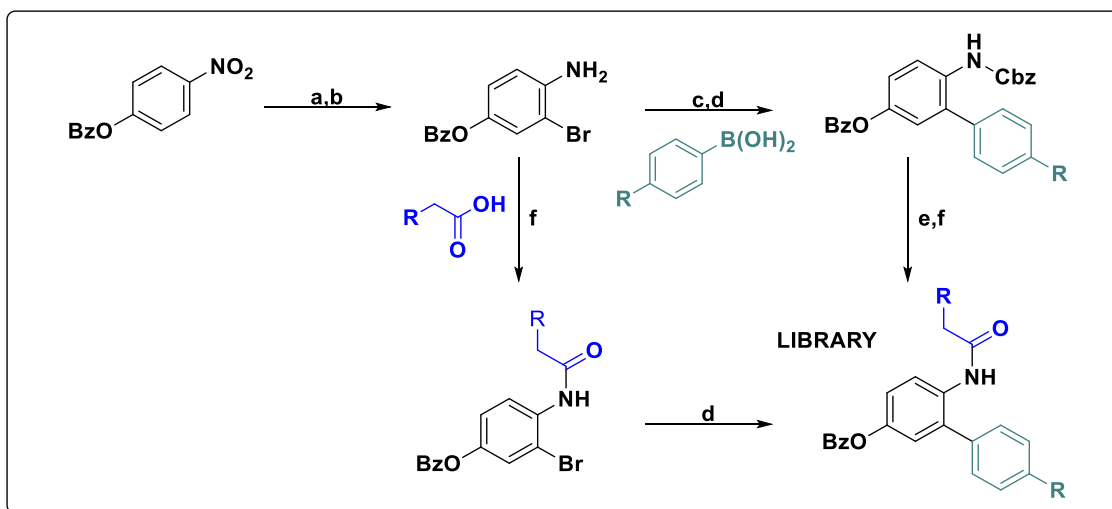


Figure 6.1 Ligand L14 in Cav(V148) obtained from molecular docking with AutoDock Vina with an estimated free binding energy of -36.40 kJ/mol.



Scheme 6.1 Modular synthesis approach of improved lead structure A for library enlargement.

Furthermore, to be able to elucidate the affinity of the ligands, hSOD1 proteins were expressed and purified. This process already showed a difference between the wild-type and the A4V protein. While a high purity could be obtained for both proteins, instability of the A4V variant was noted prior to reconstitution with the cofactors, which resulted in

a 15% reduced yield of the variant. The instability of the apo variant, the lower activity and its prompt aggregation were also confirmed. In size exclusion chromatography experiments, the monomer-dimer equilibrium of the variant was not observed, rather high molecular weights aggregates indicated an unstable, readily aggregating protein. The protein activity assay confirmed a 30-40% lower activity for the apo A4V variant compared to the hSOD1wt. The influence of DMSO (20%) as a co-solvent, which was needed for further binding studies, was investigated, and the pronounced influence on the protein activity was higher for the wt protein than the A4V variant, when compared with the buffer controls. The overall influence of DMSO on the protein activity was found to be negligible.

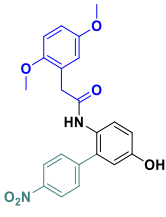
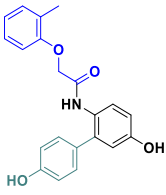
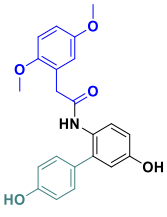
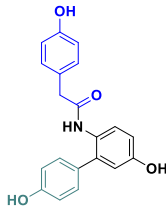
Furthermore, the influence of ligands on the protein was comprehensively studied and different assays were developed. It has been shown that various assays would be required for a decisive claim of the real binding constants. The development of the microscale thermophoresis (MST) assay enabled ligand binding affinity studies, but also indicated many pitfalls. The solubility of the ligands turned out to be a significant drawback in the assay studies. This was also reflected in the quality of the data and on the reproducibility of the binding constants. Yet, the binding affinity studies showed that the rational design and ligand scaffold variation were performed in the right direction.

The obtained ligand binding affinities were also mostly in agreement with the *in silico* predicted ligand binders. However, small differences in the binding affinity energies of less than ~ 4 kJ/mol, among the putative ligand binders from *in silico* simulations cannot be decisively used for the ligand synthesis. Ligands with aliphatic groups in their scaffold, which were expected to be inferior binders, showed a putative binding affinity of ~ 30 kJ/mol, while the others with more aromaticity had an increase in affinity for the protein of ~ 36 kJ/mol. However, with lower differences (33 kJ/mol - 35kJ/mol) among the ligands with an aromatic scaffold and differently positioned H-bond donors and acceptor groups, ligands could not precisely be ranked just from putative binding affinities. The most promising ligands are shown in Table 6.1.

First, the ligand L1 was exhaustively studied with different incubation times and DMSO concentrations. It was previously elaborated that observed differences in DMSO concentration and incubation time had an insignificant influence on the binding constant. The best binding affinity was observed for ligands L14 and L3, while L6 performed worst. It can be noted that the signal to noise ratio (S/N), response amplitude, and binding constant of L6 is the highest and with the lowest error, which represents a good assay.

Here, however, the ligand concentration has to be considered; with low solubility of L14 and L3, the highest concentration was 0.5 and 1.0 mM, respectively, and saturation could not be reached, which influenced the fit value. A comparison of the binding constants among the ligands L1, L3, L4, and L14 generally showed the tendency for a higher affinity, respectively, (Figure 5.43).

Table 6.1 Ligands with their averaged binding constants obtained from the MST assay, and putative free energy obtained as the best score by *in silico* simulations.

Ligands				
	L14	L3	L4	L1
conc. [mM]	0.50 - 1.53e-05	1.00 - 3.05e-05	4.00 - 1.22e-04	7.00 - 2.14e-04
K_a value	48 μM ± 15 μM	182 μM ± 95 μM	315 μM ± 115 μM	634 μM ± 235 μM
S/N	11.38	9.07	10.71	10.89
Response amplitude	3.42	3.78	4.05	3.67
- kJ/mol	36.40	35.98	34.72	33.47

This was complementing the initial *in silico* putative binders, however, here it is only possible to say that these ligands show a binding affinity in the middle micromolar range. For a definite binding constant, an additional method like ITC is required, as it could be seen from the obtained dissociation binding constants of L3 and L14, which differed almost 6-fold just from a different batch measurement. However, these data confirmed that the designed ligands have an affinity for the protein and could be improved further by rational design.

From the MST data, the best ligands were tested in an aggregation assay. The obtained results showed that L3 has the highest influence on the inhibition of aggregation of the apo hSOD1 A4V protein, while the other ligands do not have a significant influence.

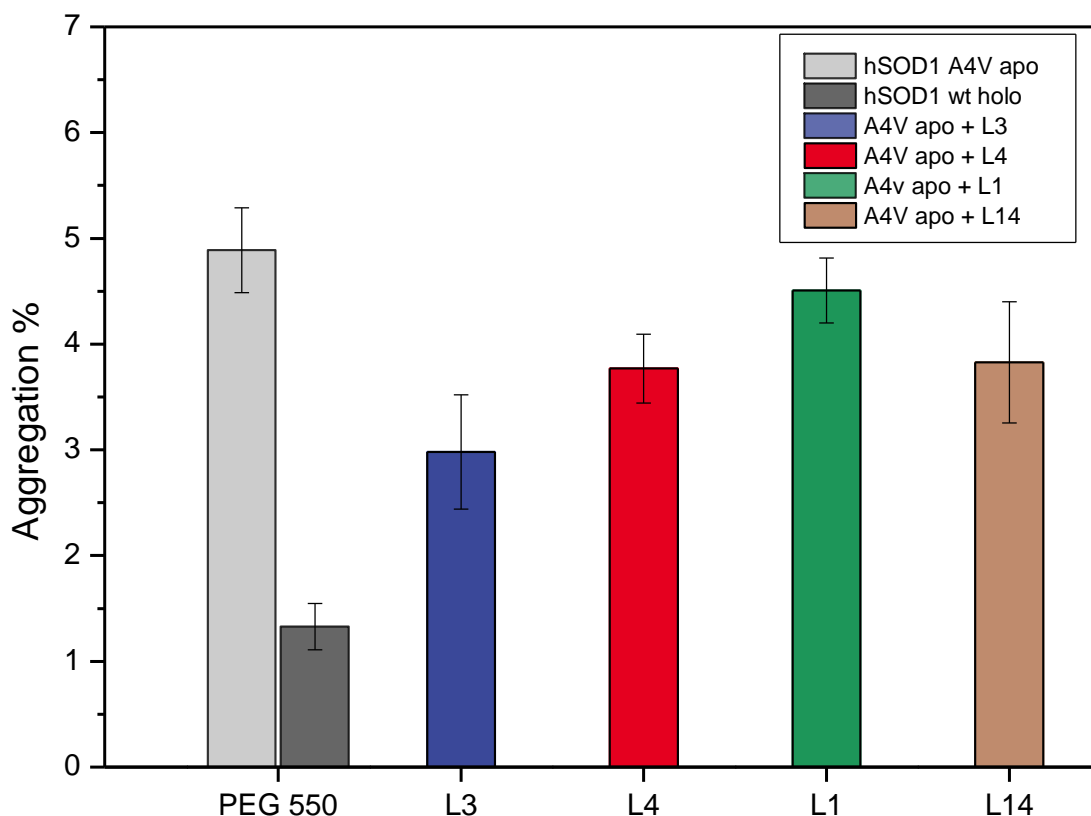


Figure 6.2 Ligands influence on the aggregation of the hSOD1 A4V apo protein. Assay conducted at 50 °C for 24 h with a final protein (20 μM) and ligands (1 mM) concentration in 50 mM sodium phosphate buffer, pH 7.4 and 20% PEG550.

The ligands designed *in silico* correlate well with the results obtained from the biophysical studies. Taken together, designed ligands showed the potential for further development.

The ligand optimization could be beneficial, especially in terms of solubility. Additional attachment of a short PEG-linker could help to increase the solubility. Moreover, the main biphenyl ring can also be considered for introducing more overall polarity to the ligands. In the MST binding affinity studies, more additives could be tested to reduce the DMSO interference. Furthermore, fluorescence studies with the protein should be employed, that can be valuable for further aggregation analysis.

Molecular dynamic studies could be employed to better understand the molecular interactions and the cavity. However, structural information from X-ray crystallography or NMR would be required in order to improve the understanding of the cavity of interest and respective ligands.

7 EXPERIMENTAL SECTION

In this chapter, applied methods and performed experiments to obtain previously mentioned results are described. It is mainly divided into two parts; biophysical protein studies that were done in close collaboration with Lisa-Marie Funk at *Schwann-Schleiden-Forschungszentrum für molekulare Enzymologie*, University of Göttingen. The second part of the experimental section include synthesis and *in silico* design, conducted at the Center for Biostructural Imaging of Neurodegeneration of the University Medical Center Göttingen and the Institute of Organic and Biomolecular Chemistry of the Georg-August University of Göttingen.

7.1 Materials

For the simplicity purpose, the materials, chemicals and other commodities used to conduct experiments in the mentioned research groups will be listed together.

i. Chemicals

Item	Supplier
Acetic acid	Carl Roth GmbH & Co. KG (Karlsruhe, Germany)
Acetonitrile	Fisher Scientific (Leicestershire, UK)
Acrylamide	Carl Roth GmbH & Co. KG (Karlsruhe, Germany)
Agar	AppliChem GmbH (Darmstadt, Germany)
Agarose	AppliChem GmbH (Darmstadt, Germany)

Ammonium sulfate	AppliChem GmbH (Darmstadt, Germany)
APS	Carl Roth GmbH & Co. KG (Karlsruhe, Germany)
Bromophenol blue, sodium salt	AppliChem GmbH (Darmstadt, Germany)
Bovine serum albumin (BSA)	AppliChem GmbH (Darmstadt, Germany)
Calcium chloride, hexahydrate	Carl Roth GmbH & Co. KG (Karlsruhe, Germany)
Carbenicillin, disodium salt	AppliChem GmbH (Darmstadt, Germany)
Coomassie Brilliant Blue G250	AppliChem GmbH (Darmstadt, Germany)
Copper (II) sulfate pentahydrate	Sigma-Aldrich (Munich, Germany)
Dimethyl sulfoxide (DMSO)	Sigma-Aldrich (Munich, Germany)
Dimethyl sulfoxide (DMSO)	ACROS Organics
Dithiothreitol (DTT)	AppliChem GmbH (Darmstadt, Germany)
Ethanol (denatured)	Frau Magerkuth Apotheke (Karlsruhe, Germany)
Ethanol (purest)	Nordhäuser Spirituosen GmbH (Nordhausen, Germany)
Ethidium bromide	Carl Roth GmbH & Co. KG (Karlsruhe, Germany)
Ethylenediaminetetraacetic acid (EDTA)	AppliChem GmbH (Darmstadt, Germany)
Glycerol (anhydrous)	AppliChem GmbH (Darmstadt, Germany)
Guanidinium chloride	AppliChem GmbH (Darmstadt, Germany)
2-[4-(2-hydroxyethyl)piperazin-1-yl] ethanesulfonic acid (HEPES)	AppliChem GmbH (Darmstadt, Germany)
Hydrochloric acid (37 %)	Th. Geyer GmbH & CoKG (Renningen, Germany)
IPTG	Carl Roth GmbH & Co. KG (Karlsruhe, Germany)
Kanamycin sulfate	AppliChem GmbH (Darmstadt, Germany)
Lithium sulfate monohydrate	Thermo Fisher GmbH (Kandel, Germany)
Magnesium chloride, hexahydrate	Carl Roth GmbH & Co. KG (Karlsruhe, Germany)
MES	AppliChem GmbH (Darmstadt, Germany)
b-Mercaptoethanol	Carl Roth GmbH & Co. KG (Karlsruhe, Germany)
Methanol	Carl Roth GmbH & Co. KG (Karlsruhe, Germany)

Phenylmethanesulfonylfluoride (PMSF)	AppliChem GmbH (Darmstadt, Germany)
Polyethylene glycol (PEG) 400	Sigma-Aldrich (Munich, Germany)
Polyethylene glycol (PEG) 550	Sigma-Aldrich (Munich, Germany)
Polyethylene glycol (PEG) 3350	Hampton Research Corp, (CA, USA)
Polyethylene glycol (PEG) 8000	Carl Roth GmbH & Co. KG (Karlsruhe, Germany)
Polysorbat 20 (TWEEN-20)	NanoTemper Technologies GmbH (Munich, Germany)
di-Potassium hydrogen phosphate anhydrous p. A	AppliChem GmbH (Darmstadt, Germany)
Potassium di-hydrogen phosphate anhydrous	AppliChem GmbH (Darmstadt, Germany)
Potassium hydroxide	AppliChem GmbH (Darmstadt, Germany)
SYPRO® Orange protein stain	BioRad Laboratories GmbH (Munich, Germany)
Sodium chloride	AppliChem GmbH (Darmstadt, Germany)
Sodium citrate	AppliChem GmbH (Darmstadt, Germany)
Sodium dodecyl sulfate (SDS)	AppliChem GmbH (Darmstadt, Germany)
Sodium di-hydrogen phosphate	AppliChem GmbH (Darmstadt, Germany)
Sodium di-hydrogen phosphate	Carl Roth GmbH & Co. KG (Karlsruhe, Germany)
Sodium hydroxide	AppliChem GmbH (Darmstadt, Germany)
Sodium sulfate anhydrous	AppliChem GmbH (Darmstadt, Germany)
N,N,N',N'-Tetramethylethylenediamine (TEMED)	Carl Roth GmbH & Co. KG (Karlsruhe, Germany)
2-Amino-2-hydroxymethylpropane-1,3-diol (Tris)	AppliChem GmbH (Darmstadt, Germany)
Tryptone	Carl Roth GmbH & Co. KG (Karlsruhe, Germany)
Zinc Sulfate	Sigma-Aldrich (Munich, Germany)
Yeast extract	AppliChem GmbH (Darmstadt, Germany)

Furthermore, all commercially obtained reagents used for synthetic purpose that are not listed were used as received without further purification if not stated otherwise. Reagents were supplied by Thermo Fisher GmbH (Kandel, Germany), Sigma-Aldrich (Munich,

Germany), ChemPur GmbH (Karlsruhe, Germany), Fluka GmbH (Ulm, Germany), J&K Scientific GmbH (Marbach, Germany), TCI Deutschland GmbH (Eschborn Taunus, Germany), Alfa Aesar and Merck (Darmstadt, Germany). Solvents used in the reactions were of analytical grade. Anhydrous solvents were from Acros Organics (Thermo Fisher Scientific brand), stored over molecular sieves under a nitrogen atmosphere and used without further purification.

ii. Enzymes

Item	Supplier
DNase I	AppliChem GmbH (Darmstadt, Germany)
Lysozyme	AppliChem GmbH (Darmstadt, Germany)
Phusion polymerase	Thermo Fisher Scientific (Braunschweig, Germany)

iii. Bacterial strains

Item	Supplier
<i>E. coli</i> -BL21 (DE3)	Invitrogen TM (Karlsruhe, Germany)
<i>E. coli</i> -BL21 Star™ (DE3)	Invitrogen TM (Karlsruhe, Germany)
<i>E. coli</i> -XL1-Blue	Stratagene, (Heidelberg, Germany)

iv. Plasmids

Name	Supplier
pET303C-hSOD1 ^{wt}	provided by Prof. Samar Hasnain (University Liverpool)

v. Kits and solutions

Item	Supplier
dNTP mix (10 mM)	Thermo Fisher Scientific (Braunschweig, Germany)
NucleoSpin™ Plasmid Kit	Macherey Nagel (Düren, Germany)
NucleoSpin™ Gel and PCR	Macherey Nagel (Düren, Germany) Clean-Up Kit

Bradford reagent, 5x concentrate	SERVA Electrophoresis GmbH (Heidelberg, Germany)
Gel Filtration Standard	Bio-Rad Laboratories GmbH (Munich, Germany)
Pierce™ Unstained Protein MW Marker	Thermo Fisher Scientific (Braunschweig, Germany)
GeneRuler DNA Ladder Mix 0.5µg/µL	Thermo Fisher Scientific (Braunschweig, Germany)
6x DNA Loading Dye	Thermo Fisher Scientific (Braunschweig, Germany)
Monolith Protein Labeling Kit RED-NHS 2nd Generation (MO-L011)	NanoTemper Technologies GmbH (Munich, Germany)
SOD Assay Kit (19160-1KT-F)	Sigma-Aldrich Chemie GmbH (Munich, Germany)

vi. Crystallization screens

Item	Supplier
Additive Screen™ HR-418	Hampton Research Corp, (CA, USA)
The AmSO ₄ Suite	QIAGEN (Hilden, Germany)
Classic Lite	QIAGEN (Hilden, Germany)
Classics	QIAGEN (Hilden, Germany)
Classic II	QIAGEN (Hilden, Germany)
Compass	QIAGEN (Hilden, Germany)
Index	Hampton Research
MBclass	QIAGEN (Hilden, Germany)
MBclassII	QIAGEN (Hilden, Germany)
PACT	QIAGEN (Hilden, Germany)
PEGs	QIAGEN (Hilden, Germany)
pHCLear	QIAGEN (Hilden, Germany)
Protein Complex	QIAGEN (Hilden, Germany)
Wizard Classic 1+2	Rigaku

vii. Commodities

Item	Supplier
Cover plates, 18 mm (siliconized)	Jena Bioscience GmbH, (Jena, Germany)
Cryoloops (0.05 - 0.5 mm)	Hampton Research Corp, (CA, USA)
Crystallization plates, greased	Hampton Research Corp, (CA, USA)
Spin-X UF® 6, 20 mL (5 kDa – 50 kDa MWCO)	Corning GmbH (Berlin, Germany)
ZelluTrans/Roth® dialysis membrane (3.5 kDa MWCO)	Carl Roth GmbH & Co. KG (Karlsruhe, Germany)

viii. Media

LB medium		LB agar plates	
Yeast extract	0.5% (w/v)	Yeast extract	0.5% (w/v)
Tryptone	1% (w/v)	Tryptone	1% (w/v)
NaCl	0.5% (w/v)	NaCl	0.5% (w/v)
		Agar	2% (w/v)

7.1.1 Utilized Primers

i. Mutagenesis primers

Name	Sequence
hSOD1A4V <i>Fwd</i>	5' – GCGACGAAG GTC GTGTGCGTG - 3'
hSOD1A4V <i>Rev</i>	5' – CACGCACAC GAC CTTCGTCGC – 3'
hSOD1C6F <i>Fwd</i>	5' – GACGAAGGCCG TGT TCGTGCTGAAGG – 3'
hSOD1C6F <i>Rev</i>	5' - CCTTCAGCACGA ACA CGGCCTTCGTC - 3'
hSOD1D90A <i>Fwd</i>	5' – CAATGTGACTGCT GCC AAAGATGGTGTGG – 3'
hSOD1D90A <i>Rev</i>	5' – CCACACCATCTTT GGC AGCAGTCACATTG -3'
hSOD1G93C <i>Fwd</i>	5' – CTGACAAAGAT TGC GTGGCCGATGTGT – 3'
hSOD1G93C <i>Rev</i>	5' – ACACATCGGCCAC GCA ATCTTTGTCAG – 3'

ii. Sequencing primers

<i>T7 promotor</i>	5' – TAATACGACTCACTATAGGG – 3'
<i>T7 terminator</i>	5' – AGCTAGTTATTGCTCAGCGG – 3'

7.1.2 Devices

i. Cell cultivation and disruption

Item	Supplier
Biofermenter, Biostat C	Sartorius AG (Göttingen, Germany)
Incubation shaker, Unitron	Infors AG (Bottmingen, Switzerland)
Microfluidizer, M-110S	Microfluidics (Newton, MA, USA)
Multifuge 1S-R	Thermo Scientific

ii. Centrifuges and rotors

Item	Supplier
Avanti™ HP-30I	Beckmann Coulter GmbH (Krefeld, Germany)
Rotor JA-10	Beckmann Coulter GmbH (Krefeld, Germany)
Rotor JA-30.50 Ti	Beckmann Coulter GmbH (Krefeld, Germany)
Avanti™ J-20XPI	Beckmann Coulter GmbH (Krefeld, Germany)
Rotor JLA-8.1000	Beckman Coulter GmbH (Krefeld, Germany)
Centrifuge tubes	Beckman Coulter GmbH (Krefeld, Germany)
Eppendorf 5810R	Eppendorf AG (Wesseling-Berzdorf, Germany)
Rotor A-4-81	Eppendorf AG (Wesseling-Berzdorf, Germany)
Mikro 200	Hettich GmbH & Co. KG (Tuttlingen, Germany)
Rotor 2424 B	Hettich GmbH & Co. KG (Tuttlingen, Germany)
Optima™ L-90K Ultracentrifuge	Beckman Coulter GmbH (Krefeld, Germany)
Rotor SW40 Ti	Beckman Coulter GmbH (Krefeld, Germany)
Rotor SW60 class GH	Beckman Coulter GmbH (Krefeld, Germany)

Universal 320R	Hettich GmbH & Co. KG (Tuttlingen, Germany)
Rotor 1420 A/B	Hettich GmbH & Co. KG (Tuttlingen, Germany)
Rotor 1617 A	Hettich GmbH & Co. KG (Tuttlingen, Germany)
Rotor 1620 A	Hettich GmbH & Co. KG (Tuttlingen, Germany)

iii. Liquid chromatography

Item	Supplier
ÄKTAprime plus	GE Healthcare Europe (Munich, Germany)
ÄKTapurifier	GE Healthcare Europe (Munich, Germany)
HiPrep™ 26/10 desalting (50 mL)	GE Healthcare Europe (Munich, Germany)
HiTrap™ 26/10 desalting (5 mL)	GE Healthcare Europe (Munich, Germany)
Superdex™ 200 HiLoad™ 16/60	GE Healthcare Europe (Munich, Germany)
Fractogel® EMD TMAE 650 (S)	Merck KGaA (Darmstadt, Germany)
Superdex™ 75 10/300 GL	GE Healthcare Europe (Munich, Germany)
Superdex™ 200 10/300 GL	GE Healthcare Europe (Munich, Germany)
Superdex® 200 Increase 10/300 GL	GE Healthcare Europe (Munich, Germany)
Superloop (10 mL, 50 mL, 150 mL)	GE Healthcare Europe (Munich, Germany)

iv. Spectroscopy

Item	Supplier
AV401 NMR spectrometer	Bruker, USA
Avance III 300	Bruker, USA
Avance III HD 500	Bruker, USA
Fluoromax 4 spectrofluorometer	HORIBA Europe GmbH, Oberursel
NanoDropOne	Thermo Scientific, USA
UV-Vis spectrometer, V-650	Jasco GmbH, (Groß-Umstade, Germany)
UV-Vis spectrometer, V-630	Jasco GmbH, (Groß-Umstade, Germany)
UV-Vis spectrophotometer, V-750	Jasco GmbH, (Groß-Umstade, Germany)

Spectrofluorometer, FP-8500	Jasco GmbH, (Groß-Umstade, Germany)
Black quartz glass cuvettes	Hellma GmbH & Co.KG (Mühlheim, Germany)
Precision cuvettes, suprasil	Hellma GmbH & Co.KG (Mühlheim, Germany)
JASCO FT/IR-4100 type A	Jasco GmbH, (Germany)
microTOF	Bruker Daltonics

v. X-ray

Name	Supplier
BeamLine P14	EMBL (Hamburg, Germany)

vi. Miscellaneous

Item	Supplier
Arium®proVF	Sartorius AG (Göttingen, Germany)
C1000 thermal cycler	BioRad Laboratories GmbH (Munich, Germany)
CFX96™ Optical Reaction Module	BioRad Laboratories GmbH (Munich, Germany)
Thermocycler TProfessional	Biometra (Göttingen, Germany)
pH-electrode Minitrode Hamilton	Mettler Toledo GmbH (Giessen, Germany)
Monolith NT.115Pico	NanoTemper Technologies GmbH (Munich, Germany)
Melting point meter (M5000)	A. KRÜSS Optronic GmbH (Hamburg, Germany)
pH-electrode	Mettler-Toledo GmbH (Giessen, Germany)

7.2 Methods

7.2.1 Molecular Biology

7.2.1.1 Plasmid Transformation

Plasmid pET303C-hSOD1wt was obtained from Prof. Samar Hasnain, university of Liverpool. The plasmid was introduced into various chemical competent *E. coli*-strains,

for a different downstream process: multiplication of plasmid (XL1-Blue), and the recombinant protein expression (BL21 (DE3), BL21 Star™ (DE3)). The chemical competent cells were purchased (see Section 7.1).

The chemical competent cells (50 µL) were thawed on ice for 15 min; 1 ng plasmid was added and mixed by flicking. The cells were incubated on ice for 25 min. The transformation was done by heat shock (20 s, 42 °C) according to Inoue et al^[181] followed by incubation on ice for 5 min. The cells were supplied with 1 mL preheated super optimal broth with catabolite repression (SOC) medium, and they were grown for 70 min at 37 °C, 800 rpm.

The transformed cells, containing plasmid of interest, were transferred onto LB-agar plates (see page 118), enriched with appropriate antibiotic carbenicillin (100 µg/mL) and incubated overnight at 37 °C.

7.2.1.2 Isolation of Plasmid DNA

As a preparation step for the isolation of the plasmid DNA, (6 x 10 mL) of LB medium containing carbenicillin (100 µg/mL) were inoculated with single colonies of previously with pET303C-hSOD1wt transformed XL1-Blue cells. The preculture was grown overnight at 37 °C, 200 rpm. Cell culture with (OD₆₀₀ = 3.0 - 3.5) was centrifuged (4 °C, 9000 rpm, 5 min), the pellet was used for plasmid isolation following the High Copy protocol from (Macherey Nagel, Germany) and using NucleoSpin™ Plasmid Kit.

7.2.1.3 Determination of DNA Concentration

The DNA concentration was determined using a Nanodrop One™ device. The absorbance (A_{260}) values were measured at 260 nm using baseline correction at 340 nm. The DNA concentration (c) was calculated according to the Beer-Lambert Equation 7.1 with the extinction coefficient of $\varepsilon = 50 \text{ ng}/\mu\text{L cm}$, and the path length of $d = 1 \text{ cm}$.

$$A_{260} = c * d * \varepsilon$$

7.1

7.2.1.4 DNA Sequencing

The sequence of the isolated plasmid constructs was done by GATC Biotech AG (Constance, Germany). The T7 primers used for sequencing reaction are listed under Section 7.1.1.

7.2.1.5 Polymerase Chain Reaction

As firstly described site-directed mutagenesis Polymerase Chain Reaction (PCR) from Mullis in 1986 ^[182] was used to exchange desired bases by using partially mismatching oligonucleotides for directed mutagenesis. The PCR conditions were adjusted for the respective variants, primers are listed, see Section 7.1.1. To obtain designed variants, QuikChange (Stratagene, La Jolla, USA) protocol was adapted for Phusion® DNA-polymerase. After the PCR, template DNA with unmodified sequence was digested by adding 5 units DpnI and incubated at 37 °C overnight. The digestion was then heat-inactivated at 80 °C for 20 min.

7.2.1.6 Horizontal Agarose Gel Electrophoresis

DNA fragments were separated by their sequence length using agarose gel electrophoresis. DNA samples were mixed with 6x DNA loading dye and loaded onto a 1% agarose gels, containing 1 x TAE buffer (40 mM Tris, 20 mM acetic acid, 1 mM EDTA, pH 7.0). The gels were stained in a 2 µg/mL ethidium bromide solution for 15 min, following visualization with UV-light. DNA fragments size was determined using 1kb DNA-Ladder as a size standard.

7.2.2 Protein preparation

7.2.2.1 Expression of hSOD1 and variants

For expression of the hSOD1 wt and variants, a preculture of 200 mL of sterilized LB medium (10 g/L tryptone, 5 g/L yeast extract, 5 g/L NaCl) with 100 µg/mL carbenicillin was inoculated with two to three colonies of *E. coli* BL21 Star™ (DE3), carrying a specific hSOD1 plasmid. The preculture was incubated overnight at 30 °C with a constant shaking of 200 rpm. The preculture at the final ($OD_{600} = 0.1$) was aliquoted and centrifuged (9000 rpm, 10 °C, 15 min), the supernatant was discarded, and the cell pellets were dissolved again in 4 mL fresh LB medium per 50 mL of preculture. The prepared preculture was used to inoculate the main cultures to an OD_{600} of 0.1 (LB medium was containing the respective antibiotic). The main culture was incubated at 37 °C while shaking at 200 rpm. At OD_{600} of (0.6 - 0.8), expression was induced by addition of 200 mM IPTG (2 mL), and 500 mM ZnSO₄ (1 mL) was added. After induction, it was incubated overnight at 25 °C with constant shaking at 200 rpm. The expression of hSOD1

protein and variants was confirmed via SDS-PAGE. The cells were transferred into 1 L beakers and harvested by centrifugation (20 min, 4800 rpm, 4 °C). The cell pellets were resuspended in approximately 5-10 mL of buffer A (20 mM Tris, pH 8.0) per beaker, transferred to 50 mL falcon tubes and centrifuged for 20 min at 4000 rpm and 4 °C. The cell pellets were flash-frozen in liquid nitrogen and stored at -80 °C for long term storage, or -20 °C for short term storage.

7.2.2.2 Purification of the hSOD1 proteins

Purification of the hSOD1 proteins was done based on the protocol received from Dr. Michael Capper (University of Liverpool), which was further optimized by Lisa-Marie Funk. The cell pellets (approx. 10 g) were resuspended in the loading buffer A (20 mM Tris, pH 8.0), using 4 mL per gram of pellet. While kept on ice it was supplemented with 0.5 mM PMSF, 5 µg/mL DNase I, 5 mM MgCl₂, and a tip of spatula of lysozyme. The cell suspension was stirred for 45 min at 6 °C. Lysis of the homogenous cell suspension was performed using three to five cycles on the Microfluidizer device at 15000 psi. Afterwards, the cells debris were removed by centrifugation (30 min, 75 000 x g, 10 °C). The supernatant was dialyzed twice against 2 L buffer A (20 mM Tris, pH 8.0) for 16 h at 4 °C. Prior to anion-exchange chromatography protein solution was centrifuged for 20 min at 75 000 x g, and 10 °C. The supernatant was loaded onto a TMAE column which was equilibrated with buffer A (20 mM Tris, pH 8.0). Chromatography was performed on the room temperature of approximately 20 °C. The column was washed with buffer A until the baseline was reached and flow-through did not contain any visible amount of unspecific bound proteins. The hSOD1 proteins were eluted in buffer B (20 mM Tris, 500 mM NaCl, pH 8.0) with a gradient of 20% over 3 column volumes (150 mL). Afterwards, the gradient was increased to 100% to elute remaining proteins from the column. SDS-PAGE was used to confirm the purified proteins. Pure fractions of the hSOD1 proteins were pooled together and concentrated via ultrafiltration using concentrator (Corning Spin-X UF, 10K MWCO) up to 5-10 mL. The proteins were then either loaded onto HiPrep 26/10 desalting column equilibrated with the chosen buffer M (100 mM HEPES, 150 mM NaCl, pH 7.4), and stored at -80 °C or utilized further without desalting for dialysis and cofactors reconstitution.

7.2.2.3 SDS-Polyacrylamide Gel Electrophoresis (SDS-PAGE)

Sodium dodecyl sulfate-polyacrylamide gel electrophoresis (SDS-PAGE) is a method used to separate denatured proteins by molecular weight and confirm their purity.^[183] To assign a molecular weight to a different band detected on the gel, protein molecular weight marker was used. The gels were prepared as following: stacking gel (5% acrylamide, 125 mM Tris, 0.1% (w/v) SDS, pH 6.8), and a separating gel (15% acrylamide, 375 mM Tris, 0.1% (w/v) SDS, pH 8.0). Samples for the SDS-PAGE were mixed with the sample buffer (0.1 M Tris, 25% (v/v) glycerol, 2% (w/v) SDS, 0.02% (w/v) bromophenol blue, 2.5% β -mercaptoethanol, pH 6.8) and incubated for 5 minutes at 95 °C. The gels were run at 35 mA, 150 W, and 300 V for 30 min. Afterwards, the gels were stained with solution of (0.25% (w/v) Coomassie Brilliant Blue G250, 30% (v/v) ethanol, and 6% (v/v) acetic acid). Non-protein bound dye was removed by washing with a destaining solution (30% (v/v) ethanol, 10% (v/v) acetic acid).

7.2.2.4 Protein concentration determination

The protein concentrations were determined spectroscopically by measuring the intrinsic absorbance of the Trp amino acid at 280 nm, using the Beer-Lambert Equation (7.1). It was measured on NanoDrop One device using molar extinction coefficients of ($\epsilon_{280} = 5500 \text{ M}^{-1} \text{ cm}^{-1}$) and molecular weight ($M_w = 15936 \text{ kDa}$) calculated with the ProtParam online-tool.^[184] Additionally, the protein concentrations were determined using an assay based on the Bradford method.^[185] Calibrations of the Bradford reagent were done using known concentration (0.1 - 0.9 mg/mL) of bovine serum albumin solutions. Both described methods gave statistically similar values for the protein concentrations. Therefore, we pursued using the intrinsic absorption signal of Trp to determine the hSOD1 protein concentrations.

7.2.2.5 Reconstitution of hSOD1 with Cofactors

Preparation of the apo proteins and further reconstitution with metals was performed after the purification step, as in Section 7.2.2.2. For demetallation of the Zn metal introduced in the expression step, purified proteins were dialyzed for 16 h against 2 L of buffer D1 (100 mM sodium acetate, 5 mM EDTA, pH 3.8) at 4 °C. Additionally, a second dialysis step was done against 2 L of buffer D2 (100 mM sodium acetate, 150 mM NaCl, pH 3.8) for 4 h at 4 °C. Reconstitution of the hSOD1^{wt} protein was performed at room temperature

firstly by incubation of the protein with 10 mM CuSO₄ for 15 min, followed by another 15 min incubation with 10 mM ZnSO₄. Reconstitution process of the hSOD1A4V variant was done on ice. The proteins were then loaded onto HiPrep 26/10 desalting column equilibrated with different buffers for each use, i.e., (20 mM Tris, pH 8.0) for crystallization, and (50 mM sodium phosphate pH 7.4) or (100 mM HEPES, 150 mM NaCl, pH 7.4) for biophysical assays. Protein fractions were pooled together, concentrated via ultrafiltration, as explained before, and stored at -80 °C.

7.2.2.6 Activity assay of the SOD1 proteins

The activity assay of the SOD1 protein, as elaborated in Section 5.3.2 was measured using a Superoxide Dismutase Activity Assay kit (Sigma Aldrich).^[157] The reaction mixture (260 µL) contained 200 µL of WST working solution and 20 µL of a sample (buffer, hSOD1 proteins or ligand and protein) it was incubated for 2 min at 25 °C. The reaction was started by addition of the 40 µL xanthine oxidase to the reaction mixture, and it was measured in the time span of 2 min. Final concentrations of the hSOD1 proteins were in the range of 0.04 µg/mL to 2 µg/mL, in the experiments with the ligand final concentration was 0.5 mM to 1 mM with a maximum of 20% DMSO.

The average triplicate absorbance values at 440 nm were plotted against time. To determine the rate of change in absorbance, the slope from each curve was taken in the time of 0-50s. The % inhibition of the SOD1 proteins was determined as shown in Equation 7.2 where the slope in the absence of the SOD1 protein was the control measurement and was taken as the 100% value.

$$\% \text{ Inhibition} = \frac{\text{slope}(\text{control}) - \text{slope}(\text{sample})}{\text{slope}(\text{control})}$$

7.2

7.2.2.7 Size exclusion chromatography (SEC)

To analyse and separate the oligomerization state of the holo and apo hSOD1 proteins, size exclusion chromatography was performed. The Superdex Increase 200 10/300 GL column was equilibrated with 50 mM sodium phosphate buffer pH 7.4 and 150 µL hSOD1 sample (0.1 mg/mL – 5 mg/mL) was loaded onto the column. The experiment was performed at 4 °C with a flow rate of 0.5 mL/min. Fractions of interest were collected, analysed, and processed for further use. To obtain a calibration curve, gel filtration standard (Bio-Rad Laboratories) was used as in the previously described

experimental setup of the sample. Using Equation 7.3 partition coefficient (K_{av}) was calculated, where V_e is elution volume, V_c geometric column volume and V_0 is void column volume. The calibration curve was plotted using calculated K_{av} versus logarithmic molecular weight values of the BioRad standard. (Figure 9.5).

The molecular weight of the hSOD1 proteins and oligomers was determined from the elution volume of the samples and the calibration curve of the standard.

$$K_{av} = \frac{V_e - V_0}{V_c - V_0}$$

7.3

7.2.3 X-Ray Crystallography

7.2.3.1 Crystallization conditions for hSOD1 proteins

Prior to the crystallization of hSOD1wt, the protein was thawed on ice, centrifuged for 15 min at 4 °C and 13 000 x g, further the protein stocks, concentration (5 - 20 mg/mL, 20 mM Tris buffer, pH 8.0) were prepared. The well solution consisted of 18-22% (w/v) PEG 8000, 0.2 M ammonium sulfate, 0.1 M MES buffer, pH 6.5 with a total volume of 500 μ L. For the crystallization, hanging drop diffusion method was used, two drops were set up per each well, 2 μ L of the protein stock (10 mg/mL) were mixed with 2 μ L of the well solution, and the plates were stored at 20 °C. Crystals grew over a period of 3-10 days. Crystals were incubated with a total time of 1-4 min, the sequentially increasing amount of PEG 8000 50% (w/v) by 5% in cryoprotectant solution with 20% (w/v) DMSO, 0.2 M ammonium sulfate, 0.1 M MES buffer, 1 mM ZnSO₄, 1 mM CuSO₄. Soaking of crystals with ligands L3 (10 mM), L4 (15 mM), L1 (20 mM), L7 (20 mM) and L14 (5 mM) was performed using cryoprotectant solution and soaking them for 1-5 min in the last step.

7.2.3.2 X-ray Data Collection and Refinement

Diffraction data collection was performed using synchrotron radiation at the P14 beamLine at DESY (Hamburg, Germany) under cryogenic conditions (100 K). Diffraction patterns were indexed, integrated and scaled with the XDS package (Kabsch, 2010).^[186] Processing data collection and refinement was done by Lisa-Marie Funk.

7.2.4 Biophysical studies

7.2.4.1 Thermal shift assay

In order to test thermal stability and protein unfolding, thermal shift assay was performed. The concentration range of the hSOD1wt protein and A4V variant were investigated to obtain the concentration for further assays with the target molecules. Typically, the reaction mixture consisted of 50 mM sodium phosphate buffer pH 7.4, with or without 20% of DMSO, 1x SYPRO® Orange protein stain (1:50 dilution of the supplied stock solution), and 1-20 μ M of the hSOD1 protein concentration.

Furthermore, to confirm the interaction, and understand the influence of the ligands (Figure 5.21) on the hSOD1 proteins, the experiment was performed with previously established conditions, with a final ligand concentration of 1 mM, and protein concentration of 1 μ M. Ligands were dissolved in 100% DMSO, with the final DMSO concentration of 20%.

The measurements were performed using a C1000 thermal cycler in the department of Molecular Structural Biology (Institute for Microbiology and Genetics, Georg-August-University Göttingen). The thermal protein unfolding was monitored using a CFX96™ Optical Reaction Module (excitation: 515 – 535 nm, detection: 560 – 580 nm). The temperature range was 20-95 °C with the temperature increment of (1 °C/30 s). Recorded raw data across 96 well plate, was exported and processed with OriginPro 8.5.0 SR1 (OriginLab Corporation, Northampton, Massachusetts, USA).

Melting curves were obtained by plotting data of fluorescence intensity against time. Fluorescence data of the sample triplicates were averaged, and the respective reference sample was subtracted. Analysis of the obtained fluorescence transition signals was done by investigation of the first derivative for a peak maximum, where it represents T_m value. In the case of our measurement, the difference in T_m values was < 1°C, therefore, to confirm the T_m values for different ligands, calculations with a second derivative were done. Linear regression curves were fitted for the specified temperature range, further, the T_m values were calculated from the obtained fit, as x-intercept, when $y=0$.

7.2.4.2 Microscale Thermophoresis

To perform binding studies of the hSOD1 proteins and respective ligands by Microscale Thermophoresis (MST) it was necessary to label the protein. As a labelling strategy, NHS

ester chemistry was used. Protein was labelled using Monolith Labeling Kit (NanoTemper Technologies).^[187] In our case, it was Red dye-NHS 2nd Generation which contains reactive NHS-ester group that can react with the primary amines in the protein (*n*-terminus or ϵ -amino group of lysine) at pH 7-9, and form an amide bond. Before the labelling, proteins were prepared in sodium phosphate buffer, as shown previously in Section 7.2.2.5 and the stock concentration was adjusted to 2-fold of the final concentration (200 μ M). The dye was dissolved in 100% DMSO to a stock concentration of 600 μ M. For the labelling reaction, final concentration of the protein and dye was adjusted to the 1:1 ratio, it was mixed shortly by pipetting, and incubated for 1.5 h in the dark at room temperature. Following, the unreacted free dye was removed via Superdex 200 10/300 GL column as described in Section 7.2.2.7.

Afterwards, protein concentration and degree-of-labelling (DOL) were calculated. Absorbance spectrum was measured using UV/Vis spectrophotometer (see Section 7.1.2). Protein absorbance values at a wavelength of 280 nm (A_{280}) and the maximum wavelength at 650 nm (A_{650}) were used for concentration determination. Protein concentration was calculated using the adjusted Beer-Lambert Equation 7.4. where: $\epsilon_{Prot} = 10\,800\,M^{-1}cm^{-1}$ is the extinction coefficient of the hSOD1 dimer^[70], absorbance value at 650 nm (A_{650}) is the maximum wavelength observed which is characteristic of the red dye, $cf = 0.04$ is the correction factor of the dye for absorbance at 280 nm, and $d = 1$ cm is the instrument path length.

$$c_{Prot} = \frac{A_{Prot}}{\epsilon_{Prot} \cdot d} = \frac{A_{280} - (A_{650} \cdot cf_{280})}{\epsilon_{Prot} \cdot d}$$

7.4

The concentration of the dye was calculated using the Beer-Lambert Equation with the extinction coefficient of the dye $\epsilon_{dye} = 195\,000\,M^{-1}cm^{-1}$. Calculation of the labelling efficiency; DOL was obtained as dye/protein concentration ratio.^[187] A degree of labelling between 0.3 - 1.1 was achieved.

Binding experiments with the ligands explained in Section 5.4.1 were performed as follows. The concentration of the labelled hSOD1wt protein was adjusted to 10 nM with the assay buffer, it consisted of 50 mM sodium phosphate pH 7.4, 20% DMSO and 0.05% Tween 20. Following, sixteen ligands concentrations were prepared in the range from 30.4 nM to 20 mM using ligand buffer (50 mM sodium phosphate buffer, pH 7.4 and 20% DMSO) with 1:1 dilution series. Thus, prepared ligand dilution series was mixed with a labelled protein, producing final concentrations i.e., (5 nM of hSOD1wt NHS labelled

protein and ligand concentrations ranging from 15.2 nM to 10 mM). Samples were centrifuged at $10\,000 \times g$ for 2 - 5 min. After 2 h incubation at room temperature samples were loaded into Monolith NT.115 Premium Capillaries (NanoTemper Technologies). MST experiment was performed using a Monolith NT.115 Pico instrument (NanoTemper Technologies) with 10% LED power and medium MST power at 22 °C. Data of three independently pipetted measurements were analysed with MO. Affinity Analysis software version 2.3 (NanoTemper Technologies) using the signal from an MST-on time of 1.5 s. The dissociation constant (K_d) was estimated from the law of mass action by fitting function with Equation 7.5.

$$f(c_L) = F_{norm T} + (F_{norm LT} - F_{norm T}) \cdot \frac{c_L + c_T + K_d - \sqrt{(c_L + c_T + K_d)^2 - 4 \cdot c_L \cdot c_T}}{2c_T} \quad 7.5$$

Where the $f(c_L)$ is the fraction bound at a given ligand concentration c_L ; F_{norm} is normalized MST trace value, it is calculated by dividing the average fluorescence signal in the heated state when the laser is turned on (F_{hot}) by the average fluorescence signal when the IR laser is turned off (F_{cold}). L , T , LT represent ligand, target protein, and ligand-protein complex, respectively.

7.2.4.3 Isothermal titration calorimetry (ITC)

For an ITC experiment, hSOD1^{wt} was reconstituted with Cu^{2+} and Zn^{2+} in 100 mM hepes, 150 mM NaCl buffer, pH 7.4, ligands were dissolved in the same buffer with 20% DMSO or glycerol. Before the experiment protein and ligands were degassed for 2 min and the measurement cell was flushed with 50 – 200 μ L of the sample before loading. In the experiment at 25 °C, 10 mM ligand in hepes buffer with 20% of respective additive was titrated into hSOD1 dimer (175 μ M) with the same additive concentration in the cell as in syringe at the rate of 2 μ L every 2 min. Experiments were conducted on MicroCal PEAQ-ITC (Malvern), and ITC data were obtained from analysis software. (Experiments were performed and evaluated by Lisa-Marie Funk).

7.2.4.4 Aggregation assay

In order to analyse the influence of the ligands to the proteins, aggregation assays were conducted. To confirm and determine a low level of aggregated protein PROTESOTAT® Protein Aggregation assay kit ENZ-51023-KP050 [188] was tested, with slightly modified

protocol, the assay was adjusted and aggregation was monitored with the use of a ThT dye (extinction coefficient used for concentration determination was $31600 \text{ M}^{-1}\text{cm}^{-1}$).^[189] hSOD1 proteins (20 μM) were incubated for up to 48 h at temperatures between 0 °C to 50 °C in 50 mM sodium phosphate buffer, pH 7.4 with or without ligands (1 mM) in presence of 20% DMSO, PEG550, or other additives where indicated. After respective incubation time, PROTESOSTAT® detection dye was added with a final concentration of 1000-fold dilution in the assay, while in the assay with the ThT dye final concentration was 15 μM . The aggregation experiment was monitored using a Cytation3 instrument, and fluorescence was read at 25 °C, with an optics set to be measured from the bottom, and the gain value set to 100. Excitation and emission were set to 550 nm and 600 nm for PROTESOSTAT® detection dye, and at 440 nm and 480 nm for the assay with the ThT dye, respectively. Aggregated and monomeric lysozyme controls were used in the assay and had the final concentration of (15 or 20 μM). For a quantitative result of the aggregates in the solution, the reference sample of aggregated IgG protein, PROTESOSTAT® aggregation standard was used.^[190] From the linear regression fit of the standard curve, the slope coefficient was obtained and was used for the calculation of aggregates % in the sample, respective blanks RFU values were subtracted. Data was exported, evaluated, and plotted with OriginPro 8.5.0 SR1 (OriginLab Corporation, Northampton, Massachusetts, USA), see Section 5.4.4.

7.3 *In silico* design and molecular docking

7.3.1 Preparation of protein and ligands structure for docking

The crystal structures of the hSOD1wt protein with a PDB codes 2V0A, 2C9U were obtained from the RCSB protein data bank.^[191] They were compared and 2V0A was used for *in silico* docking. All water molecules were removed, polar hydrogen atoms and charges were added with AutoDock Tools (ADT) software version 1.5.6 as shown by Forli *et al.*^[192] Additionally, so prepared protein structure was converted from the PDB file format to the PDBQT format that is needed for the AutoDock Vina 1.1.2 docking software.^[106,193]

Ligands structures were prepared using Chem3D software version 15.1 and saved as a PDB file format. The ligands were further prepared with AutoDock tools by assigning

and confirming rotatable bonds, all functional groups were assigned as flexible except for amide bonds. Prepared ligands were saved in PDBQT format for docking analysis.

7.3.2 Docking procedure with AutoDock Vina

Molecular docking was performed using the AutoDock Vina 1.1.2 software. Protein and ligands were prepared as described. Ligands were docked individually to the protein receptor. The big grid-box was set to the size of 38 x 30 x 42 Å in x, y and z dimensions with the centre at 20.41, -0.008, and 13.315, respectively, and a grid spacing of 1000 Å. Small grid-box was centred at x = 14.383, y = 0.003, and z = 13.503 with a size of 26 x 24 x 24. A total exhaustive search was set to 200. Docking parameters were set as default, with a total of nine output conformations without randomization of the ligand prior docking. Ligand-binding affinities were predicted as a negative Gibbs energy in kcal/mol using a scoring function from AutoDock Vina and RMSD cut off at 4Å.^[106] Visualization of ligands and proteins was performed using UCSF Chimera visualization modelling software.^[44]

7.4 Synthesis of ligand molecules

7.4.1 Analytics

i. NMR Spectroscopy

NMR spectra were recorded on one of the following devices: BRUKER Avance III 300 or BRUKER Avance III HD 500. Coupling constants are given in Hertz (Hz). Multiplicities are abbreviated as follows: singlet (s), doublet (d), triplet (t), quartet (q), doublet of doublets (dd), doublet of triplets (dt), triplet of doublets (td), doublet of doublet of triplets (ddt), triplet of doublet of doublets (tdd). The chemical shifts of the deuterated solvents acetone-d₆ (2.05 ppm; 29.84 ppm, 206.26 ppm), (CDCl₃ (7.26 ppm; 77.16 ppm), MeOD d₄ (3.31 ppm; 49.00 ppm), DMSO d₆ (2.50 ppm; 39.52 ppm), CD₂Cl₂ (5.32 ppm; 53.84 ppm), THF d₈ (1.72 ppm; 3.58 ppm, 25.31 ppm, 67.21 ppm), D₂O (4.79 ppm) were used as an internal standard for (¹H NMR; ¹³C NMR), respectively.^[194]

ii. Mass Spectrometry

Mass spectra were recorded using a microTOF mass spectrometer manufactured by BRUKER DALTONICS. For ionisation, electron ionisation (EI) or electrospray

ionization (ESI) was applied and detection was conducted using a time-of-flight (TOF) detector. All data is given in m/z values and the peak intensities are normalized in EI to the intensity of the respective mol peak.

iii. UV/Vis Spectroscopy

UV absorption of a sample was measured on a V-750 spectrometer from JASCO using the Spectra Manager software provided by the manufacturer. Black quartz glass cuvettes from Hellma Analytics 104 (Müllheim, Germany) with 10 mm light path were used. The sample volume was 120 μL . The temperature was set to 25 $^{\circ}\text{C}$, the scanning speed to 200 nm/min with fast response and the bandwidth to 2.0 nm. Typically, the absorption was monitored over 30 s and the mean value was calculated.

iv. IR spectroscopy

IR spectra were measured from the solid or oil compounds using a JASCO FT/IR 4100 type A spectrometer. Wavenumbers ν are given in cm^{-1} .

v. Melting point analysis

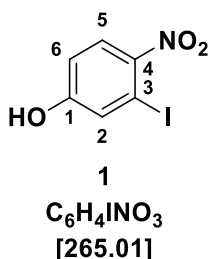
Melting points were measured using a Krüss melting point meter (M 5000) and capillary tubes for melting point determination.

vi. Reactions under anhydrous and/or oxygen-free conditions

Standard Schlenk techniques were applied for conversions under anhydrous and/or oxygen-free conditions. Argon (99.999 %) was used as a protective gas, and all glassware was flame dried in vacuo and vented with argon. This was repeated three times in total.

7.4.2 Synthetic procedures

7.4.2.1 3-Iodo-4-nitrophenol (1)



Over 15 min, fuming nitric acid (730 μ L, 17.5 mmol, 1.00 eq), which was dissolved in glacial acetic acid (3 mL) was added to a cooled solution of 3-iodophenol (3.50 g, 15.9 mmol, 0.91 eq) dissolved in glacial acetic acid (15 mL). The reaction mixture was allowed to warm up to room temperature and was stirred for 30 min, the solution was poured on ice and concentrated *in vacuo*. The mixture was dissolved in water (40 mL) and extracted with DCM (3 x 70 mL). The combined organic layers were dried over anhydrous magnesium sulfate and the solvent was removed *in vacuo*. Afterwards a flash chromatography on silica gel (*n*-hexane/EtOAc, 9:1 + 0.5% AcOH) was performed. The product was obtained as a yellow solid (1.54 g, 5.80 mmol, 37%).

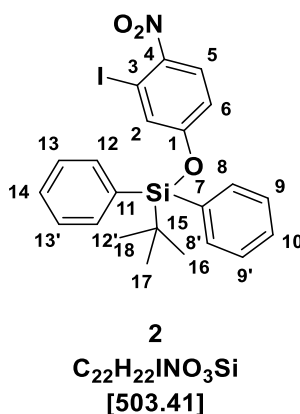
TLC: $R_f = 0.05$ (*n*-hexane/ EtOAc, 9:1 + 0.5% AcOH).

1H NMR (400 MHz, DMSO): δ (ppm) 11.08 (s, 1H, OH), 7.94 (dd, $J = 9.0, 0.6$ Hz, 1H, H-5), 7.45 (d, $J = 0.5$ Hz, 1H, H-2), 6.92 (dd, $J = 9.0, 2.6$ Hz, 1H).

^{13}C NMR (76 MHz, DMSO) δ (ppm) 161.83 (1C, C-1), 149.45 (C1, C-4), 143.89 (C1, C-5), 127.94 (1C, C-2), 115.67 (1C, C-6), 90.46 (1C, C-3).

MS (ESI-): 263.9 ([M-H]⁻).

HR-MS (ESI-): calc. for $C_6H_4NO_3I$ ([M-H]⁻): 263.9163, found: 263.9166.

7.4.2.2 *Tert*-butyl(3-iodo-4-nitrophenoxy)diphenylsilane (**2**)

In a schlenk flask under an argon atmosphere, 3-iodo-4-nitrophenol (1.00 g, 3.77 mmol, 1.0 eq) was dissolved in anhydrous DCM (11 mL), Et₃N (1.0 mL, 7.5 mmol, 2.0 eq) was added, and the reaction mixture was stirred for 5 min. Then, TBDPSCl (1.96 mL, 7.55 mmol, 2.0 eq) was added, and the reaction mixture was stirred for 48 h, and monitored by TLC (*n*-hexane/EtOAc, 19:1). The reaction mixture was washed with sat. aq. NaHCO₃ solution (20 mL), extracted with DCM (3 x 25 mL). Organic layers were washed with sat. aq. NaCl solution (50 mL), dried over MgSO₄ and concentrated *in vacuo*. The title compound was obtained as a yellow oil (1.77 g, 3.51 mmol, 93%), after purification by flash column chromatography (*n*-hexane/EtOAc, 19:1). NMR analysis confirmed that only ~50% is a product, hence the portion of the title compound was purified via HPLC in a gradient 80% to 100%, so the total final yield cannot be given.

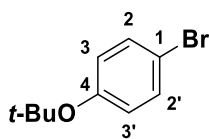
TLC: $R_f = 0.34$ (*n*-hexane/EtOAc, 19:1)

¹H NMR (300 MHz, DMSO) δ (ppm) 7.68 – 7.62 (m, 4H, H-8, H-8', H-12, H-12'), 7.59 – 7.34 (m, 7H, H-2, H-9, H-9', H-10, H-13, H-13', H-14), 6.96 (t, $J = 8.2$ Hz, 1H, H-6), 6.44 (dd, $J = 8.4, 1.0$ Hz, 1H, H-5), 0.95 (s, 9H, H-16, H-17, H-18).

¹³C NMR (76 MHz, DMSO) δ (ppm) 146.12 (1C, C-1), 134.81 (4C, C-8, C-8', C-12, C-12'), 131.48 (1C, C-5), 130.81 (1C, C-2), 128.40 (6C, C-7, C-11, C-9, C-9', C-13, C-13'), 119.31 (1C, C-6), 87.40 (1C, C-3), 25.67 (3C, C-16, C-17, C-18), 18.78 (1C, C-15).

MS (ESI⁺): 526.0 ([M+Na]⁺)

HR-MS (ESI⁺): calc. for C₂₂H₂₂INO₃Si ([M+Na]⁺): 526.0306, found: 526.0292 calc. for C₂₂H₂₂INO₃Si ([M+K]⁺): 542.0056, found: 542.0027

7.4.2.3 1-Bromo-4-(*tert*-butoxy) benzene (4)

4
 $C_{10}H_{13}BrO$
 [229.12]

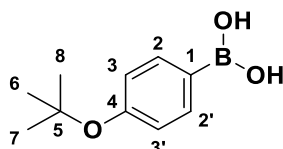
In a one-neck flask under an argon atmosphere, 4-bromophenol (15.0 g, 86.7 mmol, 10 eq) was mixed with pyridine (701 μ l, 8.67 mmol, 1.0 eq). The reaction mixture was stirred for 5 min, and *tert*-butyl bromide (973 μ l, 8.67 mmol, 1.0 eq) was added. The clear reaction mixture was stirred for 6 h. The yellowish reaction mixture was poured into a water-ethylene glycol (8/1) mixture (30 mL) and extracted with *n*-pentane (3 x 40 mL). The organic layer was washed with 5% aq. NaOH solution (40 mL), water (2 x 40 mL), and dried over $MgSO_4$. The title compound was isolated as a colourless liquid (980 mg, 4.27 mmol, 49%) after purification by flash column chromatography (*n*-hexane/ EtOAc, 95:5).

TLC: $R_f = 0.51$ (*n*-hexane/EtOAc, 95:5)

1H NMR (300 MHz, DMSO- d_6): δ (ppm) 7.43 (d, $J = 8.9$ Hz, 2H, H-2, H-2'), 6.92 (d, $J = 8.9$ Hz, 2H, H-3, H-3'), 1.28 (s, 9H, -*t*Bu).

^{13}C NMR (75 MHz, DMSO- d_6): δ (ppm) 154.18 (1C, C-4), 131.49 (2C, C-2, C-2'), 125.40 (2C, C-3, C-3'), 114.77 (1C, C-1), 78.30 (1C, -*t*Bu), 28.31 (3C, -*t*Bu).

MS (EI+): m/z (%) calc. for $C_{10}H_{13}BrO$ found: 228.0157 (80), 230.0170.

7.4.2.4 4-(*Tert*-butoxy)phenyl)boronic acid (5)

5
 $C_{10}H_{15}BO_3$
 [194.04]

In a three-neck Schlenk flask, equipped with a reflux condenser under an argon atmosphere Mg (331.2 mg, 13.62 mmol, 3.0 eq) and LiCl (240.67 mg, 5.67 mmol, 1.25 eq) were dissolved in anhydrous THF (6 mL). The solution of 4-bromophenol *t*-butyl

ether (1.05 g, 4.54 mmol, 1.0 eq) in anhydrous THF (5 mL) was added. The reaction mixture was heated up until reflux, and the colour turned dark grey/black, further it was stirred for 1 h at room temperature. Afterwards, the reaction mixture was transferred with a cannula to a one-neck flask under argon, B(OEt)₃ (2.30 mL, 13.6 mmol, 3.0 eq), and anhydrous THF (15 mL) were added. The reaction was stirred for 90 min, and then HCl (1 M, 15 mL, 3.3 eq) was added, stirred for 30 min, and extracted with EtOAc (3 x 60 mL). The organic layer was washed with sat. aq NaCl solution (30 mL), dried over MgSO₄ and concentrated *in vacuo*. The title compound was obtained as a white solid (208 mg, 1.07 mmol, 23%) after purification by flash column chromatography (DCM/MeOH, 19:1).

TLC: $R_f = 0.6$ (DCM/MeOH, 19:1)

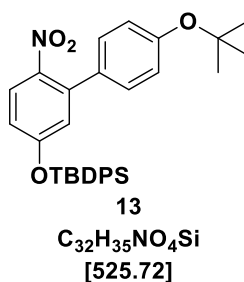
¹H NMR (300 MHz, DMSO-d₆) δ (ppm) 7.81 – 7.76 (m, 2H, H-2, H-2'), 6.97 – 6.90 (m, 2H, H-3, H-3'), 1.31 (s, 9H, H-6, H-7, H-8).

¹³C NMR (75 MHz, DMSO-d₆) δ (ppm) 156.52 (1C, C-4), 134.41 (2C, C-2, C-2'), 122.41 (2C, C-3, C-3'), 77.80 (1C, C-5), 28.67 (3C, C-6, C-7, C-8).

FT-IR (Diamond-ATR): ν (cm⁻¹) 2978, 1743, 1602, 1561, 1362, 1338, 1238, 1153, 895.

HR-MS (ESI-): calc. for C₁₀H₁₅O₃Br ([M-H]⁻): 193.1043, found: 193.1042

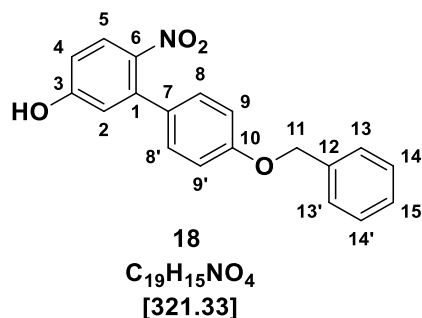
7.4.2.5 ((4'-(*Tert*-butoxy)-6-nitro-[1,1'-biphenyl]-3-yl)oxy)(*tert*-butyl)diphenylsilane (13)



In a one-neck flask under argon, *tert*-butyl(3-iodo-4-nitrophenoxy)diphenyl silane (79.0 mg, 0.160 mmol, 1.0 eq), 4-(*tert*-butoxy)phenylboronic acid (68.0 mg, 0.350 mmol, 2.2 eq), barium hydroxide (76.1 mg, 0.44 mmol, 2.8 eq), and Pd(PPh₃)₄ (20.0 mg, 0.016 mmol, 10 mol%) were dissolved in 5 mL of dioxane/water (4:1 *v/v*) mixture, which was previously degassed in an argon stream. The reaction mixture was stirred at 75 °C for 24 h. Afterwards, the TLC analysis (*n*-hexane/EtOAc, 9:1) still showed starting material, therefore it was stirred for 24 h more at 100 °C. The reaction

mixture was washed with sat. aq. NH_4Cl (40 mL) and extracted with EtOAc (3 x 50 mL). The organic layers were washed with sat. aq. NaCl (2 x 50 mL), dried over MgSO_4 and concentrated *in vacuo*, as a yellow/orange crude solid (126 mg). The title compound was not confirmed with mass analysis of the crude solid.

7.4.2.6 4'-(Benzyloxy)-6-nitro-[1,1'-biphenyl]-3-ol (18)



In a dry 100 mL two-neck Schlenk flask, which was equipped with a reflux condenser, and in an argon atmosphere, 3-iodo-4-nitrophenol (1.50 g, 5.66 mmol, 1.0 eq), (4-(benzyloxy)phenyl)boronic acid (1.94 g, 8.49 mmol, 1.5 eq), TBAI (167.25 mg, 0.45 mmol, 0.08 eq), K_2CO_3 (3.52 g, 25.47 mmol, 4.5 eq) and $\text{Pd}(\text{PPh}_3)_4$ (170 mg, 0.147 mmol, 2.6 mol%) were dissolved in MeOH/ H_2O (4/1) mixture (20 mL), which was previously degassed under an argon stream for 1.5 h. The mixture was refluxed for 6 h, while the reaction was monitored by TLC (DCM/MeOH 50:1). As the 3-iodo-4-nitrophenol has the same R_f value, as the title compound, the reaction mixture was stirred for an additional 12 h at room temperature. The mixture was filtered, washed with EtOAc (30 mL), and the filtrate was concentrated *in vacuo*. The residue was dissolved in H_2O (60 mL) and sat. aqueous NaHCO_3 solution (40 mL) and extracted with EtOAc (3 x 50 mL). The combined organic layers were washed with sat. aqueous NaCl solution (60 mL), dried over anhydrous Na_2SO_4 , filtered, and concentrated *in vacuo*. The title compound was obtained after flash column chromatography (DCM/MeOH, 50:1) as a yellow solid (1.63 g, 5.09 mmol, 90 %).

TLC: $R_f = 0.47$ (DCM/MeOH 50:1).

mp.: 130 °C - 131 °C

^1H NMR (400 MHz, DMSO) δ (ppm) 10.85 (s, 1H, -OH), 7.90 (d, $J = 8.9$ Hz, 1H, H-5), 7.51 – 7.44 (m, 2H, H-13, H-13'), 7.44 – 7.37 (m, 2H, H-14, H-14'), 7.41 – 7.30 (m, 1H, H-15), 7.26 – 7.17 (m, 2H, H-8, H-8'), 7.10 – 7.02 (m, 2H, H-9, H-9'), 6.88 (dd, $J = 8.9, 2.7$ Hz, 1H, H-4), 6.74 (d, $J = 2.6$ Hz, 1H, H-2), 5.14 (s, 2H, H-11).

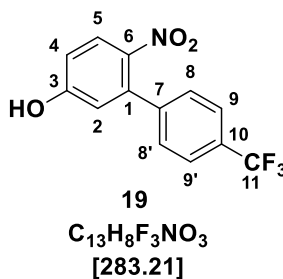
^{13}C NMR (101 MHz, DMSO) δ (ppm) 161.29 (1C, C-3), 158.18 (1C, C-10), 140.38 (1C, C-6), 138.38 (1C, C-1), 136.94 (1C, C-12), 130.29 (2C, C-8, C-8'), 128.88 (2C, C-13, C-13'), 128.46 (2C, C-14, C-14'), 127.89 (1C, C-7), 127.76 (1C, C-5), 127.35 (1C, C-15), 117.99 (1C, C-4), 114.78 (2C, C-9, C-9'), 114.45 (1C, C-2), 69.29 (1C, C-11).

MS (ESI-): 320.1 ([M-H]⁻), 641.2 ([2M-H]⁻).

HR-MS (ESI-): calc. for C₁₉H₁₅NO₄ ([M-H]⁻): 320.0928, found: 320.0925.

FT-IR (Diamond-ATR): ν (cm⁻¹) 3750.87, 3398.92, 1734.66, 1588.09, 1505.17, 1324.86, 1001.84.

7.4.2.7 6-Nitro-4'-(trifluoromethyl)-[1,1'-biphenyl]-3-ol (19)



In a dry 100 mL two-neck Schlenk flask, which was equipped with a reflux condenser, and under an argon atmosphere, 3-iodo-4-nitrophenol (1.60 g, 5.66 mmol, 1.0 eq), (4-(trifluoromethyl)phenyl)boronic acid (1.63 g, 8.49 mmol, 1.5 eq), TBAI (167.25 mg, 0.450 mmol, 0.08 eq), K₂CO₃ (3.52 g, 25.5 mmol, 4.5 eq) and Pd(PPh₃)₄ (170 mg, 0.147 mmol, 2.6 mol%) were dissolved in MeOH/H₂O (4/1) solvent mixture (20 mL), which was previously degassed under an argon stream for 1.5 h. The mixture was refluxed for 30 h, and the reaction was monitored by TLC (DCM/MeOH, 50:1). The brown/orange mixture was filtered, the precipitate washed with EtOAc (30 mL) and the filtrate concentrated *in vacuo*. The residue was suspended in H₂O (60 mL) and sat. aqueous NaHCO₃ solution (40 mL) and extracted with EtOAc (3 x 50 mL). The combined organic layers were washed with sat. aqueous NaCl solution (60 mL), dried over anhydrous MgSO₄, filtered, and the solvent was removed *in vacuo*. The title compound was obtained after purification by flash column chromatography (DCM/MeOH, 100:1) as a yellow solid (962 mg, 3.40 mmol, 60 %).

TLC: R_f = 0.5 (DCM/MeOH, 100:1)

mp.: 113 °C – 114 °C

¹H NMR (300 MHz, cd₂cl₂) δ (ppm) 8.02 (dd, *J* = 9.0, 0.3 Hz, 1H, H-5), 7.75 – 7.64 (m, 2H, H-8, H-8'), 7.50 – 7.38 (m, 2H, H-9, H-9'), 7.04 – 6.88 (m, 1H, H-2), 6.85 – 6.77 (m, 1H, H-2).

¹³C NMR (126 MHz, cd₂cl₂) δ (ppm) 159.64 (1C, C-3), 142.36 (1C, C-6), 138.72 (1C, C-7), 128.25 (4C, C-8, C-8', C-5, C-7), 127.95 (3C, C-9, C-9', C-10), 125.67 (1C, C-11), 118.84 (1C, C-4), 115.65 (1C, C-2).

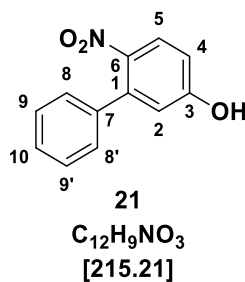
¹⁹F NMR (282 MHz, cd₂cl₂) δ (ppm) -60.62

MS (ESI-): 282.0 ([M-H]⁻), 565.0 ([2M-H]⁻)

HR-MS (ESI-): calc. for C₁₃H₈F₃NO₃ ([M-H]⁻): 282.0384, found: 282.0380.

FT-IR (Diamond-ATR): ν (cm⁻¹) 3422.06, 1589.06, 1512.88, 1319.07, 1109.83, 850.454, 702.926.

7.4.2.8 6-Nitro-[1,1'-biphenyl]-3-ol (21)



To a solution of 3-phenylphenol (2.50 g, 14.6 mmol, 1.0 eq) in acetic acid (15 mL), HNO₃ (3 mL, 6 M, 18.0 mmol) was added dropwise within 15 min, while cooling on an ice bath. Afterwards, the reaction mixture was stirred for 2.5 h at ambient temperature. To the dark brown reaction mixture water (60 mL) was added, and the mixture was extracted with DCM (4 x 60 mL). The organic phase was washed with sat. aq. NaCl solution (100 mL), dried over Na₂SO₄, filtered, and the solvent was removed *in vacuo*. The residue was purified by flash column chromatography using a gradient of (*n*-hexane/EtOAc, 10:1 to 1:1) as an eluent to give 4-nitrobiphenyl-3-ol (822 mg, 3.82 mmol, 26%) as a yellow solid and a mixture of 2-nitrobiphenyl-3-ol and 6-nitrobiphenyl-3-ol as a brown oil. The brown oily mixture was purified by silica gel flash column chromatography using (DCM/MeOH, 50:1) as eluent to give 2-nitrobiphenyl-3-ol (443 mg, 2.05 mmol, 14%) as a brown solid, and the title compound (1.29 g, 5.99 mmol, 41%) as a brown oil.

TLC: *R*_f = 0.47 (DCM/MeOH, 50:1)

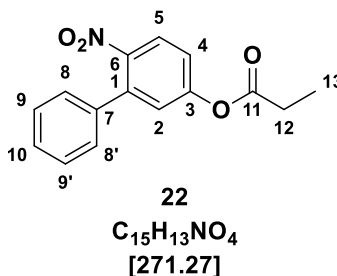
^1H NMR (600 MHz, CDCl_3) δ (ppm) 7.79 (d, $J = 9.0$ Hz, 1H, H-5), 7.30 – 7.22 (m, 2H, H-8, H-8'), 7.17 – 7.10 (m, 3H, H-9, H-9', H-10), 6.73 (dd, $J = 8.9, 2.7$ Hz, 1H, H-4), 6.67 (d, $J = 2.7$ Hz, 1H, H-2).

^{13}C NMR (126 MHz, CDCl_3) δ (ppm) 159.28 (1C, C-3), 139.66 (1C, C-1), 137.87 (1C, C-6), 128.41 (2C, C-8, C-8'), 127.99 (1C, C-7), 127.61 (2C, C-9, C-9'), 127.17 (1C, C-10), 118.48 (1C, C-4), 114.52 (1C, C-2).

MS (ESI+): 238.1 ($[\text{M}+\text{Na}]^+$)

HR-MS (ESI+): calc. for $\text{C}_{12}\text{H}_9\text{NO}_3$ ($[\text{M}+\text{H}]^+$): 216.0655, found: 216.0658. calc. for $\text{C}_{12}\text{H}_9\text{NO}_3$ ($[\text{M}+\text{Na}]^+$): 238.0475, found: 238.0478

7.4.2.9 6-Nitro-[1,1'-biphenyl]-3-yl propionate (22)



In a dry 100 mL schlenk flask, and in an argon atmosphere, 6-nitro-[1,1'-biphenyl]-3-ol (390 mg, 1.81 mmol, 1.0 eq) was dissolved in anhydrous DCM (10 mL). To this solution propionic acid (0.270 mL, 3.62 mmol, 2.0 eq), and DMAP (22.1 mg, 0.18 mmol, 0.1 eq) were added. The mixture was stirred for 15 min. In a second dry 50 mL Schlenk flask, and under argon, EDC-HCl was dissolved in anhydrous DCM (20 mL) and added to the reaction mixture. After complete addition of EDC-HCl, the flask was rinsed with additional 10 mL of anhydrous DCM. The reaction mixture was stirred at ambient temperature for 12 h. The yellowish reaction mixture was washed with aq. HCl solution (1M, 30 mL), water (30 mL), sat. aq. NaHCO_3 solution (50 mL) and sat. aq. NaCl solution (50 mL). The organic layer was dried over MgSO_4 , filtered, and the solvent was removed *in vacuo* to give a yellow oil (500 mg). The title compound was isolated as a yellow solid (420 mg, 1.56 mmol, 85%) after purification by flash column chromatography (*n*-hexane/EtOAc, 4:1).

TLC: $R_f = 0.40$ (*n*-hexane/EtOAc, 4:1)

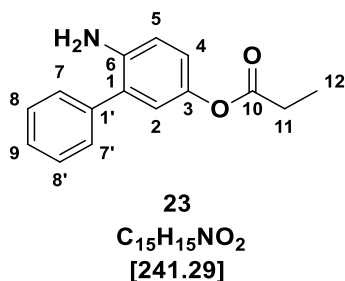
¹H-NMR (300 MHz, cd₂cl₂): δ (ppm) 7.92 (dd, *J* = 8.8, 0.4 Hz, 1H, H-5), 7.48 – 7.40 (m, 3H, H-8, H-8', H-2), 7.34 – 7.28 (m, 2H, H-9, H-9'), 7.26 – 7.18 (m, 2H, H-10, H-4), 2.62 (q, *J* = 7.5 Hz, 2H, H-12), 1.32 – 1.16 (m, 3H, H-13).

¹³C-NMR (126 MHz, cd₂cl₂) δ (ppm) 172.23 (1C, C-11), 153.51 (1C, C-3), 146.36 (1C, C-6), 138.45 (1C, C-1), 137.21 (1C, C-7), 128.86 (2C, C-9, C-9'), 128.63 (1C, C-10), 128.01 (2C, C-8, C-8'), 126.00 (1C, C-5), 125.26 (1C, C-4), 121.59 (1C, C-2), 28.02 (1C, C-12), 9.04 (1C, C-13).

MS (ESI+): 294.1 ([M+Na]⁺)

HR-MS (ESI+): calc. for C₁₅H₁₃NO₄ ([M+Na]⁺): 294.0737, found: 294.0736.

7.4.2.10 6-Amino-[1,1'-biphenyl]-3-yl propionate (23)



In a hydrogen atmosphere, 6-nitro-[1,1'-biphenyl]-3-yl propionate (728 mg, 2.66 mmol, 1.0 eq) was dissolved in a mixture of ethyl acetate (15 mL) and acetic acid (10 mL). Then, Pd/C (10%, 100 mg) was added and the pressure vessel was purged with hydrogen and set to 2 bar. The reaction mixture was stirred for 5 h at ambient temperature until no starting material was observed by TLC analysis (*n*-hexane/EtOAc, 4:1). The reaction mixture was filtered and concentrated under reduced pressure. The title compound was isolated after gradient flash column chromatography (*n*-hexane/EtOAc, 4:1 to *n*-hexane/EtOAc, 1:1) as an off-yellow oil (398.4 mg, 1.65 mmol, 62%).

TLC: *R*_f = 0.26 (*n*-hexane/EtOAc, 4:1)

¹H NMR (300 MHz, cd₂cl₂) δ (ppm) 7.51 – 7.28 (m, 5H, H-8, H-8', H-9, H-2, H-4), 6.89 – 6.78 (m, 2H, H-7, H-7'), 6.78 – 6.67 (m, 1H, H-5), 3.77 (s, 2H, H-NH₂), 2.53 (q, *J* = 7.5 Hz, 2H, H-11), 1.29 – 1.14 (m, 3H, H-12).

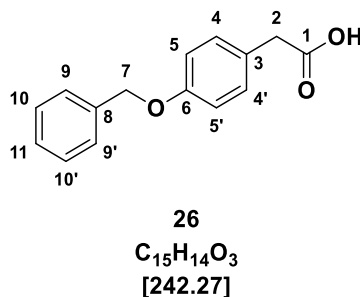
¹³C NMR (126 MHz, cd₂cl₂) δ (ppm) 173.57 (1C, C-10), 143.06 (1C, C-6), 141.74 (1C, C-3), 138.96 (1C, C-1'), 129.11 (2C, C-8, C-8'), 129.06 (2C, C-7, C-7'), 128.13 (1C, C-9), 127.63 (1C, C-1), 123.27 (1C, C-4), 121.63 (1C, C-2), 116.02 (1C, C-5), 27.93 (1C, C-11), 9.27 (1C, C-12).

MS (ESI⁺): 242.1 ([M+H]⁺)

HR-MS (ESI⁺): calc. for C₁₅H₁₅NO₂ ([M+H]⁺): 242.1176, found: 242.1178

calc. for C₁₅H₁₅NO₂ ([M+Na]⁺): 264.0995, found: 264.0996

7.4.2.11 2-(4-(Benzyloxy)phenyl)acetic acid (**26**)



In a 500 mL one-neck flask, which was equipped with a reflux condenser, 2-(4-(benzyloxy)phenyl)acetic acid (5.00 g, 32.9 mmol, 1.0 eq), (bromomethyl)benzene (4.10 mL, 34.5 mmol, 1.1 eq), KOH (4.60 g, 82.3 mmol, 2.5 eq) and NaI (99.0 mg, 0.66 mmol, 0.02 eq) were dissolved in EtOH (150 mL) and refluxed for 24 h. The reaction mixture was allowed to cool down to room temperature, and upon addition of 3 M HCl (150 mL) product precipitated. The precipitate was filtered, washed with water (100 mL), and dried *in vacuo*. The title compound was obtained as a white powder (4.60 g, 18.98 mmol, 60%).

TLC: $R_f = 0.5$ (cyclohexane/EtOAc, 1:1)

mp.: 122.6 °C

¹H NMR (300 MHz, DMSO) δ (ppm) 12.24 (s, 1H, -OH) 7.49 – 7.36 (m, 5H, H-10, H-10', H-11, H-9, H-9'), 7.17 (d, $J = 8.1$ Hz, 2H, H-4, H-4'), 6.95 (d, $J = 8.1$ Hz, 2H, H-5, H-5'), 5.09 (s, 2H, H-7), 3.49 (s, 2H, H-2).

¹³C NMR (75 MHz, DMSO) δ (ppm) 173.43 (1C, C-1), 157.57 (1C, C-6), 137.65 (1C, C-8), 130.85 (2C, C-4, C-4'), 128.89 (2C, C-10, C-10'), 128.24 (1C, C-3), 128.08 (2C, C-9, C-9'), 127.67 (1C, C-11), 115.03 (2C, C-5, C-5'), 69.61 (1C, C-7), 40.31 (1C, C-2).

FT-IR (Diamond-ATR): ν (cm⁻¹) 2360.44, 1685.48, 1508.06, 1012.45.

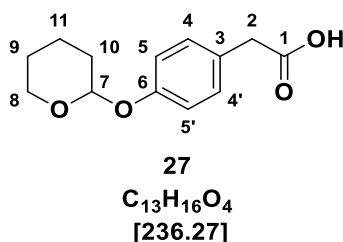
MS (ESI⁺): 265.1 ([M+Na]⁺)

HR-MS (ESI⁺): calc. for C₁₅H₁₄O₃ ([M+Na]⁺): 265.0846, found: 265.0846

MS (ESI⁻): 241.1 ([M-H]⁻)

HR-MS (ESI-): calc. for $C_{15}H_{14}O_3$ ($[M-H]^-$): 241.0870, found: 241.0869

7.4.2.12 2-(4-((Tetrahydro-2H-pyran-2-yl)oxy)phenyl)acetic acid (27)



Methyl 2-(4-hydroxyphenyl)acetate (2.50 g, 15.0 mmol, 1.0 eq) and 3,4-dihydro-2H-pyran (1.5 mL, 16.5 mmol, 1.1 eq) were dissolved in DCM (65 mL). Pyridinium 4-methylbenzenesulfonate (57.7 mg, 0.15 mmol, 0.01 eq.) was added and the solution was stirred at room temperature for 12 h and poured into saturated aqueous $NaHCO_3$ solution (50 mL). The aqueous phase was extracted three times with methylene chloride (50 mL). The combined organic phases were extracted with brine (100 mL) and dried over anhydrous Na_2SO_4 . After the removal of the solvent under reduced pressure, 3.91 g of a yellow-green oil (methyl 2-(4-((tetrahydro-2H-pyran-2-yl)oxy)phenyl)acetate) was isolated and directly used without further purification. The crude methyl ester was dissolved in THF/methanol/water (2:2:1, 75 mL) and lithium hydroxide monohydrate (930 mg, 22.5 mmol) was added. The clear solution was stirred at room temperature for 12 h, after which 1 M hydrochloric acid was added to adjust the pH to 7. The mixture was extracted with ethyl acetate (3 x 50 mL); the aqueous phase was stored. The combined organic phases were washed with brine (2x 50 mL) and dried over anhydrous $MgSO_4$ to yield 436 mg of a reddish oil, which solidified in the fridge. 1 M hydrochloric acid was added to the remaining aqueous solution until no new white precipitate appeared. The suspension was then treated as described above yielding white powder (2.72 g, 11.0 mmol, 77%).

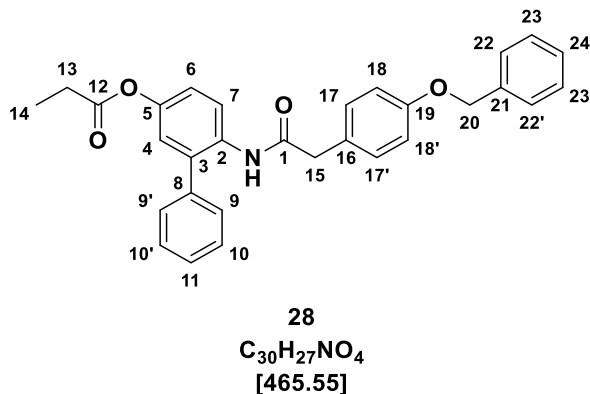
1H NMR (300 MHz, $CDCl_3$) δ (ppm) 11.09 (s, 1H, H-COOH), 7.19 (d, $J = 8.6$ Hz, 2H, H-4, H-4'), 7.01 (d, $J = 8.6$ Hz, 2H, H-5, H-5'), 5.40 (t, $J = 3.3$ Hz, 1H, H-7), 3.68 - 3.55 (m, 4H, H-2, H-8), 2.09 - 1.92 (m, 2H, H-10), 1.91 - 1.49 (m, 4H, H-9, H-11).

^{13}C NMR (75 MHz, $CDCl_3$) δ (ppm) 177.39 (1C, C-1), 156.48 (1C, C-6), 130.46 (2C, C-4, C-4'), 126.39 (1C, C-3), 116.78 (2C, C-5, C-5'), 96.52 (1C, C-7), 62.14 (1C, C-8), 40.27 (1C, C-2), 30.49 (1C, C-10), 25.35 (1C, C-9), 18.88 (1C, C-11).

HR-MS (ESI-) calc. for $C_{13}H_{16}O_4$ ($[M-H]^-$): 235.0976, found: 235.0977.

HR-MS (ESI+) calc. for $C_{13}H_{16}O_4$ ($[M+Na]^+$): 259.0941, found: 259.0942.

7.4.2.13 6-(2-(4-(Benzyloxy)phenyl)acetamido)-[1,1'-biphenyl]-3-yl propionate (28)



In a dry 50 mL Schlenk flask, under an argon atmosphere, 2-(4-(benzyloxy)phenyl)acetic acid (450 mg, 1.85 mmol, 1.0 eq) was dissolved in anhydrous DCM (10 mL) with catalytic amounts of DMF. To the reaction mixture, oxalyl chloride (0.2 mL, 2.78 mmol, 1.5 eq) was added slowly, and the reaction was stirred under an argon atmosphere for 2 h. Afterwards, excess oxalyl chloride was removed under reduced pressure. The obtained yellow solid was dissolved in anhydrous toluene (10 mL), and K_2CO_3 (978 mg, 7.20 mmol, 4.0 eq) was added to the reaction mixture. In a second dry Schlenk flask under an argon, 6-amino-[1,1'-biphenyl]-3-yl propionate (644 mg, 2.68 mmol, 1.5 eq) was dissolved in anhydrous toluene (5 mL) and added to the reaction mixture. The flask was rinsed with an additional 5 mL of anhydrous toluene. The reaction mixture was stirred for 20 h in an argon atmosphere. The yellow suspension was filtered, washed with water (20 mL), sat. aq. $NaHCO_3$ solution (40 mL) and sat. aq. $NaCl$ solution (50 mL). The organic phase was dried over $MgSO_4$ and concentrated *in vacuo* to give a crude brownish solid (714 mg). The title compound was purified by flash column chromatography (*n*-hexane/EtOAc, 5:1), and isolated as a brownish solid (340 mg, 0.73 mmol, 40%).

TLC: $R_f = 0.22$ (*n*-hexane/EtOAc, 3:1)

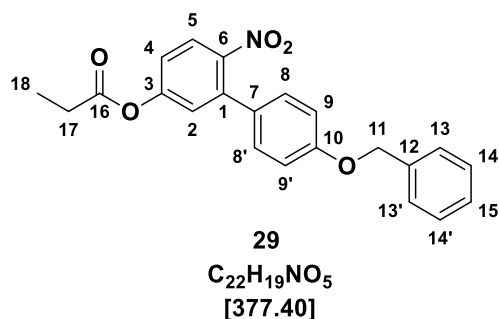
1H NMR (500 MHz, CD_3CN) δ (ppm) 7.97 (d, $J = 8.8$ Hz, 1H, H-7), 7.60 (s, 1H, H-NH), 7.48 (ddt, $J = 7.6, 1.4, 0.7$ Hz, 2H, H-22, H-22'), 7.45 – 7.38 (m, 2H, H-11, H-24), 7.38 – 7.29 (m, 4H, H-10, H-10', H-23, H-23'), 7.22 – 7.15 (m, 2H, H-17, H-17'), 7.09 – 7.01 (m, 3H, H-9, H-9', H-6), 6.97 (d, $J = 2.7$ Hz, 1H, H-4), 6.89 – 6.82 (m, 2H, H-18, H-18'), 5.08 (s, 2H, H-20), 3.46 (s, 2H, H-15), 2.56 (q, $J = 7.5$ Hz, 2H, H-13), 1.17 (t, $J = 7.5$ Hz, 3H, H-14).

^{13}C NMR (126 MHz, CD_3CN) δ (ppm) 174.08 (1C, C-12), 170.64 (1C, C-1), 158.76 (1C, C-19), 148.57 (1C, C-5), 138.26 (1C, C-8), 136.48 (1C, C-21), 133.48 (1C, C-2), 131.45 (2C, C-22, C-22'), 129.83 (2C, C-17, C-17'), 129.72 (2C, C-10, C-10'), 129.51 (1C, C-16), 128.88 (1C, C-3), 128.78 (2C, C-11, C-24), 128.64 (2C, C-23, C-23'), 128.05 (2C, C-9, C-9'), 125.28 (1C, C-7), 124.19 (1C, C-6), 122.14 (1C, C-4), 116.01 (2C, C-18, C-18'), 70.54 (1C, C-20), 43.67 (1C, C-15), 28.08 (1C, C-13), 9.23 (1C, C-14).

MS (ESI+): 488.2 ($[\text{M}+\text{Na}]^+$), 466.2 ($[\text{M}+\text{H}]^+$).

HR-MS (ESI+): calc. for $\text{C}_{30}\text{H}_{27}\text{NO}_4$ ($[\text{M}+\text{H}]^+$): 466.2013, found 466.2016

7.4.2.14 4'-(Benzyloxy)-6-nitro-[1,1'-biphenyl]-3-yl propionate (29)



In a dry 250 mL Schlenk flask under an argon atmosphere, 4'-(benzyloxy)-6-nitro-[1,1'-biphenyl]-3-ol (1.55 g, 4.85 mmol, 1.0 eq) was dissolved in anhydrous DCM (50 mL). To this solution propionic acid (0.7 mL, 9.70 mmol, 2.0 eq), and DMAP (63.0 mg, 0.50 mmol, 0.1 eq) were added. The mixture was stirred for 15 min. In a second dry 50 mL Schlenk flask, and under argon, EDC-HCl (929.75 mg, 4.85 mmol, 1.0 eq) was dissolved in anhydrous DCM (20 mL) and added to the reaction mixture. After complete addition of EDC-HCl, the flask was rinsed with an additional 10 mL of anhydrous DCM. The reaction mixture was stirred at ambient temperature for 12 h. Then, the reaction mixture was washed with aq. HCl (1M, 50 mL), water (50 mL), sat. aq. NaHCO_3 solution (50 mL) and sat. aq. NaCl solution (50 mL). The organic phase was dried over MgSO_4 , filtered, and the solvent was removed *in vacuo* to give a yellow oil (1.71 g). The title compound was isolated as a yellow solid (1.57 g, 4.17 mmol, 86%) after purification by flash column chromatography (*n*-hexane/EtOAc, 4:1).

TLC: $R_f = 0.45$ (*n*-hexane/EtOAc, 4:1)

mp.: 76.1 °C

$^1\text{H NMR}$ (300 MHz, cd_2cl_2) δ (ppm) 7.87 (dd, $J = 8.6, 0.5$ Hz, 1H, H-5), 7.51 – 7.28 (m, 5H, H-4, H-13, H-13', H-14, H-14'), 7.32 – 7.13 (m, 4H, H-8, H-8', H-15, H-2), 7.09 – 6.98 (m, 2H, H-9, H-9'), 5.10 (s, 2H, H-11), 2.62 (q, $J = 7.5$ Hz, 2H, H-17), 1.24 (t, $J = 7.5$ Hz, 3H, H-18).

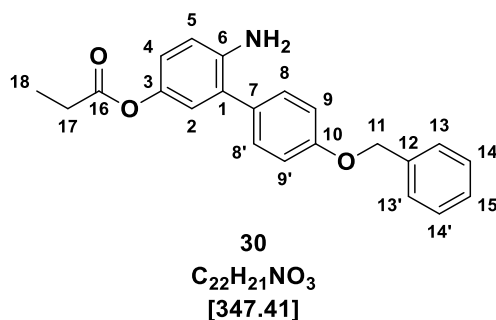
$^{13}\text{C NMR}$ (126 MHz, cd_2cl_2) δ (ppm) 172.24 (1C, C-16), 159.31 (1C, C-10), 153.37 (1C, C-3), 146.44 (1C, C-6), 137.92 (1C, C-1), 137.05 (1C, C-12), 129.47 (1C, C-7), 129.31 (2C, C-8, C-8'), 128.74 (1C, C-5), 128.23 (2C, C-14, C-14'), 127.80 (2C, C-13, C-13'), 125.90 (1C, C-15), 125.15 (2C, C-9, C-9'), 121.18 (1C, C-4), 115.21 (1C, C-2), 70.37 (1C, C-11), 28.00 (1C, C-17), 9.03 (1C, C-18).

MS (ESI+): 400.1 ($[\text{M}+\text{Na}]^+$)

HR-MS (ESI+): calc. for $\text{C}_{22}\text{H}_{19}\text{NO}_5$ ($[\text{M}+\text{Na}]^+$): 400.1155, found 400.1148

FT-IR (Diamond-ATR): ν (cm^{-1}) 1759.73, 1516.74, 1345.11, 1177.33, 1132.01.

7.4.2.15 6-Amino-4'-(benzyloxy)-[1,1'-biphenyl]-3-yl propionate (30)



In a one-neck flask, 4'-(benzyloxy)-6-nitro-[1,1'-biphenyl]-3-yl propionate (1.58 g, 4.19 mmol, 1.0 eq) was dissolved in EtOH (50 mL). Then, tin (II) chloride (4.21 g, 22.2 mmol, 5.3 eq) was added and the reaction mixture was refluxed for 4 h. After the completion of the reaction ice-cold water (100 mL) was added, and the tin hydroxide precipitate was dissolved with 20 mL of NaOH (20%). The aqueous layer was extracted with EtOAc (3 x 60mL), dried over anhydrous Na_2SO_4 , and concentrated *in vacuo*. The title compound was isolated, after purification by gradient flash column chromatography (*n*-hexane/EtOAc, 3:1 \rightarrow 2:1) as a brown oil (557 mg, 1.60 mmol, 40%).

TLC: $R_f = 0.43$ (*n*-hexane/EtOAc, 2:1)

$^1\text{H NMR}$ (300 MHz, dmsO) δ (ppm) 7.50 – 7.30 (m, 7H, H-2, H-4, H-13, H-13', H-14, H-14', H-15), 7.12 – 7.05 (m, 2H, H-8, H-8'), 6.80 – 6.68 (m, 3H, H-9, H-9', H-5), 5.13 (s,

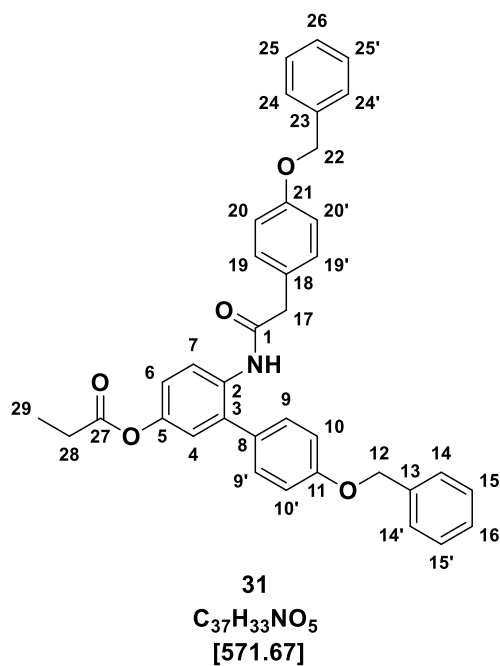
2H, H-11), 4.67 (s, 2H, H-NH₂), 2.56 – 2.47 (m, 2H, H-17), 1.11 (t, $J = 7.5$ Hz, 3H, H-18).

¹³C NMR (126 MHz, dmsO) δ (ppm) 172.79 (1C, C-16), 157.24 (1C, C-10), 142.59 (1C, C-6), 141.18 (1C, C-3), 136.92 (1C, C-12), 131.03 (1C, C-7), 129.52 (2C, C-8, C-8'), 128.28 (2C, C-14, C-14'), 127.66 (1C, C-15), 127.50 (2C, C-13, C-13'), 125.59 (1C, C-4), 122.46 (1C, C-2), 120.68 (1C, C-1), 115.27 (1C, C-5), 114.93 (2C, C-9, C-9'), 69.18 (1C, C-11), 26.84 (1C, C-17), 8.95 (1C, C-18).

MS (ESI⁺): 348.2 ([M+H]⁺), 370.1 ([M+Na]⁺).

HR-MS (ESI⁺): calc. for C₂₂H₂₁NO₃ ([M+H]⁺): 348.1594, found: 348.1592; calc. for C₂₂H₂₁NO₃ ([M+Na]⁺): 370.1414, found: 370.1411.

7.4.2.16 4'-(Benzyloxy)-6-(2-(4-(benzyloxy)phenyl)acetamido)-[1,1'-biphenyl]-3-yl propionate (31)



In a dry Schlenk flask, 2-(4-(benzyloxy)phenyl)acetic acid (698 mg, 2.88 mmol, 2.0 eq), EDC-HCl (664 mg, 3.46 mmol, 2.1 eq) and HOBT (39.02 mg, 0.288 mmol, 0.2 eq) were dissolved in DCM (30 mL) and stirred at room temperature for 10 min under an argon atmosphere. 6-Amino-4'-(benzyloxy)-[1,1'-biphenyl]-3-yl propionate (502 mg, 1.44 mmol, 1.0 eq) was dissolved in DCM (10 mL) in a second dry Schlenk flask, and added to the clear reaction solution. The mixture was stirred at room temperature for 24 h and quenched with sat. aq. NaHCO₃ solution (10 mL). The organic phase was washed with sat. aq. NaCl solution and dried over MgSO₄. After evaporation and flash column

chromatography (*n*-hexane/EtOAc, 3:1), the product was isolated as a yellowish oil (500 mg, 0.87 mmol, 60%).

TLC: $R_f = 0.21$ (*n*-hexane/EtOAc, 3:1)

$^1\text{H NMR}$ (300 MHz, acetone) δ (ppm) 8.16 (dd, $J = 8.8, 4.0$ Hz, 1H, H-7), 7.98 – 7.83 (m, 1H, H-NH), 7.54 – 7.24 (m, 9H, H-9, H-9', H-4, H-14, H-14', H-24, H-24', H-15, H-15'), 7.21 – 6.82 (m, 11H, H-16, H-6, H-26, H-10, H-10', H-19, H-19', H-20, H-20', H-25, H-25'), 5.14 (d, $J = 17.3$ Hz, 4H, H-12, H-22), 3.55 (s, 2H, H-17), 2.58 (q, $J = 7.5$ Hz, 2H, H-28), 1.18 (t, $J = 7.5$ Hz, 3H, H-29).

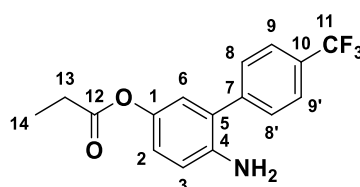
$^{13}\text{C NMR}$ (126 MHz, acetone) δ (ppm) 173.33 (1C, C-27), 170.00 (1C, C-1), 159.55 (1C, C-21), 159.05 (1C, C-11), 148.25 (1C, C-5), 138.4 (2C, C-23, C-13), 135.09 (1C, C-2), 134.98 (2C, C-9, C-9'), 133.96 (1C, C-2), 131.53 (2C, C-25, C-25'), 131.06 (2C, C-24, C-24'), 129.50 (4C, C-14, C-14', C-19, C-19'), 128.85 (2C, C-15, C-15'), 128.60 (2C, C-26, C-16), 128.31 (1C, C-7), 124.04 (1C, C-6), 121.64 (1C, C-4), 116.21 (4C, C-10, C-10', C-20, C-20') (2C, C-12, C-22) 116.06, 114.29, 70.75 (1C, C-17), 28.24 (1C, C-28), 9.60 (1C, C-29).

MS (ESI+): 594.2 ($[\text{M}+\text{Na}]^+$), 1165.4 ($[\text{2M}+\text{Na}]^+$).

HR-MS (ESI+): calc. for $\text{C}_{37}\text{H}_{33}\text{NO}_5$ ($[\text{M}+\text{H}]^+$): 572.2431, found: 572.2431; calc. for $\text{C}_{37}\text{H}_{33}\text{NO}_5$ ($[\text{M}+\text{Na}]^+$): 594.2251, found: 594.2248; calc. for $\text{C}_{37}\text{H}_{33}\text{NO}_5$ ($[\text{M}+\text{K}]^+$): 610.1990, found: 610.1981.

FT-IR (Diamond-ATR): ν (cm^{-1}) 3266.82, 2358.52, 1758.76, 1649.8, 1512.88, 1248.68, 1141.65, 1007.62, 695.212.

7.4.2.17 6-Amino-4'-(trifluoromethyl)-[1,1'-biphenyl]-3-yl propionate (32)



32
 $\text{C}_{16}\text{H}_{14}\text{F}_3\text{NO}_2$
[309.29]

In a dry 250 mL Schlenk flask, under an argon atmosphere, 6-nitro-4'-(trifluoromethyl)-[1,1'-biphenyl]-3-ol (819 mg, 2.89 mmol, 1.0 eq) was dissolved in anhydrous DCM (20 mL). To this solution propionic acid (0.430 mL, 5.78 mmol, 2.0 eq), and DMAP

(35.3 mg, 0.280 mmol, 0.1 eq) were added. The mixture was stirred for 15 min. In a second dry 50 mL schlenk flask under argon, EDC-HCl (555 mg, 2.89 mmol, 1.0 eq) was dissolved in anhydrous DCM (15 mL) and added to the reaction mixture. After complete addition of EDC-HCl, the flask was rinsed with an additional 10 mL of anhydrous DCM. The reaction mixture was stirred at ambient temperature for 12 h. The reaction mixture was washed with aq. HCl (1 M, 50 mL), water (50 mL), sat. aq. NaHCO₃ solution (50 mL) and sat. aq. NaCl solution (50 mL). The organic phase was dried over MgSO₄, filtered, and the solvent was removed *in vacuo* to give the compound as a yellow oil (922 mg, 2.71 mmol, 94%). That was used in the next step without further purification.

In a pressure vessel, 6-nitro-4'-(trifluoromethyl)-[1,1'-biphenyl]-3-yl propionate (900 mg, 2.65 mmol, 1.0 eq) was dissolved in a mixture of EtOH (10 mL), EtOAc (5 mL), and acetic acid (8 mL). Pd/C (10%, 80 mg) was added to the reaction mixture, and it was stirred in a hydrogen atmosphere (3 bar) for 36 h. TLC analysis (*n*-hexane/EtOAc, 3:1) showed full conversion of the starting material. The reaction mixture was filtered over three filtered filter papers, the filter cake was washed with EtOH and concentrated under reduced pressure. The title compound was isolated as yellowish-brown solid (491 mg, 1.58 mmol, 60%) after purification by flash column chromatography (*n*-hexane/EtOAc, 5:1 + 0.5% Et₃N).

TLC: $R_f = 0.5$ (*n*-hexane/EtOAc, 3:1)

mp.: 66.3 °C

¹H NMR (300 MHz, cd₂cl₂) δ (ppm) 7.77 – 7.67 (m, 2H, H-9, H-9'), 7.67 – 7.56 (m, 2H, H-8, H-8'), 6.95 – 6.70 (m, 3H, H-2, H-3, H-6), 3.77 (s, 3H, 13), 2.55 (q, $J = 7.5$ Hz, 2H, 16), 1.30 - 1.14 (m, 3H, 18).

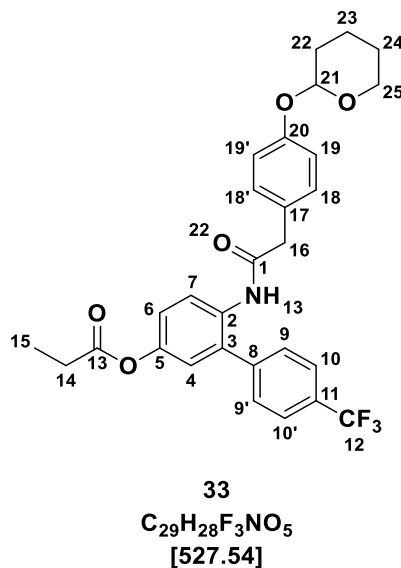
¹³C NMR (126 MHz, cd₂cl₂) δ (ppm) 173.54 (1C, C-12), 143.20 (1C, C-7), 142.86 (1C, C-4), 141.67 (1C, C-1), 129.66 (3C, C-10, C-8, C-8'), 126.48 - 125.98 (3C, C-9, C-9', C-11), 123.45 (1C, C-5), 123.21 (1C, C-2), 122.48 (1C, C-6), 116.44 (1C, C-3), 27.92 (1C, C-13), 9.24 (1C, C-14).

MS (ESI-): 308.1 ([M-H]⁻).

HR-MS (ESI-): calc. for C₁₆H₁₄F₃NO₂ ([M-H]⁻): 308.0904, found: 308.0898

FT-IR (Diamond-ATR): ν (cm⁻¹) 3492.45, 3383.5, 2359.48, 1747.19, 1626.66, 1495.53, 1323.89, 1161.90, 1105.01.

7.4.2.18 6-(2-(4-((Tetrahydro-2H-pyran-2-yl)oxy)phenyl)acetamido)-4'-(trifluoromethyl)-[1,1'-biphenyl]-3-yl propionate (33)



In a dry Schlenk flask, 2-(4-((tetrahydro-2H-pyran-2-yl)oxy)phenyl)acetic acid (312 mg, 1.32 mmol, 2.0 eq), EDC-HCl (305 mg, 1.58 mmol, 2.4 eq) and HOBT (17.6 mg, 0.132 mmol, 0.2 eq) were dissolved in anhydrous DCM (10 mL) and stirred at room temperature for 10 min under an argon atmosphere. 6-Amino-4'-(trifluoromethyl)-[1,1'-biphenyl]-3-yl propionate (204.5 mg, 0.66 mmol, 1.0 eq) was dissolved in DCM (10 mL) in a second dry Schlenk flask and added to the clear reaction solution. The mixture was stirred at room temperature for 24 h, quenched with sat. aq. $NaHCO_3$ solution (10 mL) and extracted with DCM (2 x 50 mL). The organic phase was washed with sat. aq. NaCl solution and dried over $MgSO_4$. After evaporation and flash column chromatography (*n*-hexane/EtOAc, 3:1) the product was isolated as a yellowish solid (200 mg, 0.38 mmol, 57%).

TLC: $R_f = 0.18$ (*n*-hexane/EtOAc, 3:1)

mp.: 141.9 °C

1H NMR (300 MHz, DMSO) δ 9.55 (s, 1H, NH), 7.66 (d, $J = 8.1$ Hz, 1H, H-7), 7.48 (dd, $J = 8.2, 5.0$ Hz, 3H, H-10, H-10', H-4), 7.23 – 7.12 (m, 2H, H-18, H-18'), 7.12 – 7.02 (m, 3H, H-9, H-9', H-6), 7.00 – 6.87 (m, 2H, H-19, H-19'), 5.42 (t, $J = 3.2$ Hz, 1H, H-21), 3.78 (m, 1H, H-25), 3.61 – 3.48 (m, 1H, H-25), 3.43 (s, 2H, H-16), 2.61 (q, $J = 7.5$ Hz, 2H, H-14), 1.95 – 1.48 (m, 6H, H-22, H-23, H-24), 1.14 (t, $J = 7.5$ Hz, 3H, H-15).

^{13}C NMR (75 MHz, DMSO) δ 172.64 (1C, C-13), 169.65 (1C, C-1), 155.30 (1C, C-20), 148.26 (1C, C-5), 142.18 (1C, C-8), 136.43 (1C, C-2), 129.95 (4C, C-18, C-18', C-11, C-

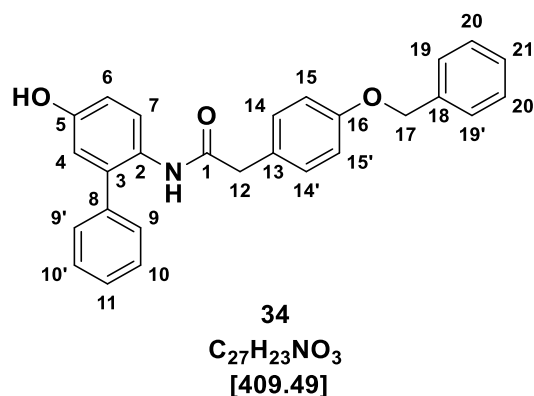
17), 129.37 (2C, C-9, C-9'), 128.50 (2C, C-10, C-10'), 125.13 (2C, C-12, C-3), 123.24 (1C, C-7), 121.90 (1C, C-6), 116.19 (3C, C-19, C-19', C-4), 95.85 (1C, C-21), 61.49 (1C, C-22), 41.71 (1C, C-16), 29.91 (1C, C-22), 26.88 (1C, C-14), 24.73 (1C, C-24), 18.67 (1C, C-23), 8.81 (1C, C-15).

MS (ESI⁺): 528.2 ([M+H]⁺), 550.2 ([M+Na]⁺).

HR-MS (ESI⁺): calc. for C₂₉H₂₈NO₅F₃ ([M+H]⁺): 528.1992, found: 528.1996 calc. for C₂₉H₂₈NO₅F₃ ([M+Na]⁺): 550.1812, found: 550.1822; calc. for C₂₉H₂₈NO₅F₃ ([M+NH₄]⁺): 545.2258, found: 545.2263.

FT-IR (Diamond-ATR): ν (cm⁻¹) 3219.58, 1761.65, 1654.62, 1509.03, 1322.93, 1174.44, 1106.94, 965.198.

7.4.2.19 2-(4-(Benzyloxy)phenyl)-N-(5-hydroxy-[1,1'-biphenyl]-2-yl)acetamide (34)



In a one neck flask equipped with a reflux condenser, 6-(2-(4-(benzyloxy)phenyl)acetamido)-[1,1'-biphenyl]-3-yl propionate (370 mg, 0.79 mmol, 1.0 eq) and KOH (312 mg, 5.56 mmol, 7.0 eq) were dissolved in MeOH (30 mL). The reaction mixture was refluxed for 3 h, full conversion of the starting material was indicated by TLC analysis. The reaction mixture was concentrated *in vacuo*, the residue was dissolved in DCM (30 mL), filtered, washed with water (20 mL), sat. aq. NaCl solution (20 mL), dried over MgSO₄ and concentrated under reduced pressure to obtain the title compound as off-yellow solid (320 mg, 0.78 mmol, 99%).

TLC: R_f = 0.37 (*n*-hexane/EtOAc, 1:1)

mp.: 128.2 °C

¹H NMR (300 MHz, CD₃CN) δ (ppm) 7.56 (dd, J = 8.7, 4.4 Hz, 1H, H-7), 7.53 – 7.27 (m, 8H, H-9, H-9', H-10, H-10', H-19, H-19', H-20, H-20'), 7.26 – 7.14 (m, 2H, H-11,

H-21), 7.06 – 6.99 (m, 2H, H-14, H-14'), 6.88 – 6.81 (m, 2H, H-15, H-15'), 6.77 (dd, $J = 8.7, 2.9$ Hz, 1H, H-6), 6.68 (d, $J = 2.8$ Hz, 1H, H-4), 5.08 (s, 2H, H-17), 3.40 (s, 2H, H-12).

^{13}C NMR (126 MHz, CD_3CN) δ (ppm) 170.62 (1C, C-1), 158.48 (1C, C-16), 155.20 (1C, C-5), 139.22 (1C, C-8), 138.30 (1C, C-18), 137.92 (1C, C-2), 131.21 (2C, C-14, C-14'), 129.54, (2C, C-10, C-10), 129.38 (2C, C-20, C-20'), 128.71 (1C, C-11), 128.47 (2C, C-19, C-19'), 128.29 (1C, C-13), 128.23 (2C, C-9, C-9'), 127.83 (1C, C-3), 127.11 (1C, C-7), 117.28 (1C, C-6), 115.83 (2C, C-15, C-15'), 115.31 (1C, C-4), 70.5 (1C, C-17), 43.42 (1C, C-12).

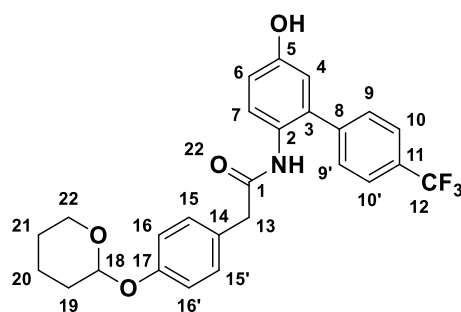
MS (ESI-): 408.16 ($[\text{M}-\text{H}]^-$), 817.33 ($[\text{2M}-\text{H}]^-$)

HR-MS (ESI-): calc. for $\text{C}_{27}\text{H}_{23}\text{NO}_3$ ($[\text{M}-\text{H}]^-$): 408.1605, found: 408.1607

HR-MS (ESI+): calc. for $\text{C}_{27}\text{H}_{23}\text{NO}_3$ ($[\text{M}+\text{H}]^+$): 410.1751, found: 410.1743 calc. for $\text{C}_{27}\text{H}_{23}\text{NO}_3$ ($[\text{M}+\text{Na}]^+$): 432.1570, found: 432.1566

FT-IR (Diamond-ATR): ν (cm^{-1}) 3459.67, 3169.43, 3024.80, 1625.7, 1237.11, 999.91.

7.4.2.20 *N*-(5-Hydroxy-4'-(trifluoromethyl)-[1,1'-biphenyl]-2-yl)-2-(4-((tetrahydro-2H-pyran-2-yl)oxy)phenyl)acetamide (35)



35

$\text{C}_{26}\text{H}_{24}\text{F}_3\text{NO}_4$
[471.48]

6-(2-(4-((tetrahydro-2H-pyran-2-yl)oxy)phenyl)acetamido)-4'-(trifluoromethyl)-[1,1'-biphenyl]-3-yl propionate (155 mg, 0.28 mmol, 1.0 eq) was dissolved in 15 mL of MeOH, and stirred for 5 min. Then, KOH (177.4 mg, 2.56 mmol, 9.0 eq) was added. The reaction mixture was stirred for 2 h at ambient temperature. The solvent was removed under reduced pressure, the residue was dissolved in EtOAc (30 mL), washed with water (20 mL), and sat. aq. NaCl (30 mL) solution. The organic phase was dried over MgSO_4 and concentrated *in vacuo*. The title compound was obtained as yellowish solid (110 mg, 0.230 mmol, 85%).

TLC: $R_f = 0.32$ (*n*-hexane/EtOAc, 3:1)

mp.: 167.4 °C

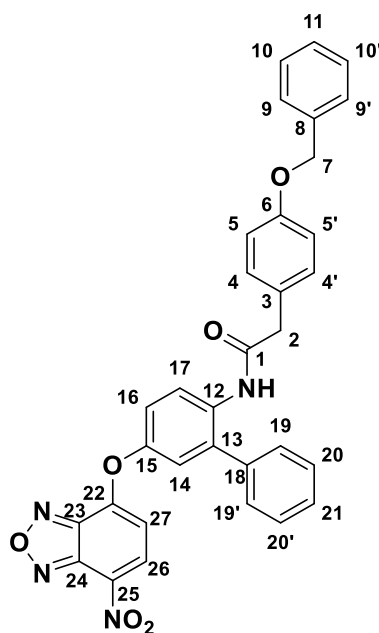
¹H NMR (300 MHz, DMSO) δ 9.62 (s, 1H, NH), 9.30 (s, 1H, OH), 7.62 (d, $J = 8.2$ Hz, 2H, H-9, H-9'), 7.43 (d, $J = 8.1$ Hz, 2H, H-10, H-10'), 7.15 (d, $J = 8.6$ Hz, 1H, H-7), 7.08 – 6.97 (m, 2H, H-15, H-15'), 6.94 – 6.84 (m, 2H, H-16, H-16'), 6.79 (dd, $J = 8.6, 2.8$ Hz, 1H, H-6), 6.72 (d, $J = 2.8$ Hz, 1H, H-4), 5.40 (t, $J = 3.2$ Hz, 1H, H-18), 3.77 (ddd, $J = 11.6, 8.3, 3.7$ Hz, 1H, H-22'), 3.53 (dt, $J = 11.3, 4.5$ Hz, 1H, H-22'), 3.35 (s, 2H, H-12), 1.95 – 1.49 (m, 6H, H-19, H-20, H-21).

¹³C NMR (75 MHz, DMSO) δ 170.05 (1C, C-1), 156.00 (1C, C-5), 155.50 (1C, C-17), 143.59 (1C, C-8), 137.68 (1C, C-2), 130.16 (3C, C-15, C-15', C-11), 129.53 (3C, C-9, C-9', C-14), 129.09 (2C, C-10, C-10'), 126.27 - 125.21 (3C, C-3, C-12), 116.43 (4C, C-16, C-16', C-6, C-7), 115.58 (1C, C-4), 96.14 (1C, C-18), 61.77 (1C, C-22), 41.91 (1C, C-13), 30.20 (1C, C-19), 25.01 (1C, C-21), 18.97 (1C, C-20).

HR-MS (ESI+): calc. for $C_{26}H_{24}F_3NO_4$ ($[M+H]^+$): 472.1730, found: 472.1728; calc. for $C_{26}H_{24}F_3NO_4$ ($[M+Na]^+$): 494.1550, found: 494.1542.

FT-IR (Diamond-ATR): ν (cm^{-1}) 3232.11, 2971.76 1655.59, 1536.99, 1510.95, 1321.96, 1166.72, 1107.9.

7.4.2.21 2-(4-(Benzyloxy)phenyl)-N-(5-((7-nitrobenzo[c][1,2,5]oxadiazol-4-yl)oxy)-[1,1'-biphenyl]-2-yl)acetamide (36)



36

$C_{33}H_{24}N_4O_6$
[572.58]

In a dry 10 mL Schlenk flask and in an argon atmosphere, 2-(4-(benzyloxy)phenyl)-N-(5-hydroxy-[1,1'-biphenyl]-2-yl)acetamide (50.0 mg, 0.120 mmol, 1.0 eq), 4-chloro-7-nitro-1,2,3-benzoxadiazole (28.3 mg, 0.130 mmol, 1.1 eq), and trimethylamine (18.6 μ L, 0.134 mmol, 1.1 eq) were dissolved in anhydrous acetonitrile (3 mL). The orange reaction mixture was protected from light and stirred at ambient temperature for 24 h. The solvent was removed under reduced pressure, the residue was dissolved in DCM (20 mL) washed with water (20 mL), dried over anhydrous $MgSO_4$, and concentrated *in vacuo*. The product was isolated as an orange solid (50.5 mg, 0.090 mmol, 73%) after purification by flash column chromatography.

TLC: $R_f = 0.23$ (*n*-hexane/EtOAc, 2:1)

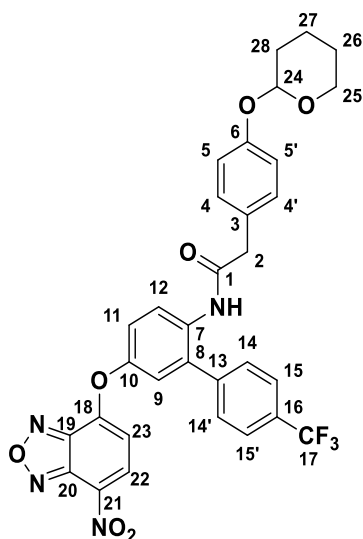
1H NMR (500 MHz, Acetone) δ (ppm) 8.62 (d, $J = 8.4$ Hz, 1H, H-26), 8.33 (d, $J = 8.9$ Hz, 1H, H-17), 7.53 – 7.47 (m, 2H, H-20, H-20'), 7.44 – 7.29 (m, 7H, H-5, H-5', H-10, H-10', H-9, H-9', H-11), 7.28 – 7.21 (m, 3H, H-19, H-19', H-21), 7.18 – 7.11 (m, 2H, H-4, H-4'), 6.95 – 6.87 (m, 3H, H-16, H-17, H-27), 5.13 (s, 2H, H-7), 3.57 (s, 2H, H-2).

^{13}C NMR (126 MHz, Acetone) δ (ppm) 170.39 (1C, C-1), 158.98 (1C, C-6), 155.07 (1C, C-15), 150.26 (1C, C-22), 146.60 (1C, C-24), 145.55 (1C, C-18), 138.50 (1C, C-8), 137.84 (1C, C-13), 136.65 (1C, C-23), 135.63 (1C, C-26), 134.94 (2C, C-3, C-12), 131.37

(2C, C-4, C-4'), 129.97 (2C, C-20, C-20'), 129.78 (2C, C-19, C-19'), 129.41 (2C, C-10, C-10'), 128.99 (1C, C-21), 128.73 (1C, C-11), 128.48 (2C, C-9, C-9'), 128.00 (1C, C-25), 125.51 (1C, C-17), 123.28 (1C, C-14), 121.10 (1C, C-16), 116.03 (2C, C-5, C-5'), 110.07 (1C, C-27), 70.41 (1C, C-7), 44.04 (1C, C-2).

HR-MS (ESI⁺): calc. for C₃₃H₂₄N₄O₆ ([M+H]⁺): 573.1769, found: 573.1769 calc. for C₃₃H₂₄N₄O₆ ([M+Na]⁺): 595.1588, found: 595.1588. calc. for C₃₃H₂₄N₄O₆ ([M+K]⁺): 611.1327, found: 611.1329.

7.4.2.22 N-(5-((7-Nitrobenzo[c][1,2,5]oxadiazol-4-yl)oxy)-4'-(trifluoromethyl)-[1,1'-biphenyl]-2-yl)-2-(4-((tetrahydro-2H-pyran-2-yl)oxy)phenyl)acetamide (37)



37

C₃₂H₂₅F₃N₄O₇
[634.57]

In a dry one-neck flask, under an argon atmosphere, *N*-(5-hydroxy-4'-(trifluoromethyl)-[1,1'-biphenyl]-2-yl)-2-(4-((tetrahydro-2H-pyran-2-yl)oxy)phenyl)acetamide (87.0 mg, 0.180 mmol, 1.0 eq), 4-chloro-7-nitro-1,2,3-benzoxadiazole (36.1 mg, 0.180 mmol, 1.1 eq) were dissolved in anhydrous acetonitrile (10 mL). The reaction mixture was stirred for 5 min. Then, triethylamine (28.13 μ L, 0.200 mmol, 1.1 eq) was added, which resulted in an intense orange colour of the reaction solution. The reaction was protected from light and stirred at ambient temperature for 24 h. As TLC analysis showed no further consumption of the starting material, the reaction was stopped. The solvent was removed under reduced pressure, the residue was dissolved in DCM (50 mL) washed with water (40 mL), dried over anhydrous MgSO₄, and concentrated *in vacuo*. The title compound

was isolated as a yellow-orange solid (56.5 mg, 0.080 mmol, 50%) after purification by flash column chromatography (*n*-hexane/EtOAc, 1:1).

TLC: $R_f = 0.5$ (*n*-hexane/EtOAc, 1:1)

mp.: 171.5 °C

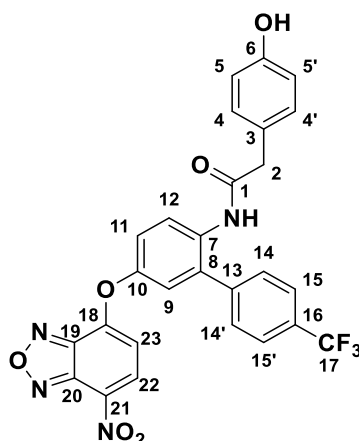
$^1\text{H NMR}$ (300 MHz, CD_2Cl_2) δ (ppm) 8.53-8.38 (m, 2H, H-22, H-NH), 7.66 – 7.55 (m, 2H, H-14, H-14'), 7.39 – 7.22 (m, 3H, H-12, H-15, H-15'), 7.20 – 7.07 (m, 2H, H-9, H-11), 7.06 – 6.96 (m, 2H, H-4, H-4'), 6.99 – 6.84 (m, 2H, H-5, H-5'), 6.64 (d, $J = 8.3$ Hz, 1H, H-23), 5.38 (t, $J = 3.3$ Hz, 1H, H-24), 3.86 (ddd, $J = 11.8, 9.0, 3.2$ Hz, 1H, H-25), 3.58 (s, 2H, H-2), 3.67 – 3.50 (m, 1H, H-25), 2.09 – 1.78 (m, 3H, H-27, H-28), 1.68-1.52 (m, 3H, H-26, H-27).

$^{13}\text{C NMR}$ (126 MHz, CD_2Cl_2) δ (ppm) 169.60 (1C, C-1), 156.91 (1C, C-6), 154.40 (1C, C-10), 149.03 (1C, C-18), 145.54 (1C, C-19), 144.58 (1C, C-20), 140.39 (1C, C-13), 134.01 (1C, C-7), 130.81 (2C, C-4, C-4'), 129.65 (2C, C-15, C-15'), 126.76 (2C, C-16, C-17), 126.48 (2C, C-14, C-14'), 125.53 (1C, C-8), 123.97 (1C, C-22), 123.37 (1C, C-3), 122.55 (2C, C-9, C-11), 121.46 (1C, C-12), 117.50 (2C, C-5, C-5'), 108.57 (1C, C-23), 96.92 (1C, C-24), 62.52 (1C, C-25), 44.49 (1C, C-2), 30.71 (1C, C-28), 25.67 (1C, C-26), 19.32 (1C, C-27).

$^{19}\text{F NMR}$ (282 MHz, CD_2Cl_2) δ (ppm) -60.97.

MS (ESI+): 635.2 ($[\text{M}+\text{H}]^+$), 657.2 ($[\text{M}+\text{Na}]^+$)

HR-MS (ESI+): calc. for $\text{C}_{32}\text{H}_{25}\text{N}_4\text{O}_7\text{F}_3$ ($[\text{M}+\text{H}]^+$): 635.1748, found: 635.1736; calc. for $\text{C}_{32}\text{H}_{25}\text{N}_4\text{O}_7\text{F}_3$ ($[\text{M}+\text{Na}]^+$): 657.1568, found: 657.1561.

7.4.2.23 2-(4-Hydroxyphenyl)-N-(5-((7-nitrobenzo[c][1,2,5]oxadiazol-4-yl)oxy)-4'-(trifluoromethyl)-[1,1'-biphenyl]-2-yl)acetamide (38)


38

 $C_{27}H_{17}F_3N_4O_6$
 [550.45]

In one-neck flask a mixture of *N*-(5-((7-nitrobenzo[c][1,2,5]oxadiazol-4-yl)oxy)-4'-(trifluoromethyl)-[1,1'-biphenyl]-2-yl)-2-(4-((tetrahydro-2H-pyran-2-yl)oxy)phenyl)acetamide (34 mg, 0.050 mmol, 1.0 eq) and pyridinium *p*-toluenesulfonate (5.00 mg, 5.00 μ mol, 0.1 eq) in MeOH (10 mL) was stirred at 50 °C for 24 h. The solvent was removed under reduced pressure, the residue was dissolved in EtOAc (15 mL) washed with water (10 mL), sat. aq. NaHCO₃ (15 mL) solution. The organic layer was separated, dried over anhydrous MgSO₄, and concentrated *in vacuo*. The title compound was obtained as a yellow-orange solid (21.0 mg, 0.040 mmol, 74%) after purification by flash column chromatography (DCM/MeOH, 100:1).

TLC: $R_f = 0.3$ (*n*-hexane/EtOAc, 1:1)

¹H NMR (400 MHz, Acetone) δ (ppm) 8.64 (d, $J = 8.4$ Hz, 1H, H-22), 8.39 (s, 1H, H-NH), 8.34 (s, 1H, H-OH), 8.23 (d, $J = 8.6$ Hz, 1H, H-12), 7.71 (d, $J = 8.0$ Hz, 2H, H-15, H-15'), 7.54 (d, $J = 8.0$ Hz, 2H, H-14, H-14'), 7.47 (d, $J = 8.9$ Hz, 1H, H-11), 7.40 (s, 1H, H-9), 7.08 (d, $J = 8.1$ Hz, 2H, H-4, H-4'), 6.95 (d, $J = 8.4$ Hz, 1H, H-23), 6.77 (d, $J = 8.2$ Hz, 2H, H-5, H-5'), 3.55 (s, 2H, H-2).

¹³C NMR (101 MHz, Acetone) δ (ppm) 169.66 (1C, C-1), 156.57 (1C, C-6), 153.89 (1C, C-10), 149.98 (1C, C-18), 145.85 (1C, C-20), 144.50 (1C, C-13), 134.55 (1C, C-22), 133.98 (1C, C-19), 130.37 (3C, C-7, C-4, C-4'), 129.68 (4C, C-14, C-14', C-3, C-16), 126.01, (1C, C-12), 125.63 (3C, C-15, C-15', C-17), 122.39 (1C, C-9), 120.87 (2C, C-8, C-11), 115.43 (3C, C-5, C-5', C-21), 109.31 (1C, C-23), 42.84 (1C, C-2).

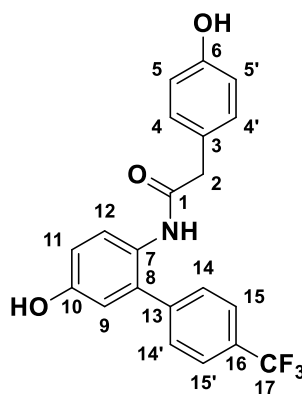
^{19}F NMR (377 MHz, Acetone) δ -62.97 (CF_3).

MS (ESI+): 573.1 ($[\text{M}+\text{Na}]^+$).

HR-MS (ESI+): calc. for $\text{C}_{27}\text{H}_{17}\text{F}_3\text{N}_4\text{O}_6$ ($[\text{M}+\text{Na}]^+$): 573.0992, found: 573.0995

FT-IR (Diamond-ATR): ν (cm^{-1}) 2367.19, 1735.62, 1653.66, 1615.09, 1540.85, 1509.03, 1323.89, 1261.22.

7.4.2.24 *N*-(5-Hydroxy-4'-(trifluoromethyl)-[1,1'-biphenyl]-2-yl)-2-(4-hydroxyphenyl)acetamide (L9)



L9

$\text{C}_{21}\text{H}_{16}\text{F}_3\text{NO}_3$
[387.36]

In a pressure vessel 2-(4-(Benzyloxy)phenyl)-*N*-(5-hydroxy-4'-(trifluoromethyl)-[1,1'-biphenyl]-2-yl)acetamide (85.0 mg, 0.160 mmol, 1.0 eq) was dissolved with EtOH (15 mL), and acetic acid (3 mL). Pd/C (30 mg) was added to the reaction mixture, which was stirred in a hydrogen atmosphere (3 bar) for 8 h. After this time, TLC analysis (*n*-hexane/EtOAc, 1:1) showed complete consumption of the starting material. The reaction mixture was filtered over three filtered filter papers, the filter cake was washed with EtOH and concentrated *in vacuo*. The title compound was isolated as an off-white solid (60.0 mg, 0.155 mmol, 97%.) after purification by flash column chromatography (*n*-hexane/EtOAc, 1:1).

TLC: R_f = 0.21 (*n*-hexane/EtOAc, 1:1)

mp.: 85 °C

^1H NMR (400 MHz, CD_3CN) δ (ppm) 7.64 – 7.55 (m, 3H, H-15, H-15'), 7.42 (d, J = 8.7 Hz, 1H, H-12), 7.40 – 7.30 (m, 2H, H-14, H-14'), 6.97 – 6.89 (m, 2H, H-4, H-4'), 6.81 (dd, J = 8.7, 2.9 Hz, 1H, H-11), 6.72 (d, J = 2.8 Hz, 1H, H-9), 6.69 – 6.63 (m, 2H, H-5, H-5'), 3.36 (s, 2H, H-2).

¹³C NMR (101 MHz, CD₃CN) δ (ppm) 171.24 (1C, C-1), 156.89 (1C, C-6), 155.88 (1C, C-10), 143.79 (1C, C-13), 137.65 (1C, C-7), 131.37 (2C, C-14, C-14'), 130.40 (3C, C-4, C-4', C-8), 128.56 (2C, C-15, C-15'), 127.77 (1C, C-3), 127.23 (1C, C-16), 126.09 (1C, C-17), 117.35 (1C, C-11), 116.25 (3C, C-5, C-5', C-9), 43.32 (1C,C-2).

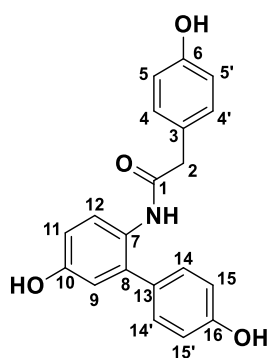
¹⁹F NMR (376 MHz, CD₃CN) δ (ppm)-62.84 (CF₃).

MS (ESI+): 410.1([M+Na]⁺), 388.2 ([M+H]⁺)

HR-MS (ESI+): calc. for C₂₁H₁₆NO₃F₃ ([M+H]⁺): 388.1155, found: 388.1155 calc. for C₂₁H₁₆NO₃F₃ ([M+Na]⁺): 410.0974, found: 410.0978

FT-IR (Diamond-ATR): ν (cm⁻¹) 3289.96, 2360.44, 1738.51, 1652.7, 1513.85, 1323.89, 1122.37, 824.42.

7.4.2.25 *N*-(4',5-Dihydroxy-[1,1'-biphenyl]-2-yl)-2-(4-hydroxyphenyl)acetamide (L1)



L1
C₂₀H₁₇NO₄
[335.36]

To a solution of 4'-(benzyloxy)-6-(2-(4-(benzyloxy)phenyl)acetamido)-[1,1'-biphenyl]-3-yl propionate (469 mg, 0.820 mmol, 1.0 eq) in EtOAc (45 mL), EtOH (50 mL), and acetic acid (5 mL), in a small pressure reactor vessel, Pd/C (10%, 60 mg) was added. The reaction mixture was stirred in a hydrogen atmosphere (3 bar) at ambient temperature for 12 h. Afterwards, TLC analysis (*n*-hexane/EtOAc, 2:1) showed complete consumption of the starting material. The mixture was filtered through three pleated filters and washed with EtOH. The filtrate was concentrated *in vacuo* to give a colourless oil (345 mg) which was used without further purification in the next step.

The oil was dissolved in MeOH (15 mL), and KOH (449 mg, 0.880 mmol, 7.0 eq) was added under stirring. The reaction was monitored by TLC analysis (DCM/MeOH, 19:1). As starting material was still observed after stirring 3 h under reflux, further KOH

(234 mg, 0.440 mmol) was added and the reaction was left to equilibrate under reflux overnight. After 20 h, no further product formation was observed. Hence, the solvent was removed under reduced pressure, the residue was dissolved in DCM (30 mL), filtered, and washed with acidified water pH (4-5). The title compound was purified by flash column chromatography (DCM/MeOH 19:1) and isolated as an off-white solid (213 mg, 0.64 mmol, 78%).

TLC: $R_f = 0.14$ (DCM/MeOH, 19:1)

mp.: 92.5 °C

$^1\text{H NMR}$ (500 MHz, Acetone) δ (ppm) 7.93 (s, 1H, H-NH), 7.72 (d, $J = 7.0$ Hz, 1H, H-12), 7.06 – 7.01 (m, 4H, H-14, H-14', H-4, H-4'), 6.83 – 6.80 (m, 2H, H-15, H-15'), 6.76 – 6.72 (m, 3H, H-11, H-5, H-5'), 6.67 (d, $J = 2.9$ Hz, 1H, H-9), 3.46 (s, 2H, H-2).

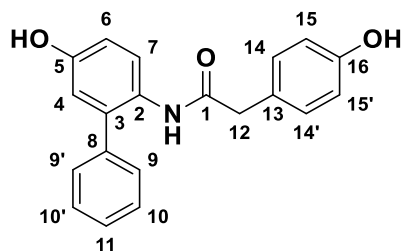
$^{13}\text{C NMR}$ (126 MHz, Acetone) δ (ppm) 170.43 (1C, C-1), 157.86 (1C, C-16), 157.32 (1C, C-6), 155.37 (1C, C-10), 136.91 (1C, C-7), 131.25 (2C, C-4, C-4'), 130.91 (2C, C-14, C-14'), 130.47 (1C, C-3), 128.20 (1C, C-13), 127.08 (1C, C-8), 126.28 (1C, C-12), 117.29 (1C, C-9), 116.42 (2C, C-15, C-15'), 116.32 (2C, C-5, C-5'), 114.75 (1C, C-11), 43.77 (1C, C-2).

MS (ESI+): 336.1 ($[\text{M}+\text{H}]^+$), 358.1 ($[\text{M}+\text{Na}]^+$).

HR-MS (ESI+): calc. for $\text{C}_{20}\text{H}_{17}\text{NO}_4$ ($[\text{M}+\text{H}]^+$): 336.1230, found: 336.1234; calc. for $\text{C}_{20}\text{H}_{17}\text{NO}_4$ ($[\text{M}+\text{Na}]^+$): 358.1050, found: 358.1046.

FT-IR (Diamond-ATR): ν (cm^{-1}) 3285.14, 1611.23, 1513.85, 1444.42, 1230.36, 821.527.

7.4.2.26 *N*-(5-Hydroxy-[1,1'-biphenyl]-2-yl)-2-(4-hydroxyphenyl)acetamide (L10)



L10
C₂₀H₁₇NO₃
[319.36]

In a reactor pressure vessel 2-(4-(Benzyloxy)phenyl)-*N*-(5-hydroxy-[1,1'-biphenyl]-2-yl)acetamide (115 mg, 0.280 mmol, 1.0 eq) was dissolved in a mixture of EtOAc (10 mL), EtOH (15 mL) and acetic acid (5 mL), and Pd/C (10%, 50 mg) was added. The reaction was stirred at room temperature in a hydrogen atmosphere (2 bar) for 24 h, after which full consumption of starting material was indicated by TLC analysis (*n*-hexane/EtOAc, 1:1). The reaction mixture was filtered over three filtered filter papers, and the filter cake was washed thoroughly with EtOH and concentrated *in vacuo*. The title compound was isolated as an off-white solid (85.0 mg, 0.280 mmol, quant.) after purification by flash column chromatography (*n*-hexane/EtOAc 1:1).

TLC: $R_f = 0.20$ (*n*-hexane/EtOAc, 1:1)

mp.: 94 °C

¹H NMR (300 MHz, dms_o) δ (ppm) 9.48 (s, 1H, NH), 9.22 (s, 1H, OH), 9.04 (s, 1H, OH), 7.41 – 7.24 (m, 4H, H-7, H-11, H-10, H-10'), 7.24 – 7.12 (m, 2H, H-9, H-9'), 6.99 – 6.88 (m, 2H, H-14, H-14'), 6.77 – 6.68 (m, 2H, H-6, H-4), 6.68 – 6.59 (m, 2H, H-15, H-15'), 3.31 (s, 2H, H-12).

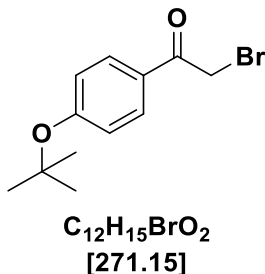
¹³C NMR (126 MHz, dms_o) δ (ppm) 169.84 (1C, C-1), 155.67 (1C, C-16), 155.16 (1C, C-5), 138.76 (C, C-2), 138.13 (1C, C-8), 129.79 (2C, C-14, C-14'), 128.70 (2C, C-10, C-10'), 128.40 (1C, C-3), 128.02 (3C, C-9, C-9', C-11), 126.87 (1C, C-13), 125.89 (1C, C-7), 116.12 (1C, C-6), 114.85 (2C, C-15, C-15'), 114.30 (1C, C-4), 41.65 (1C, C-12).

FT-IR (Diamond-ATR): ν (cm⁻¹) 3345.89, 2321.87, 1735.62, 1541.81, 1232.29, 1204.33.

MS (ESI⁺): 320.1 ([M+H]⁺), 342.1 ([M+Na]⁺), 661.3 ([2M+Na]⁺).

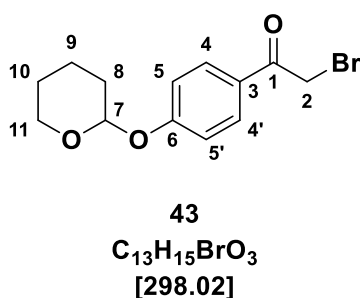
HR-MS (ESI⁺): calc. for C₂₀H₁₇NO₃ ([M+H]⁺): 320.1281, found: 320.1278 calc. for C₂₈H₂₂NO₃F₃ ([M+Na]⁺): 342.1101, found: 342.1095.

7.4.2.27 2-Bromo-1-(4-(*tert*-butoxy)phenyl)ethan-1-one (40)



In a two-neck flask, which was equipped with a reflux condenser, CuBr₂ (1.78 g, 7.98 mmol, 2.0 eq) and 1-(4-(*tert*-butoxy)phenyl)ethan-1-one were dissolved in EtOAc (40 mL) and refluxed for 36 h. The reaction mixture was cooled down to room temperature, filtered over celite, and the solvent was concentrated under reduced pressure. TLC analysis showed consumption of starting material, the crude mixture was obtained in 79% but the isolation of the pure product from the double brominated by-product was not possible.

7.4.2.28 2-Bromo-1-(4-((tetrahydro-2H-pyran-2-yl)oxy)phenyl)ethan-1-one (43)



In a Schlenk flask, and under an argon atmosphere, 3,4-dihydro-2H-pyran (1.91 mL, 0.020 mmol, 1.5 eq) and pyridinium *p*-toluenesulfonate (175 mg, 0.700 mmol, 0.1 eq) were added to the suspension of 2-bromo-1-(4-hydroxyphenyl)ethan-1-one (3.00 g, 14 mmol, 1.0 eq) in anhydrous DCM (28 mL). The reaction mixture was stirred for 72 h at room temperature while monitoring by TLC (*n*-hexane/EtOAc, 7:1). The black reaction mixture was diluted with sat. aq. NaHCO₃ (40 mL), the layers were separated, and the aqueous layer was extracted with DCM (3 x 30 mL). The combined organic layers were washed with sat. aq. NaCl (50 mL), dried over MgSO₄ and concentrated *in vacuo*. The

title compound was obtained as a brownish solid (2.50 g, 8.36 mmol, 60%), after purification by flash column chromatography (*n*-hexane/EtOAc, 7:1).

TLC: $R_f = 0.23$ (*n*-hexane/EtOAc, 7:1)

$^1\text{H NMR}$ (600 MHz, cd_2cl_2) δ (ppm) 7.97 – 7.87 (m, 2H, H-4, H-4'), 7.13 – 7.07 (m, 2H, H-5, H-5'), 5.52 (t, $J = 3.2$ Hz, 1H, H-7), 4.43 (s, 2H, H-2), 3.81 (ddd, $J = 11.3, 9.9, 3.0$ Hz, 1H, H-11"), 3.59 (dtd, $J = 11.4, 4.1, 1.5$ Hz, 1H, H-11'), 2.03 – 1.93 (m, 1H, H-10"), 1.92 – 1.79 (m, 2H, H-8), 1.74 – 1.63 (m, 2H, H-9", H-10'), 1.62 – 1.55 (m, 1H, H-9').

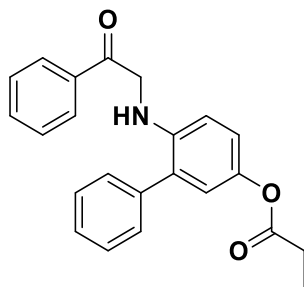
$^{13}\text{C NMR}$ (126 MHz, dms o) δ (ppm) 189.92 (1C, C-1), 160.64 (1C, C-6), 130.76 (2C, C-4, C-4'), 127.27 (1C, C-3), 116.01 (2C, C-5, C-5'), 95.45 (1C, C-7), 61.55 (1C, C-11), 30.07 (1C, C-2), 24.46 (1C, C-10), 18.28 (1C, C-9).

MS (ESI+): 321.0 [M+Na $^+$]

HR-MS (ESI+): calc. for $\text{C}_{13}\text{H}_{15}\text{BrO}_3$ ([M+Na] $^+$): 321.0097, found: 321.0101 calc. for $\text{C}_{13}\text{H}_{15}\text{BrO}_3$ ([M+Na] $^+$): 323.0077, found: 323.0082

FT-IR (Diamond-ATR): ν (cm^{-1}) 3267.79, 2941.88, 1597.73

7.4.2.29 6-((2-Oxo-2-phenylethyl)amino)-[1,1'-biphenyl]-3-yl propionate (44)

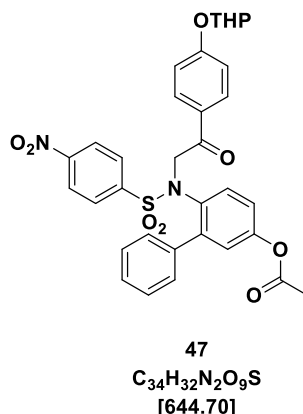


44

$\text{C}_{23}\text{H}_{21}\text{NO}_3$
[359.43]

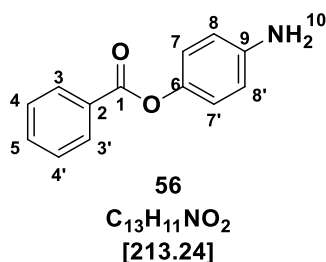
In a two-neck flask, equipped with reflux condenser, 6-amino-[1,1'-biphenyl]-3-yl propionate (161 mg, 0.670 mmol, 1.0 eq) was dissolved in MeCN (20 mL). Then K_2CO_3 (184 mg, 1.32 mmol, 2.0 eq) and 2-bromo-1-phenylethan-1-one (132 mg, 0.670 mmol, 1.0 eq) were added. While reflux for 48 h, and monitoring by TLC analysis (*n*-hexane/EtOAc, 4:1), there was no observed change on the TLC plate. Mass analysis of the crude reaction mixture didn't show any product formation.

7.4.2.30 6-((4-Nitro-N-(2-oxo-2-(4-((tetrahydro-2H-pyran-2-yl)oxy)phenyl)ethyl)phenyl)sulfonamido)-[1,1'-biphenyl]-3-yl propionate(47)



In a two-neck flask, under an argon atmosphere, 6-amino-[1,1'-biphenyl]-3-yl propionate (237 mg, 0.980 mmol, 1.1 eq) was dissolved in anhydrous DCM, followed by addition of pyridine (0.1 mL, 0.980 mmol, 1.1 eq). In a second one-neck flask, and under argon, 4-nitrobenzenesulfonyl chloride (218 mg, 0.890 mmol, 1.0 eq) was dissolved in anhydrous DCM (15 mL) and added to the reaction mixture. The reaction mixture was stirred for 12 h at room temperature and afterwards refluxed for an additional 12 h. Brown solid reaction mixture was dissolved in DCM (15 mL), washed with 1 M HCl (20 mL). The organic phase was separated, and the aqueous phase was extracted with DCM (3x10 mL). The combined organic layers were washed with sat. aq. NaCl, dried over Na₂SO₄ and concentrated *in vacuo*. After purification by flash column chromatography (*n*-hexane/EtOAc, 6:1) 6-((4-nitrophenyl)sulfonamido)-[1,1'-biphenyl]-3-yl propionate **46** was obtained as a brownish oil (223 mg, 58%). The oil (190 mg, 0.450 mmol, 1.0 eq) was dissolved in MeCN (10 mL). Then K₂CO₃ (124 mg, 0.890 mmol, 2.0 eq), and 2-bromo-1-(4-((tetrahydro-2H-pyran-2-yl)oxy)phenyl)ethan-1-one (147 mg, 0.490 mmol, 1.1 eq) were added. The yellow reaction mixture was stirred at room temperature for 24 h. TLC analysis monitoring did not show the formation of the product; hence the reaction mixture was refluxed for 4 h. The solvent was concentrated *in vacuo*, and the residue was dissolved in water (70 mL) extracted with EtOAc (3x40 mL). The organic layers were washed with sat. aq. NaCl solution (50 mL), dried over MgSO₄ and concentrated *in vacuo* to obtain a yellow oil. Mass analysis of the crude yellow oil did not show any traces of product formation.

7.4.2.31 4-Aminophenyl benzoate (56)



In a 250 mL hydrogen pressure vessel 4-nitrophenyl benzoate (1.56 g, 6.41 mmol, 1.0 eq) was dissolved in EtOH (20 mL) and EtOAc (15 mL), Pd/C (156 mg, 10%) was added to the stirring solution. The vessel was purged three times with nitrogen, followed by hydrogen. The reaction was stirred at room temperature for 3.5 h, at 2.5 bar. After 2 h pressure dropped to 1 bar, the reaction was stirred for an additional 1.5 h, there was no additional change in pressure observed. The TLC plate control (*n*-hexane/EtOAc, 2:1) showed complete consumption of the starting material. The reaction mixture was filtered over three pleated filter papers, washed thoroughly with EtOAc and dried in vacuum. Product was obtained as an off-white solid (1.29 g, 6.05 mmol, 95%).

TLC: $R_f = 0.28$ (*n*-hexane/EtOAc 2:1)

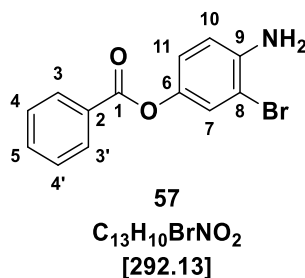
mp.: 156.1 °C

¹H NMR (300 MHz, CD₂Cl₂) δ (ppm) 8.17 (d, $J = 7.7$ Hz, 2H, H-3, H-3'), 7.65 (d, $J = 14.8$ Hz, 1H, H-5), 7.56 – 7.48 (m, 2H, H-4, H-4'), 6.98 (d, $J = 8.8$ Hz, 2H, H-7, H-7'), 6.71 (d, $J = 8.8$ Hz, 2H, H-8, H-8'), 3.75 (s, 2H, H-NH₂).

¹³C NMR (75 MHz, CD₂Cl₂): δ (ppm) 165.63 (1C, C-1), 144.73 (1C, C-9), 142.86 (1C, C-6), 133.36 (1C, C-5), 129.90 (2C, C-3, C-3'), 128.52 (2C, C-4, C-4'), 122.24 (2C, C-7, C-7') 115.27 (2C, C-8, C-8').

HR-MS (ESI⁺): calc. for C₁₃H₁₁NO₂ ([M+H]⁺): 214.0863, found: 214.0867; calc. for C₁₃H₁₁NO₂ ([M+Na]⁺): 236.0682, found: 236.0687

FT-IR (Diamond-ATR): ν (cm⁻¹) 3449.06, 3370.96, 2361.41, 1715.37, 1508.06, 1273.75, 1191.79.

7.4.2.32 4-Amino-3-bromophenyl benzoate (57)

In one neck flask in an argon atmosphere, 4-aminophenyl benzoate (630 mg, 2.97 mmol, 1.0 eq) was dissolved in anhydrous DCM (18 mL). After stirring for five minutes NBS (529 mg, 2.97 mmol, 1.0 eq) was added. The reaction was monitored by TLC plate (*n*-hexane/EtOAc 2:1) for 6h. The reaction was stopped after 20h, a dark purple solution was washed with water (3x 25 mL), aq. NaCl (50 mL), dried over MgSO₄ and concentrated in vacuum. The product was purified by flash column chromatography and obtained as a dark red solid (683 mg, 2.33 mmol, 78%).

TLC: R_f = 0.50 (*n*-hexane/EtOAc, 2:1)

mp.: 56.3 °C

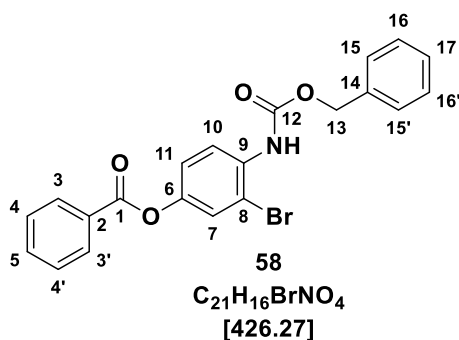
¹H NMR (300 MHz, CD₂Cl₂) δ (ppm) 8.24 – 8.14 (m, 2H, H-3, H-3'), 7.75 – 7.63 (m, 1H, H-5), 7.56 (t, *J* = 7.7 Hz, 2H, H-4, H-4'), 7.35 (d, *J* = 2.6 Hz, 1H, H-7), 7.04 (dd, *J* = 8.7, 2.6 Hz, 1H, H-11), 6.86 (d, *J* = 8.7 Hz, 1H, H-10), 4.18 (s, 2H, H-NH₂).

¹³C NMR (75 MHz, CD₂Cl₂) δ 165.32 (1C, C-1), 142.46 (1C, C-9), 133.56 (1C, C-5), 129.95 (3C, C-3, C-3', C-2), 129.48, 128.57 (2C, C-4, C-4'), 125.50 (1C, C-7), 121.82 (1C, C-11), 115.39 (1C, C-10), 108.10 (1C, C-8).

HR-MS (ESI⁺): calc. for C₁₃H₁₀BrNO₂ ([M+H]⁺): 291.9968, found: 291.9970 calc. for C₁₃H₁₀BrNO₂ ([M+Na]⁺): 313.9787, found: 313.9788

FT-IR (Diamond-ATR): ν (cm⁻¹) 3466.41, 3376.74, 1728.87, 1487.81, 1253.50, 702.96.

7.4.2.33 4-(((Benzyloxy)carbonyl)amino)-3-bromophenyl benzoate (58)



In one neck flask, 4-amino-3-bromophenyl benzoate (5.08 g, 17.3 mmol, 1.0 eq) was dissolved in EtOAc (60 mL) and pyridine (1.62 mL, 20.07 mmol, 1.3 eq) was added. The reaction mixture was cooled down while dropwise addition of CBz-Cl (4.86 mL, 34.7 mmol, 2.0 eq). Shortly after addition, white suspension occurred. The reaction was monitored by TLC plate (*n*-hexane/EtOAc, 3:1), and it was stopped after 1 h. The reaction mixture was washed with water and the aqueous phase was extracted with EtOAc (3 x 40 mL). The combined organic phases were washed with (2 x 40 mL), sat. aq. NaHCO₃ solution sat. aq. NaCl solution (50 mL), dried over MgSO₄ and the solvent was removed under reduced pressure. The obtained crude product was recrystallized from (*n*-hexane/EtOAc, 10:1) 370 mL, and the product was obtained as a light orange needle (6.48 g, 15.2 mmol, 87%).

TLC: $R_f = 0.77$ (*n*-hexane/EtOAc, 2:1)

mp.: 99.4 °C

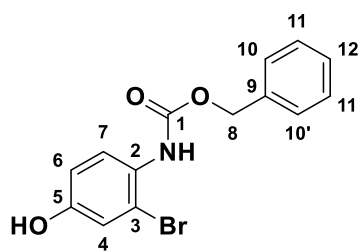
¹H NMR (300 MHz, Acetone) δ (ppm) 8.22 – 8.13 (m, 2H, H-3, H-3'), 8.09 – 8.00 (m, 1H, H-5), 7.80 – 7.68 (m, 1H, H-7), 7.68 – 7.54 (m, 3H, H-4, H-4', H-10), 7.52 – 7.29 (m, 6H, H-15, H-15', H-16, H-16', H-17, H-11), 5.23 (s, 2H, H-13).

¹³C-NMR (75 MHz, Acetone) δ (ppm) 165.35 (1C, C-1), 158.93 (1C, C-12), 154.40 (1C, C-14), 148.26 (1C, C-6), 137.51 (1C, C-2), 135.17 (1C, C-9), 134.75 (1C, C-5), 130.82 (2C, C-3, C-3'), 130.15 (1C, C-8), 129.66 (2C, C-4, C-4'), 129.32 (2C, C-16, C-16'), 128.98 (2C, C-15, C-15'), 126.89 (1C, C-17), 124.37 (1C, C-11), 122.67 (1C, C-10), 100.87 (1C, C-7), 67.52 (C-13).

HR-MS (ESI⁺): calc. for C₂₁H₁₆BrNO₄ ([M+H]⁺): 426.0335, found: 426.0331.

FT-IR (Diamond-ATR): ν (cm⁻¹) 3300.05, 3029.15, 2958.98, 1751.93, 1689.76, 1527.22, 753.62, 699.43.

7.4.2.34 Benzyl (2-bromo-4-hydroxyphenyl) carbamate (59)



59

 $C_{14}H_{12}BrNO_3$

[322.16]

In a one neck flask, 4-amino-3-bromophenyl benzoate (428 mg, 1.47 mmol, 1.0 eq) was dissolved in 10 mL of EtOAc. Pyridine (153.7 μ L, 1.90 mmol, 1.3 eq) was added and the reaction mixture was stirred for 5 min. The reaction mixture was cooled down while dropwise addition of CBZ-Cl (420 μ L, 2.93 mmol, 2.0 eq). Shortly after addition reaction mixture became a white suspension. The reaction was monitored by TLC (n-hexane/EtOAc, 2:1), and it was stopped after 1.5 h. The reaction mixture was washed with water (25 mL), sat. aq. $NaHCO_3$ solution (30 mL), sat. aq. NaCl solution (50 mL), dried over $MgSO_4$ and the solvent was removed under vacuum. The quantitatively obtained product was used further in the second step without additional purification. It was dissolved in MeOH (50 mL), stirred for 20 min, until the reaction mixture was homogenous, K_2CO_3 (261.4 mg, 1.89 mmol, 2.6 eq) was added and the reaction was stirred on room temperature for 30 min. TLC (n-hexane/EtOAc, 3:1) analysis confirmed completion of the reaction, as no educt was observed on the TLC plate. MeOH was removed under vacuum, the reaction mixture was dissolved in EtOAc (20 mL), washed with water (30 mL), sat. aq. $NaHCO_3$ solution (30 mL), sat. aq. NaCl solution (30 mL), dried over $MgSO_4$ and the solvent was removed under vacuum. The product was isolated as a white solid (388 mg, 1.20 mmol, 81%) after purification by flash column chromatography.

TLC: $R_f = 0.16$ (n-hexane/EtOAc, 5:1)

mp.: 150.3 $^{\circ}C$

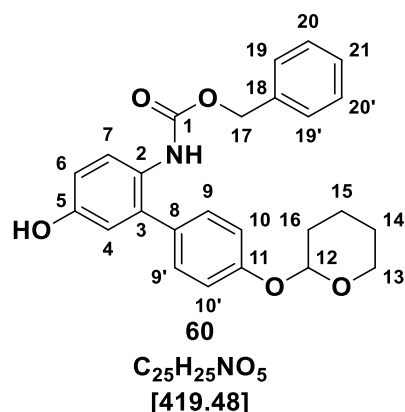
1H NMR (300 MHz, Acetone) δ 8.67 (s, 1H, H-OH), 7.79 (s, 1H, H-NH), 7.58 (d, $J = 8.8$ Hz, 2H, H-6), 7.48 – 7.25 (m, 5H, H-10, H-10', H-11, H-11', H-12), 7.10 (dd, $J = 2.8, 0.8$ Hz, 1H, H-4), 6.86 (dd, $J = 8.8, 2.7$ Hz, 1H, H-6), 5.17 (s, 2H, H-8).

^{13}C NMR (75 MHz, Acetone) δ , 155.19 (1C, C-1), 154.12 (1C, C-5), 137.00 (1C, C-9), 128.47 (1C, C-2) 128.38 (3C, C-11, C-11', C-12), 127.92 (3C, C-10, C-10', C-7), 118.81 (1C, C-4), 115.07 (1C, C-6), 66.24 (1C, C-8).

HR-MS (ESI+): calc. for $\text{C}_{14}\text{H}_{12}\text{BrNO}_3$ ($[\text{M}+\text{Na}]^+$): 343.9893, found: 343.9906.

FT-IR (Diamond-ATR): ν (cm^{-1}) 3291.89, 3031.55, 2317.05, 2116.49, 1662.34, 1528.31, 1340.28, 1216.86, 1070.3, 867.81, 757.88.

7.4.2.35 Benzyl (5-hydroxy-4'-((tetrahydro-2H-pyran-2-yl)oxy)-[1,1'-biphenyl]-2-yl)carbamate (60)



In a 10 mL microwave vial, benzyl (2-bromo-4-hydroxyphenyl)carbamate (58.0 mg, 0.16 mmol, 1.0 eq), (4-((tetrahydro-2H-pyran-2-yl)oxy)phenyl)boronic acid (37.9 mg, 0.170 mmol, 1.1 eq), Na_2CO_3 (32.85 mg, 0.310 mmol, 2.0 eq) and $\text{Pd}(\text{PPh}_3)_4$ (9.00 mg, 0.078 mmol, 5 mol%) were dissolved in 3 mL (DME/ H_2O , 3:1) solvent; previously degassed under an argon stream for 30 min. Upon addition, a light yellow solution occurred; the reaction mixture was placed into a microwave, stirred for 10 min at 110 °C, and maximal pressure was 12 psi. TLC plate control (*n*-hexane/EtOAc, 2:1) showed completion of the reaction, consecutively, the solvent was removed under reduced pressure. The reaction mixture was dissolved in EtOAc and washed with water (2 x 10 mL). The aqueous phase was extracted with EtOAc (2 x 15 mL). Afterwards, the combined organic phases were washed with sat. aq. NaHCO_3 solution (20 mL), sat. aq. NaCl solution (20 mL), dried over MgSO_4 and concentrated in vacuum resulting as crude orange-yellow oil. The pure product was obtained as a white solid (45.0 mg, 0.110 mmol, 68%) after flash column chromatography with (*n*-hexane/EtOAc, 3:1).

TLC: $R_f = 0.22$ (*n*-hexane/EtOAc, 3:1)

mp.: 46.3 °C

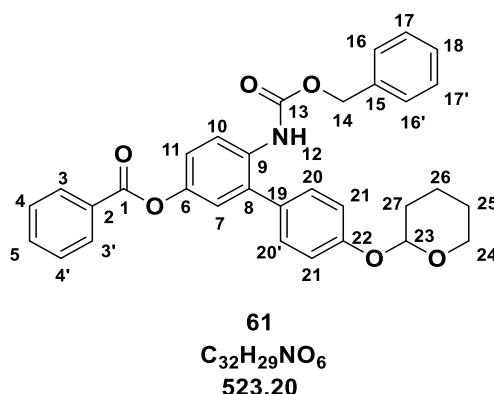
¹H NMR (300 MHz, CD₂Cl₂) δ 7.70 (d, *J* = 8.6 Hz, 1H, -OH), 7.34 (m, 5H, H-19, H-19', H-20, H-20', H-21), 7.26 – 7.18 (m, 2H, H-9, H-9'), 7.13 – 7.03 (m, 2H, H-10, H-10'), 6.76 – 6.65 (m, 2H, H-4, H-6), 6.49 (s, 1H, H-7), 5.79 (s, 1H, -NH), 5.45 (t, *J* = 3.4 Hz, 1H, H-12), 5.12 (s, 2H, H-17, H-17'), 3.92 (ddd, *J* = 11.8, 8.9, 3.2 Hz, 1H, H-13), 3.65 – 3.56 (m, 1H, H-13'), 2.07 – 1.80 (m, 3H, H-16, H-16', H-15), 1.66 (tdd, *J* = 17.6, 8.7, 4.5 Hz, 3H, H-14, H-14', H-15).

¹³C NMR (75 MHz, CD₂Cl₂) δ 157.36 (C-11), 154.81 (C-5), 153.25 (C-1), 137.03 (C-18), 131.69 (C-8), 130.67 (C-9, C-9'), 129.02 (C-20, C-20'), 128.67 (C-21), 128.58 (C-19, C-19'), 128.00 (C-3), 117.44 (C-2), 117.36 (C-6, C-10, C-10'), 115.18 (C-4, C-7), 97.09 (C-12), 67.38 (C-17), 62.85 (C-13), 30.92 (C-16), 25.76 (C-14), 19.47 (C-15).

HR-MS (ESI⁻): calc. for C₂₅H₂₅NO₅ ([M-H]⁻): 418.1660, found: 418.1655

FT-IR (Diamond-ATR): ν (cm⁻¹) 3315.15, 3052.25, 2935.89, 2881.71, 1712.85, 1612.49, 1512.12, 1434.85, 1194.15, 1116.88, 1031.61, 954.34, 923.25, 822.88, 753.61, 706.53.

7.4.2.36 6-(((Benzyloxy)carbonyl)amino)-4'-((tetrahydro-2H-pyran-2-yl)oxy)-[1,1'-biphenyl]-3-yl benzoate (61)



In a dry 100 mL Schlenk flask, benzoic acid (1.25 g, 10.2 mmol, 2.0 eq), 4-(dimethylamino)-pyridine (63.0 mg, 0.512 mmol, 0.1 eq) and EDC-HCl (1.47 g, 7.68 mmol, 1.5 eq) were dissolved in anhydrous chloroform (30 mL). Benzyl (5-hydroxy-4'-((tetrahydro-2H-pyran-2-yl)oxy)-[1,1'-biphenyl]-2-yl)carbamate (2.09 g, 4.99 mmol, 1.0 eq) was dissolved in anhydrous chloroform (40 mL) and added to the reaction mixture. It was stirred overnight at room temperature. After monitoring the reaction by TLC (*n*-hexane/EtOAc, 4:1), the reaction was stopped as it was observed the complete consumption of the starting material. The solvent was removed under reduced pressure, and the reaction mixture was diluted in EtOAc (40 mL), washed with water (50 mL). The aqueous phase was extracted with EtOAc (3 x 20 mL). The combined organic phase was

washed with 1 M HCl, sat. aq. NaHCO₃ solution, sat. aq. NaCl solution dried over MgSO₄ and concentrated in vacuum. Product was isolated as a brown solid (2.21 g, 4.22 mmol, 83%) after purification by flash column chromatography (*n*-hexane/EtOAc, 4:1).

TLC: $R_f = 0.66$ (*n*-hexane/EtOAc 4:1)

mp.: 97 °C

¹H NMR (300 MHz, CD₂Cl₂) δ (ppm) 8.25 – 8.14 (m, 3H, H-3, H-3', H-10), 7.64 – 7.44 (m, 3H, H-5, H-4, H-4'), 7.43 – 7.26 (m, 6H, H-16, H-16', H-17, H-17', H-18, H-11), 7.26 – 7.07 (m, 4H, H-20, H-20', H-21, H-21), 6.80 (s, 1H, H-12), 5.46 (t, $J = 3.3$ Hz, 1H, H-23), 5.17 (s, 2H, H-14), 3.94– 3.87 (m, 1H, H-24), 3.68 – 3.54 (m, 1H, H-24'), 2.10 – 1.77 (m, 3H, H-26, H-27), 1.77 – 1.50 (m, 3H, H-25, H-26).

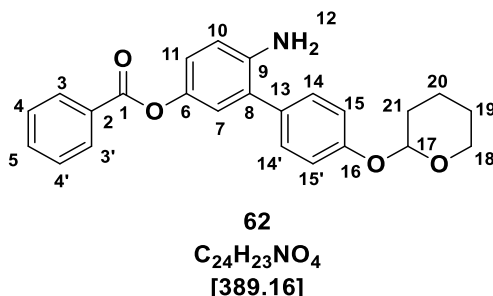
¹³C NMR (75 MHz, CD₂Cl₂) δ (ppm) 165.61 (1C, C-1), 157.61 (1C, C-22), 153.86 (1C, C-13), 146.96 (1C, C-6), 136.76 (1C, C-15), 133.22 (2C, C-5, C-8), 130.65 (5C, C-16, C-16', C-17, C-17', C-18), 130.00 (2, C-19, C-2), 129.01 (4C, C-20, C-20', C-4, C-4'), 128.90 (3C, C-9, C-3, C-3'), 123.72 (1C, C-10), 121.50 (1C, C-11), 117.44 (3C, C-21, C-21', C-7), 96.90 (1C, C-23), 67.32 (1C, C-14), 62.60 (1C, C-24), 30.74 (1C, C-27), 25.60 (1C, C-25), 19.27 (1C, C-27).

FT-IR (Diamond-ATR): ν (cm⁻¹) 3285.1433, 3028.6572, 1642.0896, 1611.234, 1512.8823, 1306.5364, 1230.3619, 1103.0831, 899.6298, 705.33.

MS (ESI+): 546.2 ([M+Na]⁺).

HR-MS (ESI+): calc. for C₃₂H₂₉NO₆ ([M+Na]⁺): 546.1887, found: 546.1887

7.4.2.37 6-Amino-4'-((tetrahydro-2H-pyran-2-yl)oxy)-[1,1'-biphenyl]-3-yl benzoate (62)



In a 250 mL pressure vessel 6-(((benzyloxy)carbonyl)amino)-4'-((tetrahydro-2H-pyran-2-yl)oxy)-[1,1'-biphenyl]-3-yl benzoate (2.15 g, 4.10 mmol, 1.0 eq) was dissolved in EtOH (25 mL) and EtOAc (30 mL), Pd/C (200 mg, 1.88 mmol, 50 mol%) was added and

stirred under hydrogen pressure at 4 bar for 5 h. TLC control (*n*-hexane/EtOAc, 4:1) confirmed complete consumption of the starting material. The reaction mixture was filtrated, the solvent was removed under reduced pressure. After purification by flash column chromatography (*n*-hexane/EtOAc, 4:1), the product was obtained as a white solid (1.55 g, 3.98 mmol, 94%).

TLC: $R_f = 0.23$ (*n*-hexane/EtOAc, 4:1)

mp.: 49 °C

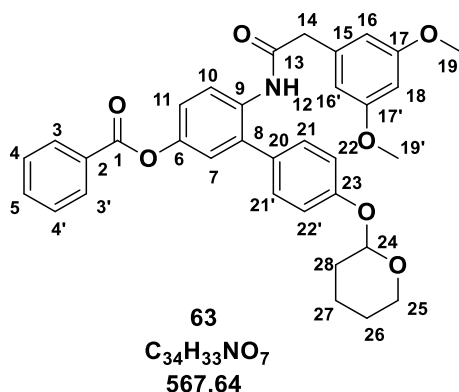
¹H NMR (300 MHz, CD₂Cl₂) δ (ppm) 8.21 – 8.14 (m, 2H, H-3, H-3'), 7.64 (dd, $J = 7.6, 0.5$ Hz, 1H, H-5), 7.57 – 7.48 (m, 2H, H-4, H-4'), 7.40 (m, 2H, H-14, H-14'), 7.16 – 7.10 (m, 2H, H-15, H-15'), 7.01 – 6.94 (m, 2H, H-11, H-7), 6.81 – 6.76 (m, 1H, H-10), 5.45 (t, $J = 3.4$ Hz, 1H, H-17), 3.98 – 3.54 (m, 2H, H-18). 1.90 – 1.54 (m, 6H, H-21, H-20, H-19).

¹³C NMR (75 MHz, CD₂Cl₂) δ (ppm) 166.03 (1C, C-1), 156.95 (1C, C-16), 143.30 (1C, C-9), 142.27 (1C, C-6), 133.76 (1C, C-5), 132.20 (1C, C-13), 130.35 (2C, C-14, C-14'), 130.32 (2C, C-3, C-3'), 128.93 (2C, C-4, C-4'), 128.16 (1C, C-8), 123.52 (1C, C-7), 121.56 (1C, C-11), 117.23 (2C, C-15, C-15'), 116.14 (1C, C-10), 96.93 (1C, C-17), 62.59 (1C, C-18), 30.78 (1C, C-19), 25.64 (1C, C-20), 19.33 (1C, C-17).

MS (ESI+): 390.2 ([M+H]⁺), 412.2 ([M+Na]⁺).

HR-MS (ESI+): calc. for C₂₄H₂₃NO₄ ([M+H]⁺): 390.1700, found: 390.1702; calc. for C₂₄H₂₃NO₄ ([M+Na]⁺): 412.1519, found: 412.1520

FT-IR (Diamond-ATR): ν (cm⁻¹) 3372.40, 2941.39, 1725.01, 1485.88, 1229.39, 1167.68.

7.4.2.38 6-(2-(3,5-Dimethoxyphenyl)acetamido)-4'-((tetrahydro-2H-pyran-2-yl)oxy)-[1,1'-biphenyl]-3-yl benzoate (63)


In a dry 100 mL two neck round bottom flask equipped with a reflux condenser (3,5-dimethoxyphenyl)acetic acid (250 mg, 1.30 mmol, 2.0 eq), EDC-HCl (390 mg, 1.90 mmol, 3.0 eq), 1-Hydroxybenzotriazole (26 mg, 0.19 mmol, 0.3 eq) and anhydrous toluene (20 mL) were added and stirred at 100°C for 10 minutes under an argon atmosphere. 6-amino-4'-((tetrahydro-2H-pyran-2-yl)oxy)-[1,1'-biphenyl]-3-yl benzoate (250 mg, 0.640 mmol, 1.0 eq) was dissolved in anhydrous toluene (5 mL) and added to the flask. The reaction mixture was refluxed at 120°C for 6 h and stirred overnight at room temperature. Reaction monitoring using TLC showed completion, water (50 mL) was added, and extracted with toluene. The organic phase was washed with 1 M HCl (50 mL) sat. aq. NaHCO₃ solution (50 mL), sat. aq. NaCl solution (50 mL), dried over MgSO₄ and concentrated in vacuum. After the purification by flash column chromatography (*n*-hexane/EtOAc, 1.5:1), the product was obtained as a brown solid (350 mg, 0.61 mmol, 95%).

TLC: $R_f = 0.47$ (*n*-hexane/EtOAc, 1.5:1)

mp.: 106 °C

¹H NMR (300 MHz, CD₂Cl₂) δ (ppm) 8.44 (d, $J = 8.9$ Hz, 1H, H-10), 8.22 – 8.12 (m, 2H, H-3, H-3'), 7.71 – 7.59 (m, 1H, H-5), 7.52 (ddt, $J = 8.3, 7.0, 1.1$ Hz, 2H, H-4, H-4'), 7.37 (s, 1H, H-12), 7.17 (dd, $J = 8.9, 2.8$ Hz, 1H, H-11), 7.09 – 6.89 (m, 5H, H-7, H-16, H-16', H-22, H-22'), 6.33 (t, $J = 2.3$ Hz, 1H, H-18), 6.26 (d, $J = 2.3$ Hz, 2H, H-16, H-16'), 5.46 (t, $J = 3.2$ Hz, 1H, H-24), 4.00 – 3.86 (m, 1H, H-25), 3.73 (s, 6H, H-19, H-19'), 3.70 – 3.58 (m, 1H, H-25), 3.56 (s, 2H, H-14), 1.97 – 1.83 (m, 2H, H-28), 1.80 – 1.59 (m, 4H, H-26, H-27).

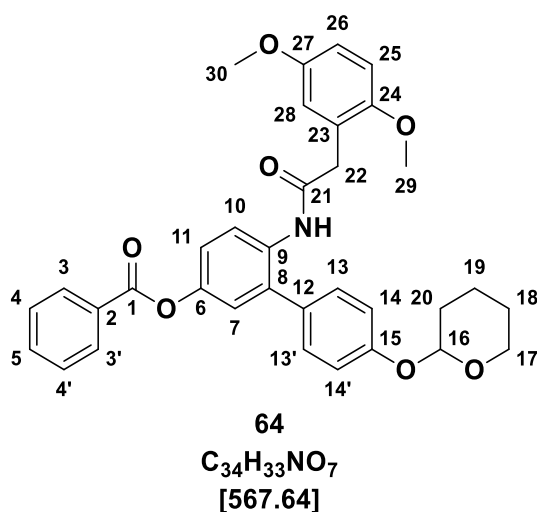
^{13}C NMR (75 MHz, CD_2Cl_2) δ (ppm) 168.89 (1C, C-13), 165.55 (1C, C-1), 161.69 (1C, C-15), 157.36 (1C, C-23), 147.14 (1C, C-6), 136.41, 133.98 (1C, C-5), 133.39 (1C, C-2), 133.20 (1C, C-9), 130.39 (2C, C-3, C-3'), 129.98 (2C, C-21, C-21'), 128.99 (2C, C-4, C-4'), 123.60 (1C, C-7), 121.61 (1C, C-10), 121.29 (1C, C-11), 120.9 (1C, C-8), 117.20 (2C, C-22, C-22'), 107.59 (2C, C-16, C-16'), 100.21 (1C, C-18), 96.97 (1C, C-24), 62.63 (1C, C-25), 60.63, 55.63 (2C, C-19, C-19'), 45.69 (1C, C-14), 30.91 (1C, C-26), 30.11, 25.65 (1C, C-27), 19.41 (1C, C-28).

MS (ESI+): 590.2 ($[\text{M}+\text{Na}]^+$), 568.3 ($[\text{M}+\text{H}]^+$).

HR-MS (ESI+): calc. for $\text{C}_{34}\text{H}_{33}\text{NO}_7$ ($[\text{M}+\text{Na}]^+$): 590.2149, found: 590.2149; calc. for $\text{C}_{34}\text{H}_{33}\text{NO}_7$ ($[\text{M}+\text{H}]^+$): 568.2330 found: 568.2338.

FT-IR (Diamond-ATR): ν (cm^{-1}) 3265.37, 2952.48, 2922.10, 1735.13, 1510.47, 1238.07, 1148.40, 816.70, 704.85.

7.4.2.39 6-(2-(2,5-Dimethoxyphenyl)acetamido)-4'-((tetrahydro-2H-pyran-2-yl)oxy)-[1,1'-biphenyl]-3-yl benzoate (64)



In a two neck flask, 6-amino-4'-((tetrahydro-2H-pyran-2-yl)oxy)-[1,1'-biphenyl]-3-yl benzoate (304.4 mg, 0.782 mmol, 1.0 eq.) was dissolved in anhydrous toluene with 2-(2,5-dimethoxyphenyl)acetic acid (307 mg, 1.56 mmol, 2.0 eq.), EDC-HCl (450 mg, 2.34 mmol, 3.0 eq) and HOBT (28.7 mg, 0.212 mmol, 0.3 eq) and refluxed for 27 h under an argon atmosphere. The reaction was controlled by TLC (*n*-hexane/EtOAc, 3:1) till the full conversion of the educt. The mixture was washed with water, and the aqueous phase was extracted with toluene (4 x 40 mL), the combined organic phases were washed with sat. aq. NaHCO_3 solution (2 x 40 mL) and sat. aq. NaCl solution (40 mL). The organic phase was dried over MgSO_4 and the solvent was removed under vacuum. The product

was purified with a *n*-hexane wash and was obtained as a light green-yellow milky oil (337 g, 0.594 mmol, 76%).

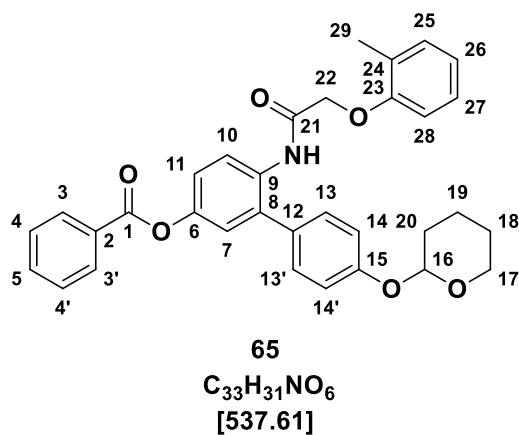
TLC: $R_f = 0.3$ (*n*-hexane/EtOAc, 3:1)

$^1\text{H-NMR}$ (300 MHz, CD_2Cl_2) δ (ppm) 8.38 (d, $J = 8.9$ Hz, 1H, H-7), 8.21 – 8.13 (m, 2H, H-3, H-3'), 7.73 (s, 1H, -NH), 7.68 – 7.60 (m, 1H, H-5), 7.56 – 7.46 (m, 2H, H-4, H-4'), 7.19 – 7.06 (m, 3H, H-11, H-13, H-13'), 7.04 – 6.95 (m, 3H, H-10, H-14, H-14'), 6.81 – 6.71 (m, 3H, H-25, H-26-H, H-28), 5.47 (t, $J = 3.3$ Hz, 1H, H-16), 3.94 (ddd, $J = 11.8, 9.0, 3.2$ Hz, 1H, H-17), 3.74 (s, 3H, H-30), 3.69 – 3.60 (m, 1H, H-17), 3.57 (d, $J = 2.2$ Hz, 2H, H-22), 3.47 (s, 3H, H-29), 2.10 – 1.84 (m, 3H, H-19, H-20), 1.76 – 1.58 (m, 3H, H-18, H-19).

$^{13}\text{C-NMR}$ (75 MHz, CD_2Cl_2) δ (ppm) 169.47 (1C, C-21), 165.74 (1C, C-1), 157.41 (1C, C-15), 154.31 (1C, C-23), 151.50 (1C, C-27), 147.19 (1C, C-24), 134.12 (1C, C-5), 133.76 (1C, C-6), 133.54 (1C, C-9), 130.67 (1C, C-12), 130.54 (2C, C-13, C-13'), 130.45 (2C, C-3, C-3'), 130.16 (1C, C-8), 129.14 (2C, C-4, C-4'), 124.16 (1C, C-2), 123.83 (1C, C-10), 122.32 (1C, C-7), 121.35 (1C, C-11), 117.46 (2C, C-14, C-14'), 117.15 (1C, C-28), 114.05 (1C, C-26), 112.42 (1C, C-25), 97.04 (1C, C-16), 62.81 (1C, C-17), 55.62 (2C, C-29, C-30), 40.30 (1C, C-22), 30.30 (1C, C-20), 25.82 (1C, C-18), 19.05 (1C, C-19).

HR-MS (ESI+): calc. for $\text{C}_{34}\text{H}_{33}\text{NO}_7$ ($[\text{M}+\text{H}]^+$): 568.2330, found: 568.2337.

7.4.2.40 4'-((Tetrahydro-2H-pyran-2-yl)oxy)-6-(2-(*o*-tolylloxy)acetamido)-[1,1'-biphenyl]-3-yl benzoate (65)



In a two neck flask 6-amino-4'-((tetrahydro-2H-pyran-2-yl)oxy)-[1,1'-biphenyl]-3-yl benzoate (249 mg, 0.640 mmol, 1.0 eq.) was dissolved in anhydrous chloroform with 2-(*o*-tolylloxy)acetic acid (213 mg, 1.28 mmol, 2.0 eq), EDC-HCl (369 mg, 1.93 mmol,

3.0 eq) and HOBt (26.0 mg, 0.192 mmol, 0.3 eq) and refluxed for 22 h under argon atmosphere. The reaction was frequently controlled via TLC (*n*-hexane/EtOAc, 2:1) till the full conversion of the educt. After that the mixture was washed with water and the aqueous phase was extracted with chloroform (4 x 40 mL), the combined organic phases were washed with sat. aq. NaHCO₃ solution (2 x 40 mL) and sat. aq. NaCl solution (40 mL). The organic phase was dried over MgSO₄ and the solvent was removed under vacuum. The product was obtained as an off-yellow solid (310 mg, 0.576 mmol, 90%) after washing with *n*-hexane.

TLC: $R_f = 0.7$ (*n*-hexane/EtOAc, 2:1)

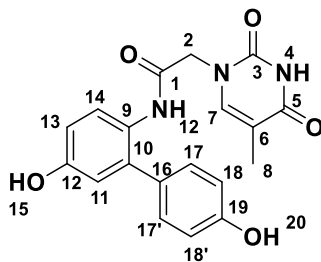
mp.: 151.6 °C

¹H-NMR (300 MHz, CD₂Cl₂) δ (ppm) 8.55 (d, $J = 8.9$ Hz, 1H, H-10), 8.47 (s, 1H, -NH), 8.22 – 8.15 (m, 2H, H-3, H-3'), 7.73 – 7.66 (m, 1H, H-5), 7.60 – 7.53 (m, 2H, H-4-H, H-4'), 7.23 (dd, $J = 8.7, 3.6$ Hz, 3H, H-7, H-13, H-13'), 7.18 – 7.08 (m, 3H, H-26, H-25, H-27), 7.07 – 7.00 (m, 2H, H-14, H-14'), 6.91 (td, $J = 7.4, 1.0$ Hz, 1H, H-11), 6.76 (d, $J = 8.1$ Hz, 1H, H-28), 5.41 (t, $J = 3.3$ Hz, 1H, H-16), 4.55 (s, 2H, H-22), 3.89 (ddd, $J = 12.2, 9.4, 3.2$ Hz, 1H, H-17), 3.63 – 3.54 (m, 1H, H-17), 2.05 – 1.84 (m, 3H, H-19, H-20), 1.80 (s, 3H, H-29), 1.74 – 1.57 (m, 3H, H-18, H-19).

¹³C-NMR (75 MHz, CD₂Cl₂) δ (ppm) 166.86 (1C, C-21), 165.71 (1C, C-1), 157.90 (1C, C-15), 155.73 (1C, C-23), 147.61 (1C, C-6), 134.18 (1C, C-5), 133.97 (C-9), 132.84 (C-12), 131.42 (C-25), 130.79 (2C, C-13, C-13'), 130.67 (2C, C-3, C-3'), 130.25 (1C, C-2), 130.11 (1C, C-8), 129.11 (2C, C-4, C-4'), 127.54 (1C, C-27), 127.26 (1C, C-24), 124.07 (1C, C-26), 122.29 (1C, C-11), 122.08 (1C, C-10), 121.61 (1C, C-7), 117.53 (2C, C-14, C-14'), 111.70 (1C, C-28), 96.94 (1C, C-16), 68.19 (1C, C-22), 62.64 (1C, C-17), 30.93 (1C, C-20), 25.79 (1C, C-18), 19.37 (1C, C-19), 16.11 (1C, C-29).

HR-MS (ESI⁺): calc. for C₃₃H₃₁NO₆ ([M+H]⁺): 538.2224, found: 538.2224

7.4.2.41 *N*-(4',5-Dihydroxy-[1,1'-biphenyl]-2-yl)-2-(5-methyl-2,4-dioxo-3,4-dihydropyrimidin-1(2H)-yl)acetamide (67)



67

$C_{19}H_{17}N_3O_5$
[367.36]

In a dry 100 mL two neck round bottom flask thymine-1-acetic acid (240 mg, 1.20 mmol, 2.0 eq), EDC-HCl (390 mg, 1.90 mmol, 3.0 eq.) and 1-hydroxybenzotriazole (26.0 mg, 0.190 mmol, 0.30 eq.) were dissolved in anhydrous toluene (20 mL) and stirred at 100 °C under an argon atmosphere. In a second flask 6-amino-4'-((tetrahydro-2H-pyran-2-yl)oxy)-[1,1'-biphenyl]-3-yl benzoate (250 mg, 0.640 mmol, 1.0 eq) was dissolved in anhydrous toluene (5 mL) and added to the flask. The reaction mixture was refluxed at 120 °C for 18 h. Reaction monitoring by TLC (DCM/EtOAc, 50:1) showed incompleteness. The toluene was evaporated, and the reaction mixture was diluted with dimethylformamide. It was stirred for 6 h at 162 °C and room temperature for 2 days. The reaction was monitored by TLC and no products were observed. EtOAc (10 mL) and water (10 mL) were added into the reaction mixture, the aqueous phase was extracted with EtOAc (3 x 20 mL). The combined organic phase was washed with water (20 mL), 1 M HCl (20 mL), sat. aq. NaHCO₃ solution (20 mL), sat. aq. NaCl solution (20 mL) dried over MgSO₄ and concentrated in vacuum. The raw product was obtained as a brown solid (127 mg, 0.35 mmol, 30%). Before biophysical studies sample was purified by preparative HPLC.

TLC: $R_f = 0.19$ (DCM/EtOAc, 50:1)

HPLC (preparative, 20 → 100% MeCN in 35 min): $t_R = 13.5$ min.

mp.: 50 °C (decomposition)

¹H NMR (400 MHz, DMSO) δ (ppm) 11.27 (s, 1H, H-4), 9.56 – 9.39 (m, 2H, H-15, H-20), 9.26 (s, 1H, H-NH), 7.35 (d, $J = 1.5$ Hz, 1H, H-13), 7.29 – 7.01 (m, 3H, H-11, H-17, H-17'), 6.85 – 6.62 (m, 4H, H-13, H-14, H-18, H-18'), 4.31 (s, 2H, H-2), 1.75 (s, 3H, H-8).

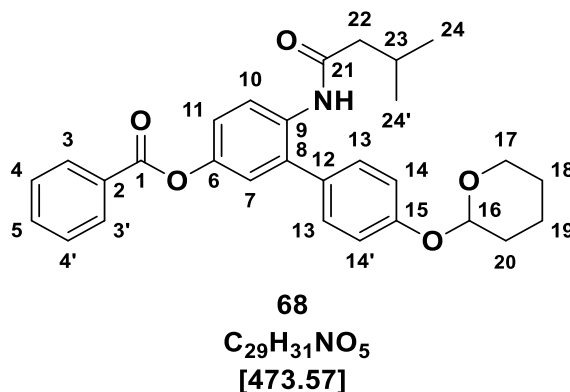
^{13}C NMR (101 MHz, DMSO) δ (ppm) 167.01 (1C, C-1), 164.94 (1C, C-5), 155.98 (1C, C-12), 151.49 (1C, C-3), 138.62 (1C, C-10), 130.28 (3C, C-9, C-17, C-17'), 129.79 (1C, C-16), 125.63 (1C, C-11), 116.60 (1C, C-13), 115.65 (2C, C-18, C-18'), 108.40 (1C, C-6), 49.99 (1C, C-2), 12.38 (1C, C-8).

FT-IR (Diamond-ATR): ν (cm^{-1}) 3736.4, 3525.24, 2969.84, 2361.41, 1964.14, 1742.37, 1363.43, 1216.86.

MS (ESI+): 390.1 ($[\text{M}+\text{Na}]^+$), 368.1 ($[\text{M}+\text{H}]^+$).

HR-MS (ESI+): calc. for $\text{C}_{19}\text{H}_{17}\text{N}_3\text{O}_5$ ($[\text{M}+\text{H}]^+$): 368.1241, found: 368.1243 calc. for $\text{C}_{19}\text{H}_{17}\text{N}_3\text{O}_5$ ($[\text{M}+\text{Na}]^+$): 390.1060, found: 390.1058.

7.4.2.42 6-(3-Methylbutanamido)-4'-((tetrahydro-2H-pyran-2-yl)oxy)-[1,1'-biphenyl]-3-yl benzoate (68)



In a two neck flask, 6-amino-4'-((tetrahydro-2H-pyran-2-yl)oxy)-[1,1'-biphenyl]-3-yl benzoate (246 mg, 0.632 mmol, 1.0 eq.) was dissolved in anhydrous chloroform with isovaleric acid (132 mg, 1.29 mmol, 2.0 eq.), EDC-HCl (364 mg, 1.90 mmol, 2.0 eq.) and HOBT (26.0 mg, 0.192 mmol, 0.3 eq.) and refluxed for 36 h under an argon atmosphere. The reaction was frequently controlled by TLC (*n*-hexane/EtOAc, 2:1) until the full conversion of the educt. After that the mixture was washed with water, then the aqueous phase was extracted with chloroform (4 x 40 mL) and the combined organic phases were washed with sat. aq. NaHCO_3 solution (2 x 40 mL) and sat. aq. NaCl solution (40 mL). The organic phase was dried over MgSO_4 and the solvent was removed under vacuum. The product was obtained as a white solid (279 mg, 0.589 mmol, 93%) after washing with *n*-hexane.

TLC: $R_f = 0.63$ (*n*-hexane/EtOAc, 2:1)

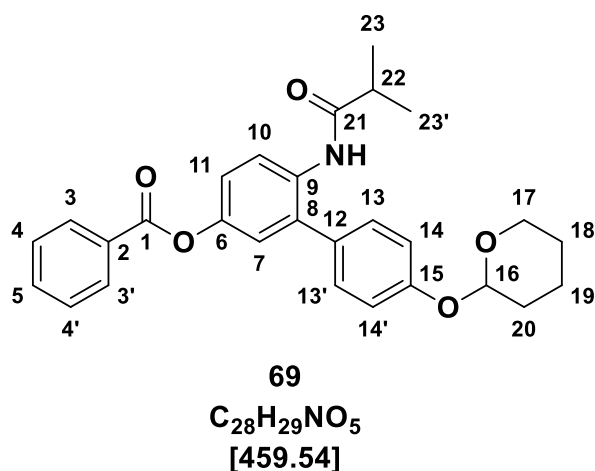
mp.: 129.9 °C

¹H-NMR (300 MHz, CD₂Cl₂) δ (ppm) 8.30 (d, *J* = 8.9 Hz, 1H, H-7), 8.22 – 8.15 (m, 2H, H-3, H-3'), 7.70 – 7.61 (m, 1H, H-5), 7.60 - 7.52 (m, 2H, H-4, H-4'), 7.36 – 7.30 (m, 2H, H-13, H-13'), 7.22 – 7.11 (m, 4H, H-10, H-11, H-14, H-14'), 5.47 (t, *J* = 3.3 Hz, 1H, H-16), 3.91 (ddd, *J* = 11.9, 9.0, 3.2 Hz, 1H, H-17), 3.66 – 3.58 (m, 1H, H-17), 2.07 (q, *J* = 2.4 Hz, 3H, H-22-H, H-23), 2.04 – 1.81 (m, 3H, H-20, H-19), 1.76 – 1.58 (m, 3H, H-18, H-19), 0.97 – 0.89 (m, 6H, H-24, H-24').

¹³C-NMR (75 MHz, CD₂Cl₂) δ (ppm) 171.31 (1C, C-21), 166.23 (1C, C-1), 158.02 (1C, C-15), 148.22 (1C, C-6), 134.37 (1C, C-5), 134.02 (1C, C-8), 133.46 (1C, C-9), 130.93 (2C, C-13, C-13'), 130.79 (1C, C-12), 131.24 (2C, C-3, C-3'), 130.93 (1C, C-2), 129.37 (2C, C-4, C-4'), 124.05 (1C, C-10), 123.08 (1C, C-7), 121.48 (1C, C-11), 117.03 (2C, C-14, C-14'), 97.49 (1C, C-16), 63.11 (1C, C-17), 47.79 (1C, C-22), 31.23 (1C, C-20), 26.68 (1C, C-23), 26.23 (1C, C-18), 23.10 (2C, C-24, C-24'), 19.66 (1C, C-19).

HR-MS (ESI⁺): calc. for C₂₉H₃₁NO₅ [M+H]⁺: 474.2275, found: 474.2276.

7.4.2.43 6-Isobutyramido-4'-((tetrahydro-2H-pyran-2-yl)oxy)-[1,1'-biphenyl]-3-yl benzoate (69)



In a two neck flask, 6-amino-4'-((tetrahydro-2H-pyran-2-yl)oxy)-[1,1'-biphenyl]-3-yl benzoate (247 mg, 0.635 mmol, 1.0 eq.) was dissolved in anhydrous chloroform with isobutyric acid (113 mg, 1.28 mmol, 2.0 eq), EDC-HCl (368 mg, 1.92 mmol, 3.0 eq) and HOBT (28.0 mg, 0.229 mmol, 0.3 eq) and refluxed for 40 h under an argon atmosphere. The reaction was frequently controlled by TLC (*n*-hexane/EtOAc, 2:1) till the full conversion of the educt. Afterwards, the reaction mixture was washed with water and the aqueous phase was extracted with chloroform (4 x 40 mL). The combined organic phases were washed with sat. aq. NaHCO₃ solution (2 x 40 mL), sat. aq. NaCl solution (40 mL), dried over MgSO₄ and the solvent was removed under vacuum. The product was purified

with an *n*-hexane wash and a white solid was obtained. Residual isobutyric acid was removed by washing with sat. aq. NaHCO₃ solution, and the product was obtained as a white solid (242.1 mg, 0.53 mmol, 83 %).

TLC: *R*_f: 0.3 (*n*-hexane/EtOAc, 2:1)

mp.: 122.4 °C

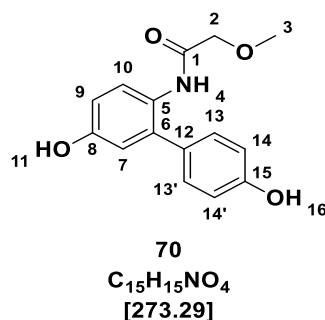
¹H-NMR (300 MHz, CD₂Cl₂) δ (ppm) 8.30 (d, *J* = 8.7 Hz, 1H, H-10), 8.23 – 8.14 (m, 2H, H-3, H-3'), 7.71 – 7.61 (m, 1H, H-5), 7.59 – 7.48 (m, 2H, H-4, H-4'), 7.34 (dd, *J* = 8.6, 4.6 Hz, 2H, H-13, H-13'), 7.23 (s, 1H, H-NH), 7.21 – 7.10 (m, 4H, H-7, H-11, H-14, H-14'), 5.47 (t, *J* = 3.2 Hz, 1H, H-16), 3.90 (dtd, *J* = 8.6, 3.3, 2.9 Hz, 1H, H-17), 3.66 – 3.56 (m, 1H, H-17), 2.42 – 2.29 (m, 1H, H-22), 2.08 – 1.82 (m, 3H, H-20, H-19), 1.77 – 1.57 (m, 3H, H-18, H-19), 1.12 (d, *J* = 8.9 Hz, 6H, H-23, H-23').

¹³C-NMR (75 MHz, CD₂Cl₂) δ (ppm) 174.74 (1C, C-21), 165.35 (1C, C-1), 157.14 (1C, C-15), 146.98 (1C, C-6), 133.97 (1C, C-5), 133.35 (1C, C-12), 130.31 (2C, C-13, C-13'), 130.15 (1C, C-2), 129.97 (2C, C-3, C-3'), 128.44 (2C, C-4, C-4'), 123.13 (1C, C-11), 122.28 (1C, C-10), 120.94 (1C, C-7), 116.87 (2C, C-14, C-14'), 96.56 (1C, C-16), 62.18 (1C, C-17), 36.55 (1C, C-22), 30.30 (1C, C-20), 25.30 (1C, C-18), 19.20 (1C, C-19), 18.87 (2C, C-23, C-23').

FT-IR (Diamond-ATR): ν (cm⁻¹) 3266.97, 2943.89, 2874.61, 1728.85, 1659.67, 1597.39, 1519.23, 1364.68, 1241.22, 1163.06, 1078.68, 1016.51, 954.35, 799.79.

HR-MS (ESI+): calc. for C₂₈H₂₉NO₅ [M+H]⁺: 460.2118, found: 460.2118

7.4.2.44 *N*-(4',5-Dihydroxy-[1,1'-biphenyl]-2-yl)-2-methoxyacetamide (70)



In a dry 100 mL two-neck round bottom flask 6-amino-4'-((tetrahydro-2H-pyran-2-yl)oxy)-[1,1'-biphenyl]-3-yl benzoate (250 mg, 0.640 mmol, 1.0 eq), EDC-HCl (390 mg, 1.90 mmol, 3.0 eq) and 1-hydroxybenzotriazole (26.0 mg, 0.190 mmol, 0.30 eq) were added and dissolved in anhydrous DMF (15 mL) under argon atmosphere. Methoxyacetic

acid (95.0 μL , 1.20 mmol, 2.0 eq) was slowly added to the flask and the reaction mixture was stirred at 160 $^{\circ}\text{C}$ overnight. Reaction monitoring by TLC (DCM/MeOH, 10:1) showed complete conversion of the starting material. The reaction mixture was diluted with EtOAc (20 mL) and water (20 mL), the aqueous phase was extracted with EtOAc (3 x 15 mL), combined organic phases were washed thoroughly with water, 1 M HCl (20 mL), sat. aq. NaHCO_3 solution (20 mL), sat. aq. NaCl (20 mL), dried over MgSO_4 and concentrated in vacuum. After purification by flash column chromatography (DCM/MeOH 10:1) product was isolated as a light orange solid (77.0 mg, 0.280 mmol, 44%), and a brown oil (57.0 mg, 0.210 mmol, 38%) as a mixture of protected and unprotected product.

TLC: $R_f = 0.62$ (DCM/MeOH, 10:1)

mp.: 76.7 $^{\circ}\text{C}$

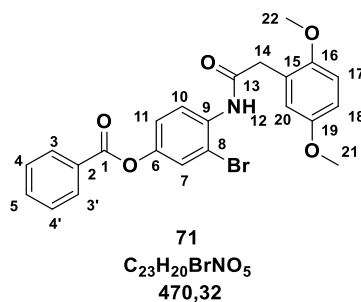
^1H NMR (400 MHz, MeOD) δ (ppm) 7.60 (m, 1H, H-10), 7.2 -7.03 (m, 2H, H-13, H-13), 7.03 -6.62 (m, 4H, H-7, H-9, H-14, H-14'), 3.83 (m, 2H, H-2), 3.27 (m, 3H, H-3).

^{13}C NMR (101 MHz, MeOD) δ (ppm) 170.87 (1C, C-1), 158.27 (1C, C-15), 156.48 (1C, C-8), 138.76 (1C, C-7), 131.16 (2C, C-13, C-13'), 130.94 (1C, C-12), 126.75 (1C, C-5), 117.78 (1C, C-10), 116.41 (1C, C-6), 116.37 (2C, C-14, C-14'), 115.19 (1C, C-9), 71.28 (1C, C-2), 59.67 (1C, C-3).

MS (ESI+): 296.1 ($[\text{M}+\text{Na}]^+$), 274.1 ($[\text{M}+\text{H}]^+$), 596.2 ($[\text{2M}+\text{Na}]^+$).

HR-MS (ESI+): calc. for $\text{C}_{15}\text{H}_{15}\text{NO}_4$ ($[\text{M}+\text{H}]^+$): 274.1074, found: 274.1073 calc. for $\text{C}_{15}\text{H}_{15}\text{NO}_4$ ($[\text{M}+\text{Na}]^+$): 296.0893, found: 296.0893.

7.4.2.45 3-Bromo-4-(2-(2,5-dimethoxyphenyl)acetamido)phenyl benzoate (71)



In a dry 250 mL two neck round bottom flask (2,5-dimethoxyphenyl)acetic acid (2.52 g, 13.7 mmol, 2.0 eq), EDC-HCl (3.95 g, 21.0 mmol, 3.0 eq) and 1-Hydroxybenzotriazole (270 mg, 2.00 mmol, 0.3 eq) were dissolved in anhydrous chloroform (10 mL) and stirred

for 15 min under an argon atmosphere. 4-amino-3-bromophenyl benzoate (2.0 g, 6.8 mmol, 1.0 eq) was dissolved in anhydrous chloroform (40 mL) and added to the flask. The reaction mixture was stirred at room temperature overnight. Monitoring of the reaction by TLC (*n*-hexane/EtOAc, 2:1) showed incompleteness, therefore additional EDC-HCl (520 mg, 0.37 eq) and HOBt (170 mg, 0.18 eq) were added. It was stirred additionally at 65 °C for 6 h and afterwards for 12 h at room temperature. After completion, the reaction mixture was washed with water, sat. aq. NaHCO₃ solution (50 mL), sat. aq. NaCl solution (50 mL) dried over MgSO₄ and concentrated in vacuum. The title compound was obtained after purification by flash column chromatography (*n*-hexane/MTBE, 2:1) as a brown solid (1.85 g, 3.93 mmol, 57%).

TLC: $R_f = 0.38$ (*n*-hexane/EtOAc, 2:1)

mp.: 117 °C

¹H NMR (300 MHz, CD₂Cl₂) δ (ppm) 8.38 (d, $J = 9.1$ Hz, 1H, H-10), 8.21 – 8.10 (m, 3H, H-12, H-3, H-3'), 7.72 – 7.60 (m, 1H, H-5), 7.59 – 7.46 (m, 2H, H-4, H-4'), 7.42 (d, $J = 2.6$ Hz, 1H, H-7), 7.22 – 7.11 (m, 1H, H-11), 6.97 – 6.87 (m, 2H, H-20, H-17), 6.85 (m, 1H, H-18), 3.89 (s, 3H, H-22), 3.75 (s, 3H, H-21), 3.72 (s, 2H, H-14).

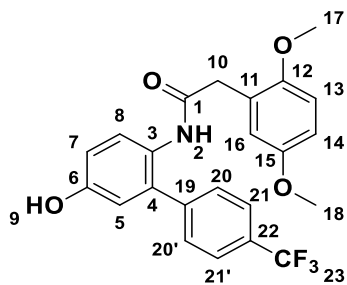
¹³C NMR (75 MHz, CD₂Cl₂) δ (ppm) 169.28 (1C, C-13), 154.03 (1C, C-19), 151.30 (1C, C-16), 134.5 (1C, C-6), 133.78 (1C, C-5), 130.03 (2C, C-3, C-3'), 128.6 (2C, C-4, C-4'), 125.4 (1C, C-7), 123.7 (1C, C-20), 121.7 (1C, C-10), 121.47 (1C, C-11), 117.05 (1C, C-5), 113.57 (1C, C-17), 111.72 (1C, C-9), 56.08 (1C, C-20), 55.68 (1C, C-21), 40.28 (1C, C-14).

MS (ESI+): 470.1 ([M+H]⁺) 390.1 ([M+Na]⁺),

HR-MS (ESI+): calc. for C₂₃H₂₀NO₅Br ([M+H]⁺): 470.0598, found: 470.0601.

FT-IR (Diamond-ATR): ν (cm⁻¹) 3287.55, 2933.19, 1736.58, 1683.06, 1499.38, 1233.73, 1187.45, 1060.17, 706.30.

7.4.2.46 2-(2,5-Dimethoxyphenyl)-N-(5-hydroxy-4'-(trifluoromethyl)-[1,1'-biphenyl]-2-yl)acetamide (72)



72

$C_{23}H_{20}F_3NO_4$
[431.13]

In a microwave vessel 3-bromo-4-(2-(2,5-dimethoxyphenyl)acetamido)phenyl benzoate (150 mg, 0.320 mmol, 1.0 eq), $Pd(PPh_3)_4$ (18.0 mg, 0.016 mmol, 5 mol%), Na_2CO_3 (67.0 mg, 0.640 mol, 2.0 eq) and 4-(trifluoromethyl)phenylboronic acid (66.0 mg, 0.350 mmol, 1.1 eq) were added and dissolved in 5 mL of the solvent mixture (DME/ H_2O 3:1) previously degassed for 30 min. The reaction mixture was placed into a microwave and stirred at 100 °C for 10 min. After cooling down, monitoring by TLC (*n*-hexane/EtOAc, 2:1) showed complete consumption of the starting material. The DME was evaporated and the reaction mixture was dissolved in EtOAc. The organic phase was washed with water (20 mL), sat. aq. $NaHCO_3$ solution (20 mL), sat. aq. $NaCl$ solution (20 mL), dried over $MgSO_4$ and concentrated in vacuum. After purification by flash column chromatography (*n*-hexane/EtOAc, 1:1), the product was obtained as a light-brown solid (124 mg, 0.280 mmol, 83%).

TLC: $R_f = 0.39$ (*n*-hexane/EtOAc 2:1)

mp.: 112 °C

1H NMR (300 MHz, DMSO) δ (ppm) 9.60 (s, 1H, H-9), 9.00 (s, 1H, H-2), 7.67 (d, $J = 8.1$ Hz, 2H, H-21, H-21'), 7.49 (d, $J = 8.0$ Hz, 2H, H-20, H-20'), 7.26 (d, $J = 8.6$ Hz, 1H, H-8), 6.90 – 6.66 (m, 5H, H-14, H-13, H-5, H-7, H-16), 3.65 (s, 3H, H-18), 3.63 (s, 3H, H-17), 3.40 (s, 2H, H-10).

^{13}C NMR (75 MHz, DMSO) δ (ppm) 169.33 (1C, C-1), 155.48 (1C, C-6), 152.90 (1C, C-15), 151.25 (1C, C-12), 143.26 (1C, C-19), 136.77 (1C, C-4), 129.26 (2C, C-20, C-20'), 128.77 (1C, C-8), 127.73 (1C, C-22), 127.31 (1C, C-3), 126.23 (1C, C-11), 125.64 (2C, C-21, C-21'), 125.00 (1C, C-23), 117.07 (1C, C-16), 115.32 (1C, C-13), 111.90 (2C, C-5, C-7), 111.67 (1C, C-14), 55.83 (1C, C-17), 55.23 (1C, C-18), 37.02 (1C, C-10).

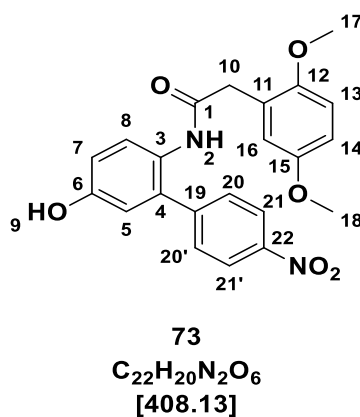
¹⁹F NMR (282 MHz, DMSO) δ (ppm) -60.94 (-CF₃).

MS (ESI+): 432.2 ([M+H]⁺), 863.3 ([2M+H]⁺).

HR-MS (ESI+): calc. for C₂₃H₂₀F₃NO₄ ([M+H]⁺): 432.1417, found: 432.1418

FT-IR (Diamond-ATR): ν (cm⁻¹) 3218.12, 3019.78, 2835.31, 1647.87, 1322.92, 1235.66, 1067.40, 854.31.

7.4.2.47 2-(2,5-Dimethoxyphenyl)-N-(5-hydroxy-4'-nitro-[1,1'-biphenyl]-2-yl)acetamide (73)



In a microwave vessel 3-bromo-4-(2-(2,5-dimethoxyphenyl) acetamido) phenyl benzoate (150 mg, 0.320 mmol, 1.0 eq), Pd(PPh₃)₄ (18.0 mg, 0.016 mmol, 5 mol%), Na₂CO₃ (67.0 mg, 0.640 mmol, 2.0 eq) and 4-nitrophenylboronic acid (58.0 mg, 0.350 mmol, 1.1 eq) were added and dissolved in previously degassed (DME/H₂O, 3:1) solvent mixture (5 mL). The reaction mixture was placed into the microwave and stirred at 110 °C for 10 min. The reaction mixture was cooled down to room temperature and checked by TLC (*n*-hexane/EtOAc, 1:1) which showed complete consumption of the starting material. DME was evaporated and EtOAc was added, the organic phase was washed with water (10 mL), sat. aq. NaHCO₃ (10 mL), sat. aq. NaCl (10 mL), dried over MgSO₄ and concentrated in vacuum. After purification by flash column chromatography (*n*-hexane/EtOAc, 1:2) product was obtained as yellow solid (102 mg, 0.250 mmol, 79%).

TLC: R_f = 0.22 (*n*-hexane/EtOAc 1:1)

mp.: 146 °C

¹H NMR (400 MHz, DMSO) δ (ppm) 9.69 (s, 1H, H-9), 9.13 (s, 1H, H-2), 8.13 (d, J = 8.0 Hz, 2H, H-21, H-21'), 7.51 (d, J = 8.8 Hz, 2H, H-20, H-20'), 7.22 (d, J = 8.6 Hz, 1H,

H-8), 6.87 – 6.79 (m, 2H, H-7, H-13,), 6.76 – 6.68 (m, 2H, H-5, H-14), 6.55 (d, $J = 3.1$ Hz, 1H, H-16), 3.63 (d, $J = 10.2$ Hz, 6H, H-17, H-18), 3.38 (s, 2H, H-10).

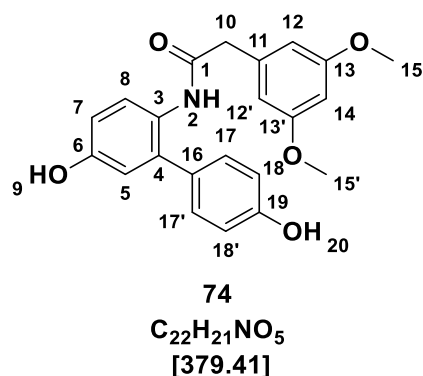
^{13}C NMR (101 MHz, DMSO) δ (ppm) 169.67(1C, C-1),, 156.08 (1C, C-6), 153.26 (1C, C-15), 151.66 (1C, C-12), 146.74 (1C, C-22), 146.64 (1C, C-19), 137.12 (1C, C-4), 130.09 (2C, C-20, C-20'), 129.33 (1C, C-8), 126.66 (1C, C-3), 125.38 (1C, C-11), 123.70 (2C, C-21, C-21'), 117.38 (1C, C-16), 116.49 (1C, C-5), 116.22 (1C, C-13), 112.06 (1C, C-14), 112.03 (1C, C-7), 56.35 (1C, C-17), 55.61 (1C, C-18), 37.24 (1C, C-10).

MS (ESI+): 409.2 ($[\text{M}+\text{H}]^+$)

HR-MS (ESI+): calc. for $\text{C}_{22}\text{H}_{20}\text{N}_2\text{O}_6$ ($[\text{M}+\text{H}]^+$): 409.1394, found: 409.1396

FT-IR (Diamond-ATR): ν (cm^{-1}) 3218.61, 3020.94, 2955.37, 1645.46, 1500.34, 1344.34, 1240.48, 990.26.

7.4.2.48 *N*-(4',5-Dihydroxy-[1,1'-biphenyl]-2-yl)-2-(3,5-dimethoxyphenyl)acetamide (74)



In a one neck flask 6-(2-(3,5-dimethoxyphenyl)acetamido)-4'-((tetrahydro-2H-pyran-2-yl)oxy)-[1,1'-biphenyl]-3-yl benzoate (300 mg, 0.5 mmol, 1.0 eq), K_2CO_3 (180 mg, 1.30 mmol, 2.5 eq) were dissolved in MeOH (44 mL) and stirred at room temperature overnight. The reaction was monitored by TLC (*n*-hexane/EtOAc, 1.5:1), upon completion, the solvent was removed, the reaction residue was diluted with EtOAc (20 mL) and washed with water (30 mL), sat. aq. NaHCO_3 solution (30 mL), sat. aq. NaCl solution (30 mL), dried over MgSO_4 and concentrated in vacuum. The product was obtained as off-white solid (230 mg, 0.490 mmol, 99.6%) which was used further in the final deprotection step. In a one neck flask 2-(3,5-dimethoxyphenyl)-*N*-(5-hydroxy-4'-((tetrahydro-2H-pyran-2-yl)oxy)-[1,1'-biphenyl]-2-yl)acetamide (150 mg, 0.320 mmol, 1.0 eq) was dissolved in MeOH (12 mL) and 1 M HCl (2 mL) was added. The reaction mixture was refluxed at 70 °C for 2 h. Reaction monitoring by TLC (*n*-hexane/EtOAc,

1:2) showed complete conversion of the starting material. Afterwards, the solvent was evaporated, and the reaction mixture was dissolved in EtOAc (2 mL), water (5 mL) was added and the aqueous phase was extracted with EtOAc (3 x 5 mL). The organic phase was washed with sat. aq. NaHCO₃ solution (5 mL), sat. aq. NaCl solution (5 mL), dried over MgSO₄ and concentrated in vacuum. Purification by flash column chromatography (*n*-hexane/EtOAc, 1:2) resulted in isolated product (110 mg, 0.290 mmol, 96 %) as a white solid. Before biophysical studies sample was purified by preparative HPLC.

TLC: $R_f = 0.36$ (*n*-hexane/EtOAc, 1:2)

HPLC (preparative, 20 → 100% MeCN in 45 min): $t_R = 23.0$ min.

mp.: 196 °C

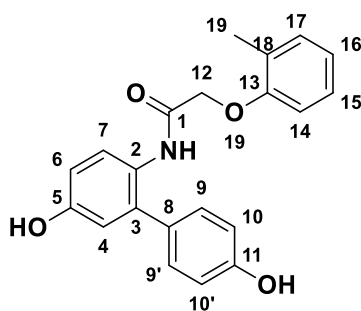
¹H NMR (300 MHz, MeOD) δ (ppm) 7.41 (d, $J = 8.6$ Hz, 1H, H-8), 7.03 – 6.93 (m, 2H, H-17, H-17'), 6.77 – 6.63 (m, 4H, H-7, H-18, H-18', H-5), 6.42 -6.33 (m, 3H, H-12, H-12', H-14), 3.74 (s, 6H, H-15, H-15'), 3.47 (s, 2H, H-10).

¹³C NMR (75 MHz, MeOD) δ (ppm) 172.40 (1C, C-1), 162.21 (2C, C-13, C-13'), 157.71 (1C, C-19), 156.38 (1C, C-6), 139.17 (1C, C-4), 137.76 (1C, C-11), 130.68 (1C, C-16), 130.61 (2C, C-17, C-17'), 127.76 (1C, C-8), 126.96 (1C, C-3), 117.44 (1C, C-5), 115.98 (2C, C-8, C-18'), 114.79 (1C, C-7), 108.03 (2C, C-2, C-12'), 99.94 (1C, C-14), 55.43 (2C, C-15, C-15'), 44.35 (1C, C-10).

MS (ESI⁺): 380.2 ([M+H]⁺), 402.1 ([M+Na]⁺).

HR-MS (ESI⁺): calc. for C₂₂H₂₁NO₅ ([M+H]⁺): 380.1492, found: 380.1495 calc. for C₂₂H₂₁NO₅ ([M+Na]⁺): 402.1312, found: 402.1315.

FT-IR (Diamond-ATR): ν (cm⁻¹) 3359.38, 3330.94, 3164.61, 2954.89, 1647.87, 1588.57, 1429.47, 1158.52, 1063.06, 813.33.

7.4.2.49 *N*-(4',5-Dihydroxy-[1,1'-biphenyl]-2-yl)-2-(*o*-tolylloxy)acetamide (75)

75

 $C_{21}H_{19}NO_4$
 [349.39]

In a one neck flask 4'-((tetrahydro-2H-pyran-2-yl)oxy)-6-(2-(*o*-tolylloxy)acetamido)-[1,1'-biphenyl]-3-yl benzoate (268 mg, 0.500 mmol, 1.0 eq) was dissolved in MeOH (20 mL) and 1 M aq. HCl solution (1 mL) was added. The mixture was stirred at room temperature for 1 h and after TLC control (*n*-hexane/EtOAc, 2:1) showed complete conversion of the starting material, the reaction was stopped. The solvent was removed under vacuum and the residue was dissolved in EtOAc. The organic phase was washed with water and the resulting aqueous phase was extracted with EtOAc (4 x 40 mL). The organic phase was washed with sat. aq. NaHCO₃ and Na₂CO₃ solution (3 x 40 mL, pH 10) and the solvent was removed under vacuum. In the following step the residue was dissolved in MeOH and K₂CO₃ (172 mg, 1.25 mmol, 2.5 eq) was added and the mixture was stirred for 1 h. The reaction was monitored by TLC plate (*n*-hexane/EtOAc, 1:1) and afterwards the solvent was removed under vacuum. The reaction mixture residue was dissolved in EtOAc and washed with water. The aqueous phase was extracted with EtOAc (4 x 30 mL) and the combined organic phases were washed with sat. aq. NaCl solution (50 mL), dried over MgSO₄ and concentrated in vacuum. The product was obtained as a light orange-brown solid (153 mg, 0.440 mmol, 88%). Before biophysical studies compound was purified by preparative HPLC.

TLC: $R_f = 0.4$ (*n*-hexane/EtOAc, 1:1)

HPLC (preparative, 20 → 100% MeCN in 30 min): $t_R = 14.0$ min.

mp.: 195.3 °C

¹H NMR (300 MHz, DMSO) δ (ppm) 9.51 (s, 2H, H-OH), 8.79 (s, 1H, H-NH), 7.61 (d, $J = 8.7$ Hz, 1H, H-7), 7.18 – 7.06 (m, 4H, H-4, H-9, H-9', H-17), 6.92 – 6.66 (m, 5H, H-

14, H-15, H-16, H-10, H-10'), 6.63 (d, $J = 2.8$ Hz, 1H, 7), 4.53 (s, 2H, H-12), 1.96 (s, 3H, H-19).

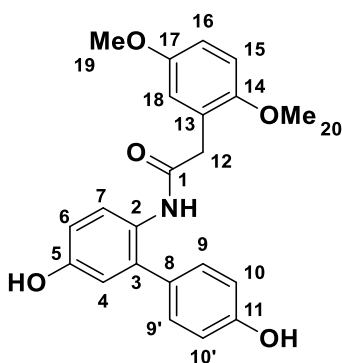
^{13}C NMR (75 MHz, DMSO) δ (ppm) 166.41 (1C, C-1), 157.01 (1C, C-13), 155.42 (1C, C-11), 154.80 (1C, C-5), 136.54 (1C, C-8), 130.55 (1C, C-2), 129.82 (2C, C-9, C-9'), 128.74 (1C, C-18), 126.90 (1C, C-15), 125.91 (1C, C-3), 121.04 (1C, C-16), 115.43 (2C, C-10, C-10'), 113.96 (1C, C-6), 111.47 (1C, C-14), 67.08 (1C, C-12), 15.68 (1C, C-19).

MS (ESI+): 350.1 ($[\text{M}+\text{H}]^+$), 699.3 ($[\text{2M}+\text{H}]^+$), 372.1 ($[\text{M}+\text{Na}]^+$).

HR-MS (ESI+): calc. for $\text{C}_{21}\text{H}_{19}\text{NO}_4$ ($[\text{M}+\text{H}]^+$): 350.1387, found: 350.1391 calc. for $\text{C}_{21}\text{H}_{19}\text{NO}_4$ ($[\text{M}+\text{Na}]^+$): 372.1206, found: 372.1206.

FT-IR (Diamond-ATR): ν (cm^{-1}) 3368.06, 2924.52, 2849.30, 1643.05, 1431.88, 1233.25, 1120.43.

7.4.2.50 *N*-(4',5-Dihydroxy-[1,1'-biphenyl]-2-yl)-2-(2,5-dimethoxyphenyl)acetamide (76)



76

$\text{C}_{22}\text{H}_{21}\text{NO}_5$
[379.41]

In a one neck flask 6-(2-(2,5-dimethoxyphenyl)acetamido)-4'-((tetrahydro-2H-pyran-2-yl)oxy)-[1,1'-biphenyl]-3-yl benzoate (304 mg, 0.540 mmol, 1.0 eq) was dissolved in MeOH and K_2CO_3 (185 mg, 1.34 mmol, 2.5 eq) was added. The mixture was stirred at room temperature for 1 h. Monitoring by TLC plate (*n*-hexane/EtOAc, 2:1) confirmed complete consumption of the starting material. The solvent was evaporated, and the reaction mixture residue was dissolved in EtOAc and washed with water. The aqueous phase was extracted with EtOAc (4 x 30 mL) and the solvent was removed under vacuum. In the next step, the residue was dissolved in MeOH and 1 M aq. HCl solution (1 mL) was added. The mixture was stirred at room temperature for 1 h and controlled by TLC (*n*-hexane/EtOAc, 1:1). The solvent was removed under vacuum and the residue was

dissolved in EtOAc. The organic phases were washed with water and the resulting aqueous phase was extracted with EtOAc (4 x 40 mL). The combined organic phase was washed with sat. aq. NaCl solution (50 mL), dried over MgSO₄ and the solvent was removed in vacuum. The product was obtained as an orange-brown oil (173 mg, 0.450 mmol, 84%). Before the biophysical studies sample was purified by semi-preparative HPLC.

TLC: $R_f = 0.2$ (*n*-hexane/EtOAc, 1:1)

HPLC (semi-preparative, 20 → 100% MeCN in 45 min): $t_R = 23.0$ min.

¹H NMR (300 MHz, CD₃CN) δ (ppm) 7.74 (d, $J = 8.8$ Hz, 1H, H-7) 7.54 (s, 1H, H-NH), 7.04 – 6.92 (m, 2H, H-9, H-9'), 6.84 – 6.67 (m, 6H, H-5, H-15, H-16, H-18, H-10, H-10'), 6.61 (d, $J = 2.9$ Hz, 1H, H-4), 3.73 (s, 3H, H-19), 3.61 (s, 3H, H-20), 3.49 (s, 2H, H-12).

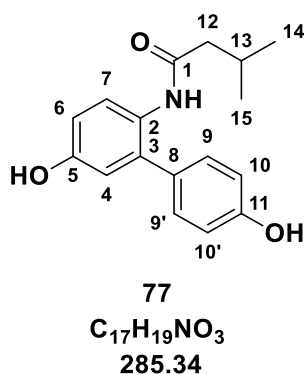
¹³C NMR (75 MHz, CD₃CN) δ (ppm) 170.30 (1C, C-1), 157.40 (1C, C-11), 154.80 (1C, C-5), 154.60 (1C, C-17), 152.32 (1C, C-14), 135.63 (1C, C-2), 129.80 (2C, C-9, C-9'), 128.40, 125.60 (1C, C-7), 124.12 (1C, C-3), 123.92 (1C, C-7), 116.43 (1C, C-4), 115.41 (1C, C-18), 114.97 (2C, C10, C-10'), 113.98 (1C, C-16), 113.94 (1C, C-6) 112.98 (1C, C-15), 55.52 (1C, C-20), 55.18 (1C, C-19), 39.83 (1C, C-12).

MS (ESI⁻): 378.1 ([M-H]⁻).

HR-MS (ESI⁻): calc. for C₂₂H₂₁NO₅ ([M-H]⁻): 378.1347, found: 378.1342

FT-IR (Diamond-ATR): ν (cm⁻¹) 3268.97, 2928.79, 2843.52, 1643.57, 1597.39, 1512.12, 1441.95, 1302.51, 714.52, 1108.88, 1031.61, 830.88.

7.4.2.51 *N*-(4',5'-Dihydroxy-[1,1'-biphenyl]-2-yl)-3-methylbutanamide (77)



In a one neck flask, 6-(3-methylbutanamido)-4'-((tetrahydro-2H-pyran-2-yl)oxy)-[1,1'-biphenyl]-3-yl benzoate (296.5 mg, 0.626 mmol, 1.0 eq) was dissolved in MeOH (10 mL)

and 6 M aq. HCl (4 mL) solution was added. The mixture was stirred at room temperature for 30 min and afterwards, TLC (*n*-hexane/EtOAc, 2:1) showed complete conversion of the starting material, the reaction was stopped. Two possible product spots were observed, one was a side product where the amide group was removed, which possibly formed because of the usage of 6 M aq. HCl solution. The solvent was removed under vacuum and the residue was dissolved in EtOAc. The organic phase was washed with water and the aqueous phase was extracted with EtOAc (4 x 40 mL). The organic phase was washed with sat. aq. NaHCO₃ and Na₂CO₃ solution (3 x 40 mL, pH = 10) and the solvent was removed under reduced pressure. In the following step the residue was dissolved in MeOH (10 mL) and K₂CO₃ (216 mg, 1.57 mmol, 2.5 eq) was added and the mixture was stirred for 1 h. Afterwards, TLC plate control (DCM/MeOH, 9:1) confirmed complete consumption of the starting material. The solvent was removed under reduced pressure, and the reaction residue was dissolved in EtOAc and washed with water. The aqueous phase was extracted with EtOAc (4 x 30 mL) and the combined organic phases were washed with sat. aq. NaCl solution (50 mL). The organic phase was dried over MgSO₄ and concentrated in vacuum. The product was obtained as a brown solid (105 mg, 0.368 mmol, 58%). Prior to biophysical studies, the compound was purified by preparative HPLC.

TLC: $R_f = 0.5$ (DCM/MeOH, 9:1)

HPLC (preparative, 20 → 100% MeCN in 45 min): $t_R = 21.5$ min.

mp.: 105 °C

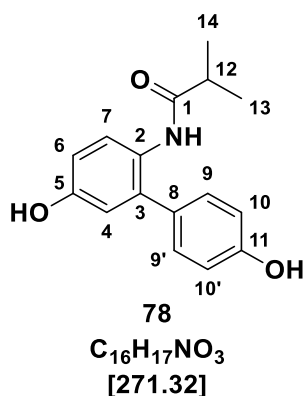
¹H NMR (300 MHz, DMSO) δ (ppm) 9.44 (s, 1H, C-11, H-OH), 9.39 (s, 1H, C-5, H-OH), 8.87 (s, 1H, H-NH), 7.19 – 7.02 (m, 3H, H-4, H-9, H-9'), 6.82 – 6.61 (m, 4H, H-6, H-7, H-10, H-10'), 2.04 – 1.88 (m, 3H, H-12, H-13), 0.84 (d, $J = 6.3$ Hz, 6H, H-14, H-15).

¹³C NMR (75 MHz, DMSO) δ (ppm) 171.16 (1C, C-1), 156.63 (1C, C-11), 155.36 (1C, C-5), 138.91 (1C, C-2), 129.41 (2C, C-9, C-9'), 126.14 (1C, C-3), 116.09 (1C, C-7), 114.91 (2C, C-10, C-10'), 113.76 (1C, C-4), 44.80 (1C, C-12), 25.43 (1C, C-13), 22.34 (2C, C-14, C-15).

FT-IR (Diamond-ATR): ν (cm⁻¹) 3254.28, 2951.51, 1614.12, 1521.56, 1190.82.

MS (ESI⁻): 284.11 ([M-H]⁻), 569.1 ([2M-H]⁻).

HR-MS (ESI⁻): calc. for C₁₇H₁₉NO₃ ([M-H]⁻): 284.1292, found: 284.1296.

7.4.2.52 *N*-(4',5'-Dihydroxy-[1,1'-biphenyl]-2-yl)isobutyramide (78)

In a one neck flask 6-isobutyramido-4'-((tetrahydro-2H-pyran-2-yl)oxy)-[1,1'-biphenyl]-3-yl benzoate (209 mg, 0.460 mmol, 1.0 eq) was dissolved in MeOH and K₂CO₃ (158 mg, 1.14 mmol, 2.5 eq) was added. The mixture was stirred at room temperature for 1 h and after TLC (*n*-hexane/EtOAc, 2:1) showed complete conversion of the starting material, the reaction was stopped, and the solvent was evaporated. The residue was dissolved in EtOAc and washed with water. The aqueous phase was extracted with EtOAc (4 x 30 mL) and the solvent removed under vacuum. In the next step, the residue was dissolved in MeOH and 1 M aq. HCl solution (1 mL) was added. It was stirred at room temperature for 40 min and monitored by TLC (*n*-hexane/EtOAc, 1:1). Afterwards, the solvent was removed under vacuum and the residue was dissolved in EtOAc. The organic phase was washed with water and the resulting aqueous phase was extracted with EtOAc (4 x 40 mL). The combined organic phase was washed with sat. aq. NaCl (50 mL), dried over MgSO₄ and the solvent was removed under vacuum. Product was obtained as light brown oil (114 mg, 0.420 mmol, 91%). Before biophysical studies compound was purified by preparative HPLC.

TLC: $R_f = 0.24$ (*n*-hexane/EtOAc, 1:1)

HPLC (preparative, 20 → 100% MeCN in 45 min): $t_R = 18.6$ min.

¹H NMR (300 MHz, CD₃CN) δ (ppm) 7.53 (s, 1H, H-NH), 7.38 (d, $J = 8.4$ Hz, 1H, H-7), 7.22 – 7.11 (m, 3H, H-9, H-9', H-4), 6.88 – 6.78 (m, 2H, H-10, H-10'), 6.78 – 6.66 (m, 1H, H-6), 2.35 (hept, $J = 7.3$ Hz, 1H, H-12), 1.03 (d, $J = 6.9$ Hz, 6H, H-13, H-14).

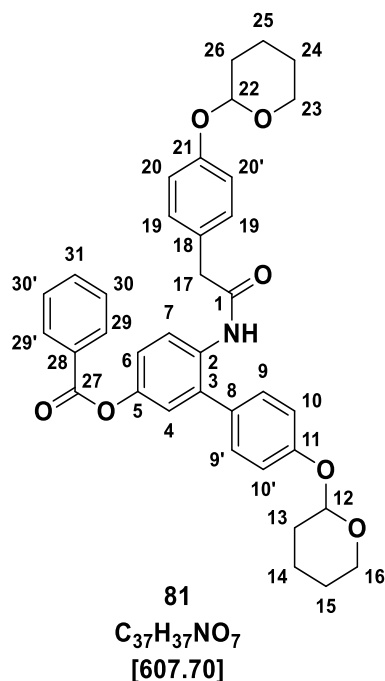
¹³C NMR (75 MHz, CD₃CN) δ (ppm) 175.91 (1C, C-1), 156.36 (1C, C-11), 154.80 (1C, C-2), 138.01 (1C, C-8), 137.99 (1C, C-3), 130.31 (2C, C-9, C-9'), 128.49, 127.50 (1C, C-7), 116.56 (2C, C-4, C-6), 115.01 (2C, C-10, C-10'), 35.30 (1C, C-12), 18.74 (2C, C-13, C-14).

MS (ESI⁺): 272.1 ([M+H]⁺), 294.1 ([M+Na]⁺).

HR-MS (ESI⁺): calc. for C₁₆H₁₇NO₃ ([M+H]⁺): 272.1281, found: 272.1284 calc. for C₁₆H₁₇NO₃ ([M+Na]⁺): 294.1101, found: 294.1101.

FT-IR (Diamond-ATR): ν (cm⁻¹) 3252.35, 2924.52, 2857.02, 1606.41, 1519.63, 1202.14.

7.4.2.53 4'-((Tetrahydro-2H-pyran-2-yl)oxy)-6-(2-(4-((tetrahydro-2H-pyran-2-yl)oxy)phenyl)acetamido)-[1,1'-biphenyl]-3-yl benzoate (81)



In a 10 mL microwave vial, benzyl (3-bromo-4-(2-(4-((tetrahydro-2H-pyran-2-yl)oxy)phenyl)acetamido)phenyl) benzoate (213 mg, 0.420 mmol, 1.0 eq), (4-((tetrahydro-2H-pyran-2-yl)oxy)phenyl)boronic acid (102 mg, 0.460 mmol, 1.1 eq), Na₂CO₃ (88.3 mg, 0.840 mmol, 2.0 eq) and Pd(PPh₃)₄ (24.1 mg, 0.021 mmol, 5 mol%) were dissolved in DME/H₂O, 3:1 solvent mixture (5 mL); previously degassed under an argon stream for 30 min. Upon addition, a light yellow solution occurred; the reaction mixture was placed into a microwave, stirred for 10 min at 110 °C, and maximal pressure was 12 psi. Monitoring by TLC plate (*n*-hexane/EtOAc, 3:1) showed completion of the reaction, consecutively, the solvent was removed under reduced pressure. The reaction mixture residue was dissolved in EtOAc and washed with water (2 x 20 mL). The aqueous phase was extracted with EtOAc (2x30 mL). Afterwards, the combined organic phases were washed with sat. aq. NaHCO₃ solution (50 mL), sat. aq. NaCl solution (50 mL), dried over MgSO₄ and concentrated in vacuum. The product was obtained as an off-white

solid (189 mg, 0.310 mmol, 75%) after purification by flash column chromatography with (*n*-hexane/EtOAc, 3:1).

TLC: $R_f = 0.20$ (*n*-hexane/EtOAc, 4:1)

mp.: 70 °C (decomposition)

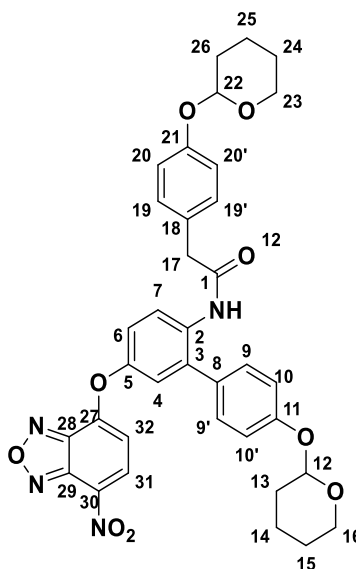
¹H NMR (300 MHz, CD₂Cl₂) δ (ppm) 8.35 (d, $J = 8.9$ Hz, 1H-7), 8.22 – 8.10 (m, 2H, H-29, H-29'), 7.72 – 7.59 (m, 1H, H-31), 7.57 – 7.47 (m, 2H, H-30, H-30'), 7.25 – 7.10 (m, 1H, H-4), 7.08-6.90 (m, 9H, H-9, H-9', H-10, H-10', H-19, H-19', H-20, H-20', H-4), 5.51 - 5.41 (m, 2H, H-12, H-22), 3.91 -3.56 (m, 4H, H-16, H-23), 3.54 (s, 2H, H-17), 2.10 – 1.51 (m, 12H, H-13, H-14, H-15, H-24, H-25, H-26).

¹³C NMR (75 MHz, CD₂Cl₂) δ (ppm) 169.12 (1C, C-1), 165.14 (1C, C-27), 156.91 (2C, C-11, C-21), 146.84 (1C, C-5), 133.57 (1C, C-2), 133.29 (1C, C-31), 132.89 (1C, C-9), 130.37 (2C, C-29, C-29') 129.98 (2C, C-19, C-19'), 129.57 (2C, C-9, C-9'), 128.58 (2C, C-30, C-30'), 123.15 (1C, C-7), 121.76 (1C, C-6), 120.86 (1C, C-4), 116.97 (4C, C-20, C-20, C-10, C-10'), 96.43 (2C, C-12, C-22), 62.12 (2C, C-16, C-23), 44.07 (1C, C-11), 30.40 (2C, C-13, C-26), 25.23 (2C, C-15, C-24), 18.95 (2C, C-14, C-25).

MS (ESI+): 630.2 ([M+Na]⁺), 608.3 ([M+H]⁺).

HR-MS (ESI+): calc. for C₃₇H₃₇NO₇ ([M+H]⁺): 608.2643, found: 608.2625 calc. for C₃₇H₃₇NO₇ ([M+Na]⁺): 630.2462, found: 630.2453

7.4.2.54 *N*-(5-((7-Nitrobenzo[*c*][1,2,5]oxadiazol-4-yl)oxy)-4'-((tetrahydro-2H-pyran-2-yl)oxy)-[1,1'-biphenyl]-2-yl)-2-(4-((tetrahydro-2H-pyran-2-yl)oxy)phenyl)acetamide (**82**)



82

$C_{36}H_{34}N_4O_9$
[666.69]

In a one neck flask *N*-(5-hydroxy-4'-((tetrahydro-2H-pyran-2-yl)oxy)-[1,1'-biphenyl]-2-yl)-2-(4-((tetrahydro-2H-pyran-2-yl)oxy)phenyl)acetamide (241 mg, 0.480 mmol, 1.0 eq) and NBD-Cl (96.0 mg, 0.480 mmol, 1.0 eq) were dissolved in anhydrous acetonitrile (12 mL). To a light orange solution, Et₃N (73.0 μL, 0.530 mmol, 1.1 eq) was added, the reaction mixture was turning gradually to a darker orange colour. The reaction was monitored by TLC (*n*-hexane/EtOAc, 1:1), and stopped after 7 h, as no starting material was observed. The solvent was removed under vacuum, reaction residual was dissolved in DCM (30 mL), washed with water (20 mL), sat. aq. NaHCO₃ solution (20 mL), sat aq. NaCl solution (30 mL) dried over MgSO₄ and concentrated in vacuum. The product was isolated as a yellow solid (221 mg, 0.330 mmol, 70%) after gradient purification (*n*-hexane/EtOAc, 3:1 → 2:1 → 1:1) by flash column chromatography.

TLC: $R_f = 0.5$ (*n*-hexane/EtOAc, 1:1)

mp.: 103 °C (decomposition)

¹H NMR (300 MHz, Acetone) δ (ppm) 8.64 (d, $J = 8.4$ Hz, 1H, H-31), 8.34 (dd, $J = 8.9, 3.9$ Hz, 1H, H-7), 8.20 (s, 1H, H-NH), 7.37 (dd, $J = 8.9, 2.9$ Hz, 1H, H-6), 7.28 – 7.14 (m, 5H, H-9, H-9', H-19, H-19', H-4), 7.09 – 6.96 (m, 4H, H-10, H-10', H-20, H-20'), 6.90 (d, $J = 8.4$ Hz, 1H, H-32), 5.57 – 5.43 (m, 2H, H-22, H-12), 3.88 (td, $J = 11.4, 5.6$ Hz,

2H, H-23, H-16), 3.69 – 3.50 (m, 4H, H-23, H-12, H-16), 1.97 – 1.52 (m, 12H, H-13, H-14, H-15, H-23, H-25, H-26).

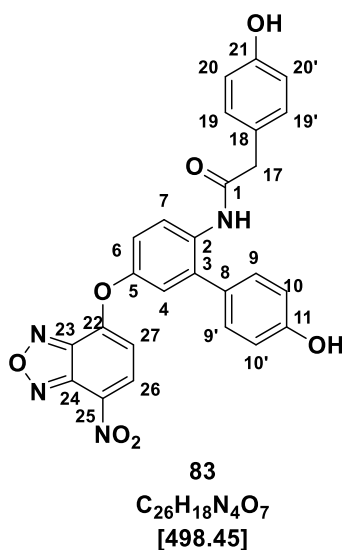
^{13}C NMR (75 MHz, Acetone) δ (ppm) 154.03(C-27), 144.65 (1C, C-29), 130.85 (1C, C-31), 124.70 (1C, C-7), 122.96 (1C, C-6), 120.62 (1C, C-4), 117.76 (4C, C-10, C-10', C-20, C-20'), 109.07 (1C, C-32) 96.98 (2C, C-22, C-12), 61.56 (2C, C-16, C-23), 43.12 (1C, C-17), 31.14 (2C, C-13, C-26), 25.96 (2C, C-15, C-24), 19.59 (2C, C-14, C-25).

MS (ESI+): 689.3 ([M+Na]⁺), 667.3 ([M+H]⁺).

HR-MS (ESI+): calc. for C₃₆H₃₄N₄O₉ ([M+H]⁺): 667.2399, found: 667.2388 calc. for C₃₆H₃₄N₄O₉ ([M+Na]⁺): 689.2218, found: 689.2212.

FT-IR (Diamond-ATR): ν (cm⁻¹) 2927.41, 2851.24, 1683.55, 1609.31, 1539.88, 1510.95, 1331.61, 1238.08, 1180.22, 1035.59, 962.305, 919.879, 812.849.

7.4.2.55 *N*-(4'-Hydroxy-5-((7-nitrobenzo[*c*][1,2,5]oxadiazol-4-yl)oxy)-[1,1'-biphenyl]-2-yl)-2-(4-hydroxyphenyl)acetamide (83) LS A1



In a one neck flask compound, **82** (181 mg, 0.270 mmol, 1.0 eq) was dissolved in MeOH (20 mL) at 50 °C, 1 M HCl (1 mL) was added, and the reaction mixture was stirred at 60 °C. The reaction was monitored by TLC (*n*-hexane/EtOAc, 1:1), after 1 h complete conversion of the educt was confirmed, and the reaction was stopped. The solvent was removed under reduced pressure, the reaction residual was dissolved in EtOAc (5 mL) and water (15 mL) was added. The aqueous phase was extracted with EtOAc (3 x 15 mL), combined organic phases were washed with sat. aq. NaHCO₃ solution (10 mL), sat aq. NaCl solution (15 mL), dried over MgSO₄ and concentrated under vacuum. Product was

isolated as a yellow solid (60.0 mg, 0.110 mmol, 44%) after purification by flash column chromatography (*n*-hexane/EtOAc, 1:1).

TLC: $R_f = 0.2$ (*n*-hexane/EtOAc, 1:1)

mp.: 103 °C

¹H NMR (300 MHz, Acetone) δ (ppm) 8.62 (d, $J = 8.4$ Hz, 1H, H-26), 8.33 (d, $J = 8.8$ Hz, 1H, H-7), 8.18 (s, 1H, H-NH), 7.33 (d, $J = 9.0$ Hz, 1H, H-6), 7.24 (d, $J = 3.4$ Hz, 1H, H-4), 7.17 – 7.04 (m, 4H, H-9, H-9', H-19, H-19'), 6.93 – 6.82 (m, 3H, H-10, H-10', H-27), 6.77 (d, $J = 8.6$ Hz, 2H, H-20, H-20'), 3.57 (s, 2H, H-17).

¹³C NMR (75 MHz, Acetone) δ (ppm) 170.48 (1C, C-1), 158.32 (1C, C-11), 157.42 (1C, C-5), 157.16 (1C, C-21), 155.12 (1C, C-22), 150.01 (1C, C-24), 135.66 (C-2), 135.05 (1C, C-8), 134.39 (1C, C-26), 130.32 (4C, C-9, C-9', C-19, C-19'), 125.88 (1C, C-18) 124.39 (1C, C-7), 122.20 (1C, C-4), 119.38 (1C, C-6), 116.00 (1C, C-27), 115.95 (2C, C-10, C-10'), 115.63 (2C, C-20, C-20'), 44.01 (1C, C-17).

MS (-): 497.1 ([M-H]⁻)

HR-MS (ESI-): calc. for C₂₆H₁₈N₄O₇ ([M-H]⁻): 497.1103, found: 497.1094.

FT-IR (Diamond-ATR): ν (cm⁻¹) 3355.53, 1653.66, 1653.66, 1539.88, 1331.61, 1260.25, 1185.04, 1089.58, 997.982, 826.348, 732.817.

8 BIBLIOGRAPHY

- [1] J. M. Statland, R. J. Barohn, A. L. McVey, J. S. Katz, M. M. Dimachkie, *Neurologic clinics* **2015**, 33, 735.
- [2] M. C. Kiernan, S. Vucic, B. C. Cheah, M. R. Turner, A. Eisen, O. Hardiman, J. R. Burrell, M. C. Zoing, *The Lancet* **2011**, 377, 942.
- [3] S. Chen, P. Sayana, X. Zhang, W. Le, *Molecular Neurodegeneration* **2013**, 8, 28.
- [4] Z.-Y. Zou, Z.-R. Zhou, C.-H. Che, C.-Y. Liu, R.-L. He, H.-P. Huang, *J Neurol Neurosurg Psychiatry* **2017**, 88, 540.
- [5] D. R. Rosen, T. Siddique, D. Patterson, D. A. Figlewicz, P. Sapp, A. Hentati, D. Donaldson, J. Goto, J. P. O'Regan, H. X. Deng, *Nature* **1993**, 362, 59.
- [6] R. A. Saccon, R. K. A. Bunton-Stasyshyn, E. M. C. Fisher, P. Fratta, *Brain* **2013**, 136, 2342.
- [7] C. G. Goetz, *Muscle Nerve* **2000**, 23, 336.
- [8] R. Tandan, W. G. Bradley, *Annals of Neurology* **1985**, 18, 271.
- [9] A. Chiò, G. Logroscino, O. Hardiman, R. Swingler, D. Mitchell, E. Beghi, B. G. Traynor, *Amyotrophic lateral sclerosis : official publication of the World Federation of Neurology Research Group on Motor Neuron Diseases* **2009**, 10, 310.
- [10] E. Longinetti, F. Fang, *Current opinion in neurology* **2019**, 32, 771.
- [11] S. J. Kaur, S. R. McKeown, S. Rashid, *Gene* **2016**, 577, 109.

- [12] R. Mejzini, L. L. Flynn, I. L. Pitout, S. Fletcher, S. D. Wilton, P. A. Akkari, *Front. Neurosci.* **2019**, *13*, 1310.
- [13] A. A. Alsultan, R. Waller, P. R. Heath, J. Kirby, *Degenerative Neurological and Neuromuscular Disease* **2016**, *6*, 49.
- [14] K. Boylan, *Neurologic clinics* **2015**, *33*, 807.
- [15] a) S. Zarei, K. Carr, L. Reiley, K. Diaz, O. Guerra, P. F. Altamirano, W. Pagani, D. Lodin, G. Orozco, A. China, *Surgical Neurology International* **2015**, *6*, 171; b) P. S. Spencer, P. B. Nunn, J. Hugon, A. C. Ludolph, S. M. Ross, D. N. Roy, R. C. Robertson, *Science (New York, N.Y.)* **1987**, *237*, 517.
- [16] M. A. van Es, O. Hardiman, A. Chio, A. Al-Chalabi, R. J. Pasterkamp, J. H. Veldink, L. H. van den Berg, *The Lancet* **2017**, *390*, 2084.
- [17] W. Robberecht, T. Philips, *Nat Rev Neurosci* **2013**, *14*, 248.
- [18] N. Geevasinga, P. Menon, P. H. Özdinler, M. C. Kiernan, S. Vucic, *Nat Rev Neurol* **2016**, *12*, 651.
- [19] T. L. Williamson, D. W. Cleveland, *Nat Neurosci* **1999**, *2*, 50.
- [20] X. Paez-Colasante, C. Figueroa-Romero, S. A. Sakowski, S. A. Goutman, E. L. Feldman, *Nat Rev Neurol* **2015**, *11*, 266.
- [21] M. R. Turner, O. Hardiman, M. Benatar, B. R. Brooks, A. Chio, M. de Carvalho, P. G. Ince, C. Lin, R. G. Miller, H. Mitsumoto et al., *The Lancet Neurology* **2013**, *12*, 310.
- [22] J. Wokke, *The Lancet* **1996**, *348*, 795.
- [23] G. Bensimon, L. Lacomblez, V. Meininger, *The New England journal of medicine* **1994**, *330*, 585.
- [24] A. Doble, *Neurology* **1996**, *47*, S233-41.
- [25] R.D. Azbill, X. Mu, J.E. Springer, *Brain Research* **2000**, *871*, 175.
- [26] D. Petrov, C. Mansfield, A. Moussy, O. Hermine, *Frontiers in Aging Neuroscience* **2017**, *9*, 68.
- [27] M. P. Cruz, *Pharmacy and Therapeutics* **2018**, *43*, 25.
- [28] H. Sawada, *Expert Opinion on Pharmacotherapy* **2017**, *18*, 735.

- [29] "Efficacy and Safety of Masitinib Versus Placebo in the Treatment of ALS Patients - Full Text View - ClinicalTrials.gov", can be found under <https://clinicaltrials.gov/ct2/show/NCT03127267?term=AB19001&draw=1&rank=1>, **2020**.
- [30] a) T. M. Miller, A. Pestronk, W. David, J. Rothstein, E. Simpson, S. H. Appel, P. L. Andres, K. Mahoney, P. Allred, K. Alexander et al., *The Lancet Neurology* **2013**, *12*, 435; b) Biogen, Ionis Pharmaceuticals, Inc., "A Study to Evaluate the Efficacy, Safety, Tolerability, Pharmacokinetics, and Pharmacodynamics of BIIB067 Administered to Adult Subjects With Amyotrophic Lateral Sclerosis and Confirmed Superoxide Dismutase 1 Mutation. NCT02623699, 233AS101", can be found under <https://clinicaltrials.gov/ct2/show/NCT02623699>, **2020**.
- [31] J. M. McCord, I. Fridovich, *The Journal of biological chemistry* **1969**, *244*, 6049.
- [32] M. S. MOHAMED, D. M. GREENBERG, *The Journal of General Physiology* **1954**, *37*, 433.
- [33] J. M. McCord, I. Fridovich, *Superoxide dismutase: The first twenty years (1968–1988)*, **1988**.
- [34] R. Rakhit, A. Chakrabarty, *Biochimica et biophysica acta* **2006**, *1762*, 1025.
- [35] Klug D, Rabani J and Fridovich **1972**, 4839.
- [36] M. J. Hitchler, F. E. Domann, *Antioxidants & redox signaling* **2014**, *20*, 1590.
- [37] M. Hayyan, M. A. Hashim, I. M. AlNashef, *Chemical Reviews* **2016**, *116*, 3029.
- [38] a) I. Fridovich, *Annual review of biochemistry* **1975**, *44*, 147; b) Y. Furukawa, T. V. O'Halloran, *Antioxidants & redox signaling* **2006**, *8*, 847.
- [39] I. N. Zelko, T. J. Mariani, R. J. Folz, *Superoxide dismutase multigene family: a comparison of the CuZn-SOD (SOD1), Mn-SOD (SOD2), and EC-SOD (SOD3) gene structures, evolution, and expression*, **2002**.
- [40] A. J. Case, *Antioxidants (Basel, Switzerland)* **2017**, *6*.
- [41] R. W. Strange, S. Antonyuk, M. A. Hough, P. A. Doucette, J. A. Rodriguez, P.J. Hart, L. J. Hayward, J. S. Valentine, S.S. Hasnain, *Journal of molecular biology* **2003**, *328*, 877.

- [42] a) J. A. Tainer, E. D. Getzoff, J. S. Richardson, D. C. Richardson, *Nature* **1983**, 306, 284; b) E. D. Getzoff, J. A. Tainer, P. K. Weiner, P. A. Kollman, J. S. Richardson, D. C. Richardson, *Nature* **1983**, 306, 287.
- [43] P. J. Hart, M. M. Balbirnie, N. L. Ogihara, A. M. Nersissian, M. S. Weiss, J. S. Valentine, D. Eisenberg, *Biochemistry* **1999**, 38, 2167.
- [44] E. F. Pettersen, T. D. Goddard, C. C. Huang, G. S. Couch, D. M. Greenblatt, E. C. Meng, T. E. Ferrin, *Journal of computational chemistry* **2004**, 25, 1605.
- [45] H. J. Forman, I. Fridovich, *The Journal of biological chemistry* **1973**, 248, 2645.
- [46] R. Rakhit, J. P. Crow, J. R. Lepock, L. H. Kondejewski, N. R. Cashman, A. Chakrabartty, *The Journal of biological chemistry* **2004**, 279, 15499.
- [47] "ALSoD", can be found under <https://alsod.ac.uk/output/gene.php#geneSummary>, **2020**.
- [48] Deng, H. X., Hentati, A., Tainer, J. A., Iqbal, Z., Cayabyab, A., Hung, W. Y., Getzoff, E. D., Hu, P., Herzfeldt, B., Roos, R. P., and et al. (1993) *Science* 261, 1047-1051 **1993**.
- [49] M. DiDonato, L. Craig, M. E. Huff, M. M. Thayer, R. M.F. Cardoso, C. J. Kassmann, T. P. Lo, C. K. Bruns, E. T. Powers, J. W. Kelly et al., *Journal of molecular biology* **2003**, 332, 601.
- [50] a) A. Tiwari, A. Liba, S. H. Sohn, S. V. Seetharaman, O. Bilsel, C. R. Matthews, P. J. Hart, J. S. Valentine, L. J. Hayward, *The Journal of biological chemistry* **2009**, 284, 27746; b) A. Tiwari, L. J. Hayward, *The Journal of biological chemistry* **2003**, 278, 5984.
- [51] M. A. Hough, J. G. Grossmann, S. V. Antonyuk, R. W. Strange, P. A. Doucette, J. A. Rodriguez, L. J. Whitson, P. J. Hart, L. J. Hayward, J. S. Valentine et al., *Proc Natl Acad Sci USA* **2004**, 101, 5976.
- [52] S. S. Ray, R. J. Nowak, K. Strokovich, R. H. Brown, T. Walz, P. T. Lansbury, *Biochemistry* **2004**, 43, 4899.
- [53] Y. Sheng, M. Chattopadhyay, J. Whitelegge, J. S. Valentine, *Current topics in medicinal chemistry* **2012**, 12, 2560.
- [54] Q. Wang, J. L. Johnson, N. Y. R. Agar, J. N. Agar, *PLOS Biology* **2008**, 6, e170.

- [55] G. S. A. Wright, S. V. Antonyuk, S. S. Hasnain, *Quart. Rev. Biophys.* **2019**, *52*, e12.
- [56] S. Antonyuk, R. W. Strange, S. S. Hasnain, *Journal of medicinal chemistry* **2010**, *53*, 1402.
- [57] R. M.F. Cardoso, M. M. Thayer, M. DiDonato, T. P. Lo, C. K. Bruns, E. D. Getzoff, J. A. Tainer, *Insights into Lou Gehrig's Disease from the Structure and Instability of the A4V Mutant of Human Cu,Zn Superoxide Dismutase*, **2002**.
- [58] A. G. Reaume, J. L. Elliott, E. K. Hoffman, N. W. Kowall, R. J. Ferrante, D. F. Siwek, H. M. Wilcox, D. G. Flood, M. F. Beal, R. H. Brown et al., *Nat Genet* **1996**, *13*, 43.
- [59] L. I. Bruijn, M. K. Houseweart, S. Kato, K. L. Anderson, S. D. Anderson, E. Ohama, A. G. Reaume, R. W. Scott, D. W. Cleveland, *Science (New York, N.Y.)* **1998**, *281*, 1851.
- [60] R. Rakhit, P. Cunningham, A. Furtos-Matei, S. Dahan, X.-F. Qi, J. P. Crow, N. R. Cashman, L. H. Kondejewski, A. Chakrabartty, *The Journal of biological chemistry* **2002**, *277*, 47551.
- [61] Y. Furukawa, K. Kaneko, K. Yamanaka, T. V. O'Halloran, N. Nukina, *The Journal of biological chemistry* **2008**, *283*, 24167.
- [62] A. Kerman, H.-N. Liu, S. Croul, J. Bilbao, E. Rogaeva, L. Zinman, J. Robertson, A. Chakrabartty, *Acta Neuropathol* **2010**, *119*, 335.
- [63] E. Sandelin, A. Nordlund, P. M. Andersen, S. S. L. Marklund, M. Oliveberg, *The Journal of biological chemistry* **2007**, *282*, 21230.
- [64] L. Banci, I. Bertini, A. Durazo, S. Giroto, E. B. Gralla, M. Martinelli, J. S. Valentine, M. Vieru, J. P. Whitelegge, *Proceedings of the National Academy of Sciences of the United States of America* **2007**, *104*, 11263.
- [65] L. Banci, I. Bertini, M. Boca, V. Calderone, F. Cantini, S. Giroto, M. Vieru, *PNAS* **2009**, *106*, 6980.
- [66] L. Lang, P. Zetterström, T. Brännström, S. L. Marklund, J. Danielsson, M. Oliveberg, *PNAS* **2015**, *112*, 9878.
- [67] M. I. Ivanova, S. A. Sievers, E. L. Guenther, L. M. Johnson, D. D. Winkler, A. Galaleldeen, M. R. Sawaya, P. J. Hart, D. S. Eisenberg, *PNAS* **2014**, *111*, 197.

- [68] T. E. Brotherton, Y. Li, J. D. Glass, *Neurobiology of Disease* **2013**, *49*, 49.
- [69] Gareth S.A. Wright, Svetlana V. Antonyuk, Neil M. Kershaw, Richard W. Strange, S Samar Hasnain, *Nat Commun* **2013**, *4*, 1.
- [70] E. A. Proctor, L. Fee, Y. Tao, R. L. Redler, J. M. Fay, Y. Zhang, Z. Lv, I. P. Mercer, M. Deshmukh, Y. L. Lyubchenko et al., *Proc Natl Acad Sci USA* **2016**, *113*, 614.
- [71] S. D. Khare, M. Caplow, N. V. Dokholyan, *Proceedings of the National Academy of Sciences of the United States of America* **2004**, *101*, 15094.
- [72] L. McAlary, J. J. Yerbury, J. A. Aquilina, *Sci Rep* **2013**, *3*, 1.
- [73] M. J. Capper, G. S. A. Wright, L. Barbieri, E. Luchinat, E. Mercatelli, L. McAlary, J. J. Yerbury, P. M. O'Neill, S. V. Antonyuk, L. Banci et al., *Nature communications* **2018**, *9*, 1693.
- [74] H. R. Broom, J. A. O. Rumfeldt, K. A. Vassall, E. M. Meiering, *Protein science : a publication of the Protein Society* **2015**, *24*, 2081.
- [75] I. P. Ermilova, V. B. Ermilov, M. Levy, E. Ho, C. Pereira, J. S. Beckman, *Protection by dietary zinc in ALS mutant G93A SOD transgenic mice*, **2005**.
- [76] J. S. Beckman, M. Carson, C. D. Smith, W. H. Koppenol, *Nature* **1993**, *364*, 584.
- [77] C. P. W. Soon, P. S. Donnelly, B. J. Turner, L. W. Hung, P. J. Crouch, N. A. Sherratt, J.-L. Tan, N. K.-H. Lim, L. Lam, L. Bica et al., *J. Biol. Chem.* **2011**, *286*, 44035.
- [78] J. R. Williams, E. Trias, P. R. Beilby, N. I. Lopez, E. M. Labut, C. S. Bradford, B. R. Roberts, E. J. McAllum, P. J. Crouch, T. W. Rhoads et al., *Neurobiology of Disease* **2016**, *89*, 1.
- [79] F. G. Vieira, T. Hatzipetros, K. Thompson, A. J. Moreno, J. D. Kidd, V. R. Tassinari, B. Levine, S. Perrin, A. Gill, *IBRO Reports* **2017**, *2*, 47.
- [80] N. E. Farrawell, M. R. Yerbury, S. S. Plotkin, L. McAlary, J. J. Yerbury, *ACS chemical neuroscience* **2019**, *10*, 1555.
- [81] J. R. Auclair, K. J. Boggio, G. A. Petsko, D. Ringe, J. N. Agar, *Proceedings of the National Academy of Sciences of the United States of America* **2010**, *107*, 21394.

- [82] L. Banci, I. Bertini, O. Blaževič, V. Calderone, F. Cantini, J. Mao, A. Trapananti, M. Vieru, I. Amori, M. Cozzolino et al., *J. Am. Chem. Soc.* **2012**, *134*, 7009.
- [83] S. S. Ray, R. J. Nowak, R. H. Brown, P. T. Lansbury, *Proc Natl Acad Sci USA* **2005**, *102*, 3639.
- [84] R. J. Nowak, G. D. Cuny, S. Choi, P. T. Lansbury, S. S. Ray, *Journal of medicinal chemistry* **2010**, *53*, 2709.
- [85] R. Manjula, G. S. A. Wright, R. W. Strange, B. Padmanabhan, *FEBS letters* **2018**, *592*, 1725.
- [86] R. Manjula, S. Unni, G. S. A. Wright, S. Bharath M M, B. Padmanabhan, *Journal of biomolecular structure & dynamics* **2019**, *37*, 3936.
- [87] a) E. Pokrishevsky, L. McAlary, N. E. Farrawell, B. Zhao, M. Sher, J. J. Yerbury, N. R. Cashman, *Sci Rep* **2018**, *8*, 15590; b) E. Pokrishevsky, R. H. Hong, I. R. Mackenzie, N. R. Cashman, *PLOS ONE* **2017**, *12*, e0184384.
- [88] J. S. Elam, A. B. Taylor, R. Strange, S. Antonyuk, P. A. Doucette, J. A. Rodriguez, S. S. Hasnain, L. J. Hayward, J. S. Valentine, T. O. Yeates et al., *Nature structural biology* **2003**, *10*, 461.
- [89] I. M. Kapetanovic, *Chemico-biological interactions* **2008**, *171*, 165.
- [90] W. P. Feinstein, M. Brylinski, *Journal of cheminformatics* **2015**, *7*, 18.
- [91] X.-Y. Meng, H.-X. Zhang, M. Mezei, M. Cui, *Current computer-aided drug design* **2011**, *7*, 146.
- [92] D.-L. Ma, D. S.-H. Chan, C.-H. Leung, *Chemical Society reviews* **2013**, *42*, 2130.
- [93] X. Xu, M. Huang, X. Zou, *Biophysics Reports* **2018**, *4*, 1.
- [94] G. Lauro, M. Masullo, S. Piacente, R. Riccio, G. Bifulco, *Bioorganic & medicinal chemistry* **2012**, *20*, 3596.
- [95] E. Fischer, *Ber. Dtsch. Chem. Ges.* **1894**, *27*, 3479.
- [96] D. E. Koshland, *Proc Natl Acad Sci USA* **1958**, *44*, 98.
- [97] Todd Holyoak in *Encyclopedia of Biophysics*, Springer, Berlin, Heidelberg, **2013**, pp. 1584–1588.

- [98] F. Spyrakis, C. N. Cavasotto, *Archives of Biochemistry and Biophysics* **2015**, 583, 105.
- [99] H. R. Bosshard, *News in physiological sciences : an international journal of physiology produced jointly by the International Union of Physiological Sciences and the American Physiological Society* **2001**, 16, 171.
- [100] V. Salmaso, S. Moro, *Front. Pharmacol.* **2018**, 9, 923.
- [101] D. B. Kitchen, H. Decornez, J. R. Furr, J. Bajorath, *Nat Rev Drug Discov* **2004**, 3, 935.
- [102] "SwissDock - The online docking web server of the Swiss Institute of Bioinformatics - Home", can be found under <http://www.swissdock.ch/>, **2020**.
- [103] "1-Click-Docking", can be found under <https://mcule.com/apps/1-click-docking/>, **2020**.
- [104] "AutoDock Vina - molecular docking and virtual screening program", can be found under <http://vina.scripps.edu/>, **2014**.
- [105] A. Grosdidier, V. Zoete, O. Michielin, *Nucleic acids research* **2011**, 39, W270-7.
- [106] O. Trott, A. J. Olson, *Journal of computational chemistry* **2010**, 31, 455.
- [107] M. W. Chang, C. Ayeni, S. Breuer, B. E. Torbett, *PLoS ONE* **2010**, 5, e11955.
- [108] M. Jerabek-Willemsen, T. André, R. Wanner, H. M. Roth, S. Duhr, P. Baaske, D. Breitsprecher, *Journal of Molecular Structure* **2014**, 1077, 101.
- [109] R. Magnez, B. Thiroux, S. Taront, Z. Segaula, B. Quesnel, X. Thuru, *Sci Rep* **2017**, 7, 17623.
- [110] J. M. Rainard, G. C. Pandarakalam, S. P. McElroy, *Slas Discovery* **2018**, 23, 225.
- [111] P. Baaske, C. J. Wienken, P. Reineck, S. Duhr, D. Braun, *Angew. Chem. Int. Ed.* **2010**, 49, 2238.
- [112] S. Duhr, D. Braun, *Proc Natl Acad Sci USA* **2006**, 103, 19678.
- [113] C. J. Wienken, P. Baaske, U. Rothbauer, D. Braun, S. Duhr, *Nat Commun* **2010**, 1, 100.

- [114] M. Jerabek-Willemsen, C. J. Wienken, D. Braun, P. Baaske, S. Duhr, *Assay and Drug Development Technologies* **2011**, 9, 342.
- [115] *MST-on time. V001 2018-03-14.*
- [116] M. W. Freyer, E. A. Lewis in *Methods in Cell Biology*, Elsevier, **2008**, pp. 79–113.
- [117] Malvern Instruments Limited, *Microcal ITC systems*, **2016**.
- [118] C. Song, S. Zhang, H. Huang, *Front. Microbiol.* **2015**, 6, 1049.
- [119] WO 2006/089221 A2.
- [120] T. Yamaguchi, M. Asanuma, S. Nakanishi, Y. Saito, M. Okazaki, K. Dodo, M. Sodeoka, *Chem. Sci.* **2014**, 5, 1021.
- [121] K. A. Ramsbottom, D. F. Carr, A. R. Jones, D. J. Rigden, *Molecular Immunology* **2018**, 101, 488.
- [122] M. Kozłowska, P. Rodziewicz, A. Kaczmarek-Kedziera, *Struct Chem* **2017**, 28, 999.
- [123] O. Llorens, J. J. Perez, A. Palomer, D. Mauleon, *Journal of Molecular Graphics and Modelling* **2002**, 20, 359.
- [124] H. Steuber, M. Zentgraf, C. Gerlach, C. A. Sotriffer, A. Heine, G. Klebe, *Journal of molecular biology* **2006**, 363, 174.
- [125] H. Merouani, N. Ouddai, M. Mokhtari, and N. Latelli, "Density Functional Theory Study of the Reactivity of Nitrobenzofurazan with a Series of 4- X - Substituted Phenols", **2009**.
- [126] A. Sharma, I. Ramos-Tomillero, A. El-Faham, E. Nicolas, H. Rodriguez, B. G. de La Torre, F. Albericio, *ChemistryOpen* **2017**, 6, 168.
- [127] C. C. C. Johansson Seechurn, M. O. Kitching, T. J. Colacot, V. Snieckus, *Angew. Chem. Int. Ed.* **2012**, 51, 5062.
- [128] Y. Shen, Q. Xie, M. Norberg, E. Sausville, G. Vande Woude, D. Wenkert, *Bioorganic & medicinal chemistry* **2005**, 13, 4960.
- [129] M. G. Banwell, M. T. Jones, D. T.J. Loong, D. W. Lupton, D. M. Pinkerton, J. K. Ray, A. C. Willis, *Tetrahedron* **2010**, 66, 9252.

- [130] P. G. M. Wuts, T. W. Greene, *Greene's Protective Groups in Organic Synthesis*, Wiley, Hoboken, **2014**.
- [131] D. Haas, J. M. Hammann, R. Greiner, P. Knochel, *ACS Catal.* **2016**, *6*, 1540.
- [132] A. Suzuki, *Angew. Chem. Int. Ed.* **2011**, *50*, 6722.
- [133] G. Bartoli, G. Palmieri, M. Bosco, R. Dalpozzo, *Tetrahedron Letters* **1989**, *30*, 2129.
- [134] B. Schmidt, M. Riemer, *The Journal of organic chemistry* **2014**, *79*, 4104.
- [135] D. Badone, M. Baroni, R. Cardamone, A. Ielmini, U. Guzzi, *The Journal of organic chemistry* **1997**, *62*, 7170.
- [136] N. E. Leadbeater, *Chemical communications (Cambridge, England)* **2005**, 2881.
- [137] T. Fukaya, T. Kodo, T. Ishiyama, H. Kakuyama, H. Nishikawa, S. Baba, S. Masumoto, *Bioorganic & medicinal chemistry* **2012**, *20*, 5568.
- [138] D. Ke, C. Zhan, X. Li, A. D.Q. Li, J. Yao, *Tetrahedron* **2009**, *65*, 8269.
- [139] A. Williamson, T. Ngouansavanh, R. Pace, A. Allen, J. Cuthbertson, M. Gaunt, *Synlett* **2015**, *27*, 116.
- [140] C. A.G.N. Montalbetti, V. Falque, *Tetrahedron* **2005**, *61*, 10827.
- [141] L. C. Chan, B. G. Cox, *The Journal of organic chemistry* **2007**, *72*, 8863.
- [142] E. Valeur, M. Bradley, *Chemical Society reviews* **2009**, *38*, 606.
- [143] M. Tissot, R. J. Phipps, C. Lucas, R. M. Leon, R. D. M. Pace, T. Ngouansavanh, M. J. Gaunt, *Angewandte Chemie (International ed. in English)* **2014**, *53*, 13498.
- [144] T. Kan, T. Fukuyama, *Chemical communications (Cambridge, England)* **2004**, 353.
- [145] V. Theuer, *Bachelor Thesis*, Georg-August-Universität Göttingen, **2018**.
- [146] J. Sheng, T. Xu, E. Zhang, X. Zhang, W. Wei, Y. Zou, *Journal of Natural Products* **2016**, *79*, 2749.
- [147] E. Blaise, A. E. Kümmerle, H. Hammoud, J. X. de Araújo-Júnior, F. Bihel, J.-J. Bourguignon, M. Schmitt, *The Journal of organic chemistry* **2014**, *79*, 10311.
- [148] J. Sherwood, J. H. Clark, I. J. S. Fairlamb, J. M. Slattery, *Green Chem.* **2019**, *21*, 2164.

- [149] J. A. La Molina de Torre, P. Espinet, A. C. Albéniz, *Organometallics* **2013**, *32*, 5428.
- [150] M. Tsakos, E. S. Schaffert, L. L. Clement, N. L. Villadsen, T. B. Poulsen, *Nat. Prod. Rep.* **2015**, *32*, 605.
- [151] R. Keller, *Bachelor Thesis*, **2020**.
- [152] J. P. Crow, J. B. Sampson, Y. Zhuang, J. A. Thompson, J. S. Beckman, *Journal of Neurochemistry* **1997**, *69*, 1936.
- [153] F. Lin, D. Yan, Y. Chen, F. E. E, H. Shi, B. Han, Y. Zhou, *Acta biochimica Polonica* **2018**, *65*, 235.
- [154] E. M. Gazdag, I. C. Cirstea, R. Breitling, J. Lukes, W. Blankenfeldt, K. Alexandrov, *Acta crystallographica. Section F, Structural biology and crystallization communications* **2010**, *66*, 871.
- [155] B. J. Tachu, K. A. Wüsten, M. C. Garza, H. Wille, G. Tamgüney, *Protein Expression and Purification* **2017**, *134*, 63.
- [156] A. S. Tan, M. V. Berridge, *Superoxide produced by activated neutrophils efficiently reduces the tetrazolium salt, WST-1 to produce a soluble formazan: a simple colorimetric assay for measuring respiratory burst activation and for screening anti-inflammatory agents*, **2000**.
- [157] can be found under <https://www.sigmaaldrich.com/content/dam/sigmaaldrich/docs/Sigma/Datasheet/6/19160dat.pdf>.
- [158] C.-Y. Wu, J. Steffen, D. J. Eide, *PLOS ONE* **2009**, *4*, e7061.
- [159] H.-T. Li, M. Jiao, J. Chen, Y. Liang, *Acta Biochim Biophys Sin (Shanghai)* **2010**, *42*, 183.
- [160] Z. W. Yang, S. W. Tendian, W. M. Carson, W. J. Brouillette, L. J. Delucas, C. G. Brouillette, *Protein science : a publication of the Protein Society* **2004**, *13*, 830.
- [161] S. Han, J.-R. Choi, K. Soon Shin, S. J. Kang, *Brain Research* **2012**, *1483*, 112.
- [162] B. Zhao, X. Zhuang, X. Bian, Z. Pi, S. Liu, Z. Liu, F. Song, *Journal of Mass Spectrometry* **2019**, *54*, 351.
- [163] "Analyzing Properties of Fluorescent Dyes Used for Labeling DNA in Microarray Experiments | Sigma-Aldrich", can be found under

<https://www.sigmaaldrich.com/technical-documents/articles/biofiles/analyzing-properties.html>, **2020**.

- [164] M. G. Acker, D. S. Auld, *Perspectives in Science* **2014**, *1*, 56.
- [165] H. Bisswanger, *Enzyme assays*, **2014**.
- [166] P. Ip, P. R. Sharda, A. Cunningham, S. Chakrabartty, V. Pande, A. Chakrabartty, *Protein Engineering, Design and Selection* **2017**, *30*, 431.
- [167] D. Cubrilovic, R. Zenobi, *Analytical chemistry* **2013**, *85*, 2724.
- [168] A. Tjernberg, N. Markova, W. J. Griffiths, D. Hallén, *Journal of biomolecular screening* **2006**, *11*, 131.
- [169] H. J. Sterling, J. S. Prell, C. A. Cassou, E. R. Williams, *Journal of the American Society for Mass Spectrometry* **2011**, *22*, 1178.
- [170] D. H. Rammler, *Annals of the New York Academy of Sciences* **1967**, *141*, 291.
- [171] P. Linke, K. Amaning, M. Maschberger, F. Vallee, V. Steier, P. Baaske, S. Duhr, D. Breitsprecher, A. Rak, *Journal of biomolecular screening* **2016**, *21*, 414.
- [172] E. Fisher, Y. Zhao, R. Richardson, M. Janik, A. K. Buell, F. I. Aigbirhio, G. Tóth, *ACS chemical neuroscience* **2017**, *8*, 2088.
- [173] R. Talhout, A. Villa, A. E. Mark, Engberts, Jan B. F. N., *J. Am. Chem. Soc.* **2003**, *125*, 10570.
- [174] R. Nelson, M. R. Sawaya, M. Balbirnie, A. Ø. Madsen, C. Riek, R. Grothe, D. Eisenberg, *Nature* **2005**, *435*, 773.
- [175] C. üinch, A. Bertolotti, *Journal of molecular biology* **2010**, *399*, 512.
- [176] S. Rajendran, C. Radha, V. Prakash, *International Journal of Peptide and Protein Research* **1995**, *45*, 122.
- [177] A. N. Rajeshwara, V. Prakash, *International Journal of Peptide and Protein Research* **1994**, *44*, 435.
- [178] A. Abdolvahabi, Y. Shi, A. Chuprin, S. Rasouli, B. F. Shaw, *ACS chemical neuroscience* **2016**, *7*, 799.
- [179] P. Crafts in *Computer Aided Chemical Engineering : Chemical Product Design: Toward a Perspective Through Case Studies* (Eds.: K. M. Ng, R. Gani, K. Dam-Johansen), Elsevier, **2007**, pp. 23–85.

- [180] C. A. Lipinski, F. Lombardo, B. W. Dominy, P. J. Feeney, *Experimental and computational approaches to estimate solubility and permeability in drug discovery and development settings IPII of original article: S0169-409X(96)00423-1. The article was originally published in Advanced Drug Delivery Reviews 23 (1997) 3–25. 1, 2001.*
- [181] H. Inoue, H. Nojima, H. Okayama, *Gene* **1990**, 96, 23.
- [182] K. Mullis, F. Faloon, S. Scharf, R. Saiki, G. Horn, H. Erlich, *Cold Spring Harbor symposia on quantitative biology* **1986**, 51 Pt 1, 263.
- [183] U. K. LAEMMLI, *Nature* **1970**, 227, 680.
- [184] Gasteiger E, Hoogland C, Gattiker A, Duvaud S, Wilkins M.R, Appel R.D., Bairoch A., *Protein Identification and Analysis Tools on the ExPASy Server*; (In John M. Walker (ed): The Proteomics Protocols Handbook, Humana Press, **2005**.
- [185] M. M. Bradford, *Analytical biochemistry* **1976**, 72, 248.
- [186] W. Kabsch, *Acta crystallographica. Section D, Biological crystallography* **2010**, 66, 125.
- [187] "MO-L011 Monolith Protein Labeling Kit RED – NHS 2nd Generation", can be found under <https://nanotempertech.force.com/explore/s/article/MO-L011-Monolith-Protein-Labeling-Kit-RED-NHS-2nd-Generation>, **2020**.
- [188] G. Schwartz, *ENZ-51023_insert PROTEOSTAT® Protein aggregation assay*.
- [189] N. P. Rodina, M. I. Sulatsky, A. I. Sulatskaya, I. M. Kuznetsova, V. N. Uversky, K. K. Turoverov, *Journal of Spectroscopy* **2017**, 2017, 1.
- [190] G. Schwartz, *ENZ-51039_insert*.
- [191] R. P. D. Bank, "RCSB PDB: Homepage", can be found under <http://www.rcsb.org/>, **2020**.
- [192] S. Forli, R. Huey, M. E. Pique, M. Sanner, D. S. Goodsell, A. J. Olson, *Nature protocols* **2016**, 11, 905.
- [193] G. M. Morris, R. Huey, W. Lindstrom, M. F. Sanner, R. K. Belew, D. S. Goodsell, A. J. Olson, *Journal of computational chemistry* **2009**, 30, 2785.
- [194] G. R. Fulmer, A. J. M. Miller, N. H. Sherden, H. E. Gottlieb, A. Nudelman, B. M. Stoltz, J. E. Bercaw, K. I. Goldberg, *Organometallics* **2010**, 29, 2176.

9 APPENDICES

9.1 Expression and purification data of hSOD1

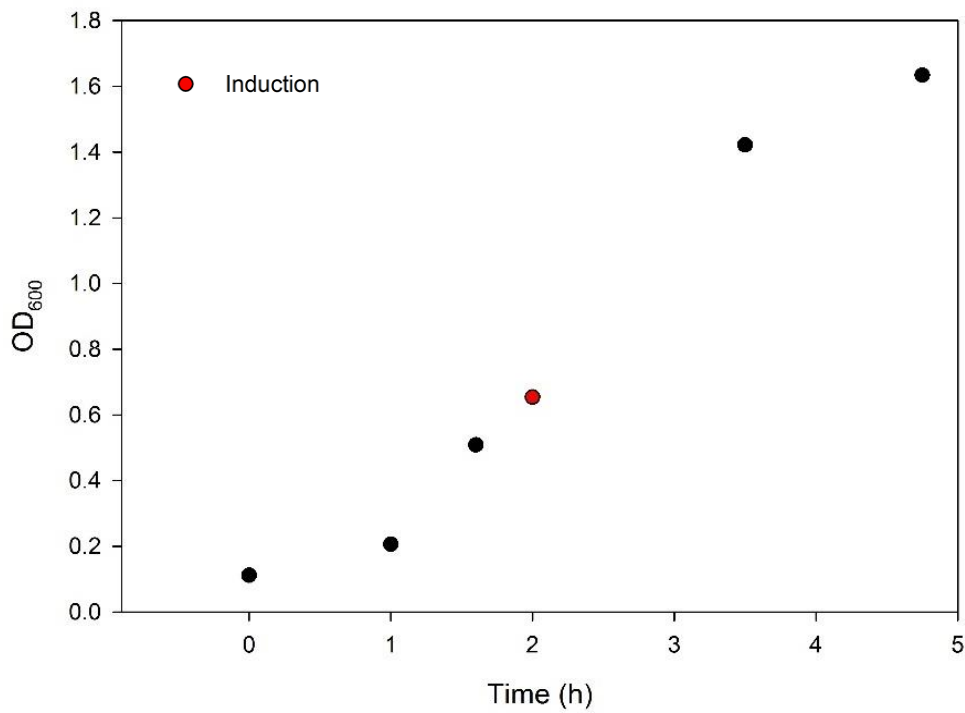


Figure 9.1 Growth rate with induction. Expression of hSOD1 in *E. coli* BL21 Star™.

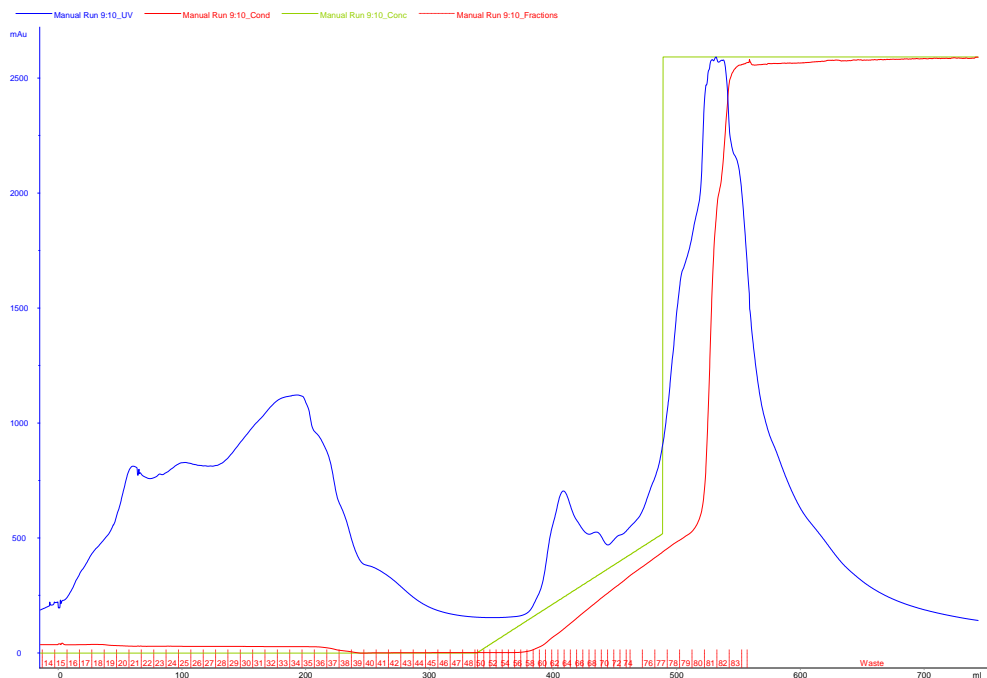
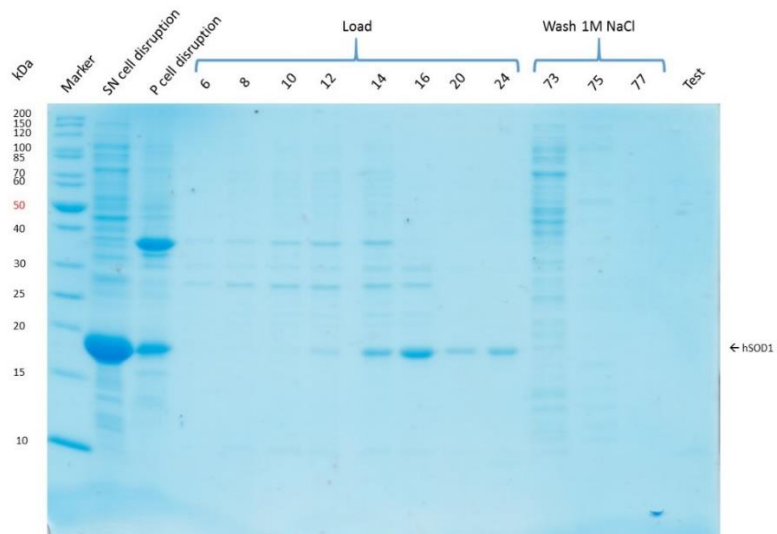
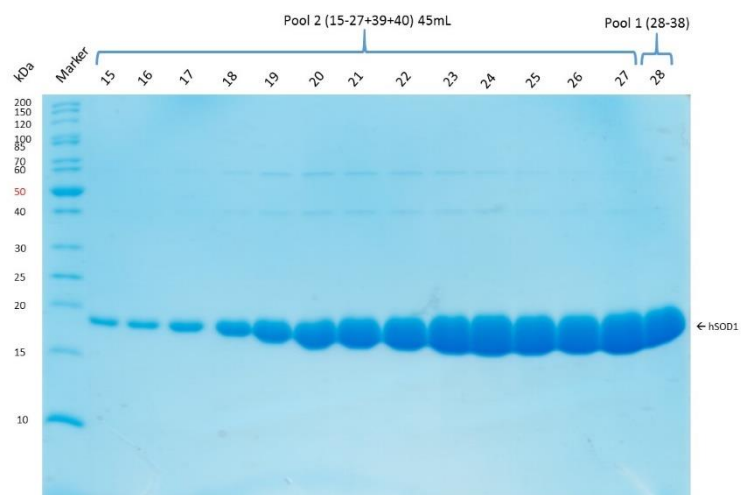


Figure 9.2 Chromatogram of hSOD1 purification on TMAE column.

TMAE Load



TMAE Elution 1



TMAE Elution 2

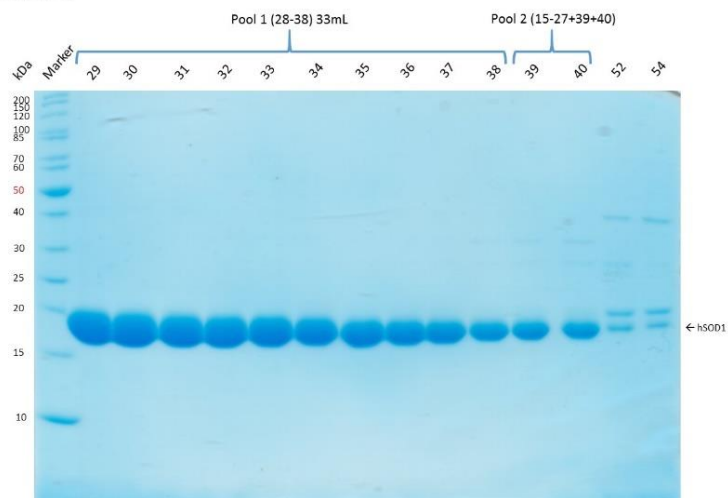


Figure 9.3 SDS-page gels from the purification of hSOD1wt

9.2 Free binding energies of the lead structures

Filename	Mode	Affinity[kcal/mol]	RMSD l.b. [Å]	RMSD u.b. [Å]
LS A	1	-9.0	0	0
LS A	2	-8.6	3.732	6.075
LS A	3	-8.5	3.63	5.26
LS A	4	-8.4	3.21	8.085
LS A	5	-8.2	1.885	3.83
LS A	6	-8.2	3.434	4.443
LS A	7	-8.2	3.143	8.024
LS A	8	-8.1	3.515	8.5
LS A	9	-8.1	2.238	3.552

Filename	Mode	Affinity[kcal/mol]	RMSD l.b. [Å]	RMSD u.b. [Å]
LS B	1	-9.1	0	0
LS B	2	-9.0	4.081	6.019
LS B	3	-9.0	4.323	6.498
LS B	4	-8.8	1.812	3.619
LS B	5	-8.8	2.396	4.402
LS B	6	-8.5	1.598	1.767
LS B	7	-8.5	1.256	1.904
LS B	8	-8.5	1.348	2.285
LS B	9	-8.3	3.539	6.33

Filename	Mode	Affinity[kcal/mol]	RMSD l.b. [Å]	RMSD u.b. [Å]
L S C	1	-8.5	0	0
L S C	2	-8.4	3.149	6.935
L S C	3	-8.4	1.977	5.918
L S C	4	-8.3	3.234	8.725
L S C	5	-8.3	3.888	5.529
L S C	6	-8.0	3.424	5.811
L S C	7	-7.9	4.625	9.928
L S C	8	-7.9	2.216	2.675
L S C	9	-7.9	2.435	5.442

9.3 Biophysical and protein studies

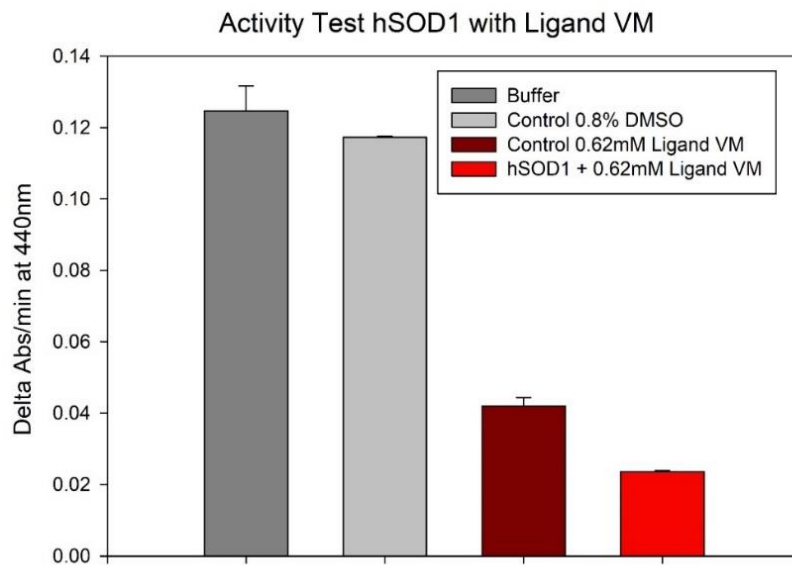


Figure 9.4 Activity assay with ligand L1 in Hepes buffer (*Experiment performed and data obtained by Lisa-Marie Funk*)

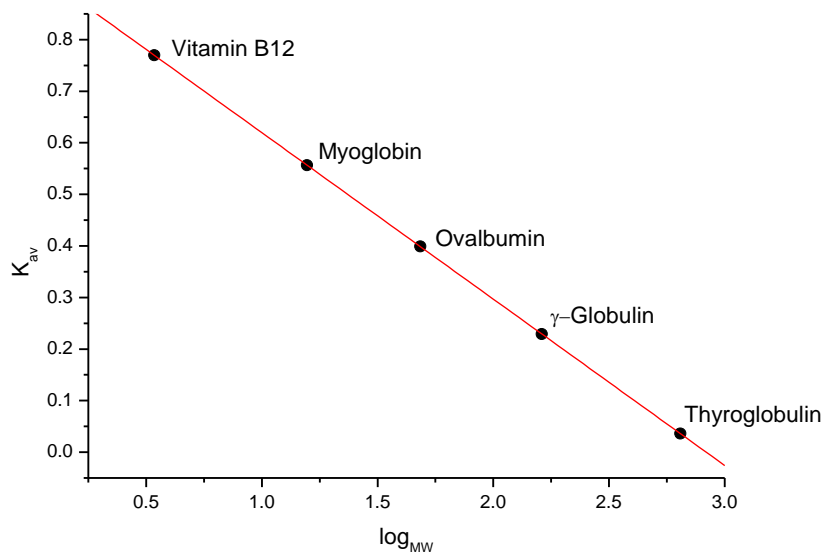


Figure 9.5 Size exclusion chromatography (SEC) Biorad standard curve

9.4 Binding affinity assay development

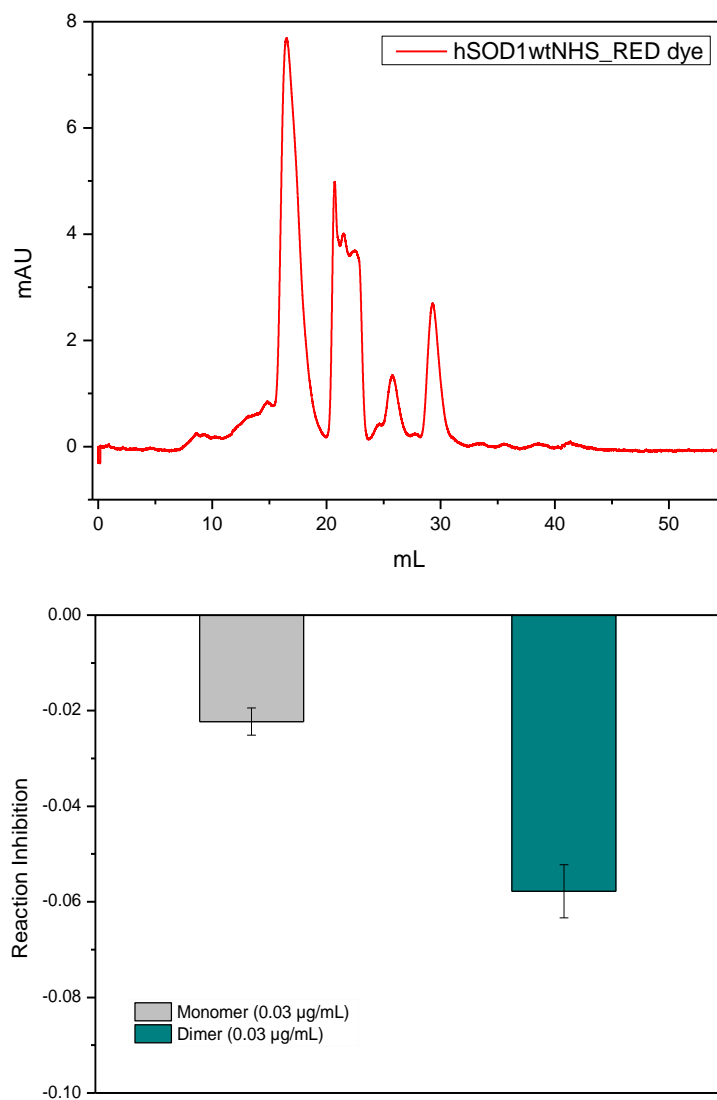


Figure 9.6 Data of NHS-ester labelled hSOD1wt protein for MST binding studies. SEC chromatogram (*top*) and activity assay of the isolated labelled hSOD1 protein, monomer and dimer (*bottom*).

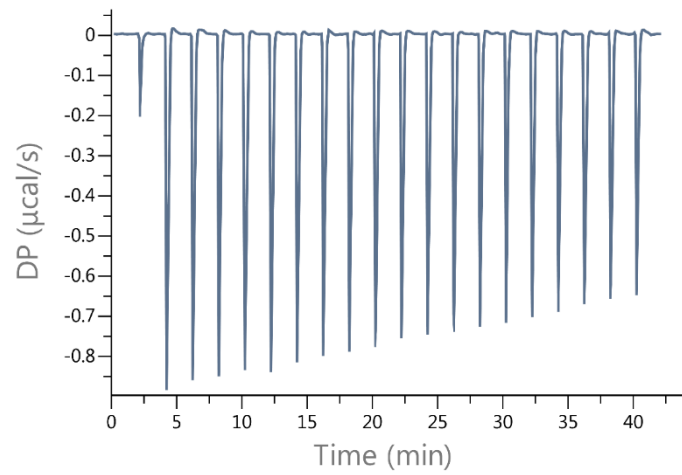


Figure 9.7 Raw data of the ITC run with L1. Titration of L1 into Hepes buffer with 20% DMSO

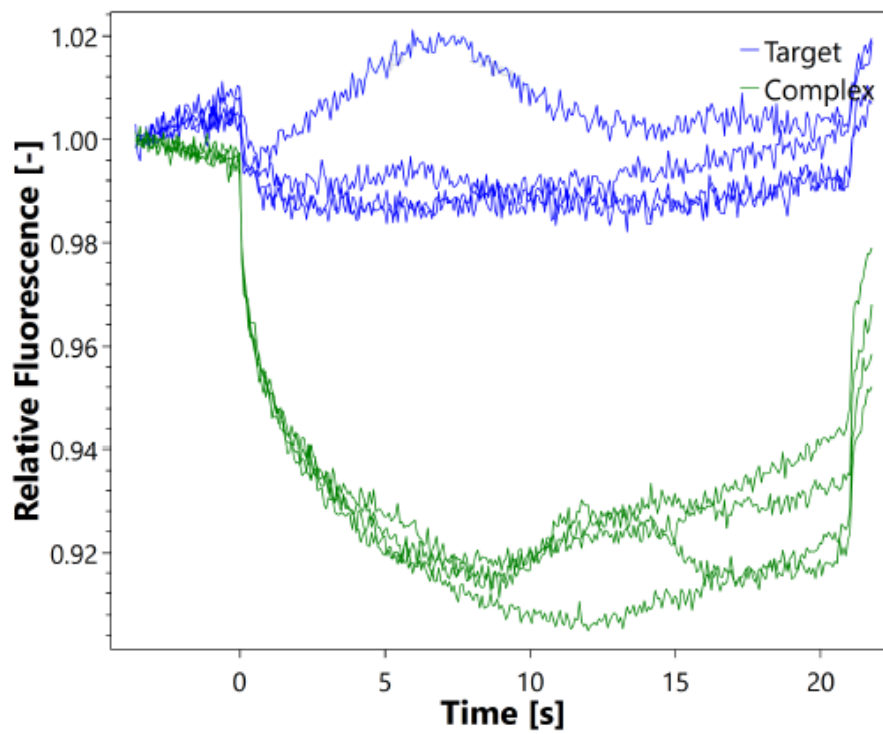


Figure 9.8 MST binding assay data. Aggregation is observed in thermophoretic signals of the complex (ligand L1 and Atto 647 labelled hSOD1wt protein target) as well as the labelled protein target only.

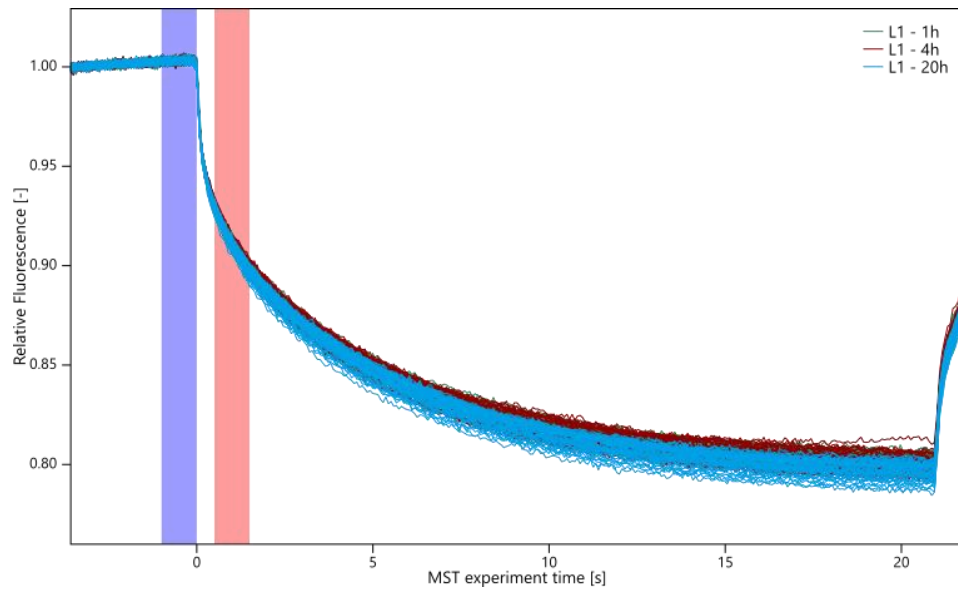


Figure 9.9 Thermophoretic traces of L1 with different incubation times

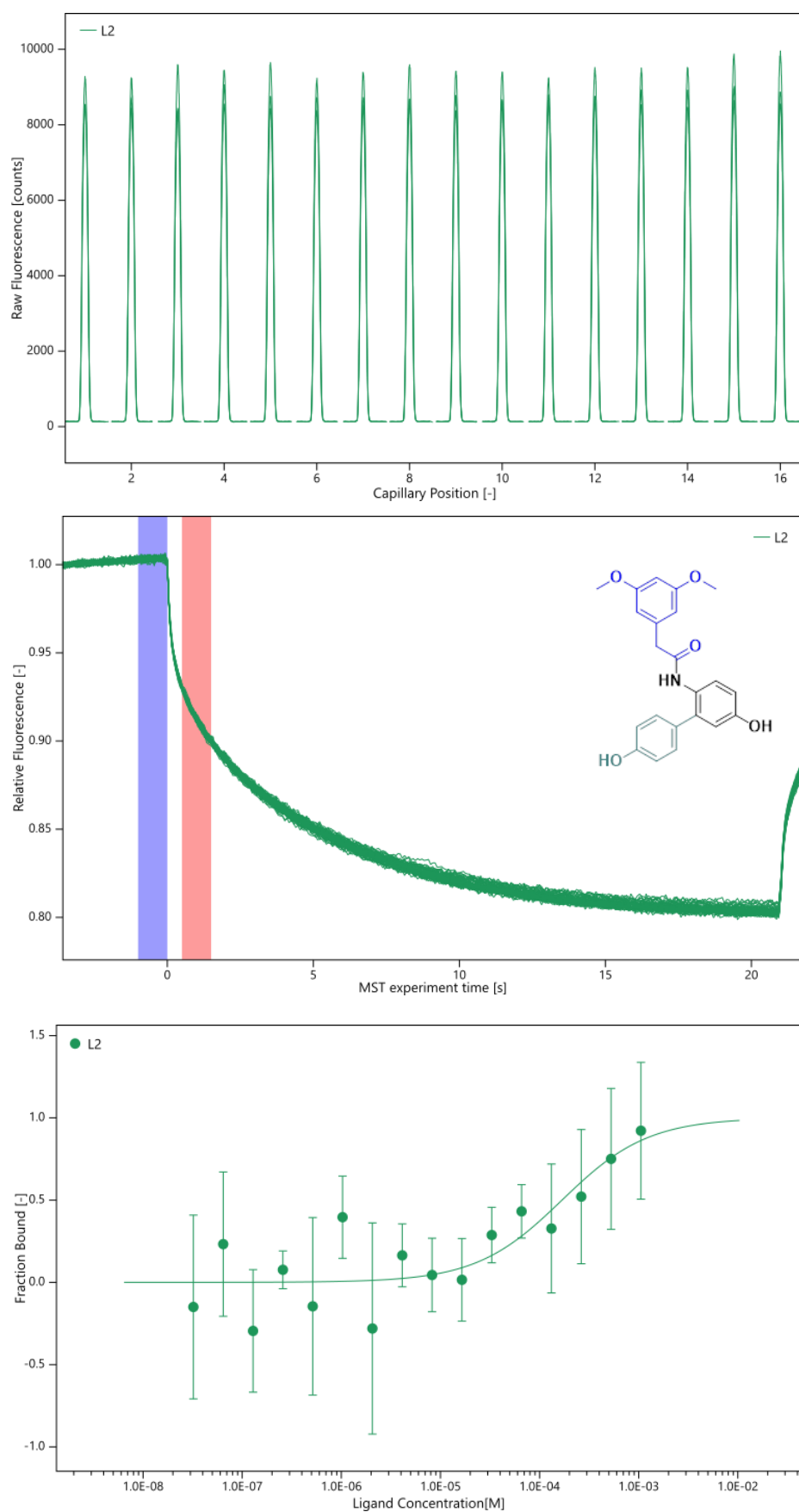


Figure 9.10 MST data of ligand L2. Fluorescence capillary scan (*top*), thermophoretic signal with 1.5 s MST-on time (*middle*), binding affinity curve of the ligand (*bottom*).

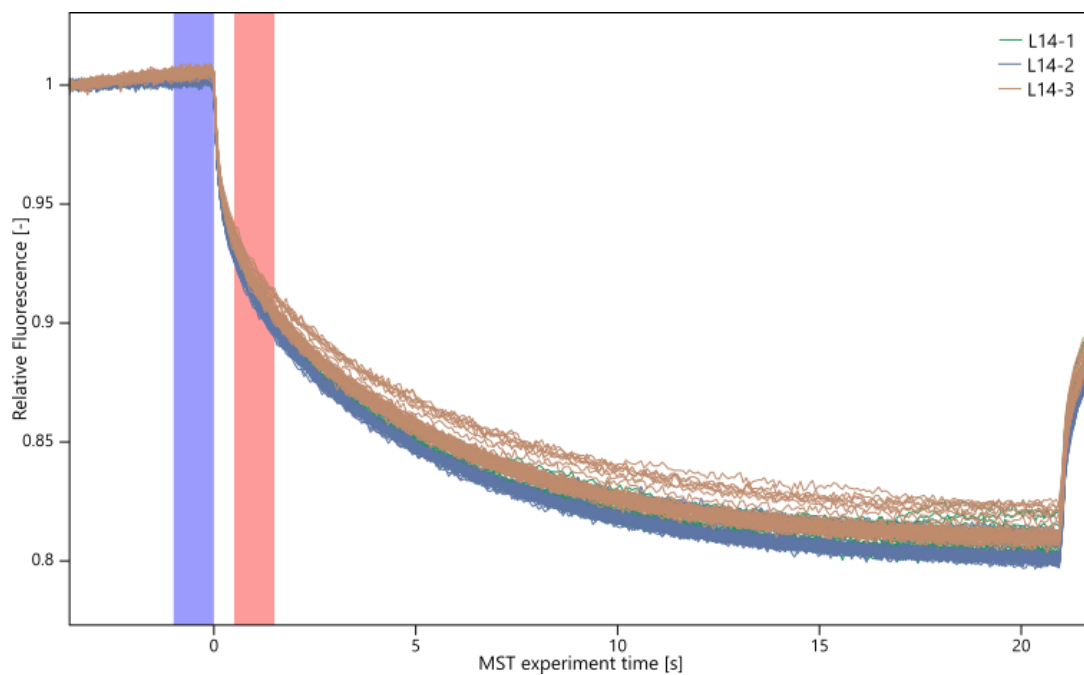


Figure 9.11 MST data of ligand L14 thermophoretic traces.

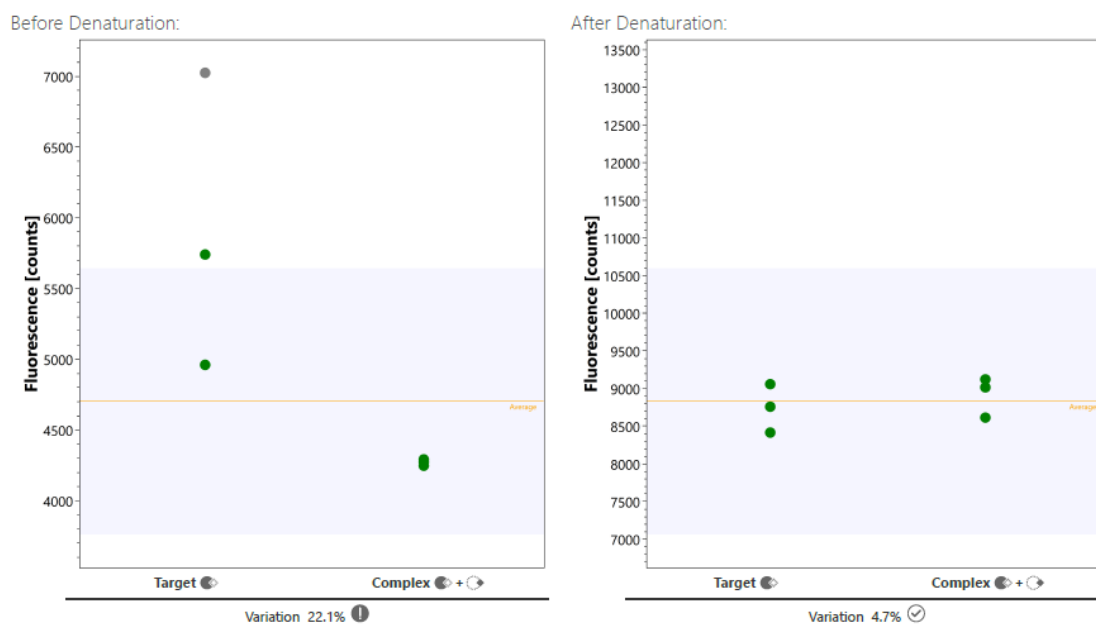


Figure 9.12 SDS denaturation test (SD test) and confirmation of fluorescent dependent binding of ligand L7. as visible from the equal fluorescence in bound and unbound state (*right*), compared to the binding assay before denaturation (*left*).

9.5 Aggregation assay data

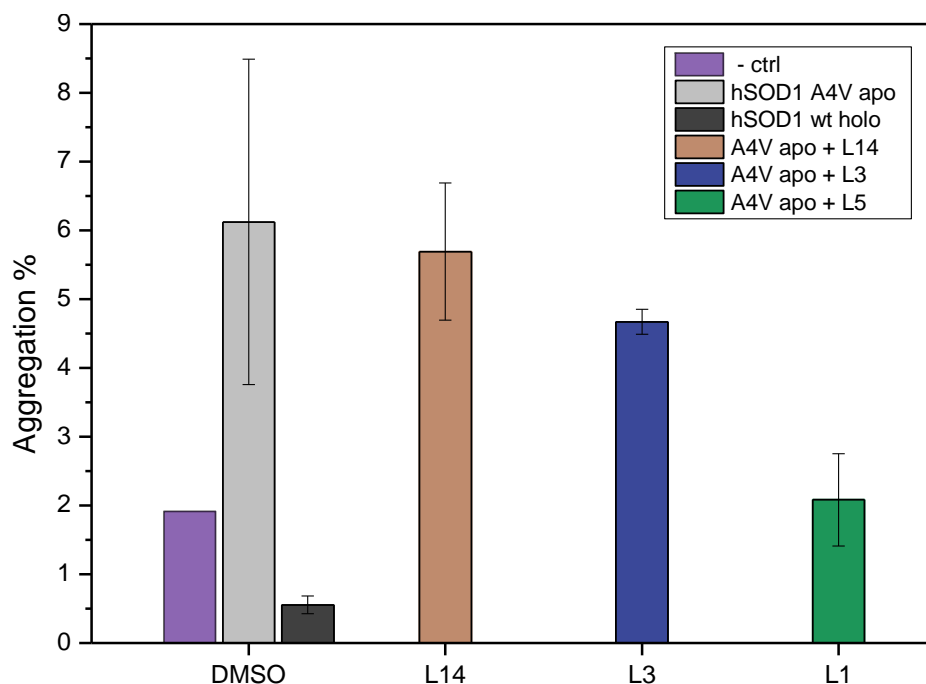


Figure 9.13 Aggregation assay in DMSO with PROTEOSTAT dye. Assay was conducted in 50 mM sodium phosphate buffer pH 7.4 and 20% DMSO, incubated at 50 °C for 24 h with final concentrations of 20 μ M and 1 mM for the protein and ligands, respectively. Monomeric lysozyme was used as a negative assay control, final concentration of 15 μ M.

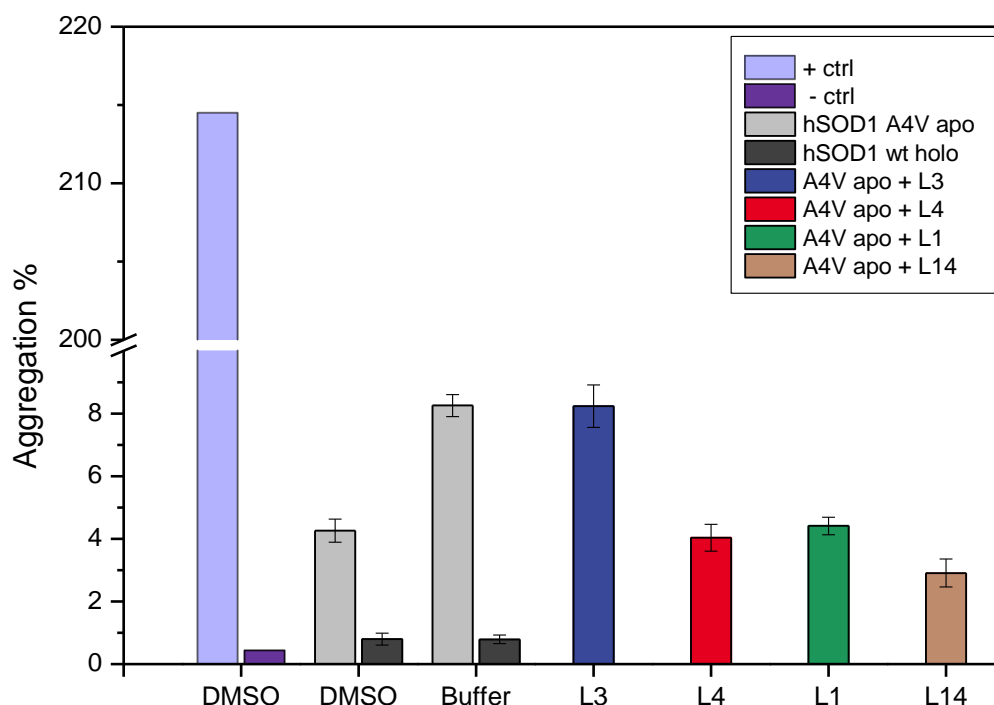
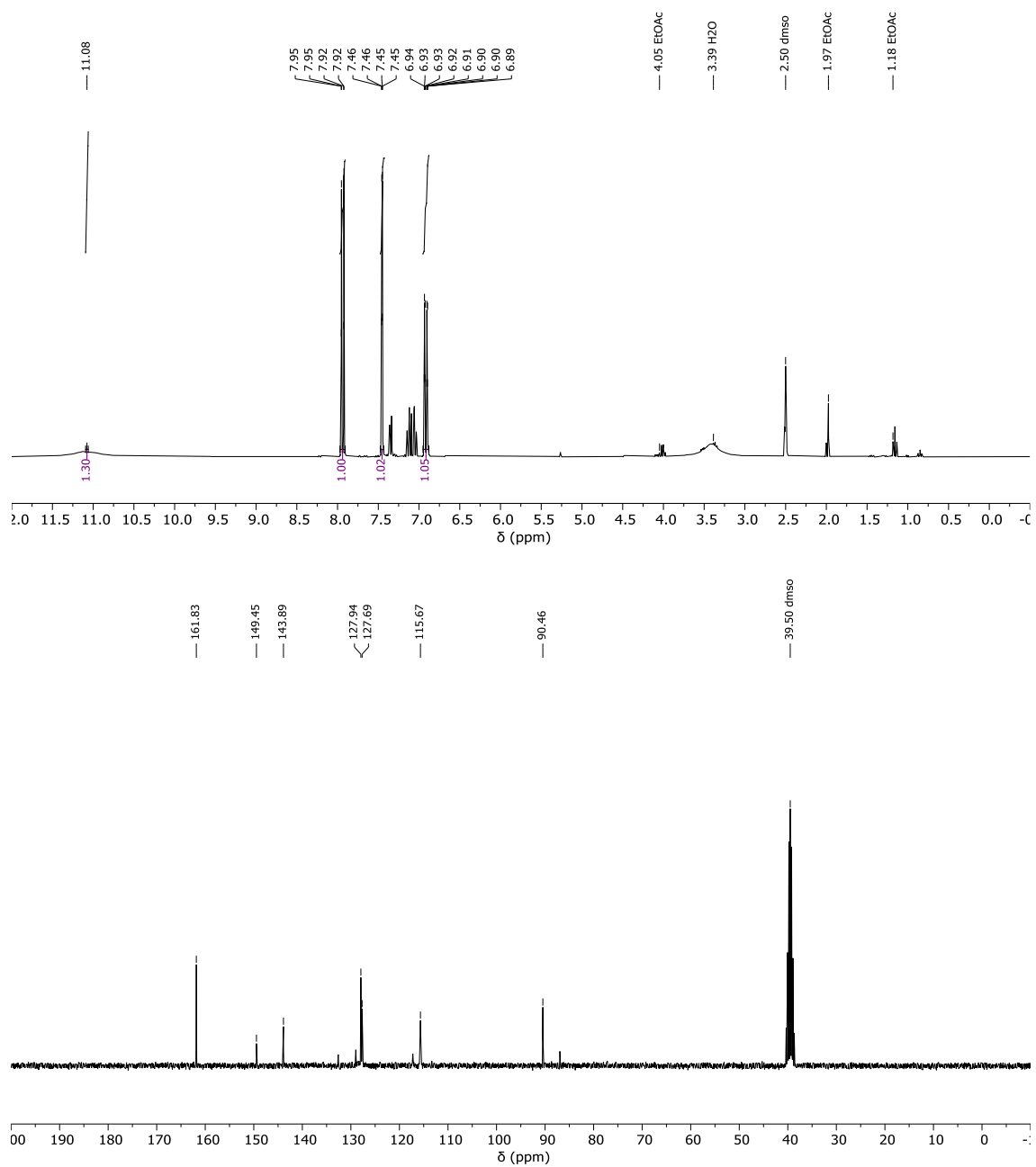


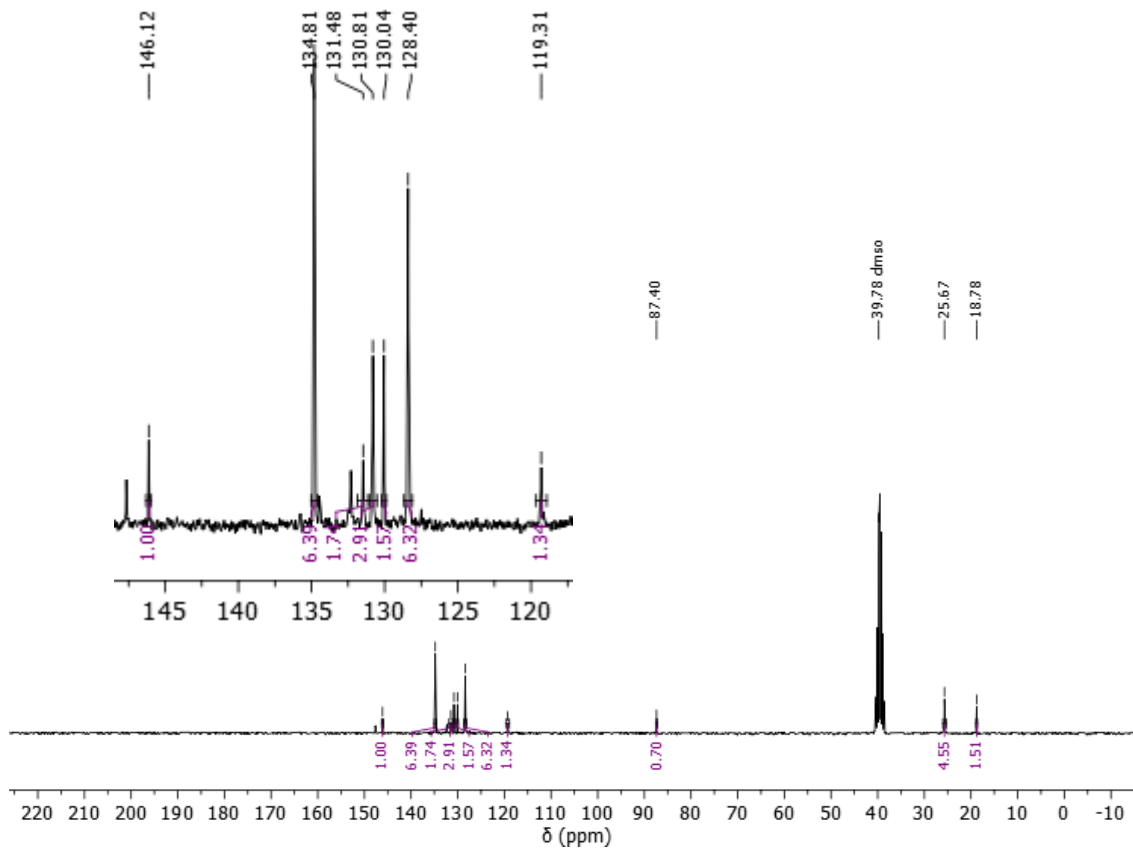
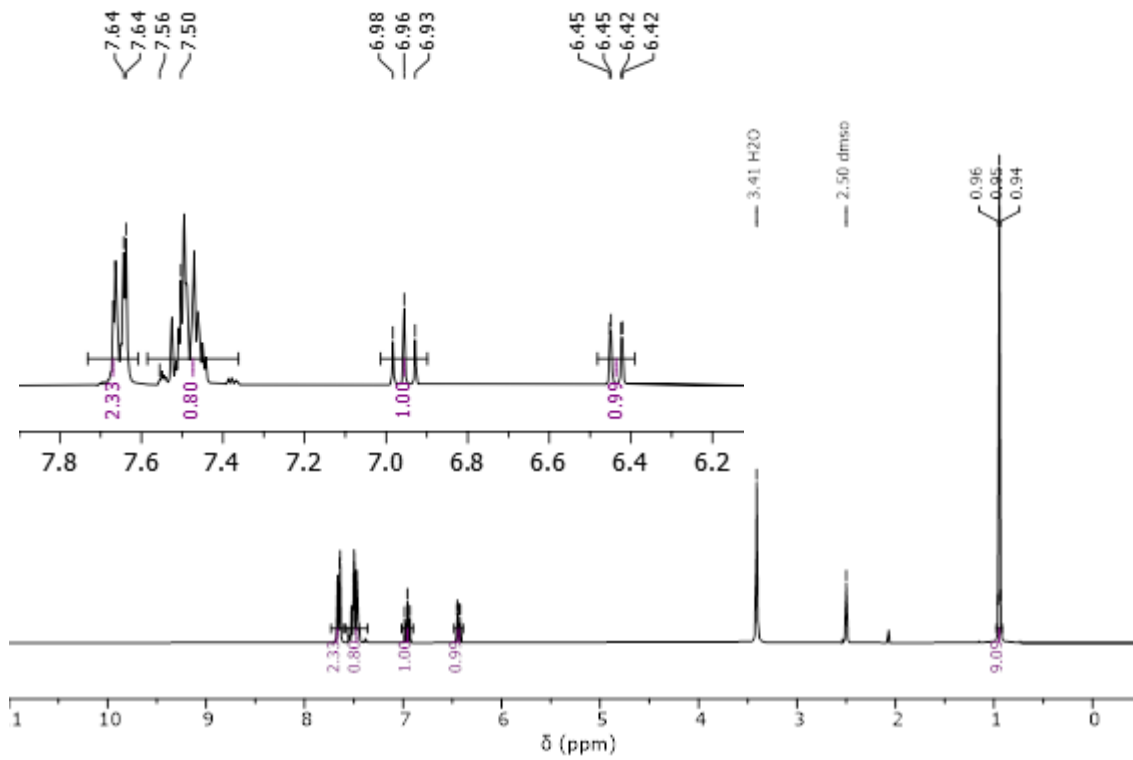
Figure 9.14 Aggregation assay in DMSO with ThT dye. Assay was conducted in 50 mM sodium phosphate buffer pH 7.4 and 20% DMSO, incubated at 50 °C for 24 h with final concentrations of 20 μ M and 1 mM for the protein and ligands, respectively. Lysozyme protein as (+) and (-) assay control; final concentration (15 μ M).

9.6 Analytics

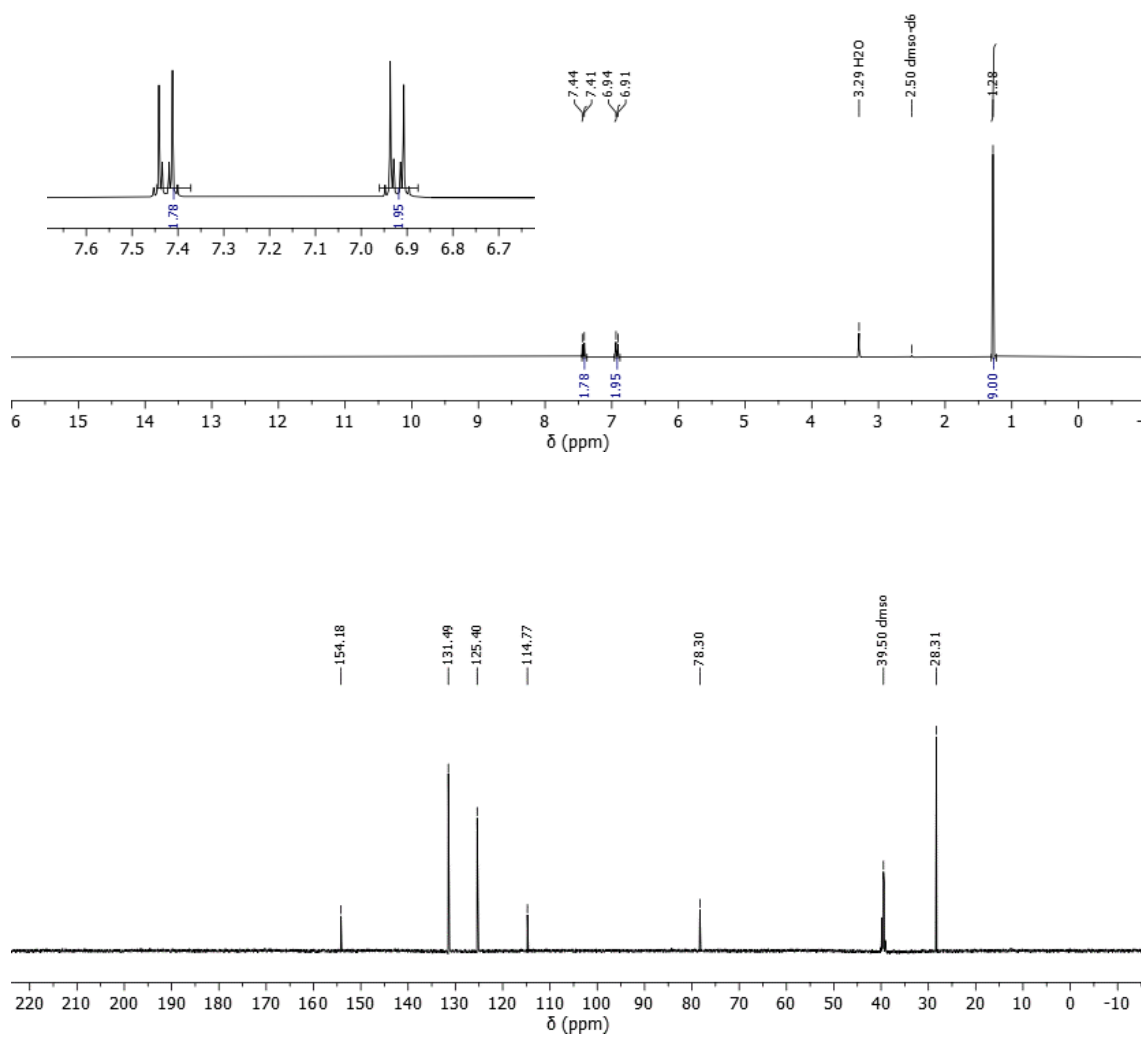
9.6.1 3-Iodo-4-nitrophenol (1)



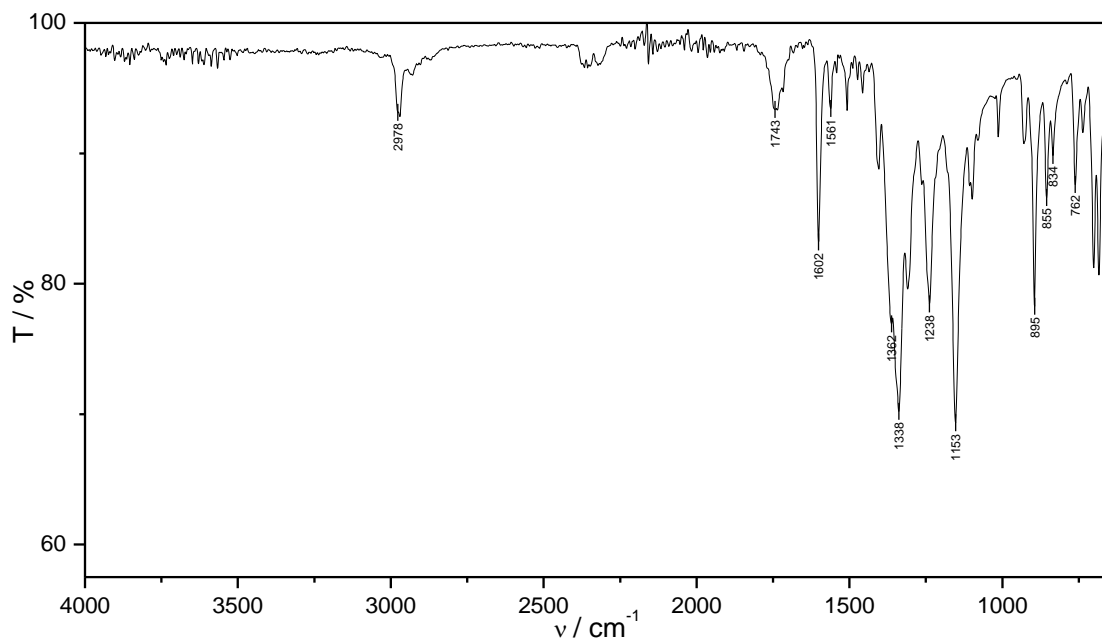
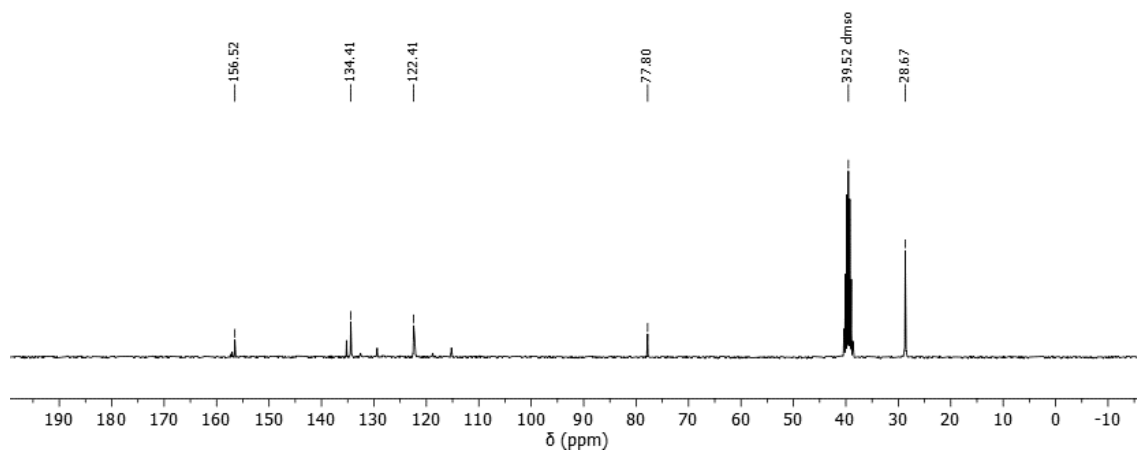
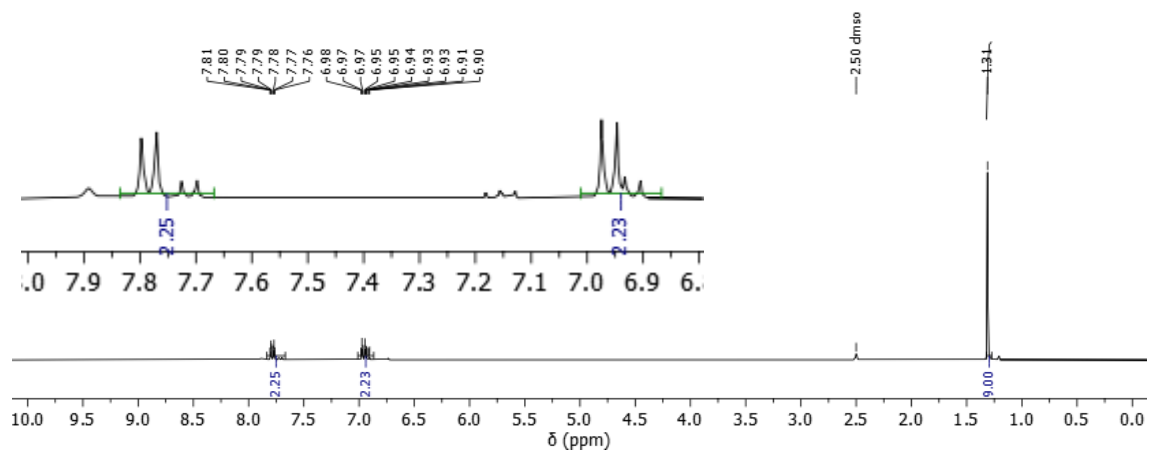
9.6.2 *Tert*-butyl(3-iodo-4-nitrophenoxy)diphenylsilane (2)



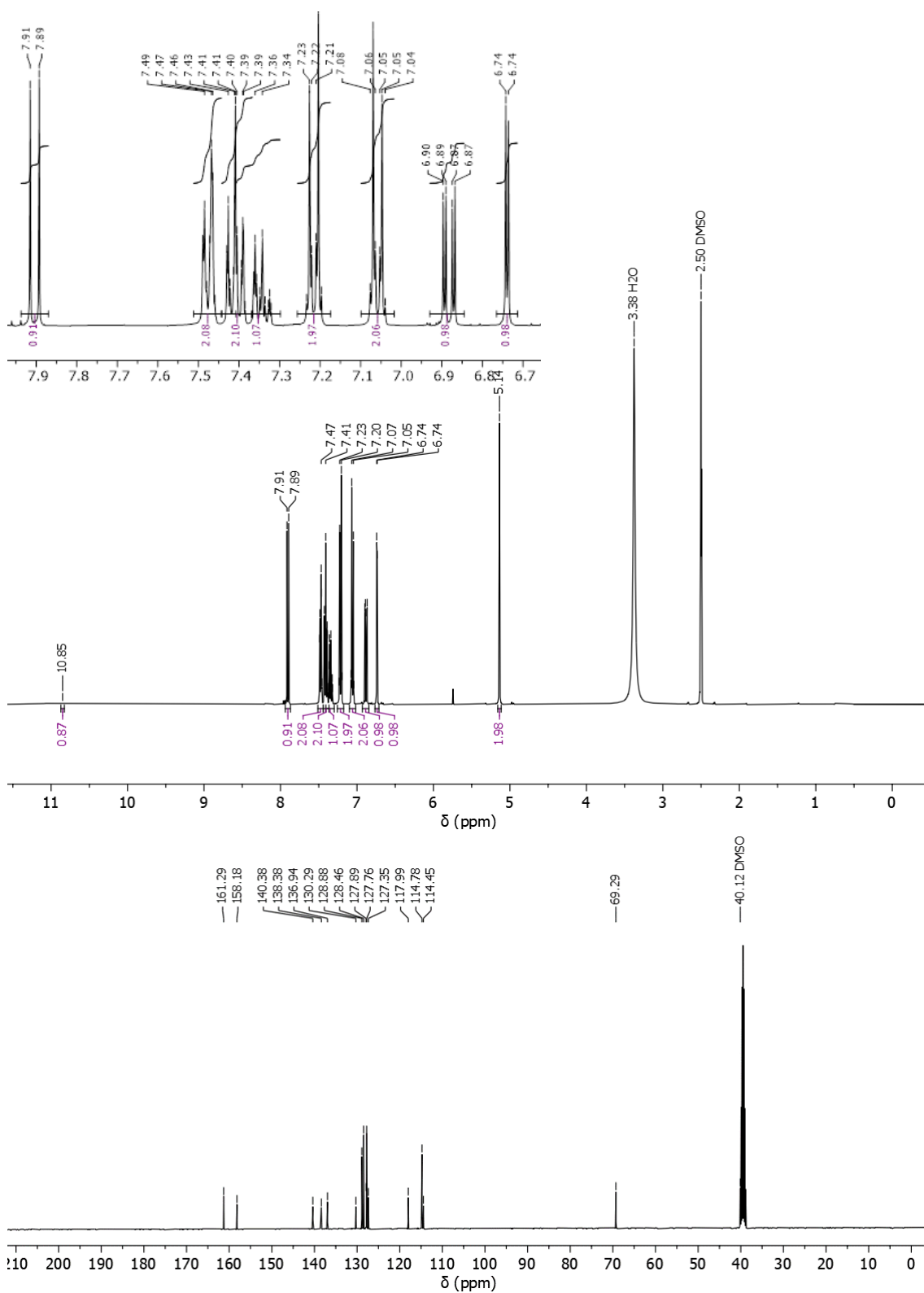
9.6.3 1-Bromo-4-(tert-butoxy)benzene (4)

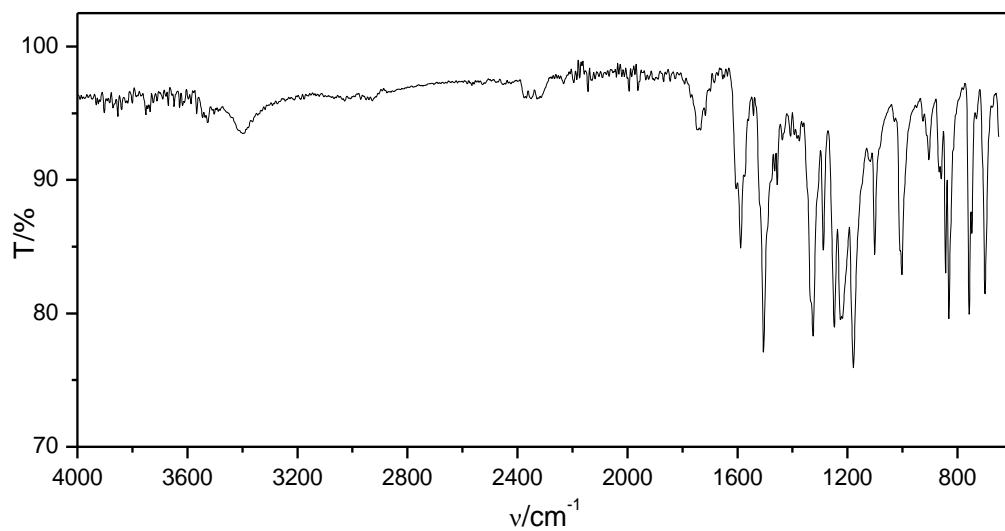


9.6.4 (4-(Tert-butoxy)phenyl)boronic acid (5)

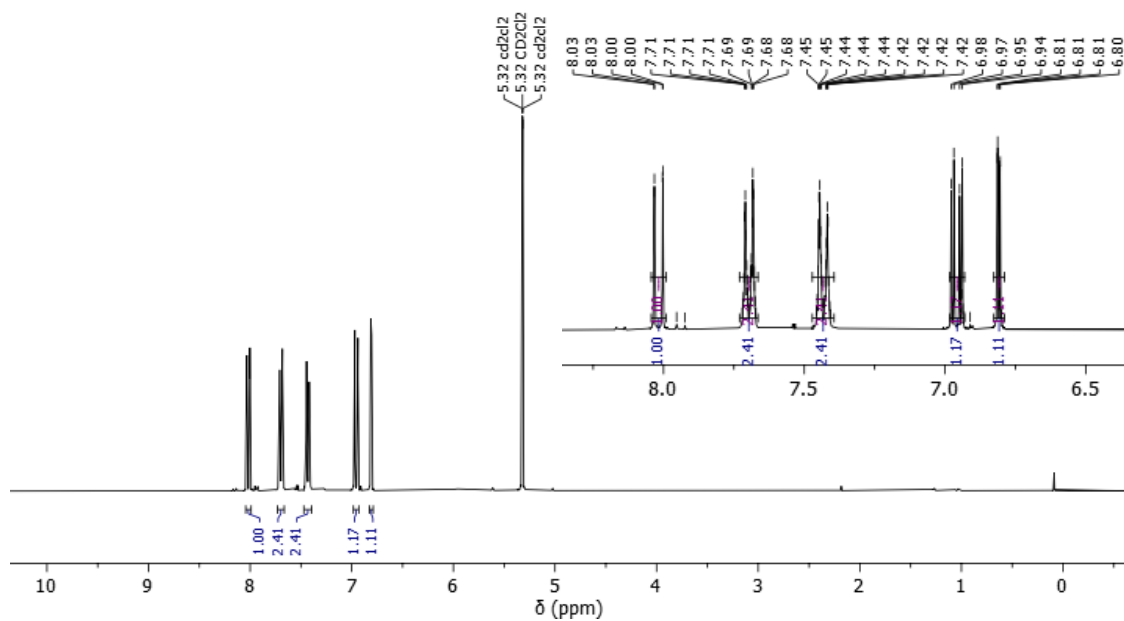


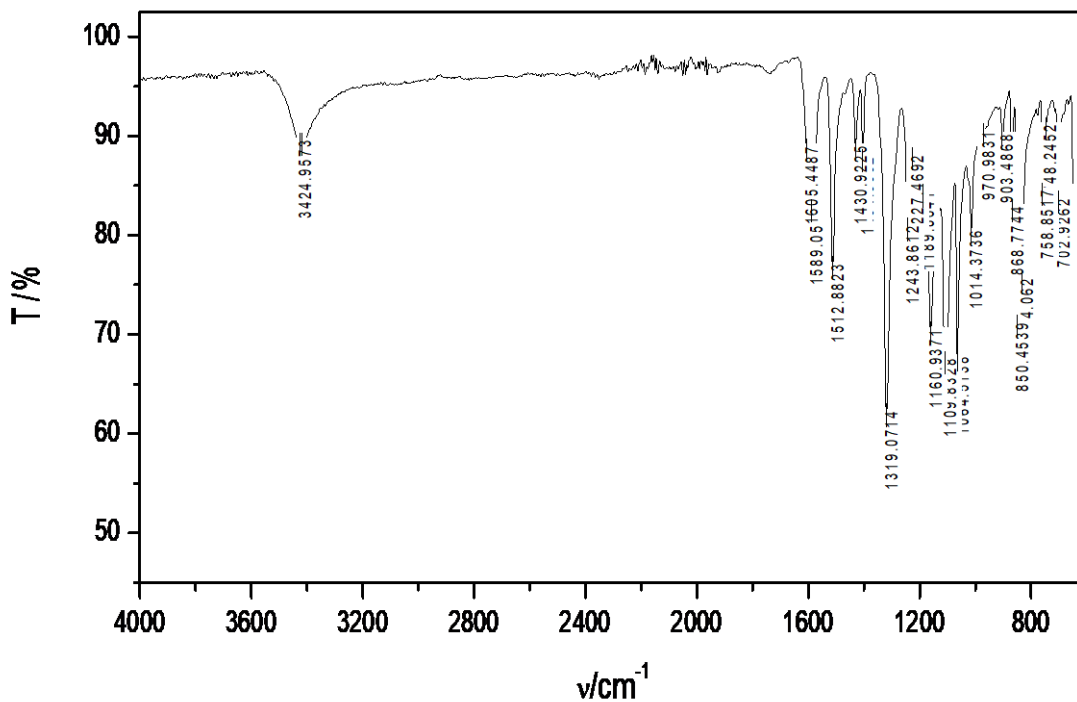
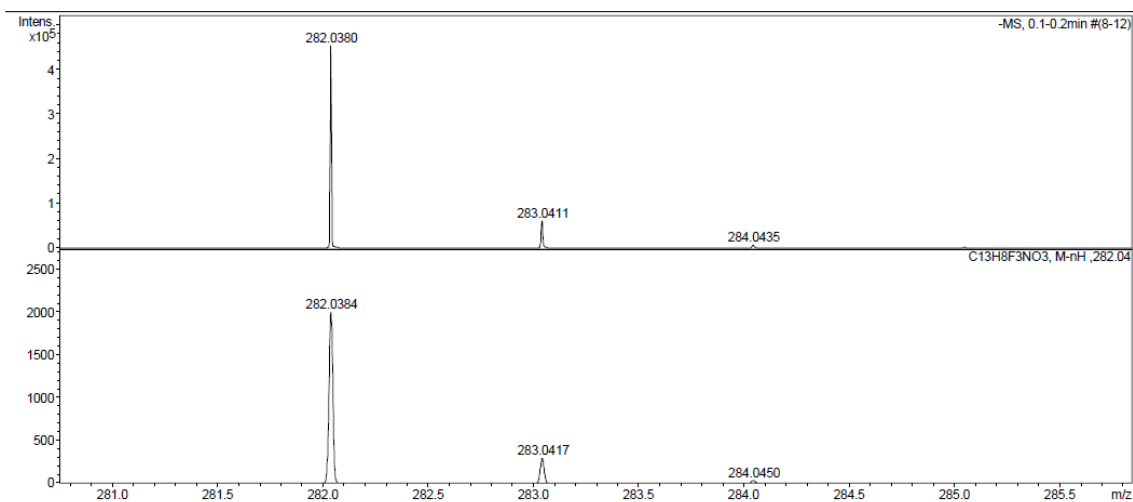
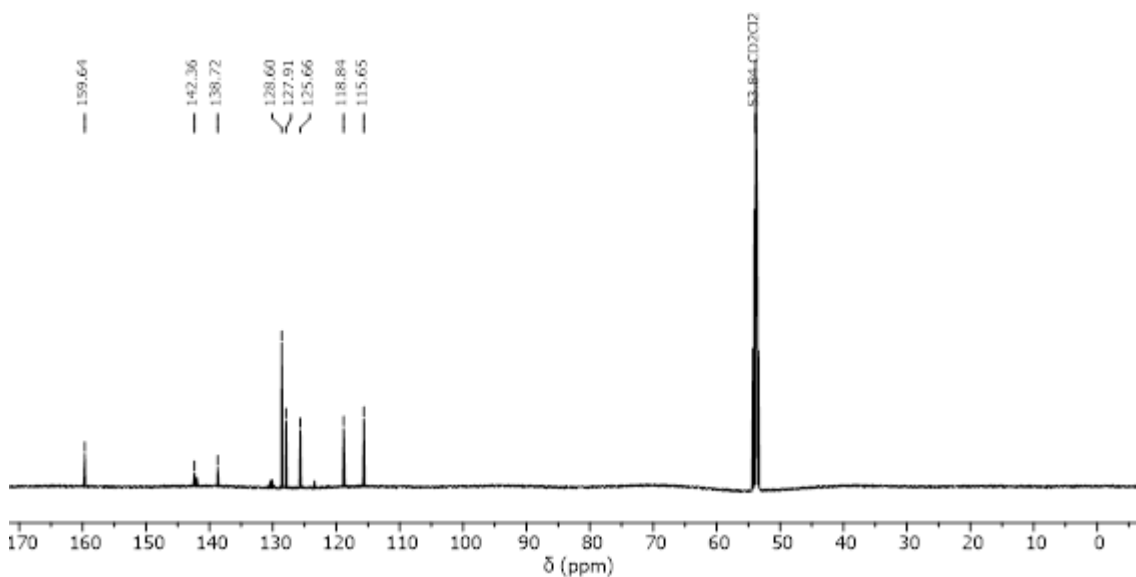
9.6.5 4'-(Benzyloxy)-6-nitro-[1,1'-biphenyl]-3-ol (18)



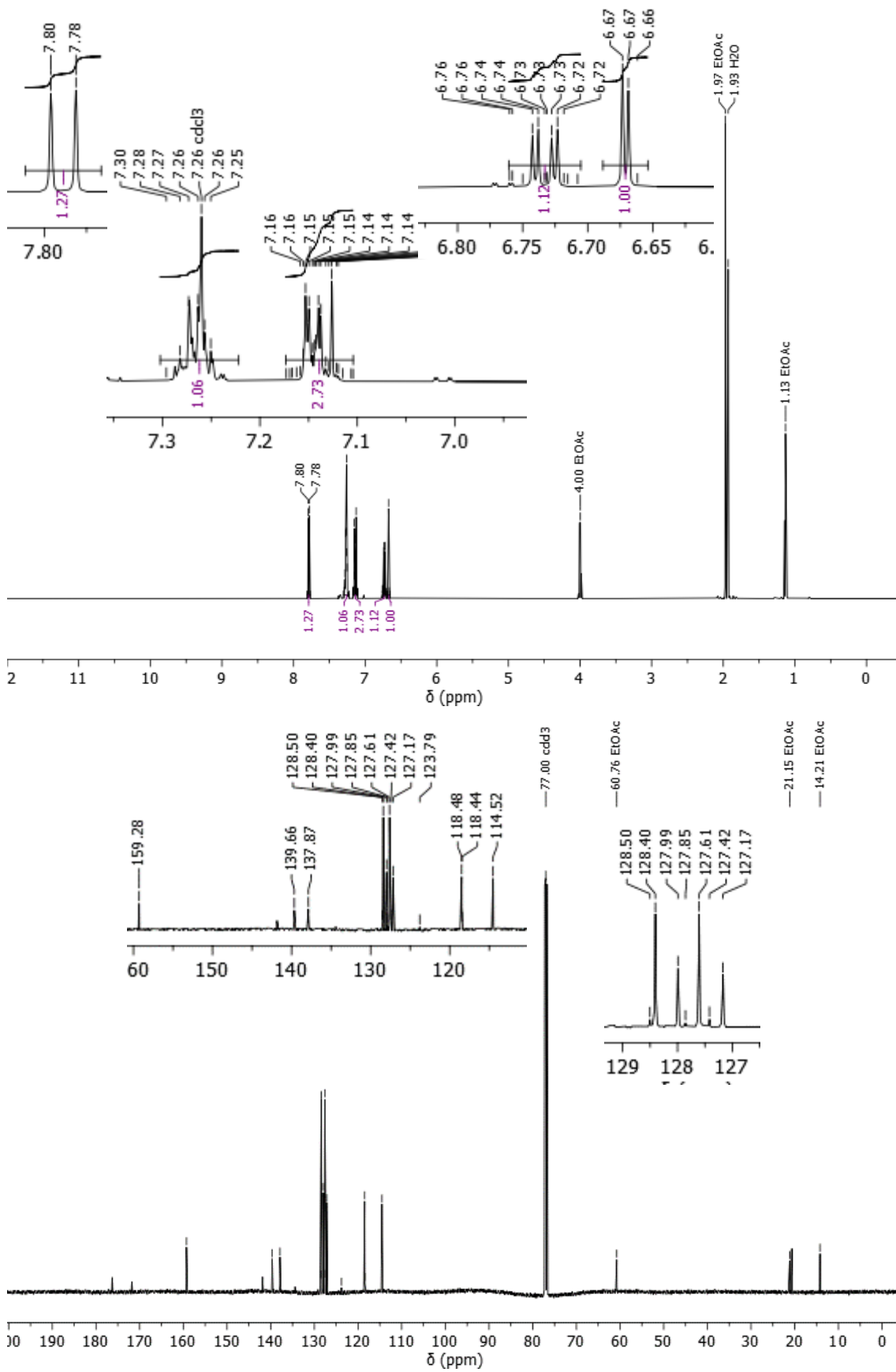


9.6.6 6-Nitro-4'-(trifluoromethyl)-[1,1'-biphenyl]-3-ol (19)

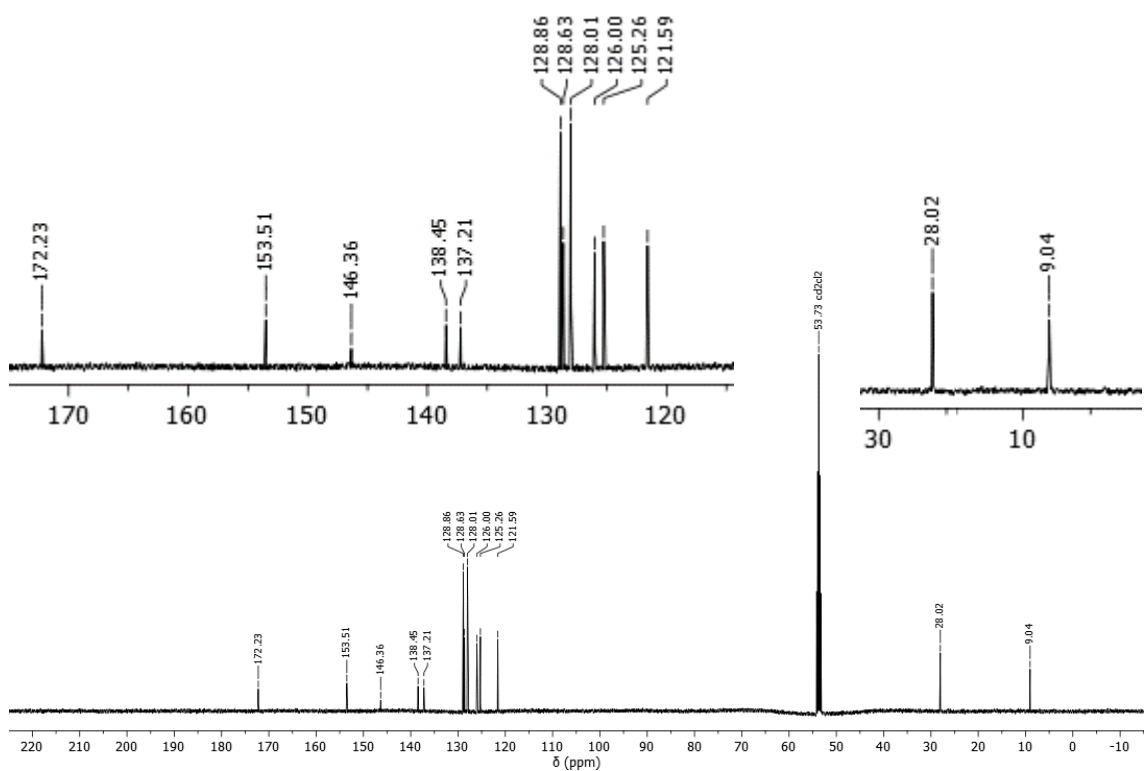
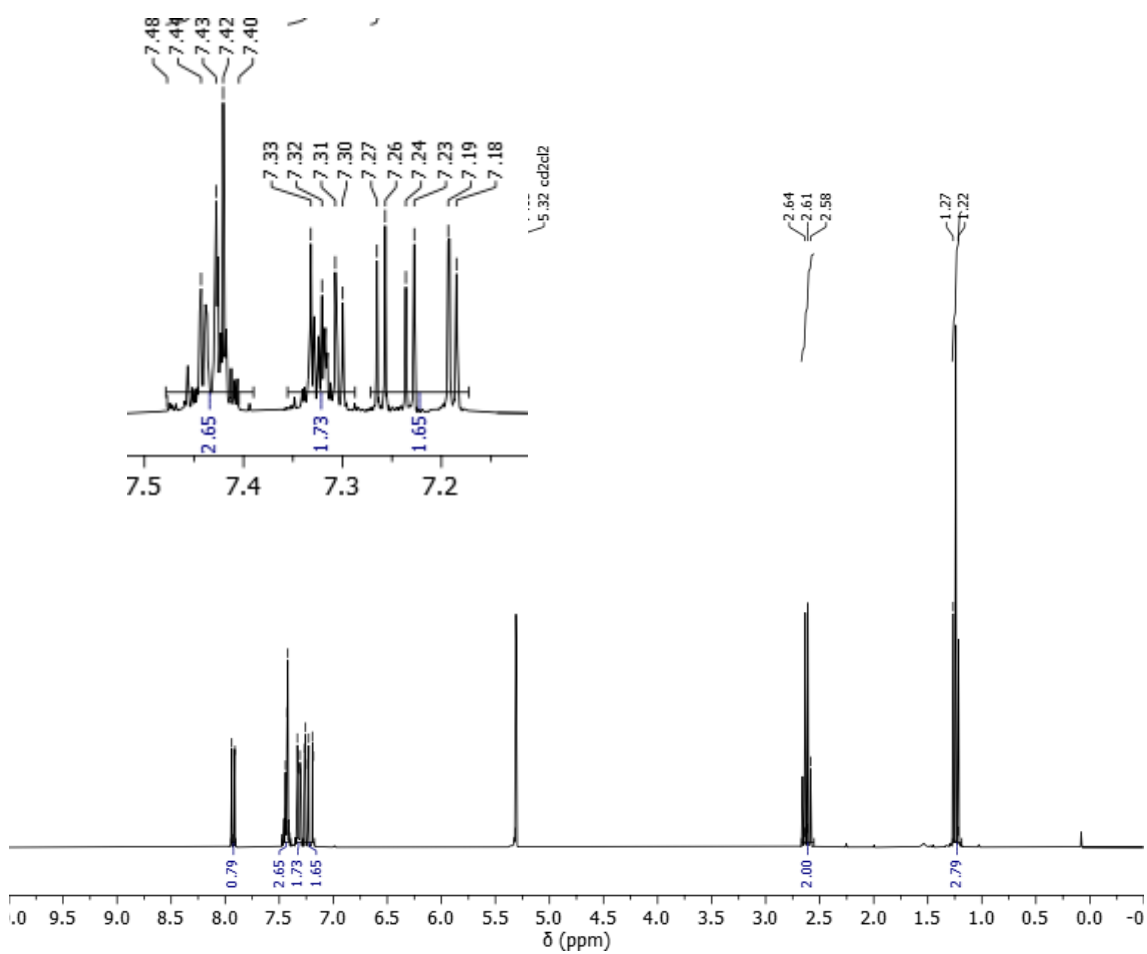




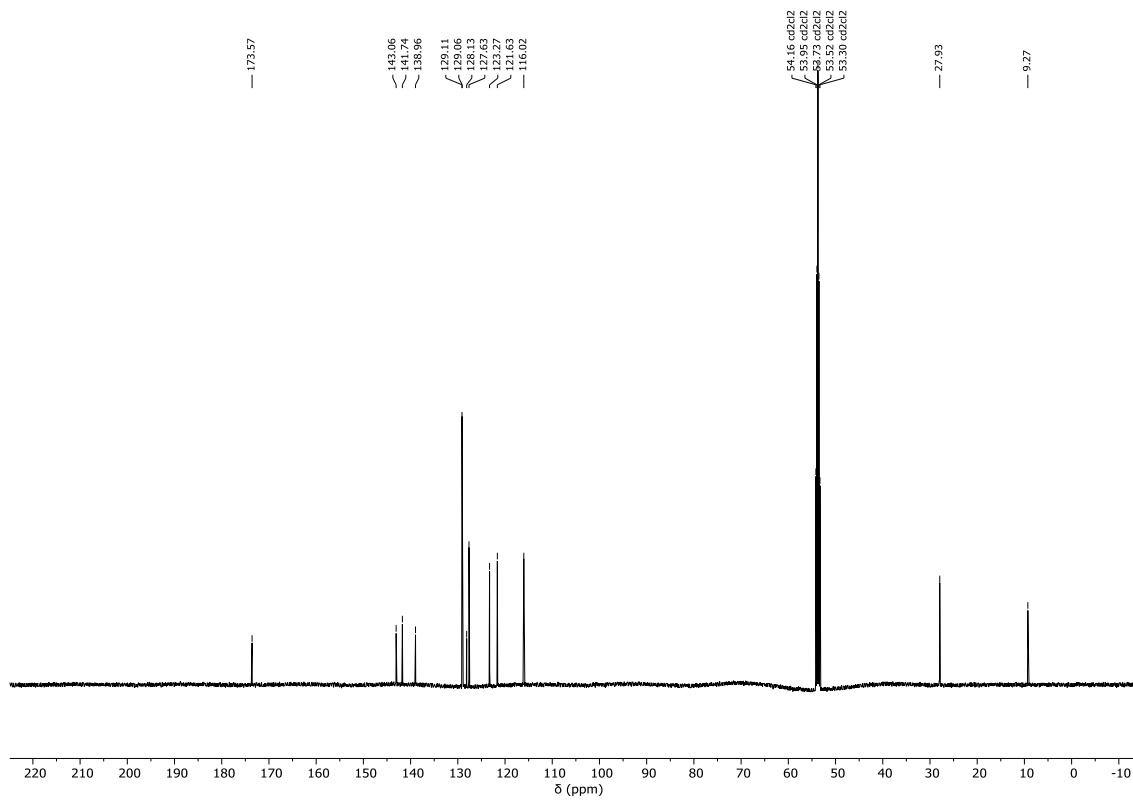
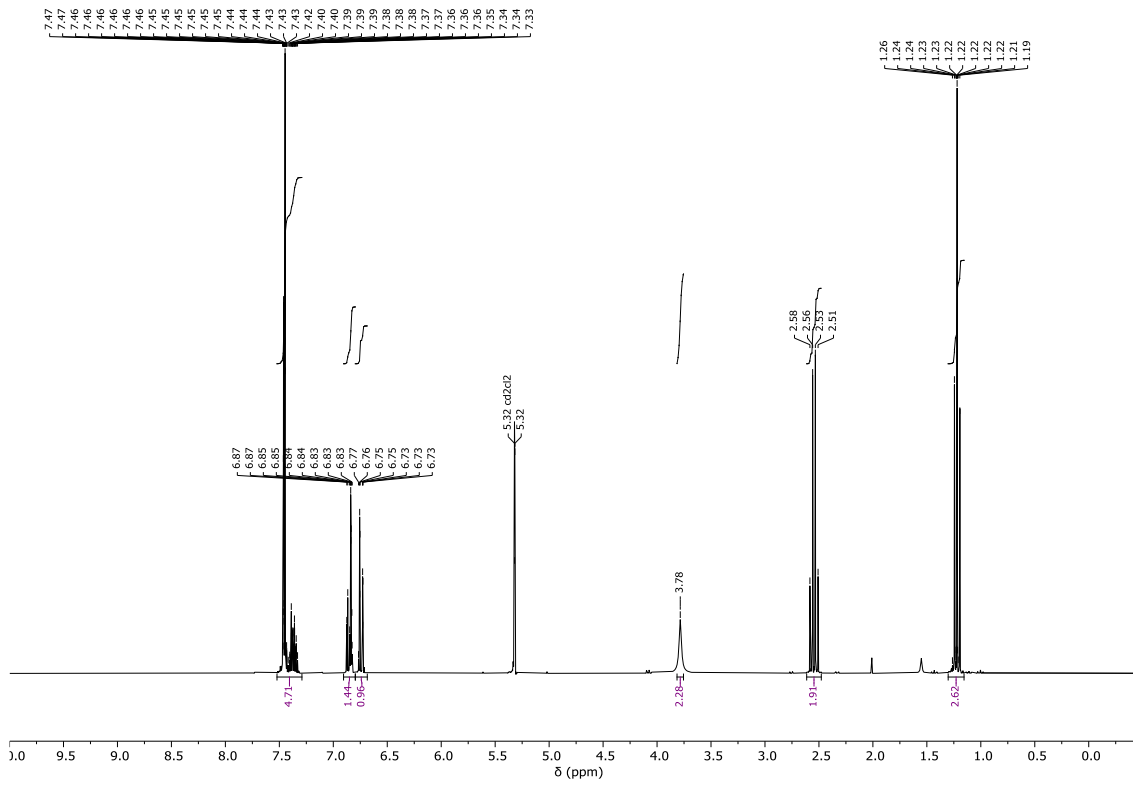
9.6.7 6-nitro-[1,1'-biphenyl]-3-ol (21)

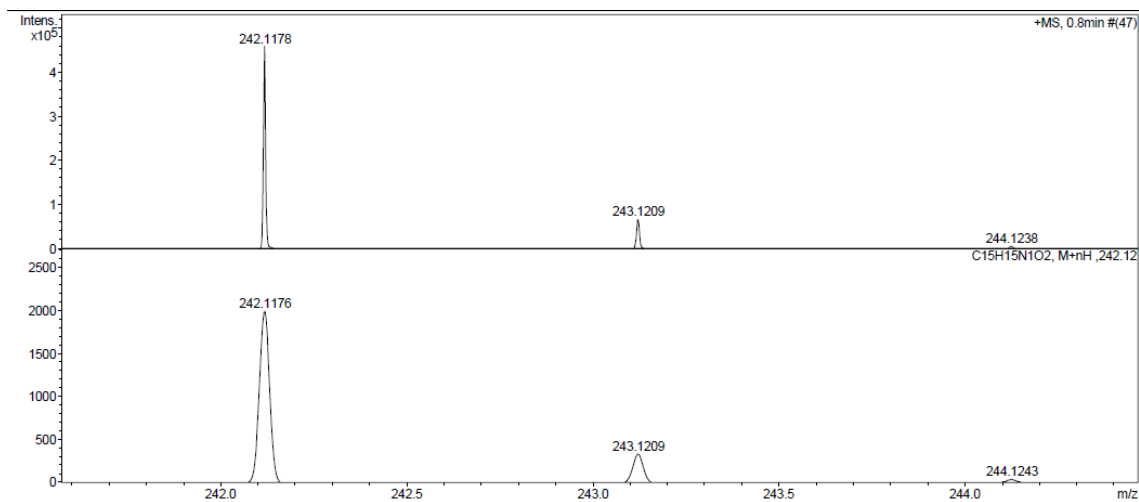


9.6.8 6-Nitro-[1,1'-biphenyl]-3-yl propionate (22)

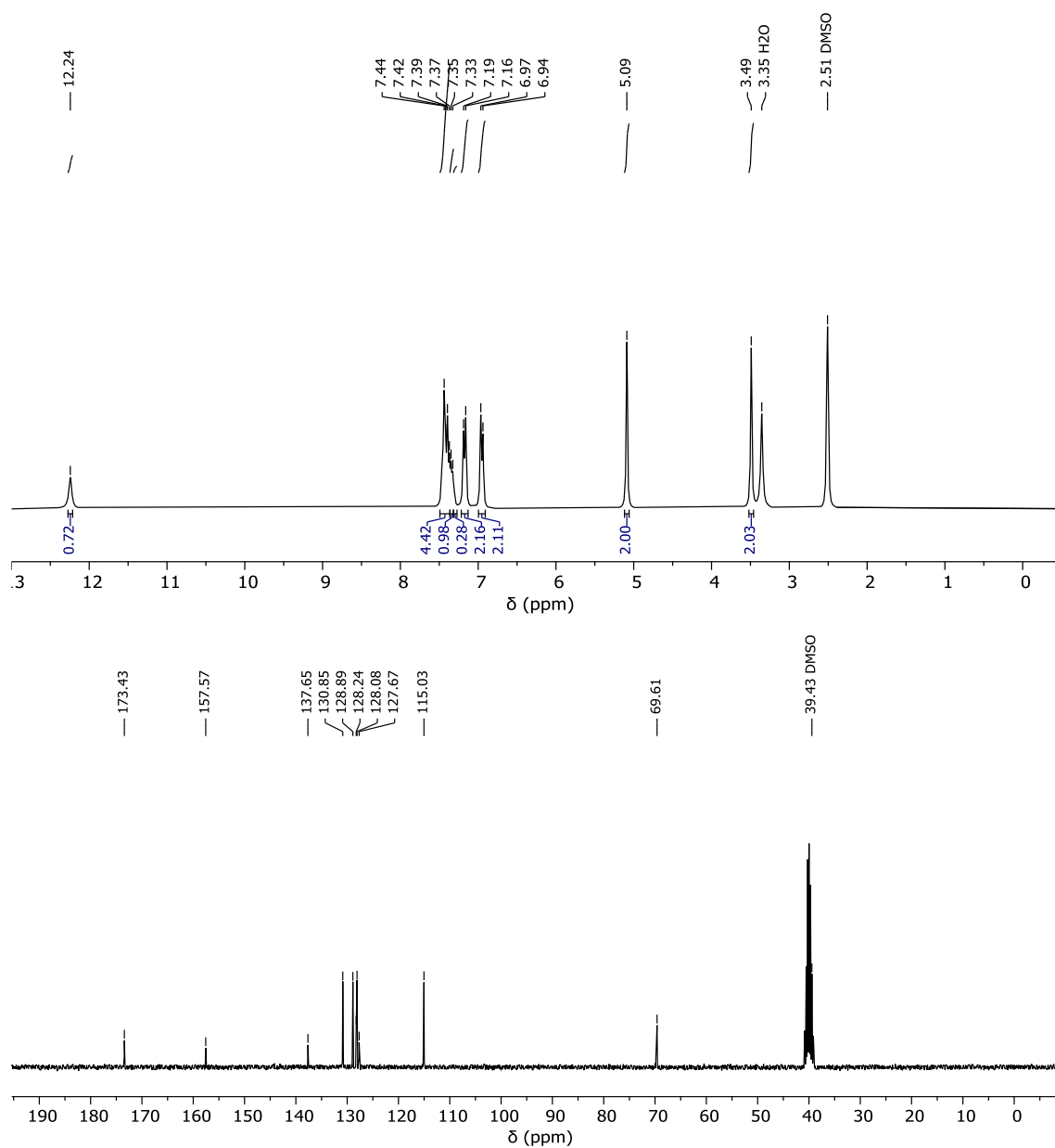


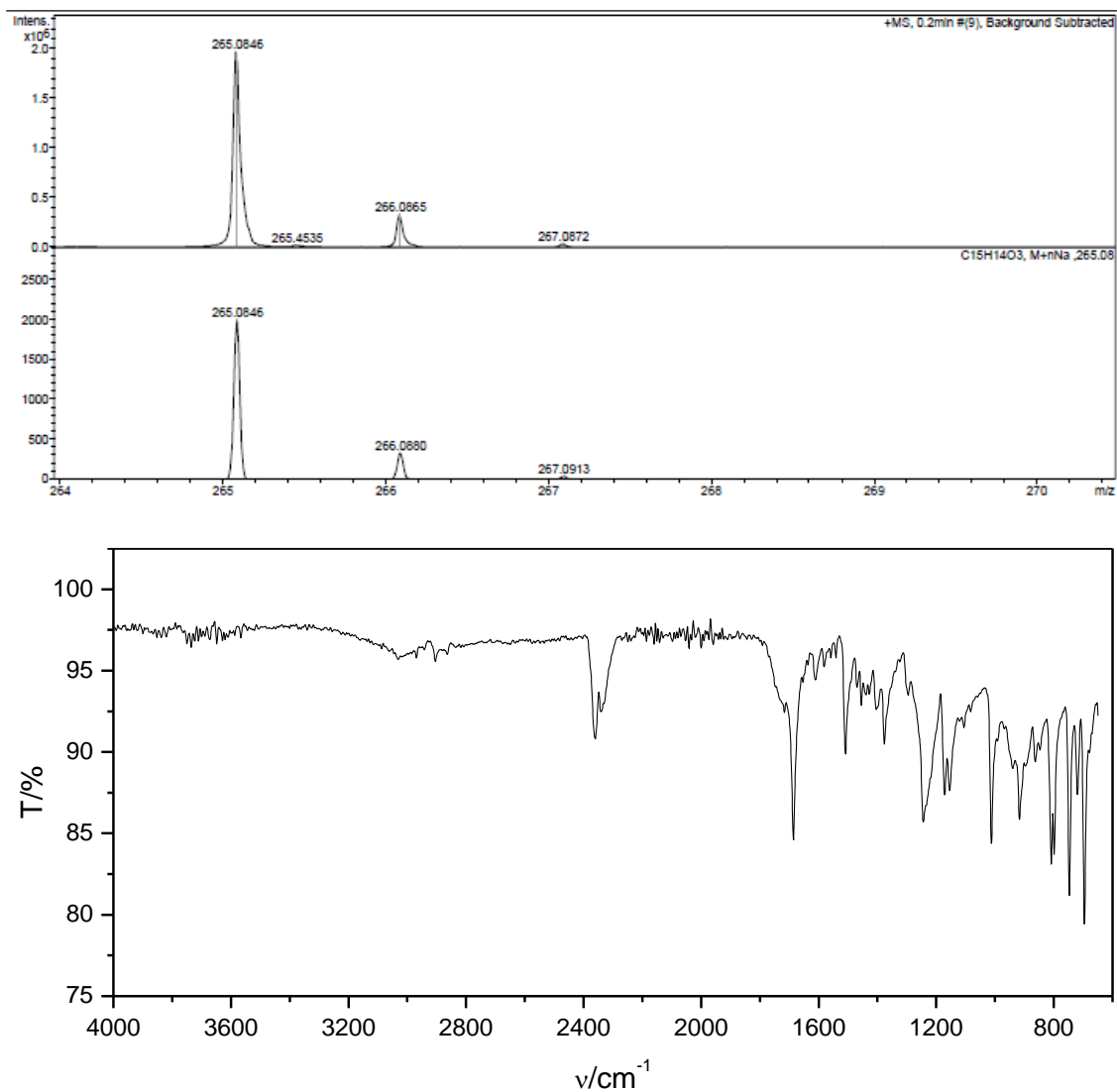
9.6.9 6-Amino-[1,1'-biphenyl]-3-yl propionate (23)



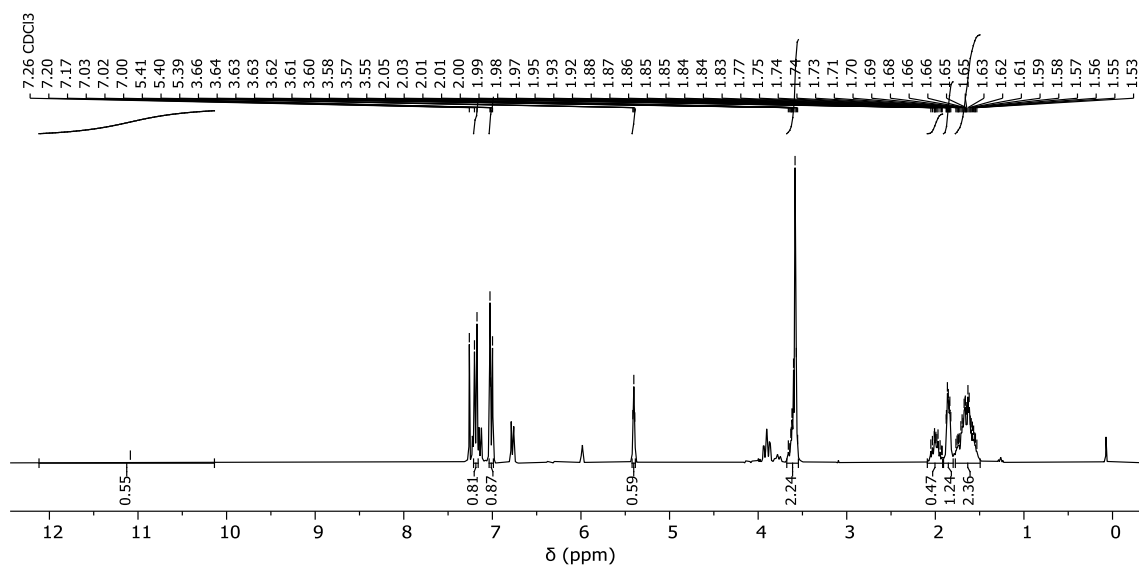


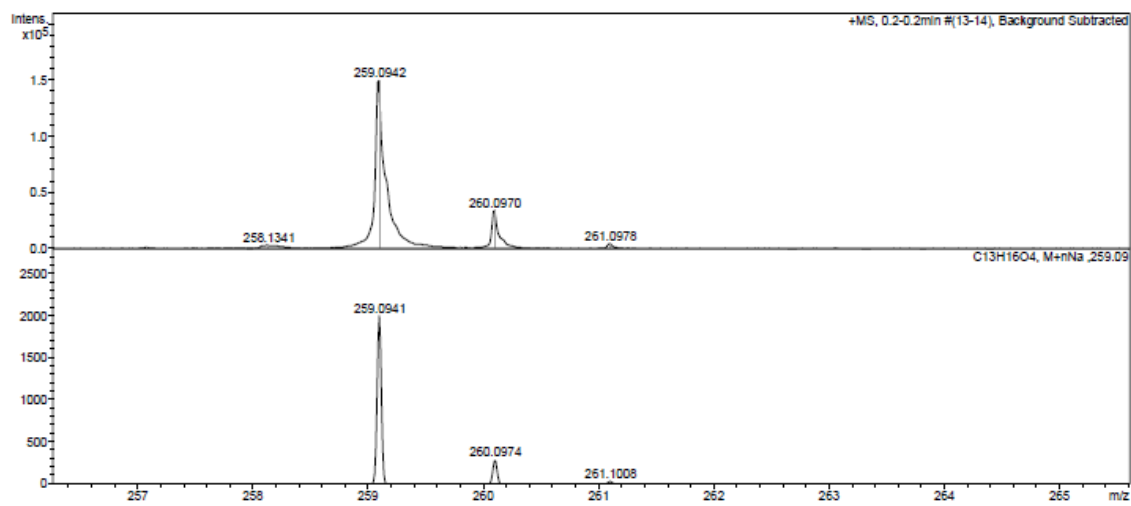
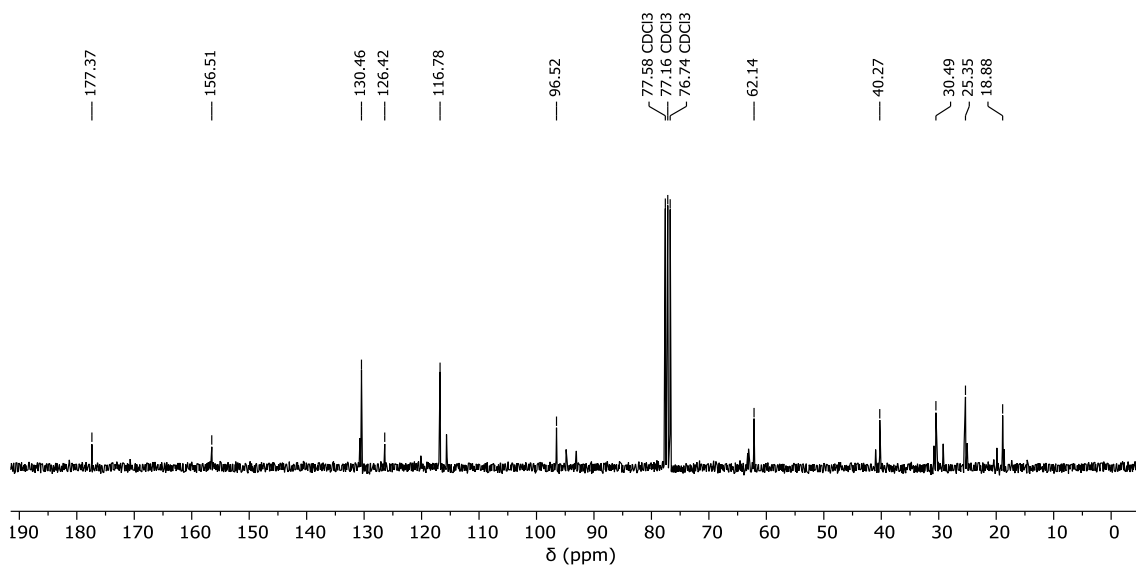
9.6.10 2-(4-(Benzyloxy)phenyl)acetic acid (26)



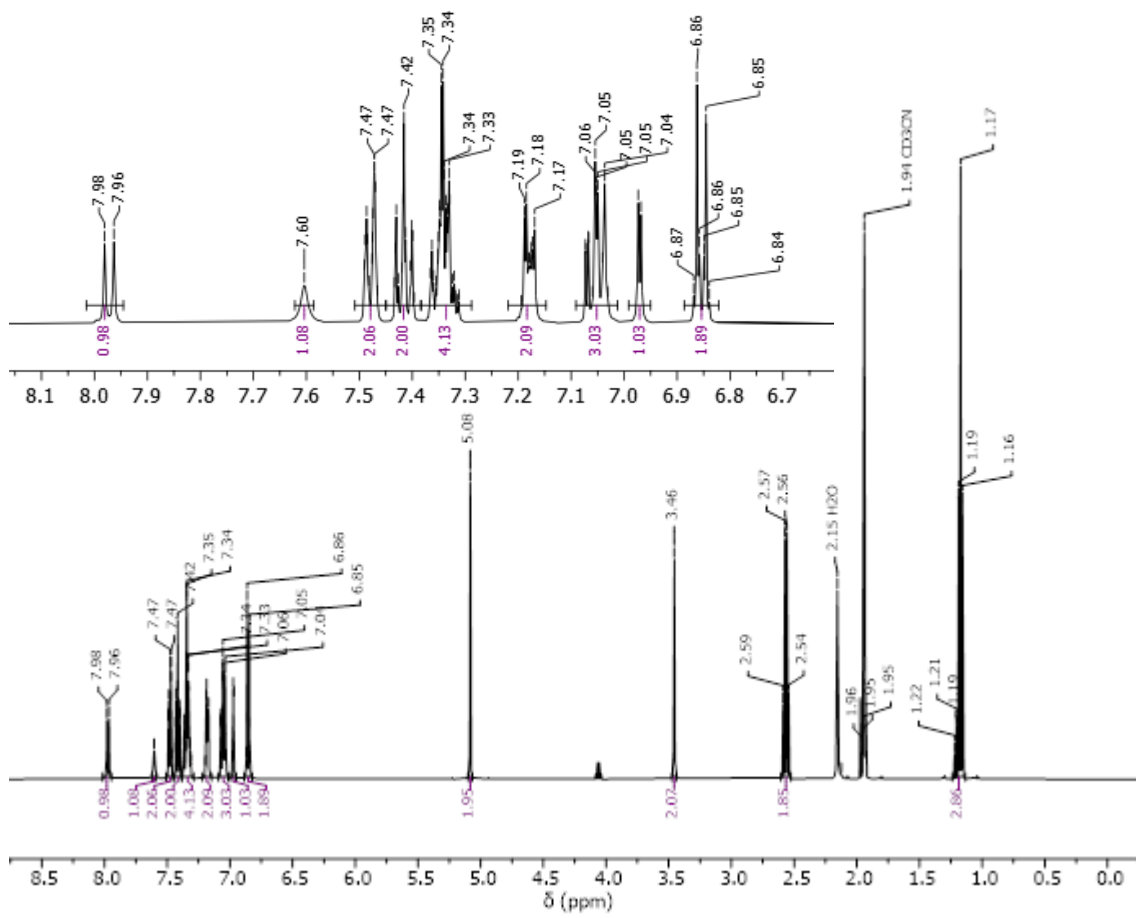


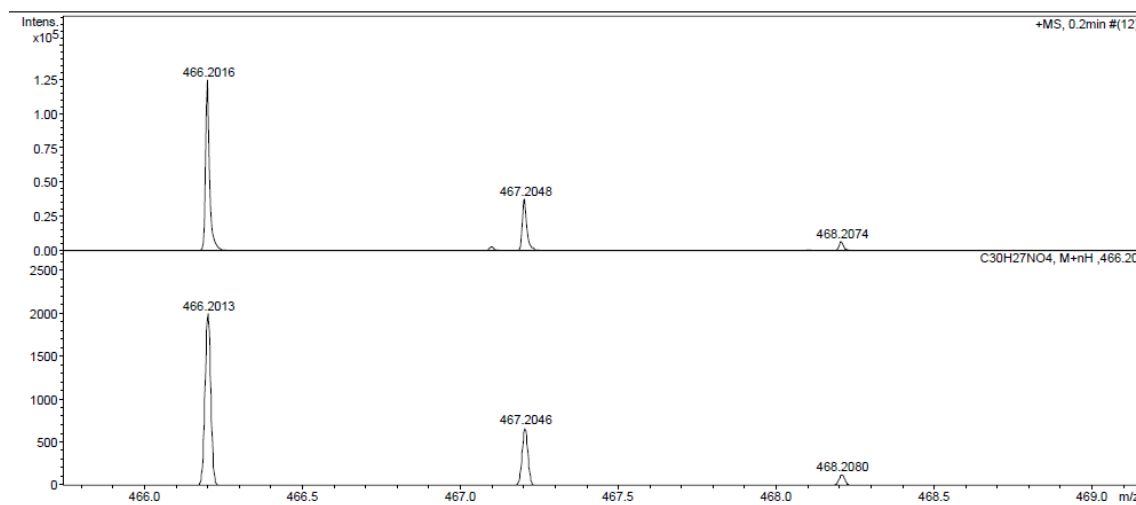
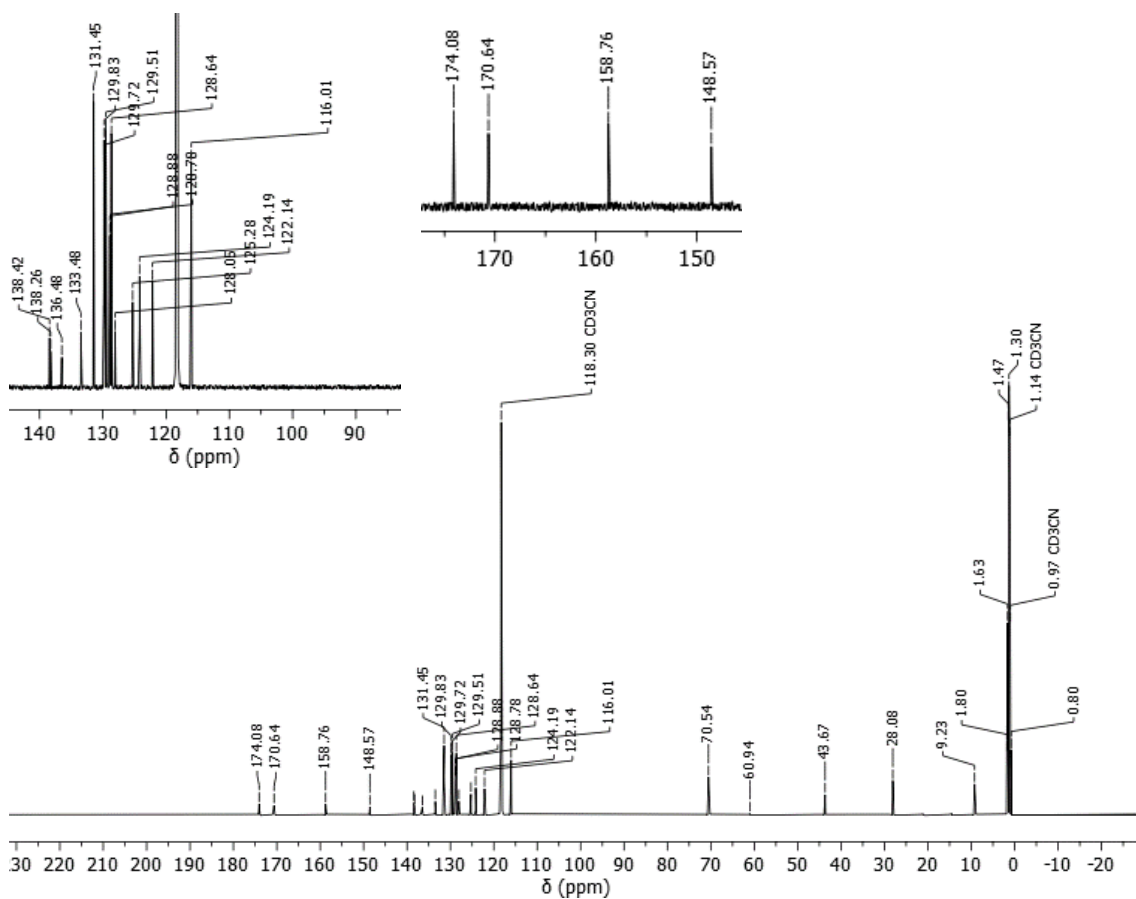
9.6.11 2-(4-((Tetrahydro-2H-pyran-2-yl)oxy)phenyl)acetic acid (27)



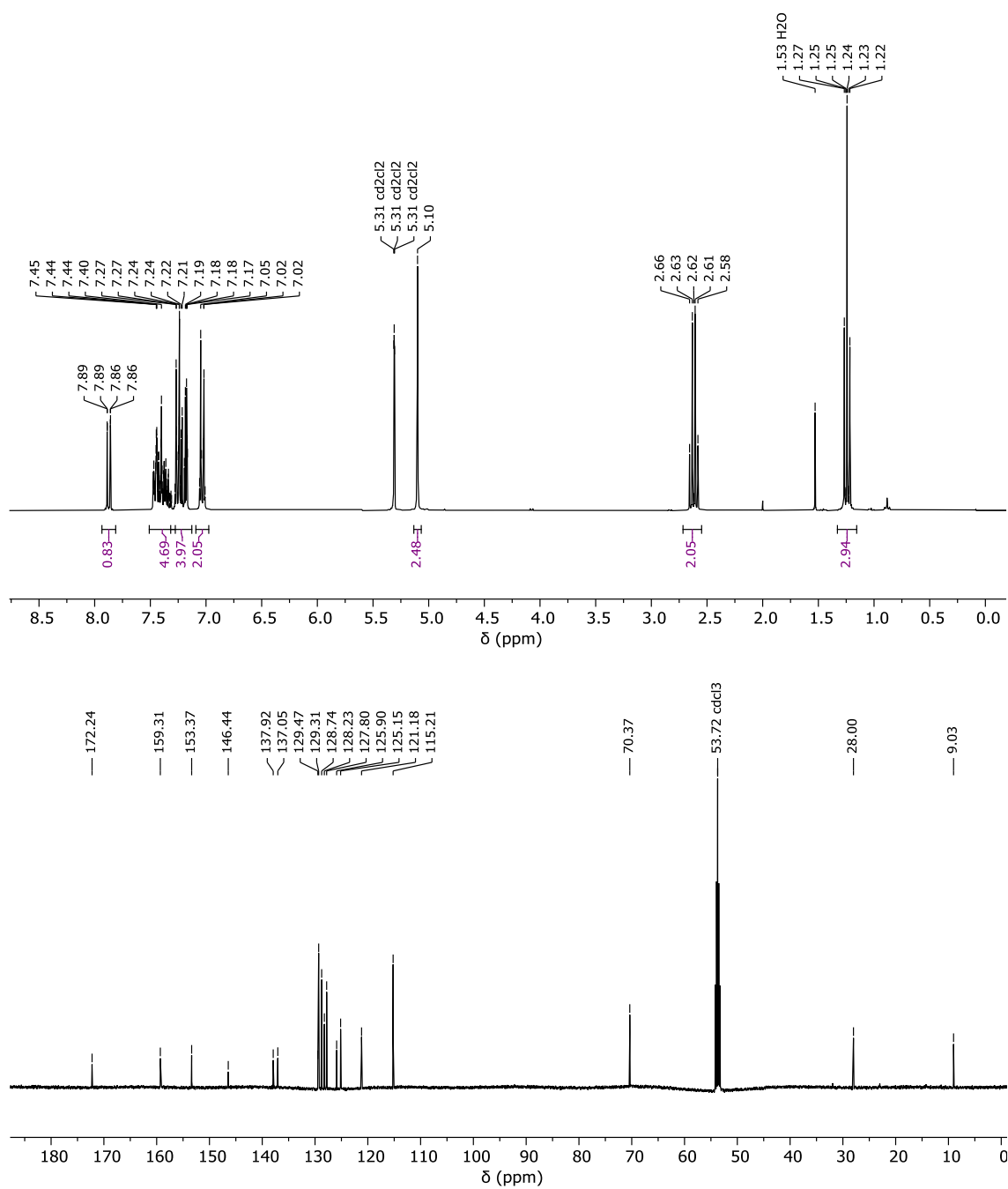


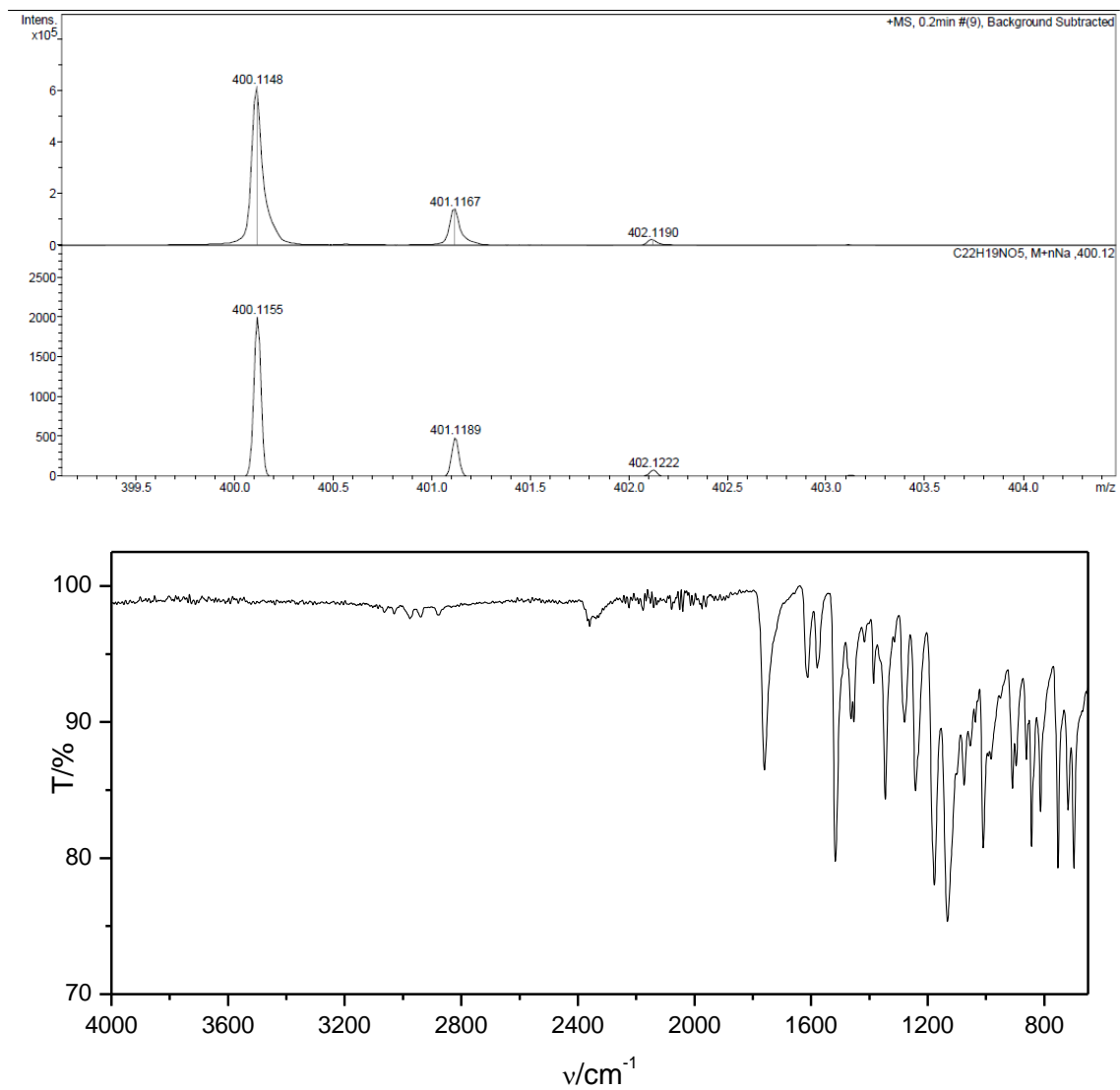
9.6.12 6-(2-(4-(Benzyloxy)phenyl)acetamido)-[1,1'-biphenyl]-3-yl propionate (28)



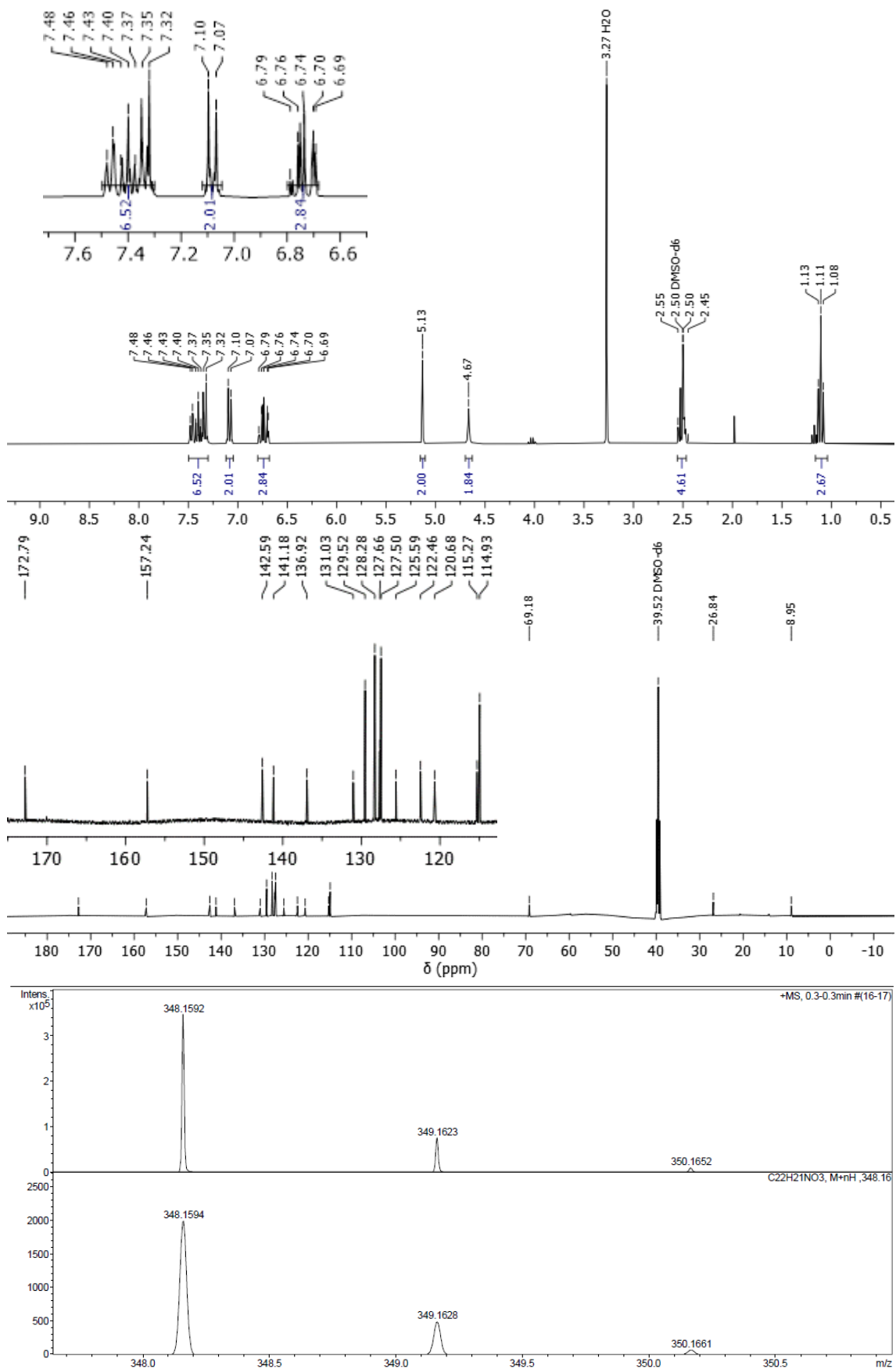


9.6.13 4'-(Benzyloxy)-6-nitro-[1,1'-biphenyl]-3-yl propionate (29)

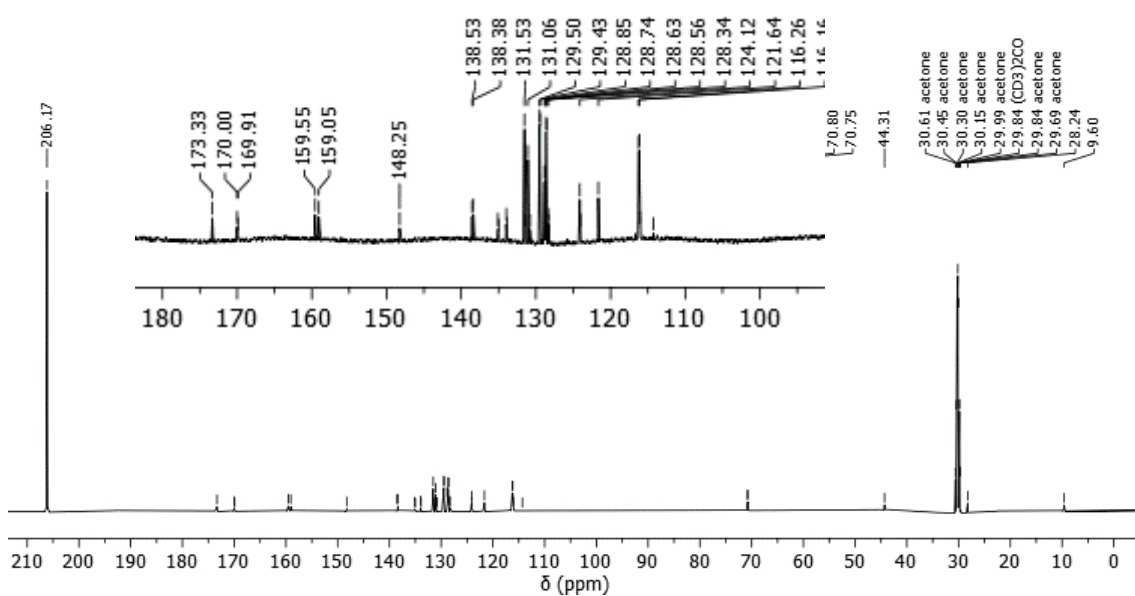
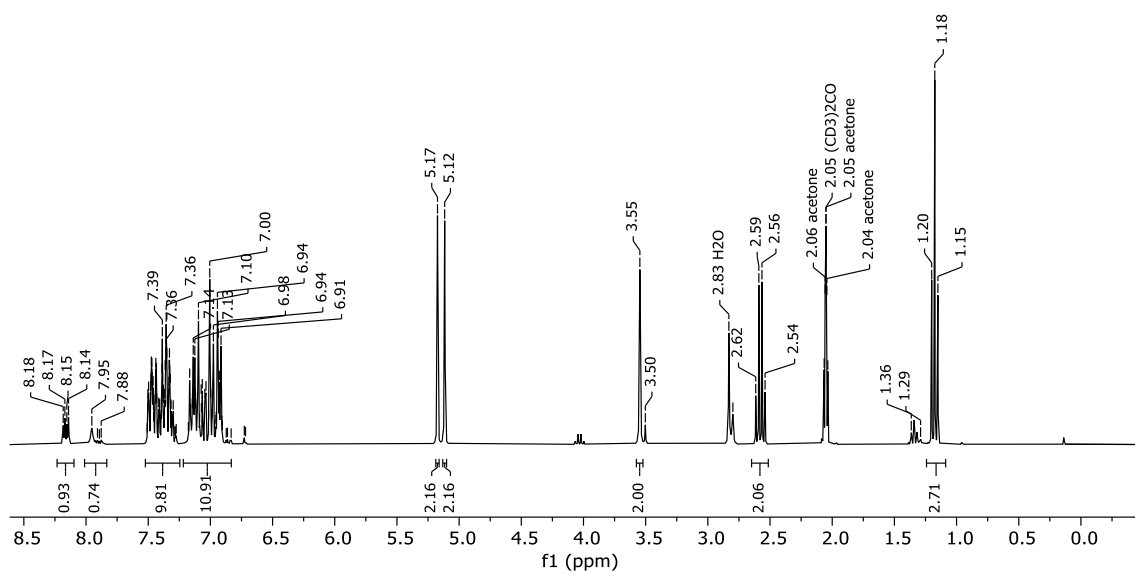


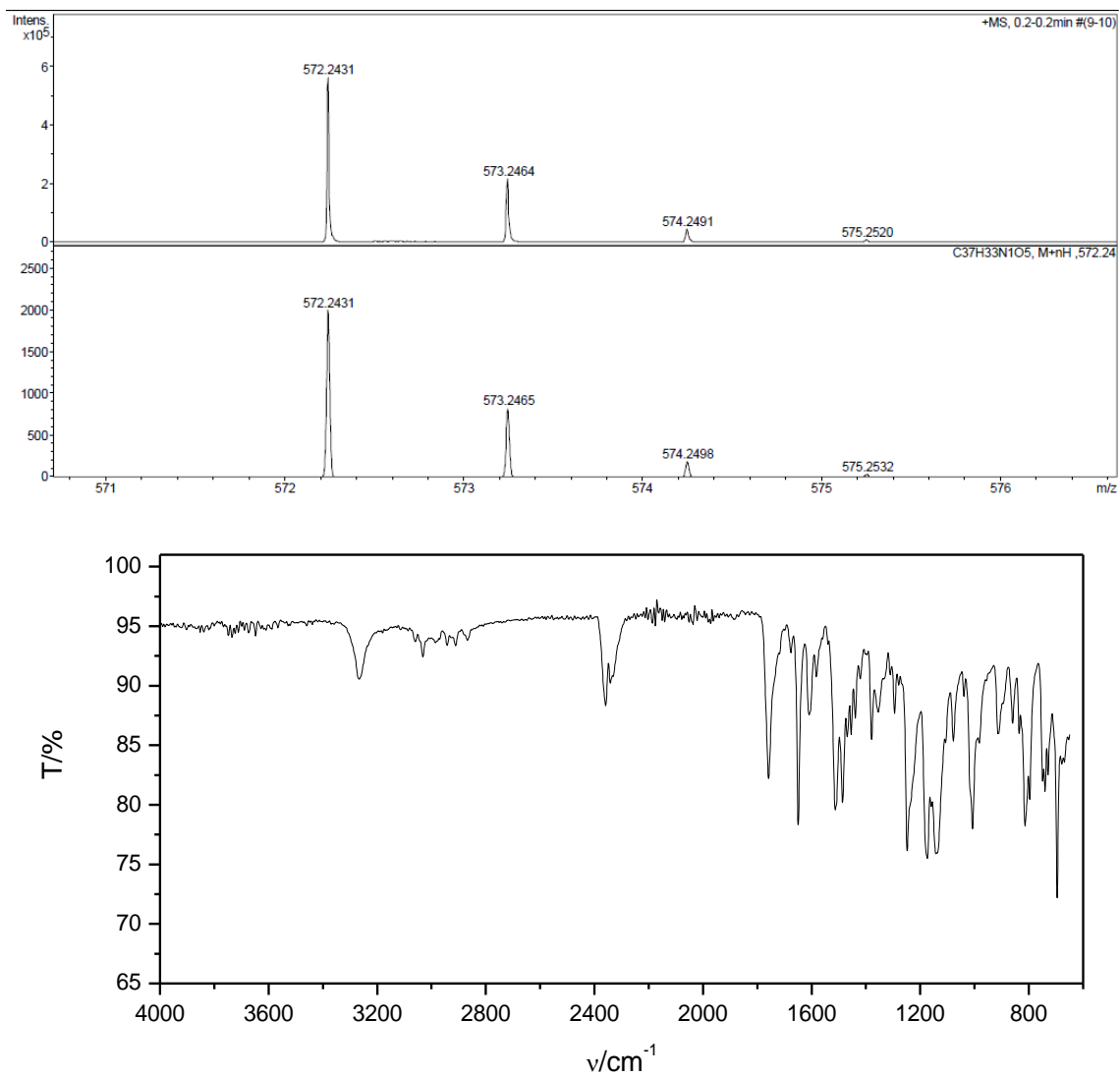


9.6.14 6-Amino-4'-(benzyloxy)-[1,1'-biphenyl]-3-yl propionate (30)

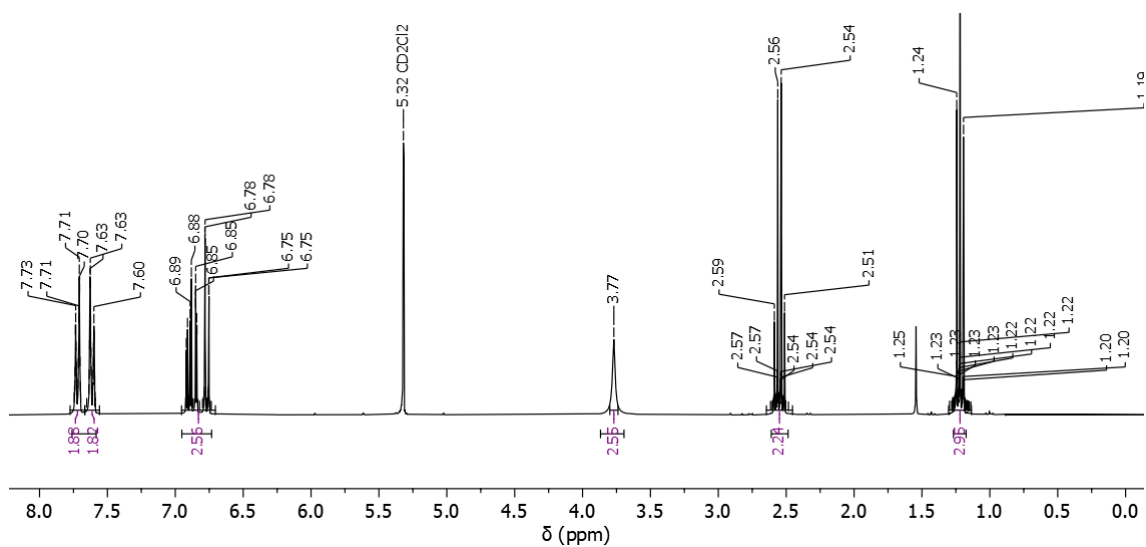


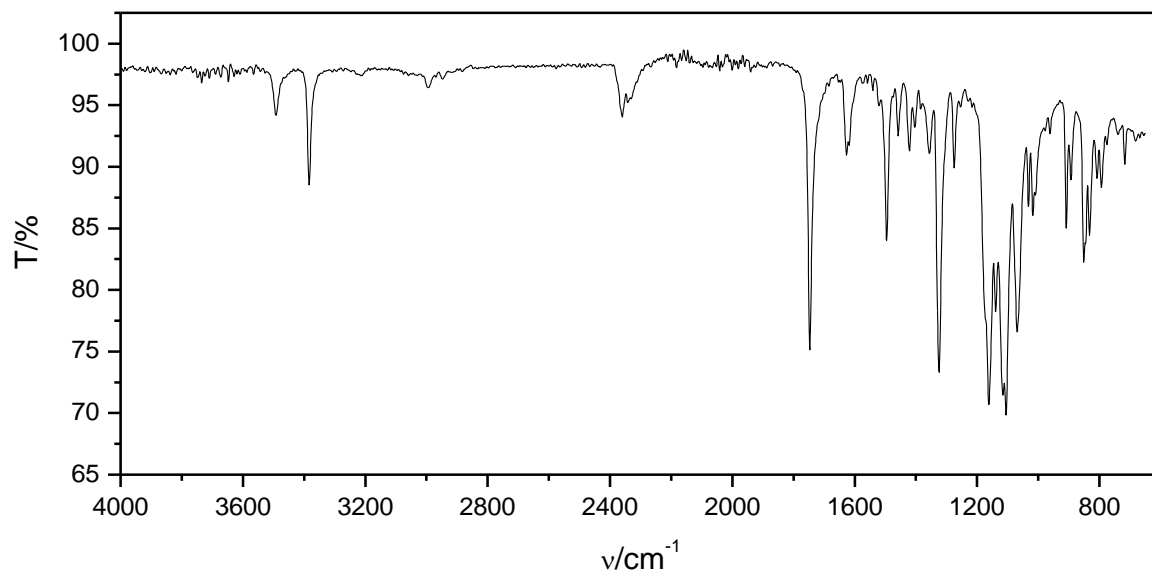
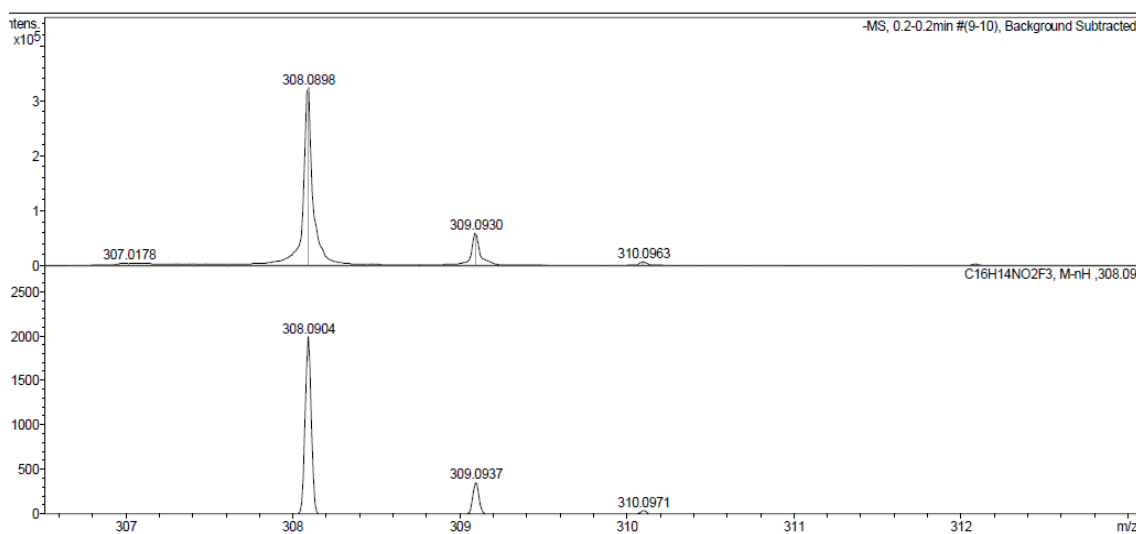
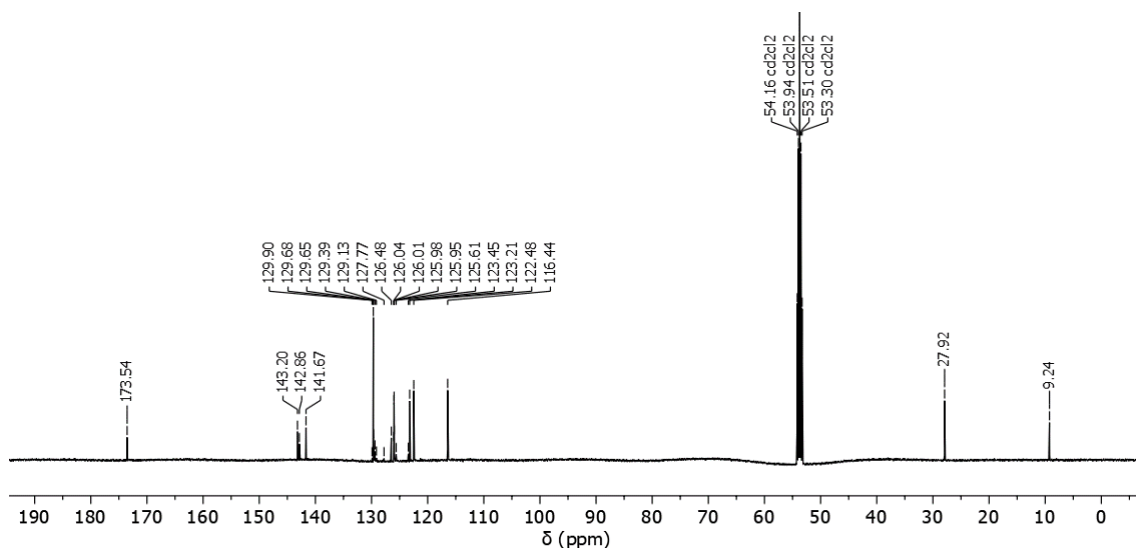
9.6.15 4'-(Benzyloxy)-6-(2-(4-phenoxyphenyl)acetamido)-[1,1'-biphenyl]-3-yl propionate (31)



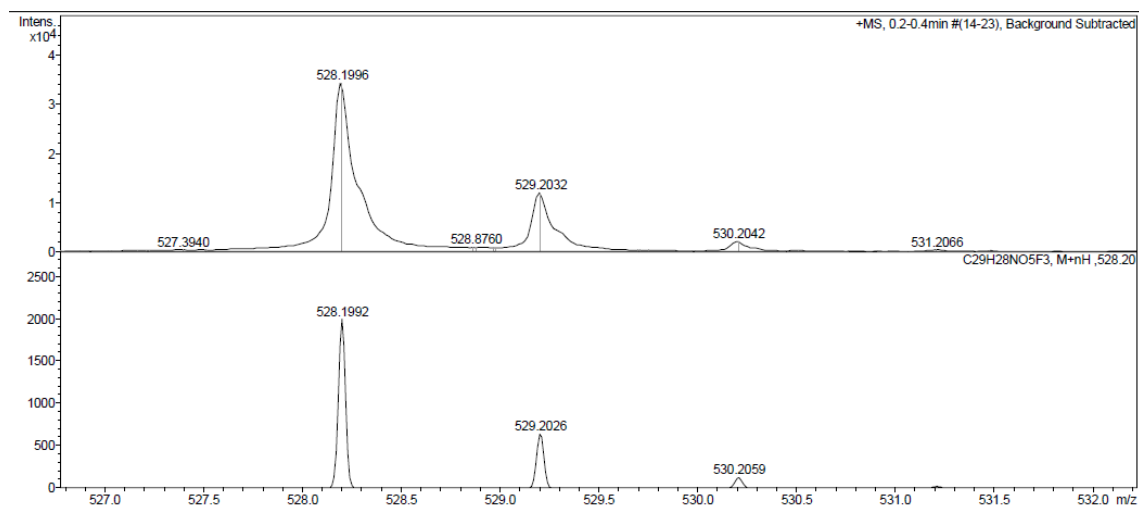
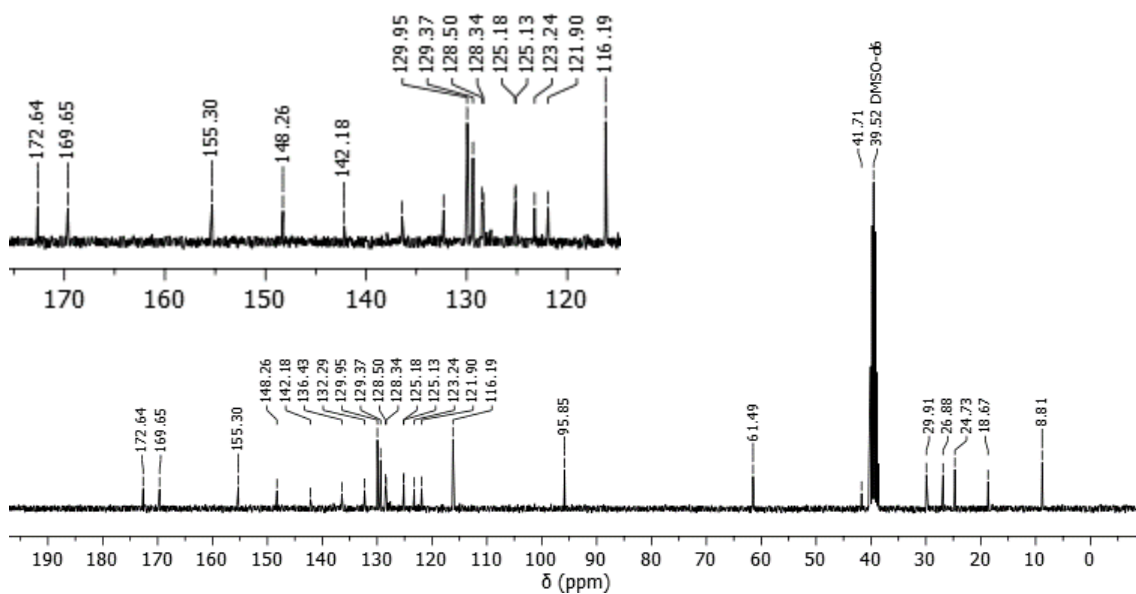
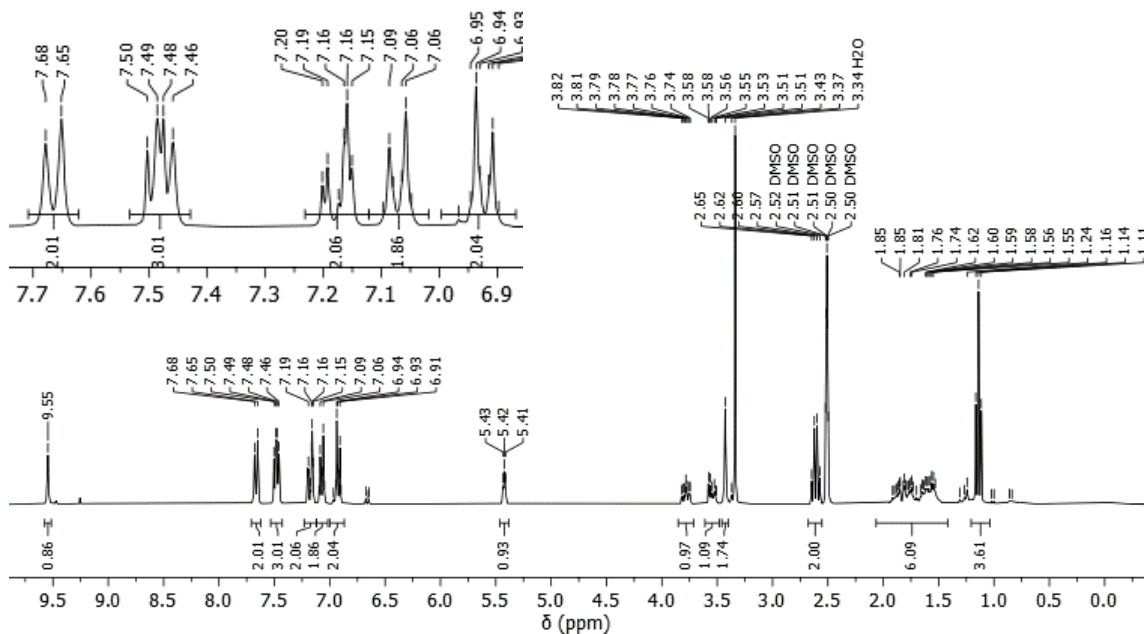


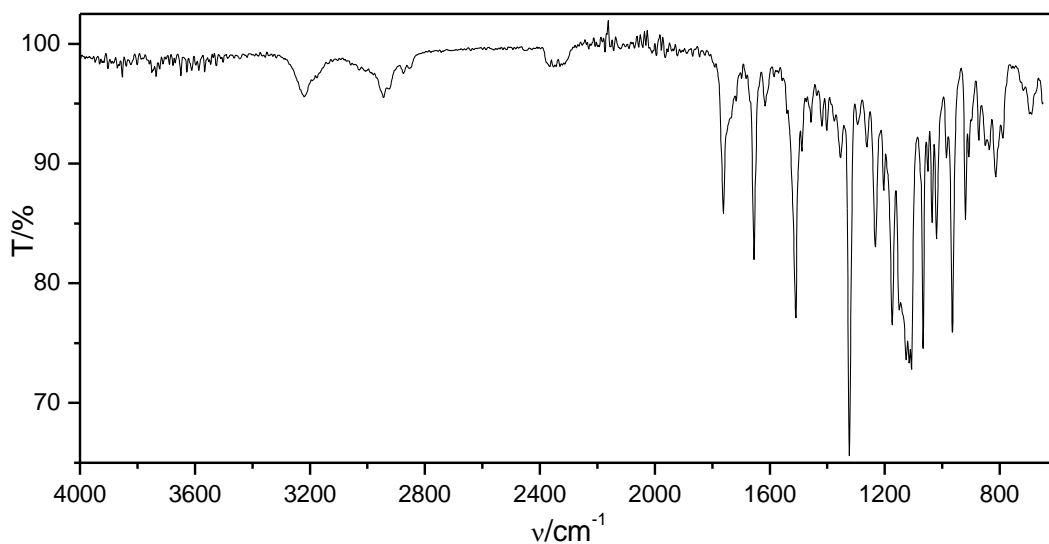
9.6.16 6-Amino-4'-(trifluoromethyl)-[1,1'-biphenyl]-3-yl propionate (32)



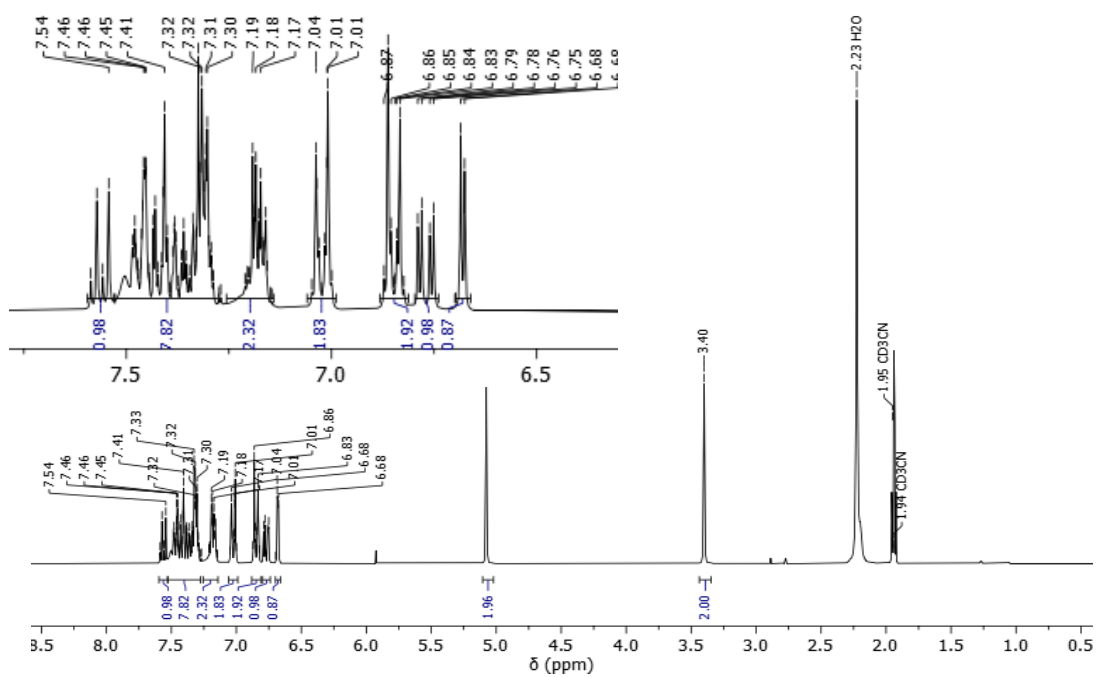


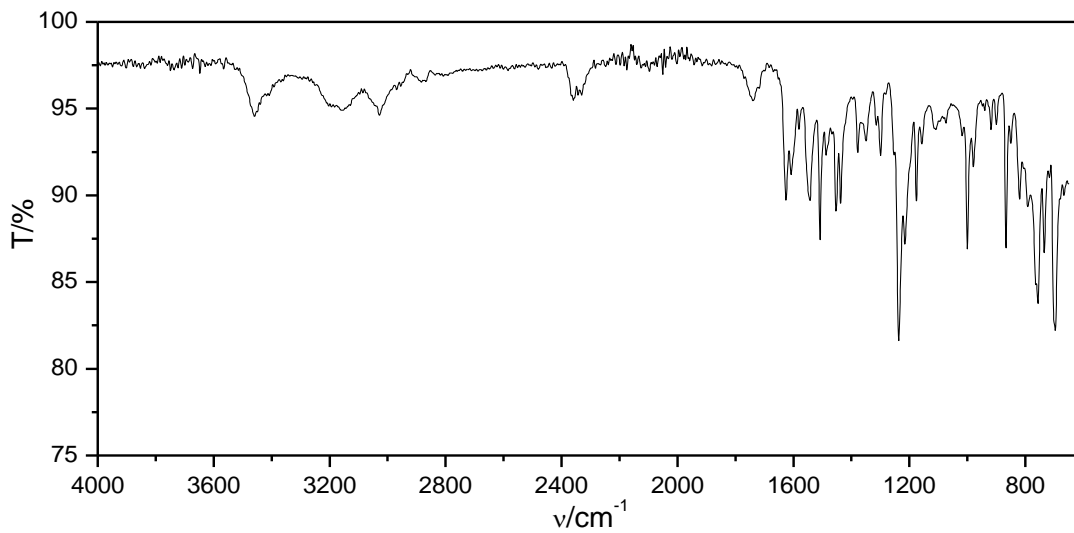
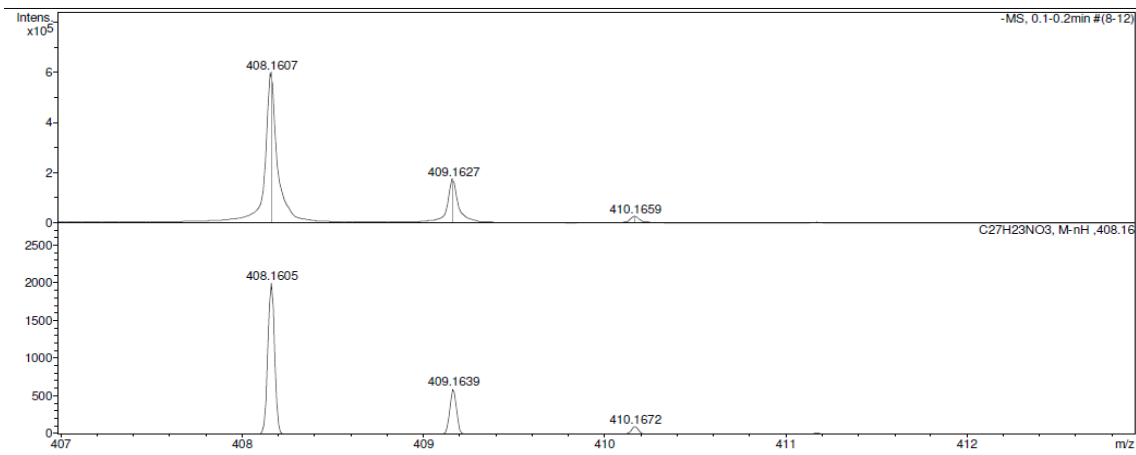
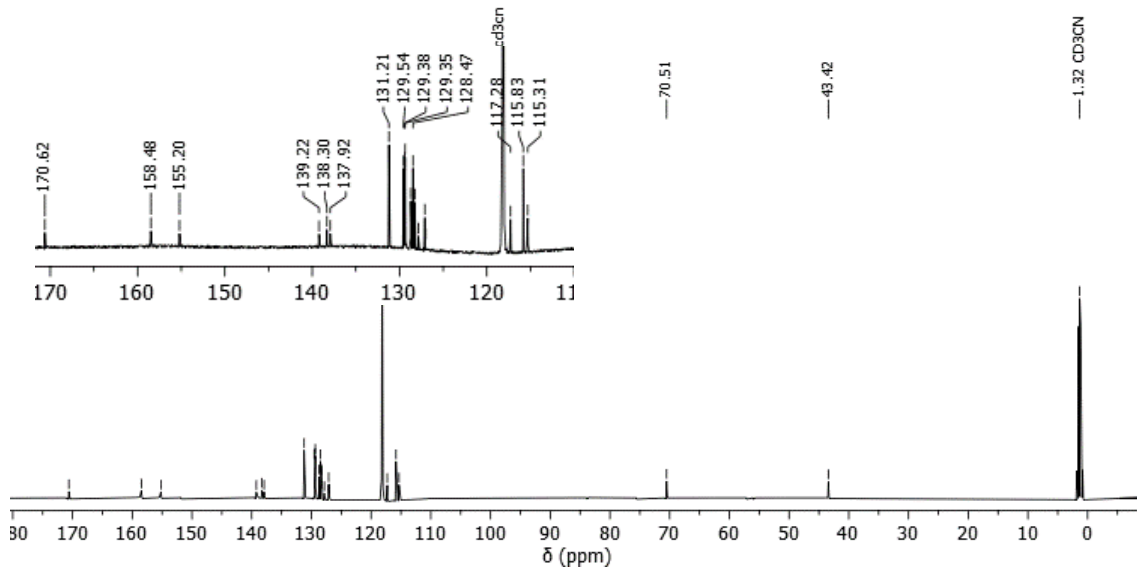
9.6.17 6-(2-(4-((Tetrahydro-2H-pyran-2-yl)oxy)phenyl)acetamido)-4'-(trifluoromethyl)-[1,1'-biphenyl]-3-yl propionate (33)



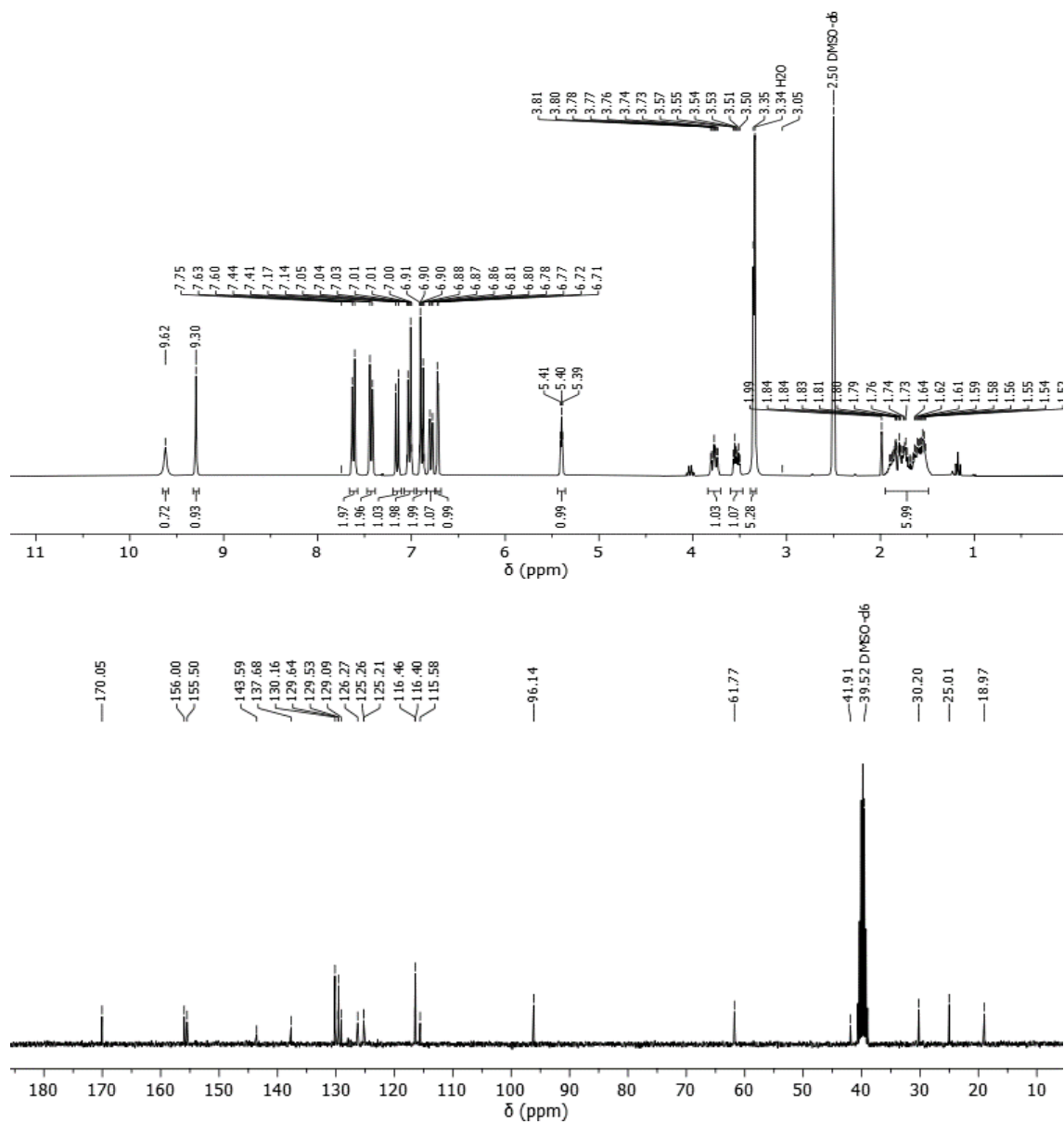


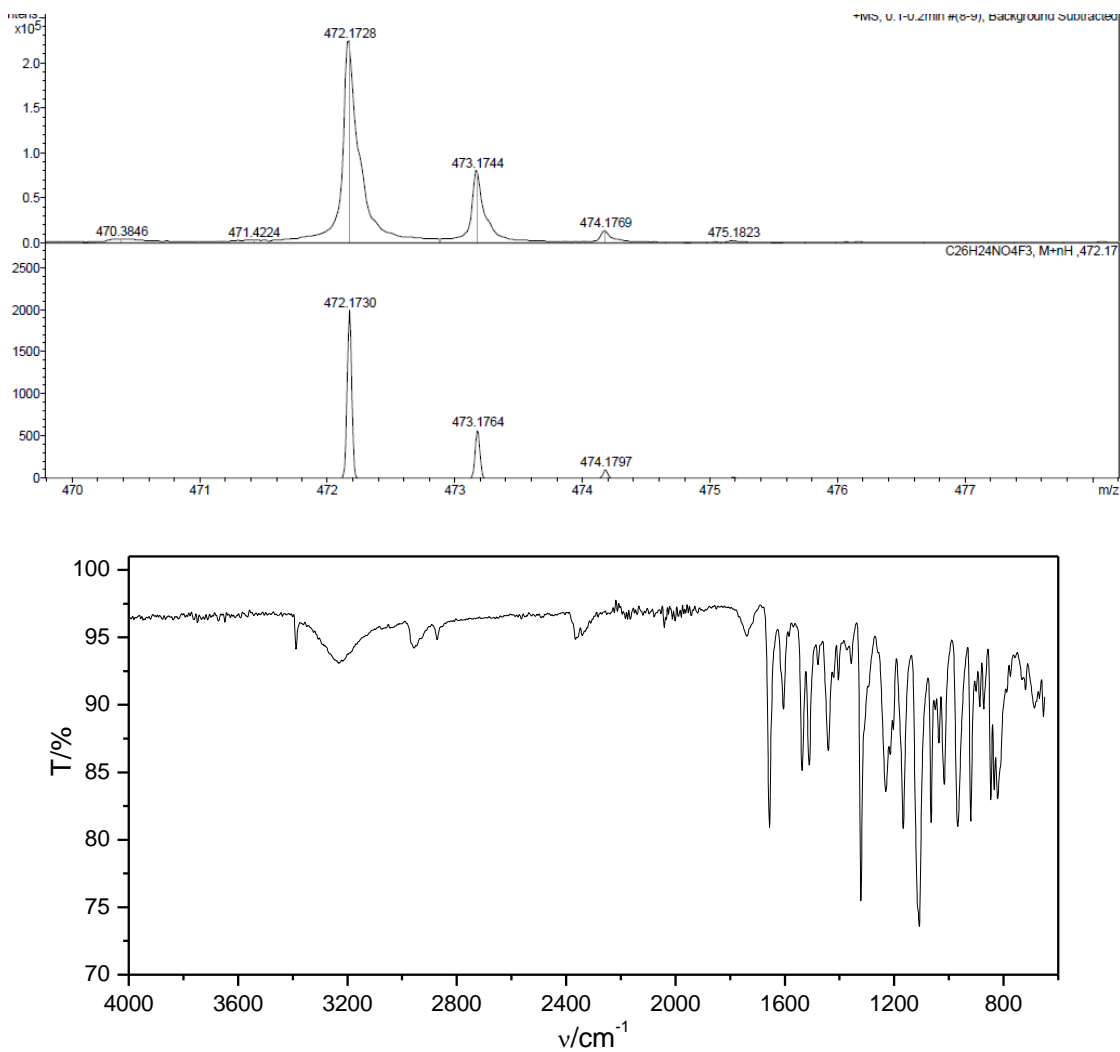
9.6.18 2-(4-(Benzyloxy)phenyl)-N-(5-hydroxy-[1,1'-biphenyl]-2-yl)acetamide (34)



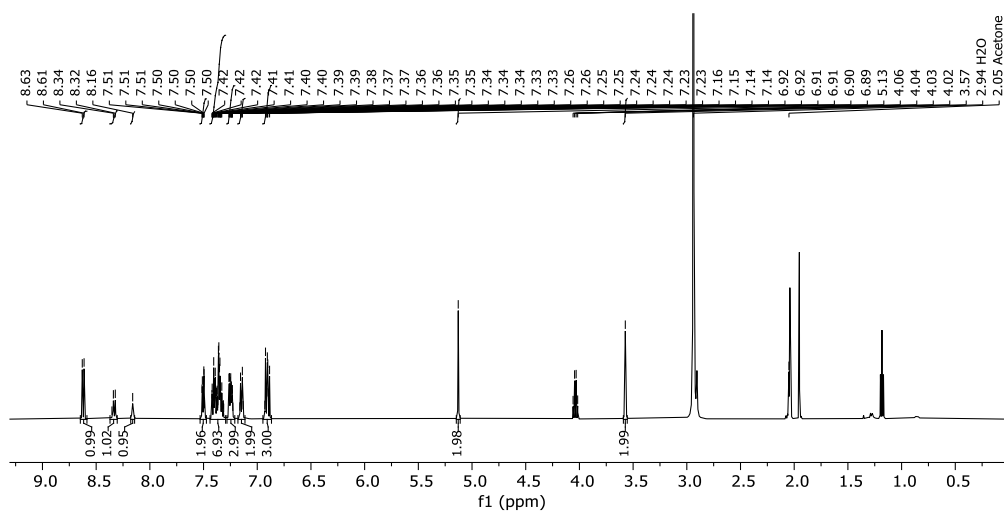


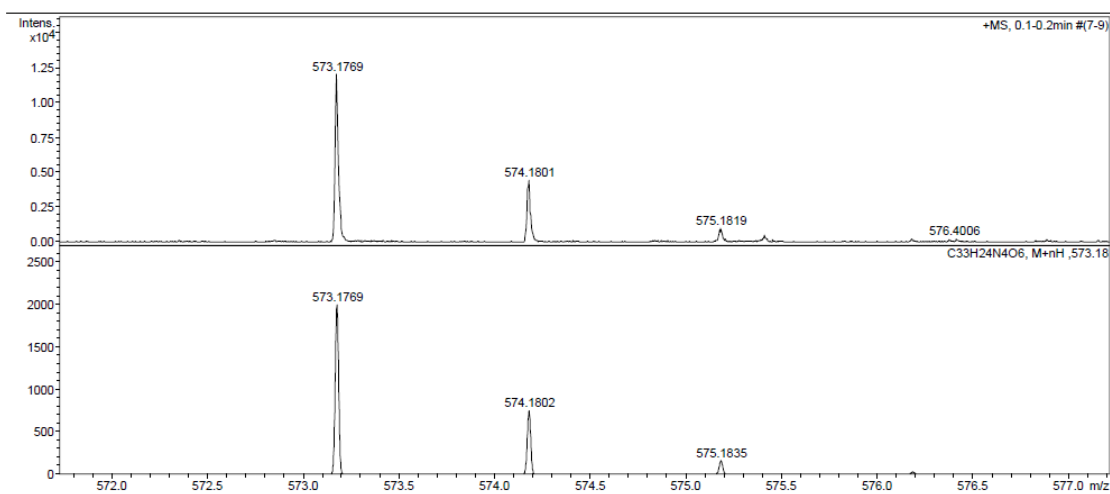
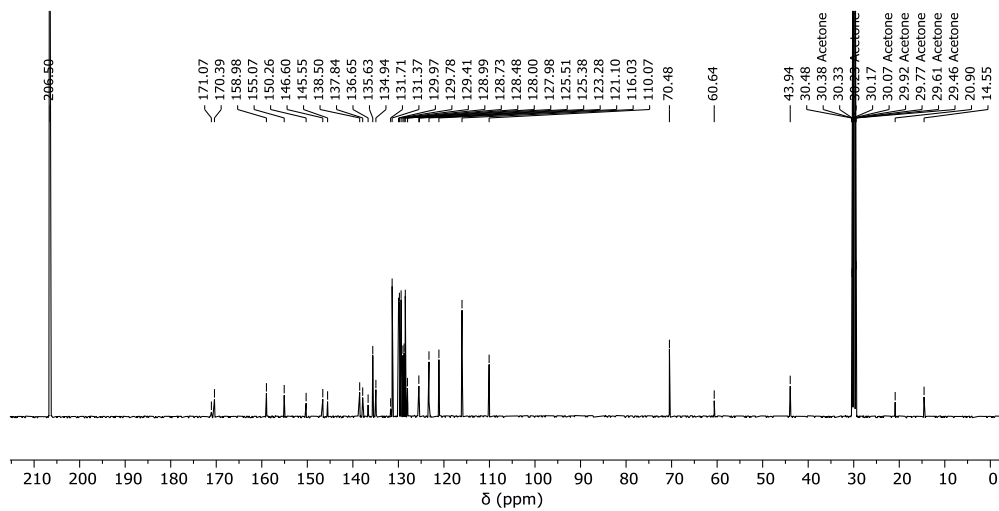
9.6.19 *N*-(5-Hydroxy-4'-(trifluoromethyl)-[1,1'-biphenyl]-2-yl)-2-(4-((tetrahydro-2H-pyran-2-yl)oxy)phenyl)acetamide (35)

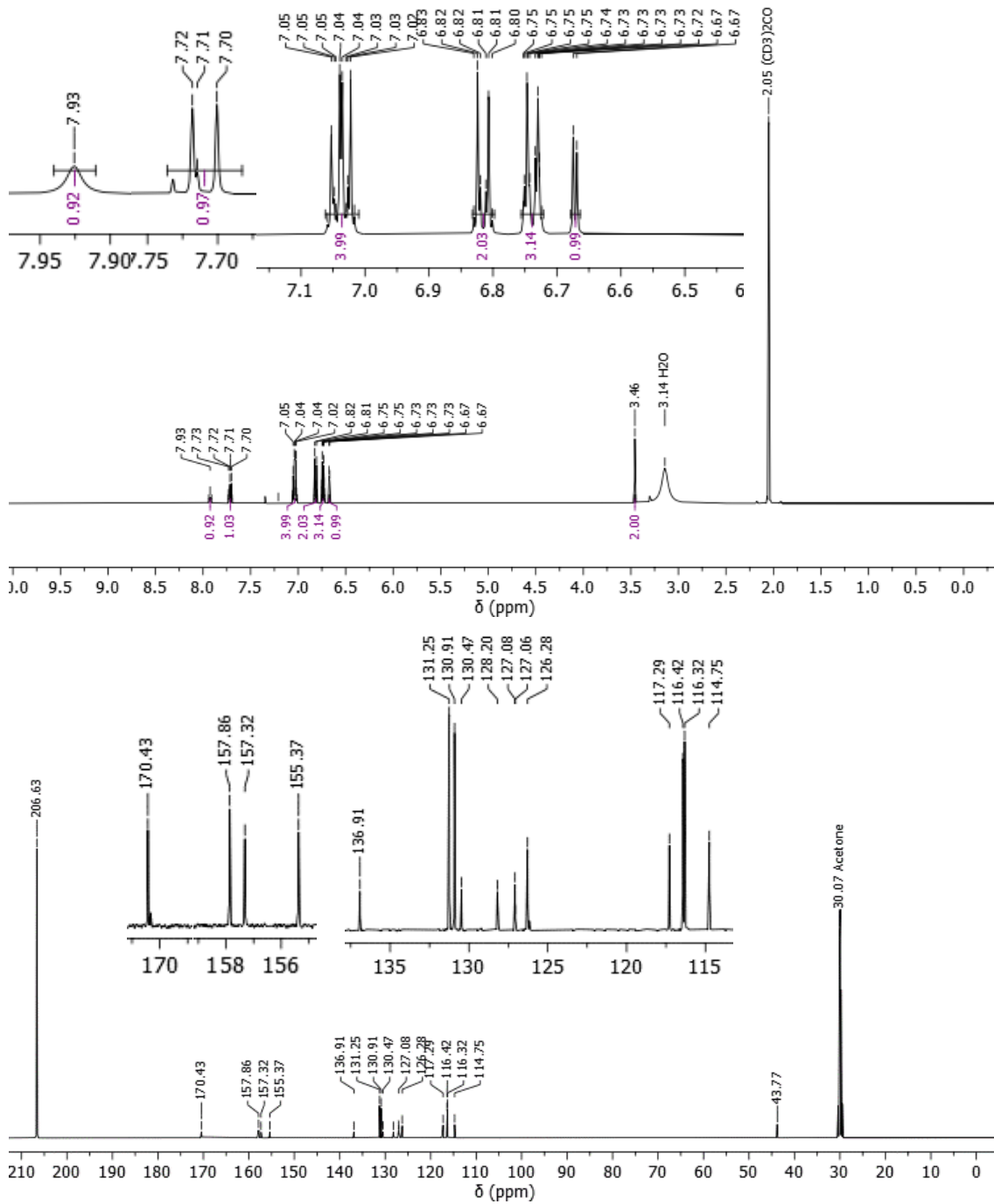


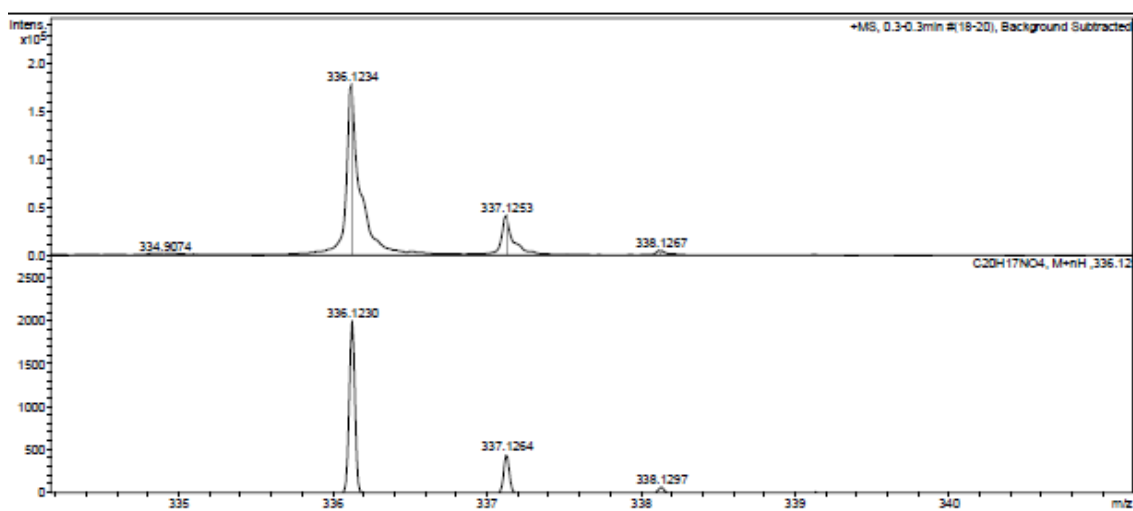
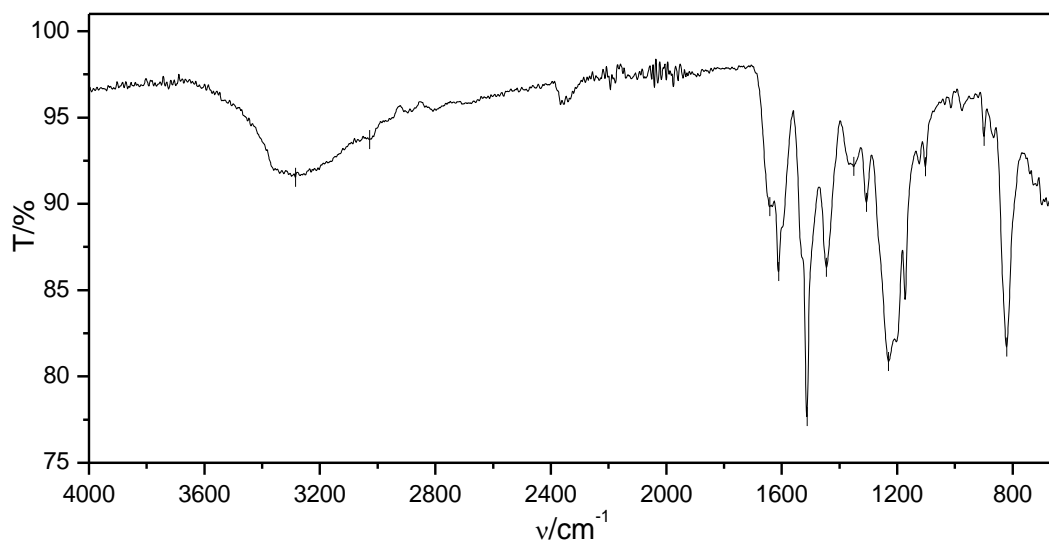


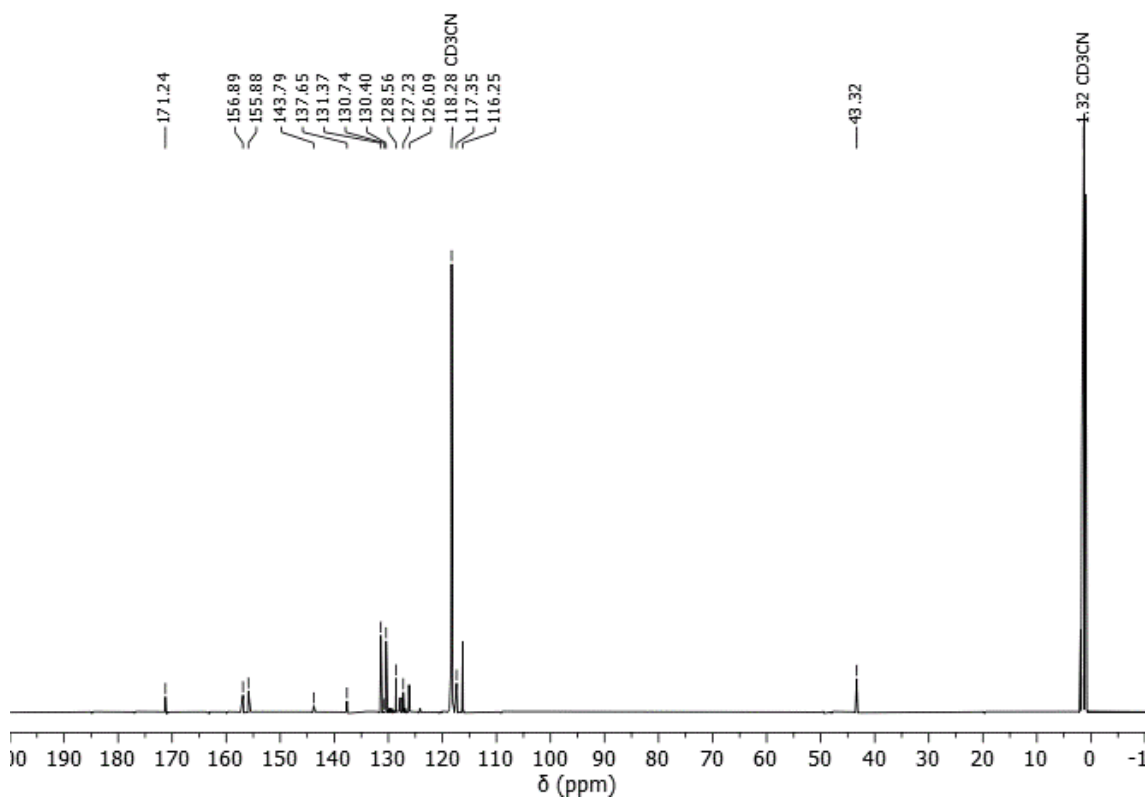
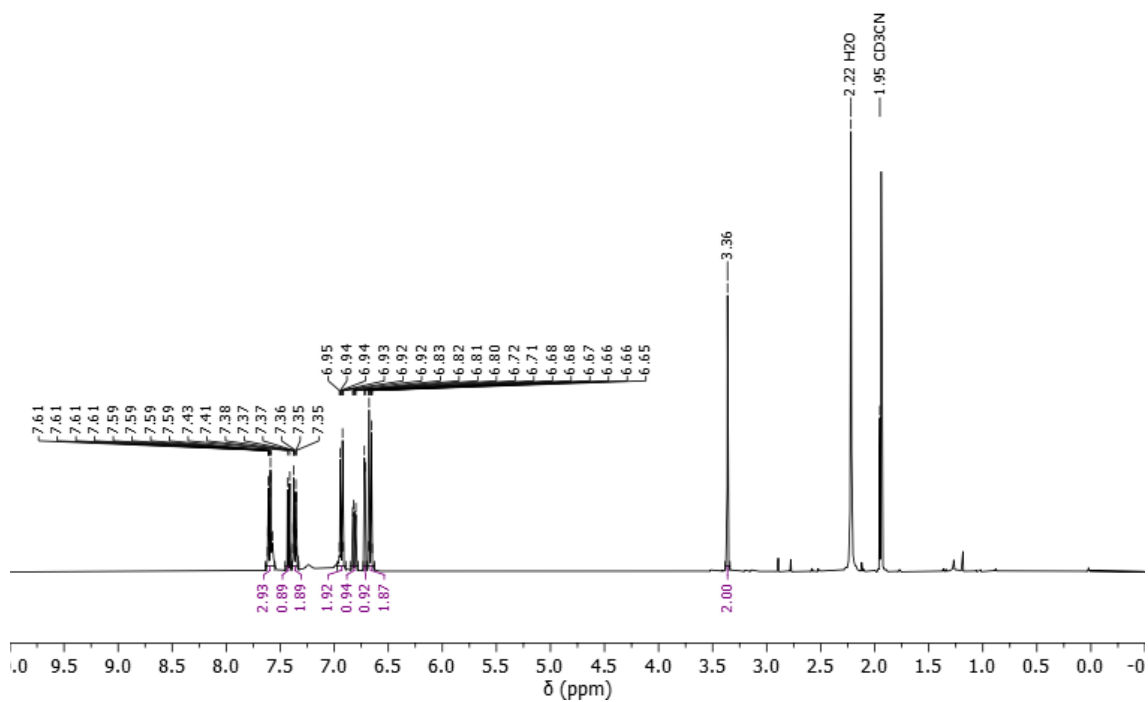
9.6.20 2-(4-(Benzyloxy)phenyl)-*N*-(5-((7-nitrobenzo[*c*][1,2,5]oxadiazol-4-yl)oxy)-[1,1'-biphenyl]-2-yl)acetamide (36)

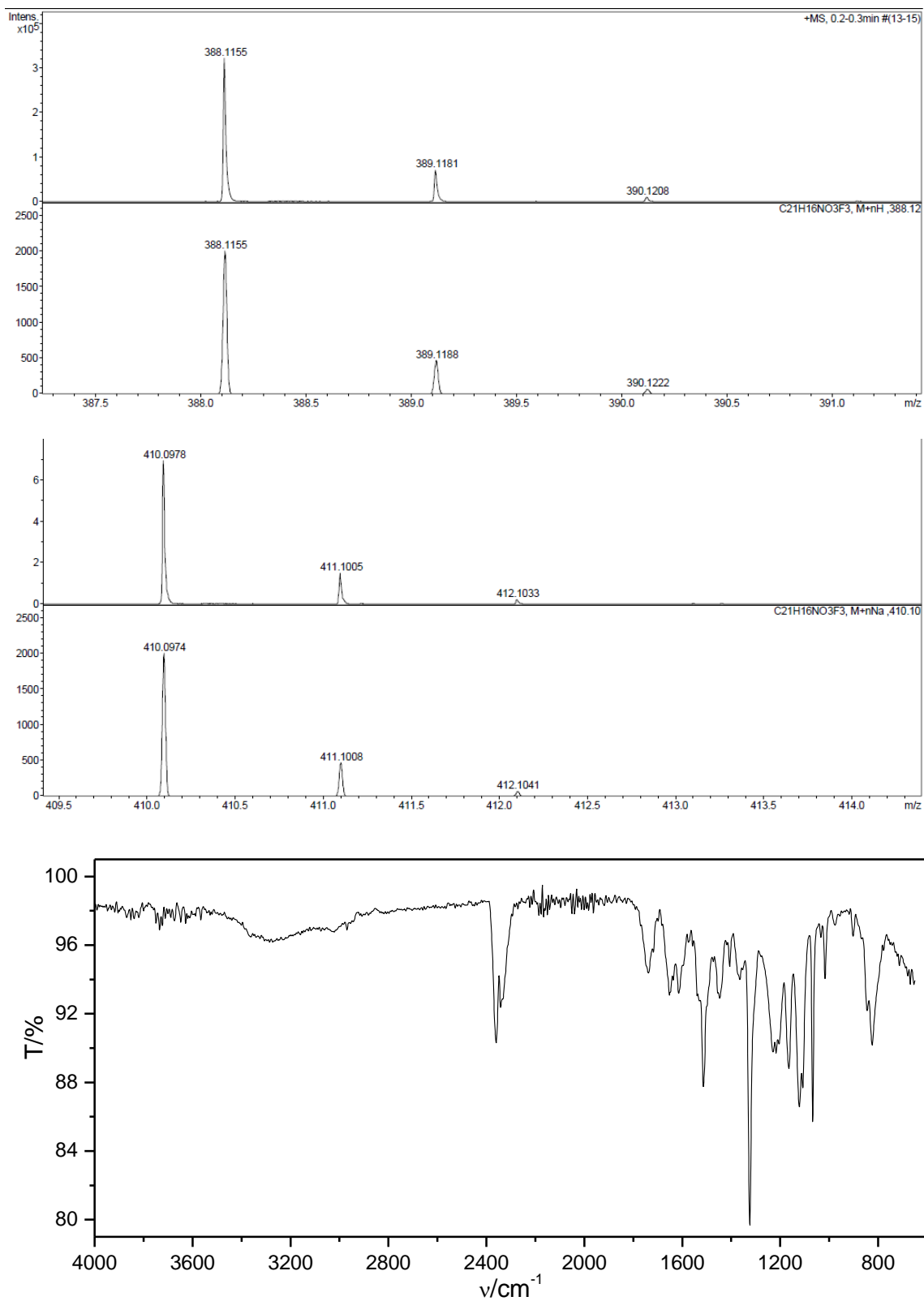




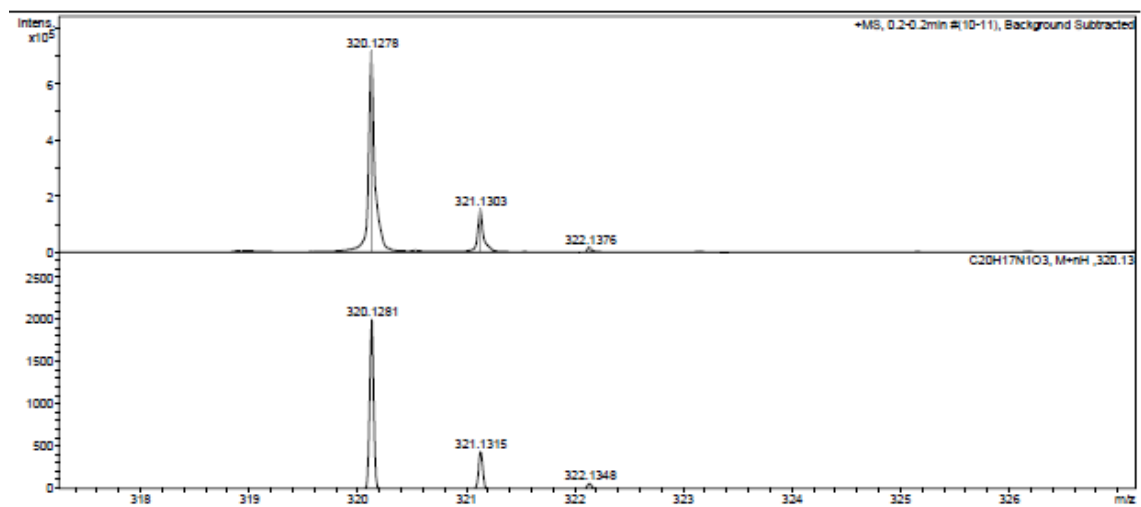
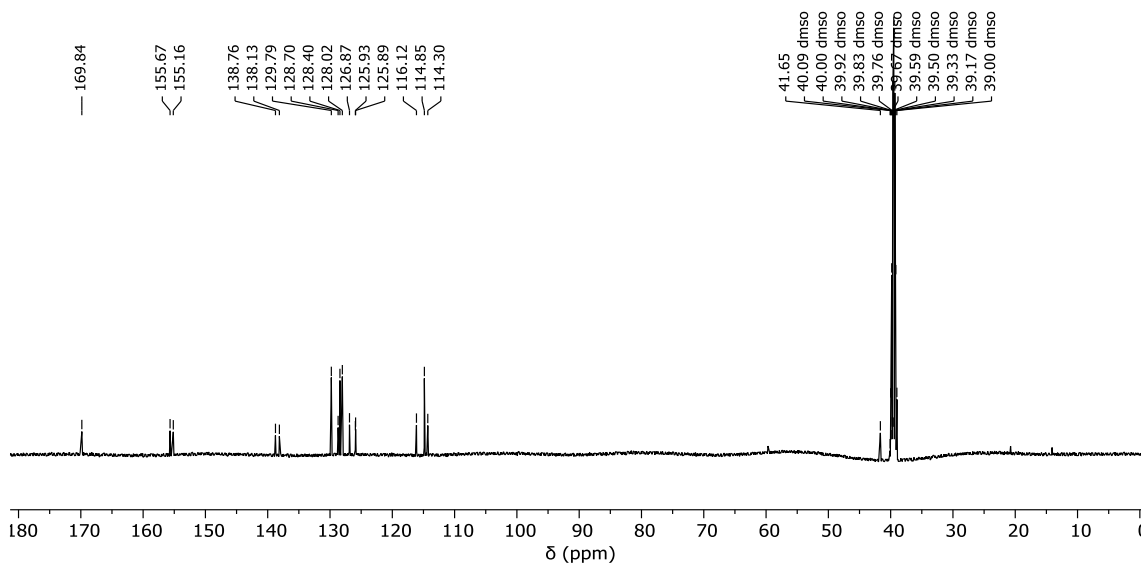
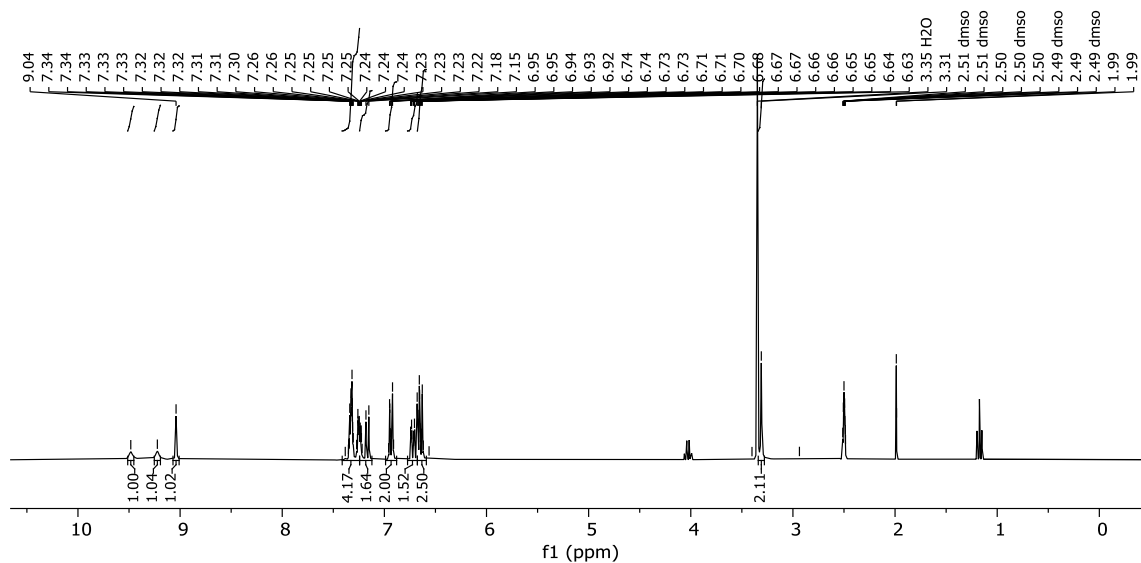
9.6.21 *N*-(4',5-Dihydroxy-[1,1'-biphenyl]-2-yl)-2-(4-hydroxyphenyl)acetamide (L1)

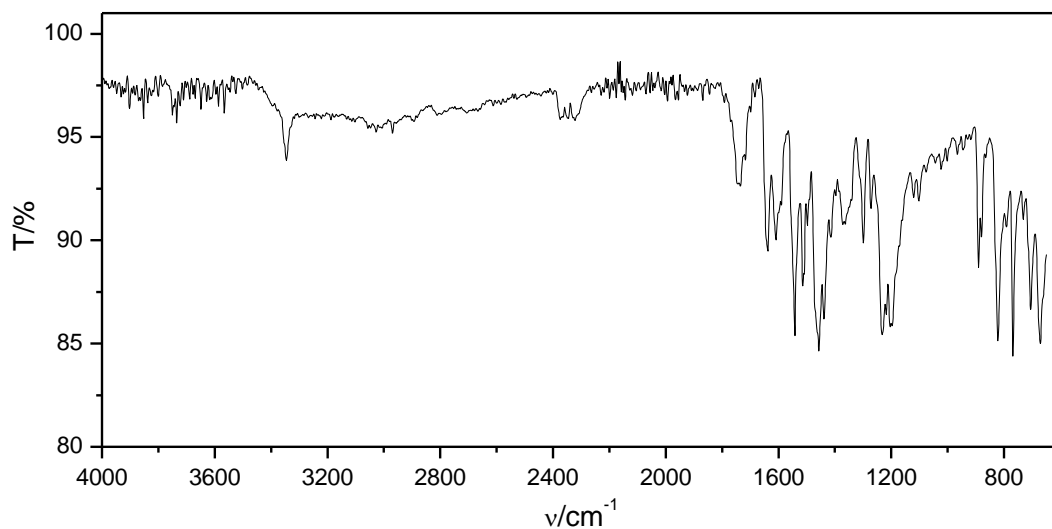


9.6.22 *N*-(5-Hydroxy-4'-(trifluoromethyl)-[1,1'-biphenyl]-2-yl)-2-(4-hydroxyphenyl)acetamide (L9)

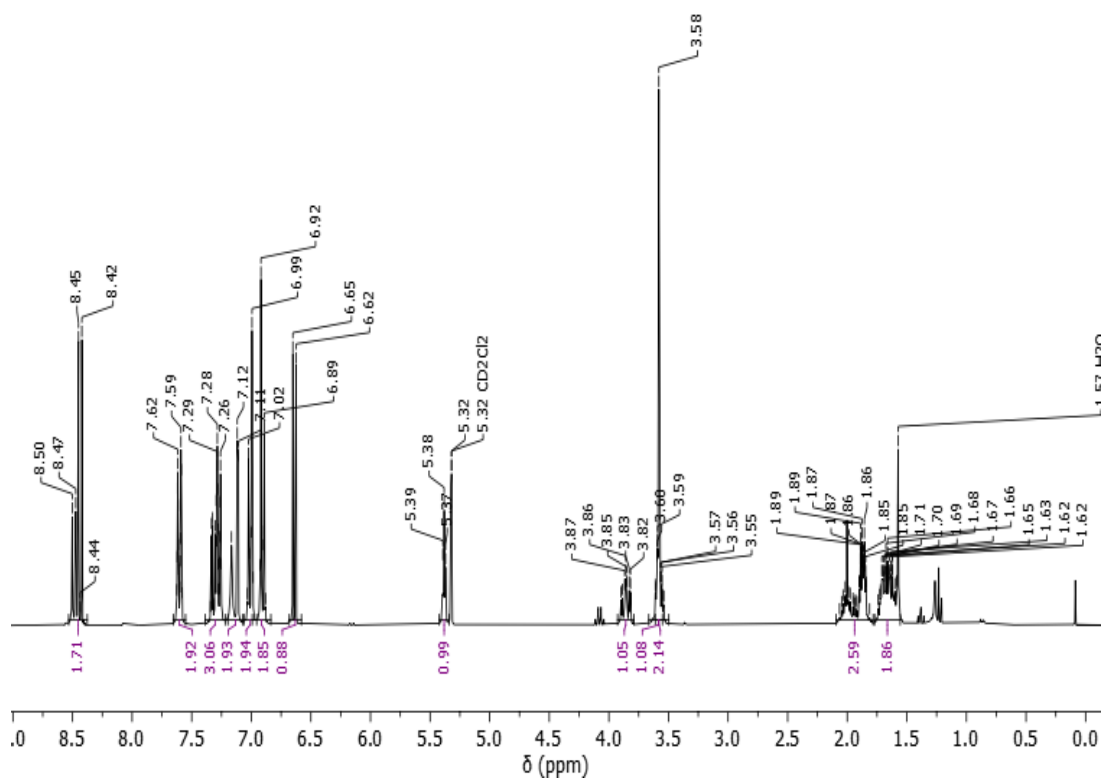


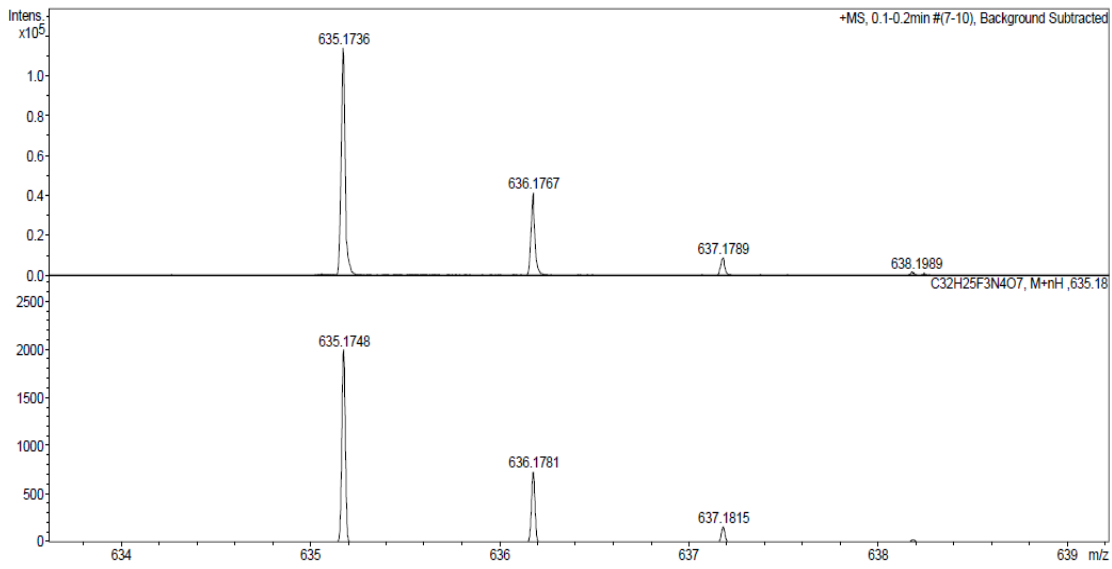
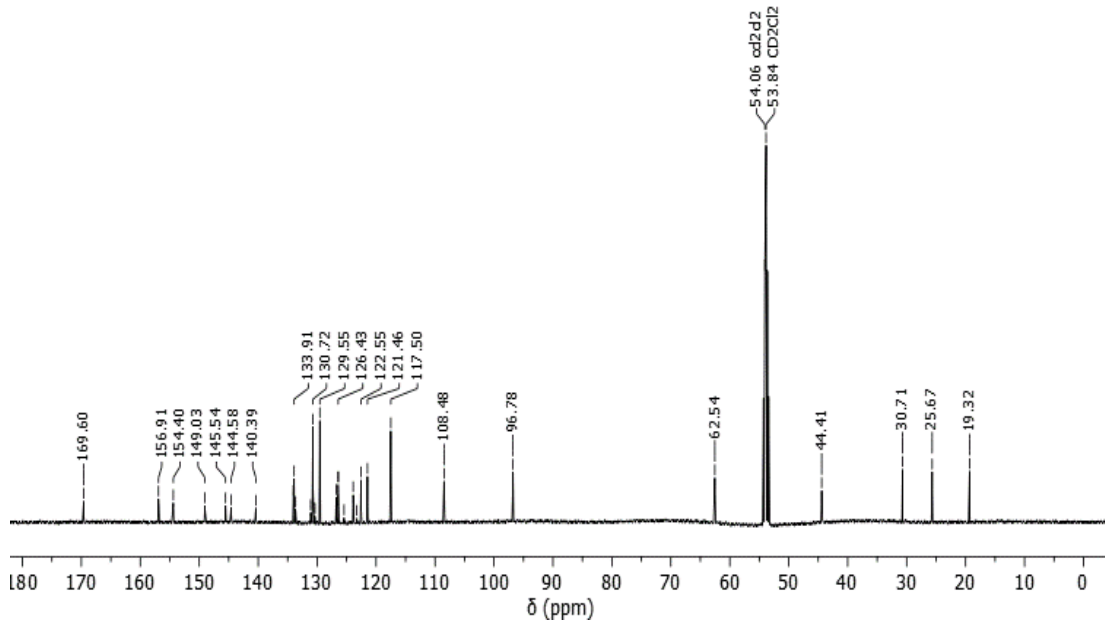
9.6.23 *N*-(5-Hydroxy-[1,1'-biphenyl]-2-yl)-2-(4-hydroxyphenyl)acetamide (L10)



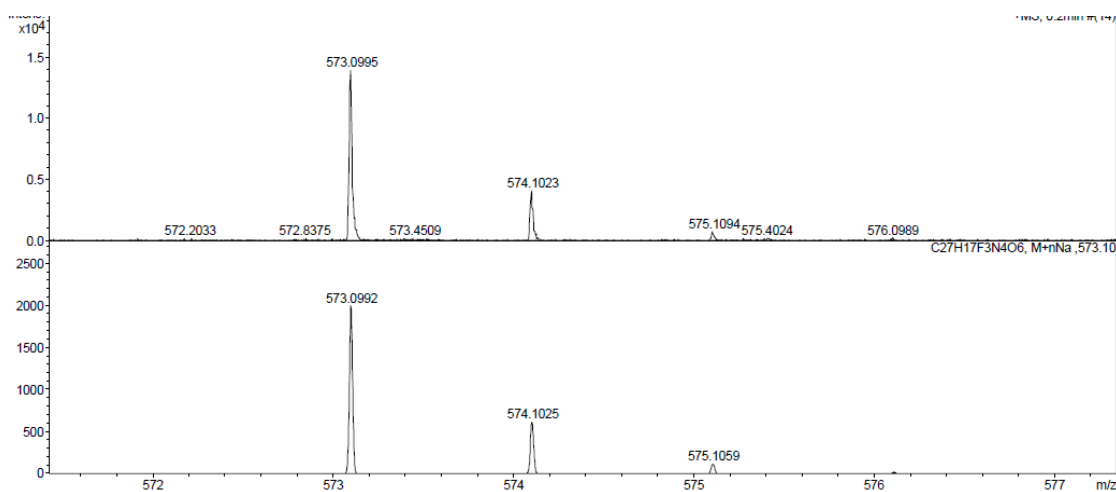
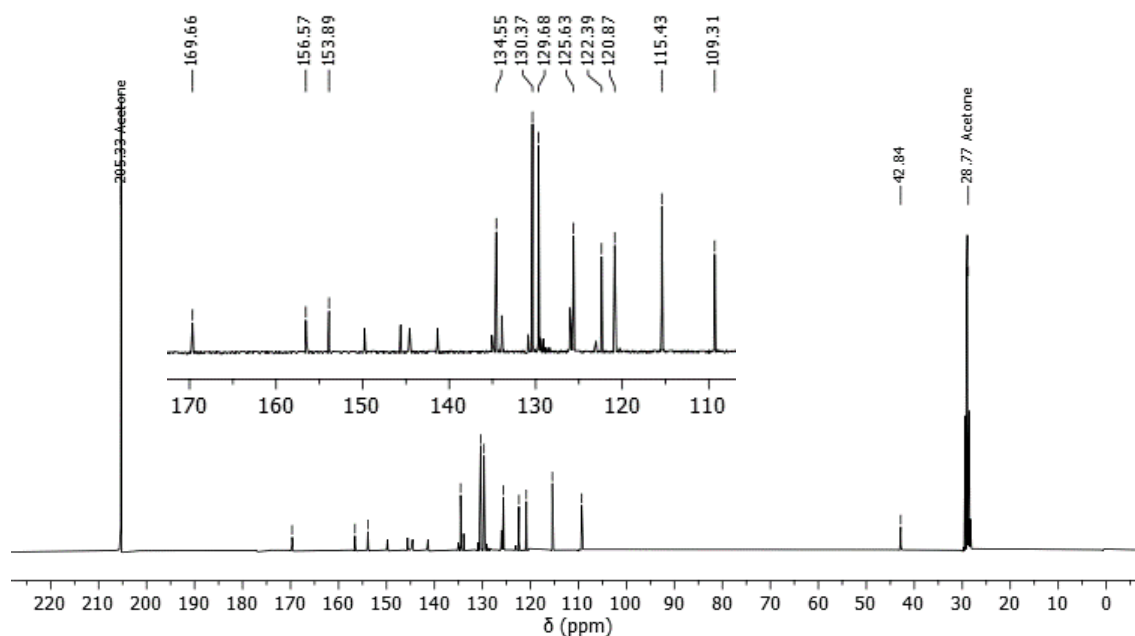
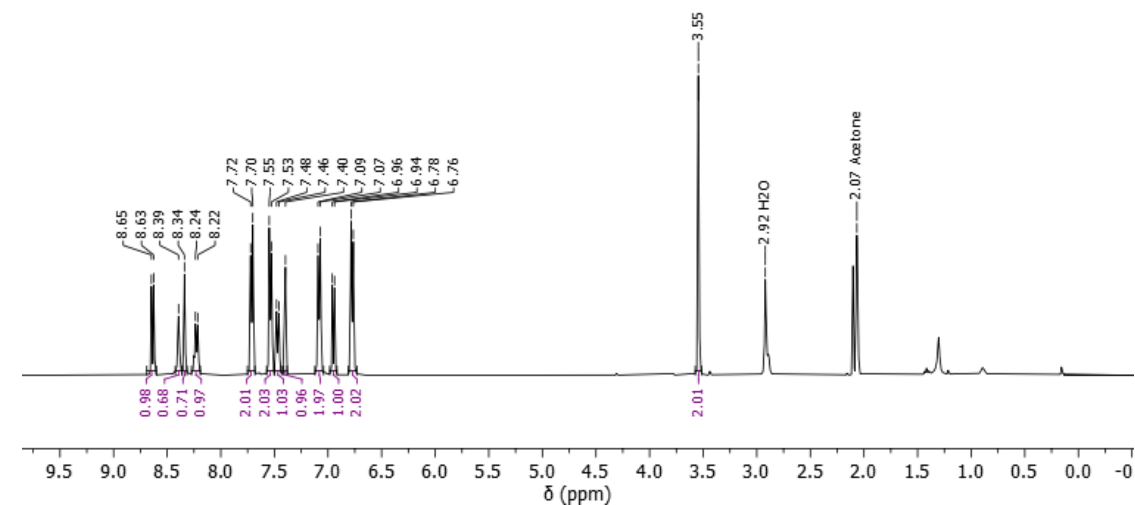


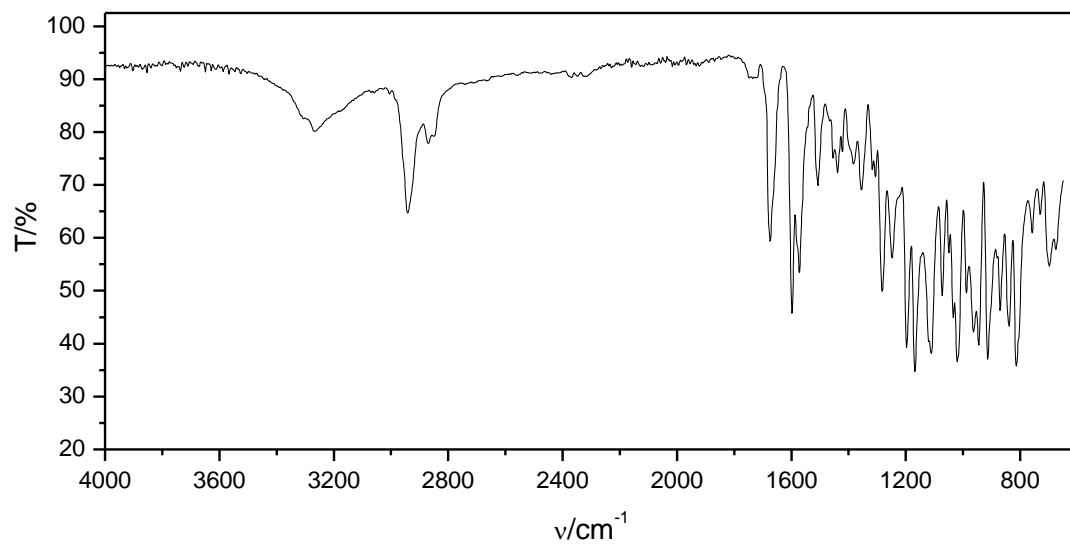
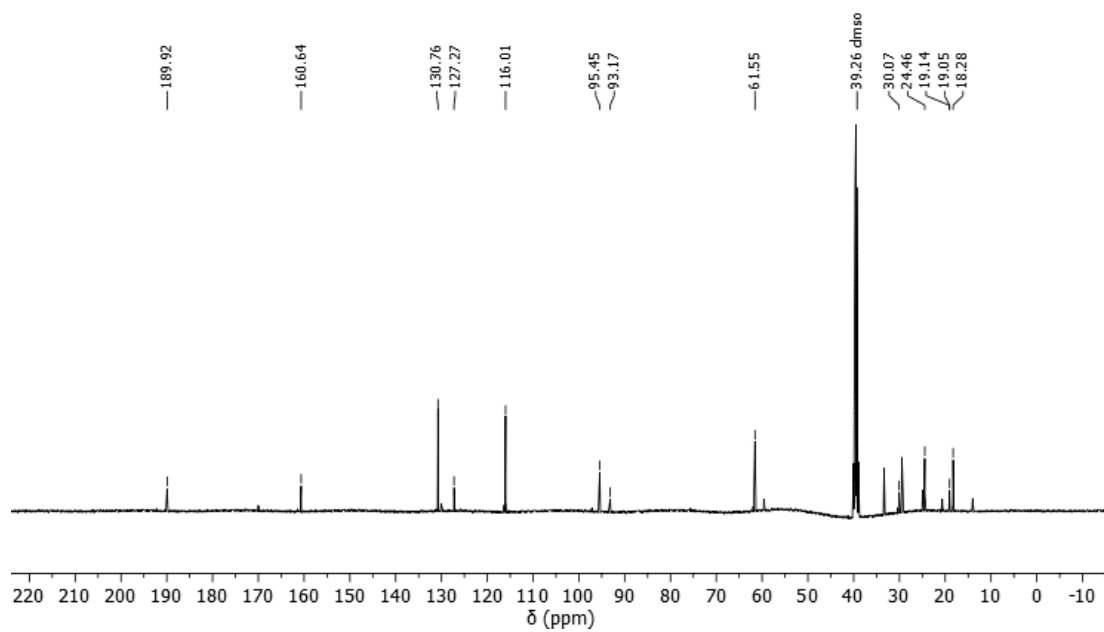
9.6.24 *N*-(5-((7-Nitrobenzo[*c*][1,2,5]oxadiazol-4-yl)oxy)-4'-(trifluoromethyl)-[1,1'-biphenyl]-2-yl)-2-(4-((tetrahydro-2H-pyran-2-yl)oxy)phenyl)acetamide (37)



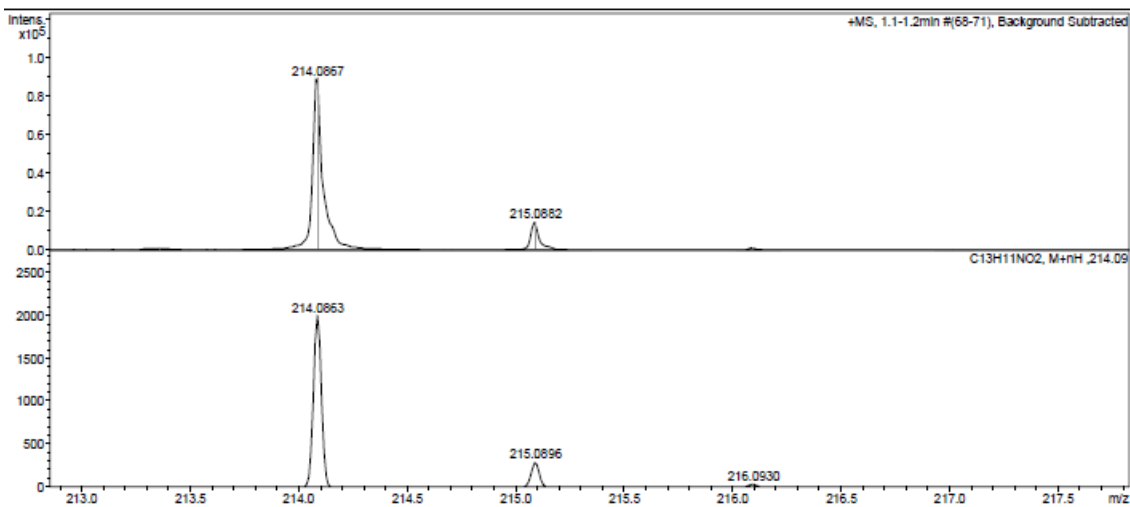
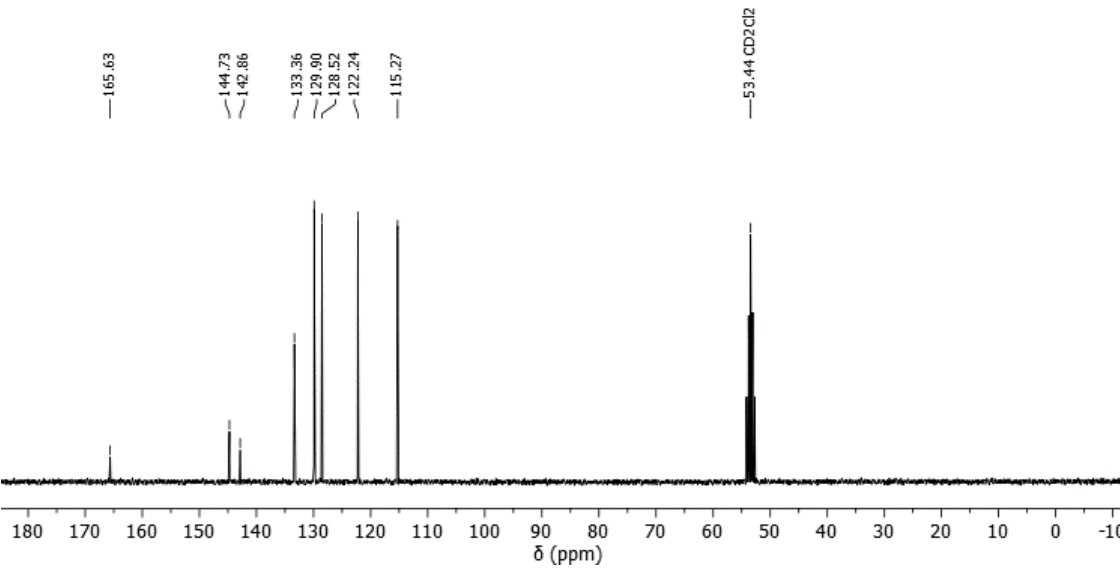
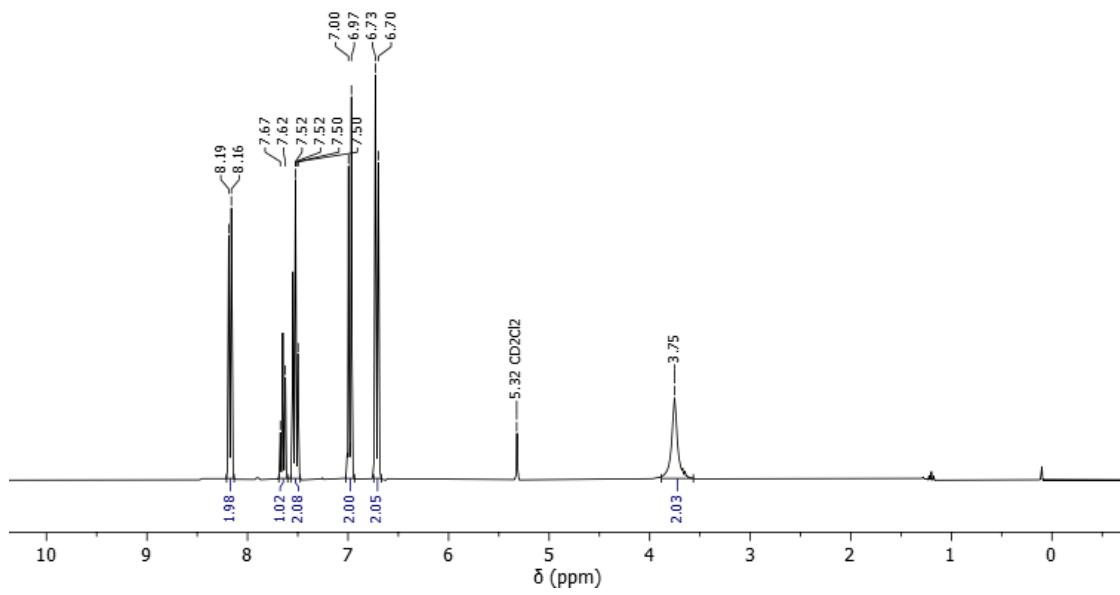


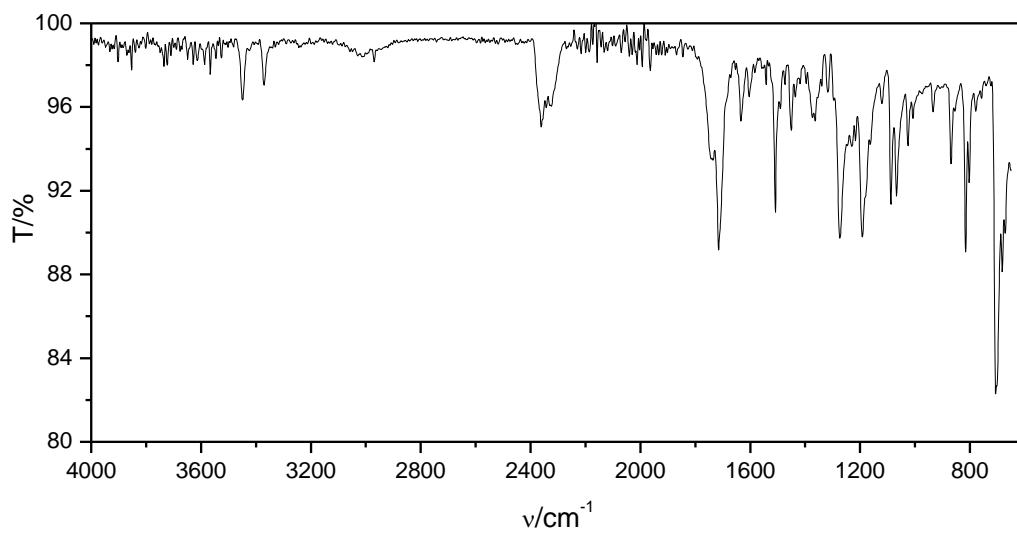
9.6.25 2-(4-Hydroxyphenyl)-*N*-(5-((7-nitrobenzo [c][1,2,5] oxadiazol-4-yl)oxy)-4'-(trifluoromethyl)-[1,1'-biphenyl]-2-yl) acetamide (38)



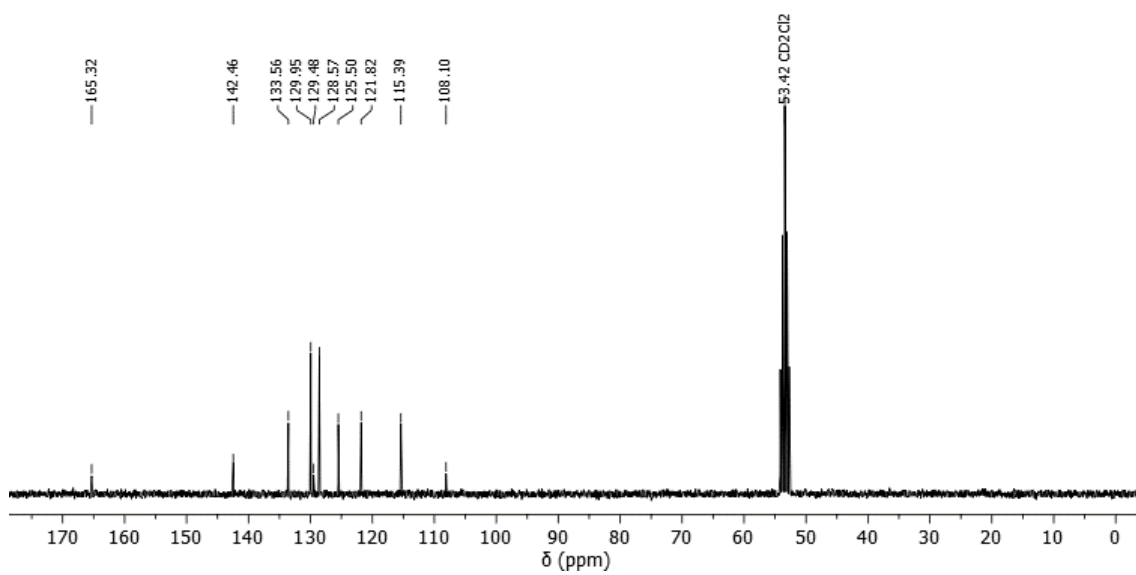
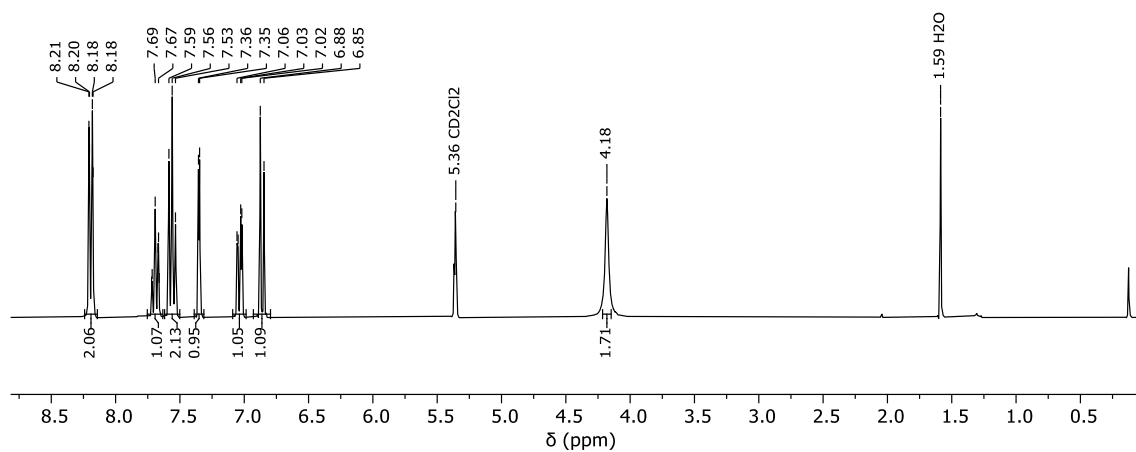


9.6.27 4-Aminophenyl benzoate (56)

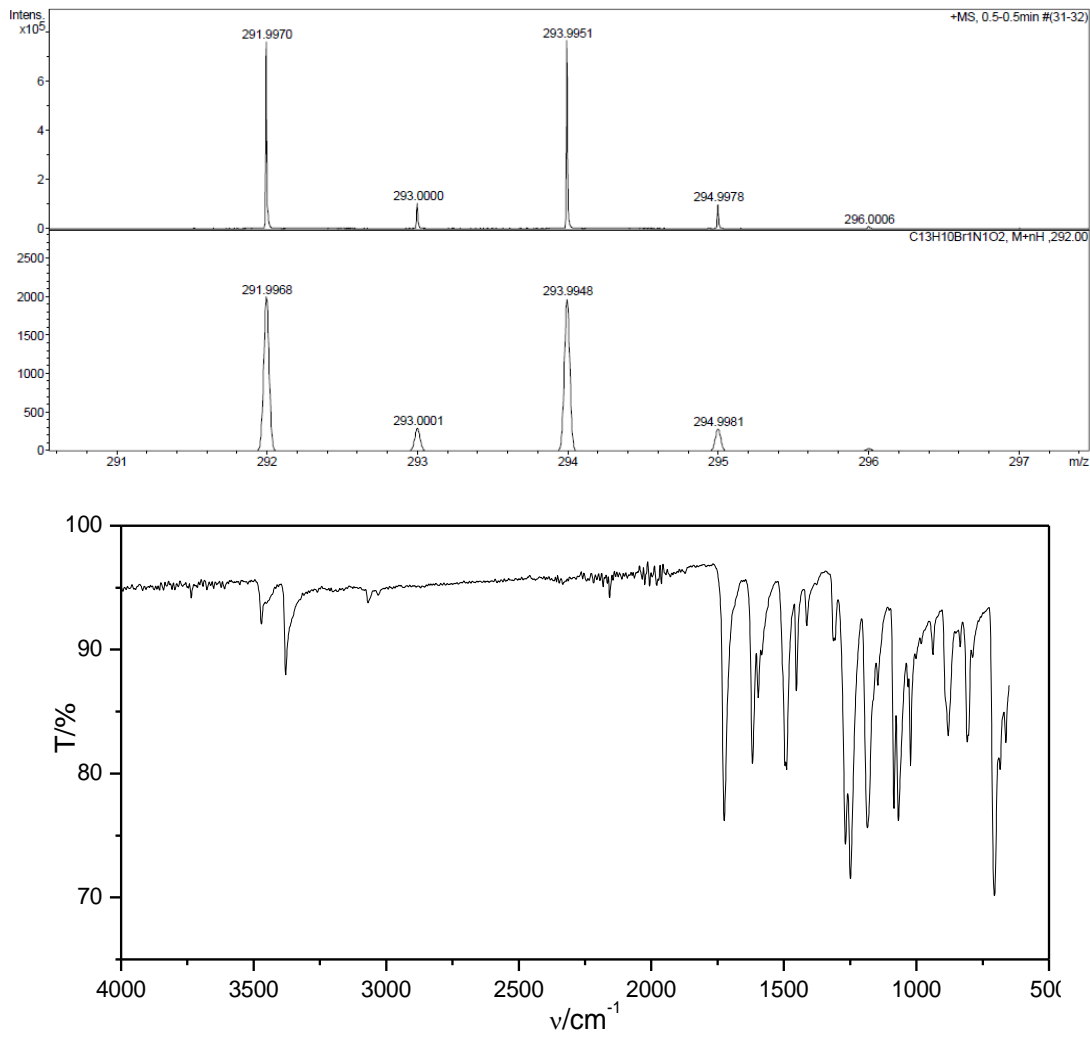




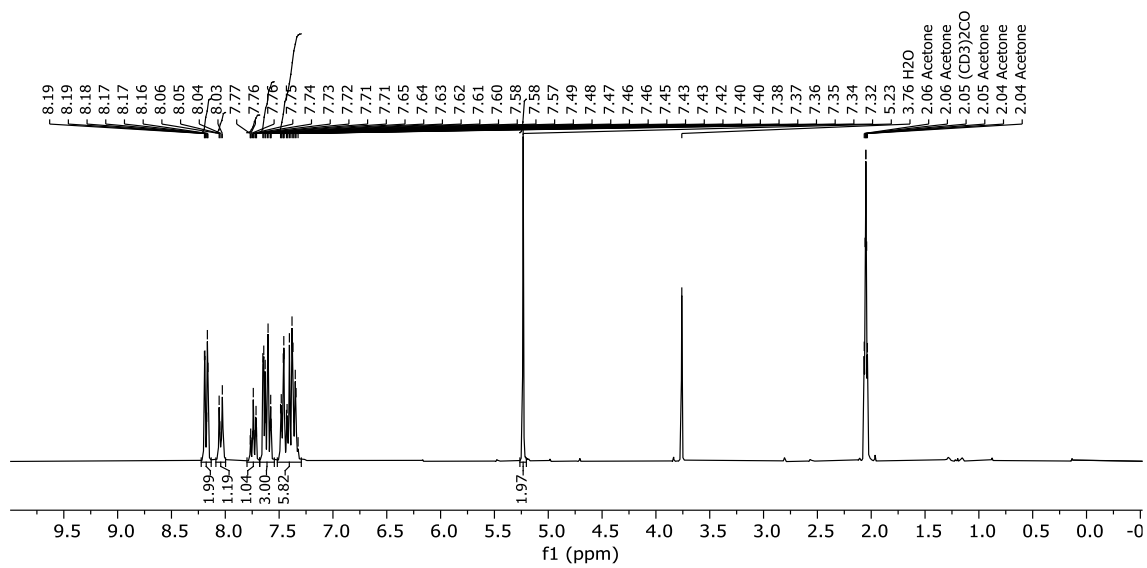
9.6.28 4-Amino-3-bromophenyl benzoate (57)

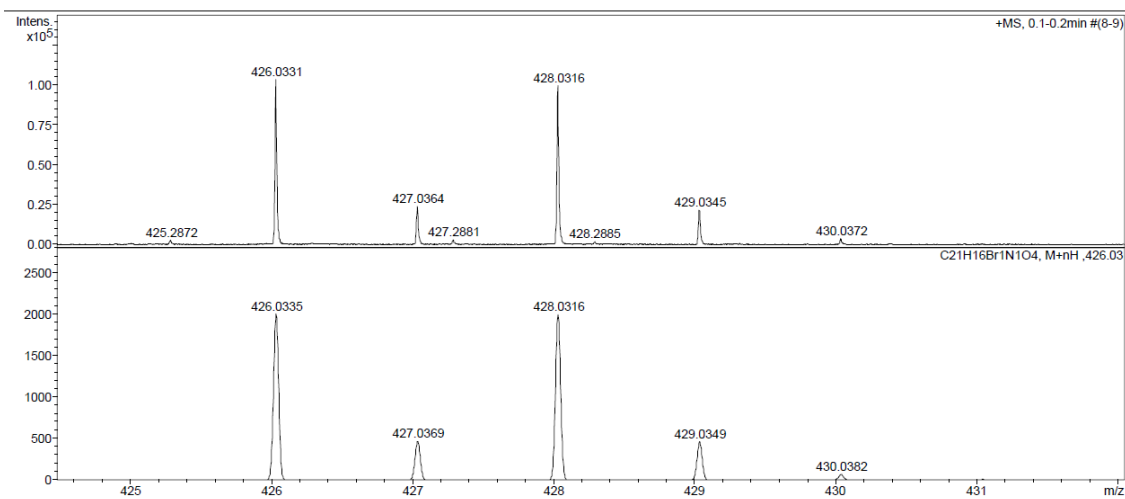
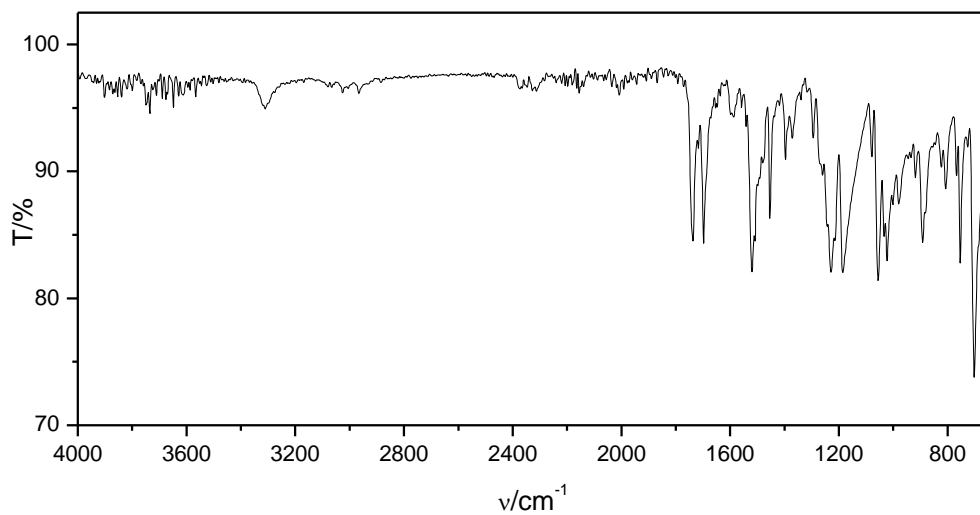
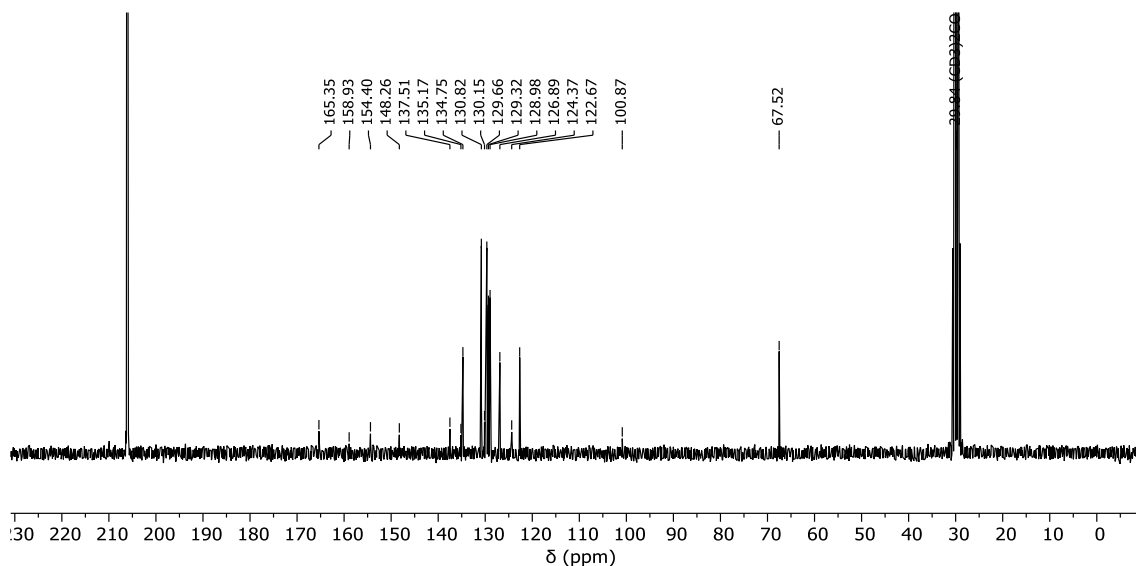


9 Appendices

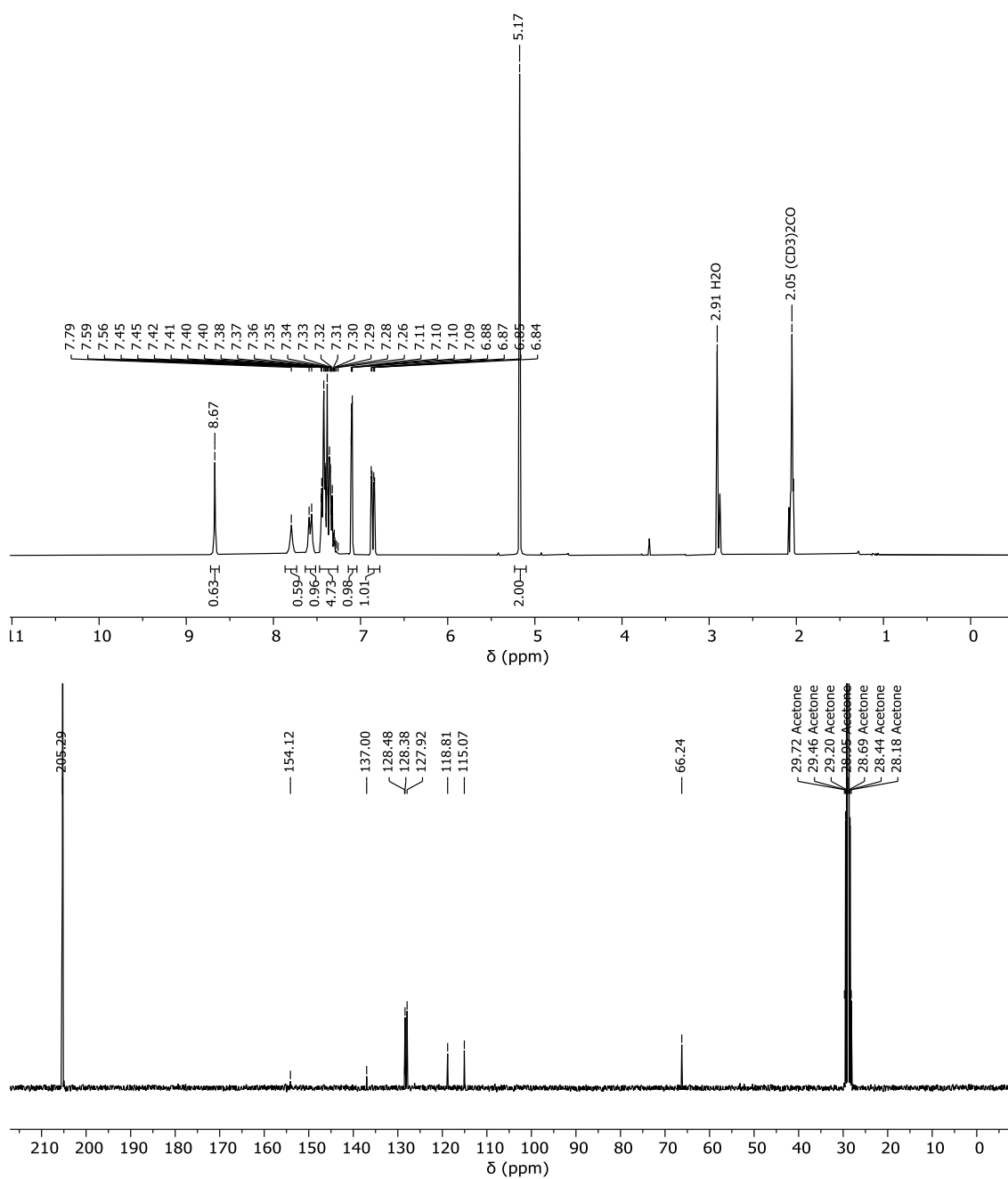


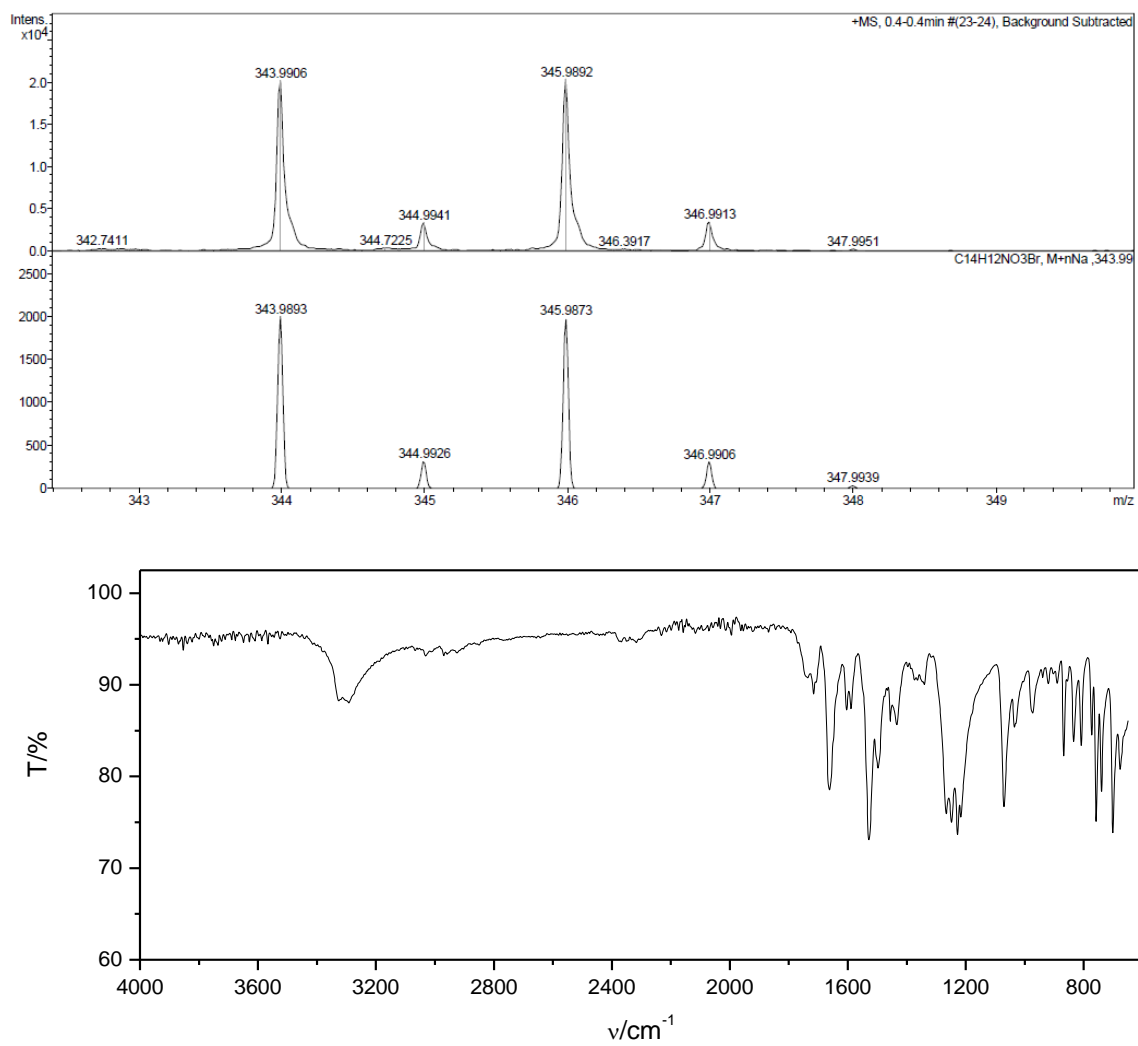
9.6.29 4-(((Benzyloxy)carbonyl)amino)-3-bromophenyl benzoate (58)



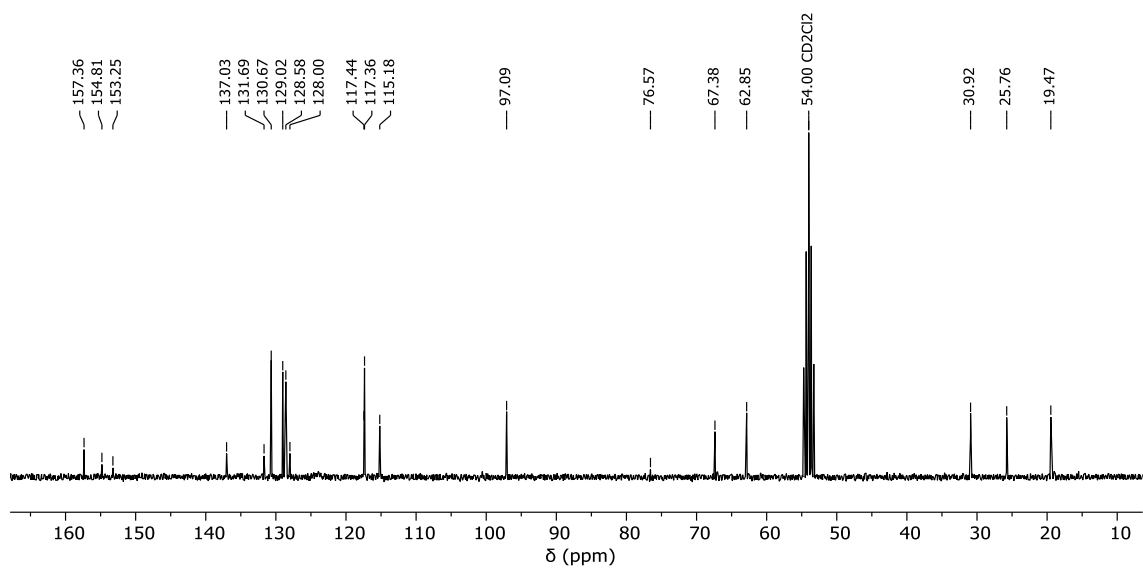
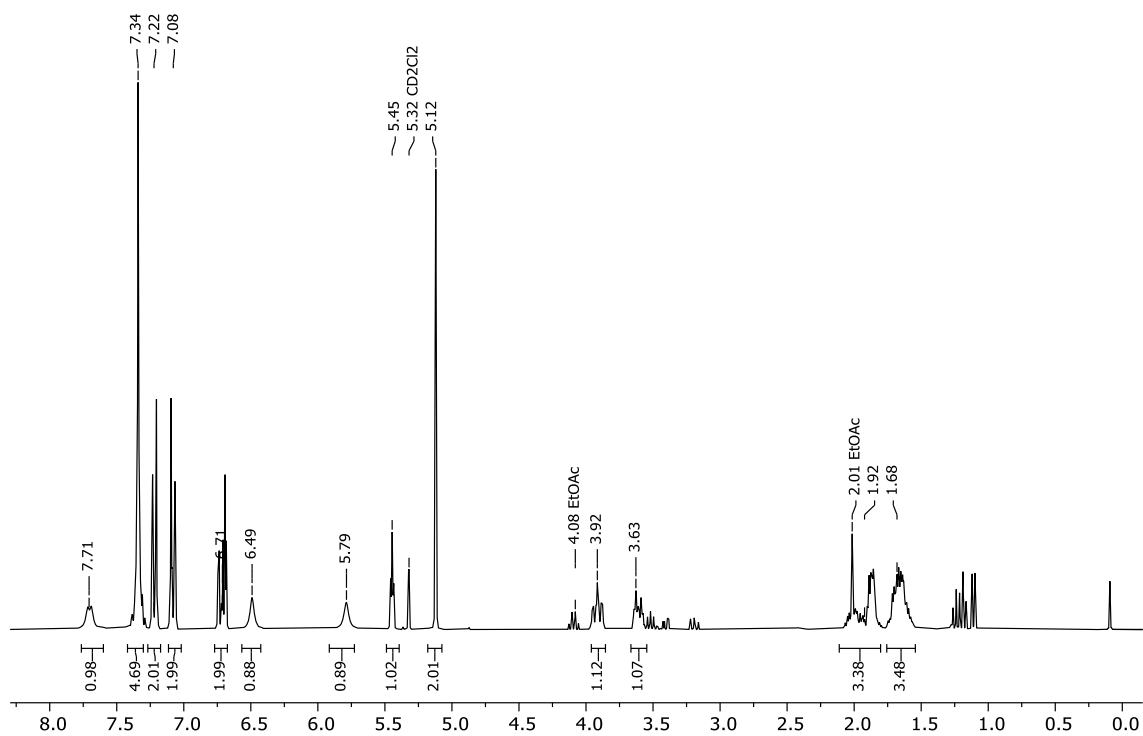


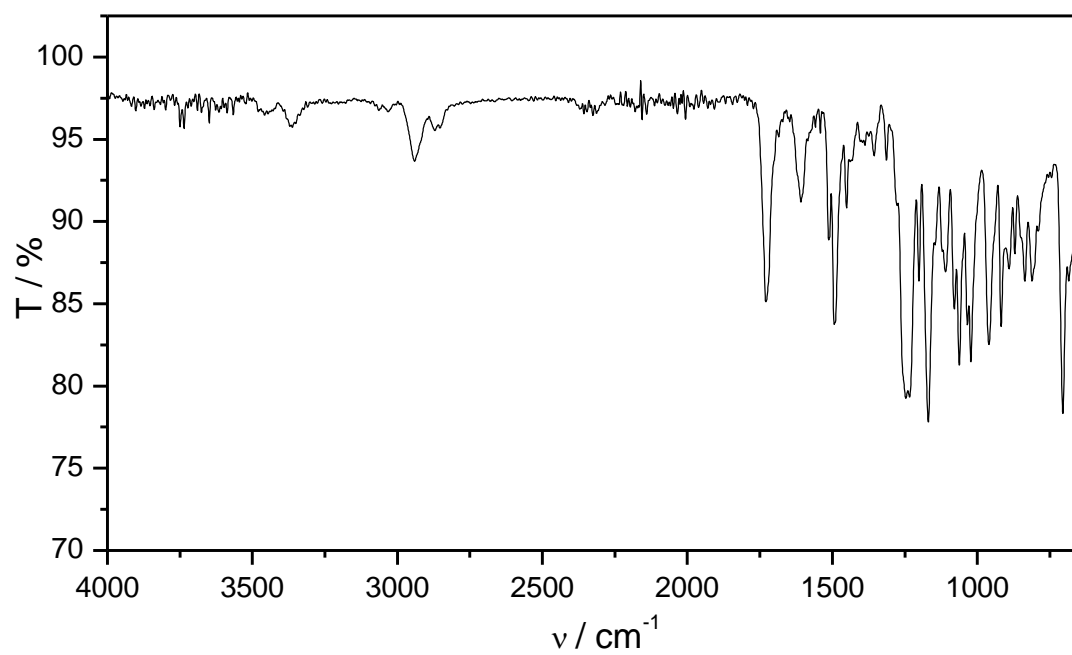
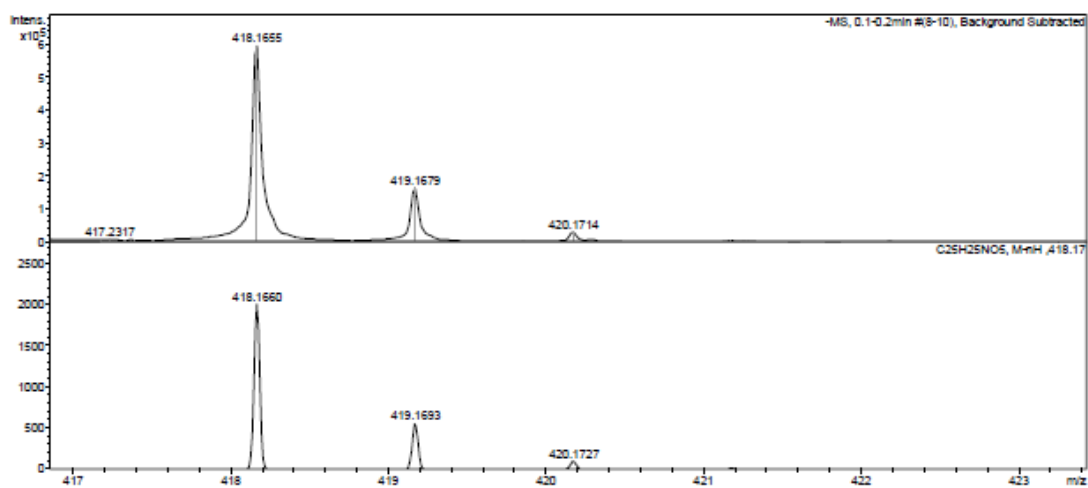
9.6.30 Benzyl (2-bromo-4-hydroxyphenyl)carbamate (59)



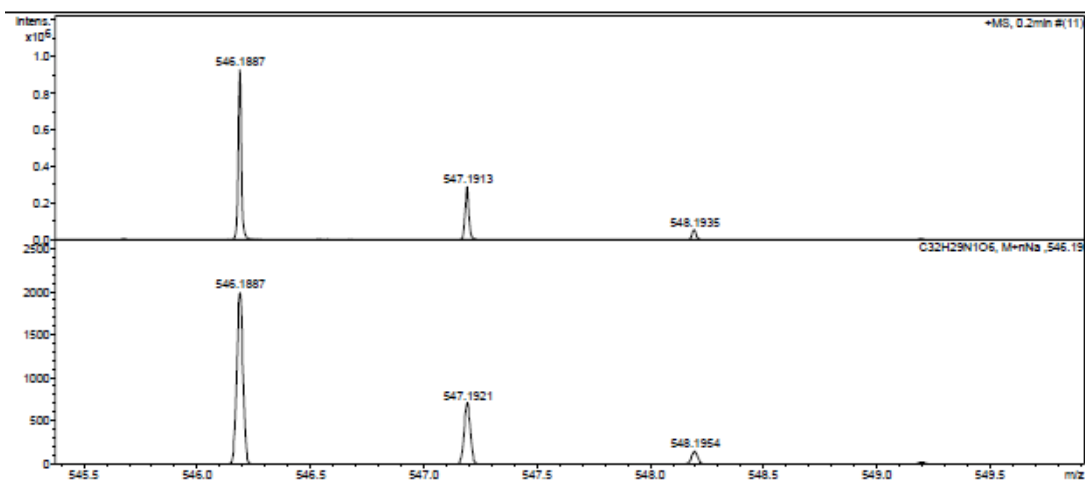
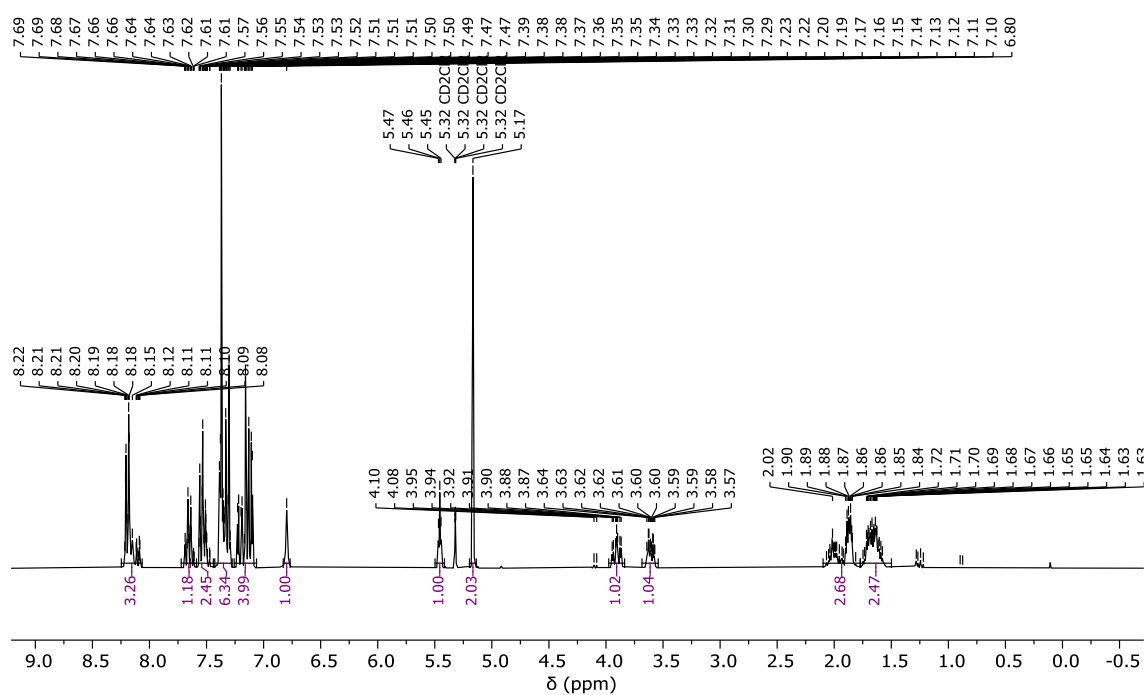
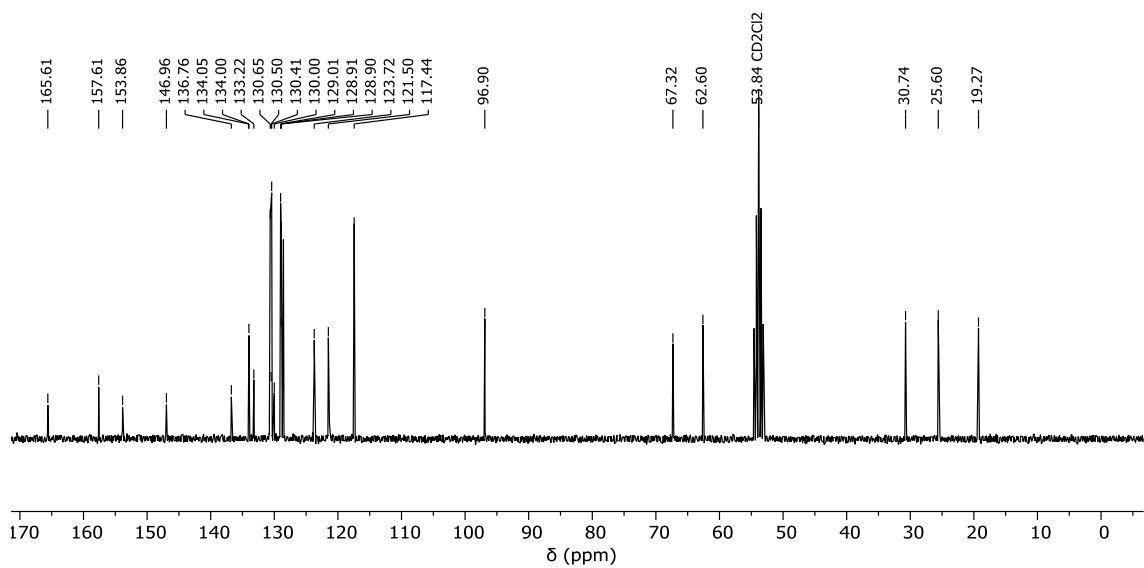


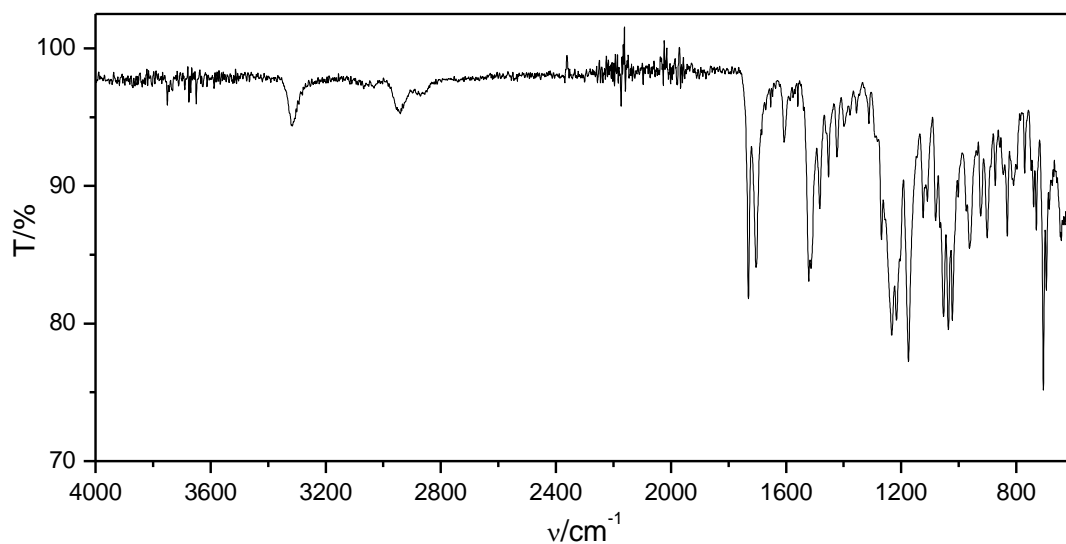
9.6.31 Benzyl (5-hydroxy-4'-((tetrahydro-2H-pyran-2-yl)oxy)-[1,1'-biphenyl]-2-yl)carbamate (60)



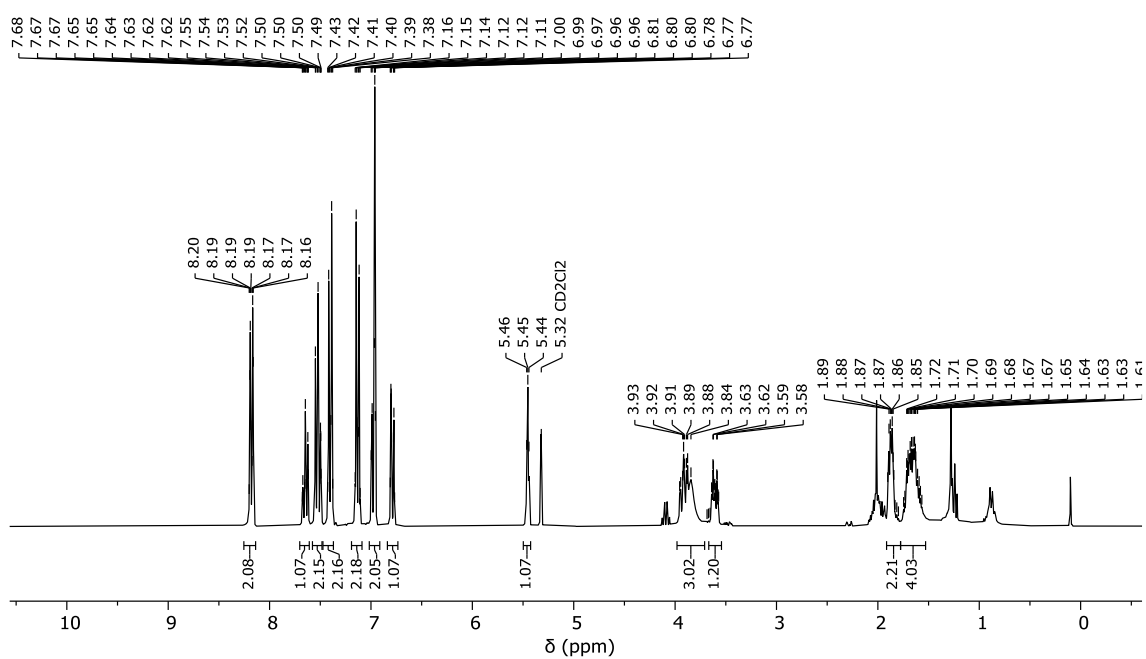


9.6.32 6-(((Benzyloxy)carbonyl)amino)-4'-((tetrahydro-2H-pyran-2-yl)oxy)-[1,1'-biphenyl]-3-yl benzoate (61)

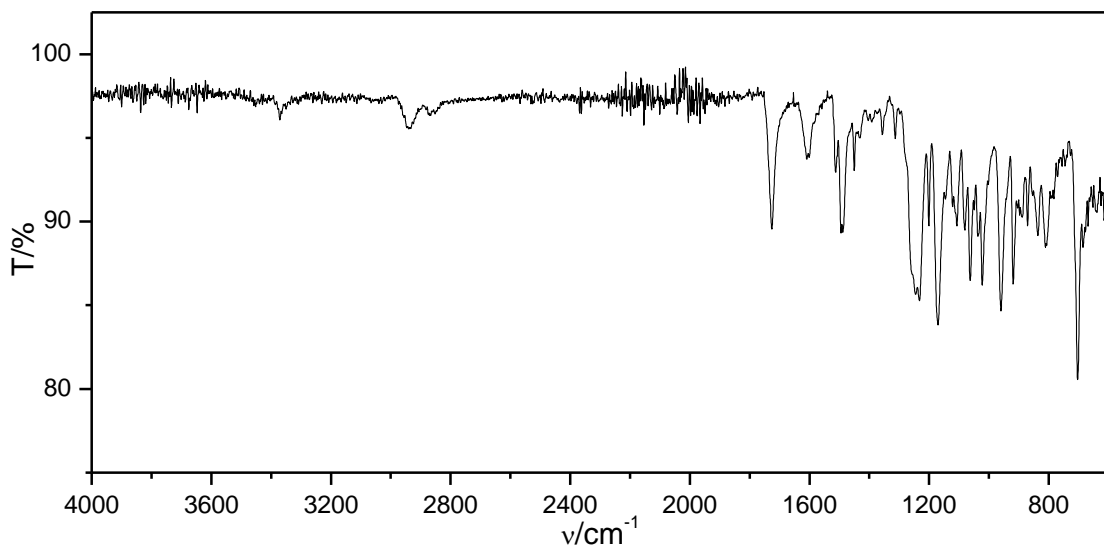
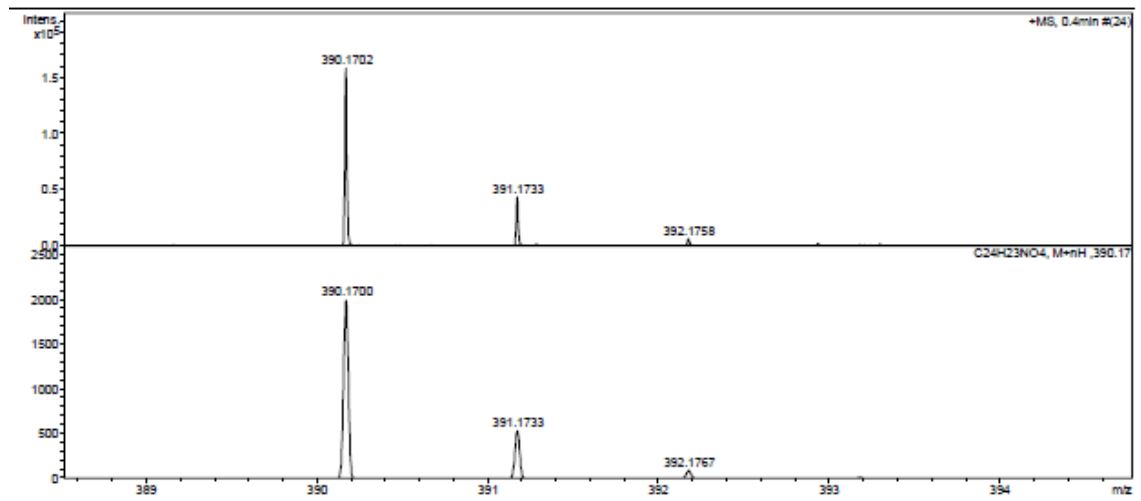
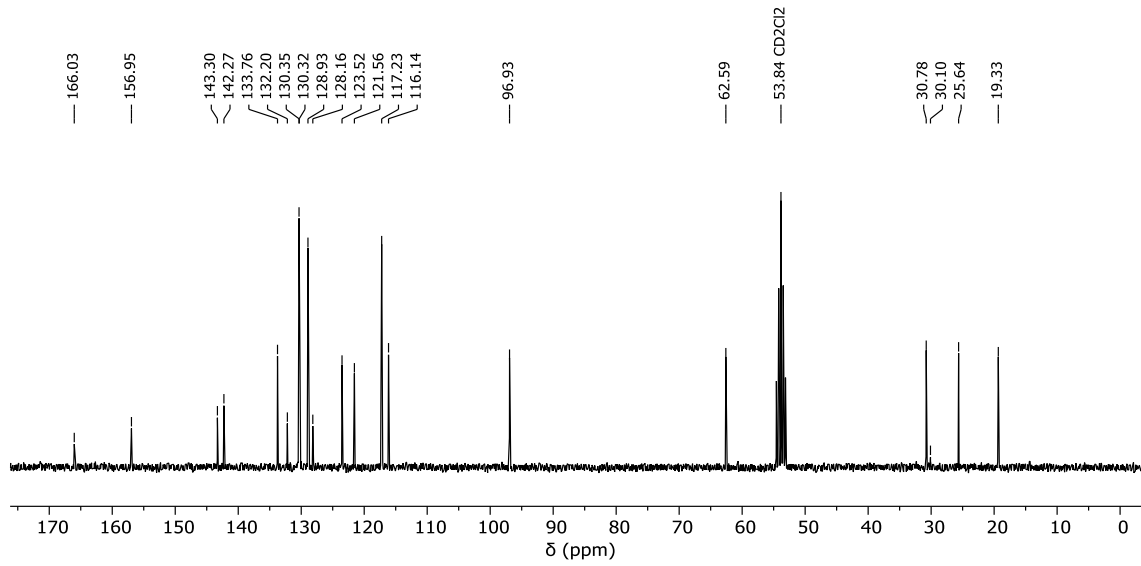




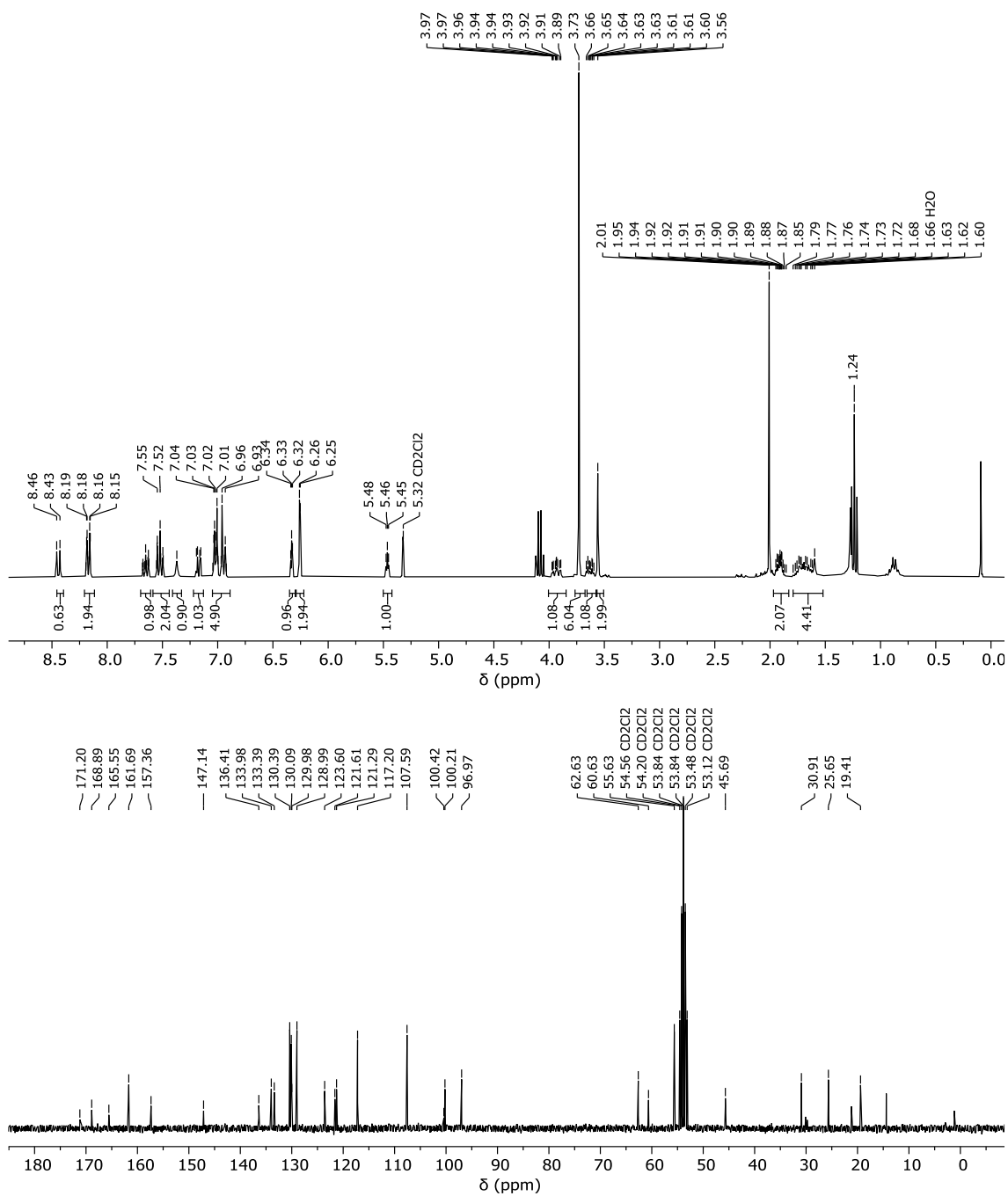
9.6.33 6-Amino-4'-((tetrahydro-2H-pyran-2-yl)oxy)-[1,1'-biphenyl]-3-yl benzoate (62)

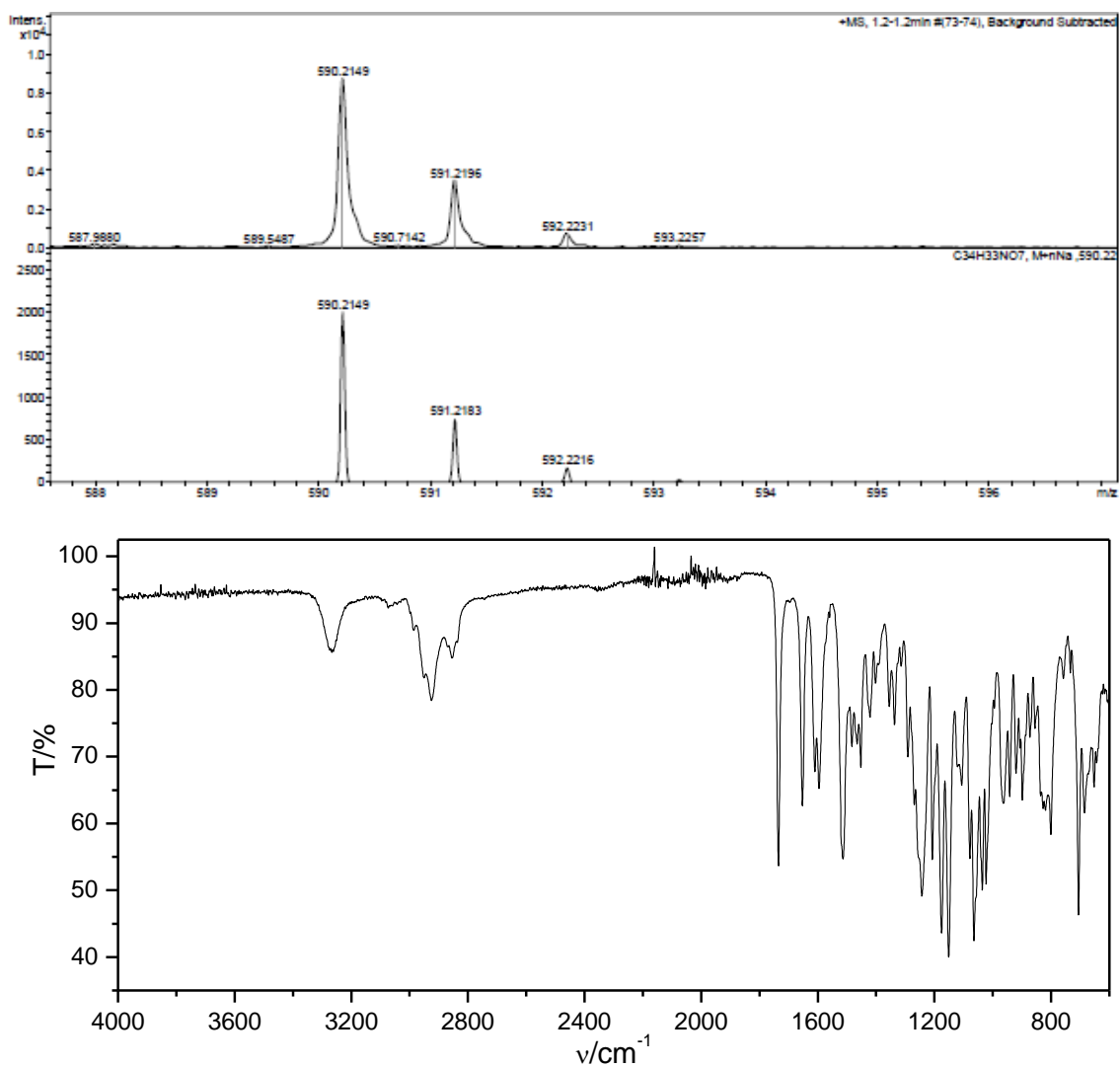


9 Appendices

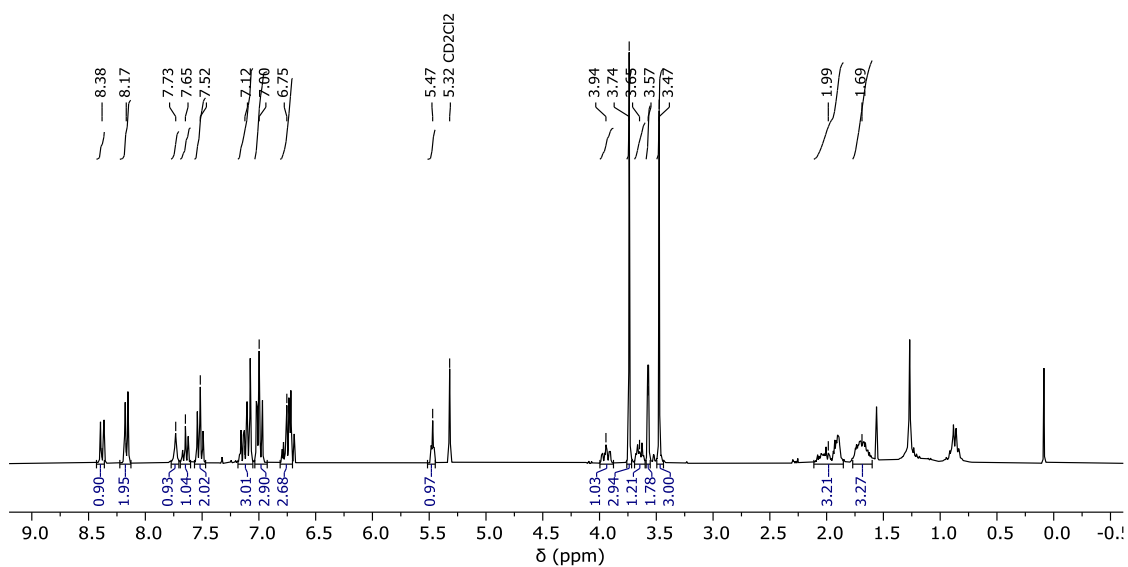


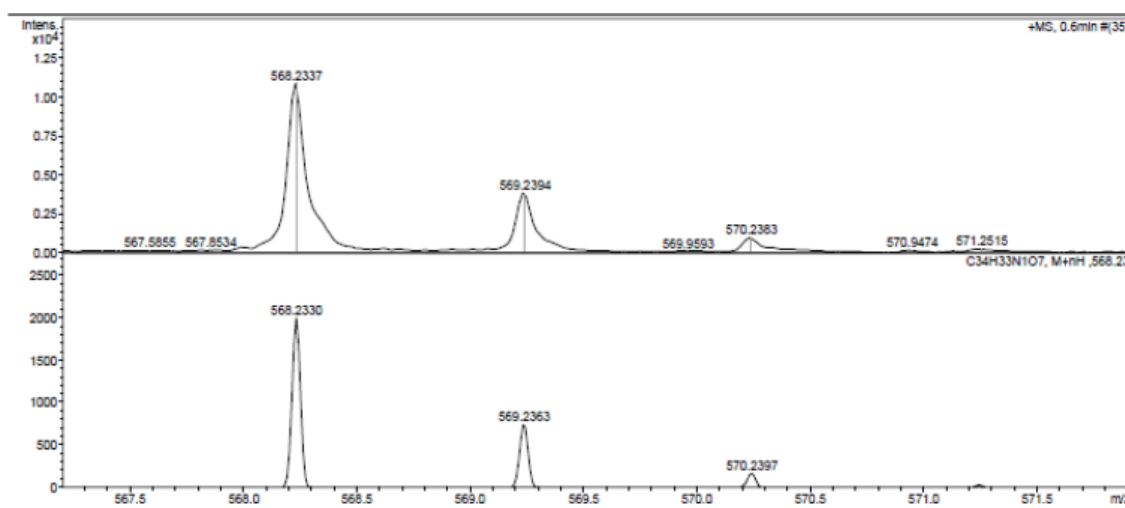
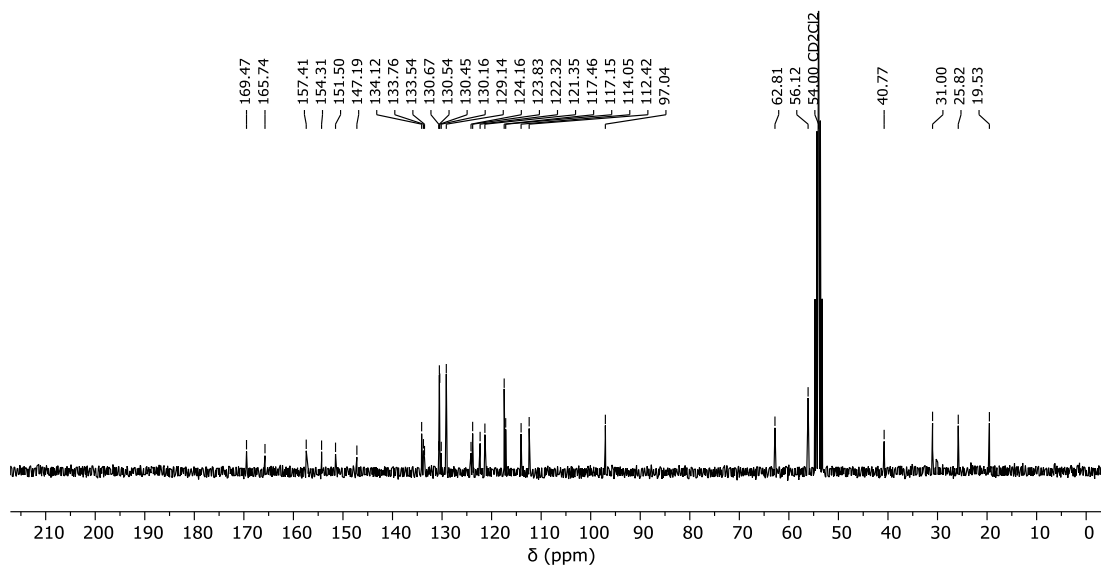
9.6.34 6-(2-(3,5-Dimethoxyphenyl)acetamido)-4'-((tetrahydro-2H-pyran-2-yl)oxy)-[1,1'-biphenyl]-3-yl benzoate (63)



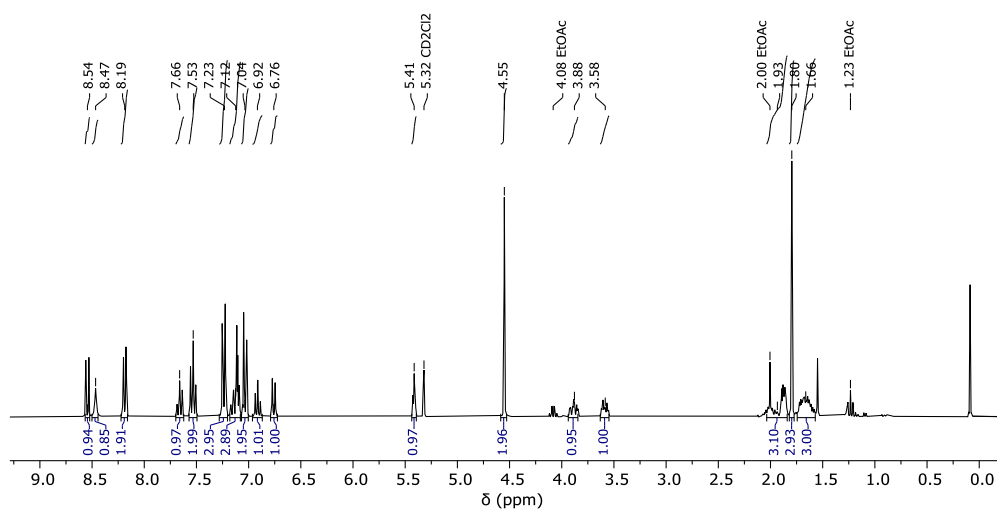


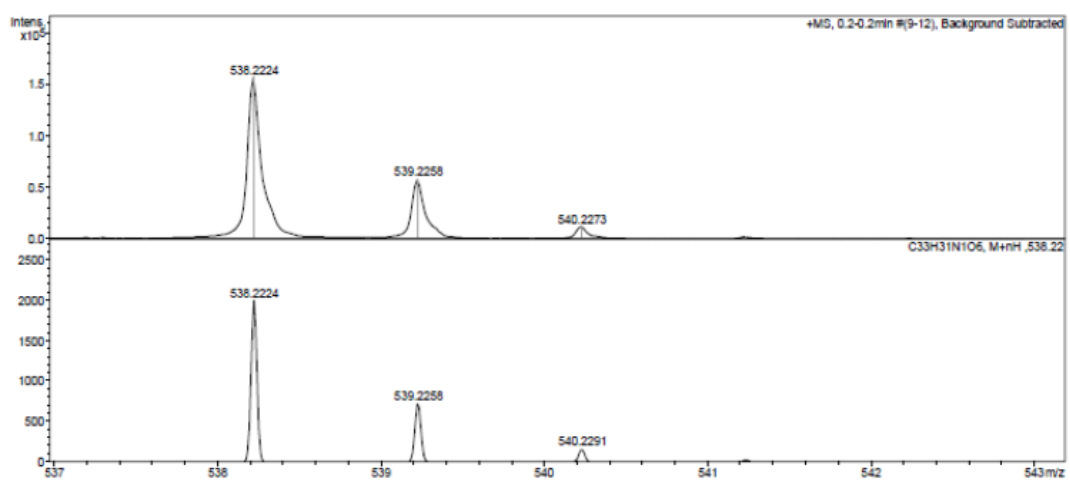
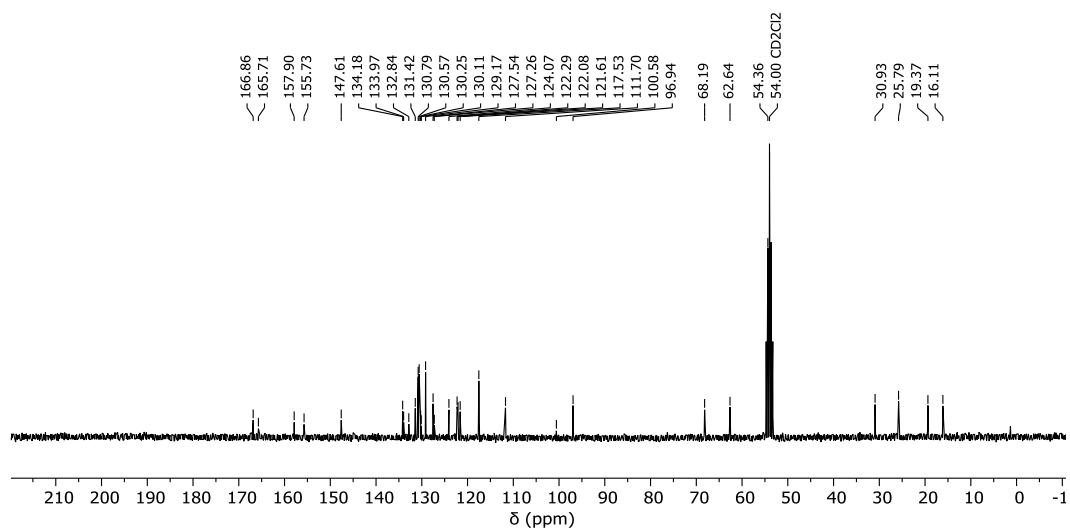
9.6.35 4'-((Tetrahydro-2*H*-pyran-2-yl)oxy)-6-(2-(*o*-tolyl)oxy)acetamido)-[1,1'-biphenyl]- 3-yl benzoate (64)



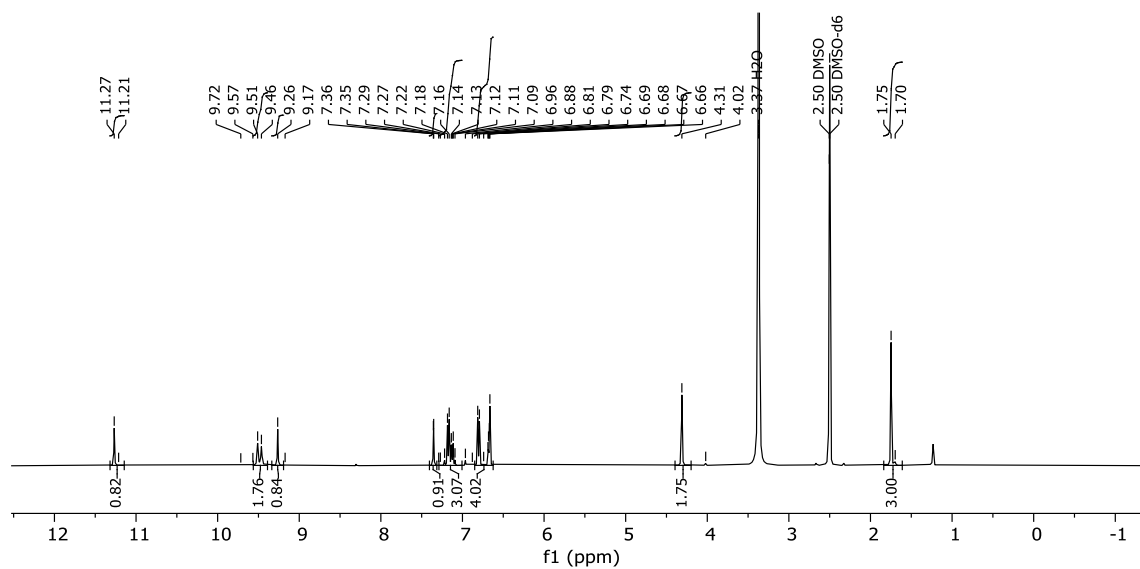


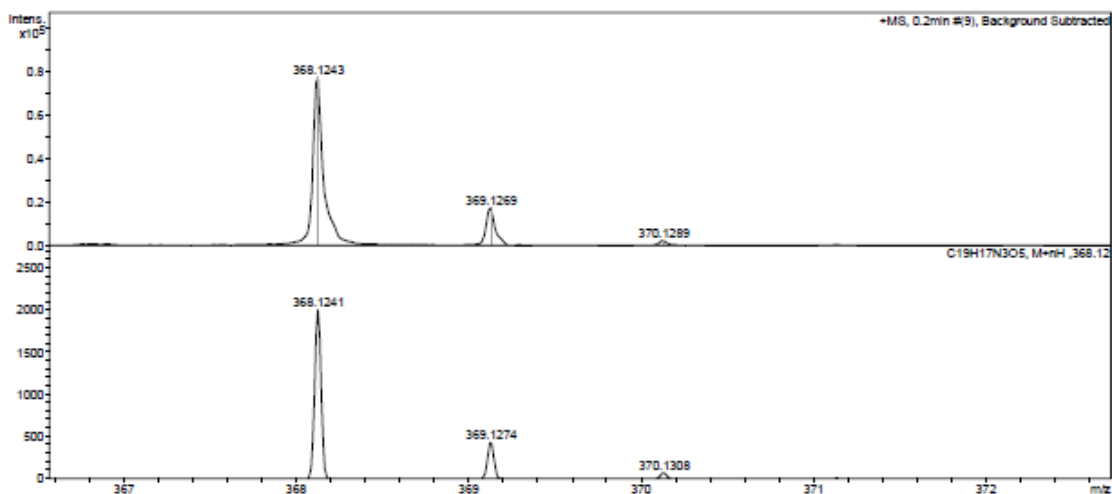
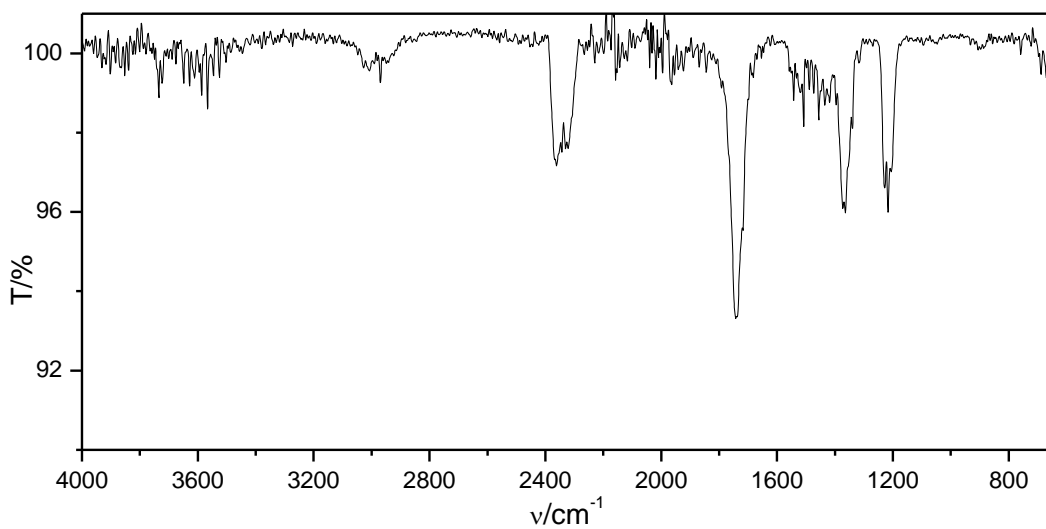
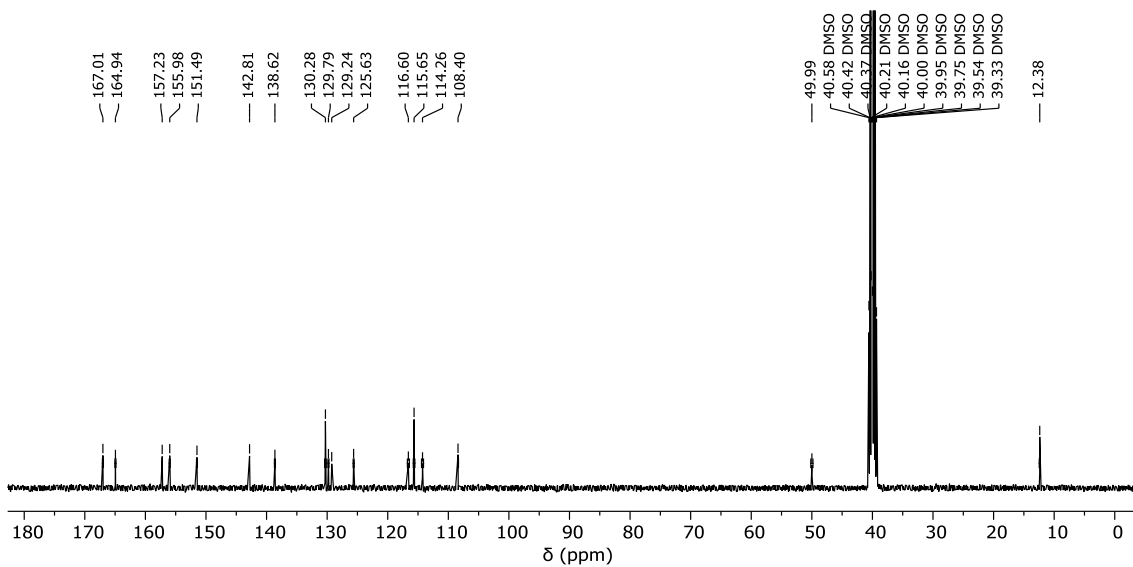
9.6.36 4'-((Tetrahydro-2H-pyran-2-yl)oxy)-6-(2-(o-tolyloxy)acetamido)-[1,1'-biphenyl]- 3-yl benzoate (65)



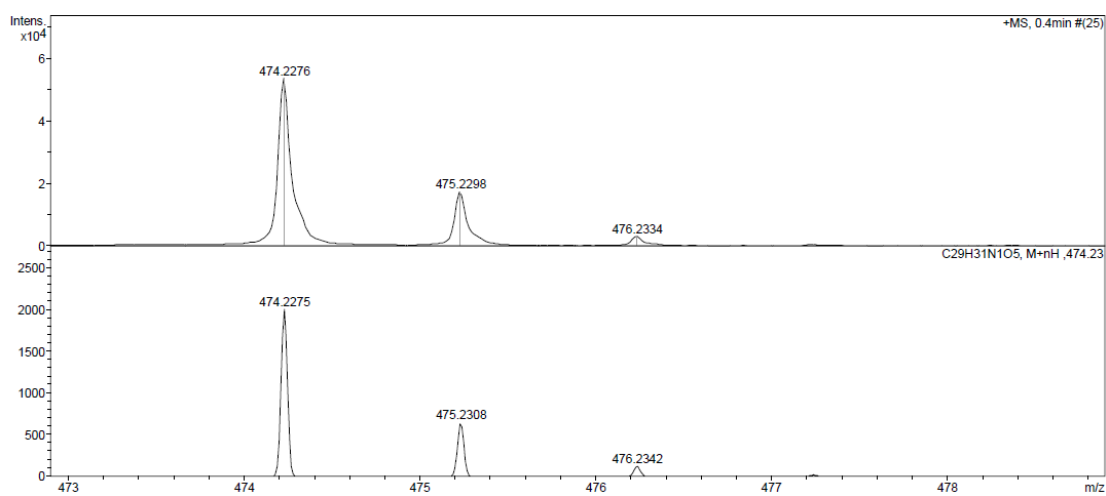
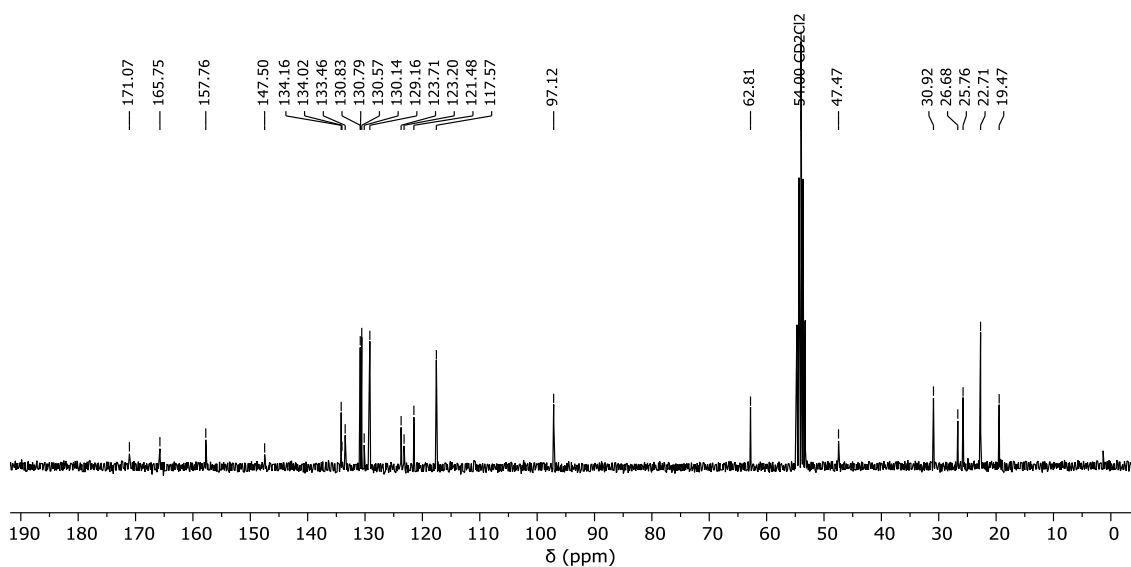
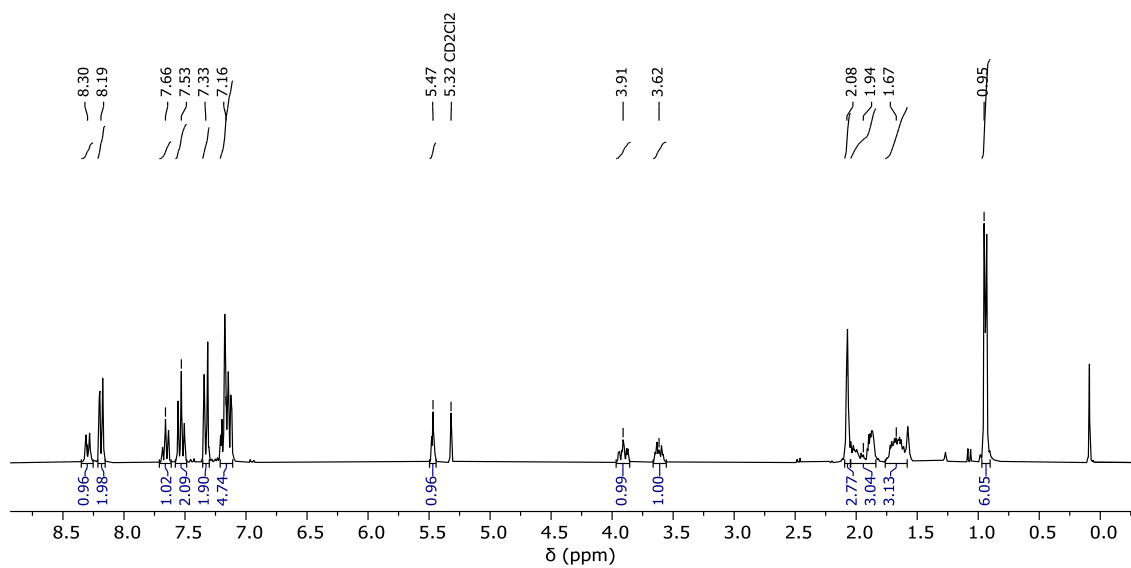


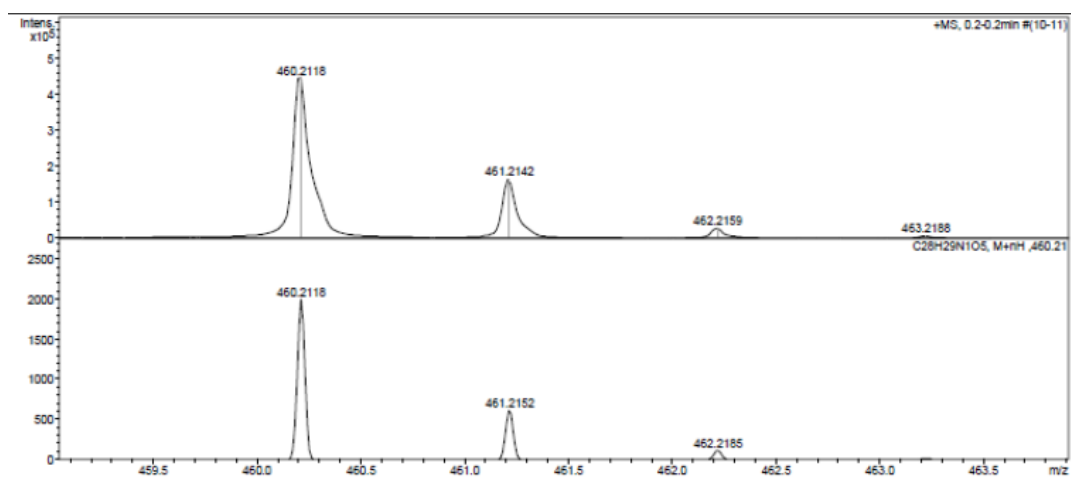
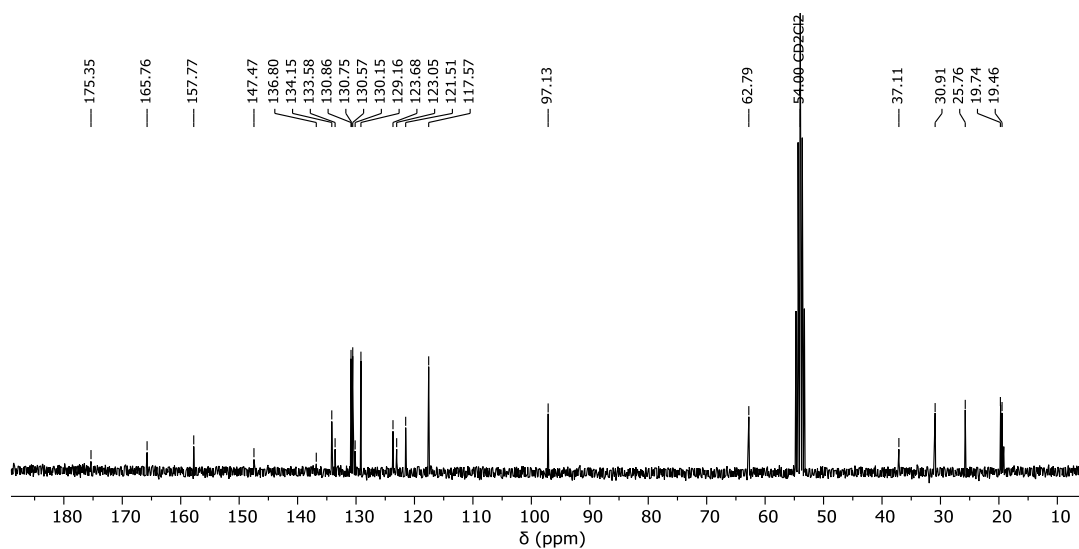
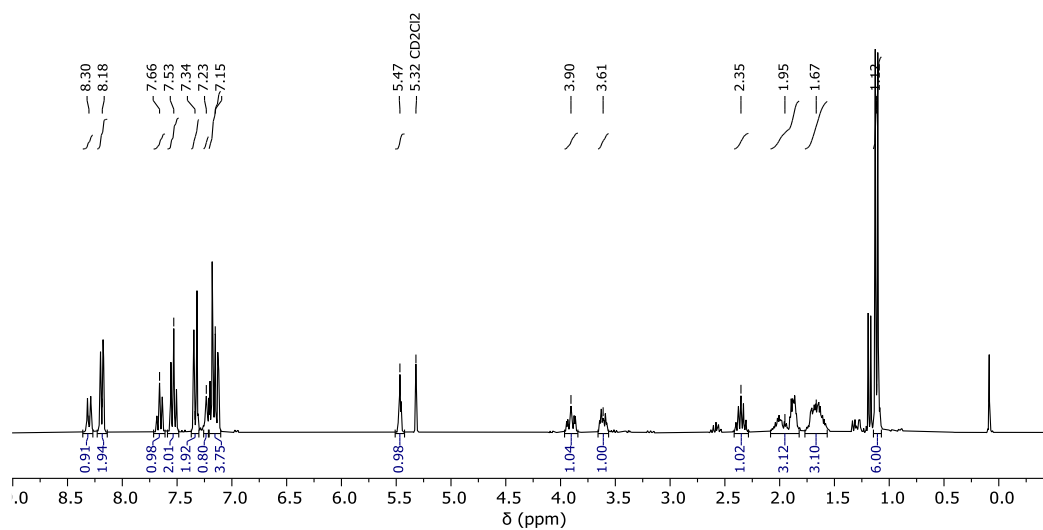
9.6.37 *N*-(4',5-Dihydroxy-[1,1'-biphenyl]-2-yl)-2-(5-methyl-2,4-dioxo-3,4-dihydropyrimidin-1(2H)-yl)acetamide (67)

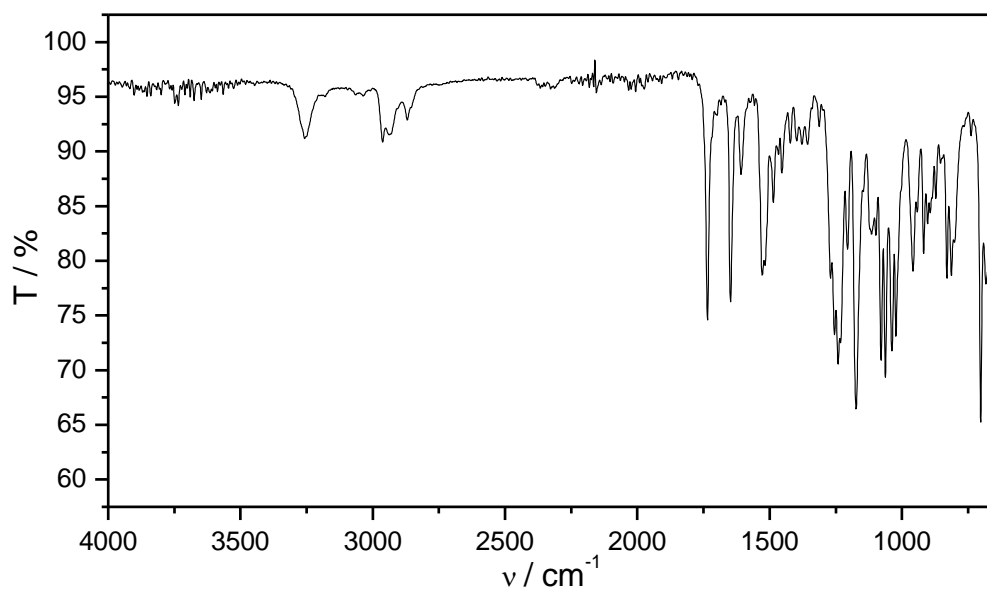


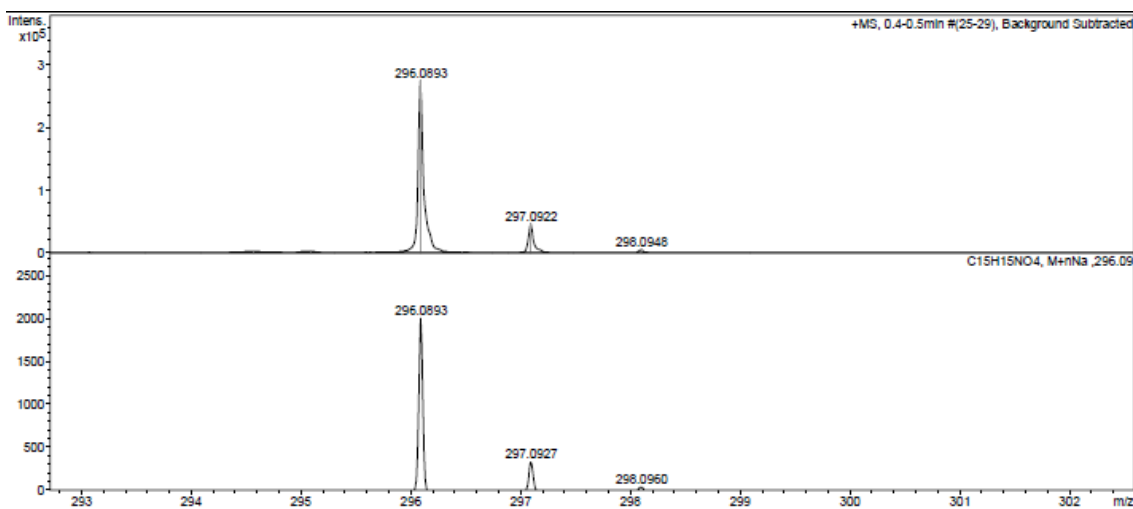
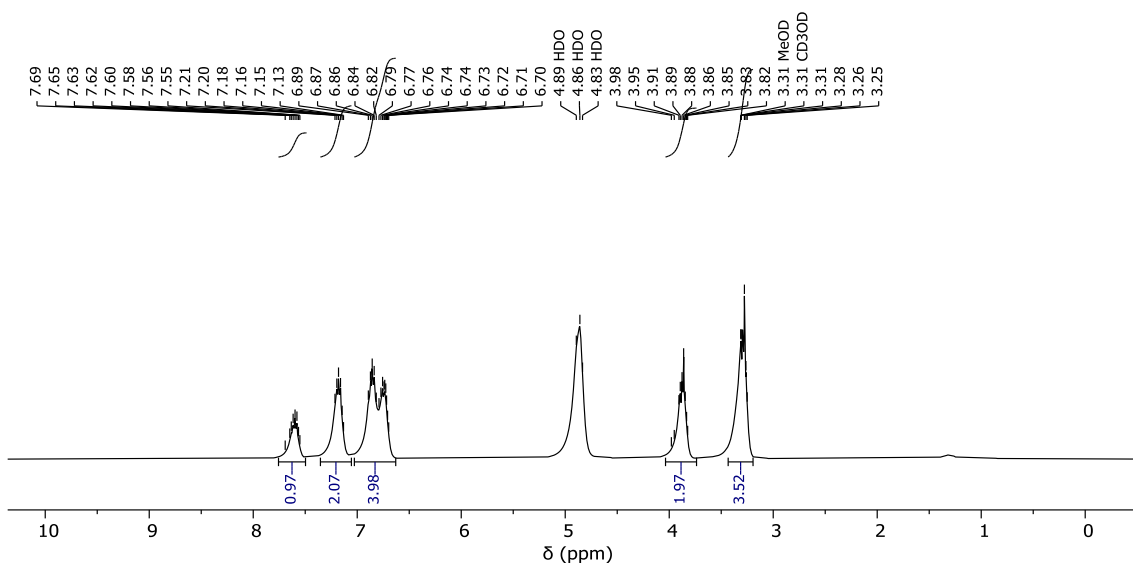
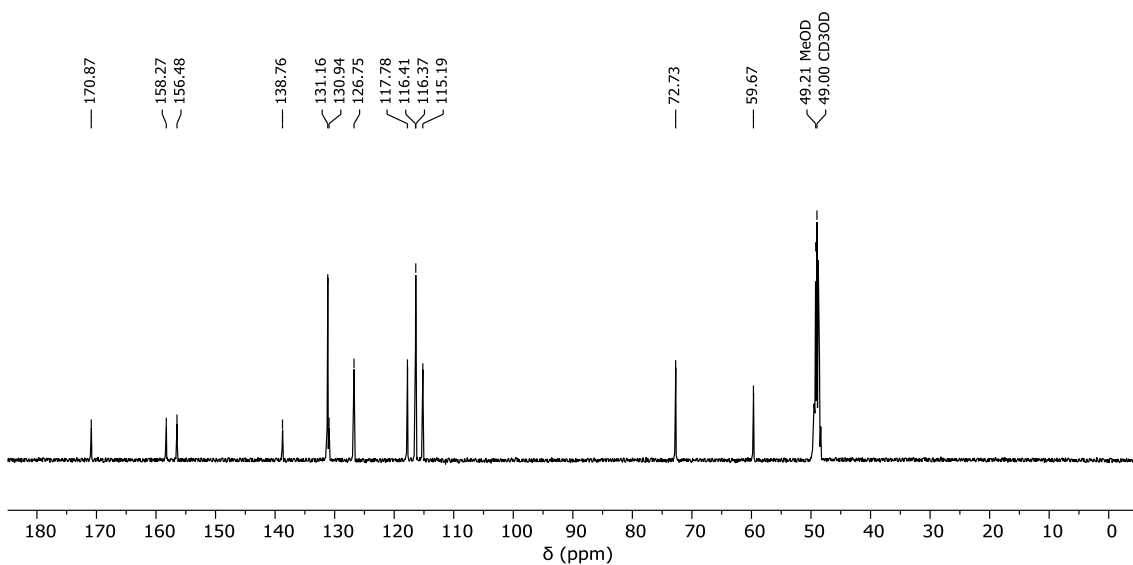


9.6.38 6-(3-Methylbutanamido)-4'-((tetrahydro-2H-pyran-2-yl)oxy)-[1,1'-biphenyl]-3-yl benzoate (68)

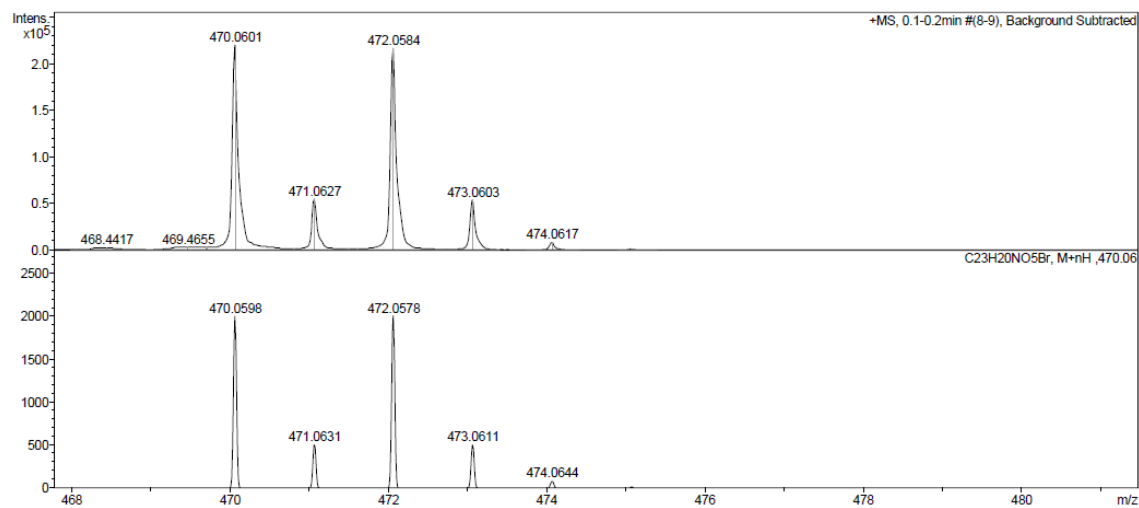
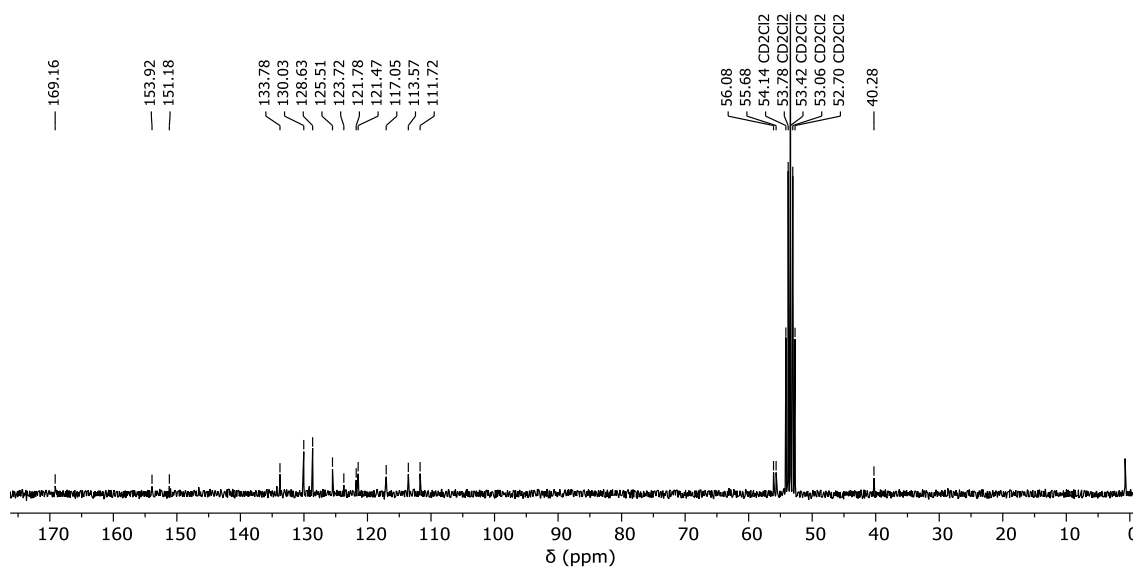
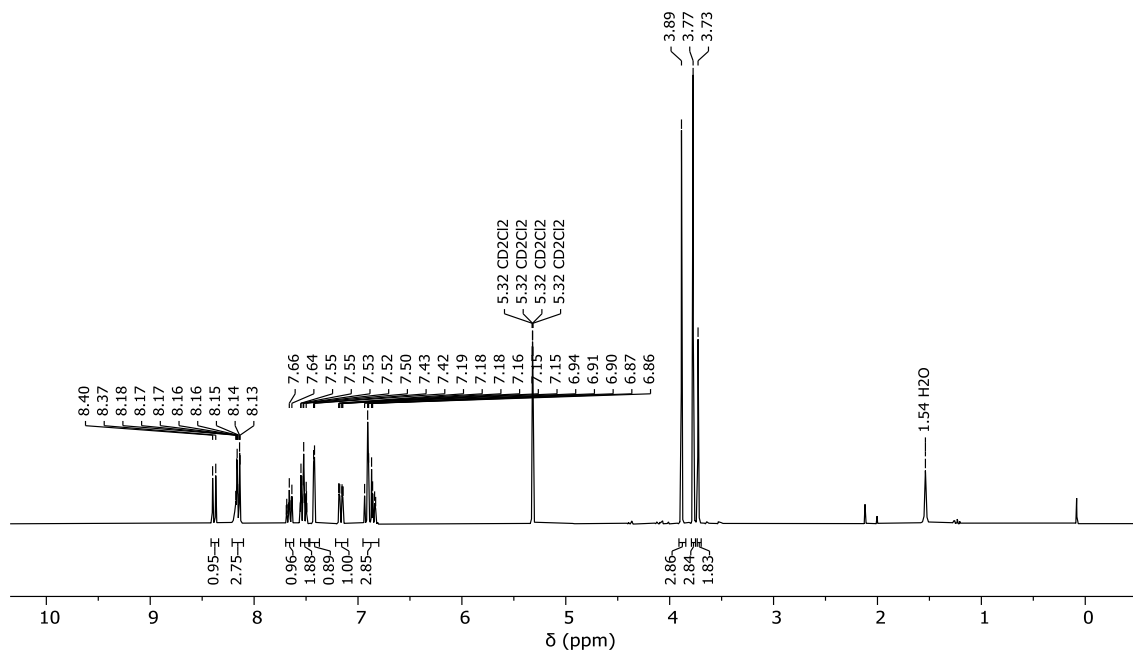


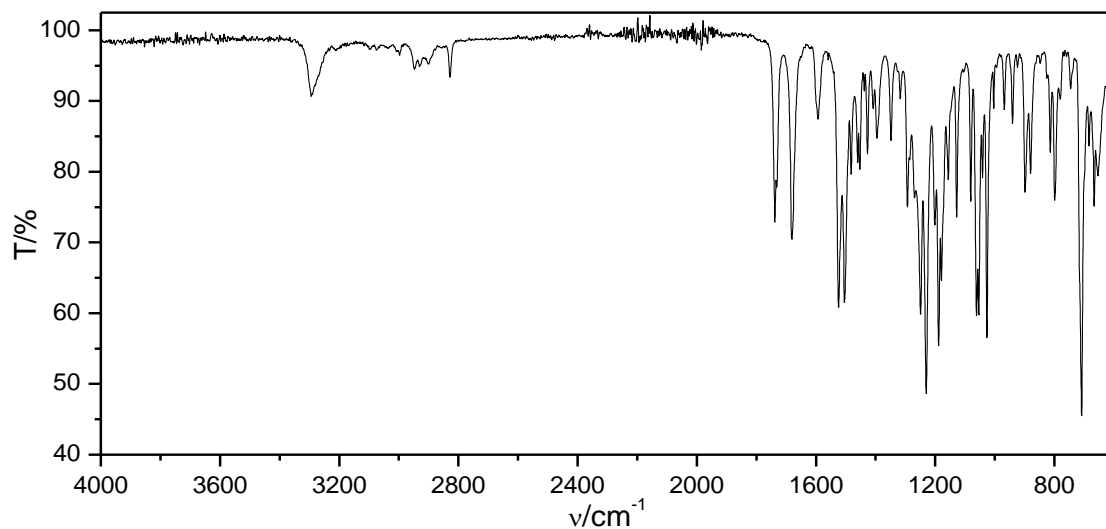
9.6.39 6-Isobutyramido-4'-((tetrahydro-2*H*-pyran-2-yl)oxy)-[1,1'-biphenyl]-3-yl benzoate (69)



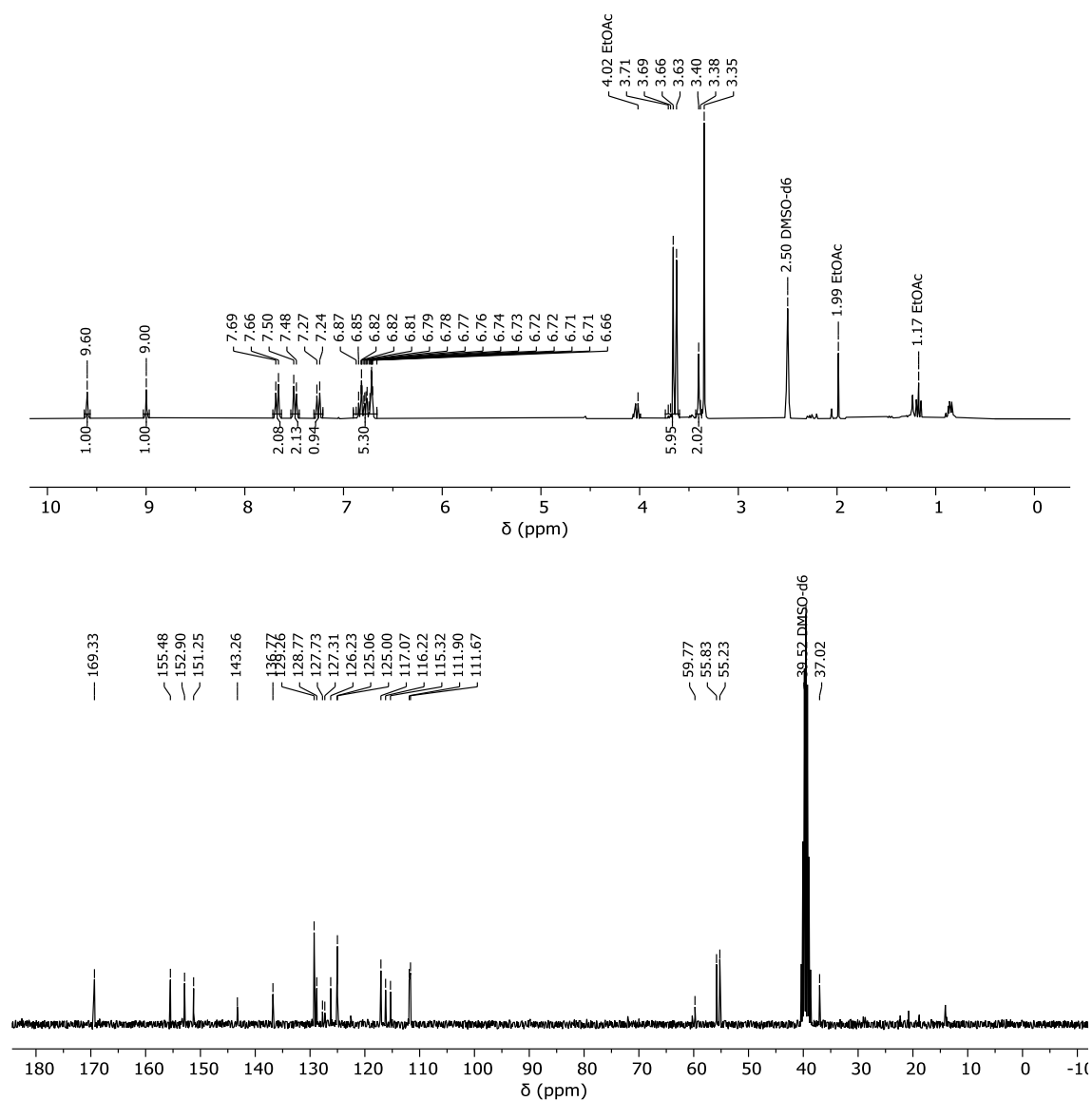
9.6.40 *N*-(4',5-Dihydroxy-[1,1'-biphenyl]-2-yl)-2-methoxyacetamide (70)

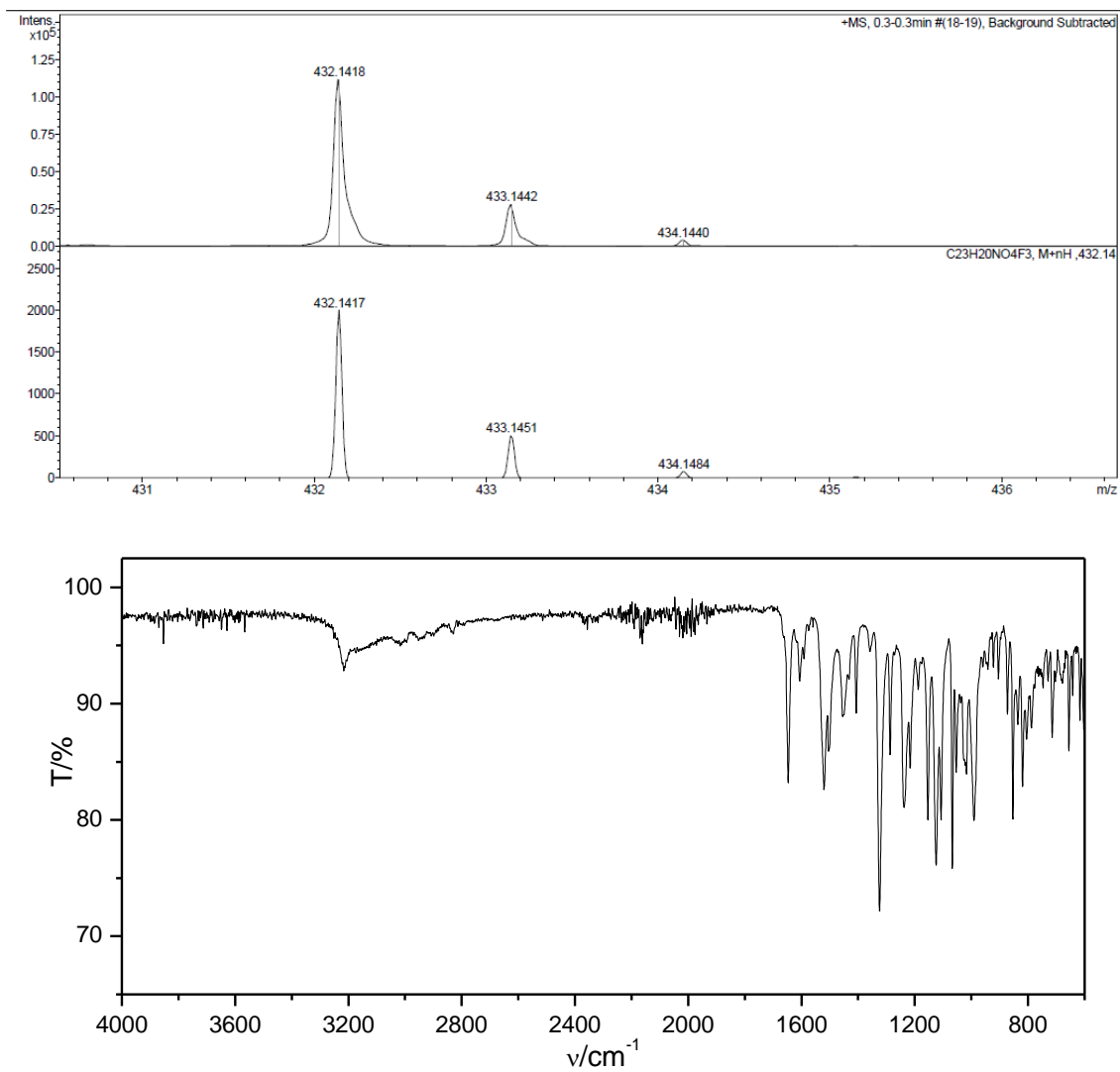
9.6.41 3-Bromo-4-(2-(2,5-dimethoxyphenyl)acetamido)phenyl benzoate (71)



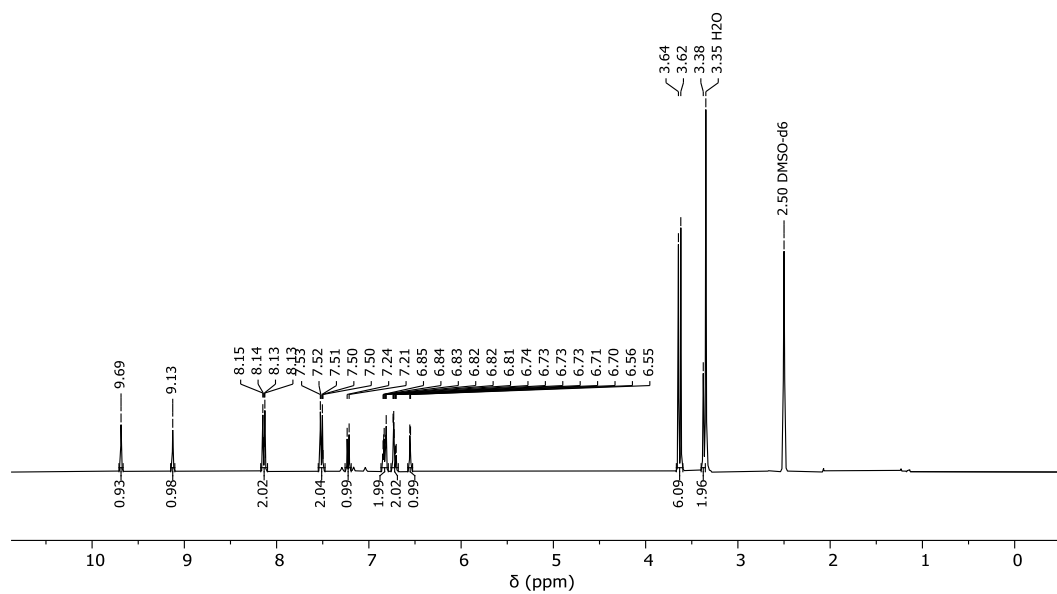


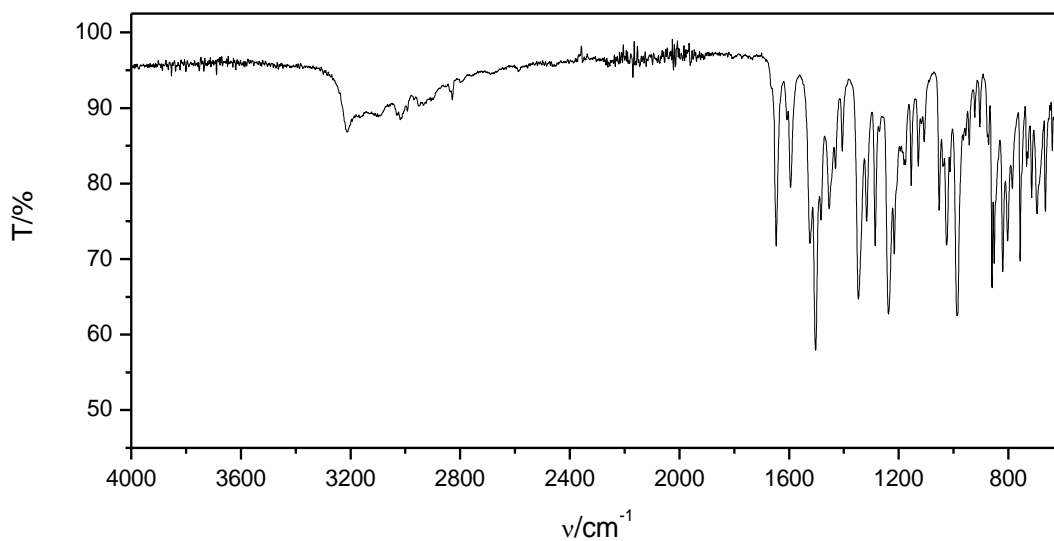
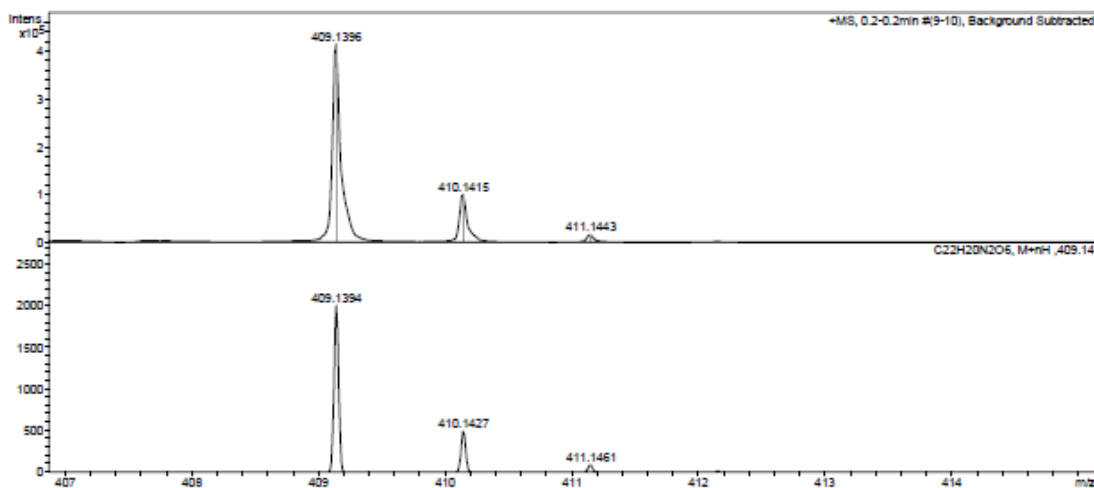
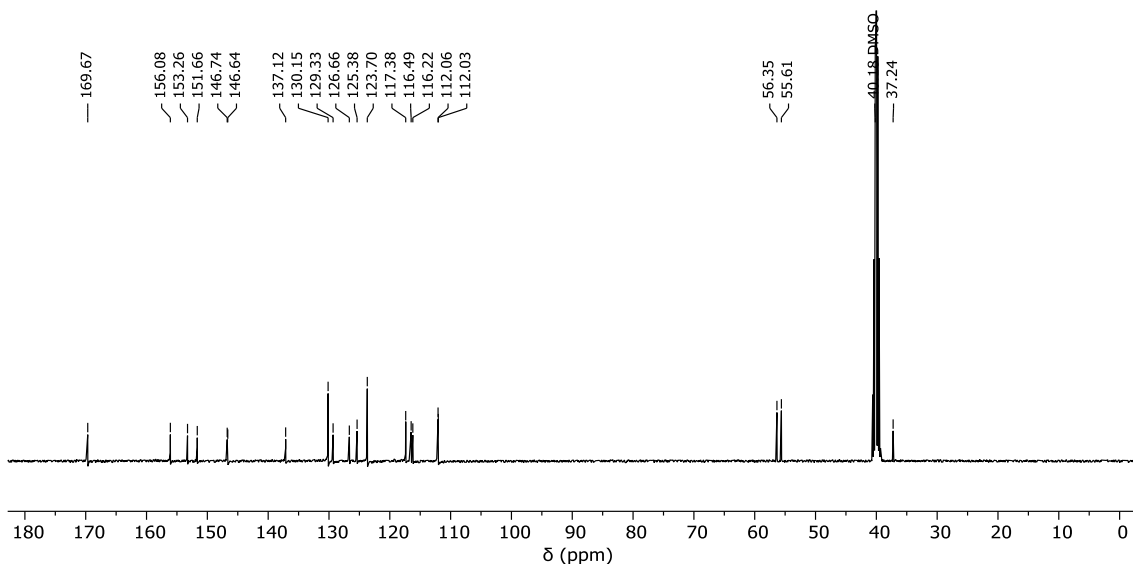
9.6.42 2-(2,5-Dimethoxyphenyl)-N-(5-hydroxy-4'-(trifluoromethyl)-[1,1'-biphenyl]-2-yl)acetamide (72)

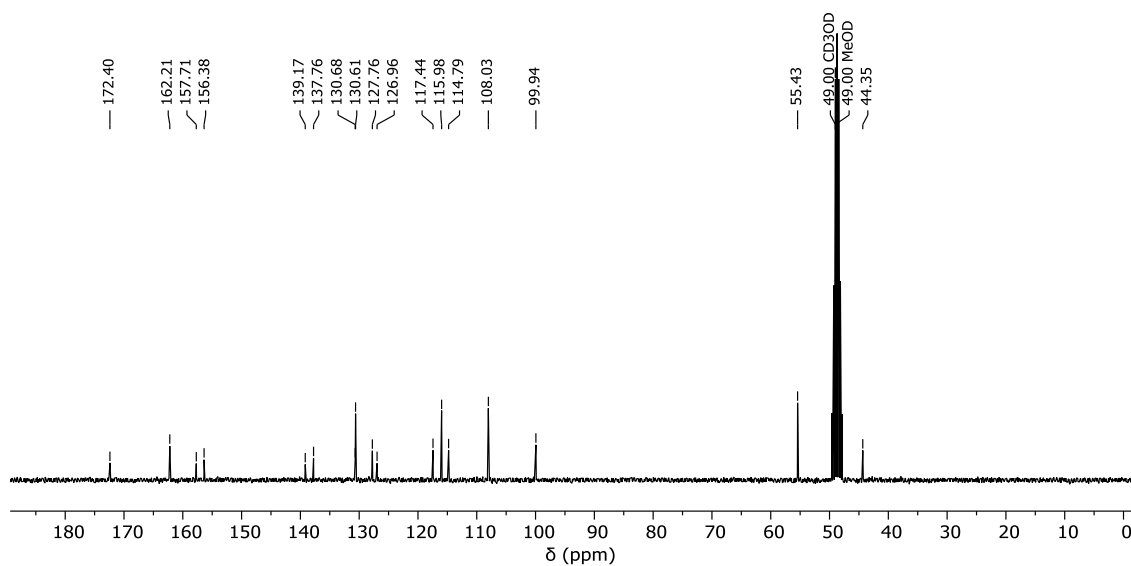
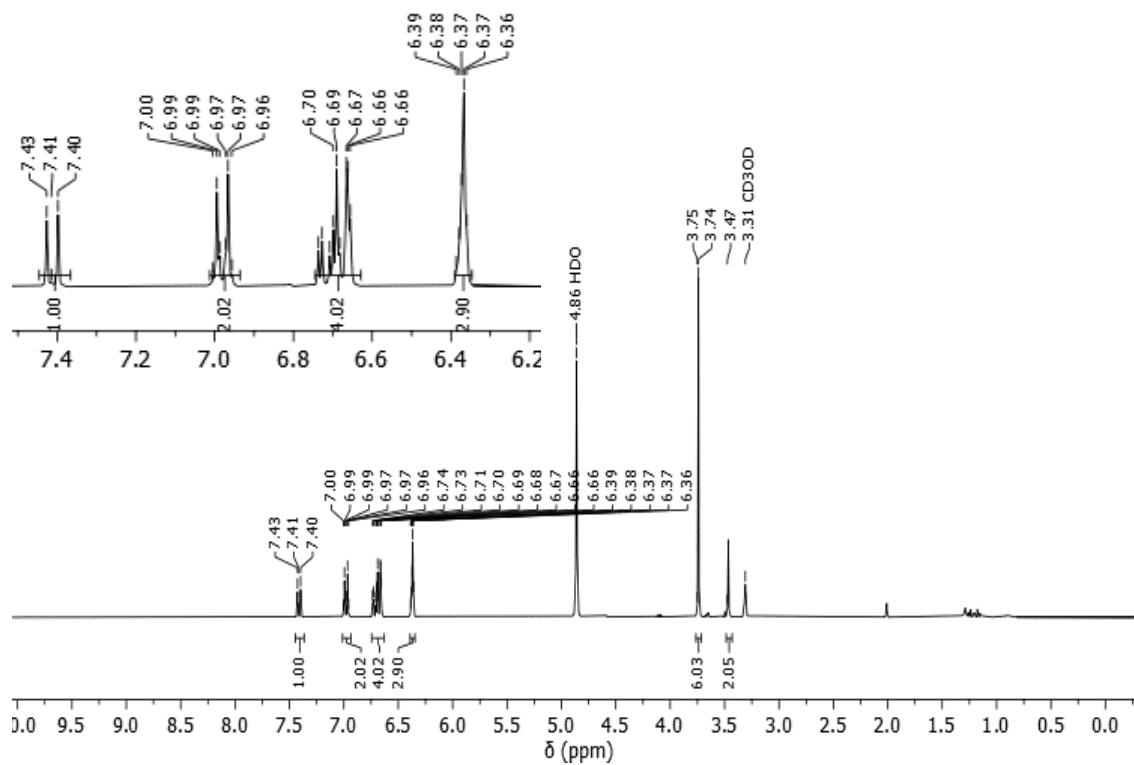


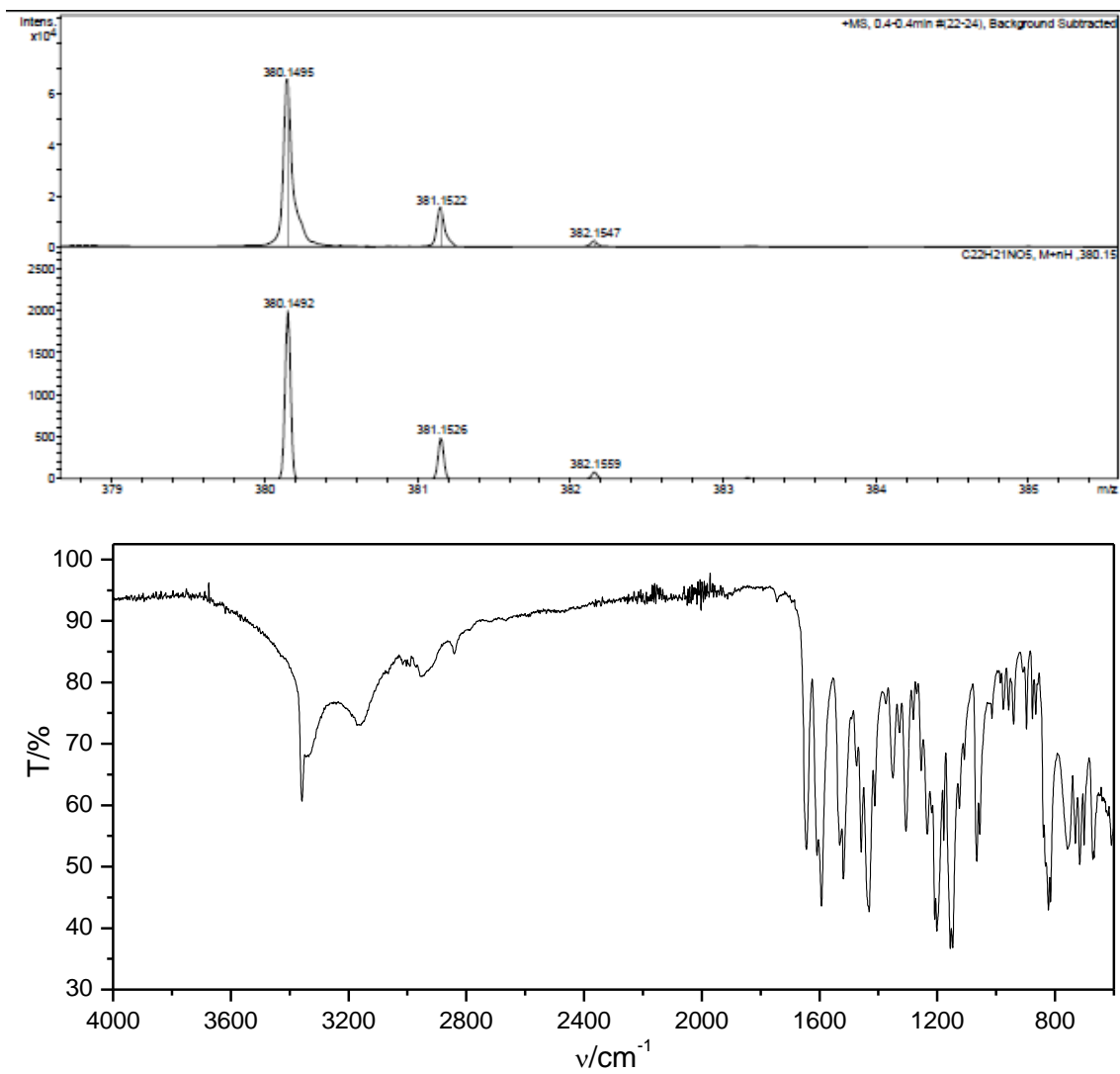


9.6.43 2-(2,5-Dimethoxyphenyl)-N-(5-hydroxy-4'-nitro-[1,1'-biphenyl]-2-yl)acetamide (73)

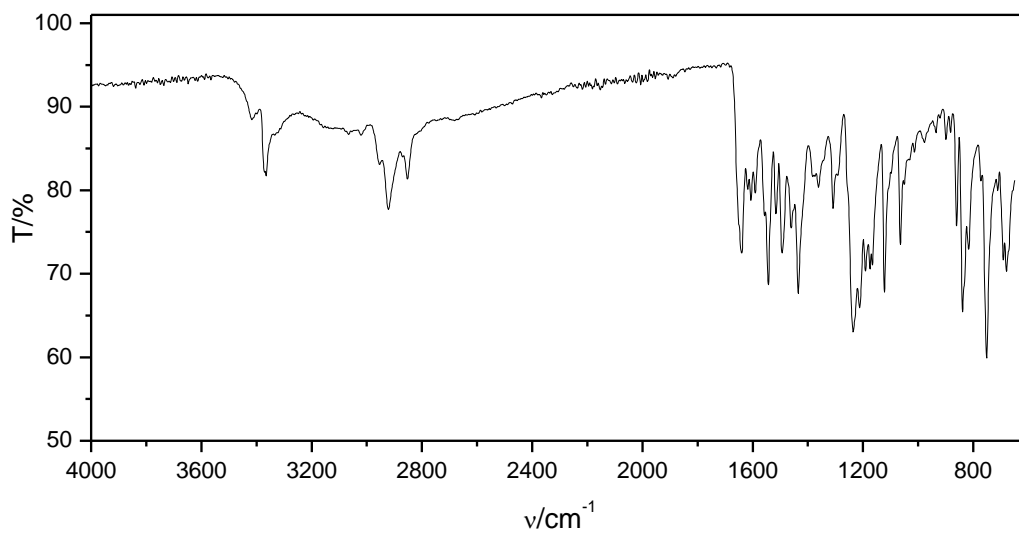
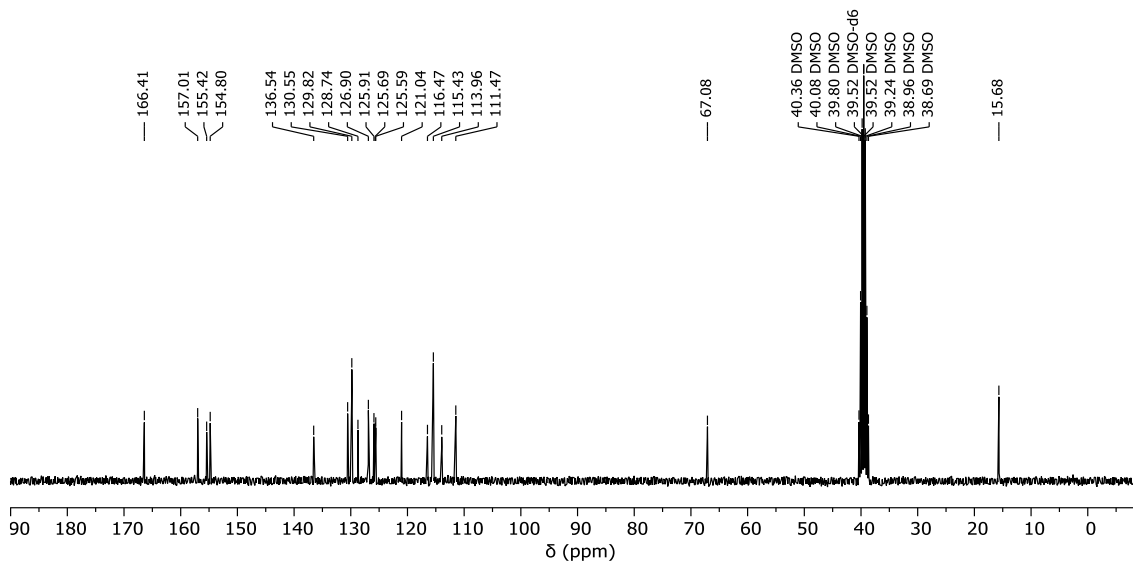
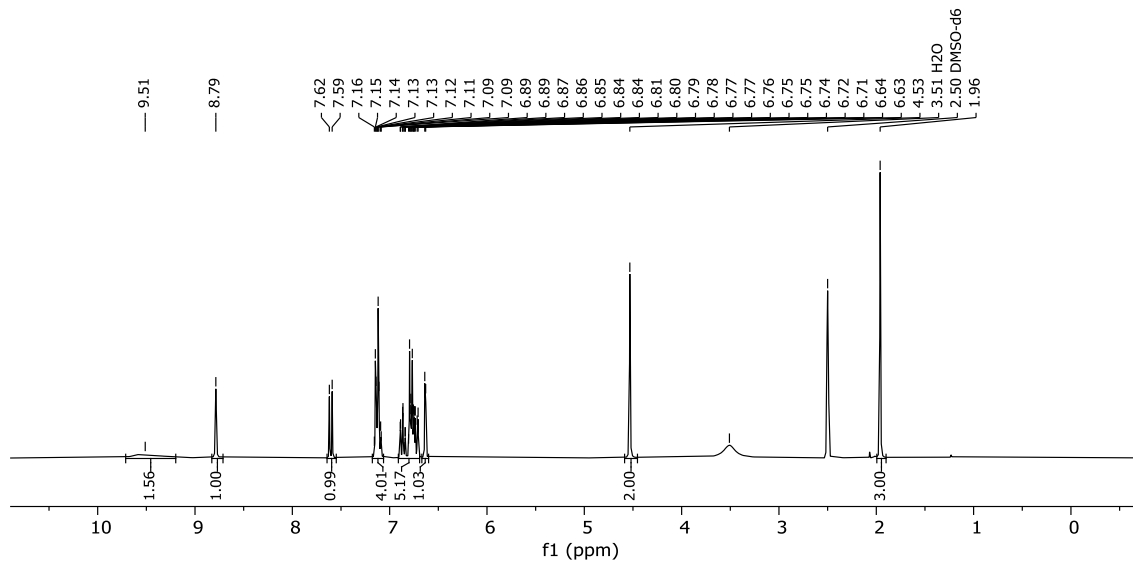


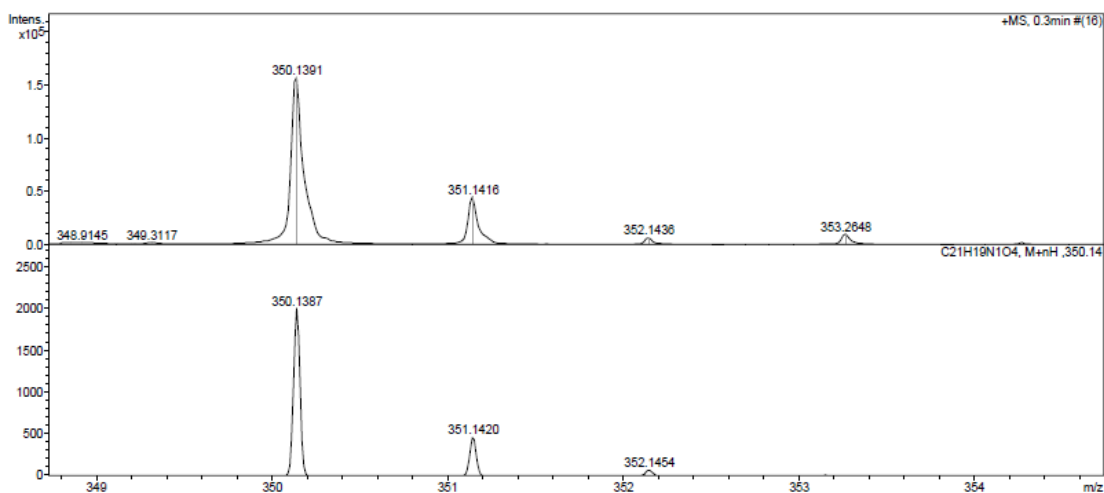


9.6.44 *N*-(4',5-Dihydroxy-[1,1'-biphenyl]-2-yl)-2-(3,5-dimethoxyphenyl)acetamide (74)

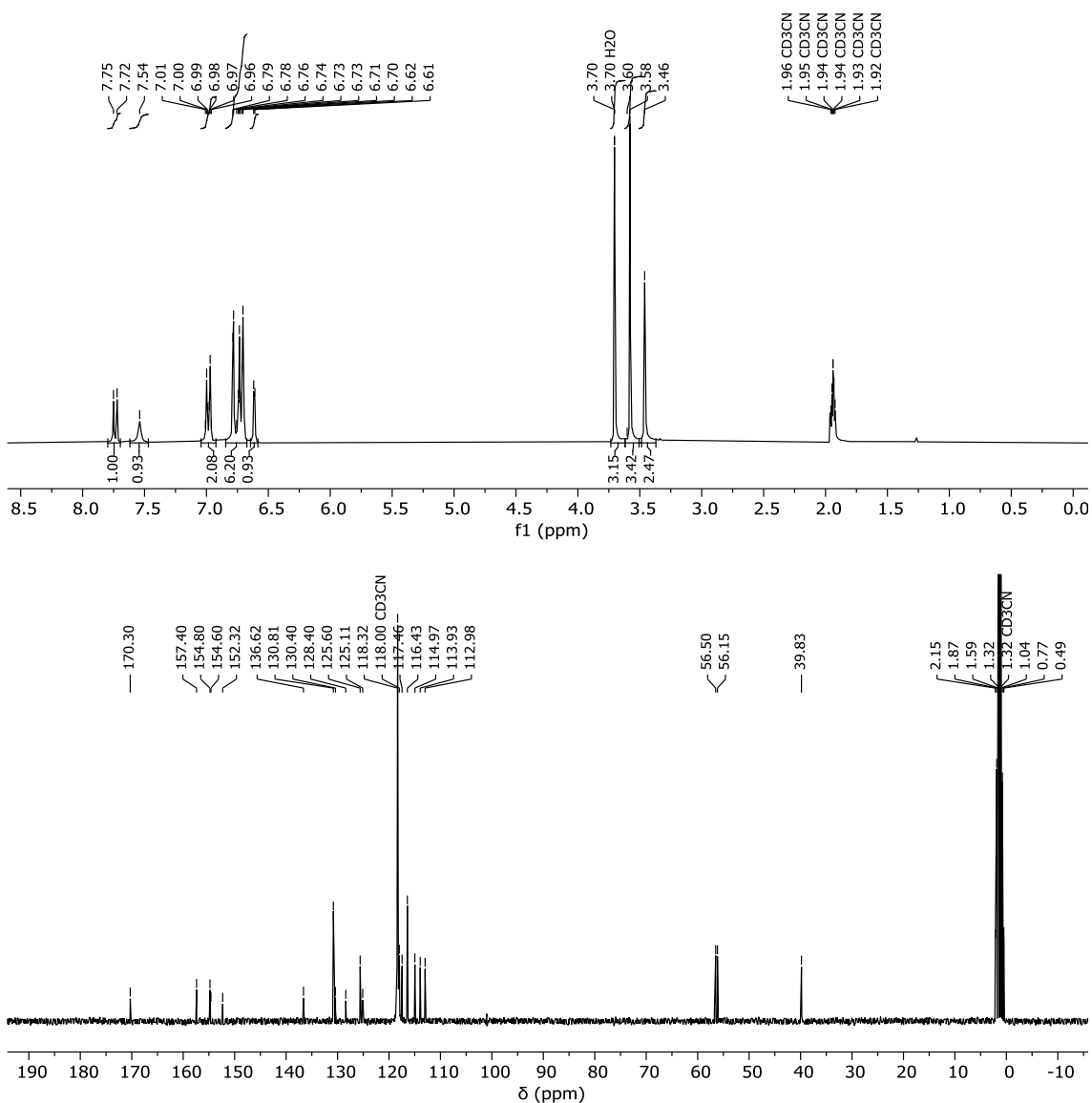


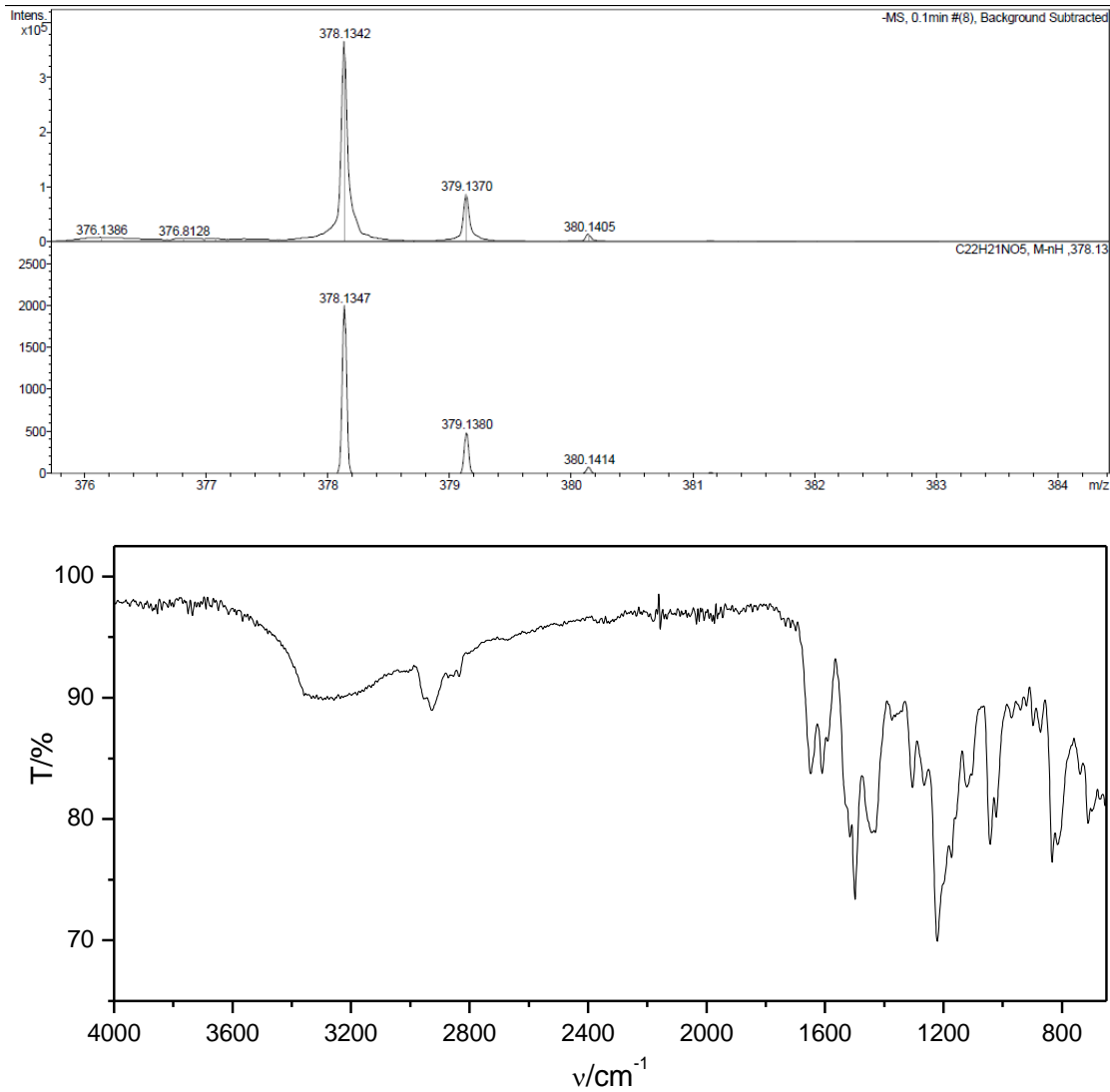
9.6.45 *N*-(4',5'-Dihydroxy-[1,1'-biphenyl]-2-yl)-2-(*o*-tolylloxy)acetamide (75)



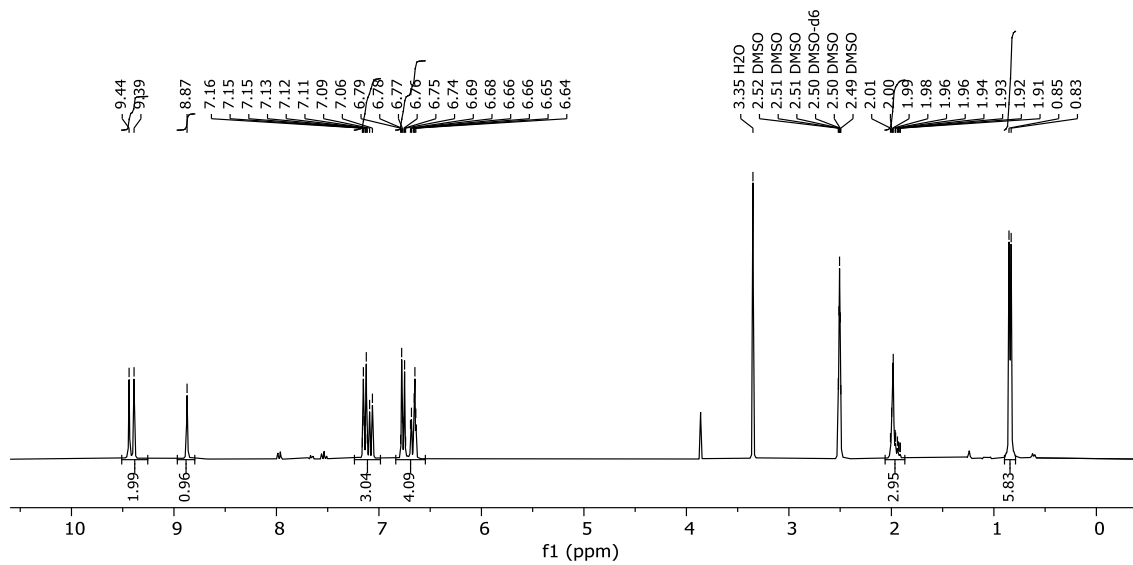


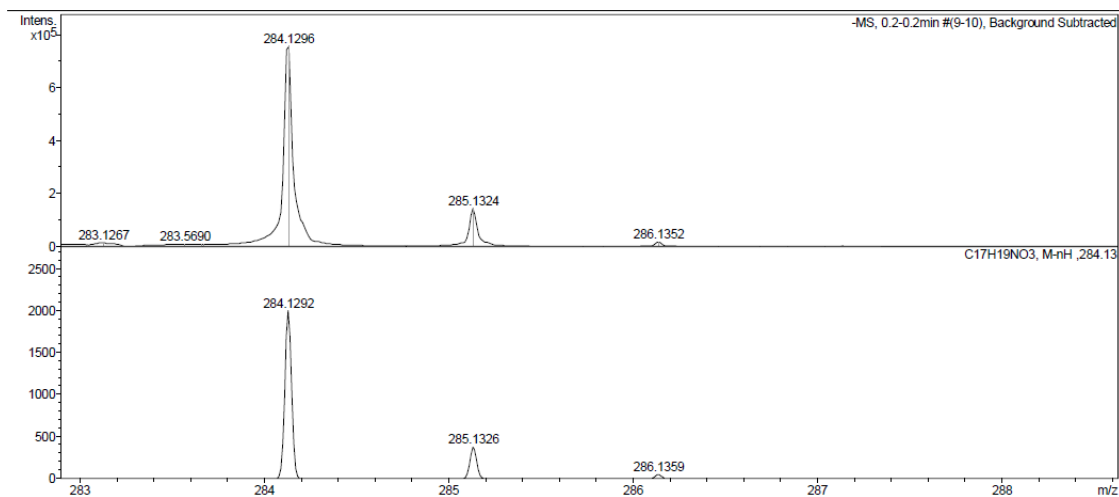
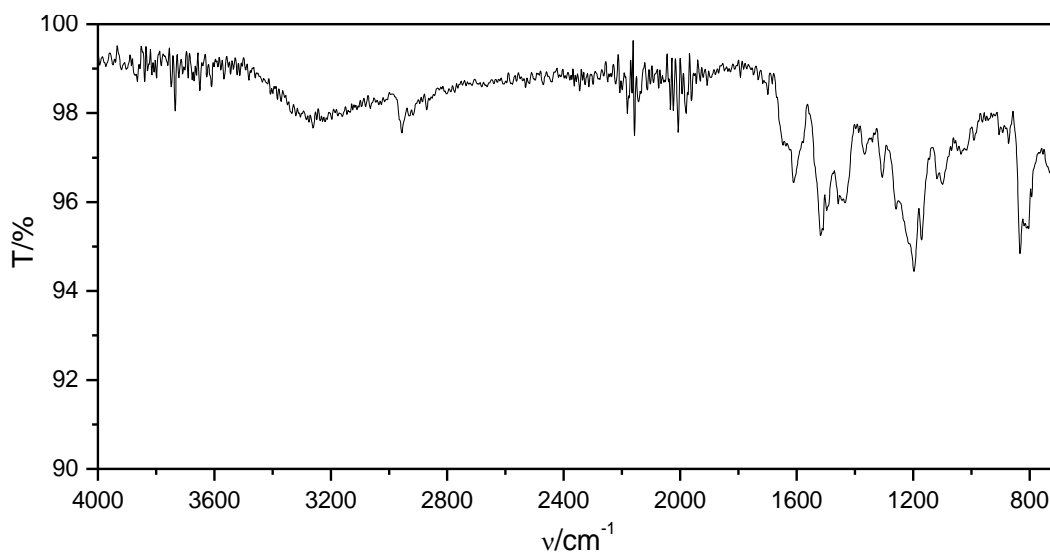
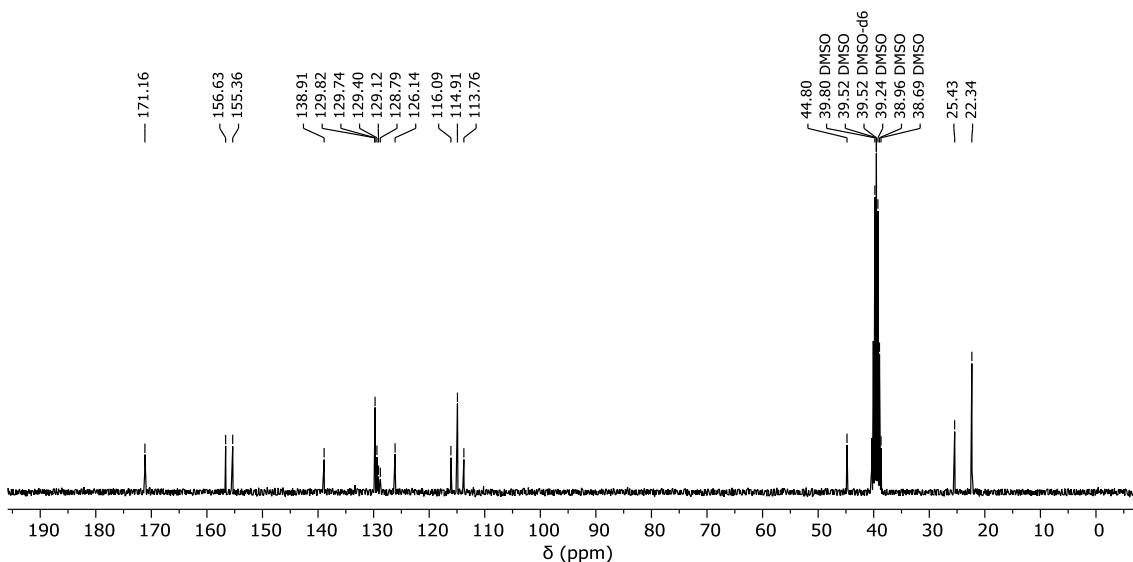
9.6.46 *N*-(4',5-Dihydroxy-[1,1'-biphenyl]-2-yl)-2-(2,5-dimethoxyphenyl)acetamide (76)



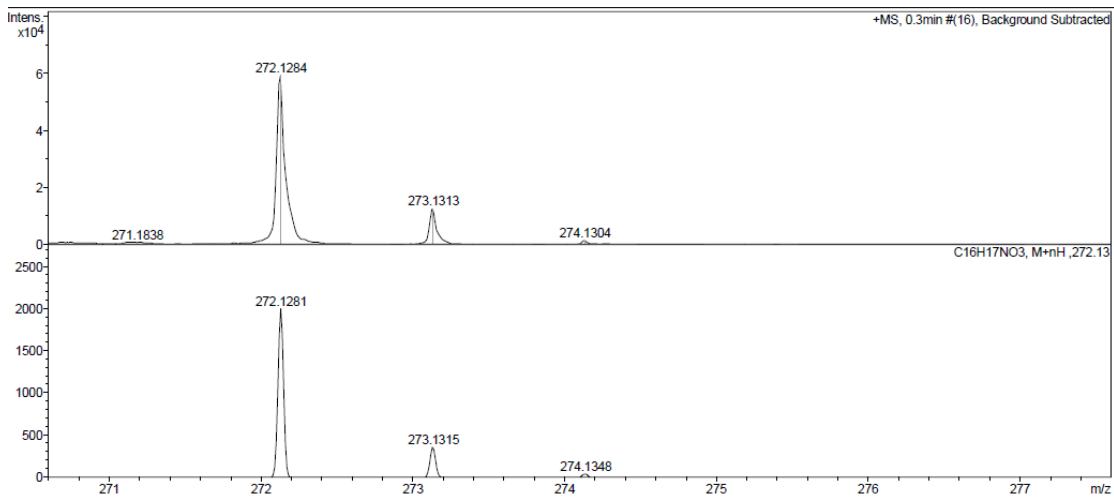
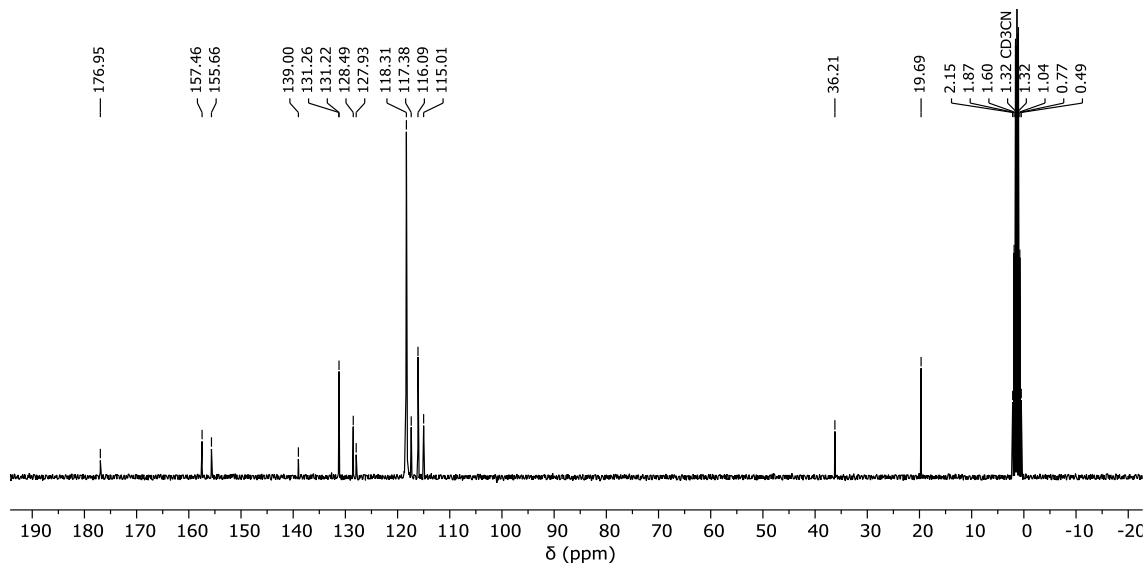
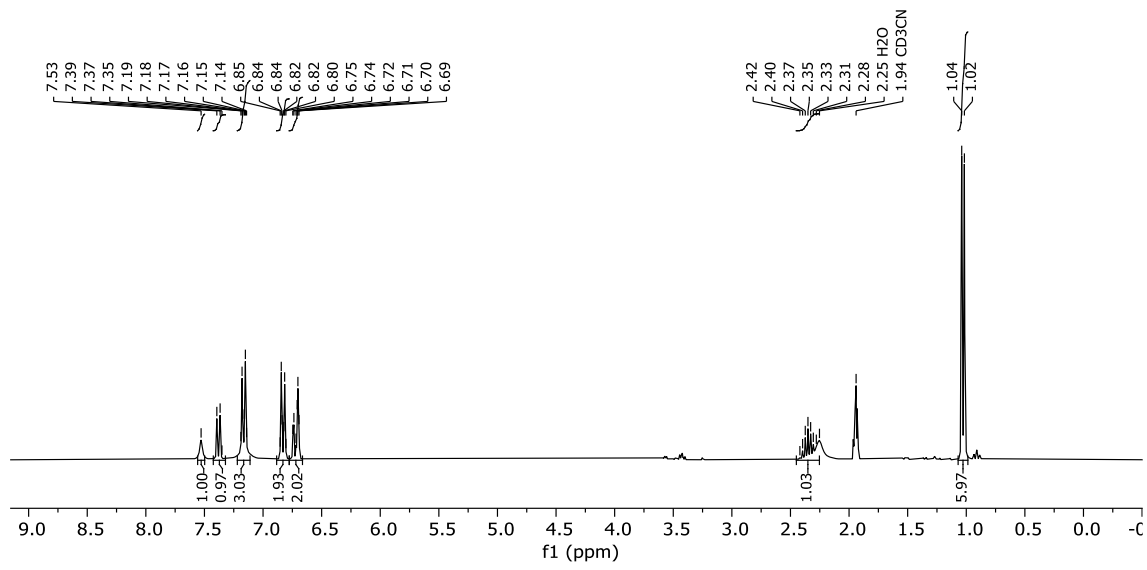


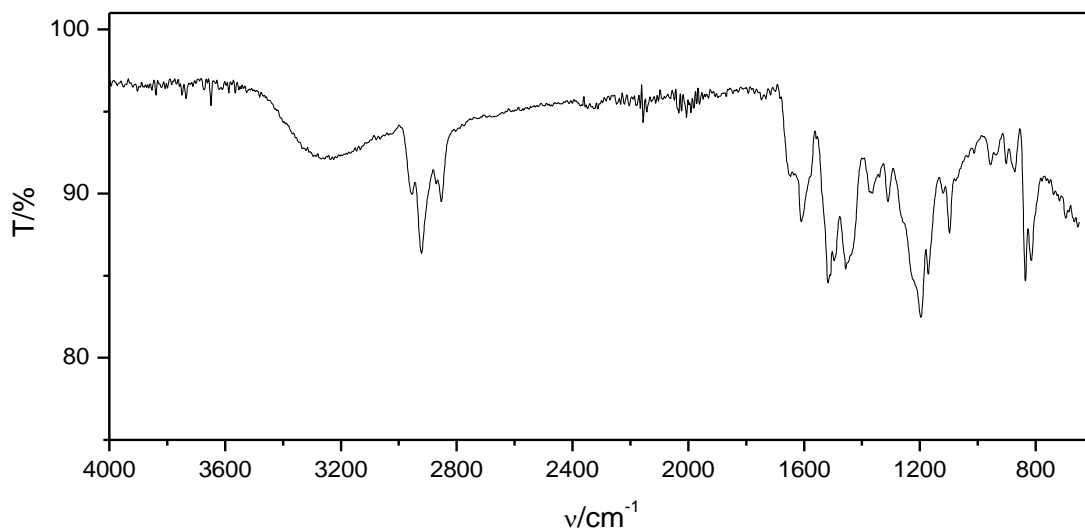
9.6.47 *N*-(4',5'-Dihydroxy-[1,1'-biphenyl]-2-yl)-3-methylbutanamide (77)



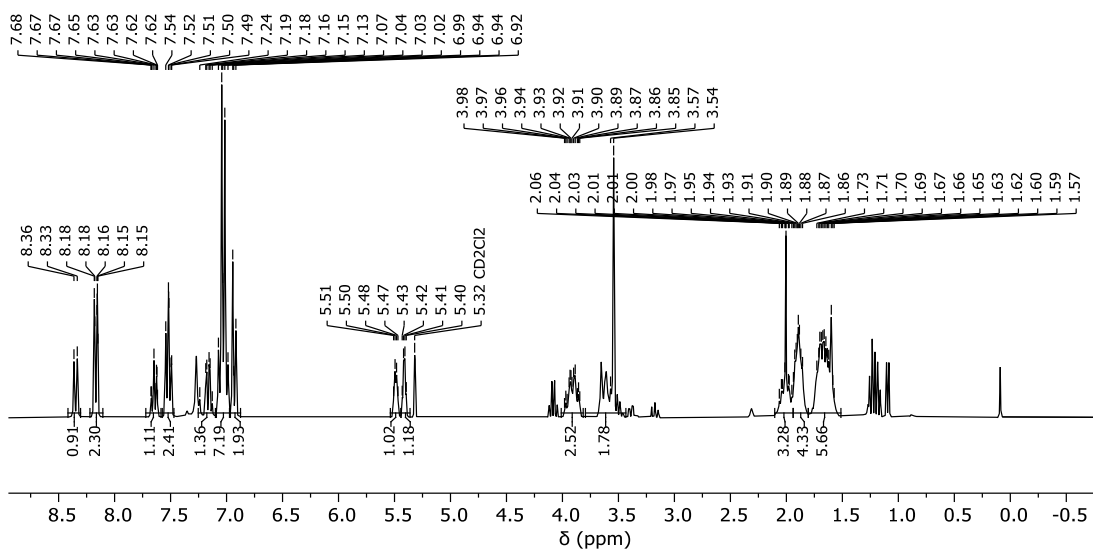


9.6.48 *N*-(4',5'-Dihydroxy-[1,1'-biphenyl]-2-yl)isobutyramide (78)

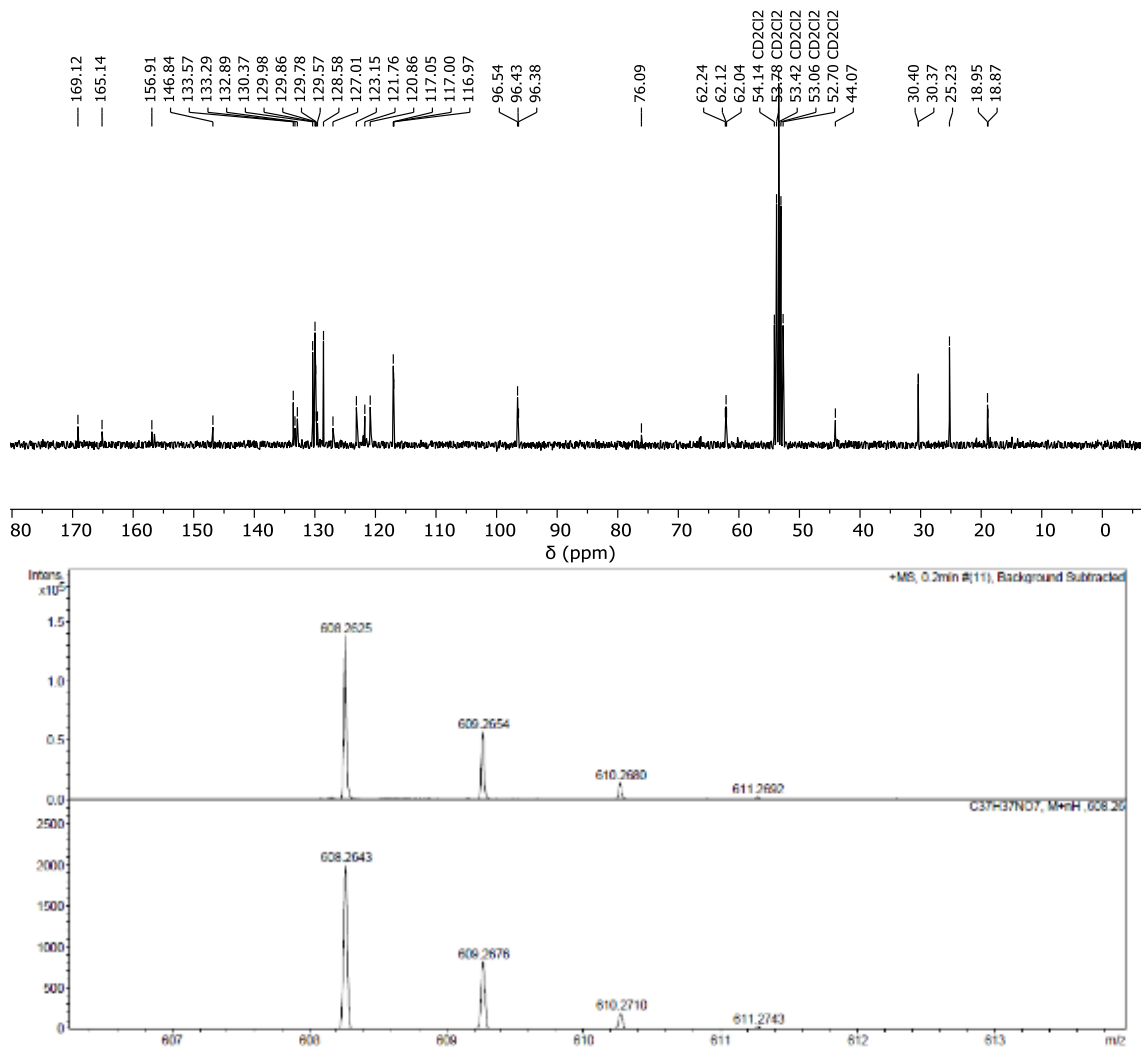




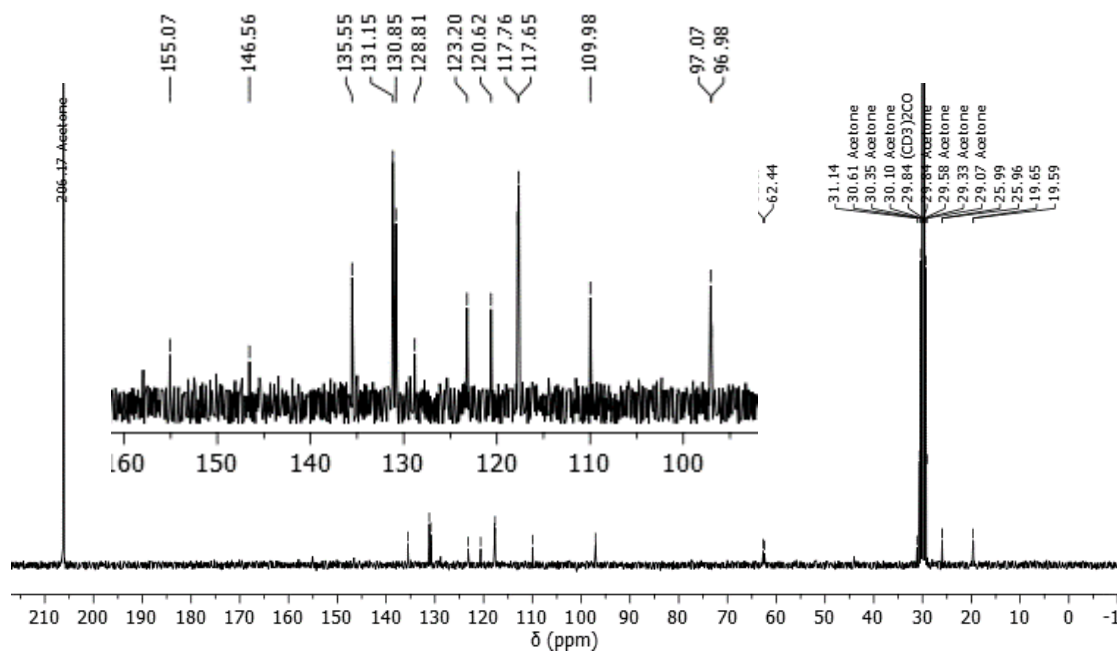
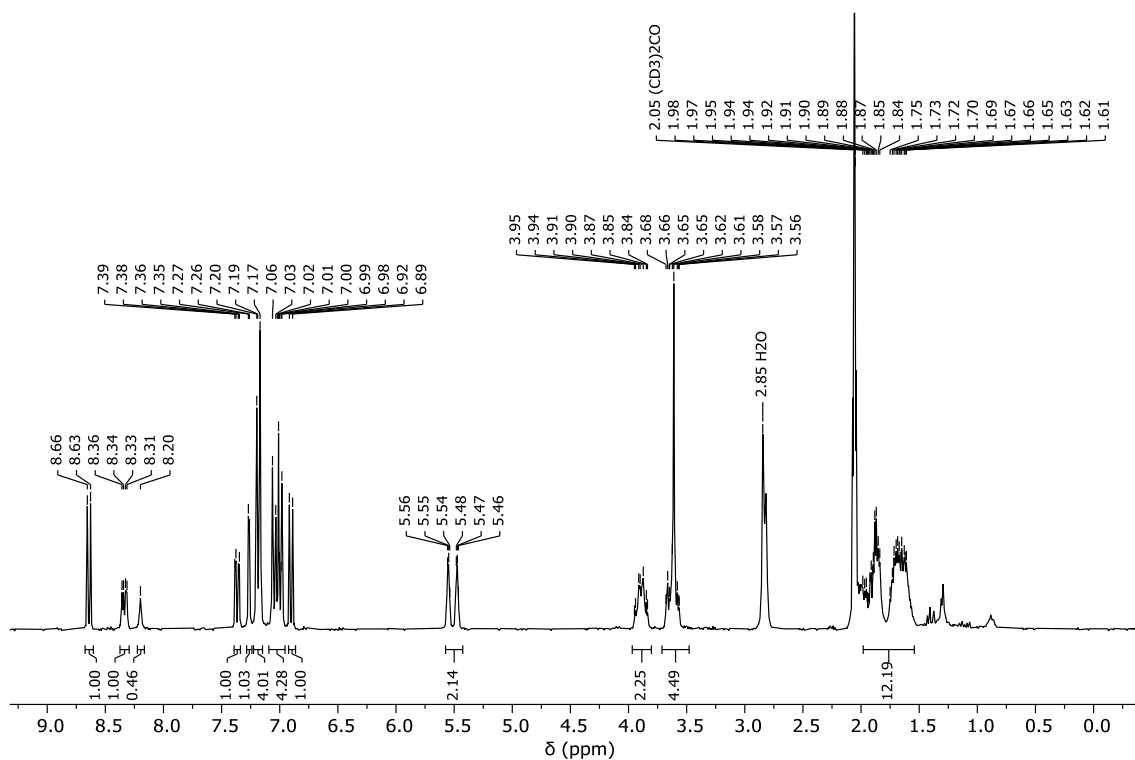
9.6.49 4'-((Tetrahydro-2H-pyran-2-yl)oxy)-6-(2-(4-((tetrahydro-2H-pyran-2-yl)oxy)phenyl)acetamido)-[1,1'-biphenyl]-3-yl benzoate (81)

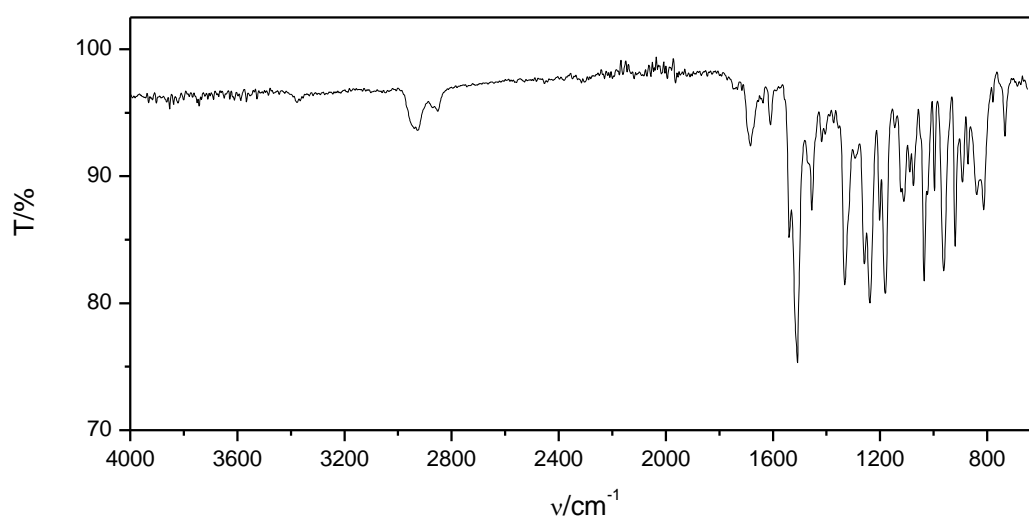
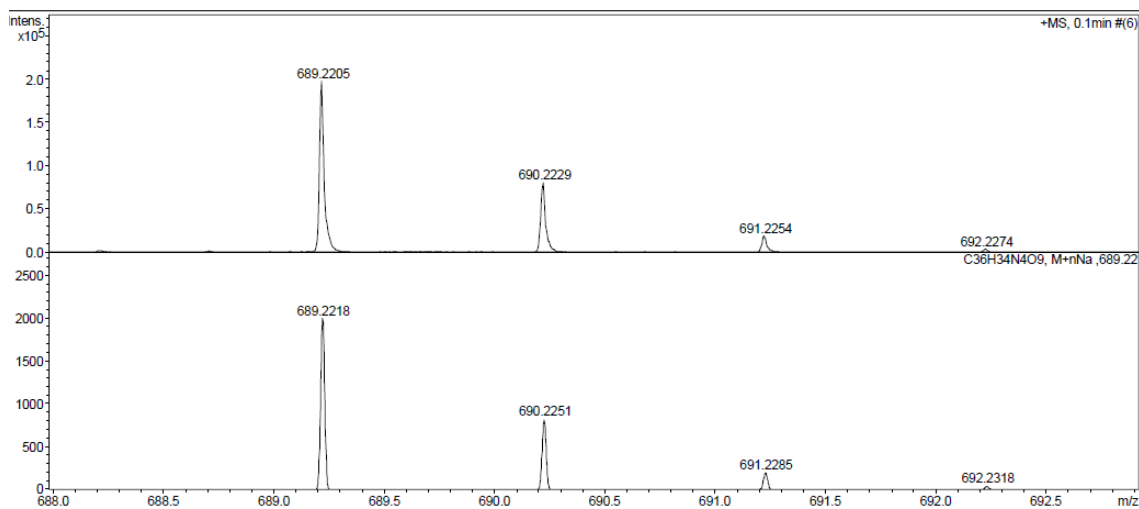


9 Appendices

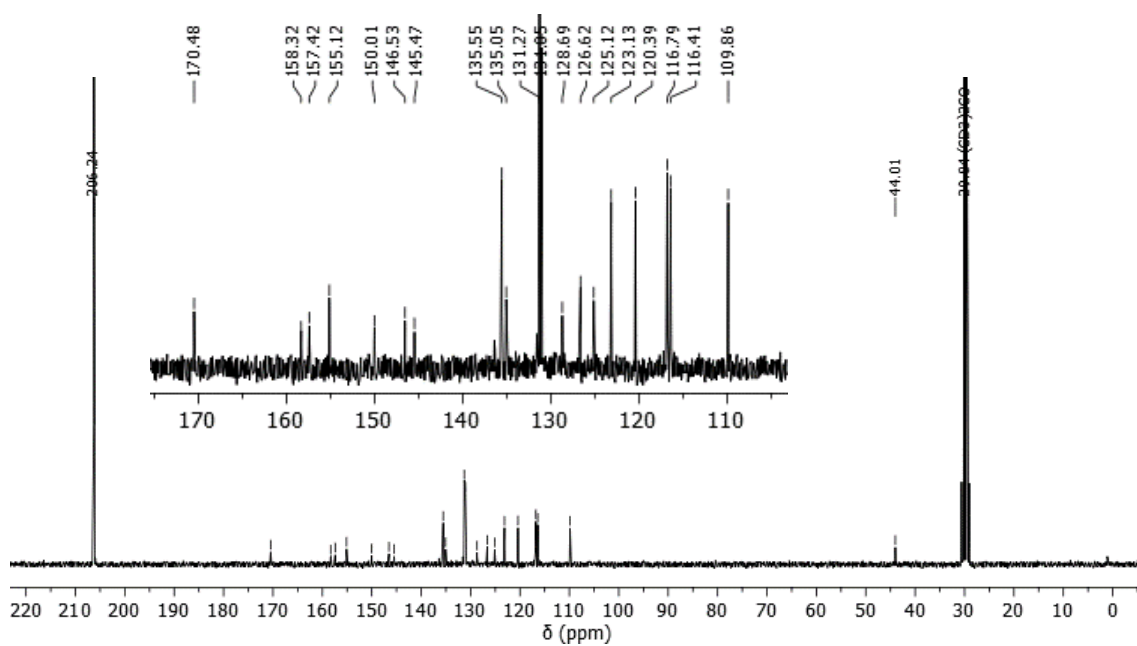


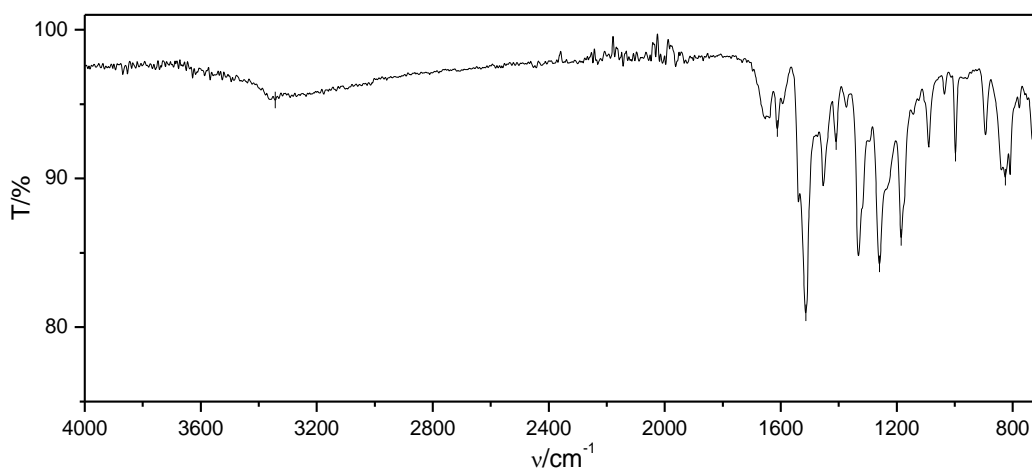
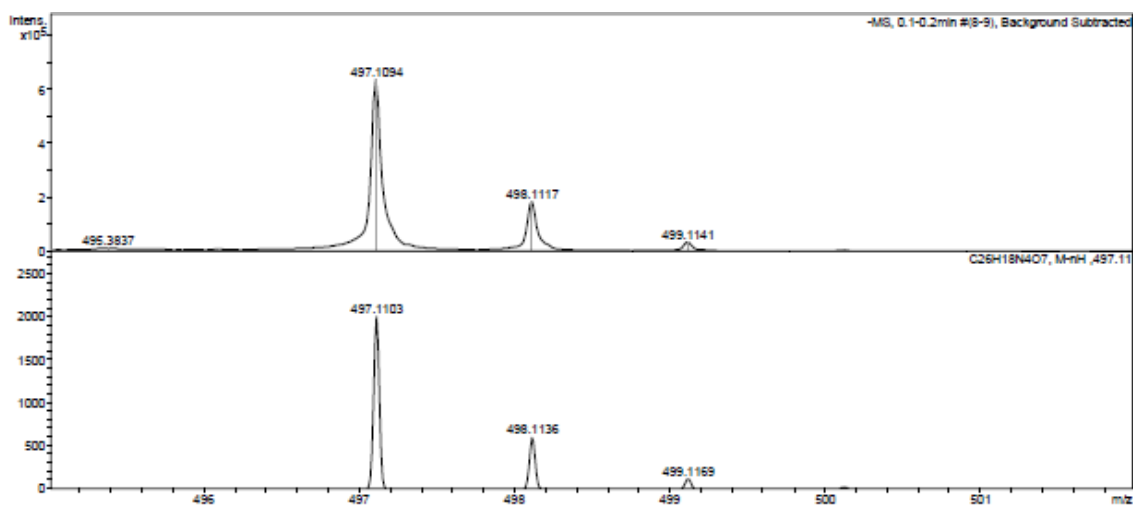
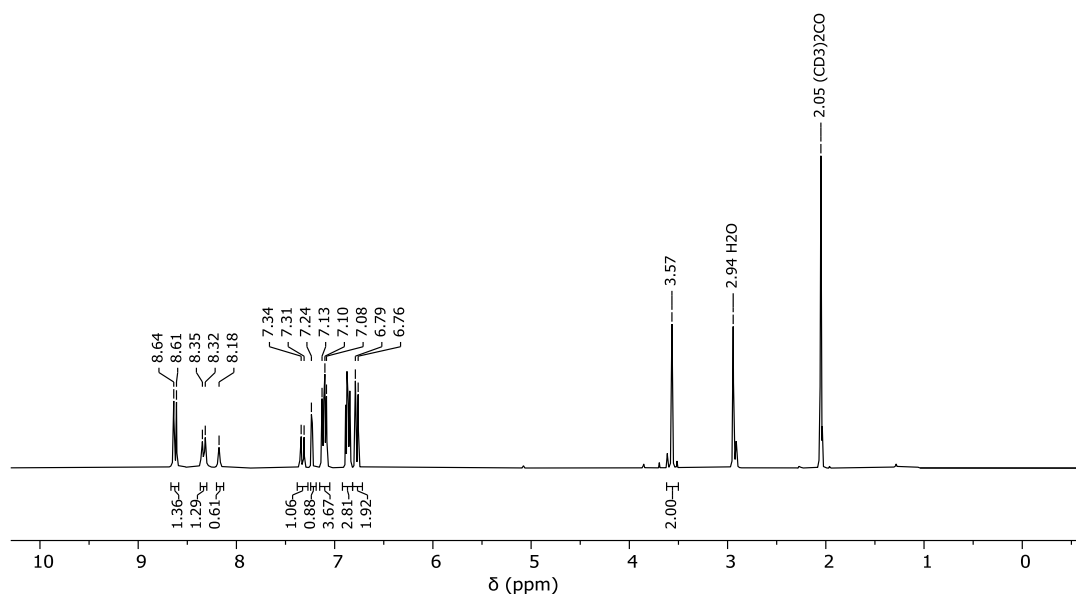
9.6.50 *N*-(5-((7-Nitrobenzo[*c*][1,2,5]oxadiazol-4-yl)oxy)-4'-((tetrahydro-2H-pyran-2-yl)oxy)-[1,1'-biphenyl]-2-yl)-2-(4-((tetrahydro-2H-pyran-2-yl)oxy)phenyl)acetamide (82)





9.6.51 *N*-(4'-Hydroxy-5-((7-nitrobenzo[*c*][1,2,5]oxadiazol-4-yl)oxy)-[1,1'-biphenyl]-2-yl)-2-(4-hydroxyphenyl)acetamide (83) LS A1





9.6.52 Proof of concept reaction

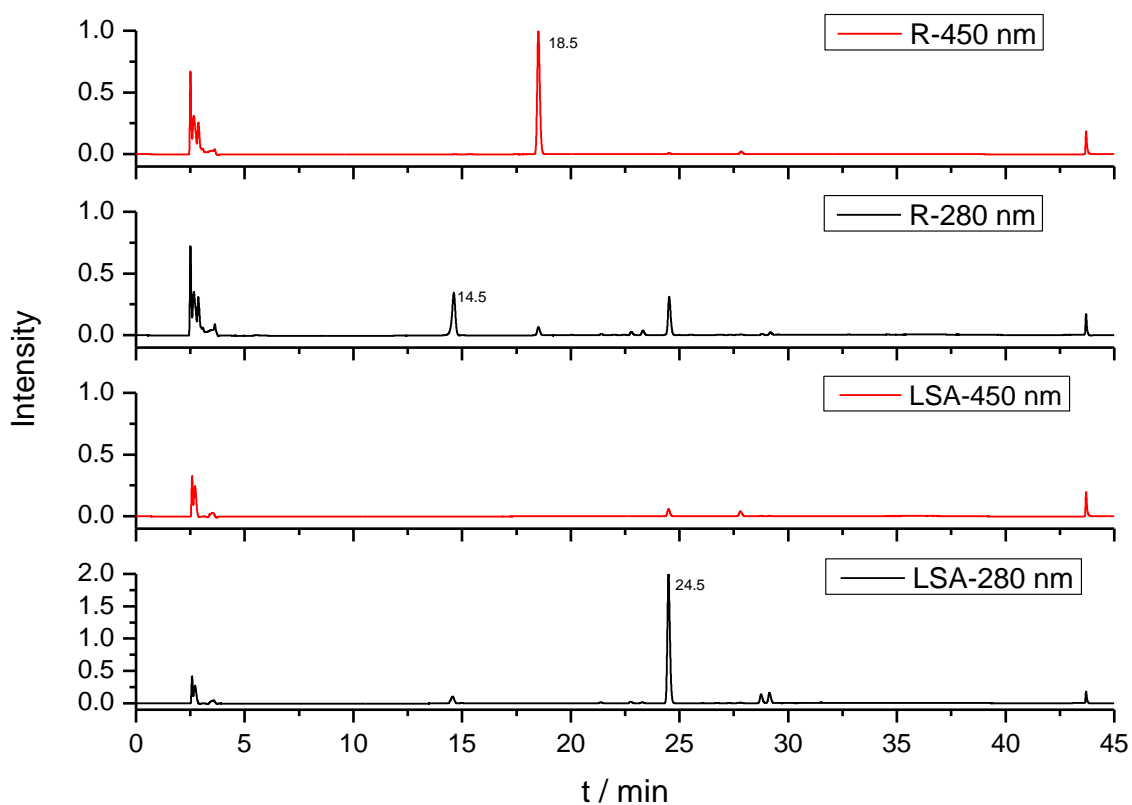


Figure 9.15 HPLC chromatograms of LS A (100 μ M) with 85 (100 μ M) in DMSO, as a proof of concept reaction after 2h incubation at 25 $^{\circ}$ C, (analytical C-18; 20 \rightarrow 100% MeCN in 35 min).